Unsupervised and Semi-Supervised Learning

Series Editor: M. Emre Celebi

Y-h. Taguchi

Unsupervised Feature Extraction Applied to Bioinformatics

A PCA Based and TD Based Approach

Springer

Unsupervised and Semi-Supervised Learning

Series Editor

M. Emre Celebi, Computer Science Department, Conway, Arkansas, USA

Springer's Unsupervised and Semi-Supervised Learning book series covers the latest theoretical and practical developments in unsupervised and semi-supervised learning. Titles – including monographs, contributed works, professional books, and textbooks – tackle various issues surrounding the proliferation of massive amounts of unlabeled data in many application domains and how unsupervised learning algorithms can automatically discover interesting and useful patterns in such data. The books discuss how these algorithms have found numerous applications including pattern recognition, market basket analysis, web mining, social network analysis, information retrieval, recommender systems, market research, intrusion detection, and fraud detection. Books also discuss semi-supervised algorithms, which can make use of both labeled and unlabeled data and can be useful in application domains where unlabeled data is abundant, yet it is possible to obtain a small amount of labeled data.

Topics of interest in include:

- Unsupervised/Semi-Supervised Discretization
- Unsupervised/Semi-Supervised Feature Extraction
- Unsupervised/Semi-Supervised Feature Selection
- Association Rule Learning
- Semi-Supervised Classification
- Semi-Supervised Regression
- Unsupervised/Semi-Supervised Clustering
- Unsupervised/Semi-Supervised Anomaly/Novelty/Outlier Detection
- Evaluation of Unsupervised/Semi-Supervised Learning Algorithms
- Applications of Unsupervised/Semi-Supervised Learning

While the series focuses on unsupervised and semi-supervised learning, outstanding contributions in the field of supervised learning will also be considered. The intended audience includes students, researchers, and practitioners.

More information about this series at http://www.springer.com/series/15892

Y-h. Taguchi

Unsupervised Feature Extraction Applied to Bioinformatics

A PCA Based and TD Based Approach

Springer

Y-h. Taguchi
Department of Physics
Chuo University
Tokyo, Japan

ISSN 2522-848X ISSN 2522-8498 (electronic)
Unsupervised and Semi-Supervised Learning
ISBN 978-3-030-22455-4 ISBN 978-3-030-22456-1 (eBook)
https://doi.org/10.1007/978-3-030-22456-1

The use of general descriptive names, registered names, trademarks, service marks, etc. in this publication does not imply, even in the absence of a specific statement, that such names are exempt from the relevant protective laws and regulations and therefore free for general use.
The publisher, the authors, and the editors are safe to assume that the advice and information in this book are believed to be true and accurate at the date of publication. Neither the publisher nor the authors or the editors give a warranty, express or implied, with respect to the material contained herein or for any errors or omissions that may have been made. The publisher remains neutral with regard to jurisdictional claims in published maps and institutional affiliations.

This Springer imprint is published by the registered company Springer Nature Switzerland AG.
The registered company address is: Gewerbestrasse 11, 6330 Cham, Switzerland

To all the scientists who have ever written at least one peer-reviewed paper. . . .

Foreword

Machine learning techniques serve as powerful tools in bioinformatics, specifically for predicting the structure and function of proteins and identifying disease-causing mutations, biomarkers, potential drug-like molecules, and so on. However, it is not straightforward to relate the features with performance. On the other hand, a simple statistical analysis can provide insights to understand the relationship; for example, the increase in long-range contacts slows down the folding of proteins, positive charged residues tend to dominate in DNA-binding domains, etc. Hence, linear algebra has the capability to reveal complicated genomic structures in a more direct manner than machine learning.

Almost 10 years ago, Prof. Taguchi and I published a paper on predicting protein folding types using principal component analysis (PCA), one of the liner algebra methods. He has continued his research to investigate the applications of PCA on various biological problems. Recently, he successfully moved to tensors. These methods provide insights to understand the concepts due to the fact that the data are easily interpreted and trace back the output from input features. It is amazing that such a simple strategy can be applied to a wide range of biological problems discussed in this book.

Prof. Taguchi has elegantly designed the book to understand the concepts easily. He has provided mathematical foundations on all important aspects followed by feature extractions. At the end of the book, he shows that PCA and tensors are powerful tools, which perform similar to machine learning techniques in the study of biological problems, namely, biomarker identification, gene expression, and drug discovery, evidenced with his numerous high-quality publications in reputed international journals.

In essence, this book is a valuable resource for students, research scholars, and faculty members to simultaneously grasp the fundamentals and applications of PCA and tensors. Although the applications listed in this book are limited to bioinformatics, the approach is extendable to other fields as well since they are general linear methods, which are easily understandable.

With these appreciations, I recommend this well-written book to the readers.

Chennai, India
25 March 2019

M. Michael Gromiha

Preface

He stole something unexpected…, your heart.
Inspector Zenigata, Lupin III: The Castle of Cagliostro, movie, Episode 1

This is a book about very classical mathematical techniques: principal component analysis and tensor decomposition. Because these two are essentially based upon linear algebra, one might think that these are no more than textbook-level matters. Actually, when I started to make use of them for the cutting-edge researches, many reviewers who reviewed my manuscripts complained about the usage of these old-fashioned techniques. They said, for example, "Why not use more modernized methods, e.g., kernel tricks?" or "Principal component analysis is a very old method for which no new findings can exist." In spite of these criticisms, I have continuously published numerous papers where I discussed how principal component analysis or tensor decomposition can be used for data science in a completely new way.

The principal reason why such old techniques can work pretty well is because of the topic targeted: feature selection in large p small n problem. Large p small n problem means that there are huge number of variables of which very small number of observations are available. In such situations, it is of course difficult to know what has happened in the system, because there are not enough number of points that cover the whole state space. This situation is also known as "the curse of dimensionality" which means the lack of enough number of observations compared with the number of dimensions. This problem remains unsolved over a long period.

In this book, I apply principal component analysis and tensor decomposition in order to tackle this difficult problem. There are several reasons why these two can work well in this difficult problem. At first, these two are unsupervised methods. In contrast to the conventional supervised methods, unsupervised methods are more robust. Especially, it is free from overfitting that can easily occur when supervised methods are applied to small number of samples with large number of dimensions, because unsupervised methods do not learn from labeling from which supervised methods must learn. Second, unsupervised methods are more stable than supervised methods, because unsupervised methods are independent of labeling. Another advantage of principal component analysis and tensor decomposition is that they consider the interaction between variables not after the features are selected but before they are selected.

The main purpose of this book is to perform feature selection that means selecting small or limited number of critical variables among huge number of variables. Although there have been numerous proposals for feature selection, there are very few fitted to apply to the large p small n problems. One typical approach among those not fitted to large p small n problems is a statistical test. When we would like to find features that satisfy some required properties, statistical test can compute the probability that the desired property can appear by chance. If some features are associated with small enough probability, we can regard that the feature is truly associated with this property. In large p small n problem, this strategy often fails. Smaller number of samples can increase the probability that the desired property can happen by chance. On the other hand, if the number of features are large, small probability can happen by chance; if the number of features is as many as 10^4, features associated with the probability as small as 10^{-4} can appear with the probability of 1 (i.e., almost always). Because of the same reason, even if we try to find the features best fitted with the desired property, it might be simply accidental.

The basic idea to resolve these difficulties using principal component analysis and tensor decomposition is as follows. First, before features are selected, a whole data set is embedded into lower-dimensional space. Because feature selection is performed within this lower-dimensional space, it is not a large p small n problem anymore. Thus, it is also free from “the curse of dimensionality.” Then the dimension in which feature selection is performed is selected with a variety of methods fitted to desired properties. As can be seen in the later parts of this book, this simple idea works surprisingly well.

In Chap. 1, I reintroduce basic concepts, including scalar, vector, matrix, and tensor, from data science point of views. Chapters 2 and 3 introduce two embedding methods by which dimensions are reduced, principal component analysis as a part of matrix factorization and tensor decomposition, respectively. The following two chapters explain how we can make use of these two for the feature selection with applying them to synthetic data sets. The last two chapters are dedicated to the applications of two methods to bioinformatics where large p small n problems are very usual.

Although the application of the proposed methods is limited to genomic science, because general workframe of the methodologies is very universal, the readers are expected to apply these two to their own problems in data science. I am happy to hear from their achievements when the methods proposed in this book are applied to various problems.

Tokyo, Japan
March 2019

Y-h. Taguchi

Acknowledgments

Unfortunately, because I have developed this method almost by my own, I have no persons to which I would acknowledge their contributions.

On the other hand, I have many researchers who would like to make use of my own methods for their problems as applications. These researchers include Prof. Yoshiki Murakami who is a medical doctor and wrote many medical papers with me, Prof. Hideaki Umeyama who is a pharmacologist and a specialist about in silico drug design and has performed a university running project with me, and Prof. Mitsuo Iwadate who was once a member of Prof. Umeyama's lab. In addition to this, two Taiwanese professors, Hsiuying Wang at the Institute of Statistics, National Chiao Tung University, and Ka-Lok Ng at the Department of Bioinformatics and Medical Engineering, Asia University, have published a few papers with me. I would like to thank all of the researchers, including these above professors, who wrote papers with me using the methods proposed in this book.

At last, but not at least, I would like to thank all of my family members, my wife, Tomoko, and sons, Yuu and Koki, for their continuous mental supports for me. Without their help, I could not write this book.

Contents

Part I Mathematical Preparations

Part II Feature Extractions

Acronyms

ALL	Acute lymphoblastic leukemia
ALS	Alternating least square
AY	Amygdala
BAHSIC	Backward elimination using Hilbert-Schmidt norm of the cross-covariance operator
BH	Benjamini Hochberg
BP	Biological process
CC	Cellular component
CHB	Chronic hepatitis B
CHC	Chronic hepatitis C
ChIP	Chromatin immunoprecipitation
CP	Canonical polyadic
DAVID	Database for Annotation, Visualization, and Integrated Discovery
DEG	Differentially expressed gene
DF	Dengue fever
DHF	Dengue hemorrhagic fever
DMS	Differentially methylated site
DNA	Deoxyribonucleic acid
FACS	Fluorescence activated cell sorting
FDR	False discovery rate
FE	Feature extraction
FN	False negative
FP	False positive
GEO	Gene Expression Omnibus
GO	Gene ontology
HC	HIPPOCAMPUS
HDAC	Histone deacetylase
HOOI	Higher-order orthogonal iteration of tensors
HOSVD	Higher-order singular value decomposition
HTS	High-throughput sequencing
KEGG	Kyoto Encyclopedia of Genes and Genomes

KO	Knockout
LBDD	Ligand-based drug design
LDA	Linear discriminant analysis
LIMMA	Linear models for microarray data
LOOCV	Leave one out cross validation
miRNA	microRNA
MF	Molecular function
MF	Matrix factorization
MPFC	Medial prefrontal cortex
MSigDB	The molecular signatures database
NASH	Nonalcoholic steatohepatitis
NP	Nondeterministic polynomial time
NSCLC	Non-small cell lung cancer
OE	Over expression
PC	Principal component
PCA	Principal component analysis
PTSD	Post-traumatic stress disorder
RFE	Recursive feature elimination
RGB	Red, green, and blue
RNA	Ribonucleic acid
RPKM	Reads per kilobase of exon per million
SAM	Significance analysis of microarrays
SBDD	Structure-based drug design
scRNA-seq	Single-cell RNA sequencing
SE	Septal nucleus
SNP	Single nucleotide polymorphism
ST	Striatum
SVD	Singular value decomposition
TD	Tensor decomposition
TF	Transcription factor
TGE	Transgenerational epigenetics
TN	True negative
TP	True positive
TSS	Transcription start site
UDB	Universal disease biomarker
UFF	Unsupervised feature filtering
UPGMA	Unweighted pair group method using arithmetic average
UTR	Untranslated region
VS	Ventral striatum

Part I
Mathematical Preparations

In this part, we briefly introduce mathematical basics required for understanding the content of this book. Most of the part is usually taught in the first grade of undergraduate course at university. Thus, some readers might skip this part. However, it tried to re-introduce basic mathematical concepts from the data science point of views.

Chapter 1
Introduction to Linear Algebra

None can extinguish souls!
Momo Minamoto, Release the Spyce, Season 1, Episode 12

1.1 Introduction

Linear algebra is composed of simple arithmetic operations: addition, subtraction, multiplication, and division. In spite of their simpleness, it is often powerful enough to represent some complicated data set. In some sense, linear algebra is something like scissors. Although scissors can do only one thing, cutting, it can be used for various purposes if it is used by skilled persons. A piece of paper can be a beautiful art called as a cutting picture that looks like a very complicated sculpture. A skilled hairdresser can use scissors to change a female outlook so beautiful. Likewise, linear algebra can be used to understand very complicated data set that is difficult to understand otherwise, if you can make use of it so as to let it demonstrate the maximum power. In this chapter, we prepare the knowledge that can be used in the later chapters for the application as data science technology.

1.2 Scalars

1.2.1 Scalars

Scalars are numbers that take real values. In the data science context, scalars are usually numbers that describe samples. Here samples correspond to some objects that will be targeted under the investigation. The examples of pairs of samples and associated scalars are

- person and weight
- food and price
- star and brightness

Y-h. Taguchi, *Unsupervised Feature Extraction Applied to Bioinformatics*,
Unsupervised and Semi-Supervised Learning,
https://doi.org/10.1007/978-3-030-22456-1_1

Thus, in contrast to the generic algebra, scalars are not always able to be added with each other; brightness cannot be added to price, price cannot be added to weight, and so on. Not only addition, but also division, multiplication or subtraction are not always possible, either. Arithmetic is possible only between same scalars; brightness plus brightness, weight plus weight. In this sense, data science algebra is more restricted than usual algebra.

In the data science, it is critically important to remember that all scalars analyzed have origins in the real world; no scalars are purely ideal numbers. This is primarily distinct from simple mathematical numbers that do not always have counterpart in the real world. Scalars in data science always represent something that exists in the real world.

Exercise
1.1 List ten pairs of samples and associated scalars.

1.2.2 Dummy Scalars

In contrast to scalars that describe samples, samples are often associated with features that cannot be described with real values. Such examples are color. Although it is possible to artificially attribute real values to colors, e.g., using RGB (red, green, and blue) color model, it is empirically useless. In RGB color system, colors are represented as combinations of three scalars. For example, red corresponds to (1,0,0) and blue corresponds to (0,0,1). Formal addition of distinct colors, e.g., red plus blue, results in completely distinct third color, (1,0,1), which corresponds to pink. Thus, it does not make sense. More severely, there are generally no ways to add distinct features. What comes if American is added to Japanese (in this case, feature is nationality)? In order to avoid this difficulty, dummy scalars are usually introduced. All features that cannot be described using real values are converted to 1 or 0. If a sample has the feature, corresponding dummy scalar takes 1 otherwise 0. In the example of colors, the number of scalars is as many as number of colors. If all samples under the investigation can take one hundred colors, we have to prepare same number of dummy scalars and add 1 or 0 to them depending on the color association with each sample. All samples with red have dummy scalar, to which red color is attributed, of 1. Introduction of dummy scalars is critically important since its introduction enables us to deal with any features that cannot be easily represented by real values.

Exercise
1.2 List ten features that must be treated as dummy scalars.

1.2.3 Generating New Features by Arithmetic

Although distinct scalars cannot be added with each other, in the real application we need to generate new features from scalars. In order to perform arithmetic between distinct scalars, multipliers are introduced. Suppose that there are three distinct scalars, x, y, and z. In order to enable addition among these, multipliers α, β, and γ are multiplied to scalars as αx, βy, and γz. Now, it is possible to add them as $\alpha x + \beta y + \gamma z$. Multipliers have two functions. The first function is make scalars non-dimensional. Non-dimensional scalars mean those without unit. For example, if one would like to add weight, price, and brightness, the multipliers of these should have unit of inverse of weight, price, and brightness. Then products of scalars and associated multipliers are non-dimensional. In order to perform arithmetic between scalars, introduction of multipliers is essential. The second function of multipliers is to equalize the amount of scalars. If weight is measured in kg, it has values between 0 and 100. If price is defined in Japanese currency, yen, it typically has values between 0 and 1,000,000. Brightness can be measured by various units. If lumen is employed as unit, brightness typically takes values as large as several thousands. Without multipliers, individual contributions of distinct scalars to newly generated feature cannot be balanced. Thus, the introduction of multipliers is required in order to control contributions of scalars to generated feature. Once scalars are multiplied with multipliers, the product of scalars and multipliers can be arguments of any arithmetic functions, e.g., sin and log. Thus, new features can be generated not only by arithmetic but also using functions, e.g., $\log(\alpha x + \beta y + \gamma z)$.

In this context, dummy scalars can also be combined with usual scalars that take real values. In this sense, any of x, y, and z can be also dummy scalars. Since dummy scalars are non-dimensional, multipliers associated with dummy scalars are also non-dimensional.

Exercise

1.3 Generate ten new features using three scalars x, y, and z as well as three associated multipliers α, β, and γ.

1.3 Vectors

1.3.1 Vectors

Vectors are composed of set of scalars. For convenience, the elements of vectors are represented by adding suffix to scalars, e.g., x_j, where x is scalar and j is suffix that spans integers. With employing this notation, we are free from introducing the numerous characters to represent a set of many scalars.

In order to be free from representing vectors as a set of many scalars with suffix, we can introduce a vector notation, $\boldsymbol{x}$,

$$\boldsymbol{x} = (x_1, x_2, \dots, x_M) \tag{1.1}$$

where M is the number of samples. In short, it is often represented as $\boldsymbol{x} \in \mathbb{R}^M$. This says that there are M samples, each of which a scalar x_j is attributed to. A typical example of $\boldsymbol{x}$ is that there are M foods, each of which prices are attributed to, e.g., (Table 1.1) where $M = 4$ and $\boldsymbol{x} = (100, 1000, 300, 200)$.

Exercise
1.4 Generate some vectors that represent a set of samples.

It is very usual that samples are accompanied with more than one scalar. For example, we can attribute weights to foods (Table 1.2).

Then, a set of foods is accompanied with additional vector, $\boldsymbol{y} = (200, 300, 100, 150)$.

1.3.2 Geometrical Interpretation of Vectors: One Dimension

It is often very useful to interpret the vectors geometrically. For example, $\boldsymbol{x} = (100, 1000, 300, 200)$ can be considered to be coordinates of four points aligned along a line (Fig. 1.1).

There are several advantages of the geometrical representation of vectors. At first, it can give samples the order that can be easily visually recognized. By simply

Table 1.1 An example of vector: foods vs prices

Foods	Prices
Bread	100 yen
Beef	1000 yen
Pork	300 yen
Fish	200 yen

Table 1.2 Another example of vector: foods vs weights

Foods	Weights
Bread	200 g
Beef	300 g
Pork	100 g
Fish	150 g

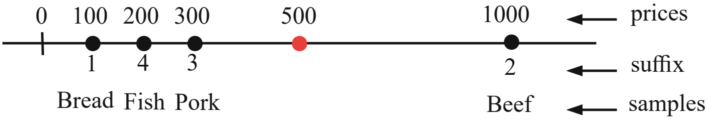

Fig. 1.1 A geometrical interpretation of vector $\boldsymbol{x} = (100, 1000, 300, 200)$. Individual components of the vector that correspond to prices of four samples are considered to be four coordinates of four points aligned along a line. Prices considered to be coordinates are displayed above the line while suffix that corresponds to four samples is displayed below the line. A red point represents an imaginary sample with the price of 500 yen

glancing the sequence of scalars, it is hard to recognize the rank order of scalars. Second, the distances between samples can be introduced. Then, from the prices, we can say that two pairs of samples, the pair of bread and fish and the pair of pork and fish, are equally separated. If we specifically define measure of distance, say Euclid distance, we can compute the distance between samples numerically as

$$\text{distance between bread and beef} = \sqrt{(100 - 1000)^2} = 900 \tag{1.2}$$

$$\text{distance between bread and fish} = \sqrt{(100 - 200)^2} = 100 \tag{1.3}$$

where Euclid distance between two points j and j' having coordinates of x_j and $x_{j'}$, respectively, can be defined as

$$\sqrt{\left(x_j - x_{j'}\right)^2} \tag{1.4}$$

Using the numerical distances, we can quantitatively compare two pairs of samples on how far they are apart from each other. In this case, bread is nine times apart from beef than fish. These two points, the definition of rank order of samples and numerical distances between pairs of samples, will turn out to be critical for data science analysis.

An additional advantage of geometrical interpretation is that any point along the line automatically has prices. For example, if a point is placed on the line with the coordinate of 500 yen (a red point in Fig. 1.1), this point represents a sample with the price of 500 yen. This allows us to think about an imaginary sample with this price without specifying what it is. This is also a great advantage for data science, which must predict something unknown. With geometrical representation, we can discuss about samples with arbitrary scalars without specifying what it is. This abstraction is very important as can be seen later.

Exercise

1.5 Draw geometrical representation of Table 1.2.

1.3.3 Geometrical Interpretation of Vectors: Two Dimensions

As denoted in Sect. 1.3.2, samples can be associated with more than one scalar (Tables 1.1 and 1.2). In this case, geometrical representation must also be altered from a line to a plane. Figure 1.2 shows geometrical representation of four foods according to the scalars shown in Tables 1.1 and 1.2.

Now, using two scalars simultaneously, the relationship among four foods becomes clearer. Beef is apart from other three, because it has the largest weight and highest price. As in the one dimension, any points in the plane are automatically associated with pairs of scalars: prices and weight. A red point in Fig. 1.2 represents an imaginary sample associated with price of 500 yen and weight of 250 g.

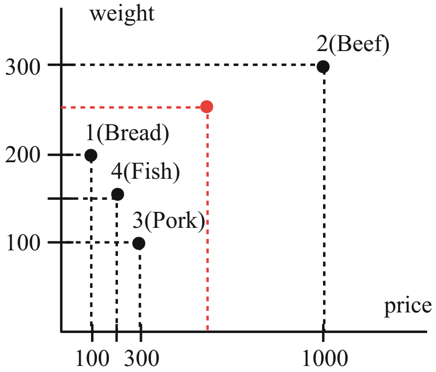

Fig. 1.2 A geometrical interpretation of Tables 1.1 and 1.2. Horizontal axis and vertical axis correspond to prices (Table 1.1) and weights (Table 1.2), respectively. A red point represents an imaginary sample with the price of 500 yen and a weight of 250 g

Table 1.3 Foods vs prices using dollar as price

Foods	Prices
Bread	1 dollar
Beef	10 dollars
Pork	3 dollars
Fish	2 dollars

If one thinks that there is nothing unclear, one might miss an important point: scale. In Fig. 1.2, length that corresponds to 100 yen does differ from length that corresponds to 100 g. Nevertheless, there are no reasons to make them equal to each other. When length of 100 yen is made to be equal to 100 g, the plot will be elongated toward horizontal direction. The problem is that there is no criterion to decide scale, since prices can never be related to weight.

One may wonder that it is not a problem, since numerical distance can be defined independent of scale. For example, the Euclidean distance between fish and pork in the plane shown in Fig. 1.2 can be defined as

$$\sqrt{(200-300)^2 + (150-100)^2} \simeq 111 \tag{1.5}$$

that is independent of scale.

Exercise

1.6 Compute Euclidean distances of any pairs of samples (points) in Fig. 1.2.

Although it apparently seems to work, it actually does not. Suppose that we use dollar instead of yen for prices. For example, if we can assume that 1 dollar costs 100 yen, Table 1.1 now becomes Table 1.3.

Then, the Euclidean distance between fish and pork is not about 111 but

$$\sqrt{(2-3)^2 + (150-100)^2} \simeq 50 \tag{1.6}$$

Now it is clear that there are many problems in two-dimensional representations. At first, the distance cannot be determined independent of the unit of scalars. As soon as the foods are imported from Japan to the USA, the distances between foods might change. It does not make sense. In addition to this, in the system of dollar-gram unit, the prices are almost ignored on the computing distances. It also does not make sense.

Unfortunately, there are no definite ways to address this problem uniquely. How we should scale different scalars must be decided depending upon what we would like to know from the data given. It is highly context dependent. Thus, we will discuss this later when we apply mathematics to real data set.

1.3.4 Geometrical Interpretation of Vectors: Features

In the previous sections, geometrical representations were applied to samples, i.e., four foods. In Sect. 1.3.1, two vectors, $\boldsymbol{x} = (100, 1000, 300, 200)$ for prices and $\boldsymbol{y} = (200, 300, 100, 150)$ for weights were defined, respectively. These two vectors can also be interpreted as a geometrical representation of two features, price and weight (Fig. 1.3). Excluding the omission of fish for easier visual recognition, Figs. 1.2 and 1.3 are mathematically equivalent. In spite of the mathematical equivalence, it is not very popular to interpret vectors as geometrical representation of not samples but features. This is primarily because we have to plot different scalars, i.e., prices and weights, on the common axes. In Sect. 1.3.3, the ambiguity of scale was pointed out. The problem of scale is more visible in the geometrical interpretation of vectors for features (Fig. 1.3) than that for samples (Figs. 1.1 and 1.2). In the third (vertical) axis in Fig. 1.3 that corresponds to pork, 300 yen is more distant from origin than 100 g. It is apparent that this spatial relationship between price and weight of bread is not informative at all, since as soon as we use dollar (Table 1.3) instead of yen, the price (now it is "only" three dollars) becomes closer to the origin than the weight (100 g). Second, it is not recommended to plot distinct units (in this case, price and weight) along the same axis in physical sciences where this kind of coordinate representation was firstly developed (for example, energy and force can never be plotted on the same axis).

In spite of these difficulties, the emphasis of the equivalence between two geometrical representations (either that of samples or that of features) will turn out to be practically very useful for the main topics of this book.

Exercise

1.7 Draw geometrical representations of prices and weights using combinations of samples distinct from those used in Fig. 1.3, e.g., beef, pork, and fish.

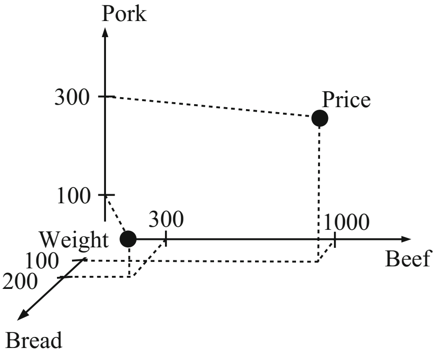

Fig. 1.3 An alternative geometrical interpretation of two vectors, $\boldsymbol{x} = (100, 1000, 300, 200)$ for prices and $\boldsymbol{y} = (200, 300, 100, 150)$ for weights. Because of the limitation of the spatial dimension that we can recognize (up to three), the fourth scalars in $\boldsymbol{x}$ and $\boldsymbol{y}$ that represent Fish are omitted

1.3.5 Generating New Features by Arithmetic

As has been down in scalars (Sect. 1.2.3), new features can be generated from vectors, too, e.g., $\alpha \boldsymbol{x} + \beta \boldsymbol{y} + \gamma \boldsymbol{z}$, where α, β, and γ are multipliers similar to the cases in scalars and $\boldsymbol{x}$, $\boldsymbol{y}$, and $\boldsymbol{z}$ are vectors. One distinction from generations of new features using scalars is that function must be applied to individual new features generated from scalars. Then, generating new feature with applying a function to vector should be denoted as $\log(\alpha x_i + \beta y_i + \gamma z_i)$, which corresponds to the ith scalar that consists of new features in the form of vectors.

Exercise
1.8 Generate new features in the vector form, using scalars shown in Tables 1.1 and 1.2 with arbitrary multipliers (and if possible, with applying functions to scalars).

1.3.6 Dummy Vectors

As features that cannot be described with real values were treated as dummy scalars, vectors can also be composed of dummy scalars. In some sense, dummy scalars themselves could be interpreted as vectors. For example, three colors in RGB representation, $(1, 0, 0)$, $(0, 0, 1)$ and $(1, 1, 0)$, can be now geometrically interpreted in three-dimensional vectors that consist of three integer scalars. They are also geometrical representations of features introduced in Sect. 1.3.4. Thus, from these points of views, i.e., unified treatment of dummy scalars with usual scalars that can be treated as real numbers, introduction of geometrical vector representation of features is critical, although it is rarely emphasized in the textbooks that introduce data science.

In the later part of this book, we try to select a part of features from all features for the practical reasons. Colors represented in geometrical vector representation are very useful for this purpose, since these allow us to select, for example, only the first scalars of RGB representations. Such a decomposition of colors never be possible without vector representations.[1]

On the other hand, in contrast to vector representation of scalars that can be represented as real values, dummy vectors can be placed only at grid points whose coordinates are composed of integer. Of course, as can be seen in RGB representation of colors, dummy scalars are often allowed to be extended to take real values as well ((0.5, 0.5, 0) can make sense in RGB representation of colors), it is not always true. For example, if the dummy scalars represent whether sample is book, chair, or stick, although dummy scalars can be represented as (1, 0, 0), (0, 1, 0), (0, 0, 1), (0.5, 0.5, 0) does not make sense at all, since (0.5, 0.5, 0) means a sample associated with a feature composed of 50% book and 50% chair.

In contrast to vectors that can be represented as real numbers, e.g., prices and weights, not all points in the geometrical representation of dummy scalars do not have anything real. For example, the dummy vector that represents if a sample is book, chair, or stick cannot take (1, 1, 0) since no samples cannot be book and chair simultaneously.

Exercise
1.9 Think about dummy vectors assuming some.

1.4 Matrices

As vectors are composed of scalars, matrices, X, are composed of vectors, as

$$X = \left(\boldsymbol{x}_1^T, \boldsymbol{x}_2^T, \ldots, \boldsymbol{x}_M^T\right) \tag{1.7}$$

where M is the number of features, e.g., price, weight, and color. $\boldsymbol{x}^T$ represents transposition of a vector $\boldsymbol{x}$ where

$$\boldsymbol{x}_j = \left(x_{1j}, x_{2j}, \ldots, x_{Nj}\right) \tag{1.8}$$

corresponds to the vector of ith feature (M is the number of samples). When prices in Table 1.1 and weights in Table 1.2 are represented as matrix, it should be Table 1.4. In this case, a matrix X is

$$X = \begin{pmatrix} 100 & 1000 & 300 & 200 \\ 200 & 300 & 100 & 150 \end{pmatrix} \tag{1.9}$$

[1] Practically, employing only the first scalars in RGB representation is equivalent to the usage of red sunglass through which only red color can penetrate. Now, colors are transformed to real values that describe red color intensity of colors, although in this example only integers are allowed since colors are treated as an example dummy scalars.

and vectors are

$$\boldsymbol{x}_1 = (100, 200) \tag{1.10}$$

$$\boldsymbol{x}_2 = (1000, 300) \tag{1.11}$$

$$\boldsymbol{x}_3 = (300, 100) \tag{1.12}$$

$$\boldsymbol{x}_4 = (200, 150) \tag{1.13}$$

where $N = 2$ and $M = 4$. For example, x_{24} is 150, since x_{ij} corresponds to the ith scalar attributed to jth sample.

Exercise
1.10 Write down the matrix X that corresponds to the table generated by merging Tables 1.2 and 1.3.

1.4.1 Equivalences to Geometrical Representation

There are several advantages for matrix representation. The first advantage is coincidence with geometrical representation. Matrix representation is highly coincident with geometrical representations. When rows in Table 1.4 are considered to be vectors as in equations, from (1.10) to (1.13), it is equivalent to Fig. 1.2; bread, beef, pork and fish correspond to $\boldsymbol{x}_1$, $\boldsymbol{x}_2$, $\boldsymbol{x}_3$, and $\boldsymbol{x}_4$.

On the other hand, when columns in Table 1.4 are considered to be vectors as

$$\boldsymbol{x}_i = (x_{i1}, x_{i2}, \ldots, x_{iM}) \tag{1.14}$$

i.e.,

$$\boldsymbol{x}_1 = (100, 1000, 300, 200) \tag{1.15}$$

$$\boldsymbol{x}_2 = (200, 300, 100, 150) \tag{1.16}$$

they are equivalent to Fig. 1.3; price corresponds to $\boldsymbol{x}_1$ and weight corresponds to $\boldsymbol{x}_2$.

Table 1.4 The matrix that represents Tables 1.1 and 1.2 in the unified format

		i	
		1	2
j	Sample	Prices (yen)	Weight (g)
1	Bread	100	200
2	Beef	1000	300
3	Pork	300	100
4	Fish	200	150

Thus, conversely $X \in \mathbb{R}^{N\times M}$ can be considered to be either M-dimensional vectors as many as N (Fig. 1.3) or N-dimensional vectors as many as M (Fig. 1.2). Thus, matrix representation is not only convenient to represent a set of vectors attributed to samples (Table 1.4) but also useful for geometrical representations. Since two distinct geometrical representations (Figs. 1.2 and 1.3) are important for the purpose of this book as mentioned in the above, matrix that can represent two distinct geometrical representations in the unified way is very important and useful.

Exercise
1.11 Write down the two geometrical interpretations of matrix X generated in the previous exercise.

1.4.2 Matrix Manipulation and Feature Generation

Any feature generation in the form, $\alpha\boldsymbol{x} + \beta\boldsymbol{y} + \gamma\boldsymbol{z}$, can be performed with matrix manipulation; it is another advantage of matrix representation in data science. Suppose $\boldsymbol{x}$, $\boldsymbol{y}$, $\boldsymbol{z}$ are vectors attributed to three features, e.g., price, weight, and color. Define matrix X as

$$X = \begin{pmatrix} \boldsymbol{x} \\ \boldsymbol{y} \\ \boldsymbol{z} \end{pmatrix} \tag{1.17}$$

Then, $\alpha\boldsymbol{x} + \beta\boldsymbol{y} + \gamma\boldsymbol{z}$ can be represented as

$$\alpha\boldsymbol{x} + \beta\boldsymbol{y} + \gamma\boldsymbol{z} = \boldsymbol{\alpha}X = (\alpha, \beta, \gamma)\begin{pmatrix} x_1 & x_2 & \cdots & x_M \\ y_1 & y_2 & \cdots & y_M \\ z_1 & z_2 & \cdots & z_M \end{pmatrix} \tag{1.18}$$

with defining multiplier vector, $\boldsymbol{\alpha}$ as

$$\boldsymbol{\alpha} = (\alpha, \beta, \gamma) \tag{1.19}$$

In data science, it is very important to describe samples with newly generated features. Otherwise, we cannot make use of newly generated features in order to describe the relationship between samples. In order to describe samples with newly generated features, we need generally at least new features as many as N that is the number of original features. Thus, the number of multiplier vectors must be as many as N as well. In this case, since there are three feature vectors, $\boldsymbol{x}$, $\boldsymbol{y}$, $\boldsymbol{z}$, the number of multiplier vectors must be three as well, i.e.,

$$\boldsymbol{\alpha}_1 = (\alpha_1, \beta_1, \gamma_1) \tag{1.20}$$

$$\boldsymbol{\alpha}_2 = (\alpha_2, \beta_2, \gamma_2) \tag{1.21}$$

$$\boldsymbol{\alpha}_3 = (\alpha_3, \beta_3, \gamma_3) \tag{1.22}$$

With multiplier matrix, A, being defined as

$$A = \begin{pmatrix} \boldsymbol{\alpha}_1 \\ \boldsymbol{\alpha}_2 \\ \boldsymbol{\alpha}_3 \end{pmatrix} = \begin{pmatrix} \alpha_1 & \beta_1 & \gamma_1 \\ \alpha_2 & \beta_2 & \gamma_2 \\ \alpha_3 & \beta_3 & \gamma_3 \end{pmatrix} \tag{1.23}$$

new features, $\boldsymbol{x}'$, $\boldsymbol{y}'$, $\boldsymbol{z}'$, that describe M samples can be obtained as matrix form

$$X' = \begin{pmatrix} \boldsymbol{x}' \\ \boldsymbol{y}' \\ \boldsymbol{z}' \end{pmatrix} = AX = \begin{pmatrix} \alpha_1 & \beta_1 & \gamma_1 \\ \alpha_2 & \beta_2 & \gamma_2 \\ \alpha_3 & \beta_3 & \gamma_3 \end{pmatrix} \begin{pmatrix} x_1 & x_2 & \cdots & x_M \\ y_1 & y_2 & \cdots & y_M \\ z_1 & z_2 & \cdots & z_M \end{pmatrix} \tag{1.24}$$

Then jth sample is now described with new feature

$$\begin{pmatrix} x'_j \\ y'_j \\ z'_j \end{pmatrix} = \begin{pmatrix} \alpha_1 x_j + \beta_1 y_j + \gamma_1 z_j \\ \alpha_2 x_j + \beta_2 y_j + \gamma_2 z_j \\ \alpha_3 x_j + \beta_3 y_j + \gamma_3 z_j \end{pmatrix} \tag{1.25}$$

Now it is obvious that Euclidean distance between two samples j and j' computed using X differs from that using X';

$$\begin{aligned} &\sqrt{(x_j - x_{j'})^2 + (y_j - y_{j'})^2 + (z_j - z_{j'})^2} \\ &\neq \sqrt{(x'_j - x'_{j'})^2 + (y'_j - y'_{j'})^2 + (z'_j - z'_{j'})^2} \end{aligned} \tag{1.26}$$

Thus, by selecting A, we can gain more suitable features adapted for the purpose (e.g., discrimination between samples that belong to more than two distinct groups). The problem is how to tune the *best* A. This is nothing but one of the critical topics that will be discussed in the later part of this book. It is also the reason why I decided to write this book.

Table 1.5 is an example of generated new features X' from X by $X' = AX$ with

$$A = \begin{pmatrix} 1 & \frac{1}{2} & 1 \\ \frac{1}{2} & 1 & 1 \\ 1 & 1 & \frac{1}{2} \end{pmatrix} \tag{1.27}$$

Figure 1.4 is the geometrical representation of X and $X' = AX$ shown in Table 1.5. It reveals various problems associated with the generation of new features. First, the separation of beef (red point) from other three foods is enhanced after the new feature, X', is generated. This means that generation of new feature can alter relationships among samples drastically. Thus, we have to be careful when

Table 1.5 An example of generation of new features

j	Sample	i		
		1	2	3
		Prices (yen)	Weight (g)	Size (cm)
X				
1	Bread	100	200	6
2	Beef	1000	300	10
3	Pork	300	100	6
4	Fish	200	150	14

j	Sample	i		
		1	2	3
		First feature	Second feature	Third feature
X'				
1	Bread	200	256	303
2	Beef	1160	810	1305
3	Pork	356	256	403
4	Fish	289	264	357

Upper: Original X, lower: generated $X' = XA$ where A is given in Eq. (1.27)

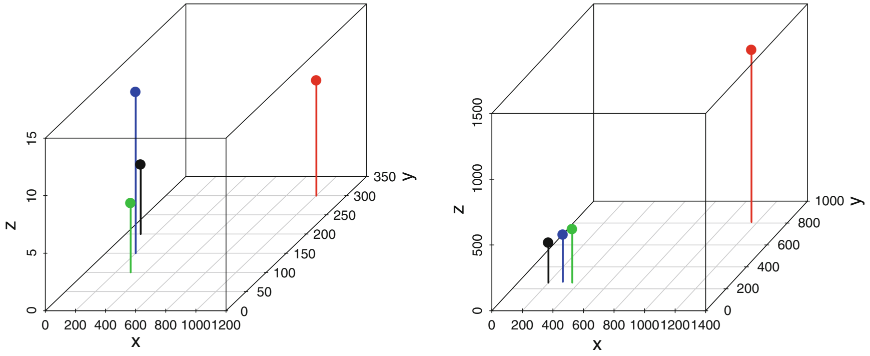

Fig. 1.4 A geometrical interpretation of X (**left**) and X' (**right**) shown in Table 1.5. Black: bread, red: beef, green: pork, blue: fish

generating new features. It might cause artifacts. Second, the dependence upon size (z-axis) in X is almost destroyed in X'. This is simply because the numerical values of sizes shown in Table 1.5 for X are much smaller than prices and weights. Basically, because A shown in Eq. (1.27) gives similar weights to three features, price, weight, and size, to generate new feature, the dependence upon size is smeared out. This is related to the problem of scale. Appreciate rescaling of individual features will recover this problem. However, we have to be also careful if rescaling is reasonable.

Exercise

1.12 Generate new features using the matrix X shown in (1.9) with arbitrary multiplier matrix A.

1.5 Tensors

1.5.1 Introduction of Tensors

As vectors are composed of scalars and matrices are composed of vectors, tensors can be composed of matrices. Suppose Table 1.6 represents foods in two shops.

Now, we can define tensor, x_{ijk}, that describes the jth feature attributed to the ith food in the kth shop. Visually, this can be represented as a cuboid (Fig. 1.5), whose three edges correspond to i (features = price and weight), j (samples = foods), and k (two shops).

Table 1.6 Two tables that describe the list of foods in two shops

		i	
		1	2
j	Sample	Prices (yen)	Weight (g)
$k=1$			
1	Bread	100	200
2	Beef	1000	300
3	Pork	300	100
4	Fish	200	150

		i	
		1	2
j	Sample	Prices (yen)	Weight (g)
$k=2$			
1	Bread	200	250
2	Beef	1500	200
3	Pork	200	150
4	Fish	100	1500

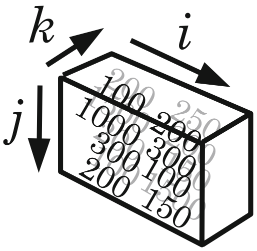

Fig. 1.5 A cuboid that represents Table 1.5. Black and gray numbers correspond to $k=1$ and $k=2$, respectively

We can even extend tensor further. For example, we can add days as the fourth suffix, ℓ. Then $x_{ijk\ell}$ represents the ith feature attributed to the jth sample (food) in the kth shop at the ℓth day. As you can easily suspect, this extension is unlimited. We can add as many suffix as we hope as long as data is available. Additional suffix can represent city, country, year, month, and so on.

As integration of scalars is named as vector, as that of vectors is named as matrix and as that of matrices is named as tensor, we can name tensors with more than three suffix alternatively. Nevertheless, we are not willing to do this, since it is unrealistic to prepare infinite sequences of names attributed to tensors with distinct number of suffix. Instead of that, we name the tensor with m suffix as m-mode tensor. Table 1.6 and Fig. 1.5 are the two distinct representations of three-mode tensor.

As long as we follow this convention, conversely, we can name scalars, vectors, and matrices as tensors as well; i.e., scalars, vectors, matrices can be considered to be zero, one, and two-mode tensors, although this kind of convention is rarely employed. What I would like to emphasize is that scalars, vectors, matrices, and tensors should be treated in the unified way, not in the distinct ways at least in the data science. This is because in contrast to conventional sciences that make use of these concepts, i.e., scalars, vectors, matrices, and tenors, distinction among these is not associated with any real distinct meaning.

In physics, potential energy is scalar, velocity is vector, and stress is tensor. This is simply because their physical realization inevitably requires them. Multiplications between distinct layers are not arbitrary, but strictly decided. Product between energy and vector does not make sense (although it may occasionally have meaning of energy flow). In data science, we can generate any kind of new features as long as they work. In this sense, in data science, scalars, vectors, matrices, and tensors should be treated similarly. Thus, introduction of tenors is natural in data science.

Exercise

1.13 Generate a three-mode tensor whose components are $x_{ijk} \in \mathbb{R}^{3\times 3\times 3}$.

1.5.2 Geometrical Representation of Tensors

In contrast to scalars, vectors, and matrices for which geometrical representations can be obtained straightly, geometrical representation of tensors is harder. This is primarily because we live in three-dimensional physical space. This difficulty has partially already existed when we introduced the concept of matrices. For example, if we have to represent 4×4 matrices geometrically, we cannot avoid dealing with four-dimensional vectors which we cannot visually represent anymore.

This limitation is severer for tensors. If we hope to get geometrical representation of data shown in Table 1.6, the most easiest way is to prepare two planes on each of which four two-dimensional vectors are drawn; $k = 1$ and $k = 2$ correspond to Figs. 1.2 and 1.6, respectively. One possible drawback of this geometrical representation is the difficulty of comparison between $k = 1$ and $k = 2$, since even scale of horizontal and vertical axes differs between Figs. 1.2 and 1.6. Although k takes only two values ($k = 1, 2$) in the present case, k can span over more shops. In that case, geometrical representation might become more difficult to interpret.

In the following, this kind of "vectoralization" can be named as unfolding. In the unfolding of the tensor $x_{ijk} \in \mathbb{R}^{2\times4\times2}$ shown in Table 1.6 as well as Figs. 1.5, 1.2 and 1.6 can be expressed as a matrix $X^{i\times(jk)}$ whose elements are $x_{i(jk)} \in \mathbb{R}^{2\times8}$

$$X^{i\times(jk)} = \begin{pmatrix} 100 & 1000 & 300 & 200 & 200 & 1500 & 200 & 100 \\ 200 & 300 & 100 & 150 & 250 & 200 & 150 & 1500 \end{pmatrix} = (\boldsymbol{x}_1, \ldots, \boldsymbol{x}_8) \tag{1.28}$$

Here, j (samples) and k (shops) are expanded as one suffix that are put in parentheses together. The first four columns, i.e., $\boldsymbol{x}_1$ to $\boldsymbol{x}_4$, and the second four columns, i.e., $\boldsymbol{x}_5$ to $\boldsymbol{x}_8$, correspond to Figs. 1.2 and 1.6, respectively. Then, the tensor can be represented as a 2(features) × 8(= 4(samples) × 2(shops)) matrix that is equivalent to eight two-dimensional vectors, $\boldsymbol{x}_1$ to $\boldsymbol{x}_8$,

In this unfolding, data set shown in Table 1.6 as well as Fig. 1.5 is represented as eight points in the two-dimensional space spanned by two features (prices and weight). It is obvious that there can be more unfolding. For example, x_{ijk} can also be unfolded as a matrix $X^{k\times(ij)}$ whose elements are $x_{k(ij)} \in \mathbb{R}^{2\times8}$,

$$X^{k\times(ij)} = \begin{pmatrix} 100 & 1000 & 300 & 200 & 200 & 300 & 100 & 150 \\ 200 & 1500 & 200 & 100 & 250 & 200 & 150 & 1500 \end{pmatrix} = (\boldsymbol{x}_1, \ldots, \boldsymbol{x}_8) \tag{1.29}$$

Here each column represents a combination of feature and sample. For example, the first column, i.e., $\boldsymbol{x}_1$, represents prices ($i = 1$) of bread ($j = 1$) at two shops and the seventh column, i.e., $\boldsymbol{x}_7$, represents weights ($i = 2$) of pork ($j = 2$) at two shops (see Table 1.6).

Because these two unfolding, Eqs. (1.28) and (1.29), are occasionally represented as two-dimensional vectors, geometrical representations are possible. However, there is yet another unfolding, which is represented as a matrix $X^{j\times(ik)}$ whose elements are $x_{k(ij)} \in \mathbb{R}^{4\times4}$,

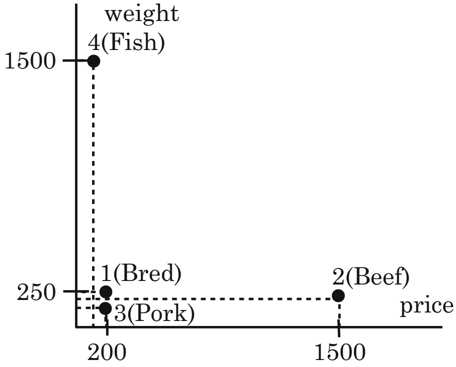

Fig. 1.6 A geometrical interpretation of $k = 2$ in Table 1.6. Horizontal axis and vertical axis correspond to prices and weights, respectively

$$X^{j \times (ik)} = \begin{pmatrix} 100 & 200 & 200 & 250 \\ 1000 & 300 & 1500 & 200 \\ 300 & 100 & 200 & 150 \\ 200 & 150 & 100 & 1500 \end{pmatrix} = (\boldsymbol{x}_1, \ldots, \boldsymbol{x}_4) \tag{1.30}$$

Because they are represented as four four-dimensional vectors, $\boldsymbol{x}_1$ to $\boldsymbol{x}_4$, unfortunately nothing can be represented visibly anymore. Here, $\boldsymbol{x}_1$ to $\boldsymbol{x}_4$ correspond to $(ik) = (11), (12), (21)$, and (22). In other words, they correspond to price at the first shop, weight and the first shop, price at the second shop and the weight at the second shop (see Table 1.6).

Generally, m-mode tensors have m kinds of representations of unfolding. This makes difficult to interpret geometrical representation. Moreover, because unfolding mixes more than one features into one, the interpretation becomes more difficult. These difficulties of interpretation are possibly the reason why tensor is not employed frequently in data science. In data science, how to interpret outcomes is the central topic; if the introduction of tensor makes the interpretation more difficult, it is not hard to imagine that people will avoid the tensor representation of data set.

Exercise
1.14 Unfold the three-mode tensor generated at the last exercise as $X^{i \times (jk)}$.

1.5.3 Generating New Features

In contrast to the matrix representation where generating new features can be easily represented as linear algebra, generating new features in tensor representation of data set is much harder.

The primary reason of this is mixture of the features. For example, in Eq. (1.30), $\boldsymbol{x}_1$ and $\boldsymbol{x}_3$ represent prices while $\boldsymbol{x}_2$ and $\boldsymbol{x}_4$ represent weights. Thus, manipulation of this matrix inevitably results in mixture of distinct features, i.e., price and weights. On the other hand, $\boldsymbol{x}_1$ and $\boldsymbol{x}_2$ are the data at the first shop while $\boldsymbol{x}_3$ and $\boldsymbol{x}_4$ are the data at the second shop. Thus, careless manipulation makes the interpretation of generation of new features also difficult. Simple mixing of distinct columns includes both mixture of price and weight and that between two shops.

In order to avoid these difficulties, it is better to generate new feature before unfolding. This inevitably requires "tensor" algebra.

1.5.4 Tensor Algebra

As in the case of matrix, it is possible to introduce algebra to tensor. Addition and subtraction are straightforward; simply adding or subtracting two corresponding components of tensor: x_{ijk} and x'_{ijk}.

Nevertheless, multiplication is not easy. In order to extend matrix multiplication to tensor, we introduce tensor multiplication between three-mode tensor $\mathcal{X}$ whose component is x_{ijk} and vector $\boldsymbol{x}$ whose length is as large as the first mode of $\mathcal{X}$

$$\{\mathcal{X} \times_i \boldsymbol{x}\}_{jk} = \sum_i x_{ijk} x_i \tag{1.31}$$

where $\{X\}_{jk}$ is the jth row and kth column component of generated matrix X.

Scalar, vector, and matrix can be considered to be zero, one, two-mode tensor. Similarly, tensor multiplication includes scalar, vector, and matrix multiplication. For example, inner product between two vectors can be represented as tensor product between two one-mode tensor,

$$\boldsymbol{x} \cdot \boldsymbol{y} = \sum_i x_i y_i = \boldsymbol{x} \times_i \boldsymbol{y} \tag{1.32}$$

Matrix product can also be represented as multiplication between two two-mode tensors,

$$\{XY\}_{ij} = \sum_k x_{ik} y_{kj} = \{X \times_k Y\}_{ij} \tag{1.33}$$

Using tensor multiplication operator, we can easily generate new features as

$$\mathcal{X}' = A \times_i \mathcal{X} \tag{1.34}$$

Here $x_{ijk} \in \mathbb{R}^{N \times M \times K}$ is the element of $\mathcal{X}$ and A is the multiplier matrix whose element is $a_{\ell i} \in \mathbb{R}^{N \times N}$ where new features are defined as

$$x'_{\ell jk} = \sum_i a_{\ell i} x_{ijk} \tag{1.35}$$

In order to be coincident with matrix representation, Eq. (1.24), we introduce the notation $\mathcal{X}^{\cdot k} \in \mathbb{R}^{N \times M}$ which represent the matrix generated from $\mathcal{X} \in \mathbb{R}^{N \times M \times K}$. In this representation, Eq. (1.34) can also be written

$$\mathcal{X}'^{\cdot k} = A\mathcal{X}^{\cdot k} \tag{1.36}$$

Exercise

1.15 Execute Eq. (1.34) using a three-mode tensor $\mathcal{X}$ whose elements are $x_{ijk} \in \mathbb{R}^{3 \times 3 \times 3}$ and a 3×3 matrix A.

In order for later use, we further introduce additional tensor multiplication. Zero multiplication is defined as

$$\left\{\boldsymbol{x} \times^0 \boldsymbol{y}\right\}_{ij} = x_i y_j \tag{1.37}$$

Generally, multiplication of m-mode tensor and m'-mode tensor with the operator $\times^0$results in $(m + m')$-mode tensor.

We can further extend the operator $\times^0$ into the other way as

$$\{\mathcal{X} \times^k \mathcal{X}'\}_{i_1 i_2 \ldots i_{m-1} k j_1 j_2 \ldots j_{m'-1}} = x_{i_1 i_2 \ldots i_{m-1} k} x'_{k j_1 j_2 \ldots j_{m'-1}} \tag{1.38}$$

where $\mathcal{X}$ and $\mathcal{X}'$ are m-mode and m'-mode tensors whose components are $x_{i_1 i_2 \ldots i_{m-1} k}$ and $x'_{k j_1 j_2 \ldots j_{m'-1}}$, respectively. Thus, the multiplication of m-mode tensor and m'-mode tensor with the operator $\times^k$ results in $(m + m' - 1)$-mode tensor.

The number of suffix attached to the operator $\times$ does not have to be restricted to one. When the number of suffix attached to the operator $\times$ is more than one, they are defined as

$$\{\mathcal{X} \times_{k\ell} \mathcal{X}'\}_{i_1 i_2 \ldots i_{m-2} j_1 j_2 \ldots j_{m-2}} = \sum_{k\ell} x_{i_1 i_2 \ldots i_{m-2} k\ell} x'_{k\ell j_1 j_2 \ldots j_{m-2}} \tag{1.39}$$

and

$$\{\mathcal{X} \times^{k\ell} \mathcal{X}'\}_{i_1 i_2 \ldots i_{m-2} k\ell j_1 j_2 \ldots j_{m-2}} = x_{i_1 i_2 \ldots i_{m-2} k\ell} x'_{k\ell j_1 j_2 \ldots j_{m'-2}} \tag{1.40}$$

These are $(m + m' - 4)$-mode tensor and $(m + m' - 2)$-mode tensor, respectively. In this sense the operator to which lower suffix is added can be represented using the operator to which upper suffix is added as

$$\mathcal{X} \times_{k\ell} \mathcal{X}' = \sum_{k\ell} \mathcal{X} \times^{k\ell} \mathcal{X}' \tag{1.41}$$

We can also add upper and lower suffix to the operator $\times$ together as

$$\{\mathcal{X} \times_k^\ell \mathcal{X}'\}_{i_1 i_1 \ldots i_{m-2} j_1 k j_2 \ldots j_{m'-2}} = \sum_{\ell} x_{i_1 i_2 \ldots i_{m-2} \ell k} x'_{k\ell j_1 j_2 \ldots j_{m'-2}} \tag{1.42}$$

Adding multiple upper and lower suffix is straightforward.

There is one problem in adding both upper and lower suffix to the operator $\times$ when the same suffix is added as both lower and upper suffix. This is equivalent to adding the suffix as lower suffix only, e.g.,

$$\begin{aligned}\{\mathcal{X} \times_k^k \mathcal{X}\}_{i_1 i_2 \ldots i_{m-1} j_1 j_2 \ldots j_{m'-1}} &= \{\mathcal{X} \times_k \mathcal{X}'\}_{i_1 i_2 \ldots i_{m-1} j_1 j_2 \ldots j_{m'-1}} \\ &= \sum_k x_{i_1 i_2 \ldots i_{m-1} k} x'_{k j_1 j_2 \ldots j_{m'-1}} \end{aligned} \tag{1.43}$$

Thus as a rule, when the same suffix appears as both upper and lower suffix, we erase upper one since it does not make any changes.

$$\times_k^k \rightarrow \times_k \tag{1.44}$$

The usefulness of these additional tensor multiplications from equations from (1.37) to (1.44) might be unclear. For example, by applying (1.37) to Eqs. (1.15) and (1.16), although we can get

$$\boldsymbol{x}_1^T \times^0 \boldsymbol{x}_2^T = \begin{pmatrix} 100 \\ 1000 \\ 300 \\ 200 \end{pmatrix} \times^0 \begin{pmatrix} 200 \\ 300 \\ 100 \\ 150 \end{pmatrix} = \begin{pmatrix} 20000 & 30000 & 10000 & 15000 \\ 200000 & 300000 & 100000 & 150000 \\ 60000 & 90000 & 30000 & 45000 \\ 40000 & 60000 & 20000 & 30000 \end{pmatrix} \tag{1.45}$$

it is unclear how this generated matrix can help us to interpret the data; these represent prices × weight that does not seemingly make any sense. In order to make use of the matrix representation (1.45), we need mathematical technique to be introduced later in this book.

Exercise
1.16 Generate a matrix with applying $\times^0$ to a pair of arbitrary vectors.

Appendix

Rank

In this appendix, rank of matrix is briefly introduced because the concept of rank is important in the next chapter. Suppose that matrix $X \in \mathbb{R}^{N\times M}$ is represented as M N-dimensional vectors, $\boldsymbol{x}_j \in \mathbb{R}^N$, as

$$X = \left(\boldsymbol{x}_1, \ldots, \boldsymbol{x}_j, \ldots, \boldsymbol{x}_M\right). \tag{1.46}$$

If there are vectors, $\boldsymbol{c}_j \in \mathbb{R}^{M'}$, $1 \le j \le M$, such that

$$\boldsymbol{x}_j = \sum_{j' \in J} c_{jj'} \boldsymbol{x}_{j'} \tag{1.47}$$

where J is a set of M' integers taken from $[1, M]$ without repetitions; the smallest M' is called as the rank of matrix, otherwise the rank of matrix is equal to M. In other words, not all $\boldsymbol{x}_j$s are independent but at most M' out of M $\boldsymbol{x}_j$s are independent. This means that $\boldsymbol{x}_j$s span not M dimensional space but at most $M'(< M)$ dimensional space. Thus, the rank of tensor is at most min(M,N) because the number of independent vectors cannot exceed the number of dimensions.

Chapter 2
Matrix Factorization

Don't tie me down!
Zero Two, Darling in the FranXX, Season 1, Episode 12

2.1 Introduction

Similar to scalars that can be represented as a product of smaller numbers, e.g., $18 = 3 \times 3 \times 2$, matrices can also be represented as a product of smaller (lower ranked) matrices. As can be seen in the following, there are no unique ways to represent a matrix as a product of smaller matrices. Presenting a matrix as a product of smaller matrices is called as matrix factorization (MF). What kind of MF should be employed highly depends upon the purpose. In this chapter, I introduce some MFs fitted for the later applications in this book.

2.2 Matrix Factorization

The aim of MF is to represent an $N \times M$ matrix $X \in \mathbb{R}^{N \times M}$ as a matrix product of a $N \times K$ matrix $Y \in \mathbb{R}^{N \times K}$ and a $K \times M$ matrix $Z \in \mathbb{R}^{K \times M}$ as

$$X = YZ \tag{2.1}$$

Generally, whether Eq. (2.1) has at least a solution or not depends upon many factors. When

$$(N + M)K \geq NM \tag{2.2}$$

stands, a MF can exit, because the number, NM, of equations that must be fulfilled is smaller than the number of variables, $(N + M)K$. Even when Eq. (2.2) is not satisfied, in some case when the rank of X is equal to or smaller than $\min(N, M)$,

Y-h. Taguchi, *Unsupervised Feature Extraction Applied to Bioinformatics*,
Unsupervised and Semi-Supervised Learning,
https://doi.org/10.1007/978-3-030-22456-1_2

Eq. (2.1) can be performed. For example, in the case of Eq. (1.37), it is obvious that Eq. (2.1) is possible with $K = 1$.

On the other hand, it is also obvious that Eq. (2.1) cannot always have the unique solution. Let's consider when $X = I$ where I is a $K \times K$ unit matrix whose diagonal components are 1 while other components are 0, i.e.,

$$I = AB \tag{2.3}$$

where A and B are $K \times L$ and $L \times K$ matrices, respectively. Using this, Eq. (2.1) can be rewritten as

$$X = YZ = YIZ = YABZ = (YA)(BZ) \tag{2.4}$$

Now, a pair of YA and BZ is also a MF of an $N \times M$ matrix, X. Thus, in order to perform MF, we need some additional restriction to Y and Z other than simple requirement that Y and Z are $N \times K$ and $K \times M$ matrices, respectively. Depending upon the restriction applied, there are several fashions of MF.

Although there are numerous MFs, most of them are limited to be applied to square matrices, X. Because matrix representation of data set in data science is not generally restricted to square matrix, here we consider only MFs applicable to non-square matrices.

Exercise
2.1 For $I \in \mathbb{R}^{2\times 2}$, generate $A, B \in \mathbb{R}^{2\times 2}$ that satisfy Eq. (2.3).

2.2.1 Rank Factorization

Rank factorization is a MF applicable to any $N \times M$ non-square rank K matrix. Thus, in this case, Eq. (2.2) does not need to be fulfilled.

Rank factorization is directly related to geometrical representation. Without losing generality, we can assume $N \geq M$ (if not, we can consider the transposed matrix). Then $N \times M$ matrix can be interpreted as M N-dimensional vectors as

$$X = (\boldsymbol{x}_1^T, \ldots \boldsymbol{x}_M^T) \tag{2.5}$$

where $\boldsymbol{x}_j \in \mathbb{R}^N$. Suppose that X is rank K matrix. Then, the number of independent vectors in $\boldsymbol{x}_j$ is K. Then each $\boldsymbol{x}_j$ can be represented by linear combination of K independent N dimensional vectors, $\boldsymbol{c}_k \in \mathbb{R}^N$ as

$$\boldsymbol{x}_j = \sum_{k=1}^{K} \boldsymbol{c}_k f_{kj} \tag{2.6}$$

where f_{kj} are coefficients of linear combination. If we define matrix F such that kth row and jth column component is f_{kj} and a matrix $C \in \mathbb{R}^{N \times K}$ as

$$C = (\boldsymbol{c}_1^T, \ldots, \boldsymbol{c}_K^T) \tag{2.7}$$

then we can write

$$X = CF \tag{2.8}$$

This is nothing but rank factorization. Computing F is nothing but solving simultaneously linear equations that correspond to Eq. (2.6), thus it is not difficult at all.

Now the data set is not M points in N-dimensional space, but those in $K(< N)$-dimensional space spanned by K $\boldsymbol{c}_j$s. In this sense, rank factorization is directly related to geometrical representation of data set in the sense that rank factorization is a projection of N dimensional space to K dimensional space.

Exercise
2.2 Apply rank factorization to Eq. (1.30) with

$$C = \begin{pmatrix} -1 & 1 & 1 & 1 \\ 1 & -1 & 1 & 1 \\ 1 & 1 & -1 & 1 \\ 1 & 1 & 1 & -1 \end{pmatrix} \tag{2.9}$$

2.2.2 Singular Value Decomposition

Singular value decomposition (SVD) is one of the special cases of rank factorization. In SVD, an $N \times M$ matrix is represented not by a product of two matrices but by a product of three matrices,

$$X = U\Sigma V^T \tag{2.10}$$

where U is an $N \times N$ orthogonal matrix, V is an $M \times N$ orthogonal matrix,[1] and Σ is $N \times N$ diagonal matrix if $N < M$. Oppositely, if $N > M$, U is an $N \times M$ orthogonal matrix, V is an $M \times M$ orthogonal matrix, and Σ is $M \times M$ diagonal matrix. Here orthogonal matrix is that multiplication with its transposition results in unit matrix, i.e.,

[1] The term "orthogonal matrix" can be used only for square matrix. In this sense, when U or V is not a square matrix, it is not very correct to call them "orthogonal matrix," but it is true that Eq. (2.11) is satisfied even when U or V is not a square matrix, because column vectors of them are orthogonal to each other.

$$U^T U = V^T V = I \tag{2.11}$$

Since a matrix X is represented not by a product of two matrices but by a product of the matrices, arbitrarity of MF shown in Eq. (2.4) is removed because

$$X = U\Sigma V^T = UI\Sigma V^T = UAB\Sigma V^T \neq UA\Sigma BV^T. \tag{2.12}$$

Thus, SVD can be a unique representative MF of a matrix X.

Here, I am not willing to mathematically prove the existence of SVD for arbitrary matrix, because any fundamental linear algebra textbook should have a proof. Instead of that, I briefly introduce SVD from data science point of views.

2.2.2.1 How to Compute SVD

Suppose that Eq. (2.10) is obtained. In the following we assume $N < M$. Then,

$$XX^T = U\Sigma V^T \left(U\Sigma V^T\right)^T = U\Sigma V^T V\Sigma^T U^T = U\Sigma^2 U^T \tag{2.13}$$

$$XX^T U = U\Sigma^2 U^T U = U\Sigma^2. \tag{2.14}$$

Because Σ is a diagonal matrix, Σ can be expressed as

$$\Sigma = \begin{pmatrix} \lambda_1 & & & \\ & \lambda_2 & & \\ & & \ddots & \\ & & & \lambda_N \end{pmatrix} \tag{2.15}$$

and $N \times N$ matrix U can be expressed using $\boldsymbol{u}_i \in \mathbb{R}^N$,

$$U = (\boldsymbol{u}_1^T, \boldsymbol{u}_2^T, \ldots, \boldsymbol{u}_N^T) \tag{2.16}$$

then Eq. (2.14) can be rewritten as

$$XX^T \boldsymbol{u}_i = \lambda_i^2 \boldsymbol{u}_i, 1 \leq i \leq N. \tag{2.17}$$

Thus, computing U is equivalent to the diagonalization of XX^T if we also require $|\boldsymbol{u}_i| = 1$ such that U is an orthogonal matrix as required, because eigenvectors, $\boldsymbol{u}_i$s, are known to be orthogonal to one another.

From Eq. (2.10),

$$X^T = \left(U\Sigma V^T\right)^T = V\Sigma U^T \tag{2.18}$$

$$X^T U \Sigma^{-1} = V \Sigma U^T U \Sigma^{-1} = V \Sigma \Sigma^{-1} = V \tag{2.19}$$

$$V = X^T U \Sigma^{-1}. \tag{2.20}$$

Thus we can get

$$\boldsymbol{v}_i = \frac{1}{\lambda_i} X^T \boldsymbol{u}_i \tag{2.21}$$

if we express $M \times N$ matrix $V \in \mathbb{R}^{M \times N}$ using $\boldsymbol{v}_i \in \mathbb{R}^M$ as

$$V = \left(\boldsymbol{v}_1^T, \boldsymbol{v}_2^T, \ldots, \boldsymbol{v}_N^T \right). \tag{2.22}$$

Then from Eqs. (2.17) and (2.21)

$$X^T X X^T \boldsymbol{u}_i = \lambda_i^2 X^T \boldsymbol{u}_i \tag{2.23}$$

$$X^T X \cdot \lambda_i \boldsymbol{v}_i = \lambda_i^2 \cdot \lambda_i \boldsymbol{v}_i \tag{2.24}$$

$$X^T X \boldsymbol{v}_i = \lambda_i^2 \boldsymbol{v}_i. \tag{2.25}$$

Thus, $\boldsymbol{v}_i$ is an eigenvector of $X^T X$. This means, V, defined by Eq. (2.22), is an orthogonal matrix if we also require $|\boldsymbol{v}_i| = 1$.

Thus performing diagonalization of Eq. (2.17) together with applying Eq. (2.21), or performing diagonalization of Eq. (2.25) together with applying Eq. (2.26),

$$\boldsymbol{u}_i = \frac{1}{\lambda_i} X \boldsymbol{v}_i \tag{2.26}$$

that is equivalent to

$$U = X V \Sigma^{-1}, \tag{2.27}$$

which can be derived as $V = X^T U \Sigma^{-1}$, we can perform SVD shown in Eq. (2.10).

Exercise

2.3 Apply SVD to

$$X = \begin{pmatrix} 1 & 1 \\ 1 & 1 \\ -1 & 1 \\ 1 & -1 \end{pmatrix} \tag{2.28}$$

2.2.2.2 Applying SVD to Shop Data

Here we apply SVD to transposed matrix $X_1 = X^T \in \mathbb{R}^{4\times 2}$ of the matrix $X \in \mathbb{R}^{2\times 4}$ defined in Eq. (1.9).

$$X_1^T X_1 = \left(X^T\right)^T X^T = XX^T = \begin{pmatrix} 100 & 1000 & 300 & 200 \\ 200 & 300 & 100 & 150 \end{pmatrix} \begin{pmatrix} 100 & 200 \\ 1000 & 300 \\ 300 & 100 \\ 200 & 150 \end{pmatrix}$$

$$= \begin{pmatrix} 1140000 & 380000 \\ 380000 & 162500 \end{pmatrix}. \tag{2.29}$$

We diagonalize $X_1^T X_1$, Eq. (2.29). Eigen equation that eigenvalue λ should satisfy is

$$\begin{vmatrix} \lambda - 1140000 & 380000 \\ 380000 & \lambda - 162500 \end{vmatrix} = 0 \tag{2.30}$$

$$(\lambda - 1140000)(\lambda - 162500) - 380000^2 = 0 \tag{2.31}$$

$$\lambda^2 - (1140000 + 162500)\lambda + 114000 \cdot 162500 - 380000^2 = 0 \tag{2.32}$$

$$\lambda^2 - 1302500\lambda + 185250000000 - 144400000000 = 0 \tag{2.33}$$

$$\lambda^2 - 1302500\lambda + 40850000000 = 0 \tag{2.34}$$

$$\lambda_\pm = \frac{1302500 \pm \sqrt{1302500^2 - 4 \cdot 40850000000}}{2} \tag{2.35}$$

$$= \frac{1302500 \pm \sqrt{1533106250000}}{2} \tag{2.36}$$

$$= \frac{1302500 \pm 2500\sqrt{245297}}{2} = 651250 \pm 1250\sqrt{245297} \tag{2.37}$$

Eigenvector $\boldsymbol{v} = (v_1, v_2)^T$ should satisfy

$$\begin{pmatrix} \lambda_\pm - 1140000 & 380000 \\ 380000 & \lambda_\pm - 162500 \end{pmatrix} \boldsymbol{v} = 0 \tag{2.38}$$

$$\begin{pmatrix} -488750 \pm 1250\sqrt{245297} & 380000 \\ 380000 & 488750 \pm 1250\sqrt{245297} \end{pmatrix} \boldsymbol{v} = 0 \tag{2.39}$$

Then we get

$$v_1^\pm = \frac{488750 \pm 1250\sqrt{245297}}{380000} v_2^\pm = \frac{391 \pm \sqrt{245297}}{304} v_2^\pm \tag{2.40}$$

In order that $V = (\boldsymbol{v}^+, \boldsymbol{v}^-)$ is orthogonal matrix, $|\boldsymbol{v}^+| = |\boldsymbol{v}^-| = 1$.

$$(v_1^\pm)^2 + (v_2^\pm)^2 = 1 \tag{2.41}$$

$$\left(\frac{391 \pm \sqrt{245297}}{304}\right)^2 (v_2^+)^2 + (v_2^+)^2 = 1 \tag{2.42}$$

$$\frac{391^2 \pm 2 \cdot 391\sqrt{245297} + 245297 + 304^2}{304^2}(v_2^\pm)^2 = 1 \tag{2.43}$$

$$\frac{490594 \pm 782\sqrt{245297}}{92416}(v_2^\pm)^2 = 1 \tag{2.44}$$

$$v_2^\pm = \sqrt{\frac{92416}{490594 \pm 782\sqrt{245297}}} \simeq 0.3244, 0.9459 \tag{2.45}$$

$$v_1^\pm = \frac{391 \pm \sqrt{245297}}{304} v_2^\pm \simeq 0.9459, -0.3244 \tag{2.46}$$

$\boldsymbol{u}^\pm$ can be computed via Eq. (2.26),

$$\boldsymbol{u}^\pm = \frac{1}{\lambda^\pm} X_1 \boldsymbol{v}^\pm = \frac{1}{\lambda^\pm} \begin{pmatrix} 100 & 200 \\ 1000 & 300 \\ 300 & 100 \\ 200 & 150 \end{pmatrix} \begin{pmatrix} v_1^\pm \\ v_2^\pm \end{pmatrix}. \tag{2.47}$$

Here we consider what $\boldsymbol{u}^\pm$ represent. Because X_1 can be considered to be a set of two four-dimensional vectors $\boldsymbol{x}_1 \in \mathbb{R}^4$ and $\boldsymbol{x}_2 \in \mathbb{R}^4$ as $X_1 = (\boldsymbol{x}_1, \boldsymbol{x}_2)$, their relations should be represented in two-dimensional space, since there can be only two independent vectors. In this sense, $\boldsymbol{u}^\pm$ represent how $\boldsymbol{x}_1$ and $\boldsymbol{x}_2$ should be combined to form two-dimensional space that represents the relation between $\boldsymbol{x}_1$ and $\boldsymbol{x}_2$.

In Fig. 1.3, we had to omit the fourth scalar, fish, in order to represent the geometrical relationship between price ($\boldsymbol{x}_1$) and weight ($\boldsymbol{x}_2$). Nevertheless, we can represent the relation between price and weight in the plane using $\boldsymbol{u}^\pm$. From Eq. (2.47), we can get

$$\left(\lambda^+ \boldsymbol{u}^+, \lambda^- \boldsymbol{u}^-\right) = X_1 \left(\boldsymbol{v}^+, \boldsymbol{v}^-\right) \tag{2.48}$$

Then

$$X_1 = \left(\lambda^+ \boldsymbol{u}^+, \lambda^- \boldsymbol{u}^-\right) \left(\boldsymbol{v}^+, \boldsymbol{v}^-\right)^T = \left(v_1^+ \lambda^+ \boldsymbol{u}^+ + v_1^- \lambda^- \boldsymbol{u}^-, v_2^+ \lambda^+ \boldsymbol{u}^+ + v_2^- \lambda^- \boldsymbol{u}^-\right) \tag{2.49}$$

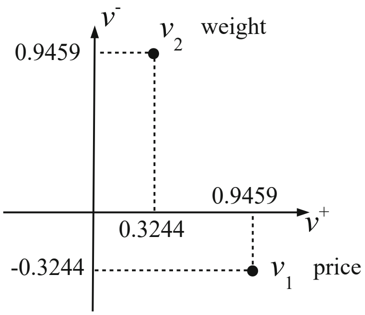

Fig. 2.1 A geometrical interpretation of price and weight originally shown in Fig. 1.3. $\boldsymbol{v}_1$: price, $\boldsymbol{v}_2$: weight

since $\left(\boldsymbol{v}^+, \boldsymbol{v}^-\right)$ is orthogonal matrix. Thus in the plane spanned by $\lambda^\pm \boldsymbol{u}^\pm$, price ($\boldsymbol{x}_1$) and weight ($\boldsymbol{x}_2$) can be two points having coordinates $\left(v_1^+, v_1^-\right)$ and $\left(v_2^+, v_2^-\right)$, respectively.

Figure 2.1 shows the geometrical interpretation of price and weight using the results given by SVD. In contrast to Fig. 1.3 where fish must be inevitably omitted, Fig. 2.1 does not omit anything but keeps all information. Instead of that, it is difficult to interpret the meaning of axes, each of which simply represent foods: bread, beef, pork, in Fig. 1.3. Two axes in Fig. 2.1 represents linear combination of foods represented as the four-dimensional vectors, $\lambda^+ \boldsymbol{u}^+$ and $\lambda^- \boldsymbol{u}^-$, respectively, although we do not write down them here because they are at most confusing and are not helpful for our understanding at all.

Thus, it turns out that there is a trade-off; if we would like to keep interpretability of axes, we cannot represent the relation of features in the easily visible lower dimensional space. On the other hand, if we would like to have geometrical representation that can be easy to understand as shown in Fig. 2.1, we cannot avoid to lose the interpretability of axes. In some sense, the purpose of data science is to make balance between these two problems, i.e., interpretability of axes or that of relation of features. Most of the popular methods ever proposed are aiming to achieve this purpose. The fact that so many methods are proposed definitely suggests that there is still not a unique (the best) solution for this problem. The purpose of this book is also to add yet another solution to solve this problem effectively.

2.3 Principal Component Analysis

In the previous section, we demonstrated that SVD can give the plane that can represent the relation between two features, price and weight, in lower dimensional space, which is more easily interpreted than original four-dimensional space spanned by four foods: bread, pork, beef, and fish. It is also shown that SVD can be performed via diagonalization of matrix products, $X^T X$ or $X X^T$. Apparently, although they seem to be nothing but mathematical or technical relationships, they actually do not. Diagonalization of these two matrix products is deeply related to principal component analysis (PCA) [2].

PCA is mathematically defined as the diagonalization of covariance matrix $S_{ii'} \in \mathbb{R}^{N \times N}$,

$$
\begin{aligned}
S_{ii'} &= \left\langle \left(x_{ij'} - \left\langle x_{ij} \right\rangle_j \right) \cdot \left(x_{i'j'} - \left\langle x_{i'j} \right\rangle_j \right) \right\rangle_{j'} && (2.50)\\
&= \left\langle x_{ij'} x_{i'j'} - \left\langle x_{ij} \right\rangle_j x_{i'j'} - x_{ij'} \left\langle x_{i'j} \right\rangle_j + \left\langle x_{ij} \right\rangle_j \left\langle x_{i'j} \right\rangle_j \right\rangle_{j'} && (2.51)\\
&= \left\langle x_{ij'} x_{i'j'} \right\rangle_{j'} - \left\langle \left\langle x_{ij} \right\rangle_j x_{i'j'} \right\rangle_{j'} - \left\langle x_{ij'} \left\langle x_{i'j} \right\rangle_j \right\rangle_{j'} + \left\langle \left\langle x_{ij} \right\rangle_j \left\langle x_{i'j} \right\rangle_j \right\rangle_{j'} && (2.52)\\
&= \left\langle x_{ij'} x_{i'j'} \right\rangle_{j'} - \left\langle x_{ij} \right\rangle_j \left\langle x_{i'j'} \right\rangle_{j'} - \left\langle x_{ij'} \right\rangle_{j'} \left\langle x_{i'j} \right\rangle_j + \left\langle x_{ij} \right\rangle_j \left\langle x_{i'j} \right\rangle_j && (2.53)\\
&= \left\langle x_{ij'} x_{i'j'} \right\rangle_{j'} - \left\langle x_{ij} \right\rangle_j \left\langle x_{i'j'} \right\rangle_{j'} && (2.54)
\end{aligned}
$$

where

$$\left\langle x_{ij} x_{i'j} \right\rangle_j = \frac{1}{M} \sum_j x_{ij} x_{i'j} \tag{2.55}$$

$$\left\langle x_{ij} \right\rangle_j = \frac{1}{M} \sum_j x_{ij} \tag{2.56}$$

and $x_{ij} \in \mathbb{R}^{N \times M}$.

It is obvious that Eq. (2.50) is equivalent to XX^T if $\langle x_{ij} \rangle_j = 0$. Thus, PCA is equivalent to SVD in special cases.

Exercise
2.4 Apply PCA to Eq. (2.28).

2.4 Equivalence Between PCA and SVD

As can be seen in the previous section, the difference between SVD and PCA is simply if $\left\langle x_{ij} \right\rangle_j = 0$ or not. Nonetheless, it is not frequently discussed from the view point of data science how the difference affects the outcome. Suppose that S is the matrix whose component is $S_{ii'}$ given in Eq. (2.54). We also define vectors $\langle \boldsymbol{S}_i \rangle$,

$$\langle \boldsymbol{S}_i \rangle = \left(\left\langle x_{1j} \right\rangle_j, \left\langle x_{2j} \right\rangle_j, \ldots \left\langle x_{ij} \right\rangle_j, \ldots \left\langle x_{Nj} \right\rangle_j \right) \tag{2.57}$$

whose components are columnwise mean of X. Then using Eq. (2.10), S can be decomposed as

$$
\begin{aligned}
S &= \frac{XX^T}{M} - \langle \boldsymbol{S}_i \rangle \times^0 \langle \boldsymbol{S}_i \rangle = \frac{1}{M} U \Sigma V^T \left(U \Sigma V^T \right)^T - \langle \boldsymbol{S}_i \rangle \times^0 \langle \boldsymbol{S}_i \rangle \\
&= U \frac{\Sigma^2}{M} U^T - \langle \boldsymbol{S}_i \rangle \times^0 \langle \boldsymbol{S}_i \rangle
\end{aligned} \tag{2.58}
$$

On the other hand, applying PCA to S, we should get

$$
SU' = U' \Lambda \tag{2.59}
$$

where $U' \in \mathbb{R}^{N \times N}$ is an orthogonal matrix and $\Lambda \in \mathbb{R}^{N \times N}$ is a diagonal matrix. Then

$$
S = U' \Lambda U'^T \tag{2.60}
$$

Thus generally $U \neq U'$ and there are no ways to compute U' directly from U and $\langle \boldsymbol{S}_i \rangle$.

SVD can also be performed by the diagonalization of $X^T X$. Covariance matrix $S_{jj'} \in \mathbb{R}^{M \times M}$ is redefined as

$$
S_{jj'} = \left\langle x_{ij} x_{ij'} \right\rangle_i - \left\langle x_{ij} \right\rangle_i \left\langle x_{ij'} \right\rangle_i \tag{2.61}
$$

Then using

$$
\langle \boldsymbol{S}_j \rangle = \left(\langle x_{i1} \rangle_i , \langle x_{i2} \rangle_i , \ldots , \left\langle x_{ij} \right\rangle_i \ldots \langle x_{iM} \rangle_i \right) \tag{2.62}
$$

we get

$$
\begin{aligned}
S &= \frac{X^T X}{M} - \left\langle \boldsymbol{S}_j \right\rangle \times^0 \left\langle \boldsymbol{S}_j \right\rangle = \frac{1}{M} \left(U \Sigma V^T \right)^T U \Sigma V^T - \left\langle \boldsymbol{S}_j \right\rangle \times^0 \left\langle \boldsymbol{S}_j \right\rangle \\
&= V \frac{\Sigma^2}{M} V^T - \left\langle \boldsymbol{S}_j \right\rangle \times^0 \left\langle \boldsymbol{S}_j \right\rangle
\end{aligned} \tag{2.63}
$$

Applying PCA to $S = X^T X \in \mathbb{R}^{M \times M}$, we get

$$
SV' = V' \Lambda \tag{2.64}
$$

where $V' \in \mathbb{R}^{M \times M}$ is an orthogonal matrix and $\Lambda \in \mathbb{R}^{M \times M}$ is a diagonal matrix. Then

$$
S = V' \Lambda V'^T \tag{2.65}
$$

Again, generally $V \neq V'$ and there are no ways to generate V' only from the information of V and $\langle \boldsymbol{S}_j \rangle$.

Thus, although diagonalization of $X^T X$ is equivalent to that of XX^T in SVD, this does not stand for PCA because of columnwise or rowwise mean extraction. Once mean is extracted from a matrix X columnwisely, it is impossible to reproduce original matrix X or rowwisely mean extracted matrix. Since PCA is more frequently employed than SVD in data science, this inequality between PCA applied to $S_{ii'}$ and $S_{jj'}$ should be taken care of. From the data science point of views, if columnwise or rowwise mean extraction should be performed is not easy to decide in advance. It cannot be determined without the knowledge about the data set to which PCA is applied. This knowledge is often quoted as domain knowledge, which is often considered to be “untouched” by data scientists. Nonetheless, even when simple linear algebra like PCA is considered, domain knowledge cannot be avoided as shown in the above.

Exercise

2.5 Compare the solutions of problems 2.3 and 2.4.

2.5 Geometrical Representation of PCA

In contrast to SVD, PCA is often discussed from the geometrical point of views. In this section, I would like to summarize some of the geometrical interpretations of PCA, since it is also beneficial to interpret the geometrical representation of SVD.

2.5.1 PCA Selects the Axis with the Maximal Variance

Suppose that $U \in \mathbb{R}^{N \times N}$ is an orthogonal matrix. $X \in \mathbb{R}^{N \times M}$ is considered to be M N-dimensional vectors as Eq. (2.5). Next, we apply columnwise mean extraction, i.e.,

$$\bar{X} = X - \underbrace{\left(\langle S_i \rangle^T, \ldots, \langle S_i \rangle^T \right)}_{M} \tag{2.66}$$

where the second term of the right-hand side is $N \times M$ matrix. Multiplying U to $\bar{X}$, we get a new matrix X' as

$$X' = U^T \bar{X} \tag{2.67}$$

Thus

$$\frac{X' X'^T}{N} = \frac{1}{N} U^T \bar{X} (U^T \bar{X})^T = U^T \frac{\bar{X} \bar{X}^T}{N} U = U^T S U \tag{2.68}$$

where $\frac{\bar{X}\bar{X}^T}{N} = S \in \mathbb{R}^{N \times N}$ is covariance matrix. If we can choose U such that $\frac{X'X'^T}{N}$ is diagonal, Λ, this is nothing but PCA, Eq. (2.59).

In this calculation, Eq. (2.67) can be considered to be coordinate transformation since

$$x'_{ij} = \sum_{i'} u_{ii'} \bar{x}_{i'j} \tag{2.69}$$

What does the requirement that $X'X^T$ should be diagonal correspond to? As can be seen below, it is equivalent to the condition that x'_{ij} should have maximal variances, S_{ii}. Because of mean extraction defined in Eq. (2.66),

$$\left\langle \bar{x}_{ij} \right\rangle_j = 0. \tag{2.70}$$

Thus,

$$\left\langle x'_{ij} \right\rangle_j = 0 \tag{2.71}$$

as well. Then $S_{ii} = \left\langle x'_{ij} x'_{ij} \right\rangle_j$ and maximizing S_{ii} is equivalent to maximizing

$$\sum_j x'^2_{ij} - \lambda \left(\sum_{i'} u^2_{ii'} - 1 \right) = \sum_{i_1} \sum_{i_2} u_{ii_1} u_{ii_2} \left(\sum_j \bar{x}_{i_1 j} \bar{x}_{i_2 j} - \lambda \delta_{i_1 i_2} \right) + \lambda \tag{2.72}$$

where Eq. (2.69) is substituted. The terms multiplied by λ are required such that

$$\boldsymbol{u}_i = (u_{i1}, u_{i2}, \ldots, u_{iN}) \tag{2.73}$$

is a unit vector; this requirement must be fulfilled in order that U is orthogonal. In order that, $u_{ii'}$ should satisfy

$$\frac{\partial}{\partial u_{ii_1}} \left\{ \sum_j x'^2_{ij} - \lambda \left(\sum_{i'} u^2_{ii'} - 1 \right) \right\} = \sum_{i_2} u_{ii_2} \left(\sum_j \bar{x}_{i_1 j} \bar{x}_{i_2 j} - \lambda \delta_{i_1 i_2} \right) = 0 \tag{2.74}$$

In order to have solutions other than the trivial solution, $\boldsymbol{u}_i = 0$, we need to solve the eigenvalue problem,

$$\sum_{i_2} u_{ii_2} \sum_j \bar{x}_{i_1 j} \bar{x}_{i_2 j} = \lambda u_{ii_1} \tag{2.75}$$

Or equivalently,

$$NSU = U\Lambda \tag{2.76}$$

which is nothing but PCA, Eq. (2.59), excluding a prefactor N in the left-hand side. Thus applying PCA is nothing but generating the new feature x'_{ij} from $\bar{x}_{ij}$ so as to have maximum variance along the new axis.

Eigenvalue problem gives us more than one eigenvalues. The largest one corresponds to the maximal S_{ii}. We would like to discuss what the second largest eigenvalue corresponds to. In the subspace to the eigenvector $\boldsymbol{u}_i$ that corresponds to the largest eigenvalues, try to find direction $\boldsymbol{u}'_i$ along which the largest variance is given. This can be achieved by maximizing

$$\sum_j x'^2_{ij} - \lambda\left(\sum_{i'} u'^2_{ii'} - 1\right) - \alpha\left(\sum_{i'} u_{ii'}u'_{ii'}\right) \tag{2.77}$$

$$= \sum_{i_1}\sum_{i_2} u'_{ii_1}u'_{ii_2}\left(\sum_j \bar{x}_{i_1 j}\bar{x}_{i_2 j} - \lambda\delta_{i_1 i_2}\right) + \lambda - \alpha\left(\sum_{i'} u_{ii'}u'_{ii'}\right) \tag{2.78}$$

$$= \sum_{i_1} u'_{ii_1}\sum_{i_2}\left(u'_{ii_2}\sum_j \bar{x}_{i_1 j}\bar{x}_{i_2 j} - u'_{ii_2}\lambda\delta_{i_1 i_2} - \alpha u_{ii_2}\delta_{i_1 i_2}\right) + \lambda \tag{2.79}$$

The last term in Eq. (2.78) is required such that $\boldsymbol{u}_i \perp \boldsymbol{u'}_i$.

Maximization is performed by

$$\frac{\partial}{\partial u'_{ii_1}}\left\{\sum_{i_1} u'_{ii_1}\sum_{i_2}\left(u'_{ii_2}\sum_j \bar{x}_{i_1 j}\bar{x}_{i_2 j} - u'_{ii_2}\lambda\delta_{i_1 i_2} - \alpha u_{ii_2}\delta_{i_1 i_2}\right) + \lambda\right\} \tag{2.80}$$

$$= \sum_{i_2}\left(u'_{ii_2}\sum_j \bar{x}_{i_1 j}\bar{x}_{i_2 j} - u'_{ii_2}\lambda\delta_{i_1 i_2} - \alpha u_{ii_2}\delta_{i_1 i_2}\right) = 0 \tag{2.81}$$

$$\sum_{i_2} u'_{ii_2}\sum_j \bar{x}_{i_1 j}\bar{x}_{i_2 j} - \lambda u'_{ii_1} = \alpha u_{ii_1} \tag{2.82}$$

Multiplying u_{ii_1} and taking summation of i_1, we get

$$\sum_{i_2} u'_{ii_2}\sum_{i_1}\sum_j \bar{x}_{i_1 j}\bar{x}_{i_2 j}u_{ii_1} - \lambda\sum_{i_1} u_{ii_1}u'_{ii_1} = \alpha\sum_{i_1} u^2_{ii_1} = \alpha \tag{2.83}$$

Because of Eq. (2.75), we get

$$\sum_{i_2} u'_{ii_2}\lambda u_{ii_2} - \lambda\sum_{i_1} u_{ii_1}u'_{ii_1} = \alpha = 0 \tag{2.84}$$

Thus Eq. (2.82) is now

$$\sum_{i_2} u'_{ii_2} \sum_j \bar{x}_{i_1 j} \bar{x}_{i_2 j} = \lambda u'_{ii_1} \tag{2.85}$$

This is the same eigenvalue problem as PCA. Because

$$\frac{\partial}{\partial \alpha} \left\{ \sum_j x'^2_{ij} - \lambda \left(\sum_{i'} u'^2_{ii'} - 1 \right) - \alpha \left(\sum_{i'} u_{ii'} u'_{ii'} \right) \right\} = \sum_{i'} u_{ii'} u'_{ii'} = 0 \tag{2.86}$$

$\boldsymbol{u'}_i \perp \boldsymbol{u}_i$. This is satisfied by restricting eigenvectors other than the first eigenvector. Since the second eigenvector has maximum eigenvalues among those other than the first eigenvector, the second eigenvector represents the direction that is both associated with the maximum variance and perpendicular to the first eigenvectors. As such, the nth eigenvalue, λ_n, is always equivalent to the maximal variance along the axis included in the subspace perpendicular to all eigenvectors $\boldsymbol{u}_i, i < n$.

Thus, if we employ the first n eigenvectors, $\boldsymbol{u}_i, i \leq n$, in order to represent samples or features, it is the geometrical representation to include maximal variance that can be expressed within n dimensional space. In this sense, PCA can be considered to be a most effective (i.e., minimum loss of information) geometrical representation of given data set expressed as a matrix.

Exercise
2.6 Compute variances along the directions parallel to the eigenvectors given in problem 2.4.

2.5.2 PCA Selects the Axis with Minimum Residuals

In the previous section, it was shown that PCA can give us the most effective geometrical representation within given number of dimension n. In this section, though it is equivalent, the geometrical representation given by PCA supports minimum residuals.

In order to compute residuals when Eq. (2.69) is employed, we need to find projection of $\bar{\boldsymbol{x}}_j = (\bar{x}_{1j}, \bar{x}_{2j}, \ldots, \bar{x}_{Nj})$ onto $\boldsymbol{u}_i$. The ith component of the projection is computed as

$$\sum_{i'} u_{ii'} \bar{x}_{i'j} \tag{2.87}$$

Thus, the projection itself is defined as

$$\left(\boldsymbol{u}_i^T \cdot \bar{\boldsymbol{x}}_j \right) \boldsymbol{u}_i \tag{2.88}$$

Then squared residual R^2 can be computed as

$$R^2 = \sum_j \left\{ \bar{\boldsymbol{x}}_j - \left(\boldsymbol{u}_i^T \cdot \bar{\boldsymbol{x}}_j \right) \boldsymbol{u}_i \right\}^2 \tag{2.89}$$

$$= \sum_j \left\{ \bar{\boldsymbol{x}}_j^T \bar{\boldsymbol{x}}_j - 2 \left(\boldsymbol{u}_i^T \cdot \bar{\boldsymbol{x}}_j \right)^2 + \left(\boldsymbol{u}_i^T \cdot \bar{\boldsymbol{x}}_j \right)^2 \boldsymbol{u}_i^T \cdot \boldsymbol{u}_i \right\} \tag{2.90}$$

$$= \sum_j \left\{ \bar{\boldsymbol{x}}_j^T \bar{\boldsymbol{x}}_j - \left(\boldsymbol{u}_i^T \cdot \bar{\boldsymbol{x}}_j \right)^2 \right\} \tag{2.91}$$

Since $\bar{\boldsymbol{x}}_j^T \bar{\boldsymbol{x}}_j$ is constant, minimizing R^2 is equivalent to maximizing $\sum_j \left(\boldsymbol{u}_i^T \cdot \bar{\boldsymbol{x}}_j \right)^2$. Because of Eq. (2.69), $\sum_j \left(\boldsymbol{u}_i^T \cdot \bar{\boldsymbol{x}}_j \right)^2 = \sum_j \boldsymbol{x}_j'^T \boldsymbol{x}_j' = N S_{ii}$. Since PCA is proven to maximize S_{ii}, PCA is now proven to minimizing residuals, too. Thus, also in this sense, PCA can be considered to be a most effective (i.e., minimum loss of information) geometrical representation of given data set expressed as a matrix, too.

Exercise

2.7 Compute residuals around the directions of eigenvectors given in problem 2.4.

2.5.3 Non-equivalence Between Two PCAs

In the previous two subsections, I have shown two equivalent geometrical interpretations of low dimensional representation given by the PCA, in the sense,

1. The geometrical space spanned by n principal components, $\boldsymbol{u}_i$, represents those with the maximum variance.
2. The geometrical space spanned by n principal components, $\boldsymbol{u}_i$, represents those with the minimum residuals.

On the other hand, in contrast to SVD, since PCA diagonalizes covariance matrix, applying PCA to X and X^T differ. This is because $S_{ii'}$ defined by Eq. (2.54) differs from $S_{jj'}$ defined by Eq. (2.61). Then the next question is how these two n dimensional representation if $S_{ii'}$ or $S_{jj'}$ is employed differ with each other.

Generally speaking, it is completely unpredictable. It is very easy to add some matrix X^0 that satisfies

$$\langle x_{ij}^0 \rangle_j = 0 \tag{2.92}$$

$$\langle x_{ij}^0 \rangle_i \neq 0 \tag{2.93}$$

i.e., a matrix with zero columnwise mean and non-zero rowwise mean, to matrix X. This procedure does not affect $S_{ii'}$ at all while it changes $S_{jj'}$. Thus they do towards

n dimensional representation, too. Therefore, we cannot expect any equivalence between two PCAs diagonalizing $S_{ii'}$ or $S_{jj'}$. This often matters in data sciences. In contrast to the physical or social sciences where the target of study is clear, in data science, even what should be targeted is decided in the data driven way. In Fig. 2.1, the relation between weight and price can be viewed only after applying SVD. It is impossible to decide how we apply PCA to data set in advance.

2.6 PCA as a Clustering Method

Usually, PCA is considered to be a kind of embedding method that represents the relationship among objects as geometrical fashion as demonstrated in the previous sections. Nonetheless, PCA can also be considered as a sort of clustering analysis that represents the relationship between objects by grouping [1]. Although there are many methods that cluster data points, clustering method whose equivalence with PCA is proven is K-means. K-means is one of the so-called centroid methods that define multiple centroids to be used as centers of generated clusters. K-means requires to find centroids, $\boldsymbol{m}_k \in \mathbb{R}^N, k = 1, \ldots, K$ when matrix $X \in \mathbb{R}^{N \times M}$ is considered to be a set of M N-dimensional vectors, $\boldsymbol{x}_j \in \mathbb{R}^N$, $j = 1, \ldots, M$, that minimizes

$$J_K = \sum_{k=1}^{K} \sum_{j \in C_k} \left(\boldsymbol{x}_j - \boldsymbol{m}_k\right)^2 \tag{2.94}$$

where

$$\boldsymbol{m}_k = \frac{1}{n_k} \sum_{j \in C_k} \boldsymbol{x}_j \tag{2.95}$$

with n_k being the number of $j \in C_k$. Equation (2.94) represents squared summation of deviations between centroids and $\boldsymbol{x}_j$ within each cluster C_k. Here each j is supposed to belong to C_k whose centroid $\boldsymbol{m}_k$ is the nearest to $\boldsymbol{x}_j$. Thus the task is to identify a set of $(\boldsymbol{m}_k, C_k), k = 1, \ldots, K$.

Suppose we define centroid subspace as that spanned by K centroids. Then the projection to centroids can be defined as

Definition 2.1 The projection of any vector $\boldsymbol{x}$ to centroid subspace is

$$S_b \boldsymbol{x} = \sum_{k=1}^{K} n_k \left(\boldsymbol{m}_k^T \cdot \boldsymbol{x}\right) \boldsymbol{m}_k \tag{2.96}$$

where

$$S_b = \sum_{k=1}^{K} n_k \boldsymbol{m}_k \times^0 \boldsymbol{m}_k \tag{2.97}$$

is the between center scattered matrix with n_k being the number of $j \in C_k$. The centroid subspace is generally considered to be the subspace in which K clusters are visibly well separated. Thus, obtaining centroid subspace is essential to see how K clusters are separated with each other.

In order to demonstrate that the projection onto the centroid subspace exhibits the clustered structure, we applied it to artificial data set. This data set consists of a matrix $X \in \mathbb{R}^{10\times 30}$. All components x_{ij} obey normal distribution, $\mathcal{N}(\mu, \sigma)$, with the mean of μ and the standard deviation of σ; $\sigma = 1$ while mean, μ, varies as follows:

$$\mu = \begin{cases} \sqrt{2}, & 1 \le j \le 10, \quad 1 \le i \le 5 \\ -1, & 11 \le j \le 20, \\ -1, & 21 \le j \le 30, \quad 1 \le i \le 5 \\ 1, & 21 \le j \le 30, \; 6 \le i \le 10 \\ 0, & \text{otherwise} \end{cases} \tag{2.98}$$

This says that js are divided into three clusters as $C_1 = \{1 \le j \le 10\}$, $C_2 = \{11 \le j \le 20\}$ and $C_3 = \{21 \le j \le 30\}$ (see also Fig. 2.2). Although no $\boldsymbol{x}_i$ represents clear separation between three clusters, C_1, C_2, and C_3 (see Fig. 2.3), it is rather

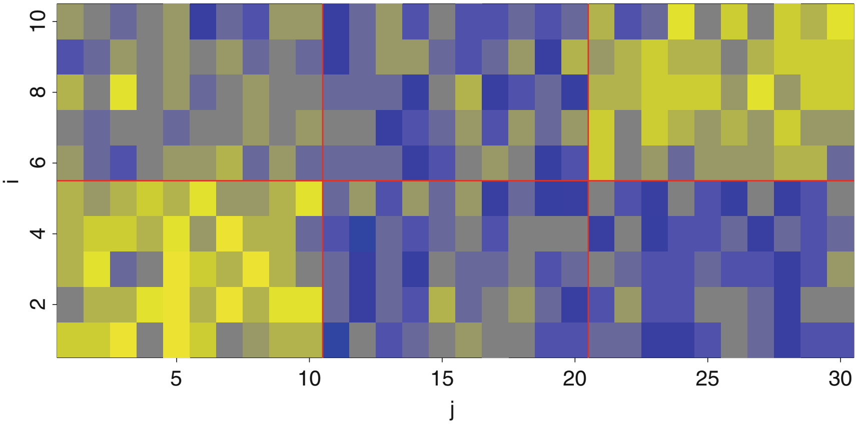

Fig. 2.2 Visualization of $x_{ij} \sim \mathcal{N}(\mu, 1)$, where μ is given by Eq. (2.98). Vertical red lines represent boundary between clusters, C_1, C_2 and C_3. The horizontal red line indicates the boundary between $1 \le i \le 5$ and $6 \le i \le 10$. Yellow(blue) corresponds to larger(smaller) values

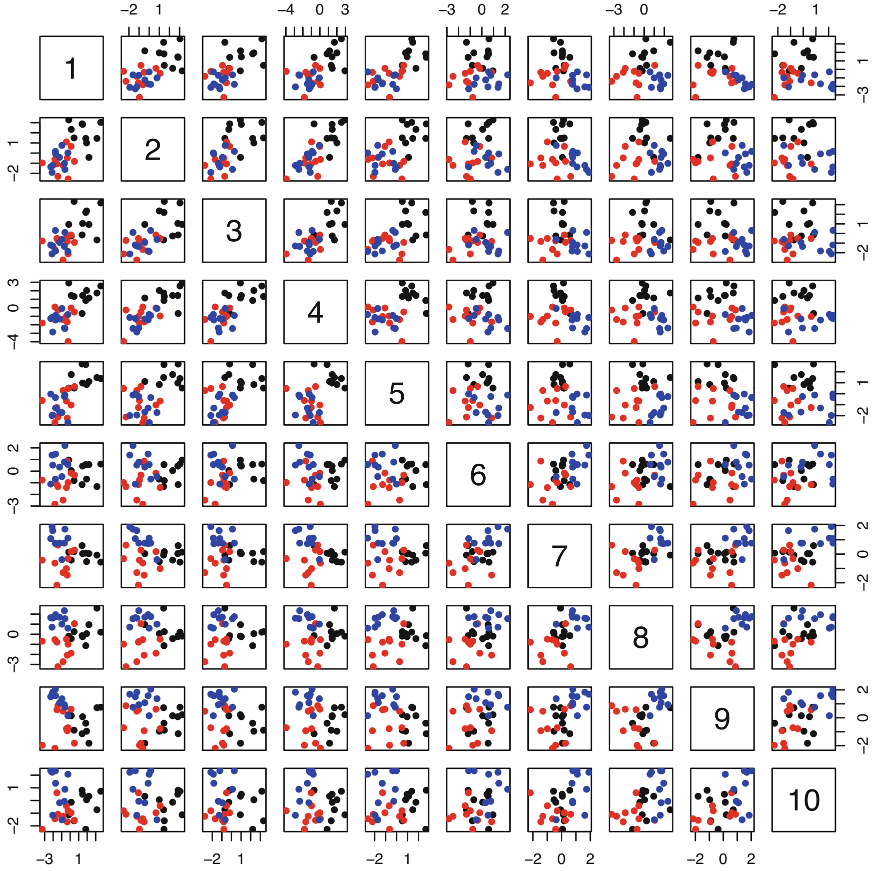

Fig. 2.3 Pairwise scatterplot of $\boldsymbol{x}_i \sim \mathcal{N}(\mu, 1), 1 \leq i \leq 10$ where μ is defined in Eq. (2.98). js that belong to clusters C_1, C_2, and C_3 are represented in black, red, and blue

obvious that $S_b\boldsymbol{x}_i, 1 \leq i \leq 10$ shown in Fig. 2.4 exhibits the more pronounced cluster structure than $\boldsymbol{x}_i$ (see also Appendix).

Now we would like to relate PCA to K-means.

Theorem 2.1 *Cluster centroid subspace is spanned by the first $K - 1$ principal directions, i.e.,*

$$S_b = \sum_{k=1}^{K-1} \lambda_k \boldsymbol{u}_k \times^0 \boldsymbol{u}_k \tag{2.99}$$

where $\boldsymbol{u}_k \in \mathbb{R}^N$ is the kth principal component (PC) given by PCA.

Proof See Appendix □

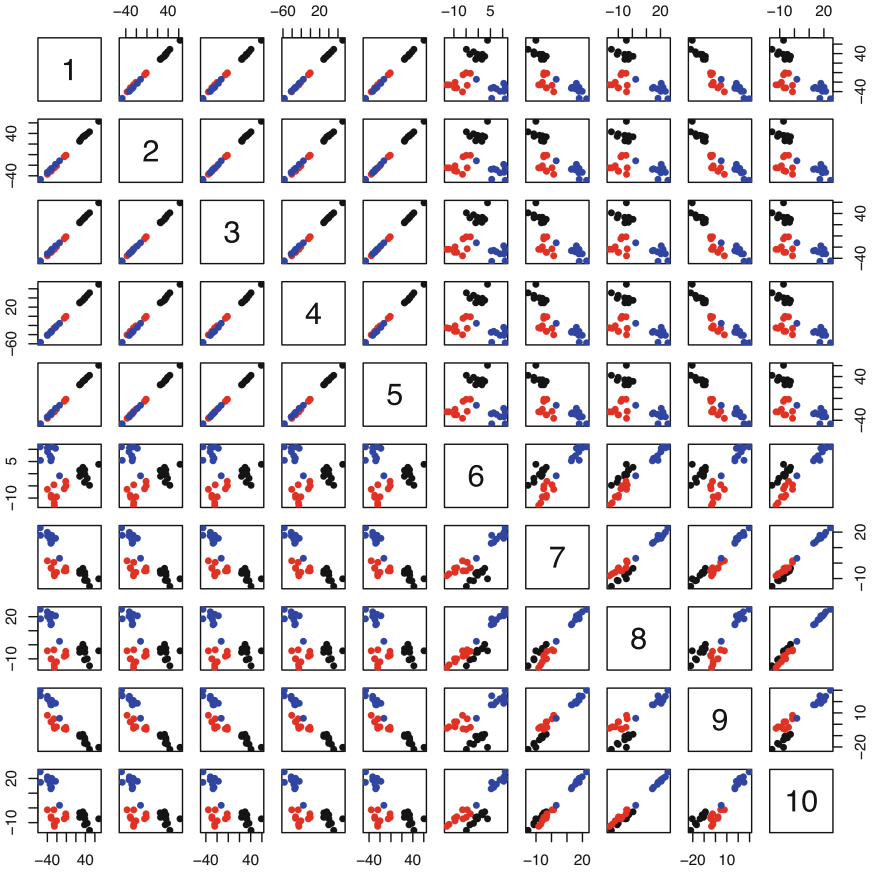

Fig. 2.4 Pairwise scatterplot of $S_b \boldsymbol{x}_i$, $1 \leq i \leq 10$ using S_b defined in Eq. (2.97). js that belong to clusters C_1, C_2, and C_3 are represented in black, red, and blue

In order to show equivalence of S_b defined in Eq. (2.99) presented by Theorem 2.1 and that defined in Eq. (2.97), we have shown the pairwise scatterplot of $S_b \cdot \boldsymbol{x}_i$ using S_b computed by Eq. (2.99) in Fig. 2.5. It is also obvious that scatter plots in Fig. 2.5 are coincident with the three clusters. In order to further emphasize the equivalence between Eqs. (2.97) and (2.99), we have shown the scatterplot between $N^2 = 100$ elements of S_bs defined by Eqs. (2.97) and (2.99), respectively in Fig. 2.6. The lack of complete coincidence is because proof of Theorem 2.1 requires complete clustering while it can never be fulfilled in the real data set.

Anyway, it is obvious that PCA can be used for cluster realization when there are more or less clear clusters. In the general data science course, it is usually taught that embedding methods including PCA can visualize something different from those by clustering method. However, as we could see here, it is not very true since PCA can also visualize clustering if there are clusters, by projecting data onto the space.

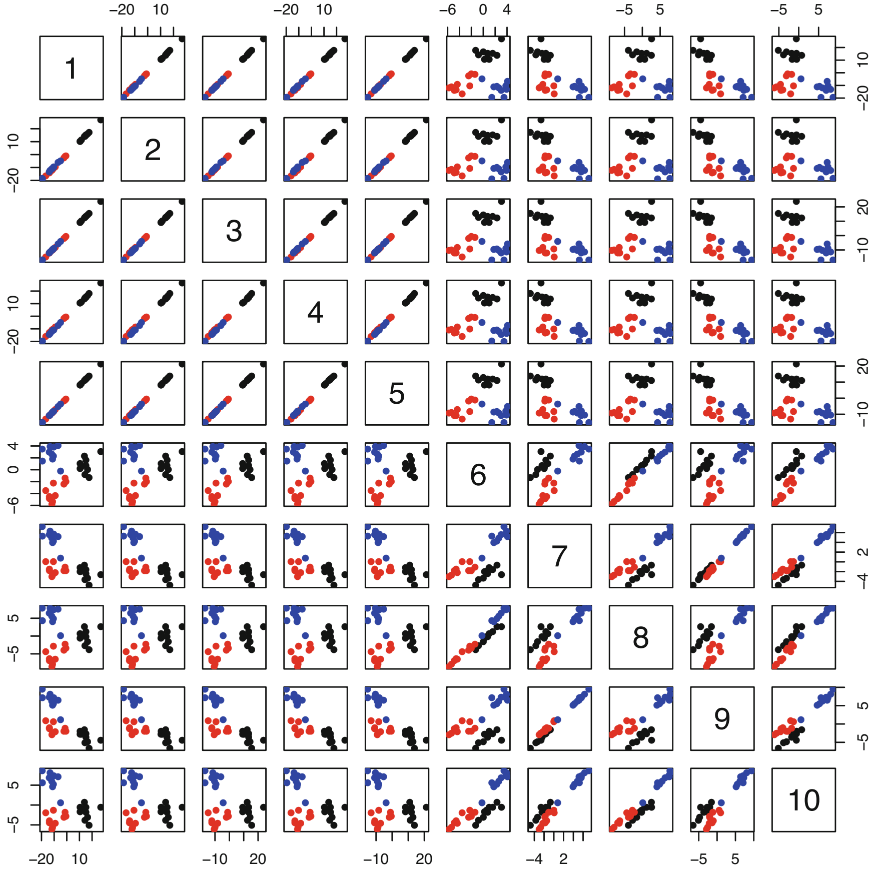

Fig. 2.5 Pairwise scatterplot of $S_b \boldsymbol{x}_i$, $1 \leq i \leq 10$ using S_b defined in Eq. (2.99). js that belong to clusters C_1, C_2, and C_3 are represented in black, red, and blue

Fig. 2.6 Pairwise scatterplot of $N^2 = 100$ elements of S_bs defined in Eqs. (2.97) and (2.99), respectively

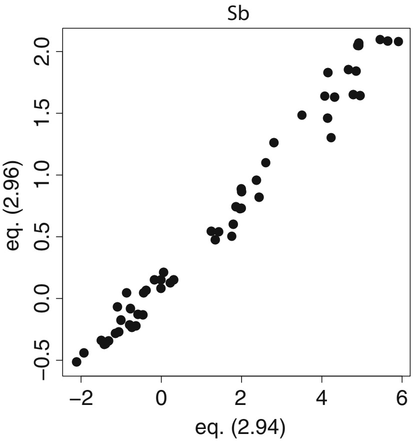

Exercise

2.8 Apply PCA to the matrix X,

$$X = \begin{pmatrix} 1\ 1\ 1\ 0\ 0\ 0\ 0\ 0\ 0 \\ 1\ 1\ 1\ 0\ 0\ 0\ 0\ 0\ 0 \\ 1\ 1\ 1\ 0\ 0\ 0\ 0\ 0\ 0 \\ 0\ 0\ 0\ 1\ 1\ 1\ 0\ 0\ 0 \\ 0\ 0\ 0\ 1\ 1\ 1\ 0\ 0\ 0 \\ 0\ 0\ 0\ 1\ 1\ 1\ 0\ 0\ 0 \\ 0\ 0\ 0\ 0\ 0\ 0\ 1\ 1\ 1 \\ 0\ 0\ 0\ 0\ 0\ 0\ 1\ 1\ 1 \\ 0\ 0\ 0\ 0\ 0\ 0\ 1\ 1\ 1 \end{pmatrix} \tag{2.100}$$

and see if three clusters can be seen. Use any kinds of script language, e.g., R or python, to do this if necessary.

Appendix

Proof of Theorem 2.1

If we define vectors

$$\boldsymbol{h}_k = (0, \dots, 0, \overbrace{1, \dots, 1}^{n_k}, 0, \dots, 0)^T / n_k^{1/2} \tag{2.101}$$

which represents the members that belong to kth cluster, $\boldsymbol{m}_k$ can be rewritten as

$$\boldsymbol{m}_k = \frac{1}{n_k} \sum_{j \in C_k} \boldsymbol{y}_j = \frac{1}{\sqrt{n_k}} \sum_j \boldsymbol{h}_k(j) \boldsymbol{y}_j = \frac{1}{\sqrt{n_k}} Y \boldsymbol{h}_k \tag{2.102}$$

with defining

$$\boldsymbol{y}_j = \boldsymbol{x}_j - \langle \boldsymbol{x}_j \rangle_j \tag{2.103}$$

and

$$Y = \left(\boldsymbol{y}_1, \dots, \boldsymbol{y}_M \right). \tag{2.104}$$

In the above, we redefined $\boldsymbol{m}_k$ using $\boldsymbol{y}_j$ instead of $\boldsymbol{x}_j$ in order to relate K-means to PCA more easily. Then S_b can be also rewritten as

$$S_b = \sum_{k=1}^{K} Y\boldsymbol{h}_k \times^0 Y\boldsymbol{h}_k = Y\left(\sum_{k=1}^{K} \boldsymbol{h}_k \times^0 \boldsymbol{h}_k\right) Y^T \tag{2.105}$$

J_k, Eq. (2.94), can be rewritten with Eq. (2.95) as

$$J_k = \sum_{k=1}^{K} \sum_{j \in C_k} \left(\boldsymbol{x}_j - \frac{1}{n_k} \sum_{j' \in C_k} \boldsymbol{x}_{j'}\right)^2 \tag{2.106}$$

$$= \sum_{k=1}^{K} \sum_{j \in C_k} \left(\boldsymbol{x}_j^2 - \frac{2}{n_k} \sum_{j' \in C_k} \boldsymbol{x}_j \cdot \boldsymbol{x}_{j'} + \frac{1}{n_k^2} \sum_{j', j'' \in C_k} \boldsymbol{x}_{j'} \cdot \boldsymbol{x}_{j''}\right) \tag{2.107}$$

$$= \sum_{k=1}^{K} \sum_{j \in C_k} \boldsymbol{x}_j^2 - \frac{2}{n_k} \sum_{k=1}^{K} \sum_{j, j' \in C_k} \boldsymbol{x}_j \cdot \boldsymbol{x}_{j'} + \sum_{k=1}^{K} \left(\frac{\sum_{j \in C_k} 1}{n_k^2}\right) \sum_{j', j'' \in C_k} \boldsymbol{x}_{j'} \cdot \boldsymbol{x}_{j''} \tag{2.108}$$

$$= \sum_{j} \boldsymbol{x}_j^2 - \frac{1}{n_k} \sum_{k=1}^{K} \sum_{j, j' \in C_k} \boldsymbol{x}_j \cdot \boldsymbol{x}_{j'} \tag{2.109}$$

Using

$$X = \left(\boldsymbol{x}_1, \ldots, \boldsymbol{x}_j, \ldots, \boldsymbol{x}_M\right) \tag{2.110}$$

$$H_K = (\boldsymbol{h}_1, \ldots, \boldsymbol{h}_K) \tag{2.111}$$

J_k can be represented as

$$J_k = \mathrm{Tr}\left(X^T X\right) - \mathrm{Tr}\left(H_K^T X^T X H_K\right) \tag{2.112}$$

Since H_k that minimizes J_k is not altered even if X is replaced with Y as

$$J_k = \mathrm{Tr}\left(Y^T Y\right) - \mathrm{Tr}\left(H_K^T Y^T Y H_K\right). \tag{2.113}$$

H_k that minimizes J_k maximizes Tr (S_b), which is also represented as

$$\mathrm{Tr}\,(S_b) = \mathrm{Tr}\left(H_K^T Y^T Y H_K\right). \tag{2.114}$$

There is a theorem:

Theorem 2.2 *Let A be a symmetric matrix with eigenvalues $\lambda_1 \geq \cdots \geq \lambda_n$ and corresponding eigenvectors $(\boldsymbol{v}_1, \ldots, \boldsymbol{v}_n)$. The maximization of Tr$(QAQ)$ subject to constraints $Q^T Q = I_K$ has the solution $Q = (\boldsymbol{v}_1, \ldots, \boldsymbol{v}_K)R$, where R is an arbitrary $K \times K$ orthogonal matrix. And max Tr$(QAQ) = \lambda_1 + \cdots + \lambda_K$.*

Thus, max S_b can be given as

$$\max_{H_K} \mathrm{Tr}\,(S_b) = \mathrm{Tr}\left(V^T Y^T Y V\right) = \mathrm{Tr}\left(\sum_{k=1}^{K-1} \lambda_k \boldsymbol{u}_k \times^0 \boldsymbol{u}_k\right) \tag{2.115}$$

since $Y\boldsymbol{v}_k = \lambda_k^{1/2}\boldsymbol{u}_k$, where $V = (\boldsymbol{v}_1, \ldots, \boldsymbol{v}_K)$. This completes the proof.

Although Ding and He [1] insist that it proves Eq. (2.99), it does not, because it does not guarantee that there is a R such that $RV = H_K$. Although all components of H_K must be 0 or 1 in order that H_K represents clusters given by K-means, Theorem 2.2 does not have such a restriction that Q must be represented as $H_K R^T$. Actually, as can be seen in Fig. 2.6, S_b given by K-means, Eq. (2.97), does not completely match with S_b given by PCA, Eq. (2.99), but deviates from S_b given by PCA. Thus S_b given by PCA should be considered as not an alternative derivation, but at most a good approximation of S_b given by K-means.

References

1. Ding, C., He, X.: *K*-means clustering via principal component analysis. In: Proceedings of the Twenty-first International Conference on Machine Learning, ICML '04, p. 29. ACM, New York (2004). http://doi.acm.org/10.1145/1015330.1015408
2. Jolliffe, I.T.: Principal Component Analysis. Springer, New York (2002). https://doi.org/10.1007/b98835

Chapter 3
Tensor Decomposition

I painted her as an unapproachable enigma and never even tried to see her for who she was.
Ichigo, Darling in the FranXX, Season 1, Episode 16

3.1 Three Principal Realizations of TD

As has been mentioned in the previous sections, among huge realizations of TD [2], we discuss the three most popular ones: canonical polyadic (CP) decomposition, Tucker decomposition, and tensor train decomposition.[1] These three decompositions of tensor $\mathcal{X} \in \mathbb{R}^{N \times M \times K}$ whose element is x_{ijk} are expressed as CP decomposition

$$\mathcal{X} = \sum_{\ell=1}^{L} \lambda_\ell \boldsymbol{u}_\ell^{(i)} \times^0 \boldsymbol{u}_\ell^{(j)} \times^0 \boldsymbol{u}_\ell^{(k)} \tag{3.1}$$

and L is positive integer, λ_ℓ is weight, $\boldsymbol{u}_\ell^{(i)} \in \mathbb{R}^N$, $\boldsymbol{u}_\ell^{(j)} \in \mathbb{R}^M$, and $\boldsymbol{u}_\ell^{(k)} \in \mathbb{R}^K$.

Using Tucker decomposition,

$$\mathcal{X} = G \times_{\ell_1} U^{(i)} \times_{\ell_2} U^{(j)} \times_{\ell_3} U^{(k)} \tag{3.2}$$

where $U_{\ell_1}^{(i)} \in \mathbb{R}^{N \times N}$,$U_{\ell_2}^{(j)} \in \mathbb{R}^{M \times M}$,$U_{\ell_3}^{(k)} \in \mathbb{R}^{K \times K}$ are singular value vectors, and $G \in \mathbb{R}^{N \times M \times K}$ is a core tensor. The components of $U^{(i)}$, $U^{(j)}$, $U^{(k)}$, and G are denoted as $u_{\ell_1 i}^{(i)}$, $u_{\ell_2 j}^{(j)}$, $u_{\ell_3 k}^{(k)}$, and $G(\ell_1, \ell_2, \ell_3)$, respectively.

Using tensor train decomposition,

[1] Although the detailed algorithms of individual TDs will be presented in the later sections, readers might feel that they would like to try them in advance with reading prior sections that demonstrate examples. In that case, see Appendix A where I list some of the implementations on various platforms.

Y-h. Taguchi, *Unsupervised Feature Extraction Applied to Bioinformatics*,
Unsupervised and Semi-Supervised Learning,
https://doi.org/10.1007/978-3-030-22456-1_3

$$\mathcal{X} = G^{(i)} \times_{\ell_1} G^{(j)} \times_{\ell_2} G^{(k)} \tag{3.3}$$

where $G^{(i)} \in \mathbb{R}^{N \times R_1}$, $G^{(j)} \in \mathbb{R}^{M \times R_1 \times R_2}$, and $G^{(k)} \in \mathbb{R}^{K \times R_2}$ with R_1 and R_2 being positive integer. $G^{(i)}$s' components, $G^{(j)}$s' components, and $G^{(k)}$s' components are denoted as $G^{(i)}(i, \ell_1)$, $G^{(j)}(j, \ell_1, \ell_2)$, and $G^{(k)}(k, \ell_2)$, respectively. Although we employed three-mode tensor, x_{ijk}, in the above, the extension to the higher mode should be straightforward.

All of these are in some sense the extension of SVD. In SVD, matrix $X \in \mathbb{R}^{N \times M}$ is represented as

$$X = \sum_{\ell=1}^{L} \lambda_\ell \boldsymbol{u}_\ell \times^0 \boldsymbol{v}_\ell \tag{3.4}$$

where $L = \min(N, M)$ and $\boldsymbol{u}_\ell \in \mathbb{R}^N$, $\boldsymbol{v}_\ell \in \mathbb{R}^M$. It is obvious that CP decomposition is straight extension of SVD toward higher mode tensors. One problem of CP decomposition is that there are no ways to determine L in Eq. (3.1) a priori.

Tucker decomposition, Eq. (3.2), can also be considered to be the extension of SVD to higher dimension, since Eq. (3.2) can also be represented as

$$\mathcal{X} = \sum_{\ell_1} \sum_{\ell_3} \sum_{\ell_2} G(\ell_1, \ell_2, \ell_3) \boldsymbol{u}_{\ell_1}^{(i)} \times^0 \boldsymbol{u}_{\ell_2}^{(j)} \times^0 \boldsymbol{u}_{\ell_3}^{(k)} \tag{3.5}$$

where

$$\boldsymbol{u}_\ell^{(i)} = (u_{\ell 1}, \ldots, u_{\ell i}, \ldots, u_{\ell N}) \tag{3.6}$$

$$\boldsymbol{u}_\ell^{(j)} = (u_{\ell 1}, \ldots, u_{\ell j}, \ldots, u_{\ell M}) \tag{3.7}$$

$$\boldsymbol{u}_\ell^{(k)} = (u_{\ell 1}, \ldots, u_{\ell k}, \ldots, u_{\ell K}) \tag{3.8}$$

Only difference from CP decomposition is that individual vectors appear more than once in the right-hand side.

Tensor train decomposition can be interpreted as an extension of SVD because Eq. (3.3) can be rewritten as

$$\mathcal{X} = \sum_{\ell_1=1}^{R_1} \sum_{\ell_2=1}^{R_2} \boldsymbol{G}_{\ell_1}^{(i)} \times^0 \boldsymbol{G}_{\ell_1,\ell_2}^{(j)} \times^0 \boldsymbol{G}_{\ell_2}^{(k)} \tag{3.9}$$

where $\boldsymbol{G}_{\ell_1}^{(i)} \in \mathbb{R}^N$, $\boldsymbol{G}_{\ell_1 \ell_2}^{(j)} \in \mathbb{R}^M$, and $\boldsymbol{G}_{\ell_2}^{(k)} \in \mathbb{R}^K$ are

$$\boldsymbol{G}_{\ell_1}^{(i)} = \left(G^{(i)}(1, \ell_1), \ldots, G^{(i)}(N, \ell_1) \right) \tag{3.10}$$

$$\boldsymbol{G}^{(j)}_{\ell_1\ell_2} = \left(G^{(j)}(1,\ell_1,\ell_2),\ldots,G^{(j)}(M,\ell_1,\ell_2)\right) \tag{3.11}$$

$$\boldsymbol{G}^{(k)}_{\ell_2} = \left(G^{(k)}(1,\ell_2),\ldots,G^{(k)}(K,\ell_2)\right) \tag{3.12}$$

Thus all of the three tensor decompositions listed in the above can be considered to be linear combinations of vector product, $\boldsymbol{a} \times^0 \boldsymbol{b} \times^0 \boldsymbol{c}$, although the number of terms differs; L for CP decomposition, $N \times M \times K$ for Tucker decomposition, and $R_1 \times R_2$ for tensor train decomposition. These three TDs have their own pros and cons. CP decomposition has an advantage of interpretability; individual vectors in the right hand of Eq. (3.1) appear only once, thus it is easy to understand what each term means. A disadvantage of CP decomposition is that obtaining CP decomposition is non-deterministic polynomial-time (NP) hard. Thus, no one knows how long it takes until convergence. Tucker decomposition does not have this disadvantage; it is expected to converge within polynomial time. Disadvantages of Tucker decomposition are twofold. The first disadvantage is that it is hard to interpret; because individual vectors in the right-hand side of Eq. (3.2) appear multiple times, it is unclear what each vector represents. The second disadvantage is non-uniqueness. In actuality, we may use any orthogonal matrix, $R \in \mathbb{R}^{N\times N}$ whose components are denoted as $R_{\ell\ell_1}$, that satisfies $R^T R = I$ with the components R^T being denoted as $R_{\ell'_1\ell}$, where I is a unit matrix whose components are $\delta_{\ell'_1\ell_1}$, Eq. (3.2) is rewritten as, with denoting the components of G as $G(\ell'_1,\ell_2,\ell_3)$,

$$\mathcal{X} = G \times_{\ell'_1} I \times_{\ell_1} U^{(i)} \times_{\ell_2} U^{(j)} \times_{\ell_3} U^{(k)} \tag{3.13}$$

$$= G \times_{\ell'_1} \left(R^T \times_{\ell} R\right) \times_{\ell_1} U^{(i)} \times_{\ell_2} U^{(j)} \times_{\ell_3} U^{(k)} \tag{3.14}$$

$$= \left\{G \times_{\ell'_1} R^T\right\} \times_{\ell} \left\{R \times_{\ell_1} U^{(i)}\right\} \times_{\ell_2} U^{(j)} \times_{\ell_3} U^{(k)} \tag{3.15}$$

If we define

$$G'(\ell,\ell_2,\ell_3) = \sum_{\ell'_1} G(\ell'_1,\ell_2,\ell_3) R_{\ell'_1\ell} \tag{3.16}$$

$$u'^{(i)}_{\ell i} = \sum_{\ell_1} R_{\ell\ell_1} u^{(i)}_{\ell_1 i} \tag{3.17}$$

Eq. (3.2) can be expressed as

$$\mathcal{X} = G' \times_{\ell} U'^{(i)} \times_{\ell_2} U^{(j)} \times_{\ell_3} U^{(k)} \tag{3.18}$$

which is nothing but an alternative representation of Tucker decomposition. It is also obvious that there are infinitely many solutions of Tucker decomposition since we can employ any orthogonal matrix R to derive alternative representations of Tucker decomposition.

Similarly, tensor train decomposition, Eq. (3.3), does not have uniqueness, either. Using R, Eq. (3.3) can be rewritten as, with denoting the components of $G^{(i)}$ as $G^{(i)}(i, \ell'_1)$,

$$\mathcal{X} = G^{(i)} \times_{\ell'_1} I \times_{\ell_1} G^{(j)} \times_{\ell_2} G^{(k)} \tag{3.19}$$

$$= G^{(i)} \times_{\ell'_1} \left(R^T \times_\ell R\right) \times_{\ell_1} G^{(j)} \times_{\ell_2} G^{(k)} \tag{3.20}$$

$$= \left\{G^{(i)} \times_{\ell'_1} R^T\right\} \times_\ell \left\{R \times_{\ell_1} G^{(j)}\right\} \times_{\ell_2} G^{(k)} \tag{3.21}$$

If we define

$$G'^{(i)}(i, \ell) = \sum_{\ell'_1} G^{(i)}(i, \ell'_1) R_{\ell'_1 \ell} \tag{3.22}$$

$$G'^{(j)}(j, \ell, \ell_2) = \sum_{\ell_1} R_{\ell \ell_1} G^{(j)}(j, \ell_1, \ell_2) \tag{3.23}$$

Eq. (3.3) can be rewritten

$$\mathcal{X} = G'^{(i)} \times_\ell G'^{(j)} \times_{\ell_2} G^{(k)} \tag{3.24}$$

which is nothing but an alternative representation of tensor train decomposition. It is also obvious that there are infinitely many solutions of tensor train decomposition since we can employ any orthogonal matrix R to derive alternative representations of tensor train decomposition.

The advantage of tensor train decomposition is the small number of parameters. For CP decomposition, Eq. (3.1), the number of parameters must be decided is $(N + M + K + 1)L$ and for Tucker decomposition, Eq. (3.2), the number of parameters that must be determined is $NMK + N^2 + M^2 + M^2$. On the other hand, in tensor train decomposition, Eq. (3.3), the number of parameters that must be decided is as many as $NR_1 + MR_1R_2 + KR_2$. In other words, the number of parameters that must be determined in tensor train decomposition is much smaller than the number of parameters that must be decided for CP and Tucker decomposition. This means, if we need to obtain the tensor decomposition of higher order modes, computational time and memory required is logarithmically small. This does not mean unfortunately that tensor train decomposition is always superior to CP decomposition and Tucker decomposition. There is no free lunch. In contrast to CP decomposition and Tucker decomposition, the order of suffix must be fixed in tensor train decomposition prior to executing tensor decomposition. In Eq. (3.3), the order of suffix in the left-hand side is $i \rightarrow j \rightarrow k$ and is not commutable. This restriction of the suffix order does not exist in either CP decomposition or Tucker decomposition. This restriction might prevent tensor train decomposition from getting optimal solutions that can be obtained by CP decomposition or Tucker decomposition. At the moment, there are no guidelines on how to order suffix in order to get optimal solutions in tensor train decomposition; if the parameter space searched is narrow, the opportunity to get optimal solution is limited, too.

Exercise

3.1 Get CP decomposition, Tucker decomposition, and tensor train decomposition of three-mode tensor, $x_{ijk} = 1 \in \mathbb{R}^{3\times3\times3}$, though it might be trivial.

3.2 Performance of TDs as Tools Reducing the Degrees of Freedoms

In contrast to the MF that are associated with geometrical representations, TD generally lacks the interpretations based upon geometrical representation. Thus, it is important how TD can help us to interpret complex data set from the data science point of views. As an intuitive example that demonstrates the usefulness of TD as data mining tools, we consider the following simple case

$$x_{ijk} = i + j + k \tag{3.25}$$

In principle, we do not need any complicated procedures like TD to understand this simple three-mode tensor. Because we know what the tensor, Eq. (3.25), represents, it is also easy for us to understand how TD works when it is applied to this simple tensor. For the simplicity, I use only the case $x_{ijk} \in \mathbb{R}^{3\times4\times5}$. However, the essential result obtained by this assumption will be kept for larger tensors, too.

3.2.1 *Tucker Decomposition*

We start this analysis with applying Tucker decomposition, Eq. (3.2), to the tensor shown in Eq. (3.25). HOSVD algorithm (detailed explanation will be given later) is employed to obtain Tucker decomposition. Excluding those having essentially zero values with considering numerical accuracy, $G(\ell_1, \ell_2, \ell_3)$s in Eq. (3.2) are in Table 3.1. Thus, although the total number of G is $3 \times 4 \times 5 = 60$, as little as eight Gs have non-zero values. Therefore, singular value vectors that can contribute to the decomposition, Eq. (3.2), are limited to $1 \le \ell_1, \ell_2, \ell_3 \le 2$. The number of them is only six. Because $\boldsymbol{u}_{\ell_1}^{(i)}, \boldsymbol{u}_{\ell_2}^{(j)}$, and $\boldsymbol{u}_{\ell_3}^{(k)}$ have three, four, and five components, these six vectors have in total $3 \times 2 + 4 \times 2 + 5 \times 2 = 24$ components. As a result, the total number of real numbers composed of Tucker decomposition, Eq. (3.2), applied to the tensor Eq. (3.25) is $8 + 24 = 32$. This number, 32, is about half of the number of elements of original tensor, $3 \times 4 \times 5 = 60$. This means, TD is effective to reduce the degrees of freedom in tensor, although it is not necessary because Eq. (3.25) is easy to understand without any kind of data reduction.

Table 3.1 Core tensors having non-zero values when Tucker decomposition, Eq. (3.2), is applied to the tensor Eq. (3.25)

$G(\ell_1, \ell_2, \ell_3)$				
	$\ell_1 = 1$		$\ell_1 = 2$	
	$\ell_2 = 1$	$\ell_2 = 2$	$\ell_2 = 1$	$\ell_2 = 2$
$\ell_3 = 1$	-60.04	5.06×10^{-3}	-8.57×10^{-3}	-1.13
$\ell_3 = 2$	6.32×10^{-3}	1.57	-0.88	-0.32

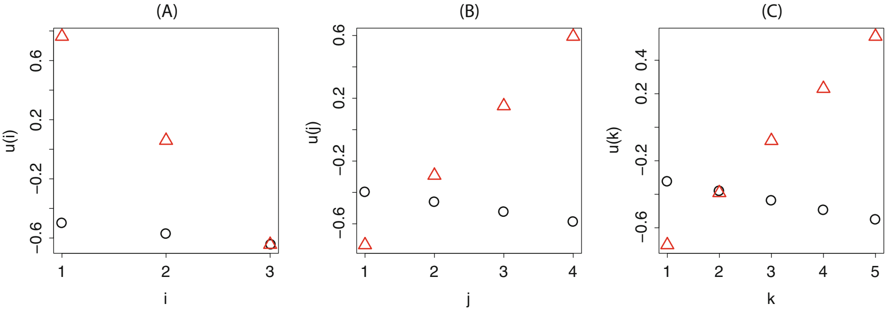

Fig. 3.1 Singular value vectors computed by applying Tucker decomposition, Eq. (3.2), to the tensor Eq. (3.25). (**a**) $\boldsymbol{u}^{(i)}_{\ell_1}$ (**b**) $\boldsymbol{u}^{(j)}_{\ell_2}$ (**c**) $\boldsymbol{u}^{(k)}_{\ell_3}$. open circle: $\ell_1, \ell_2, \ell_3 = 1$, red triangle: $\ell_1, \ell_2, \ell_3 = 2$

It is also important to see how the tensor Eq. (3.25) is decomposed by Tucker decomposition (Fig. 3.1). Firstly, all of these vectors represent monotonic dependence upon i, j, or k. This suggests that TD can capture fundamental dependence of x_{ijk} in Eq. (3.25) upon i, j, or k, since Eq. (3.25) shows the monotonic dependence upon i, j, or k as well.

In addition to this, TD can also be used as an approximation to the tensor. As can be seen in Table 3.1, $G(1, 1, 1)$ has the maximum absolute values among eight G with non-zero values. Moreover, considering that Gs play a role of weight factors in Eq. (3.2), $G(1, 1, 1)$ have most of contributions since $\frac{G(1,1,1)^2}{\sum_{\ell_1,\ell_2,\ell_3} G(\ell_1,\ell_2,\ell_3)^2} = 0.998$. In actuality, the scatterplot between x_{ijk} and the right-hand side of Eq. (3.2) with only considering $\ell_1 = \ell_2 = \ell_3 = 1$ shows almost complete reproduction (Fig. 3.2).

In conclusion, Tucker decomposition, Eq. (3.2), has the ability to reduce the degrees of freedoms (about half of them) with keeping essential dependence upon i, j, k (monotonic dependence).

Exercise

3.2 Draw something that corresponds to Fig. 3.2 with employing more terms than $\ell_1 = \ell_2 = \ell_3 = 1$.

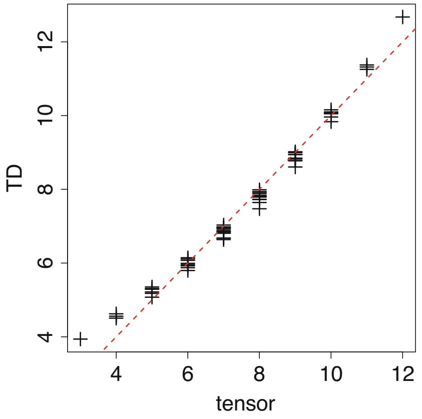

Fig. 3.2 Comparison between x_{ijk} in Eq. (3.25) and the recomputation from Tucker decomposition, Eq. (3.2), with considering only $\ell_1 = \ell_2 = \ell_3 = 1$. Red broken line represents diagonal line (i.e., complete agreement)

3.2.2 CP Decomposition

Next, we consider CP decomposition, Eq. (3.1). It is usual that CP decomposition, Eq. (3.1), is more interpretable than Tucker decomposition, Eq. (3.2). This is because CP decomposition is a simple linear combination of tensor product of individual vectors while individual vectors are repeatedly used in Tucker decomposition, Eq. (3.2). Thus, apparently CP decomposition has more ability to relate vectors one by one; it is expected to make interpretation easier than Tucker decomposition.

Since we know that x_{ijk} in Eq. (3.25) can be well approximated by the single term in the right-hand side of Eq. (3.2), we try to check if CP decomposition, Eq. (3.1), can represent x_{ijk} in Eq. (3.25) with $L = 1$. Figure 3.3 shows the comparison between x_{ijk} in Eqs. (3.25) and (3.1) with $L = 1$ when CP decomposition is applied to x_{ijk} in Eq. (3.25). Figures 3.2 and 3.3 look identical; these two are really identical within numerical accuracy. Thus, CP decomposition can approximate x_{ijk} in Eq. (3.25) as well as Tucker decomposition did.

In order to estimate the degrees of freedom that CP decomposition can represent x_{ijk} in Eq. (3.25) not approximately but completely, we try to find minimum L that can perform complete CP decomposition. Then we found that $L = 4$ is minimum. Thus, the total number of real numbers required is $(3 + 4 + 5) \times 4 = 48$. Because this number is larger than 34 which is the number of real values to obtain Tucker decomposition that can perform complete decomposition, CP decomposition has less ability to reduce the degrees of freedom than Tucker decomposition.

The difference between Tucker decomposition and CP decomposition takes place when considering the second term. One might expect that Eq. (3.1) with $L = 2$ might be identical to summation of two terms composed of singular value vectors shown in Fig. 3.1. Figure 3.4 shows $\boldsymbol{u}_\ell^{(i)}$, $\boldsymbol{u}_\ell^{(j)}$, and $\boldsymbol{u}_\ell^{(k)}$ for $\ell = 1, 2$. In contrast to the expectation, Fig. 3.4 does not look like Fig. 3.1. In contrast to Fig. 3.1 where

Fig. 3.3 Comparison between x_{ijk} in Eq. (3.25) and the recomputation from CP decomposition, Eq. (3.1), with $L = 1$. Red broken line represents diagonal line (i.e., complete agreement)

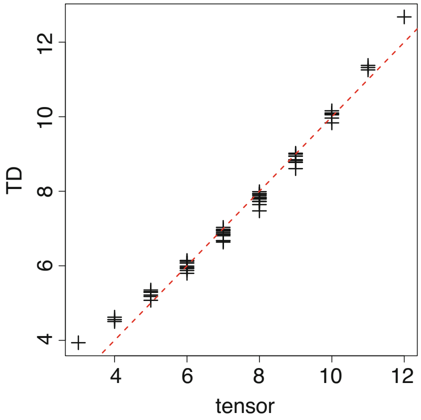

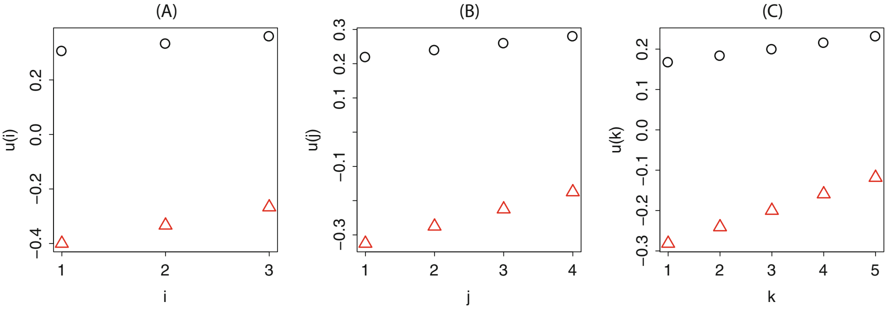

Fig. 3.4 Singular value vectors computed by applying CP decomposition, Eq. (3.1), to the tensor Eq. (3.25) with $L = 2$. (**a**) $\boldsymbol{u}_\ell^{(i)}$ (**b**) $\boldsymbol{u}_\ell^{(j)}$ (**c**) $\boldsymbol{u}_\ell^{(k)}$. Open circle: $\ell = 1$, red triangle: $\ell = 2$

Table 3.2 λ_ℓs with $L = 1$ and $L = 2$ when CP decomposition, Eq. (3.1), is applied to the tensor Eq. (3.25)

λ_ℓ	$L = 1$	$L = 2$
$\ell = 1$	450.6	533.7
$\ell = 2$	–	83.7

singular value vectors associated with distinct ℓ_1, ℓ_2, ℓ_3 values look different, those with distinct ℓ look similar excluding parallel vertical displacements in Fig. 3.4.

Table 3.2 shows the λ_ℓs with $L = 1$ and $L = 2$. The absolute ratio, $\left|\frac{\lambda_2}{\lambda_1}\right|$, of weights between the first term, λ_1, and the second term, λ_2, when $L = 2$ is comparatively larger than that between terms with the first and the second largest absolute values in Table 3.1, $\left|\frac{G(1,2,2)}{G(1,1,1)}\right|$. It is coincident with the fact that singular value vectors with $\ell = 1, 2$ in CP decomposition does not look distinct, because similar singular value vectors unlikely have very distinct weights. On the other hand, this suggests that CP decomposition fails to compute the additional small correction with keeping the contribution from the main term as large as Tucker decomposition did.

Although actual numerical algorithms to execute various TDs are not yet explained (see later part of this chapter), CP decomposition is not guaranteed to converge to the unique solution (see the following sections). Thus, in contrast to the apparent interpretability of CP decomposition, because TD itself is not unique but depends upon the initial values for the iterative computation, CP decomposition cannot be considered to have superior interpretability to Tucker decomposition.

Since the Tucker decomposition is easier to compute and has more converging algorithm, I prefer Tucker to CP in the approximations shown in the following application examples mentioned in this book in spite of the apparent interpretability of CP decomposition.

Exercise
3.3 Draw something that corresponds to Fig. 3.3 with employing more terms than $L = 1$.

3.2.3 *Tensor Train Decomposition*

Finally, I apply tensor train decomposition, Eq. (3.3), to x_{ijk} in Eq. (3.25). The result is

$$G^{(i)}_{\ell_1,i} = (i, 1) \tag{3.26}$$

$$G^{(j)}_{\ell_1,\ell_2,j} = \begin{pmatrix} 1 & 0 \\ j & 1 \end{pmatrix} \tag{3.27}$$

$$G^{(k)}_{\ell_2,k} = (1, k) \tag{3.28}$$

because

$$G^{(i)}_{\ell_1,i} \times_{\ell_1} G^{(j)}_{\ell_1,\ell_2,j} \times_{\ell_2} G^{(k)}_{\ell_2,k} = (i, 1) \begin{pmatrix} 1 & 0 \\ j & 1 \end{pmatrix} \begin{pmatrix} 1 \\ k \end{pmatrix} = (i + j, i) \begin{pmatrix} 1 \\ k \end{pmatrix} = i + j + k \tag{3.29}$$

The number of $G^{(i)}$ is three, that of $G^{(j)}$ is four and that of $G^{(k)}$ is five, thus the total number of real numbers that compose tensor train decomposition is $2 \times 3 + 4 \times 4 + 2 \times 5 = 32$. Since this number is smaller than 34 and 48, which are the minimum degrees of freedom to execute complete decomposition when Tucker and CP decomposition are applied to x_{ijk} in Eq. (3.25), respectively, tensor train decomposition has superior ability to reduce the degrees of freedom. In this example, the amount of superiority might look small, but if we consider tensors with the higher dimensions or modes, this difference matters.

On the other hand, tensor train decomposition has some disadvantages. The first disadvantage is that Eq. (3.3) is not invariant when the order of i, j, k is exchanged.

It is obvious that i, j, k must be exchanged when the order of i, j, k in Eqs. (3.26)–(3.28) is exchanged. In actuality, the ability of reducing the number of freedoms itself is also altered. If the order of i, j, k is modified as j, i, k such that the number of matrices used is minimized, the total number of real numbers required decreases from 32 to $2 \times 4 + 4 \times 3 + 2 \times 5 = 30$. This might be problematic for the application of data science that requires interpretation of the obtained singular value vectors. If the order of i, j, k matters, we have to decide this order in advance, or select the best order after investigating the results. This is really problematic because the number of possibility on how to order i, j, k grows exponentially if we have to consider tensors with more number of modes. Selecting one of them might not be easy.

The second disadvantage is that tensor train decomposition does not have weight, by which we can know the primary terms in decomposition as in the cases of CP decomposition and Tucker decomposition. In the case of tensor train decomposition, we have no ways to know which combination among Eq. (3.3) is dominant. For the application of TD towards real data sets, it is not an ignorable point. Thus, in the application that will be discussed in the later parts of this text, I do not employ tensor train decomposition, either, as CP decomposition is not employed.

Exercise
3.4 Draw something that corresponds to Fig. 3.2 or 3.3 for tensor train decomposition.

3.2.4 TDs Are Not Always Interpretable

When applying TDs to x_{ijk} in Eq. (3.25), no matter how many degrees of freedom are required, three TDs, CP decomposition, Tucker decomposition, and tensor train decomposition can acquire essential feature of the tensor, i.e., monotonic dependence upon i, j, k. Although readers might trust the usefulness of these TDs as the tool for the application in data science, the situation is actually not so straightforward. Instead of the x_{ijk} in Eq. (3.25) we consider the tensor

$$x_{ijk} = \left(i - \frac{N+1}{2}\right) + \left(j - \frac{M+1}{2}\right) + \left(k - \frac{K+1}{2}\right) \tag{3.30}$$

such that average over either i, j, or k is equal to zero. Although this may not seem to dramatically change the results of TD, it actually does. Table 3.3 shows the list of Gs with non-zero values when Tucker decomposition is applied to x_{ijk} defined in Eq. (3.30). Compared with Table 3.1, although the number of Gs with non-zero values is eight which is the same as that in Table 3.1, individual absolute values of Gs are larger excluding $G(1, 1, 1)$. This suggests that $G(1, 1, 1)$ cannot acquire most of the contributions in contrast to Table 3.3 but other Gs have substantial contributions. Figure 3.5 shows the singular value vectors, which are very different from those in Fig. 3.1 that represent monotonic dependence upon

Table 3.3 Core tensors having non-zero values when Tucker decomposition, Eq. (3.2), is applied to the tensor Eq. (3.30)

$G(\ell_1, \ell_2, \ell_3)$				
	$\ell_1 = 1$		$\ell_1 = 2$	
	$\ell_2 = 1$	$\ell_2 = 2$	$\ell_2 = 1$	$\ell_2 = 2$
$\ell_3 = 1$	15.67	1.70	−1.71	5.69
$\ell_3 = 2$	1.86	−3.69	3.39	−3.04

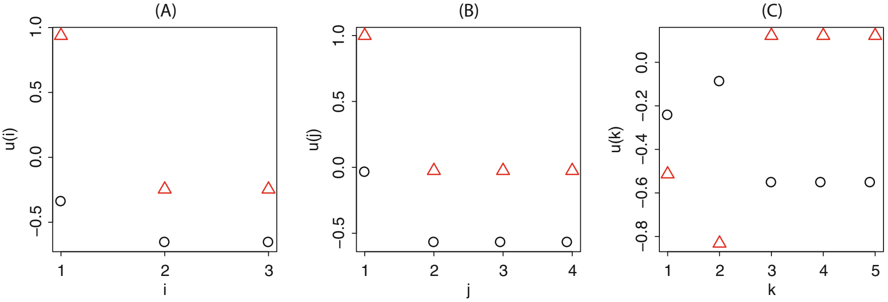

Fig. 3.5 Singular value vectors computed by applying Tucker decomposition, Eq. (3.2), to the tensor Eq. (3.30). **(a)** $\boldsymbol{u}_{\ell_1}^{(i)}$ **(b)** $\boldsymbol{u}_{\ell_2}^{(j)}$ **(c)** $\boldsymbol{u}_{\ell_3}^{(k)}$. Open circle: $\ell_1, \ell_2, \ell_3 = 1$, red triangle: $\ell_1, \ell_2, \ell_3 = 2$

i, j, k. Singular value vectors in Fig. 3.5 have lost monotonic dependence upon i, j, k in spite of that x_{ijk} itself in Eq. (3.30) still keeps monotonic dependence upon i, j, k as in Eq. (3.25). This drastic change is caused because x_{ijk}s in Eq. (3.30) take both negative and positive values while those in Eq. (3.25) take positive values only. Because the product between two negative values results in positive values, expressing the distinct signs of x_{ijk} with the products of vectors is not straightforward. Thus, singular value vectors inevitably lost the simple monotonic dependence upon i, j, k.

Thus, from the point of data science, tensors whose elements are both negatively and positively signed are not easy to be dealt with TDs. For the cases of matrix factorization, extraction of means affected the outcomes in unpredictable ways (see Sect. 2.5.3). Similarly, the outcomes of TDs are affected by whether means are extracted or not, because of the effect discussed in the above. How to extract means is also a key on the application of TD to real datasets, although this point is rarely emphasized.

Exercise

3.5 Draw something that corresponds to Fig. 3.2 for Tucker decomposition applied to Eq. (3.30).

3.3 Various Algorithms to Compute TDs

In this section, I introduce various algorithms to derive various TDs.

3.3.1 CP Decomposition

Firstly, I introduce how to compute CP decomposition, Eq. (3.1). Before introducing algorithm, I would like to mention about non-uniqueness of approximation of tensor by CP decomposition as demonstrated when CP decomposition, Eq. (3.1), with $L = 2$ is applied to x_{ijk}, Eq. (3.25), in the previous section. In §3.3 of Kolda and Bader [2], there is an example of non-uniqueness when a specific three-mode tensor is decomposed by CP decomposition with $L = 2$. The tensor $X \in \mathbb{R}^{N \times M \times K}$ has the form of

$$\mathcal{X} = \boldsymbol{a}_1 \times^0 \boldsymbol{b}_1 \times^0 \boldsymbol{c}_2 + \boldsymbol{a}_1 \times^0 \boldsymbol{b}_2 \times^0 \boldsymbol{c}_1 + \boldsymbol{a}_2 \times^0 \boldsymbol{b}_1 \times^0 \boldsymbol{c}_1 \tag{3.31}$$

where $A = (\boldsymbol{a}_1, \boldsymbol{a}_2) \in \mathbb{R}^{N \times 2}$, $B = (\boldsymbol{b}_1, \boldsymbol{b}_2) \in \mathbb{R}^{M \times 2}$, and $C = (\boldsymbol{c}_1, \boldsymbol{c}_2) \in \mathbb{R}^{K \times 2}$. Then consider the specific form of CP decomposition with $L = 2$ as

$$\mathcal{Y} = \alpha \left(\boldsymbol{a}_1 + \frac{\boldsymbol{a}_2}{\alpha} \right) \times^0 \left(\boldsymbol{b}_1 + \frac{\boldsymbol{b}_2}{\alpha} \right) \times^0 \left(\boldsymbol{c}_1 + \frac{\boldsymbol{c}_2}{\alpha} \right) - \alpha \boldsymbol{a}_1 \times^0 \boldsymbol{b}_1 \times^0 \boldsymbol{c}_1 \tag{3.32}$$

Then

$$\begin{aligned} ||\mathcal{X} - \mathcal{Y}|| = \frac{1}{\alpha} \Big|\Big| & \boldsymbol{a}_2 \times^0 \boldsymbol{b}_2 \times^0 \boldsymbol{c}_1 + \boldsymbol{a}_2 \times^0 \boldsymbol{b}_1 \times^0 \boldsymbol{c}_2 + \boldsymbol{a}_1 \times^0 \boldsymbol{b}_2 \times^0 \boldsymbol{c}_2 \\ & - \frac{1}{\alpha} \boldsymbol{a}_2 \times^0 \boldsymbol{b}_2 \times^0 \boldsymbol{c}_2 \Big|\Big| \end{aligned} \tag{3.33}$$

can be made arbitrarily small. Thus, CP decomposition with $L = 2$ for Eq. (3.31) can never be unique. The reason why this can happen is because two oppositely signed arbitrarily large terms can result in small value with canceling each other. In this sense, no matter what algorithm is employed for CP decomposition, there is no unique approximation using CP decomposition.

Consequently, the algorithm of CP decomposition is inevitably empirical and does not guarantee neither uniqueness nor convergence. Here I introduce a specific algorithm that employs alternating least square (ALS). ALS is a general algorithm that minimizes multi arguments functions by alternating one argument with fixing other arguments. Suppose the case that minimization of the function $f(x, y, z)$ is difficult while $f(x, y_0, z_0)$ with fixing y_0 and z_0 is easy (this also stands for y and z). Then ALS algorithm repeatedly minimizes $f(x, y_0, z_0)$, $f(x_0, y, z_0)$, and $f(x_0, y_0, z)$ in turn until convergence. For example, let us consider the minimization of $f(x, y, z) = x^2 + y^2 + z^2$ with starting $x = y = z = 1$. Applying ALS to this problem is as follows. At first, try to minimize $f(x, 1, 1) = x^2 + 2$. It is obvious that $x = 0$ minimizes $x^2 + 2$. Then, x is decided to be 0. Then, we try to minimize $f(0, y, 1) = y^2 + 1$. It is again obvious $y = 0$ does. Then, y is decided to be 0. Finally, we try to minimize $f(0, 0, z) = z^2$. We get $z = 0$. The minimum value $f(0, 0, 0) = 0$ can be obtained by ALS algorithm.

In order to apply ALS to obtain CP decomposition, Eq. (3.1), we need some mathematics [2]. At first, Eq. (3.1) needs to be rewritten in the unfolded matrix form, $X^{i\times(jk)}$, of tensor $\mathcal{X} \in \mathbb{R}^{N\times M\times K}$

$$X^{i\times(jk)} = \hat{U}^{(i)} \times_\ell \left(U^{(j)} \times^\ell U^{(k)}\right)^{\ell\times(jk)} \tag{3.34}$$

with introducing matrices $\hat{U}^{(i)} = \left(\lambda_1 \boldsymbol{u}_1^{(i)}, \lambda_2 \boldsymbol{u}_2^{(i)}, \dots, \lambda_L \boldsymbol{u}_L^{(i)}\right) \in \mathbb{R}^{N\times L}$, $U^{(j)} = \left(\boldsymbol{u}_1^{(j)}, \boldsymbol{u}_2^{(j)}, \dots, \boldsymbol{u}_L^{(j)}\right) \in \mathbb{R}^{M\times L}$ and $U^{(k)} = \left(\boldsymbol{u}_1^{(k)}, \boldsymbol{u}_2^{(k)}, \dots, \boldsymbol{u}_L^{(k)}\right) \in \mathbb{R}^{K\times L}$ and $\left(U^{(j)} \times^\ell U^{(k)}\right)^{\ell\times(jk)} \in \mathbb{R}^{L\times MK}$ is an unfolding of the tensor, $U^{(j)} \times^\ell U^{(k)} \in \mathbb{R}^{L\times M\times K}$. Then, we try to find $\hat{U}^{(i)}$ with fixing $U^{(j)}$ and $U^{(k)}$ such that

$$\min_{\hat{U}^{(i)}} \left|\left| X^{i\times(jk)} - \hat{U}^{(i)} \times_\ell \left(U^{(j)} \times^\ell U^{(k)}\right)^{\ell\times(jk)} \right|\right|_F \tag{3.35}$$

where $||\cdots||_F$ is the Frobenius norm which is defined as the root of the squared summation of matrix elements. This is the same as linear regression problem with having NL elements of $\hat{U}^{(i)}$ as variables.

The solution of Eq. (3.35) can be obtained to compute Moore-Penrose pseudoinverse as

$$\hat{U}^{(i)} = X^{i\times(jk)} \times_{jk} \left[\left(U^{(j)} \times^\ell U^{(k)}\right)^{\ell\times(jk)}\right]^\dagger \tag{3.36}$$

where $A^\dagger$ is the Moore-Penrose pseudoinverse of a matrix A. Moore-Penrose pseudoinverse is known to give the solution of $A\boldsymbol{x} = \boldsymbol{b}$ as the form $\boldsymbol{x} = A^\dagger \boldsymbol{b}$ including the cases that A is not a square matrix. Computing $A^\dagger$ from A is implemented in various application software, thus it is not discussed in detail here.[2] After getting $\hat{U}^{(i)}$ with Eq. (3.36), we normalize the columns of $\hat{U}^{(i)}$ to get $U^{(i)}$. Then, $U^{(i)}$ is replaced with either $U^{(j)}$ or $U^{(k)}$ which can be obtained by repeating the above procedure until the convergence.

In order to see how ALS works for CP decomposition, we apply this algorithm to the simplest case. X is supposed to be a matrix instead of tensor as

$$X = \begin{pmatrix} 1 & 2 & 3 \\ 4 & 5 & 6 \\ 7 & 8 & 9 \end{pmatrix} \tag{3.37}$$

In CP decomposition with $L = 1$, X is supposed to be decomposed as

[2] See Appendix for more details about Moore-Penrose pseudoinverse. Alternatively, one can simply execute linear regression analysis, Eq. (3.35).

$$X = \boldsymbol{a} \times^0 \boldsymbol{b} \tag{3.38}$$

where $\boldsymbol{a}, \boldsymbol{b} \in \mathbb{R}^3$. Although it is nothing but SVD, since we simply would like to demonstrate the usefulness of CP decomposition, it does not matter. Then we get

$$a_1 b_1 = 1 \tag{3.39}$$

$$a_1 b_2 = 2 \tag{3.40}$$

$$a_1 b_3 = 3 \tag{3.41}$$

$$a_2 b_1 = 4 \tag{3.42}$$

$$a_2 b_2 = 5 \tag{3.43}$$

$$a_2 b_3 = 6 \tag{3.44}$$

$$a_3 b_1 = 7 \tag{3.45}$$

$$a_3 b_2 = 8 \tag{3.46}$$

$$a_3 b_3 = 9 \tag{3.47}$$

In order to perform ALS, we need to express $\boldsymbol{a}$ by $\boldsymbol{b}$ and $\boldsymbol{b}$ by $\boldsymbol{a}$. This can be done by performing Eq. (3.39) + Eq. (3.40) + Eq. (3.41), Eq. (3.42) + Eq. (3.43) + Eq. (3.44), Eq. (3.45) + Eq. (3.46) + Eq. (3.47), Eq. (3.39) + Eq. (3.42) + Eq. (3.45), Eq. (3.40) + Eq. (3.43) + Eq. (3.46), and Eq. (3.41) + Eq. (3.44) + Eq. (3.47). This results in

$$\boldsymbol{a} = \frac{1}{\sum_i b_i} \begin{pmatrix} 6 \\ 15 \\ 24 \end{pmatrix} \tag{3.48}$$

$$\boldsymbol{b} = \frac{1}{\sum_i a_i} \begin{pmatrix} 12 \\ 15 \\ 18 \end{pmatrix} \tag{3.49}$$

ALS can be performed, by computing $\boldsymbol{a}$ by Eq. (3.48) then $\boldsymbol{b}$ by Eq. (3.49) and repeat them iteratively.

Starting from $\boldsymbol{b} = \begin{pmatrix} 1 \\ 1 \\ 1 \end{pmatrix}$, after one iteration, we get

$$\boldsymbol{a} = \begin{pmatrix} 2 \\ 5 \\ 8 \end{pmatrix} \tag{3.50}$$

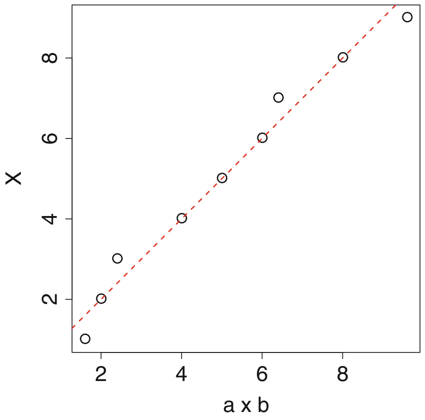

Fig. 3.6 Scatterplot of X, Eq. (3.37), and the approximation by CP decomposition, $\boldsymbol{a} \times^0 \boldsymbol{b}$ where $\boldsymbol{a}$ and $\boldsymbol{b}$ are given as Eqs. (3.50) and (3.51). Red broken lines indicate complete match

$$\boldsymbol{b} = \begin{pmatrix} 0.8 \\ 1.0 \\ 1.2 \end{pmatrix} \tag{3.51}$$

This satisfies Eqs. (3.48) and (3.49). Thus, they are converged solutions.

Next we would like to see how good it is. Figure 3.6 shows the comparison between X, Eq. (3.37), and $\boldsymbol{a} \times^0 \boldsymbol{b}$. It is obvious that they are highly coincident. Thus, CP decomposition implemented using ALS works well.

Here readers should notice that we need initial values of $U^{(i)}$, $U^{(j)}$, and $U^{(k)}$ in CP decomposition implemented using ALS (in the above example, we needed to initialize $\boldsymbol{b}$). Since uniqueness of approximate solution by CP decomposition is not guaranteed as demonstrated in Eq. (3.33), CP decomposition cannot give unique approximation but generally gives various approximations depending upon initial values. From this point of view, employing CP decomposition for data science is not recommended because data science requires interpretation of obtained decomposition. If the results of CP decomposition have initial value dependence, it is not easy to interpret the outcome uniquely.

In order to extend the above calculation to tensors, $X \in \mathbb{R}^{N_1 \times N_1 \times \cdots \times N_m}$ with arbitrary number of modes m, Eq. (3.1) is generalized as

$$\mathcal{X} = \sum_{\ell=1}^{L} \lambda_\ell \boldsymbol{u}_\ell^{(i_1)} \times^0 \boldsymbol{u}_\ell^{(i_2)} \times^0 \cdots \times^0 \boldsymbol{u}_\ell^{(i_m)} \tag{3.52}$$

Figure 3.7 shows the generalized algorithm of CP decomposition aiming tensors with arbitrary number of modes m, which is the straight extension of ALS based CP decomposition algorithm described for the three-mode tensor in the above.

```
Procedure CP decomposition
    Initialize $U^{(i_\alpha)}, \alpha \in [1, m]$
    repeat
        do $\alpha \in [1, m]$
            $\hat{U}^{(i_\alpha)} \longleftarrow X^{i_\alpha \times (i_1 i_2 \ldots i_{\alpha-1} i_{\alpha+1} \ldots i_m)} \times_{(i_1 i_2 \ldots i_{\alpha-1} i_{\alpha+1} \ldots i_m)}$
                $\left[\left(U^{(i_1)} \times^\ell U^{(i_2)} \times^\ell \cdots \times^\ell U^{(i_{\alpha-1})} \times^\ell U^{(i_{\alpha+1})} \times^\ell \cdots \times^\ell U^{(i_m)}\right)^{\ell \times (i_1 i_2 \cdots i_{\alpha-1} i_{\alpha+1} \cdots i_m)}\right]^\dagger$
            normalize columns of $\hat{U}^{(i_\alpha)}$ (storing norms as $\boldsymbol{\lambda}$)
        end do
    until fit ceases to improve or maximum iterations exhausted
    return $\boldsymbol{\lambda}$, $U^{(i_\alpha)}, \alpha \in [1, m]$
end procedure
```

Fig. 3.7 Algorithm of CP decomposition for tensors with arbitrary number of modes m

Exercise
3.6 Apply CP decomposition implemented using ALS to the tensor $\mathcal{X} \in \mathbb{R}^{2 \times 2 \times 2}$

$$X_{ij1} = \begin{pmatrix} 1 & 2 \\ 3 & 4 \end{pmatrix} \tag{3.53}$$

$$X_{ij2} = \begin{pmatrix} 5 & 6 \\ 7 & 8 \end{pmatrix} \tag{3.54}$$

3.3.2 Tucker Decomposition

Tucker decomposition, Eq. (3.2), is not as popular as CP decomposition that has apparent ease to apply to dataset. As discussed in the previous section, this apparent ease is not always true. Since I found that Tucker decomposition has numerous advantages in spite of its unpopularity and I can almost always make use of it in the applications described in the later part of this textbook, I would like to discuss about it in more detail in this section.

There are two popular implementations of Tucker decomposition, ALS based one and SVD based one. Since Tucker decomposition does not have uniqueness at all as discussed in the above, these two distinct implementations generally give distinct outcomes. The first one that makes use of ALS is named higher orthogonal iteration of tensors (HOOI). HOOI, as its name says, computes TD iteratively with orthogonalizing column vectors, because Tucker decomposition requires the orthogonal matrices as outcomes, although CP decomposition does not always require orthogonality between obtained singular value vectors. Using $U^{(i)} \in \mathbb{R}^{L_1 \times N}$, $U^{(j)} \in \mathbb{R}^{L_2 \times M}$, and $U^{(k)} \in \mathbb{R}^{L_3 \times K}$ defined in the previous subsection, Eq. (3.2) can be rewritten as

$$\mathcal{X} = G \times_{\ell_1} U^{(i)} \times_{\ell_2} U^{(j)} \times_{\ell_3} U^{(k)} \tag{3.55}$$

In order to perform ALS, we need to express $U^{(i)}$ with $U^{(j)}$ and $U^{(k)}$. Since $U^{(i)}$, $U^{(j)}$, and $U^{(k)}$ are orthogonal matrices, it can be easily done as follows. First, we need to define a tensor $\mathcal{Y} \in \mathbb{R}^{N \times \ell_2 \times \ell_3}$

$$\mathcal{Y} = \mathcal{X} \times_j U^{(j)} \times_k U^{(k)} \tag{3.56}$$

Since $U^{(j)}$ and $U^{(k)}$ are orthogonal matrices, $U_{(j)} \times_j U_{(j)} = I$ and $U_{(k)} \times_k U_{(k)} = I$. Then we get

$$\mathcal{Y} = G \times_{\ell_1} U^{(i)} \tag{3.57}$$

Applying SVD to unfolded matrix $Y^{i \times (\ell_2 \ell 3)}$ of $\mathcal{Y}$, we get

$$Y^{i \times (\ell_2 \ell_3)} = G^{\ell_1 \times (\ell_2 \ell_3)} \times_{\ell_1} U^{(i)} \tag{3.58}$$

Thus Eqs. (3.56)–(3.58) give the procedure to compute $U^{(i)}$ from $U^{(k)}$ and $U^{(j)}$. Based upon ALS, we can repeatedly compute either of $U^{(i)}$, $U^{(j)}$ and $U^{(k)}$ from the other two of them until these are converged. After the convergence, we can compute G as

$$G = \mathcal{X} \times_i U^{(i)} \times_j U^{(j)} \times_k U^{(k)} \tag{3.59}$$

because $U^{(i)}$, $U^{(j)}$, and $U^{(k)}$ are orthogonal matrices.

One might notice that HOOI also needs the initialization of $U^{(i)}$, $U^{(j)}$, and $U^{(k)}$. In contrast to CP decomposition that has no ways to perform initialization uniquely, Tucker decomposition can have unique way to decide the initialization. It is called as higher order singular value decomposition (HOSVD). In order to perform HOSVD, we apply SVD to unfolded matrix $X^{i \times (jk)}$ in order to obtain $U^{(i)}$, because we get $U^{(i)}$ through getting the tensor $\mathcal{Y} \in \mathbb{R}^{L_1 \times M \times K}$ and its unfolded matrix $Y^{i \times (jk)}$ as

$$X^{i \times (jk)} = Y^{\ell_1 \times (jk)} \times_{\ell_1} U^{(i)} \tag{3.60}$$

$$\mathcal{Y} = G \times_{\ell_2} U^{(j)} \times_{\ell_3} U^{(k)} \tag{3.61}$$

Similarly, $U^{(j)}$ and $U^{(k)}$ can be obtained with applying SVD to unfolded matrices $X^{j \times (ik)}$ and $X^{k \times (ij)}$, respectively. Finally, using obtained $U^{(i)}$, $U^{(j)}$, and $U^{(k)}$, we can compute G as

$$G = \mathcal{X} \times_i U^{(i)} \times_j U^{(j)} \times_k U^{(k)} \tag{3.62}$$

In order to extend the above computations to tensors with arbitrary modes m, Eq. (3.2) is extended as

$$\mathcal{X} = G \times_{\ell_1} U^{(i_1)} \times_{\ell_2} U^{(i_2)} \times_{\ell_3} \cdots \times_{\ell_m} U^{(i_m)} \tag{3.63}$$

where $\mathcal{X}, G \in \mathbb{R}^{N_1 \times N_2 \times \cdots \times N_m}$ and $U^{(i_\alpha)} \in \mathbb{R}^{N_\alpha \times N_\alpha}$, $1 \leq \alpha \leq m$.

```
Procedure HOSVD
    do $i_\alpha, \alpha \in [1, m]$
        compute $U^{(i_\alpha)}$ with applying SVD to $X^{i_\alpha \times (i_1 i_2 \cdots i_{\alpha-1} i_{\alpha+1} \cdots i_m)}$ as
        $X^{i_\alpha \times (i_1 i_2 \cdots i_{\alpha-1} i_{\alpha+1} \cdots i_m)} = Y^{\ell_\alpha \times (i_1 i_2 \cdots i_{\alpha-1} i_{\alpha+1} \cdots i_m)} \times_{\ell_\alpha} U^{(i_\alpha)}$
    end do
    $G = \mathcal{X} \times_{i_1} U^{(i_1)} \times_{i_2} U^{(i_2)} \times_{i_3} \cdots \times_{i_m} U^{(i_m)}$
    return $G$, $U^{(i_\alpha)}, \alpha \in [1, m]$
end procedure
```

Fig. 3.8 Algorithm of HOSVD for tensors with arbitrary number of modes m

```
Procedure HOOI
    Initialize $U^{(i_\alpha)}, \alpha \in [1, m]$ with HOSVD
    repeat
        do $i_\alpha \in [1, m]$
            compute $U^{(i_\alpha)}$ with applying SVD to $Y^{i_\alpha \times (\ell_{i_1} \ell_{i_2} \cdots \ell_{\alpha-1} \ell_{\alpha+1} \cdots \ell_m)}$ as
            $Y^{i_\alpha \times (\ell_1 \ell_2 \cdots \ell_{\alpha-1} \ell_{\alpha+1} \cdots \ell_m)} = G^{\ell_\alpha \times (\ell_1 \ell_2 \cdots \ell_{\alpha-1} \ell_{\alpha+1} \cdots \ell_m)} \times_{\ell_\alpha} U^{(i_\alpha)}$
            with $\mathcal{Y} = \mathcal{X} \times_{i_1} U^{(i_1)} \times_{i_2} U^{(i_2)} \times_{i_3} \cdots \times_{i_{\alpha-1}} U^{(i_{\alpha-1})} \times_{i_{\alpha+1}} U^{(i_{\alpha+1})} \times_{i_{\alpha+2}} \cdots \times_{i_m} U^{(i_m)}$
        end do
    until fit ceases to improve or maximum iterations exhausted
    $G = \mathcal{X} \times_{i_1} U^{(i_1)} \times_{i_2} \cdots \times_{i_m} U^{(i_m)}$
    return $G$, $U^{(i_\alpha)}, \alpha \in [1, m]$
end procedure
```

Fig. 3.9 Algorithm of HOOI for tensors with arbitrary number of modes. "…" means the operation over modes excluding the selected ith mode for do loop

Figure 3.8 shows the HOSVD algorithm for tensors with general number of modes and Fig. 3.9 shows the HOOI algorithm for tensors with general number of modes starting from initialization by HOSVD. In these definitions, we can get two algorithms to obtain Tucker decomposition, Eq. (3.2), for tensors with general number of modes. They are also free from arbitrary initialization in contrast to CP decomposition, because HOSVD does not need initialization while HOOI can be initialized uniquely with HOSVD.

I would like to mention some additional comments for these two algorithms. In Figs. 3.8 and 3.9, we do not specify the dimensions of $U^{(i)}, U^{(j)}, \ldots$. If we employ full rank, i.e., $U^{(i)} \in \mathbb{R}^{N \times N}$, $U^{(j)} \in \mathbb{R}^{M \times M}$, $U^{(k)} \in \mathbb{R}^{K \times K}$ …, HOSVD and HOOI do not differ from each other, since initialization using HOSVD gives complete solution, thus there is no way for HOOI to optimize. If we assign smaller dimensions to $U^{(i)}, U^{(j)}, \ldots$, there are possibilities that HOOI can optimize the results by HOSVD. If HOOI differs from HOSVD, it is completely data dependent. For the tensor Eq. (3.25), $U^{(i)}, U^{(j)}, \ldots$ whose ranks are much smaller than full rank can give complete solution. Thus, we cannot say that assignment of smaller dimensions to $U^{(i)}, U^{(j)}, \ldots$ always results in more optimal results by HOOI than that by HOSVD.

One should also notice that HOSVD has superiority to CP decomposition (Fig. 3.7) and HOOI (Fig. 3.9) because arbitrary $U^{(i)}$ can be computed independent of others. Although anyway we cannot avoid computing other singular matrices,

$U^{(j)}, U^{(k)}, \ldots$ because we cannot get G without computing all $U^{(i)}, U^{(j)}, U^{(k)}, \ldots$, it is a great advantage of HOSVD when considering applications.

Exercise

3.7 Apply HOSVD to the tensor $X \in \mathbb{R}^{2\times2\times2}$

$$X_{ij1} = \begin{pmatrix} 1 & 2 \\ 3 & 4 \end{pmatrix} \tag{3.64}$$

$$X_{ij2} = \begin{pmatrix} 5 & 6 \\ 7 & 8 \end{pmatrix} \tag{3.65}$$

3.3.3 Tensor Train Decomposition

After recognizing how to compute Tucker decomposition, it is relatively easy to understand how to compute tensor train decomposition [3] as well. Essentially, it is iterative application of SVD to unfolded matrices of a tensor. In order to show the algorithm that computes tensor train decomposition for the tensor with arbitrary number of modes m, tensor train decomposition, Eq. (3.3), is generalized as

$$\mathcal{X} = G^{(i_1)} \times_{\ell_1} G^{(i_2)} \times_{\ell_2} \cdots \times_{\ell_{\alpha-1}} G^{(i_\alpha)} \times_{\ell_\alpha} \cdots \times_{\ell_{m-1}} G^{(i_m)} \tag{3.66}$$

where $G^{(i_1)} \in \mathbb{R}^{N_1 \times R_1}$, $G^{(i_2)} \in \mathbb{R}^{N_2 \times R_1 \times R_2}$, $\ldots$, $G^{(i_\alpha)} \in \mathbb{R}^{N_\alpha \times R_{\alpha-1} \times R_\alpha}$, $\ldots$, $G^{(i_m)} \in \mathbb{R}^{N_m \times R_{m-1}}$. The components of $G^{(i_1)}$, $G^{(i_\alpha)}$, and $G^{(i_m)}$ are denoted as $G^{(i_1)}(i_1, \ell_1)$, $G^{(i_\alpha)}(i_\alpha R_{\alpha-1}, R_\alpha)$, and $G^{(i_m)}(i_m, R_{m-1})$, respectively.

Figure 3.10 shows the tensor train decomposition algorithm applied to tensor with arbitrary number of modes m. In order to perform the algorithm shown in Fig. 3.10, we need to know $R_\alpha, \alpha \in [1, m-1]$ in advance ($R_0 = 1$). It is known that [3]

```
Procedure Tensor train decomposition
    $C \leftarrow \mathcal{X}$
    do $i_\alpha, \alpha \in [1, m-1]$
        compute $G^{(i_\alpha)} \in \mathbb{R}^{N_\alpha \times R_{\alpha-1} \times R_\alpha}$
            with applying SVD to unfolded matrix $C^{(i_\alpha \ell_{\alpha-1}) \times (i_{\alpha+1} \cdots i_m)}$ as
        $C^{(i_\alpha \ell_{\alpha-1}) \times (i_{\alpha+1} \cdots i_m)} = \left[G^{(i_\alpha)}\right]^{(i_\alpha \ell_{\alpha-1}) \times \ell_\alpha} \times_{\ell_\alpha} Y^{\ell_\alpha \times (i_{\alpha+1} \cdots i_m)}$
            with $\mathcal{Y} \in \mathbb{R}^{R_\alpha \times N_{\alpha+1} \times \cdots \times N_m}$
        $C \leftarrow \mathcal{Y}$
    end do
    $G^{(i_m)} \leftarrow C$
    return $G$s
end procedure
```

Fig. 3.10 Algorithm of tensor train decomposition for tensors with arbitrary number of modes m

$$R_\alpha = \text{rank}\left[X^{(i_1 i_2 \cdots i_\alpha)\times(i_{\alpha+1}\cdots i_m)}\right]. \tag{3.67}$$

In order to see how well the algorithm shown in Fig. 3.10 works, it is applied to the tensor Eq. (3.25) with $(R_0, R_1, R_2, R_3) = (1, 2, 2, 1)$ (Fig. 3.11). Here R_1 and R_2 are estimated by Eq. (3.67) with applying SVD to unfolded matrices, $X^{i\times(jk)}$ and $X^{(ij)\times k}$, respectively. If Fig. 3.11 is compared with Eqs. (3.26)–(3.28), it is a little bit more complicated. However, if it is inserted to Eq. (3.3), it turns out that Eq. (3.25) is reproduced completely. Thus, as far as the reduction of degrees of freedom is considered, algorithm shown in Fig. 3.10 has the solution (Fig. 3.11) with the same performance as Eqs. (3.26)–(3.28).

Using tensor train decomposition to obtain approximation is easy. Simply employing R_α which is smaller than Eq. (3.67) such that SVD is truncated up to the first R_α components. Of course, this truncated tensor train decomposition is not guaranteed to be an optimal solution with fixed $R_\alpha, \alpha \in [1, m]$. If the truncated tensor train decomposition does not work well, further optimization might be required. In this case, it is rather straightforward to apply ALS to tensor train decomposition computed by the algorithm shown in Fig. 3.10. In order that, we need to introduce frame matrix $G^{(\neq i_\alpha)} \in \mathbb{R}^{(N_1\cdots N_{\alpha-1}N_{\alpha+1}\cdots N_m)\times(R_{\alpha-1}R_\alpha)}$ as

$$G^{(\neq i_\alpha)} = \Big[G^{(i_1)} \times_{\ell_1} \cdots \times_{\ell_{\alpha-2}} G^{(i_{\alpha-1})} \times^{\ell_{\alpha-1}\ell_\alpha} G^{(i_{\alpha+1})} \cdots \times \ell_{m-1} G^{(i_m)}\Big]^{(i_1 i_2\cdots i_{\alpha-1} i_{\alpha+1}\cdots i_m)\times(\ell_{\alpha-1}\ell_\alpha)} \tag{3.68}$$

Then ALS that optimizes $G^{(i_\alpha)}$ with fixing $G^{(i_{\alpha'})}, \alpha' \neq \alpha$ can be done as

$$G^{(i_\alpha)} = \mathcal{X} \times_{i_1 i_2\cdots i_{\alpha-1} i_{\alpha+1}\cdots i_m} [G^{(\neq i_\alpha)}]^\dagger \tag{3.69}$$

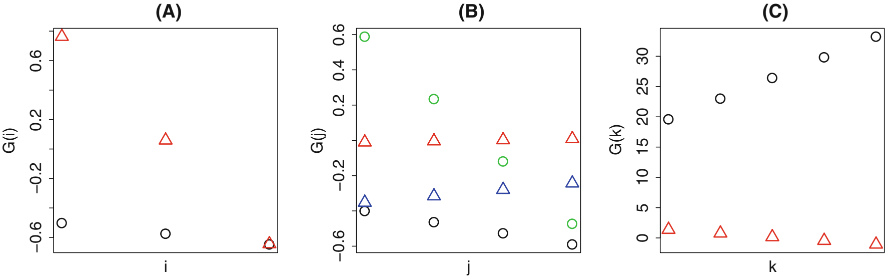

Fig. 3.11 Singular value vectors computed by applying tensor train decomposition (Fig. 3.10) to the tensor Eq. (3.25). (**a**) $G^{(i)}(i, \ell_1)$, Open circle: $\ell_1 = 1$, red triangle: $\ell_1 = 2$ (**b**) $G^{(j)}(j, \ell_1, \ell_2)$, Open circle: $(\ell_1, \ell_2) = (1, 1)$, red triangle: $(\ell_1, \ell_2) = (2, 1)$, green circle : $(\ell_1, \ell_2) = (1, 2)$, blue triangle: $(\ell_1, \ell_2) = (2, 2)$ (**c**) $G^{(k)}(k, \ell_2)$, open circle: $\ell_2 = 1$, red triangle: $\ell_2 = 2$

```
Procedure Tensor train decomposition with ALS
    initialize $G^{(i_\alpha)}, \alpha \in [1, m]$ with the algorithm shown in Fig. 3.10
    repeat
        do $i_\alpha \in [1, m]$
            compute $G^{(i_\alpha)}$ with eq. (3.69)
        end do
    until fit ceases to improve or maximum iterations exhausted
    return $G^{(i_\alpha)}, \alpha \in [1, m]$
end procedure
```

Fig. 3.12 Algorithm of tensor train decomposition with ALS for tensors with arbitrary number of modes m

Figure 3.12 shows the algorithm of tensor train decomposition with ALS. Unfortunately, the algorithm shown in Fig. 3.12 still does not guarantee globally optimal solution.

Exercise
3.8 Apply tensor train decomposition to the tensor $X \in \mathbb{R}^{2\times2\times2}$

$$X_{ij1} = \begin{pmatrix} 3 & 4 \\ 4 & 5 \end{pmatrix} \tag{3.70}$$

$$X_{ij2} = \begin{pmatrix} 4 & 5 \\ 5 & 6 \end{pmatrix} \tag{3.71}$$

3.4 Interpretation Using TD

In order to demonstrate how effective use of TD is to interpret the data set, we apply TDs to data set shown in Table 1.6. We have already applied SVD to data set with $k = 1$ in Table 1.6 in order to visualize the relation between price and weight (Fig. 2.1). Here we show the integrated analysis of $k = 1$ and $k = 2$ with TD. Because ks represent two shops, the integrated analysis by TD should represent how similar two shops are as well as how much they differ from each other. Figure 3.13 shows the results of SVD applied to data sets shown in Table 1.6 ($k = 2$). The difference between Figs. 2.1 and 3.13 represents the distinction between two shops ($k = 1$ and $k = 2$). v^+ axis represents the same contribution to price and weight while v^- axis represents the opposite contribution to them. $k = 1$ (shop 1, Fig. 2.1) has more distinct contribution between v^+ and v^- while that of $k = 2$ (shop 2, Fig. 3.13) is less. This represents the primary difference between $k = 1$ and $k = 2$ (two shops).

Next we apply Tucker decomposition (HOSVD algorithm, Fig. 3.8) to the data set shown in Table 1.6 that is formatted as $\mathcal{X} \in \mathbb{R}^{4\times2\times2}$ where is stand for goods, js stand for price ($j = 1$) and weight ($j = 2$), and ks stand for shops. Figure 3.14

shows that scatterplot of $U^{(j)}_{\ell_2 j}$; $U^{(j)}_{1j}$ and $U^{(j)}_{2j}$ correspond to v^+ and v^- in Figs. 2.1 and 3.13, respectively. It is rather obvious that Fig. 3.14 represents, in some sense, "in between" feature of Figs. 2.1 and 3.13, because $U^{(j)}_{11}$ is larger than v^+ for price in Fig. 3.13 and smaller than that in Fig. 2.1, $U^{(j)}_{21}$ is larger than v^- for price in Fig. 3.13 and smaller than that in Fig. 2.1, $U^{(j)}_{12}$ is smaller than v^+ for price in Fig. 3.13 and larger than that in Fig. 2.1, and $U^{(j)}_{21}$ is larger than v^- for price in Fig. 3.13 and smaller than that in Fig. 2.1. Thus, integrated analysis using TD of two shops' data is seemingly successful.

The next question is how these factors, i.e., simultaneous and opposite effects between price and weight, affect dataset. It can be also understood by investigating Gs that represent the interaction between distinct three features, i.e., foods (bread, beef, pork, and fish), properties (price and weight), and two shops. Table 3.4 shows Gs. Gs associated with larger absolute values correspond to is associated with the combination of foods, properties and shops singular vectors that contribute more to the right-hand side of Eq. (3.55). It is obvious that two combinations, $(\ell_1 \ell_2, \ell_3) =$ $(1, 1, 1)$ and $(2, 2, 1)$, outperform other combinations. First, we investigate what $U^{(k)}$ represents, because $U^{(k)}_{2k}$ does not seem to be important at all. As can be seen in Fig. 3.15c, $\ell_3 = 2$ represents the distinction between two shops because $U^{(k)}_{21}$

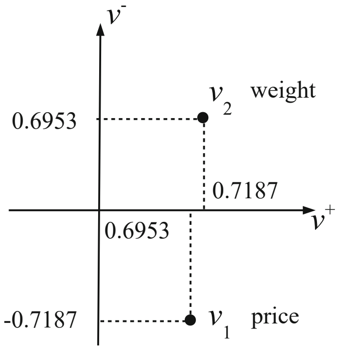

Fig. 3.13 A geometrical interpretation of price and weight originally shown in Table 1.6, $k = 2$. $\boldsymbol{v}_1$: price, $\boldsymbol{v}_2$: weight

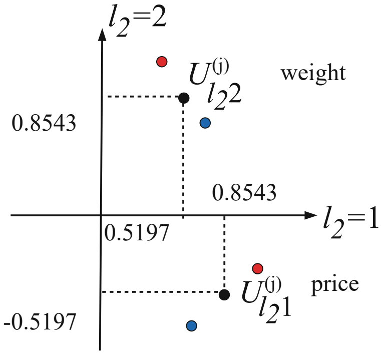

Fig. 3.14 A geometrical interpretation of price and weight originally shown in Table 1.6 with applying HOSVD (Fig. 3.8). $U^{(j)}_{\ell_2 1}$: price, $U^{(j)}_{\ell_2 2}$: weight. Red and blue dots correspond to the location of price and weight in Figs. 2.1 and 3.13, respectively

Table 3.4 $G(\ell_1, \ell_2, \ell_3)$s computed by HOSVD (Fig. 3.8) applied to data set shown in Table 1.6

	$\ell_2 = 1$		$\ell_2 = 2$	
ℓ_3	1	2	1	2
ℓ_1				
1	1964	−283	46	−208
2	−25	−275	1316	427
3	18	13	−42	141
4	17	126	28	−5

ℓ_1: foods (bread, beef, pork, and fish), ℓ_2: properties (price and weight), ℓ_3: two shops

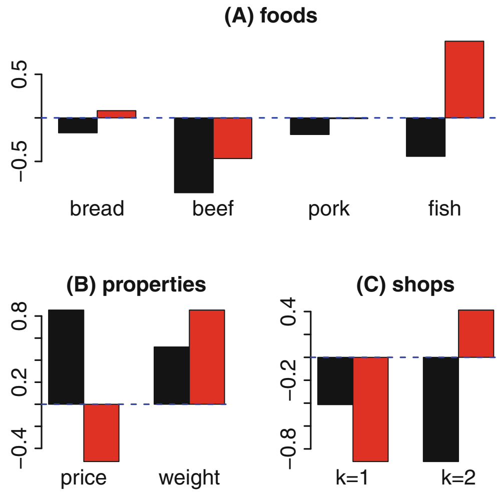

Fig. 3.15 $U^{(i)}$, $U^{(j)}$ and $U^{(k)}$ when HOSVD (Fig. 3.8) is applied to dataset originally shown in Table 1.6. (**a**) $U^{(i)}$, foods, (**b**) $U^{(j)}$, properties, (**c**) $U^{(k)}$, shops. Black: $\ell_1 = \ell_2 = \ell_3 = 1$, red: $\ell_1 = \ell_2 = \ell_3 = 2$

and $U^{(k)}_{22}$ are oppositely signed. Thus, the smaller absolute values of Gs associated with $\ell_3 = 2$ suggests the unimportance of the difference between two shops. In Fig. 3.14, we demonstrated that the difference between two shops is comparatively smaller than mean between two shops with comparing the results obtained by SVD and those by HOSVD. Nevertheless, even without comparison between SVD and HOSVD, by investigating the results by SVD and HOSVD independently, we can easily recognize the unimportance of the difference between two shops as shown here.

Next, we try to understand what the combinations $(\ell_1, \ell_2) = (1, 1)$ and $(2, 2)$ mean. $\ell_2 = 1$ and $\ell_2 = 2$ (Fig. 3.15b) correspond to the coincidence and distinction between price and weight as shown in Fig. 3.14. Thus, $\ell_1 = 1$ and $\ell_2 = 1$ (Fig. 3.15a) show that as well. $U^{(i)}_{1i}$ shows the coincidence between four foods. On the other hand, $U^{(i)}_{2i}$ shows the distinct signs between four foods, especially opposite signs between fish and beef. From this analysis, we can understand that applying TD to the dataset enables us to understand many characteristic features hidden in

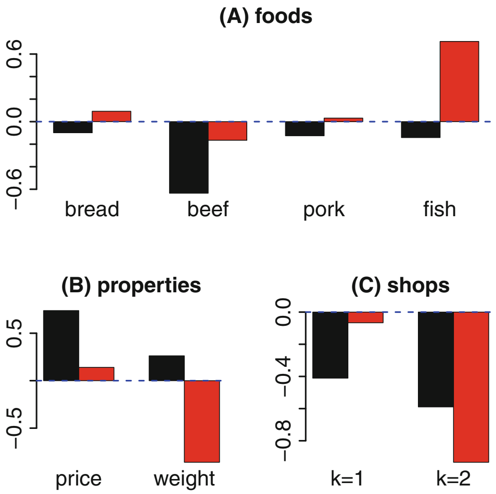

Fig. 3.16 $U^{(i)}$, $U^{(j)}$ and $U^{(k)}$ when CP decomposition with $L = 2$ is applied to dataset originally shown in Table 1.6. (**a**) $\boldsymbol{u}_\ell^{(i)}$, foods, (**b**) $\boldsymbol{u}_\ell^{(j)}$, properties, (**c**) $\boldsymbol{u}_\ell^{(k)}$, shops. Black: $\ell = 1$, red: $\ell = 2$

dataset. This ability of TD will be further demonstrated in the application of TDs to more extensive dataset in the following sections.

One might wonder how other TDs work as well. In order to see if CP decomposition works as well, we apply CP decomposition to data set shown in Table 1.6. The reason why we use $L = 2$ because we know that there are only two important combinations of singular value vectors when HOSVD is applied to the same dataset in the above. Figure 3.16 shows $\boldsymbol{u}_\ell^{(i)}, \boldsymbol{u}_\ell^{(j)}, \boldsymbol{u}_\ell^{(k)}$. It is rather obvious that they are coincident with Fig. 3.15 excluding some reversed signs that are not critical. This might suggest that CP decomposition works as well, but we need to remind that we assumed $L = 2$ based upon the results by HOSVD. In order to see if we can identify that $L = 2$ is enough without the support of HOSVD, we apply CP decomposition with $L = 4$ to the same data set (Fig. 3.17). The result is rather disappointing. Not only it is not easily understood, but also there are no ways to identify which ℓs are important. Since λ_ℓs are 6052 ($\ell = 1$), 4109 ($\ell = 2$), 3810 ($\ell = 3$), and 9771.689 ($\ell = 4$), there are no outstandingly important ones in contrast to Gs in Table 3.4 where only $(\ell_1, \ell_2, \ell_3) = (1, 1, 1)$ and $(2, 2, 1)$ have outstandingly large contributions. Thus, CP decomposition has less ability to identify fewer number of important singular value vectors.

Finally, we apply tensor train decomposition, Fig. 3.10, to the same data set with $R_1 = R_2 = 2$ that enables us to retain supposedly important two combinations. In this setup, although js (properties, i.e., price and weight) must be associated with $R_1 \times R_2 = 4$ singular value vectors, there are no ways to restrict the number of singular value vectors attributed to j to two in the tensor train framework. Figure 3.18 shows the results of tensor train decomposition. Figure 3.18 is also coincident with Fig. 3.15 where HOSVD is employed if excluding $G^{(j)}(j, \ell_1, \ell_2)$, $(\ell_1, \ell_2) = (2, 1), (2, 2)$. Nevertheless, we cannot exclude these two without the knowledge from HOSVD, because there are no weight factors like λ_ℓs for CP decomposition

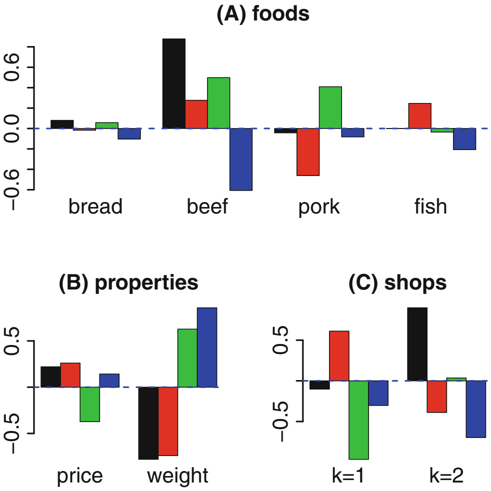

Fig. 3.17 $U^{(i)}$, $U^{(j)}$ and $U^{(k)}$ when CP decomposition with $L = 4$ is applied to dataset originally shown in Table 1.6. (**a**) $\boldsymbol{u}_\ell^{(i)}$, foods, (**b**) $\boldsymbol{u}_\ell^{(j)}$, properties, (**c**) $\boldsymbol{u}_\ell^{(k)}$, shops. Black: $\ell = 1$, red: $\ell = 2$, green: $\ell = 3$, blue: $\ell = 4$

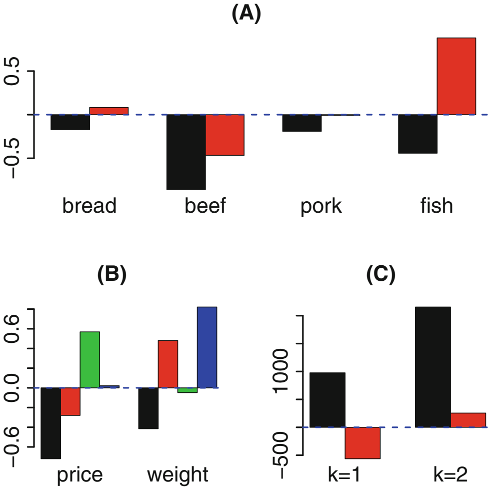

Fig. 3.18 $G^{(i)}(i, \ell_1)$, $G^{(j)}(j, \ell_1, \ell_2)$, and $G^{(k)}(k, \ell_2)$ when tensor train decomposition with $R_1 = R_2 = 2$ is applied to dataset originally shown in Table 1.6. (**a**) $G^{(i)}(i, \ell_1)$, foods, (**b**) $G^{(j)}(j, \ell_1, \ell_2)$, properties, (**c**) $G^{(k)}(k, \ell_2)$, shops. Black: (**a**) $\ell_1 = 1$, (**b**) $(\ell_1, \ell_2) = (1, 1)$, (**c**) $\ell_2 = 1$, red: (**a**) $\ell_1 = 2$, (**b**) $(\ell_1, \ell_2) = (1, 2)$, (**c**) $\ell_2 = 1$, green: (**b**) $(\ell_1, \ell_2) = (2, 1)$, blue: (**b**) $(\ell_1, \ell_2) = (2, 2)$

and Gs for HOSVD that can be used for the selection of important terms in TDs. In this sense, tensor train decomposition is also inferior to HOSVD because it cannot select primarily important two combinations.

3.5 Summary

In this section, I have introduced three popular TD methods, CP decomposition, Tucker decomposition, and tensor train decomposition. All three TDs have their own advantages and disadvantages.

3.5.1 *CP Decomposition*

3.5.1.1 Advantages

The advantages of CP decomposition are as follows:

- Easy interpretability. CP decomposition can result in one-to-one correspondence between singular value vectors. Thus, the interpretation is easier than the other two methods.
- The number of terms in the right-hand side of decomposition can be decided freely without any restriction.
- Because of freely decidable number of decomposition terms, truncation is uniquely decided.
- It has weights, λ_ℓ, that can evaluate importance of each term.

3.5.1.2 Disadvantages

The disadvantages of CP decomposition are as follows:

- With using known algorithms, it is not guaranteed to converge to global optimum.
- In some worst cases, there is no global optimum in the sense complete solution (i.e., no residuals) can achieve the limit when the absolute values of each terms go to infinity.
- It needs to have initial values to start and it reaches the local minimums depending upon the initial values.
- No known algorithm to converge within polynomial times.

3.5.2 *Tucker Decomposition*

3.5.2.1 Advantages

The advantages of Tucker decomposition are as follows:

- There are algorithms that can converge in polynomial times (e.g., HOSVD), although convergence to the global minimum is not guaranteed.
- It has weight, G, that can evaluate importance of each term.
- ALS can be used to optimize the solution obtained by the method with the guarantee of convergence within polynomial time.
- Although it is limited to the product of truncated rank of each mode, i.e., $\prod_{\alpha=1}^{m} R_\alpha$ where R_α is the truncated rank of αth mode, truncation decomposition is straightforward.
- We do not need to assign initial values to perform ALS since initial values can be computed by HOSVD which requires only polynomial time.

3.5.2.2 Disadvantages

The disadvantages of Tucker decomposition are as follows:

- Since all possible combinations of singular value vectors are present, selection of important terms based upon weight G is inevitably subjective.
- In the full rank TD, i.e. $R_\alpha = N_\alpha$ where N_α is the number of variables in αth mode, the number of degrees of freedom increases to $\prod_{\alpha=1}^m N_\alpha + \sum_{\alpha=1}^m N_\alpha^2$ from that of original tensor, $\prod_{\alpha=1}^m N_\alpha$.
- It does not have unique solutions, because applying unitary transformation does not alter the amount of residues.

3.5.3 Tensor Train Decomposition

3.5.3.1 Advantages

The advantages of tensor train decomposition are as follows:

- It has superior ability to reduce degrees of freedoms to other two TDs. In CP decomposition, degrees of freedom is as many as $L \sum_{\alpha=1}^m N_\alpha$. That in Tucker decomposition is as many as $\prod_{\alpha=1}^m N_\alpha + \sum_{\alpha=1}^m N_\alpha^2$. On the other hand, that of tensor train decomposition is as many as $N_1 R_1 + \sum_{\alpha=1}^m R_{\alpha-1} R_\alpha N_\alpha + N_m R_{m-1}$. Thus, degrees of freedom increases are only proportional to logarithmic order of terms in decomposition.
- It has algorithm that converges in polynomial time.
- ALS can be applied to optimize the obtained solution.
- We do not need to assign initial values to perform ALS since initial values can be computed by algorithm which requires only polynomial time.

3.5.3.2 Disadvantages

- It does not have unique solutions, because applying unitary transformation does not alter the amount of residues.
- It does not have weight that evaluates importance of each term.

3.5.4 Superiority of Tucker Decomposition

Considering the advantages and disadvantages of three TDs, we decided to employ Tucker decomposition implemented by HOSVD to be applied to real problems in the following sections. It is primarily because it has weight to select relevant terms. Tensor train decomposition does not have weight, thus it is not suitable to employ the application that needs the interpretation of the outcome of TDs. In other applications, e.g., image analysis, because it is not required to interpret TDs themselves, tensor train decomposition does not have to be excluded. Nevertheless, in this monograph, the application to the biological problem is the main topic. In the application to biological problems, interpretability is important. Tensor train decomposition that lacks the weight to evaluate each term is not suitable.

On the other hand, CP decomposition apparently has more interpretability than Tucker decomposition because it provides one-to-one correspondence between singular value vectors. The apparent superior interpretability of this method is not fully trustable because of heavy initial value dependence. It is not also ideal one because increasing L often results in distinct results obtained by smaller L. In this case, it is unsure how large L should be.

Because of the above reasons, HOSVD is considered to be the best method that can be applied to tensors when interpretability is important. In addition to this, because HOSVD is natural extension of SVD to higher mode tensors, we can discuss the application of SVD (or PCA) and that of HOSVD in the integrated manner.

Appendix

Moore-Penrose Pseudoinverse

Moore-Penrose pseudoinverse [1], which is denoted as $A^\dagger$, of matrix A satisfies the following conditions:

- $AA^\dagger A = A$
- $A^\dagger A A^\dagger = A^\dagger$
- $(A^\dagger A)^T = A^\dagger A$
- $(AA^\dagger)^T = AA^\dagger$

Suppose we need to find $\boldsymbol{x} \in \mathbb{R}^M$ that satisfies

$$A\boldsymbol{x} = \boldsymbol{b} \tag{3.72}$$

where $A \in \mathbb{R}^{N \times M}$ and $\boldsymbol{b} \in \mathbb{R}^N$. It is known that there is a unique solution only when $N = M$.

Moore-Penrose pseudoinverse can *solve* Eq. (3.72) because

$$\boldsymbol{x} = A^\dagger \boldsymbol{b} \tag{3.73}$$

gives

- the unique solution of Eq. (3.72) when $N = M$.
- the $\boldsymbol{x}$ that satisfies Eq. (3.72) with minimum $|\boldsymbol{x}|$ when $N < M$ (i.e., when no unique solutions are available).

- the $\boldsymbol{x}$ with minimum $|A\boldsymbol{x} - \boldsymbol{b}|$ when $N > M$ (equivalent to the so-called linear regression analysis).

When $N < M$, there are infinitely large number of solutions that satisfy Eq. (3.72). Moore-Penrose pseudoinverse allows us to select one of them, which has minimum $|\boldsymbol{x}|$. On the other hand, when $N > M$, there are not always solutions that satisfy Eq. (3.72). Moore-Penrose pseudoinverse allows us to select the solution having the minimum $|A\boldsymbol{x} - \boldsymbol{b}|$, i.e., the smallest residuals. Thus, by computing Moore-Penrose pseudoinverse, we can always compute $\boldsymbol{x}$ that satisfies Eq. (3.72) as much as possible in some sense.

How to compute $A^\dagger$ is as follows. Apply SVD to A as

$$A = U\Sigma V^T \tag{3.74}$$

$U \in \mathbb{R}^{N\times M}$, $\Sigma, V \in \mathbb{R}^{M\times M}$ for $N > M$ and $U, \Sigma \in \mathbb{R}^{N\times N}, V \in \mathbb{R}^{M\times N}$ for $N < M$. When U or V is not a square matrix, $U^TU = V^TV = I$, but $UU^T \neq I$ and $VV^T \neq I$. When U and V are square matrices, $U^TU = UU^T = V^TV = VV^T = I$.

Then $A^\dagger$ can be defined as

$$A^\dagger = V\Sigma^{-1}U^T \tag{3.75}$$

It is not difficult to show that $A^\dagger = V\Sigma^{-1}U^T$ satisfies the required conditions because

$$AA^\dagger = \left(U\Sigma V^T\right)\left(V\Sigma^{-1}U^T\right) = U\Sigma\Sigma^{-1}U^T = UIU^T = \begin{cases} UU^T, N > M \\ I, N \leq M \end{cases} \tag{3.76}$$

and

$$A^\dagger A = \left(V\Sigma^{-1}U^T\right)\left(U\Sigma V^T\right) = V\Sigma^{-1}\Sigma V^T = VIV^T = \begin{cases} I, N \geq M \\ VV^T, N < M \end{cases} \tag{3.77}$$

where $V^TV = I$ for $N > M$ and $U^TU = I$ for $N < M$ are used.

Then when $N > M$,

$$AA^\dagger A = A\left(A^\dagger A\right) = AI = A, \tag{3.78}$$

$$A^\dagger AA^\dagger = \left(A^\dagger A\right)A^\dagger = IA^\dagger = A^\dagger \tag{3.79}$$

$$\left(AA^\dagger\right)^T = \left(UU^T\right)^T = \left(U^T\right)^T U^T = UU^T = AA^\dagger \tag{3.80}$$

$$\left(A^\dagger A\right)^T = I^T = I = A^\dagger A \tag{3.81}$$

On the other hand, when $N < M$,

$$AA^\dagger A = \left(AA^\dagger\right) A = IA = A, \tag{3.82}$$

$$A^\dagger AA^\dagger = A^\dagger \left(AA^\dagger\right) = A^\dagger I = A^\dagger \tag{3.83}$$

$$\left(AA^\dagger\right)^T = I^T = I = AA^\dagger \tag{3.84}$$

$$\left(A^\dagger A\right)^T = \left(VV^T\right)^T = \left(V^T\right)^T V^T = VV^T = A^\dagger A \tag{3.85}$$

When $N = M$, these are obvious because $AA^\dagger = A^\dagger A = I$.

The reason why we can treat Eq. (3.72) using Moore-Penrose pseudoinverse as mentioned in the above is as follows. Define

$$\boldsymbol{x}_0 = A^\dagger \boldsymbol{b} + \left(I - A^\dagger A\right) \boldsymbol{w} \tag{3.86}$$

with arbitrary vector $\boldsymbol{w}$. Then because

$$A\boldsymbol{x}_0 = AA^\dagger \boldsymbol{b} + \left(A - AA^\dagger A\right) \boldsymbol{w} = AA^\dagger \boldsymbol{b} \tag{3.87}$$

when $AA^\dagger = I$, i.e., $N \leq M$, $A\boldsymbol{x}_0 = \boldsymbol{b}$, $\boldsymbol{x}_0$ is a solution of Eq. (3.72). This corresponds to the cases where there are no unique solutions because the number of variables, M, is larger than the number of equations, N. $\boldsymbol{x}_0$ can be a unique solution only when $A^\dagger A = I$ as well, i.e., $N = M$ because of Eq. (3.86). This corresponds to the cases where there is a unique solution because the number of variables, M, is equal to the number of equations, N.

Here one should notice that $A^\dagger \boldsymbol{b} \perp \left(I - A^\dagger A\right) \boldsymbol{w}$ because

$$\begin{aligned}\left(I - A^\dagger A\right) \boldsymbol{w} \cdot A^\dagger \boldsymbol{b} &= \left(\left(I - A^\dagger A\right) \boldsymbol{w}\right)^T A^\dagger \boldsymbol{b} = \boldsymbol{w}^T \left(I - A^\dagger A\right)^T A^\dagger \boldsymbol{b} \\ &= \boldsymbol{w}^T \left(I - A^\dagger A\right) A^\dagger \boldsymbol{b} = \boldsymbol{w}^T (A^\dagger - A^\dagger AA^\dagger) \boldsymbol{b} \\ &= \boldsymbol{w}^T 0 \boldsymbol{b} = 0.\end{aligned} \tag{3.88}$$

Thus from Eq. (3.86)

$$|\boldsymbol{x}_0|^2 = \left|A^\dagger \boldsymbol{b}\right|^2 + \left|\left(I - A^\dagger A\right) \boldsymbol{w}\right|^2 \tag{3.89}$$

This means $|\boldsymbol{x}_0| > \left|A^\dagger \boldsymbol{b}\right|$. Therefore, $A^\dagger \boldsymbol{b}$ is the solution that satisfies Eq. (3.72) and has the smallest $|x_0|$ (in other words, the solution with the $L2$ regulation term).

When $AA^\dagger \neq I$, i.e., $N > M$, there are no solutions. This corresponds to the cases where there are no solutions because the number of variables, M, is smaller than the number of equations, N. In this case, $\boldsymbol{x} = A^\dagger \boldsymbol{b}$ is known to be optimal (i.e., the solution with minimum $|A\boldsymbol{x} - \boldsymbol{b}|$). In order to prove this, first we need to compute $A^T(AA^\dagger \boldsymbol{b} - \boldsymbol{b})$ as

$$\begin{aligned} A^T\left(AA^\dagger \boldsymbol{b} - \boldsymbol{b}\right) &= A^T\left(\left(AA^\dagger\right)^T \boldsymbol{b} - \boldsymbol{b}\right) = \left(\left(AA^\dagger A\right)^T - A^T\right)\boldsymbol{b} \\ &= \left(AA^\dagger A - A\right)^T \boldsymbol{b} = 0\boldsymbol{b} = 0 \end{aligned} \tag{3.90}$$

With taking transposition of the above, we can also get

$$\left(AA^\dagger \boldsymbol{b} - \boldsymbol{b}\right)^T A = 0 \tag{3.91}$$

Using these, we can show

$$|A\boldsymbol{x} - \boldsymbol{b}|^2 = \left|\left(A\boldsymbol{x} - AA^\dagger \boldsymbol{b}\right) + \left(AA^\dagger \boldsymbol{b} - \boldsymbol{b}\right)\right|^2 \tag{3.92}$$

$$\begin{aligned} &= \left|A\boldsymbol{x} - AA^\dagger \boldsymbol{b}\right|^2 + \left(A\boldsymbol{x} - AA^\dagger \boldsymbol{b}\right)^T \left(AA^\dagger \boldsymbol{b} - \boldsymbol{b}\right) \\ &\quad + \left(AA^\dagger \boldsymbol{b} - \boldsymbol{b}\right)^T \left(A\boldsymbol{x} - AA^\dagger \boldsymbol{b}\right) + \left|AA^\dagger \boldsymbol{b} - \boldsymbol{b}\right|^2 \end{aligned} \tag{3.93}$$

$$\begin{aligned} &= \left|A\boldsymbol{x} - AA^\dagger \boldsymbol{b}\right|^2 + \left(\boldsymbol{x} - A^\dagger \boldsymbol{b}\right)^T A^T \left(AA^\dagger \boldsymbol{b} - \boldsymbol{b}\right) \\ &\quad + \left(AA^\dagger \boldsymbol{b} - \boldsymbol{b}\right)^T A \left(\boldsymbol{x} - A^\dagger \boldsymbol{b}\right) + \left|AA^\dagger \boldsymbol{b} - \boldsymbol{b}\right|^2 \end{aligned} \tag{3.94}$$

$$\begin{aligned} &= \left|A\boldsymbol{x} - AA^\dagger \boldsymbol{b}\right|^2 + \left(\boldsymbol{x} - A^\dagger \boldsymbol{b}\right)^T 0 \\ &\quad + 0\left(\boldsymbol{x} - A^\dagger \boldsymbol{b}\right) + \left|AA^\dagger \boldsymbol{b} - \boldsymbol{b}\right|^2 \end{aligned} \tag{3.95}$$

$$= \left|A\boldsymbol{x} - AA^\dagger \boldsymbol{b}\right|^2 + \left|AA^\dagger \boldsymbol{b} - \boldsymbol{b}\right|^2 \tag{3.96}$$

$$\geq \left|AA^\dagger \boldsymbol{b} - \boldsymbol{b}\right|^2 \tag{3.97}$$

This means that $\boldsymbol{x} = A^\dagger \boldsymbol{b}$ is an optimal solution of Eq. (3.72).

References

1. Barata, J.C.A., Hussein, M.S.: The Moore–Penrose pseudoinverse: a tutorial review of the theory. Braz. J. Phys. **42**(1), 146–165 (2012). https://doi.org/10.1007/s13538-011-0052-z
2. Kolda, T., Bader, B.: Tensor decompositions and applications. SIAM Rev. **51**(3), 455–500 (2009). https://doi.org/10.1137/07070111X
3. Oseledets, I.: Tensor-train decomposition. SIAM J. Sci. Comput. **33**(5), 2295–2317 (2011). https://doi.org/10.1137/090752286

Part II
Feature Extractions

Feature extraction is a generation of new feature in the data-driven way. In this part, two methods, PCA and TD are extensively considered. Although both are supposed to be fully linear methods, because they decompose variables to products of new variables, it can include non-linear transformation partly. In addition to this, both have the ability to reduce degrees of freedom. They are discussed from the data science point of views, with the applications to the data sets, for the usage in the later chapters.

Chapter 4
PCA Based Unsupervised FE

There is no sound that I do not need.
Rio Kazumiya, Sound of the Sky, Season 1, Episode 3

4.1 Introduction: Feature Extraction vs Feature Selection

In this chapter, I mainly discuss about the situation where feature extraction or feature selection is inevitable. When or under what kind of conditions, do we need either or both of two? Here are some examples of such situations.

- **Case 1**: The number of features attributed to individual samples is larger than the number of samples.
- **Case 2**: Features attributed to individual samples are not independent of one another.
- **Case 3**: Some of the features attributed to samples are not related to some properties that we would like to relate features to.

Although these above three cases are not comprehensive, they are good examples by which we can discuss the reason why we need feature extraction and/or feature selection. An example of case 1 is linear equations that can be represented as $A\boldsymbol{x} = \boldsymbol{b}$ where $A \in \mathbb{R}^{N \times M}, \boldsymbol{x} \in \mathbb{R}^{M}, \boldsymbol{b} \in \mathbb{R}^{N}$ and $\boldsymbol{x}$ represents variables, A represents coefficients, and $\boldsymbol{b}$ represents constants. When $N < M$, not only there are no unique solutions, but also there are always solutions, even when A and $\boldsymbol{b}$ are purely random numbers. The fact that there are no unique solutions prevents us from interpreting outcome, because there can be multiple distinct unique solutions. The fact that there are always solutions means that there might be meaningless solutions. In this case, we need feature extraction and/or feature selection such that we can have limited number of features that is smaller than the number of samples. An example of case 2 is multicollinearity. In this case, although apparently, $A\boldsymbol{x} = \boldsymbol{b}$ is uniquely solvable, it is actually not because coefficient matrix A is not regular (in other words, row vectors are not independent of one another). In this case, we need to apply feature extraction or feature selection in order to obtain reduced number of features that

Y-h. Taguchi, *Unsupervised Feature Extraction Applied to Bioinformatics*,
Unsupervised and Semi-Supervised Learning,
https://doi.org/10.1007/978-3-030-22456-1_4

enables us to get unique solutions. An example of case 3 is that some elements of A are zero. Especially, if A includes column vectors totally filled with zero, variables that correspond to these columns are not related to $\boldsymbol{b}$ at all. When A is given, we can simply discard these variables. Nevertheless, when A is required to be inferred from $\boldsymbol{x}$ and $\boldsymbol{b}$ (e.g., linear regression analysis), it is impossible to exclude there variables in advance. This might result in the incorrect estimation of A. In this case, we need feature selection that enables us to exclude variables not related to $\boldsymbol{b}$ in advance.

From these examples, we can know that the need of feature selection and feature extraction is very ubiquitous. So, the next question is which strategy is better to address these problems. Unfortunately, the answer is highly context dependent and cannot be decided based upon mathematical considerations. For example, let us consider image analysis, e.g., face recognition. In this case, it is rather obvious that not all pixels of digital images but only a limited number of them is useful for the purpose. If small number of features generated from large number of pixels work well, there is no need to go further. On the other hand, suppose that the problem is the inference about bankruptcy, in other words, the prediction of who will bankrupt. In this case, even if a newly generated feature composed of numerous personal information, e.g., income, age, education history, address, and so on, works pretty well, it might not be a final goal. This is because collecting these information might cost or is impossible at all. If another feature composed of more limited number of features works, even if the performance is a little bit less, another one might be employed because of easiness to use. Thus, it is inevitable to specify situation that we want to discuss.

As for the targeted field, I would like to say that the targeted field is bioinformatics as the title of this book says. In bioinformatics analysis, it is very usual that feature selection is more favorable than feature extraction because of the following reasons. In bioinformatics analysis (or in biology although it means the same), measuring individual features often costs. Thus, measuring less number of features can reduce the cost spent to individual observations. This results in the increased number of observations that often leads to better outcome. Even when measuring individual features does not cost, e.g. in the case of high throughput measurements, feature selection is often better than feature extraction, because each feature has its own meaning. For example, if features are genes, the selected limited number of genes are more interpretable than features generated by the combination of large number of genes. Thus, in the following I assume the situation where feature selection is more favorable than feature extraction even if not explicitly denoted.

4.2 Various Feature Selection Procedures

Although there are various ways to classify numerous number of previously proposed feature selection procedures, I would like to employ the one shown in Table 4.1. Feature selection strategies can be classified into two groups in two ways. One way is supervised ones vs unsupervised ones. Not to mention, supervised ones

Table 4.1 Classification of feature selections

	One by one	Collective
Supervised	Statistical tests[a]	Random forest, LASSO
Unsupervised	Highly variable genes, bimodal genes	PCA based unsupervised FE

[a] *t* test, limma, SAM

are definitely more popular than unsupervised ones. This is because the purpose of feature selection is usually purpose oriented. For example, if the study aims to investigate diseases, it is natural to consider genes expressed differently between patients and healthy controls. If the study aims to predict who will bankrupt, it is reasonable to consider features related to something financial. On the other hand, unsupervised feature selection might sound self-discrepancy, because it is unlikely possible to select features without any clear purposes. In spite of that, unsupervised feature selection is still possible. For example, it is natural to select features with maximum variance, because large variance might reflect the ability of the feature that represents diverse categories hidden in the considered sample. Thus, although it is less popular, unsupervised feature selection is still possible. Another way to classify feature selection strategies is one by one vs collective. The former means that feature selection is performed without the consideration of interaction between features. For example, when conventional statistical tests are applied to a feature of samples composed of two categories, the P-value that rejects the null hypothesis that a feature of members of two samples obeys the same distribution is computed. Then, if P value is small enough, say less than 0.01, the feature is identified as distinct between two categories. This means that each P-value attributed to each feature is not affected by other features at all. On the other hand, the latter considers the interaction between features. For example, when dummy variables are attributed to each of two categories, we can make linear regression using arbitrary number of features to predict dummy variables. In this case, the interaction between features included into regression equation is considered. Then, features used to construct regression equation with good performance are selected.

In order to demonstrate how differently feature selections that belong to four categories listed in Table 4.1 work, I prepare two synthetic data sets. Both are matrices $x_{ij} \in \mathbb{R}^{N \times M}$ where i and j correspond to features' index and samples' index, respectively. In both data sets, the only first $N_1 (< N)$ features, $x_{ij}, i \leq N_1$, are distinct between two classes where $j \leq \frac{M}{2}$ and $j > \frac{M}{2}$ belong to the first and second class, respectively. x_{ij} is also drawn from Gaussian or mixed Gaussian distribution where $\mathcal{N}(\mu, \sigma)$ represents Gaussian distribution that has mean of μ and standard deviation σ, respectively.

- Data set 1:

$$x_{ij} \sim \begin{cases} \mathcal{N}(0, \sigma) & j \leq \frac{M}{2},\ i \leq N_1 \\ \mathcal{N}(\mu_0, \sigma) & j > \frac{M}{2},\ i \leq N_1 \\ \frac{1}{2}\mathcal{N}(0, \sigma) + \frac{1}{2}\mathcal{N}(\mu_0, \sigma) & i > N_1. \end{cases} \tag{4.1}$$

- Data set 2:

$$x_{ij} \sim \begin{cases} \mathcal{N}(0,\sigma) & j \le \frac{M}{2},\ i \le N_1 \\ \mathcal{N}(\mu_0,\sigma) & j > \frac{M}{2},\ i \le N_1 \\ \mathcal{N}(\mu_1,\sigma) & \quad\quad i > N_1. \end{cases} \tag{4.2}$$

Thus, the only difference between two synthetic data sets is if the $N - N_1$ features (i.e., $i > N_1$) not distinct between two classes are drawn from bimodal [Eq. (4.1)] or unimodal [Eq. (4.2)] distributions. Specifically, $N = 100$, $M = 20$, $\mu_0 = 4$, $\mu_1 = \frac{\mu_0}{2} = 2$, $N_1 = 10$ and $\sigma = 1$ in the following. Performance is averaged over one hundred independent trials. The number of features distinct between two categories, N_1, is assumed to be known in advance. μ_1 is selected such that the sample mean of ith feature, $\langle x_{ij} \rangle_j$ defined by Eq. (2.56), does not differ between two models.

The statistical tests used belong to either of four categories. t test is employed as a representative of one by one, supervised feature selection. P values computed by t test are attributed to individual features. Top N_1 features with smaller P values are selected. As a representative of collective supervised feature selection, linear regression is employed. The dummy variable $y_j \in [0, 1]^M$ is given such that $y_j = 0, j \le \frac{M}{2}$ and $y_j = 1, j > \frac{M}{2}$. Then using regression coefficient vector, $a_i \in \mathbb{R}^N$, $X\boldsymbol{a} = \boldsymbol{y}$ is assumed. $\boldsymbol{a}$ is computed with $\boldsymbol{a} = X^\dagger \boldsymbol{y}$ using Moore-Penrose pseudoinverse, $X^\dagger$, because there are no unique solutions due to $N > M$. Top N_1 features with larger absolute a_i are selected. As for representatives of one by one, unsupervised feature selections, two methods are employed. One is highly variable features. Sample variance of each feature,

$$\frac{1}{M}\left(x_{ij} - \frac{1}{M}\sum_{j=1}^{M} x_{ij}\right)^2, \tag{4.3}$$

is computed and top $N_1 = 10$ features associated with larger variance are selected. Another is unimodal test. Unimodal test computes P-values that reject the null hypothesis that x_{ij}s with fixed i are drawn from unimodal distribution; Hartigan's dip test, which rejects the null hypothesis that the distribution is unimodal [1] is used for this purpose. Then top $N_1 = 10$ features associated with smaller P-values are selected. Finally, as a representative of collective unsupervised feature selections, we employ PCA. PCA is applied to x_{ij} such that kth PC score vectors, $\boldsymbol{u}_k \in \mathbb{R}^N$, are attributed to features. In other words, $\boldsymbol{u}_k$ is computed as the eigenvectors of $S_{ii'}$, Eq. (2.50), $S_{ii'}\boldsymbol{u}_k = \lambda_k \boldsymbol{u}_k$ where λ_k is eigenvalue. Then, top $N_1 = 10$ features associated with the larger absolute first PC score, $|u_{1i}|$, are selected (the reason why this procedure works as feature selection will be discussed later).

Table 4.2 shows the number of features that are distinct between two classes and are also selected by individual methods. When tests are applied to data sets 1 and 2, two supervised methods samely achieved well although the collective method achieved a little bit worse than one by one method. The performance achieved by

Table 4.2 Performance of statistical tests applied to two synthetic data set 1 defined by Eq. (4.1) and data set 2 defined by Eq. (4.2)

	Supervised		Unsupervised		
	One by one	Collective	One by one		Collective
Data set	*t* test	Linear regression	Variance	Unimodal test	PCA
1	10.00	9.88	1.20	1.68	8.75
2	10.00	9.79	9.99	5.68	10.00
1 (shuffled)	1.03	0.08	1.34	1.66	8.78
2 (shuffled)	0.94	0.89	10.00	5.76	10.00

Numbers represent mean number of features selected by each method, among N_1 features distinct between two classes, $i < N_1 (= 10)$. Shuffled means that class labels are shuffled

unsupervised method is quite distinct between two data sets. Two unsupervised one by one methods fail when data set 1 is considered while they performed better for data set 2. This is reasonable because all N features obey the identical distribution if class labels are not considered. Thus, unsupervised methods have no ways to distinguish features with and without distinction between two classes. In this sense, it is remarkable that PCA, an unsupervised and collective method, can perform similarly well for both data sets 1 and 2.

One might wonder why unsupervised method must be considered, because supervised methods perform better. This impression changes once the class labels are shuffled. It is reasonable that no supervised methods work well. On the other hand, it is also reasonable that the performance by unsupervised method does not change because of class label shuffling. This suggests that unsupervised feature selections are better choices when class labels are not available or not trustable.

Unsupervised collective feature selection, PCA, is successful for data set 1, for which other unsupervised methods fail, and shuffled data set, for which supervised collective methods fail. It is important why it can happen. In order to see this, we investigate the first PC loading vectors, $\boldsymbol{v}_1 \in \mathbb{R}^M$, which is defined as $\boldsymbol{v}_1 = \frac{1}{\lambda_1} X^T \boldsymbol{u}_1$ (see Eq. (2.21)). Figure 4.1 shows the first PC loading vectors. For all cases, u_{ij}s with $j \le \frac{M}{2}$ take positive values while u_{ij}s with $j > \frac{M}{2}$ take negative value. Since $\boldsymbol{u}_1 = \lambda_1 \boldsymbol{X} \boldsymbol{v}_1$, u_{1i} reflects the difference between two classes. Thus, selecting is associated with absolutely larger u_{1i} can identify correctly features associated with distinction between two classes for all four cases. This is the reason why PCA can always perform well.

4.3 PCA Applied to More Complicated Patterns

In the previous section, feature selection with two classes was discussed. Nevertheless, it is the simplest case. There are many more complicated feature selections. One direction is to have more classes than two. Another direction is to have more than one classifications simultaneously. Here, let us discuss both together,

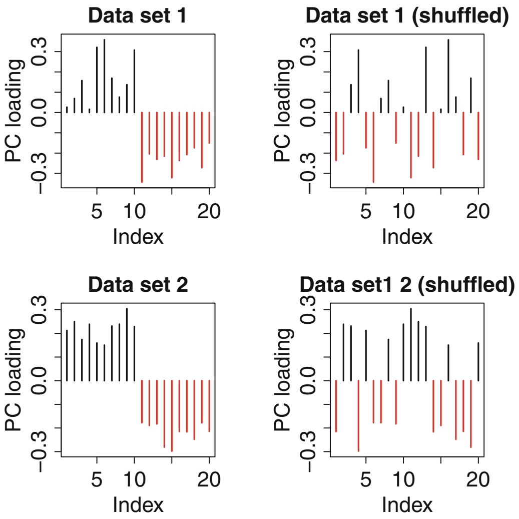

Fig. 4.1 The first PC loading vectors, $\boldsymbol{v}_1 \in \mathbb{R}^M$, for data set 1, shuffled data set 1, data set 2, and shuffled data set 2. Black and red bars correspond to classes 1 and 2, respectively

i.e., feature extraction under the conditions having more than one classification with more than two classes. In order to demonstrate feature selections under this condition, we extend data set 2, Eq. (4.2), as follows.

Data set 3

$$x_{ij} \sim \begin{cases} \mathcal{N}(0,\sigma) & j \le \frac{M}{2}, \quad i \le N_1 \\ \mathcal{N}(\mu_0,\sigma) & j > \frac{M}{2}, \quad i \le N_1 \\ \mathcal{N}(0,\sigma) & j \le \frac{M}{4}, \quad N_1 < i \le N_1 + N_2 \\ \mathcal{N}(\mu_1,\sigma) & \frac{M}{4} < j \le \frac{M}{2}, \quad N_1 < i \le N_1 + N_2 \\ \mathcal{N}(2\mu_1,\sigma) & \frac{M}{2} < j \le \frac{3M}{4}, \quad N_1 < i \le N_1 + N_2 \\ \mathcal{N}(3\mu_1,\sigma) & j > \frac{3M}{4}, \quad N_1 < i \le N_1 + N_2 \\ \mathcal{N}(\mu_2,\sigma) & i > N_1 + N_2. \end{cases} \tag{4.4}$$

Features $i \le N_1$ are composed of two classes, those $N_1 < i \le N_1 + N_2$ are composed of four classes, and those $i > N_1 + N_2$ are composed of no classes. Thus the feature selection aims to identify which features are composed of how many classes.

Now the problem is more difficult. For example, simply trying to identify which features are composed of two classes does not help us to distinguish between features composed of two classes and those composed of four classes, because four classes can be also considered to be two classes if each two of four classes are considered as one class. Thus in order to perform feature selections under such a complicated condition, we usually need more detailed information about class labeling.

It is not very easy to adapt to this situation. Suppose that we have already known 20 samples classified into the four classes as

$$(A, A, A, A, A, B, B, B, B, B, C, C, C, C, C, D, D, D, D, D) \tag{4.5}$$

or into the two classes as

$$(E, E, E, E, E, E, E, E, E, E, F, F, F, F, F, F, F, F, F, F). \tag{4.6}$$

Even if this is the case, identification of features with four classes is not straightforward. Simple linear regression analysis is not applicable, because we know only that four classes differ from one another. In order to perform linear regression analysis, we need to assign numbers to each of four classes. If we do not know practical relationship between four classes, there are no ways to assign numbers to four classes. Pairwise comparison between four classes might be possible, but might not work well, because we need to integrate pairwise comparisons in order to rank features. Suppose we try all possible six pairwise comparisons in Eq. (4.5), as

$$(A, B), (A, C), (A, D), (B, C), (B, D), (C, D). \tag{4.7}$$

If we consider this is occasionally applied to Eq. (4.6), they correspond to comparisons of

$$(E, E), (E, F), (E, F), (E, F), (E, F), (F, F). \tag{4.8}$$

Thus, in contrast to the expectation, four out of six comparisons will report that they differ. Thus, if difference between two classes, E and F, is greater than that between pairs in four classes, A, B, C, and D, integration of six pairwise comparison might report that Eq. (4.8) more fits to four classes than Eq. (4.7). In the following, we consider occasions where integration of six pairwise comparisons occasionally report that Eq. (4.8) is more likely to be four classes than Eq. (4.7). For the simplicity, we assume that all pairwise comparisons (E,F) in Eq. (4.8) are higher ranked than all pairwise comparisons in Eq. (4.7). The requirement that difference between two classes among four classes should be smaller than that among two classes is not unrealistic. It is very usual that values of features have both upper and lower boundary. In this case, the distinction between two classes when samples are classified into two classes is that between the upper and the lower halves. On the other hand, the distinction between two classes when samples are classified into four classes is that between any pairs of four quantiles. If region is divided into two, the distinction is larger than that when region is divided into four. In this case, the following happens (Table 4.3). Four pairwise comparisons (E,F) in Eq. (4.8) is always higher ranked than corresponding four pairwise comparisons, (A,C), (A,D), (B,C), and (B, D) in Eq. (4.7). On the other hand, two pairwise comparisons (E, E) and (F, F) in Eq. (4.8) are always lower ranked than corresponding two pairwise comparisons, (A, B) and (C, D). There are N_1 features composed of two classes and N_2 features composed of four classes. Thus mean rank of pairs (A, B) and (C, D) are $\frac{N_2}{2}$ because N_2 features composed of four classes are ranked higher

Table 4.3 Mean (expected) rank, mean lowest rank, and mean top ranks of pairwise comparisons

							Integrated rank
Pairs in Eq. (4.7)	(A, B)	(A, C)	(A, D)	(B, C)	(B, D)	(C, D)	
Mean rank	$\frac{N_2}{2}$	$N_1 + \frac{N_2}{2}$	$N_1 + \frac{N_2}{2}$	$N_1 + \frac{N_2}{2}$	$N_1 + \frac{N_2}{2}$	$\frac{N_2}{2}$	$3N_2 + 4N_1$
Pairs in Eq. (4.8)	(E, E)	(E, F)	(E, F)	(E, F)	(E, F)	(F, F)	
Mean rank	$\frac{N+N_2}{2}$	$\frac{N_1}{2}$	$\frac{N_1}{2}$	$\frac{N_1}{2}$	$\frac{N_1}{2}$	$\frac{N+N_2}{2}$	$N + 2N_1 + N_2$
Pairs in Eq. (4.7)	(A, B)	(A, C)	(A, D)	(B, C)	(B, D)	(C, D)	
Mean lowest rank	N_2	$N_1 + N_2$	$N_1 + N_2$	$N_1 + N_2$	$N_1 + N_2$	N_2	$4N_1 + 6N_2$
Pairs in Eq. (4.8)	(E, E)	(E, F)	(E, F)	(E, F)	(E, F)	(F, F)	
Mean top rank	$\frac{N_2+N-N_1}{2}$	1	1	1	1	$\frac{N_2+N-N_1}{2}$	$N - N_1 + N_2 + 4$

Integrated rank is summation of ranks of six pairwise comparisons

than other features. Mean rank of (A, C), (A, D), (B, C), and (B, D) are $\frac{N_2}{2} + N_1$ because N_1 features composed of two classes are always ranked higher than N_2 features composed of four classes. Mean rank of four pairs (E, F) in Eq. (4.8) is $\frac{N_1}{2}$ because N_1 features composed of two classes are higher ranked than other features. Mean rank of two pairs (E, E) and (F, F) are $\frac{N+N_2}{2}$ because N_2 features composed of four classes are higher ranked than others. Next, integrated rank is computed as the summation over six pairwise comparisons. Then, integrated rank of features composed of four classes is

$$2 \times \frac{N_2}{2} + 4 \times \left(N_1 + \frac{N_2}{2}\right) = 4N_1 + 3N_2 \tag{4.9}$$

and integrated rank of features composed of two classes is

$$2 \times \frac{N + N_2}{2} + 4 \times \frac{N_1}{2} = N + 2N_1 + N_2 \tag{4.10}$$

In order that N_2 features composed of four classes are higher ranked than N_1 features composed of two classes based upon integrated rank in average, Eq. (4.9) < Eq. (4.10). Thus

$$\text{Eq. (4.10)} - \text{Eq.(4.9)} > 0 \tag{4.11}$$

$$N + 2N_1 + N_2 - (4N_1 + 3N_2) > 0 \tag{4.12}$$

$$N - 2N_1 - 2N_2 > 0 \tag{4.13}$$

$$N > 2(N_1 + N_2) \tag{4.14}$$

is required. Otherwise, integrated rank based upon six pairwise comparisons, Eq. (4.7), cannot select N_2 features composed of four classes more likely than N_1

features composed of two classes. This means that total number of features distinct between any pairs of classes must not exceed the half of total number of features. This requirement is unlikely fulfilled always.

Equation (4.14) that cannot always be expected to be satisfied is only for average. Even if Eq. (4.14) stands, at most only half of selected features is correctly composed of four classes. If we require that there should not be any false positives, requirement can become more strict (Table 4.3). In order that, we have to require that top ranked features among those composed of two classes must be always ranked lower than the lowest ranked features among those composed of four classes. The rank of bottom ranked feature among those composed of four classes by the two pairwise comparison (A, B) and (C, D) in Eq. (4.7) is N_2 because there are N_2 features that are composed of four classes and are ranked higher than other features. The rank of feature ranked as bottom by the four pairwise comparisons (A, C), (A, D), (B, C), and (B, D) in Eq. (4.7) among those composed of four classes is $N_1 + N_2$ because N_1 features that are composed of two classes and are ranked higher than N_2 features composed of four classes. On the other hand, features ranked as top by two pairwise comparisons (E, E) and (F, F) in Eq. (4.8) among those composed of two classes are ranked uniformly between N_2 and $N - N_1$. This is because N_2 features composed of four classes are higher ranked than N_1 features composed of two classes and there are N_1 features ranked lower than top ranked features among those composed of two classes. Thus, mean top ranked features among those composed of two classes by two pairwise comparisons (E, E) and (F, F) in Eq. (4.8) is $\frac{N-N_1+N_2}{2}$. The rank of feature ranked as top by four pairwise comparisons (E, F) in Eq. (4.8) among those composed of two classes is 1, because N_2 features composed of two classes are higher ranked than other features. Thus integrated bottom rank among N_2 features composed of four classes is

$$2 \times N_2 + 4 \times (N_1 + N_2) = 4N_1 + 6N_2 \tag{4.15}$$

while integrated top rank among N_1 features composed of two classes is

$$2 \times \left(\frac{N - N_1 + N_2}{2} \right) + 4 = N - N_1 + N_2 + 4. \tag{4.16}$$

In order that there are no false positives, i.e., N_2 features composed of four classes is always ranked higher than N_1 features composed of two classes, Eq. (4.16) > Eq. (4.15),

$$\text{Eq. (4.16)} - \text{Eq. (4.15)} > 0 \tag{4.17}$$

$$N - N_1 + N_2 + 4 - (4N_1 + 6N_2) > 0 \tag{4.18}$$

$$N - 5N_1 - 5N_2 + 4 > 0 \tag{4.19}$$

$$N + 4 > 5(N_1 + N_2). \tag{4.20}$$

This means that the number of features composed of two classes and that of four classes must be less than 10% of N if $N_1 = N_2$. This is a less likely fulfilled requirement than Eq. (4.14). Thus integration of six pairwise comparisons unlikely correctly identifies N_2 features composed of four classes when features composed of two classes coexist with them.

Because pairwise comparisons are not expected to work well to identify features composed of multiple classes when more than two kinds of multiple classes coexist, e.g. Eq. (4.4), usually any other alternative strategies are recommended to employ; ones of such alternative strategies are categorical regressions. In categorical regression, class labels are converted to dummy variables, δ_{kj} that takes 1 when jth sample belongs to kth class otherwise 0. Then, categorical regression analysis of x_{ij} is

$$x_{ij} = a_i + \sum_k b_{ik}\delta_{kj} \tag{4.21}$$

where a_i and b_{ik} are the regression coefficients specific to ith feature. Pairwise comparisons that assume four classes could not distinguish features composed of four classes from those composed of two classes well. This problem does not exist in categorical regression analysis anymore. Suppose the simplest cases correspond to two classes, Eq. (4.6), and four classes, Eq. (4.5), as

$$(1, 1, 1, 1, 1, 1, 1, 1, 1, 1, 2, 2, 2, 2, 2, 2, 2, 2, 2, 2) \tag{4.22}$$

and

$$(1, 1, 1, 1, 1, 2, 2, 2, 2, 2, 3, 3, 3, 3, 3, 4, 4, 4, 4, 4) \tag{4.23}$$

respectively. It is obvious that there are no residual errors when Eq. (4.21) assuming four classes (Table 4.4) is applied to Eq. (4.22) if $a_i = \frac{3}{2}$, $b_{i1} = b_{i2} = -\frac{1}{2}$, $b_{i3} = b_{i4} = \frac{1}{2}$. Because there are no residual errors when Eq. (4.21) assuming four classes (Table 4.4) is applied to Eq. (4.23) as well if $a_i = \frac{5}{2}$, $b_{i1} = -\frac{3}{2}$, $b_{i2} = -\frac{1}{2}$, $b_{i3} = \frac{1}{2}$, and $b_{i4} = \frac{3}{2}$, this cannot discriminate four classes from two classes. Nevertheless, Eq. (4.21) assuming two classes (Table 4.4) can discriminate two

Table 4.4 δ_{kj} in categorical regression, Eq. (4.21), assuming either four classes, Eq. (4.5), and two classes, Eq. (4.6), respectively

	Four classes				Two classes	
k	$1 \leq j \leq 5$,	$6 \leq j \leq 10$,	$11 \leq j \leq 15$,	$16 \leq j \leq 20$,	$1 \leq j \leq 10$,	$11 \leq j \leq 20$
1	1	0	0	0	1	0
2	0	1	0	0	0	1
3	0	0	1	0		
4	0	0	0	1		

classes from four classes. If $a_1 = \frac{3}{2}$, $b_{i1} = -\frac{1}{2}$ and $b_{i2} = \frac{1}{2}$, there are no residual errors for Eq. (4.22). On the other hand, there are no solutions with no residual errors when Eq. (4.21) assuming two classes (Table 4.4) is applied to Eq. (4.23). Thus, integration of categorical regression analyses assuming four classes and two classes can identify features composed of two classes and those composed of four classes successfully.

In order to see if categorical regression analysis, Eq. (4.21), can identify features composed of two classes and those composed of four classes simultaneously, we apply categorical regression, Eq. (4.21), to data set 3, Eq. (4.4), as follows. First we apply categorical regression, Eq. (4.21), assuming four classes to data set 3. Because categorical regression assuming four classes are simultaneously coincident with features composed of four classes and those composed of two classes, we select top ranked $N_1 + N_2$ features, which is the total number of features that are composed of either two or four classes, i.e. $i \leq N_1 + N_2$. Then, we apply categorical regression assuming two classes to data set 3. Because categorical regression assuming two classes are coincident with only features composed of two classes, we select top ranked N_1 features, which is the total number of features that are composed of two classes, i.e. $i \leq N_1$. Features selected by categorical regression assuming two classes are considered as features composed of two classes. On the other hand, features selected by categorical regression assuming four classes but not selected by categorical regression assuming two classes are considered as features composed of four classes. Table 4.5 shows the performance of this integrated categorical regression assuming two classes and four classes when $N = 100, M = 20, \mu_0 = 8, \mu_1 = \mu_2 = \frac{\mu_0}{2} = 2, N_1 = 10, N_2 = 10$ and $\sigma = 1$ in data set 3, Eq. (4.4). Performance is averaged over one hundred independent trials. Categorical regression can identify features composed of two classes and four classes completely.

In order to see if PCA based unsupervised FE is applicable, it is applied to the same data set, too. In this case, we selected top 10 features and the second top 10 features (i.e., ranked between 11th and 20th) associated with absolutely larger u_{1i}. Since we do not know which one corresponds to two classes or four classes, after investigating coincidence, we assign top 10 to four classes and the second top 10 to two classes. PCA based unsupervised FE is also successful (Table 4.5). The only disadvantage of PCA based unsupervised FE is that it cannot find the correspondence between selected sets of features and the number of classes in advance.

Table 4.5 Performance of statistical tests applied to synthetic data sets 3 defined by Eq. (4.4)

Categorical regression		PCA based unsupervised FE	
Two classes	Four classes	Two classes	Four classes
10.00	10.00	9.97	9.97

Numbers represent mean number of features distinct between two classes, $i < N_1 (= 10)$, and four classes, $N_1 < i \leq N_1 + N_2$, among N_1 features selected by each method, respectively

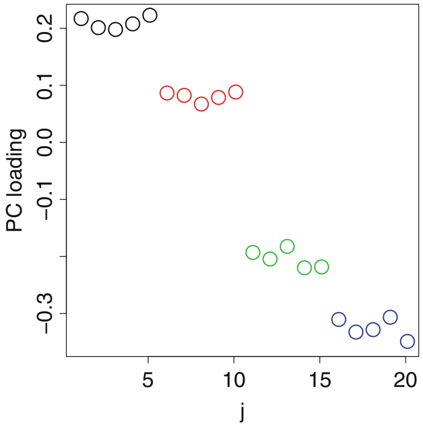

Fig. 4.2 The first PC loading vectors, $\boldsymbol{v}_1 \in \mathbb{R}^M$, for data set 3

In order to see this, we can observe the first PC loading vector, $\boldsymbol{v}_1$ (Fig. 4.2). It is obvious the first PC loading vector is coincident with four classes. This is the reason why the top ranked 10 features are coincident with, not two classes, but four classes. Although we do not repeat the application to shuffled data, it is obvious that categorical regression does not work toward shuffled data because feature selection is performed with class labeling. PCA based unsupervised FE is not affected by shuffling, because PC score vectors, $\boldsymbol{u}_k$s, which is used for feature selection, are not affected by the order of samples, thus are not affected by the class labeling as well. Thus, in this complicated situation, i.e., coexistence of features composed of two classes and four classes, PCA based unsupervised FE is the most favorable method.

4.4 Identification of Non-sinusoidal Periodicity by PCA Based Unsupervised FE

Identification of periodicity, no matter whether it is spatial or temporal, has ever been central issue of data science. In order to identify periodicity, sinusoidal regression is often used. Sinusoidal regression is defined as

$$x_{ij} = a_i + b_i \sin\left(\frac{2\pi}{T} j\right) + c_i \cos\left(\frac{2\pi}{T} j\right) \tag{4.24}$$

where a_i, b_i, c_i are regression coefficients specific to ith feature and T is period. In the following, for the simplicity, $T \in \mathbb{N}$. There are multiple practical problems on regression analysis. At first, we need to know period T in advance in order to apply regression analysis to data set. Of course, it is possible to estimate T from the data set with considering T to be a fitting parameter as well. Nevertheless, there is no known algorithm to find best T values, because any minimization algorithm applied to residues might fall in local minimum that differs from true T. Second, and more critical problem is that not all periodicity is sinusoidal. Only requirement of x_{ij} to be periodic with the period T is

$$x_{ij} = x_{ij+T} \tag{4.25}$$

which does not restrict functional forms to be sinusoidal at all.

In order to see how well sinusoidal regression, Eq. (4.24), can work, we apply it to the data set 4 with period of T

Data set 4

$$x_{ij} = \begin{cases} f_{(i+j) \bmod T} + a\varepsilon_{ij} & i \leq N_1 \\ a\varepsilon_{ij} & i > N_1 \end{cases} \tag{4.26}$$

where $f_j \in \mathbb{R}^T$ and $\varepsilon_{ij} \in \mathbb{R}^{N \times M}$ are drawn from normal distribution $\mathcal{N}(0, \sigma)$, mod is modulo operation, and $0 < a < 1$ is the coefficient that represents signal noise ratio. Because of the term $(i + j) \bmod T$, $\left\{x_{ij} \middle| 1 \leq j \leq M\right\}$s have distinct phases from one another. Performance is averaged over 100 independent trials. Table 4.6 shows the performance when $N = 100, M = 50, T = 10, a = 0.1, \sigma = 1, N_1 = 10$. It is as small as 5.72 which is hardly said to be a good performance. This low performance is because of f_j's non-sinusoidal functional form (Fig. 4.3).

Table 4.6 Performance of statistical tests applied to synthetic data sets 4 defined by Eq. (4.26)

Sinusoidal regression	PCA based unsupervised FE
5.72	10

Numbers represent mean number of features with period T, $i \leq N_1(= 10)$ among N_1 features selected by each method, respectively

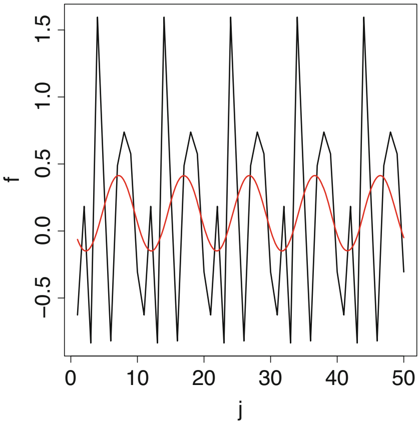

Fig. 4.3 Typical $f_{j \bmod T} \in \mathbb{R}^M (M = 50, T = 10)$ in Eq. (4.26) (black) and its sinusoidal regression, Eq. (4.24) (red)

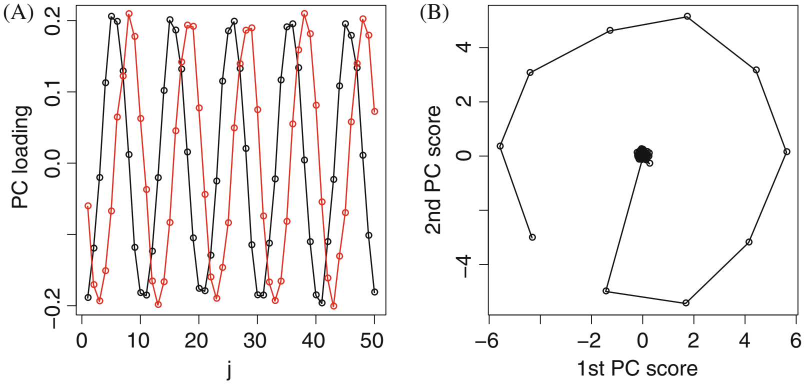

Fig. 4.4 (**a**) A typical first PC loading (black), v_{1j}, and second PC loading (red), v_{2j}. (**b**) Scatterplot of typical first PC score, u_{1i}, and the second PC score, u_{2i}, that correspond to PC loading shown in (**a**)

Next, we apply PCA based unsupervised FE to data set 4, Eq. (4.26), as in Sect. 4.2 excluding one point; instead of ranking features based on the absolute value of the first PC score, $|u_{1i}|$, features are ranked based upon squared sum of the first and second PC scores $u_{1i}^2 + u_{2i}^2$. Table 4.6 shows the performance which is as large as 10, i.e., no errors.

The reason why we need to employ, not only the first PC score, u_{1i}, but also the second PC score, u_{2i}, can be seen in Fig. 4.4. As can be seen in Fig. 4.4a, the first and second PC loading represent periodic function of period $T(= 10)$. And the first 10 pairs of the first and the second PC scores, $u_{ki}, i \leq N_1(= 10), k \leq 2$, form circular trajectory in the plain spanned by the first and the second PC (Fig. 4.4b). This is because of the term $(i + j)$ mod T in Eq. (4.26) that generates phase shift between features $x_{ij}, i \leq N_1(= 10)$. In some cases, the corresponding PC loading, v_{1j} and v_{2j}, represent not the period T, but the period $\frac{T}{2}$ or $\frac{T}{3}$. Nevertheless, in data set 4, Eq. (4.26), only features $i \leq N_1(= 10)$ can be coincident with higher modes, $\frac{T}{2}$ or $\frac{T}{3}$. Thus, these cases also can identify periodic features $i \leq N_1(= 10)$ correctly.

In the above explanation, we use circular trajectory shown in Fig. 4.4b to reasons why we need to employ the first two PC scores for feature selection. Nevertheless, in the practical application, the order of analysis can be reversed. First, we might observe the pairwise scatterplots of PC scores to identify which pairs of features have periodicity because periodic features should draw circular trajectory. Next, we can see individual PC loading as in Fig. 4.4a in order to see period T. This is possible because it is unsupervised method that assumes no specific periodic functional forms in advance. In this sense, PCA based unsupervised FE is superior to the sinusoidal regression to select periodic features.

In order to see if PCA based unsupervised FE can recognize periodicity under the more complicated situation, I modified data set 4, Eq. (4.26), such that cycles with two period, T and T', coexist, i.e.

Data set 5

$$x_{ij} = \begin{cases} f_{(i+j) \bmod T} + a\varepsilon_{ij} & i \le N_1 \\ g_{(i+j) \bmod T'} + a\varepsilon_{ij} & N_1 < i \le N_2 \\ a\varepsilon_{ij} & i > N_2 \end{cases} \tag{4.27}$$

where $g_j \in \mathbb{R}^{T'}$ is drawn from normal distribution $\mathcal{N}(0, \sigma)$. Figure 4.5 shows the typical g that is far from sinusoidal profile ($T' = 5, N_2 = 20$, other parameters are the same as those in Eq. (4.26)). Figure 4.6 shows the typical first to fourth PC scores, $\boldsymbol{u}_k, 1 \le k \le 4$, and PC loading, $\boldsymbol{v}_k, 1 \le k \le 4$. It is obvious that Fig. 4.6a, c corresponds to period $T' = 5$ and Fig. 4.6b, d corresponds to period $T = 10$, respectively. Thus, PCA based unsupervised FE basically has the ability to identify features with two distinct periods even when they coexist. The problem is that the first four PCs do not always correspond to two periods, $T' = 5$ and $T = 10$, but other four PCs, e.g., the second, third, seventh, and eighth PCs, correspond to these two periods, in contrast to data set 4, Eq. (4.26), where the first two PC loading always correspond to period $T = 10$. Thus, in order to make use of PCA to identify features with two distinct periods, we need to identify which PC loading corresponds to two periods, $T = 10$ and $T' = 5$, respectively, by applying sinusoidal regression, Eq. (4.24) with $T = 10$ and $T = T' = 5$. Thus, detailed procedure is as follows:

1. Apply PCA to data set 5, x_{ij} (Eq. (4.27)).
2. Apply sinusoidal regression, Eq. (4.24), with $T = T' = 5$ to PC loading, $\boldsymbol{v}_k$ and select top two, k_1 and k_2.
3. Apply sinusoidal regression, Eq. (4.24), with $T = 10$ to PC loading, $\boldsymbol{v}_k$ and select top two, k'_1 and k'_2.

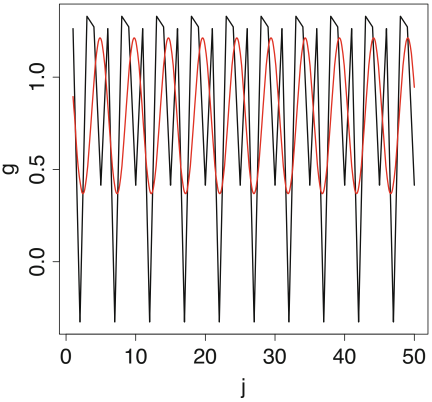

Fig. 4.5 Typical $g_{j \bmod T'} \in \mathbb{R}^M (T' = 5)$ in Eq. (4.27) (black) and its sinusoidal regression, Eq. (4.24) with $T = T' = 5$ (red)

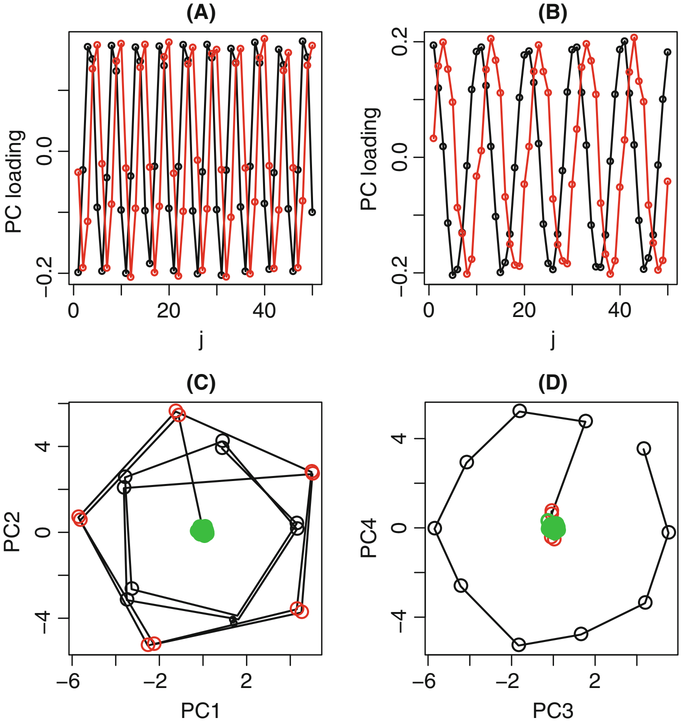

Fig. 4.6 (**a**) Typical first PC loading (black), v_{1j}, and the second PC loading (red), v_{2j}. (**b**) Typical third PC loading (black), v_{3j}, and the fourth PC loading (red), v_{4j}. (**c**) Scatterplot of typical first PC score, u_{1i}, and the second PC score, u_{2i}, that correspond to PC loading shown in (**a**). (**d**) Scatterplot of typical third PC score, u_{3i}, and the fourth PC score, u_{4i}, that correspond to PC loading shown in (**b**). Black open circles: $j \leq N_1(= 10)$, red open circles: $N_1 < j \leq N_2(= 20)$, green open circles: $N_2 < j$

4. Select top ranked $N_2(= 20)$ features using squared sum of two v_{ki}s, $v^2_{k'_1 i} + v^2_{k'_2 i}$, selected in step 3 (this is because PC score, $\boldsymbol{u}_k$ with period $T' = 5$, identifies features with periods $T' = 5$ and $T = 10$ as can be seen in Fig. 4.6c).
5. Select top ranked $N_1(= 10)$ features using squared sum of two v_{ki}s, $v^2_{k_1 i} + v^2_{k_2 i}$, selected in step 2 (this is because PC score, $\boldsymbol{u}_k$ with period $T = 10$, identifies only features with periods $T = 10$ as can be seen in Fig. 4.6d).
6. Identify features selected in step 5 as those with period $T = 10$.
7. Identify features selected in step 4 but not in step 5 as those with period $T = 5$.

Performance is averaged over 100 independent trials (Table 4.7). PCA based unsupervised FE obviously can identify features with two distinct periods almost completely.

In order to see if sinusoidal regressions, Eq. (4.24) with $T = 10$ and $T = T' = 5$, can perform as well as PCA based unsupervised FE, we applied sinusoidal

Table 4.7 Performance of statistical tests applied to synthetic data sets 5 defined by Eq. (4.27)

Sinusoidal regression		PCA based unsupervised FE	
$T = 10$	$T = T' = 5$	$T = 10$	$T = T' = 5$
6.32	6.75	9.73	9.99

Numbers represent mean number of features with period $T = 10, i \leq N_1(= 10)$ among N_1 features selected by each method and that of features with period $T = T' = 5, N_1 < i \leq N_2(= 20)$ among $N_2 - N_1(= 10)$ features selected by each method, respectively

regression to data set 5, Eq. (4.27), too. Top $10(= N_1 = N_2 - N_1)$ features were selected with $T = 10$ and $T = T' = 5$, respectively (Table 4.7). Sinusoidal regression is clearly inferior to PCA based unsupervised FE, possibly because of non-sinusoidal nature of f_j (Fig. 4.3) and g_j (Fig. 4.5) in Eq. (4.27).

4.5 Null Hypothesis

In the above examples, the number of features considered, e.g., those composed of multiple classes or those with specific period, is known in advance. Nevertheless, in the real application, it is unrealistic to assume that the number of features that should be selected is known in advance. In this case, usually P-values are attributed to individual features. These P-values represent the possibility that observation can happen accidentally under the null hypothesis that represents something opposite to the nature that selected features should obey.

For example, when we search features composed of two classes, the P-values represent the possibility that absolute difference of means between two classes can become accidentally larger than observed values when all observations are drawn from the same distribution (e.g., normal distribution with the same mean and standard deviation). If P-values are small enough, we can consider these features to be those composed of two classes, because the observed difference can unlikely appear if there are no classes.

There are some issues in this strategy. The first one is how we can select the null hypothesis. P-values are obviously dependent upon the selection of null hypothesis. Thus, it is important to select "correct" null hypothesis to address proper P-values to features. Unfortunately, there is no known established strategy to select the correct null hypothesis. Null hypothesis, which should be rejected, cannot be observable. Even if majority of features do not always follow null hypothesis, it might simply mean that most of the features are associated with properties searched. Therefore, only requirement is to present clearly null hypothesis together with the P-values attributed to features.

Another issue is how small P-values should be. Generally, P-values are considered to be false ratio. In other words, if we select n features associated with P-values smaller than p, there can be at most np features selected wrongly in spite of that they obey the null hypothesis. Thus, ideally, p should be as small as $\frac{1}{n}$ such that there are no false positives. Nonetheless, it is often unrealistic to require $p < \frac{1}{n}$ especially when n is large and data is noisy. Therefore, practically, p is set to be 0.01 or 0.05, because it is enough if the 99% or 95% of selected feature are correct, for the usual purpose.

The third and the most critical issue is the problem of multiple comparisons. When there are N features to which P-values are attributed, P-values can be accidentally as small as $\frac{1}{N}$. When N is large, e.g., $N \sim 10^4$, it causes a problem. Even if some features have P-values as small as 10^{-4}, we cannot reject null hypothesis. Thus, we cannot select these features as those associated with properties searched, e.g., composed of two classes. In spite of that, it is often unrealistic to require that P-values should be as small as 10^{-4}. Although there are many ways to address this difficulty, we employ Benjamini Hochberg (BH) criterion, because it is known to work practically well, in the applications described in the following chapters.

The basic idea of BH criterion is very simple. If the features obey null hypothesis completely, e.g., apparently two classes features are drawn from the same distribution, e.g., normal distribution, the distribution of P-values should be uniform distribution $\in [0, 1]$, because this is the definition of probability. Thus, if we order P-values in ascending order, the ith largest P-value should be as large as $\frac{i}{N}$. In other words, if the ith largest P-value is smaller than $\frac{i}{N}$, it unlikely occurs under the null hypothesis.

Considering these discussions, BH criterion is as follows:

1. Order P-values attributed to ith feature, P_i, in ascending order.
2. Find the smallest i_0 such that $P_{i_0} > \frac{i_0}{N} p$ where p is threshold P-values.
3. Select features, $i \leq i_0$, such that their attributed P-values are practically supposed to be less than p.

Throughout the remaining part of this book, we employ this criterion to adjust P-values with considering multiple comparisons as many as the number of features, N.

4.6 Feature Selection with Considering *P*-Values

In order to perform feature selection with considering P-values, we select null hypothesis for the distribution of PC score, u_{ki}, as normal distribution. In order to assign P-values to features, we employ χ^2 distribution as

$$P_i = P_{\chi^2}\left[> \sum_k \left(\frac{u_{ki}}{\sigma_k}\right)^2 \right] \tag{4.28}$$

where $P_{\chi^2}[> x]$ is the cumulative probability that the argument is larger than x. The summation is taken over PCs selected for identification of ith feature that fulfills desired condition. The degrees of freedom of χ^2 distribution is equal to the number of PCs included in the summation. σ_k is the standard deviation of u_{ki}. Then features associated with adjusted P-values less than 0.01 are selected.

Other methods compared with PCA based unsupervised FE in the previous section can also attribute P-values to individual features. Using these P-values, features associated with adjusted P-values less than 0.01 can be selected. This enables us to compare performance between the various methods.

At first, we perform analysis shown in Table 4.2 with replacing identification of features based upon top ranked $N_1 (= 10)$ features with that based upon features associated with adjusted P-values less than 0.01. Unfortunately, not all tests shown in Table 4.2 can derive P-values. Evaluation based upon variance has no ways to attribute to P-values, because no null hypothesis can exist. Regression analysis cannot either, because complete fitting is always possible because the number of features, N, is larger than the number of samples, M. Thus, only remaining three, t test, unimodal test, and PCA based unsupervised FE can be employed. We do not employ shuffling in this case, because the effect of shuffling was presented in Table 4.2.

Evaluations based upon adjusted P-values do not always give us N_1 features selected. Thus, instead of presenting the number of correctly selected features as in Table 4.2, we need to present confusion matrix, which is demonstrated in Table 4.8. Suppose that there are two classes, positive set and negative set (in the case of feature selection, positive corresponds to features with considered properties, e.g., those composed of two classes, and negative corresponds to features without considered properties, e.g., those without any classes). The number of positives predicted as positive is true positive (TP). The number of positives predicted as not positive is false negative (FN). The number of negatives predicted as positive is false positive (FP). The number of negatives predicted as not positive is true negative (TN). If FN = FP = 0, it is complete prediction.

Confusion matrices when three statistical tests are applied to data set 1, Eq. (4.1), and data set 2, Eq. (4.2), are shown in Tables 4.9 and 4.10, respectively. The performance is averaged over 100 independent trials. t test performs almost equally between data sets 1 and 2, although the performance decreases as M decreases or N increases. PCA based unsupervised FE totally fails for data set 1, while it is successful for larger N in data set 2. Unimodal test has never been successful. One

Table 4.8 Confusion matrix

	Real	
Prediction	Positive	Negative
Positive	TP	FP
Negative	FN	TN

TP true positive, *FP* false positive, *FN* false negative, *TN* true negative

Table 4.9 Confusion matrices when statistical tests are applied to synthetic data sets 1 defined by Eq. (4.1) and features associated with adjusted P-values less than 0.01 are selected

	t test		Unimodal test		PCA	
	$i \le N_1$	$N_1 < i$	$i \le N_1$	$N_1 < i$	$i \le N_1$	$N_1 < i$
Data set 1: $N = 100$, $M = 20$						
Selected	10.00	0.10	0.03	0.08	0.00	0.00
Not selected	0.00	89.90	9.97	89.92	10.00	90.00
Data set 1: $N = 100$, $M = 10$						
Selected	5.96	0.18	0.01	0.06	0.00	0.00
Not selected	4.04	89.82	9.99	89.94	10.00	90.00
Data set 1: $N = 1000$, $M = 20$						
Selected	9.98	0.2	0.0	0.2	0.00	0.00
Not selected	0.02	989.8	10	989.8	10.00	990.00
Data set 1: $N = 1000$, $M = 10$						
Selected	1.16	0.2	0.0	0.04	0.00	0.00
Not selected	8.84	989.8	10	989.96	10.00	990.00

$N_1 = 10$

Table 4.10 Confusion matrices when statistical tests are applied to synthetic data sets 2 defined by Eq. (4.2) and features associated with adjusted P-values less than 0.01 are selected

	t test		Unimodal test		PCA	
	$i \le N_1$	$N_1 < i$	$i \le N_1$	$N_1 < i$	$i \le N_1$	$N_1 < i$
Data set 2: $N = 100$, $M = 20$						
Selected	10.00	0.07	0.0	0.07	0.00	0.01
Not selected	0.00	89.93	10.00	89.93	10.00	89.99
Data set 2: $N = 100$, $M = 10$						
Selected	6.08	0.06	0.00	0.00	0.00	0.00
Not selected	3.92	89.94	10.00	90.00	10.00	90.00
Data set 2: $N = 1000$, $M = 20$						
Selected	9.98	0.1	0.00	0.00	9.97	0.07
Not selected	0.02	989.9	10.00	990.0	0.03	989.03
Data set 2: $N = 1000$, $M = 10$						
Selected	1.09	0.01	0.0	0.04	9.4	0.00
Not selected	8.91	989.99	10	989.96	0.6	990.0

$N_1 = 10$

remarkable point is that PCA based unsupervised FE can outperform t test when $N = 1000$ and $M = 10$. This suggests that PCA based unsupervised FE might be the best when $N \gg M$; the situation $N \gg M$ is very usual in the bioinformatics. This is the basic motivation that this textbook is written.

In spite of that PCA based unsupervised FE is an unsupervised method that does not fully make use of available information while t test is a supervised method that fully makes use of available information, the reason why PCA based unsupervised FE can outperform t test when $N \gg M$ is as follows. In t test, P-values increase as M decreases (i.e., less significant). On the other hand, the correction of P-values considering multiple comparisons is enhanced as N increases. Thus, adjusted P-values become larger (less significant) as N increases. This means, if $N \gg M$, t test hardly computes small enough P-values. On the other hand, in PCA based unsupervised FE where P-values are computed by u_{1i} which is less affected by varying M, P-values are less dependent on M. In Table 4.10, TPs computed by PCA based unsupervised FE do not change much between $M = 10$ and $M = 20$ when $N = 1000$. In addition to this, in this setup, N_1 that represents the number of positives remains unchanged while N increases. This means, the number of negatives increases. Generally, negatives are associated with smaller absolute values of u_{1i} because u_{1i} is associated with v_{1j} that represents distinction between two classes (Fig. 4.1). P-values are computed based upon normalized u_{1i}, Eq. (4.28), thus absolute values u_{1i} attributed to positives become relatively larger as the number of negatives increases. This process has the tendency that increasing the number of negatives reduces P-values attributed to positives (i.e., more significant). Because of that, in Table 4.10, PCA based unsupervised FE is successful only when $N = 1000$.

This is the reason why PCA based unsupervised FE is employed for the feature selection in bioinformatics where $N \gg M$ is quite usual. P-values computed by PCA based unsupervised FE is less affected by M that is typically small in bioinformatics while P-values decrease for larger N that is typically very large in bioinformatics. Thus, PCA based unsupervised FE is very fitted to the problems in bioinformatics.

One might be interested in what will happen if selection based upon adjusted P-values is applied to other examples discussed in the above. The answer is that it is dependent upon various parameters. In the examples analyzed in this section, PCA based unsupervised FE can outperform t test only when $N = 1000$ and $M = 10$. Thus, whether it works well or not when it is applied to real data set is also dependent upon the properties of data sets. The general tendency that PCA based unsupervised FE works well only when $N \gg M$ is universal independent of the data sets considered. Thus, the discussion about in which situation PCA based unsupervised FE that selects features based upon adjusted P-values works well is postponed to the later chapters where PCA based unsupervised FE is applied to real data sets. The readers can see many examples where PCA based unsupervised FE works well or not in these later chapters.

4.7 Stability

Weaker sensitivity of PCA based unsupervised FE on the number of samples, M, naturally results in the stability of feature selection. The stability of feature selection is defined as the robustness of feature selection when samples change. Suppose that samples are drawn from some distributions. If selected features vary every time samples are drawn from distribution, it is problematic in biology where individual features, e.g., genes, have meanings.

In PCA based unsupervised FE, P-values are less dependent upon the number of samples. In other words, every time we select half of samples among the available samples, P-values attributed to individual features do not change. If P-values attributed to individual features do not change, the selected features do not change, either. This is definitely equivalent to the stability. In the applications of PCA based unsupervised FE to real data sets described in the following chapters, readers will see many examples that PCA based unsupervised FE outperforms other methods from the point of stability. This is yet another reason why PCA based unsupervised FE is a recommended method to be used in bioinformatics.

4.8 Summary

In this chapter, I proposed to make use of PCA as a tool of feature selection. PCA based unsupervised FE can identify features composed of multiple classes better than conventional supervised methods, e.g., t test and categorical regression. When it is applied to identification of non-sinusoidal periodic features, PCA based unsupervised FE can outperform another conventional method, sinusoidal regression. With attributing P-values to features under the null hypothesis that PC scores obey χ^2 distribution, PCA based unsupervised FE correctly identifies features composed of two classes only when $N \gg M$, i.e., the number of features is much larger than the number of samples.

Reference

1. Hartigan, J.A., Hartigan, P.M.: The dip test of unimodality. Ann. Stat. **13**(1), 70–84 (1985). https://doi.org/10.1214/aos/1176346577

Chapter 5
TD Based Unsupervised FE

Although our world might have no reason to exist, it sounds fantastic, because we can make the reason for ourselves.
Filicia Heideman, Sound of the Sky, Season 1, Spisode 7

5.1 TD as a Feature Selection Tool

In this chapter, I would like to make use of TD as a feature selection tool. Suppose that $x_{ijk} \in \mathbb{R}^{N \times M \times K}$ represents the value of the ith feature of the samples having jth and kth properties as

Data set 6:

$$x_{ijk} \sim \begin{cases} \mathcal{N}(\mu, \sigma), \ i \leq N_1, \ j \leq \frac{M}{2}, \ k \leq \frac{K}{2} \\ \mathcal{N}(0, \sigma), \qquad\qquad \text{otherwise} \end{cases} \tag{5.1}$$

In this example, j and k are supposed to be classified into two classes, $j \leq \frac{M}{2}$, $K \leq \frac{M}{2}$ and $j > \frac{M}{2}$ or $j > \frac{K}{2}$ for $i \leq N_1$. Then, x_{ijk} is drawn from normal distribution, $\mathcal{N}(\mu, \sigma)$, with positive mean, $\mu > 0$, only when $j \leq \frac{M}{2}, k \leq \frac{K}{2}$, otherwise $\mu = 0$. The purpose of feature selection is to find N_1 features associated with two classes shown in Eq. (5.1).

Tucker decomposition, Eq. (3.2), with HOSVD algorithm, Fig. 3.8, is applied to data set 6, Eq. (5.1), with $N = 1000$, $M = K = 6$, $N_1 = 10$, $\mu = 2$, $\sigma = 1$, as

$$x_{ijk} = \sum_{\ell_1=1}^{N} \sum_{\ell_2=1}^{M} \sum_{\ell_3=1}^{K} G(\ell_1, \ell_2, \ell_3) u_{\ell_1 i}^{(i)} u_{\ell_2 j}^{(j)} u_{\ell_3 k}^{(k)} \tag{5.2}$$

where $\boldsymbol{u}_{\ell_1}^{(i)} \in \mathbb{R}^N$, $\boldsymbol{v}_{\ell_2}^{(i)} \in \mathbb{R}^M$, $\boldsymbol{u}_{\ell_3}^{(k)} \in \mathbb{R}^K$, $G(\ell_1, \ell_2, \ell_3) \in \mathbb{R}^{N \times M \times K}$. Figure 5.1a, b shows a typical realization of $\boldsymbol{u}_1^{(j)}$ and $\boldsymbol{u}_1^{(k)}$, respectively. It is obvious that these two correctly reflect the distinction between $j > \frac{M}{2}, k > \frac{K}{2}$ and $j \leq \frac{M}{2}, k \leq \frac{K}{2}$. Next,

Y-h. Taguchi, *Unsupervised Feature Extraction Applied to Bioinformatics*,
Unsupervised and Semi-Supervised Learning,
https://doi.org/10.1007/978-3-030-22456-1_5

we would like to identify which $\boldsymbol{u}_{\ell_1}^{(i)}$ can be used for feature selection. In contrast to PCA based unsupervised FE, it is not clear which $\boldsymbol{u}_{\ell_1}^{(i)}$ should be used, because there is no one-to-one correspondence among $\boldsymbol{u}_{\ell_1}^{(i)}, \boldsymbol{u}_{\ell_2}^{(j)}, \boldsymbol{u}_{\ell_3}^{(k)}$; instead of that, their relationship is represented through the core tensor, G.

In order to see this relationship, we order $G(\ell_1, 1, 1)$ with descending order of absolute values; Table 5.1 shows the core tensors, $G(\ell_1, 1, 1)$, sorted in this order. Table 5.1 suggests that $\boldsymbol{u}_1^{(i)}$ is most likely associated with $\boldsymbol{u}_1^{(j)}$ and $\boldsymbol{u}_1^{(k)}$, because $G(1, 1, 1)$ has the largest absolute value among $G(\ell_1, 1, 1)$. Actually, $\boldsymbol{u}_1^{(i)}$ shown in Fig. 5.1c obviously has larger absolute values for $i \leq N_1$ than others. Thus, the strategy proposed here, i.e., first find singular value vectors attributed to samples and associated with desired class dependence, then identify singular value vectors, attributed to features, that share G having larger absolute values with them, can identify features with not known in advance j, k dependence in fully unsupervised manner. The reason why it works so well is obvious. If we see $\boldsymbol{u}_{\ell_2}^{(j)} \times^0 \boldsymbol{u}_{\ell_3}^{(k)}$ that is shown in Fig. 5.1d, it is fully associated with the j, k dependence defined in Eq. (5.1) that means only $j, k < \frac{M}{2}$ are drawn from normal distribution with positive mean while others are drawn from those with zero mean.

Next issue might be if TD based unsupervised FE can outperform conventional methods. As a representative of conventional methods, we employ again categorical regression analysis, Eq. (4.21), that is modified to be adapted to co-existence of two kinds of classes,

Table 5.1 $G(\ell_1, 1, 1)$s that correspond to Fig. 5.1

ℓ_1	1	4	2	6
$G(\ell_1, 1, 1)$	−35.484412	2.137686	1.748955	−1.705922

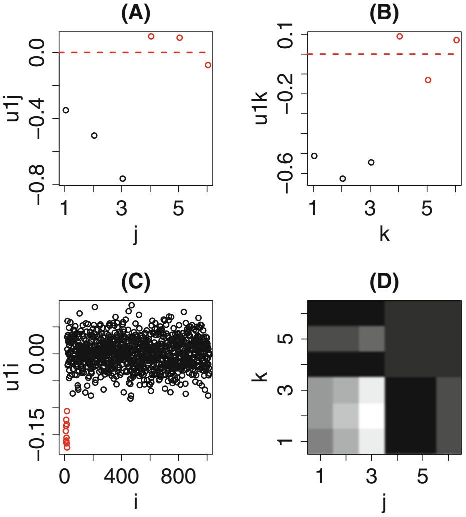

Fig. 5.1 A typical realization of $\boldsymbol{u}_1^{(i)}, \boldsymbol{u}_1^{(j)}, \boldsymbol{u}_1^{(k)}$ when Tucker decomposition, Eq. (3.2), with HOSVD algorithm, Fig. 3.8 is applied to data set 6, Eq. (5.1) with $N = 1000, M = K = 6, N_1 = 10, \mu = 2, \sigma = 1$. (**a**) $\boldsymbol{u}_1^{(j)}$, (**b**) $\boldsymbol{u}_1^{(k)}$, black and red circles correspond to $j \leq \frac{M}{2}, k \leq \frac{K}{2}$ and $j > \frac{M}{2}, k > \frac{K}{2}$, respectively. Red broken lines show baseline. (**c**) $\boldsymbol{u}_1^{(i)}$. Red open circle corresponds to $i \leq N_1$, i.e., features associated with j, k dependence. (**d**) $\boldsymbol{u}_1^{(j)} \times^0 \boldsymbol{u}_1^{(k)}$. Brighter squares indicate larger values

$$x_{ijk} = a_i + \sum_{s=1}^{2} b_{is}\delta_{sj} + \sum_{s=1}^{2} c_{is}\delta_{sk} \tag{5.3}$$

where a_i, b_{is}, c_{is} are the regression coefficients. δ_{sj} and δ_{sk} are the function that takes 1 only when sample j or k belongs to the sth class otherwise 0.

In order to perform feature selection, P-values need to be addressed to features. For categorical regression analysis, P-values computed by categorical regression analysis is used as it is. For TD based unsupervised FE,

$$P_i = P_{\chi^2}\left[> \left(\frac{u_{1i}^{(i)}}{\sigma_1}\right)^2 \right] \tag{5.4}$$

is used to attribute P-values to features where σ_1 is the standard deviation of $u_{1i}^{(i)}$. Both P-values, i.e., computed with TD based unsupervised FE and categorical regression analysis, are corrected by BH criterion and features associated with adjusted P-values less than 0.01 are selected. Table 5.2 shows the performances achieved by TD based unsupervised FE and categorical regression, Eq. (5.3). Performance is averaged over 100 independent examples. In contrast to TD based unsupervised FE that can identify more than 60% of features associated with searched j, k dependence, categorical regression, Eq. (5.3), could identify almost no features. The cause of this drastic low performance is obvious. Equation (5.3) assumes four classes, because j and k are composed of two classes, respectively. Thus, two classes times two classes are equal to four classes. Nevertheless, Eq. (5.1) obviously admits two classes, i.e., $j \leq \frac{M}{2}, k \leq \frac{K}{2}$ versus others. This not proper assumption in the model (categorical regression analysis) results in poor performance. In actuality, if we employ categorical regression as

$$x_{ijk} = a_i + \sum_{s=1}^{2} b_{is}\delta_{sjk} \tag{5.5}$$

Table 5.2 Confusion matrices when statistical tests are applied to synthetic data sets 6 defined by Eq. (5.1) and features associated with adjusted P-values less than 0.01 are selected

	TD based unsupervised FE		Categorical test(four classes)		Categorical test(two classes)	
Data set 6	$i \leq N_1$	$N_1 < i$	$i \leq N_1$	$N_1 < i$	$i \leq N_1$	$N_1 < i$
Selected	6.34	0.00	0.63	0.00	7.35	0.00
Not selected	3.66	990	9.37	990	2.65	990

	TD based unsupervised FE		Categorical test(nine classes)		Categorical test(two classes)	
Data set 7	$i \leq N_1$	$N_1 < i$	$i \leq N_1$	$N_1 < i$	$i \leq N_1$	$N_1 < i$
Selected	8.73	0.00	4.58	0.00	10.0	0.00
Not selected	1.27	990	5.42	990	0.00	990

$N_1 = 10$. "categorical test(two classes)" corresponds to Eq. (5.3), "categorical test(four classes)" corresponds to Eq. (5.5), and "categorical test(nine classes)" corresponds to Eq. (5.7) where δ_{sjk} is a function that takes 1 only when

$s = 1$: $j \leq \frac{M}{2}$ and $k \leq \frac{K}{2}$
$s = 2$: $j > \frac{M}{2}$ or $k > \frac{K}{2}$

otherwise 0 and a_i, b_{sjk} are the regression coefficients, categorical regression can outperform TD based unsupervised FE as expected (Table 5.2). The only problem is that it is usually impossible to assume two classes in spite of that there are four classes based upon the apparent category. In this case, unsupervised method can outperform supervised method.

In order to confirm these tendencies, we prepare additional synthetic data.

Data set 7:

$$x_{ijk} \sim \begin{cases} \mathcal{N}(\mu, \sigma), \; i \leq N_1, \; \frac{M}{3} < j \leq \frac{2M}{3}, \; \frac{K}{3} < k \leq \frac{2K}{3} \\ \mathcal{N}(0, \sigma), \qquad\qquad \text{otherwise} \end{cases}. \tag{5.6}$$

Equation (5.3) is modified as

$$x_{ijk} = a_i + \sum_{s=1}^{3} b_{is}\delta_{sj} + \sum_{s=1}^{3} c_{is}\delta_{sk} \tag{5.7}$$

with three classes, $1 \leq j \leq \frac{M}{3}$ or $1 \leq k \leq \frac{K}{3}$ for $s = 1$, $\frac{M}{3} < j \leq \frac{2M}{3}$ or $\frac{K}{3} < k \leq \frac{2K}{3}$ for $s = 2$, and $\frac{2M}{3} < j \leq M$ or $\frac{2K}{3} < k \leq K$ for $s = 3$. On the other hand, Eq. (5.5) remains unchanged although δ_{sjk} takes 1 only when

$s = 1$: $\frac{M}{3} < j \leq \frac{2M}{3}$ and $\frac{K}{3} < k \leq \frac{2K}{3}$
$s = 2$: $j \leq \frac{M}{3}$ or $j > \frac{2M}{3}$ or $k \leq \frac{K}{3}$ or $k > \frac{2K}{3}$

otherwise 0. $M = K = 12$ and other parameters remain unchanged. As expected (Table 5.2), the performances of categorical regressions applied to set 7 are improved from those applied to data set 6, because the number of samples, MK, increases while the number of features, N, remains unchanged. In spite of these improved performances of categorical regression analyses, TD based unsupervised FE still outperforms three classes × three classes = nine classes categorical regression analysis, Eq. (5.7) (see Table 5.2). Thus, as far as apparent categories that do not correctly reflect true category are considered, TD based unsupervised FE can outperform supervised method. It is very usual in genomic data analysis that it is unclear if apparent categories are coincident with true, but unknown, classes. This is possibly the reason why TD based unsupervised FE often outperforms supervised methods in the applications to bioinformatics that will be introduced in the later part of this book.

It should be also emphasized that TD based unsupervised FE can outperform supervised methods only when $N \gg MK$, i.e., the number of features is much larger than the number of samples. Although we do not demonstrate this using more synthetic data sets, one should remember this point when one would like to employ TD based unsupervised FE.

5.2 Comparisons with Other TDs

Here I employed only Tucker decomposition, Eq. (3.2), with HOSVD algorithm, Fig. 3.8, for feature selection. Since I have already argued the superiority of Tucker decomposition toward other two TDs, CP decomposition and tensor train decomposition, it might not be necessary to demonstrate superiority of Tucker decomposition to other two TDs. Nevertheless, it is not meaningless to see what we can get when the other two TDs are applied to data set 6.

First, tensor train decomposition, Eq. (3.3), with $R_1 = R_2 = M = K = 6$ is applied to data set 6, whose results obtained by Tucker decomposition are shown in Fig. 5.1 (Fig. 5.2). Figure 5.2 looks very similar to Fig. 5.1. In spite of that, tensor train decomposition is still inferior to Tucker decomposition. First of all, we have no idea how we should choose R_is that decide the rank of tensor train decomposition. In the present case, we can try to find R_is that result in the same result as that in Fig. 5.1. If not, we can have no ways to decide R_is. Second, we do not know how to relate $G^{(j)}(j, 1, 1)$, $G^{(k)}(k, 1)$, and $G^{(i)}(i, 1)$ with one another, because there is no core tensor that plays the role to connect singular vectors in Tucker decomposition (Table 5.1) where we know what I should search. If not as in the present case, i.e., tensor train decomposition, we have no idea which core tensors given by tensor train decomposition are selected for the feature selection.

Next, we apply CP decomposition, Eq. (3.1), with $L = 1$ to data set 6, whose results obtained by Tucker decomposition are shown in Fig. 5.1. Figure 5.3

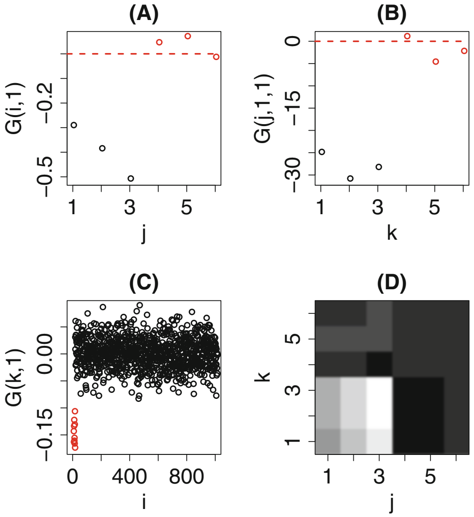

Fig. 5.2 $G^{(j)}(j, 1, 1)$, $G^{(k)}(k, 1)$, $G^{(i)}(i, 1)$ when tensor train decomposition, Eq. (3.3), with $R_1 = R_2 = M = K = 6$ is applied to data set 6, Eq. (5.1) whose results obtained by Tucker decomposition are shown in Fig. 5.1. (**a**) $G^{(j)}(j, 1, 1)$, (**b**) $G^{(k)}(k, 1)$, black and red circles correspond to $j \leq \frac{M}{2}, k \leq \frac{K}{2}$ and $j > \frac{M}{2}, k > \frac{K}{2}$, respectively. Red broken lines show baseline. (**c**) $G^{(i)}(i, 1)$. Red open circle corresponds to $i \leq N_1$, i.e., features associated with j, k dependence. (**d**) $G^{(j)}(j, 1, 1) \cdot G^{(k)}(k, 1)$. Brighter squares indicate larger values

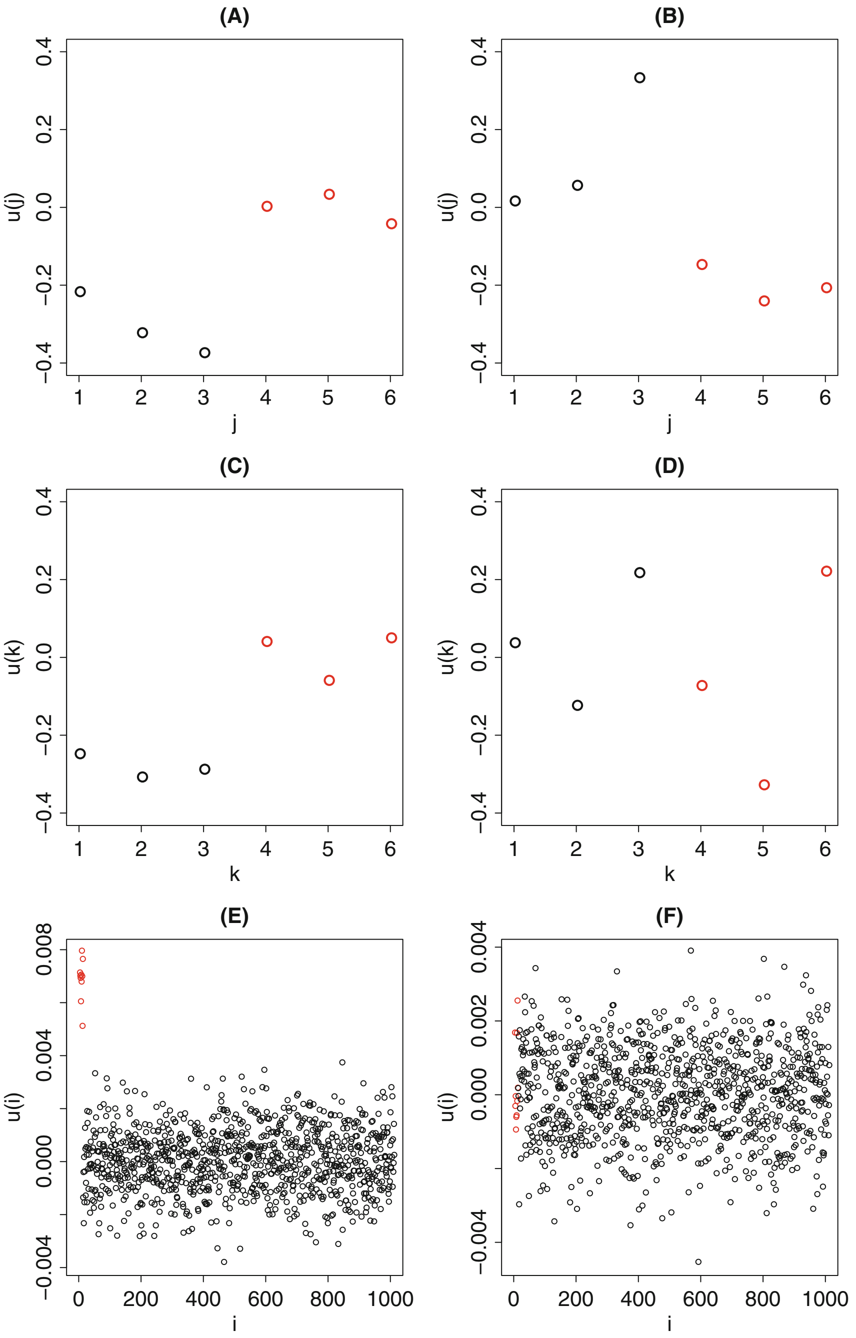

Fig. 5.3 Two typical convergent realizations starting from different initial values of CP decomposition, Eq. (3.1), with $L = 1$ applied to data set 6, Eq. (5.1), whose results obtained by Tucker decomposition is shown in Fig. 5.1. (**a**) and (**b**) $\boldsymbol{u}_1^{(j)}$, black and red circles correspond to $j \leq \frac{M}{2}$ and $j > \frac{M}{2}$, respectively. (**c**) and (**d**) $\boldsymbol{u}_1^{(k)}$, black and red circles correspond to $k \leq \frac{K}{2}$ and $k > \frac{K}{2}$, respectively. (**e**) and (**f**) $\boldsymbol{u}_1^{(i)}$. Red open circle corresponds to $i \leq N_1$, i.e., features associated with j, k dependence

represents the two independent results starting from different initial values (one should remember that CP decomposition need to be given by initial values from where computation starts). At first, they clearly differ from each other. Second, the second realizations, (b), (d), and (f), do not correspond to the distinction between two classes and fail to identify features with not known in advance j, k dependence, $i \leq N_1$. Thus, CP decomposition is inferior to Tucker decomposition because of initial condition dependence as discussed earlier.

These comparisons suggest that Tucker decomposition is superior to tensor train decomposition and CP decomposition as a tool of feature selection.

5.3 Generation of a Tensor From Matrices

In the previous section, we showed that TD based unsupervised FE can outperform conventional supervised feature selection, categorical regression analysis, when the number of features is much larger than the number of samples and true classification is a complex function of apparent labeling. Although TD based unsupervised FE is shown to be effective, it is unfortunately not so frequent that there are data sets formatted as tensor, because getting tensor requires more observation than matrices. In order to get $N \times M$ matrix that represents M samples with N features, required number of observations is as many as the number of samples, i.e., M. On the other hand, in order to get $N \times M \times K$ tensors that correspond to N features observed under the combination of M times and K times measurements, the required number of observation is as many as $K \times M$. If we need to have tensors with more modes, the number of observation will increase, too. Thus, even if TD based unsupervised FE is an effective method, we usually cannot have data set formatted as tensors, to which TD based unsupervised FE is applicable.

In order to have more opportunities to which we can apply TD based unsupervised FE, we can propose to generate tensors from matrices [1], which are obtained more easily than tensors. Suppose that we have two matrices, $x_{ij} \in \mathbb{R}^{N \times M}$ and $x_{ik} \in \mathbb{R}^{N \times K}$, which represent i features under the jth experimental conditions and the kth experimental conditions, respectively. A typical observation is that N health conditions, blood pressure, body mass, body temperature, height, weight, etc. are observed M individuals in Japan and K individuals in the USA. Then we can get tensor $x_{ijk} \in \mathbb{R}^{N \times M \times K}$ by simply multiplying x_{ij} and x_{ik},

$$x_{ijk} = x_{ij} x_{ik} \tag{5.8}$$

TD can be applied to x_{ijk} as usual. It does not have to be restricted to the product of two matrices. We can generate $m + 1$ mode tensor by multiplying m matrices, $x_{ij_1}, x_{ij_2}, \ldots, x_{ij_m}$ as

$$x_{ij_1 j_2 \cdots j_m} = \prod_{s=1}^{m} x_{ij_s} \tag{5.9}$$

On the other hand, we can consider the alternative cases where not features but samples are common between two matrices. Suppose that for K individuals two distinct N and M observations are performed and are recorded as matrices form, $x_{ik} \in \mathbb{R}^{N \times K}$ and $x_{jk} \in \mathbb{R}^{M \times K}$. A typical example is that there are N goods in kth shop and x_{ik} represents a price of ith good in kth shop. On the other hand, x_{jk} represents the number of customers at jth time point at kth shop. We can generate tensor $x_{ijk} \in \mathbb{R}^{N \times M \times K}$ as

$$x_{ijk} = x_{ik} x_{jk} \tag{5.10}$$

Again we can employ more matrices as

$$x_{i_1 i_2 \cdots i_m j} = \prod_{s=1}^{m} x_{i_s j} \tag{5.11}$$

From the mathematical point of view, although there are no needs to distinguish between equations Eqs. (5.11) and (5.9), they should be considered separately from the data science point of view. Then hereafter we denote Eq. (5.11), i.e., the cases sharing samples, as case I while Eq. (5.9), i.e., the cases sharing features, as case II, respectively.

5.4 Reduction of Number of Dimensions of Tensors

It is possible to produce tensors from matrices. However, it increases the number of features. When two matrices, $x_{ij} \in \mathbb{R}^{N \times M}$ and $x_{ik} \in \mathbb{R}^{N \times K}$ are multiplied in order to generate a tensor $x_{ijk} \in \mathbb{R}^{N \times M \times K}$ (case II), the number of features increases from $N \times (M + K)$ to $N \times M \times K$. Thus, we need some way to reduce the number of dimensions of generated tensors. Here we propose taking summation of shared features, i.e.,

$$\tilde{x}_{i_1 i_2 \cdots i_m} = \sum_j x_{i_1 i_2 \cdots i_m j} \tag{5.12}$$

$$\tilde{x}_{j_1 j_2 \cdots j_m} = \sum_i x_{i j_1 j_2 \cdots j_m} \tag{5.13}$$

Then the number of dimensions increases from $N \times (M + K)$ not to $N \times M \times K$ but to $M \times K$ for case II while from $(N + M) \times K$ not to $N \times M \times K$ but to $N \times M$ for case I.

One might wonder how we can compute singular value matrices that correspond to indices of which are taken summation when TD is applied to $\tilde{x}_{i_1 i_2 \cdots i_m}$ or $\tilde{x}_{j_1 j_2 \cdots j_m}$. These missing singular value matrices are recovered by the following computations,

Table 5.3 Distinction between cases and types

	Type I		Type II	
Case I	$x_{i_1 i_2 \cdots i_m j} = \prod_{s=1}^{m} x_{i_s j}$	Eq. (5.11)	$\tilde{x}_{i_1 i_2 \cdots i_m} = \sum_j x_{i_1 i_2 \cdots i_m j}$	Eq. (5.12)
Case II	$x_{i j_1 j_2 \cdots j_m} = \prod_{s=1}^{m} x_{i j_s}$	Eq. (5.9)	$\tilde{x}_{j_1 j_2 \cdots j_m} = \sum_i x_{i j_1 j_2 \cdots j_m}$	Eq. (5.13)

$$\boldsymbol{u}_\ell^{(i;j_s)} = X^{(ij_s)} \times_{j_s} \boldsymbol{u}_\ell^{(j_s)} \tag{5.14}$$

$$\boldsymbol{u}_\ell^{(j;i_s)} = X^{(ji_s)} \times_{i_s} \boldsymbol{u}_\ell^{(i_s)} \tag{5.15}$$

where $X^{(ij_s)} \in \mathbb{R}^{N \times M_s}$ and $X^{(ji_s)} \in \mathbb{R}^{M \times N_s}$, respectively. Thus, we have m singular value matrices that correspond to i_s or j_s, instead of one singular value matrix. This might look problematic. Nevertheless, practically, if m singular value matrices obtained are mutually highly correlated, it is not practically problematic. Thus, case to case, we might employ this approximate strategy. In order to distinguish these tensors from the previous one, we call those generated after the partial summation of index, Eqs. (5.12) and (5.13) as type II while those without partial summation, Eqs. (5.9) and (5.11), as type I. Table 5.3 summarizes the distinction between cases and types.

5.5 Identification of Correlated Features Using Type I Tensor

The purpose of introduction of tensors summarized in Table 5.3 is simply because we would like to make use of TD based unsupervised FE when no tensors are available. Nevertheless, we can make use of tensors listed in Table 5.3 for the additional alternative purpose as bi-product: identification of mutually correlated features. Suppose we have two sets of observations to K samples formatted as matrices, $x_{ik} \in \mathbb{R}^{N \times K}$ and $x_{jk} \in \mathbb{R}^{M \times K}$. The question is to search pairs of features between two sets.

The standard strategy is to compute pairwise correlation between x_{ik} and x_{jk},

$$r_{ij} = \frac{\frac{1}{K} \sum_k \left(x_{ik} - \frac{1}{K} \sum_{k'} x_{ik'} \right) \left(x_{jk} - \frac{1}{K} \sum_{k'} x_{jk'} \right)}{\sqrt{\frac{1}{K} \sum_k \left(x_{ik} - \frac{1}{K} \sum_{k'} x_{ik'} \right)^2 \frac{1}{K} \sum_k \left(x_{jk} - \frac{1}{K} \sum_{k'} x_{jk'} \right)^2}} \tag{5.16}$$

and to identify pairs of i and j associated with significant correlation. In the following, we will show some synthetic data set where pairwise computation of correlation does not work well while TD applied to a tensor generated from the product of two matrices, $x_{ijk} = x_{ik} x_{jk}$, can identify correlated pairs successfully.

In order for this purpose, we prepare data set 8 as follows.

Data set 8:

$$x_{ik} \sim \begin{cases} k + \mathcal{N}(\mu, \sigma) & i \leq N_1 \\ \mathcal{N}(\mu, \sigma) & \text{otherwise} \end{cases} \tag{5.17}$$

$$x_{jk} \sim \begin{cases} k + \mathcal{N}(\mu, \sigma) & j \leq M_1 \\ \mathcal{N}(\mu, \sigma) & \text{otherwise} \end{cases} \tag{5.18}$$

This means, only features $i \leq N_1$ and $j \leq M_1$ share the k dependence while no other pairs are correlated. In this setup, the number of positive (correlated) pairs is $N_1 \times M_1$ among total number of pairs, $N \times M$.

In order to see if pairwise correlation analysis can identify correlated pairs, we compute Pearson's correlation coefficients between all $N \times M$ pairs, x_{ik} and x_{jk}. Then computed correlation coefficient, r_{ij}, is converted to t_{ij} as

$$t_{ij} = \frac{r_{ij}(K-2)}{\sqrt{1-r^2}} \tag{5.19}$$

that is known to obey t distribution with the degrees of freedom of $K - 2$. Then P-values are computed using t distribution and are attributed to all of $N \times M$ pairs. These P-values are corrected by BH criterion and pairs associated with adjusted P-values less than 0.05 are considered to be correlated. Table 5.4 shows the confusion matrix averaged over 100 independent trials when $N = M = 100$, $N_1 = M_1 = 10$, $K = 6$, $\mu = \sigma = 1$. In this setup, the number of positive pairs is $N_1 \times M_1 = 100$. It is obvious that there are more false positives (38.49) than true positives (15.47). Thus, it unlikely works well. Next, we apply TD based unsupervised FE to data set 8 with generating case I type I tensor (Table 5.4) as Eq. (5.10). We apply HOSVD algorithm, Fig. 3.8, to data set 8. Figure 5.4a and b shows typical $\boldsymbol{u}_1^{(i)}$ and $\boldsymbol{u}_1^{(j)}$ obtained when HOSVD is applied to data set 8, respectively. These two have obviously larger absolute values for $i \leq N_1$ and $j \leq M_1$ than $i > N_1$ and $j > M_1$, respectively. This suggests that $\boldsymbol{u}_1^{(i)}$ and $\boldsymbol{u}_1^{(j)}$ can successfully identify features with correlations ($i \leq N_1$ or $j \leq M_1$) from those without correlations ($i > N_1$ or $j > M_1$). How it comes to be possible can be understood by observing $\boldsymbol{u}_1^{(k)}$ (Fig. 5.5). $\boldsymbol{u}_1^{(k)}$ clearly reflects the dependence upon k shown in Eqs. (5.17)

Table 5.4 Confusion matrices when statistical tests are applied to synthetic data sets 8 defined by Eqs. (5.17) and (5.18) and features associated with adjusted P-values less than 0.05 are selected for pairwise correlation and 0.1 for TD based unsupervised FE

	Pairwise correlation		TD based unsupervised FE			
Data set 8	$i \leq N_1$ and $j \leq M_1$	Otherwise	$i \leq N_1$	$N_1 < i$	$j \leq M_1$	$M_1 < j$
Selected	15.47	38.49	6.20	0.00	6.14	0.00
Not selected	84.53	9861.51	3.80	90.00	3.86	90.00

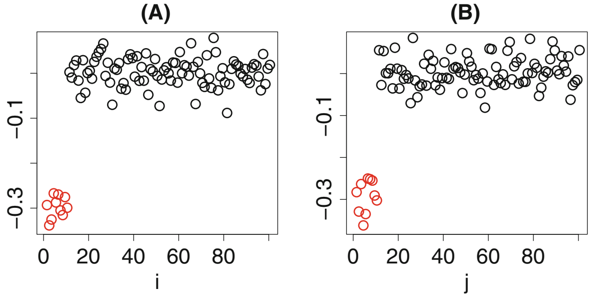

Fig. 5.4 A typical realization of $\boldsymbol{u}_1^{(i)}$ and $\boldsymbol{u}_1^{(j)}$ when Tucker decomposition, Eq. (3.2), with HOSVD algorithm, Fig. 3.8 is applied to data set 8, Eqs. (5.17) and (5.18) with $N = M = 100$, $N_1 = M_1 = 10$, $K = 6$, $\mu = \sigma = 1$. (**a**) $\boldsymbol{u}_1^{(i)}$, red and black open circles correspond to $i \leq N_1$ and $i > N_1$, respectively. (**b**) $\boldsymbol{u}_1^{(j)}$, red and black open circles correspond to $j \leq M_1$ and $j > M_1$, respectively

Fig. 5.5 $\boldsymbol{u}_1^{(k)}$ that corresponds to $\boldsymbol{u}_1^{(i)}$ and $\boldsymbol{u}_1^{(j)}$ shown in Fig. 5.4

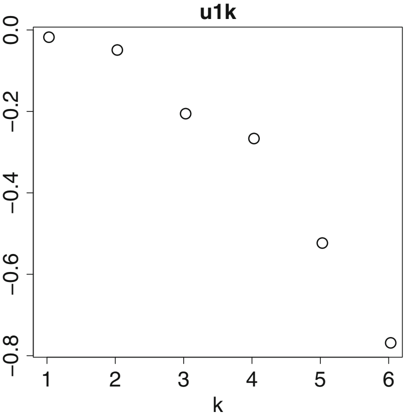

and (5.18). Since $G(1, 1, 1)$ is the largest among $G(\ell_1, \ell_2, 1)$, $\boldsymbol{u}_1^{(i)}$ and $\boldsymbol{u}_1^{(j)}$ naturally assign larger absolute values to $u_{1i}^{(i)}$ and $u_{1j}^{(j)}$ that shares embedded k dependence, i.e., $i \leq N_1$ or $j \leq M_1$.

In order to see if $u_{1i}^{(i)}$ and $u_{1j}^{(j)}$ are useful for the feature selection, P-values are attributed to i as Eq. (5.4) and j as

$$P_j = P_{\chi^2}\left[> \left(\frac{u_{1j}^{(j)}}{\sigma_1'} \right)^2 \right] \tag{5.20}$$

where σ_1' is the standard deviation of $u_{1j}^{(j)}$. Then is and js associated with adjusted P-value less than 0.1 are selected (performances are averaged over 100 independent trials). Table 5.4 shows the corresponding confusion matrices. Although the performance cannot be said very good, it is remarkable that there are no FP which are as many as 38.49 in pairwise correlation analysis (Table 5.4). TD based unsupervised FE also has more TPs than correlation analysis; 6.20 or 6.14 TPs among 10 positives versus 15.47 TP among 100 positives.

Only from this specific example, we cannot conclude that TD based unsupervised FE can always outperform the conventional methods. Nevertheless, in the application to the real data set that will be shown later, we will see that TD based unsupervised FE can achieve better performances than conventional supervised methods.

5.6 Identification of Correlated Features Using Type II Tensor

In the previous section, we can see that TD based unsupervised FE can correctly recognize the features with mutual correlation that cannot be recognized by conventional pairwise correlation analysis. In this section, we would like to see if type II tensor, Eq. (5.12), can samely identify features with mutual correlations using the same data set 8, Eqs. (5.17) and (5.18). In the present specific case, type II tensor can be defined as

$$\tilde{x}_{ij} = \sum_{k=1}^{K} x_{ijk} = \sum_{k=1}^{K} x_{ik} x_{jk}. \tag{5.21}$$

TD, or essentially it is SVD because HOSVD is equivalent to SVD when it is applied to matrix, is applied to $\tilde{x}_{ij}$. Figure 5.6 shows the comparison of $\boldsymbol{u}_1^{(i)}$ and $\boldsymbol{u}_1^{(j)}$ between type I and type II tensors. Although slight deviation can be observed, they

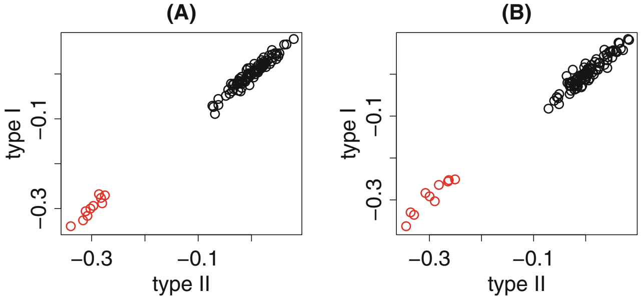

Fig. 5.6 Comparison between $\boldsymbol{u}_1^{(i)}$ and $\boldsymbol{u}_1^{(j)}$ in Fig. 5.4 and those when SVD is applied to type II tensor (matrix), $\tilde{x}_{ij}$, defined in Eq. (5.21). (**a**) $\boldsymbol{u}_1^{(i)}$, red and black open circles correspond to $i \leq N_1$ and $i > N_1$, respectively. (**b**) $\boldsymbol{u}_1^{(j)}$, red and black open circles correspond to $j \leq M_1$ and $j > M_1$, respectively

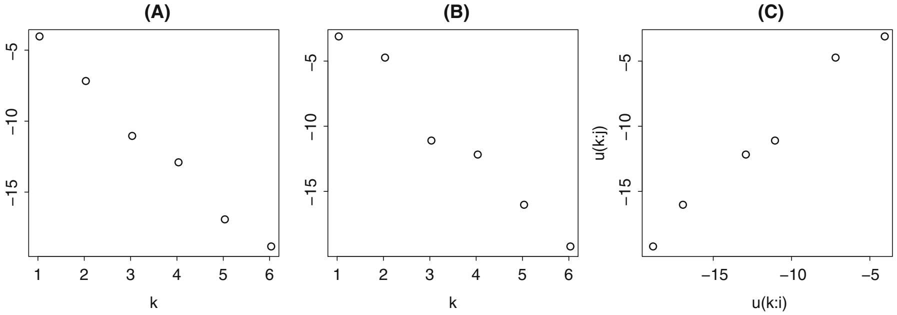

Fig. 5.7 Comparison between $\boldsymbol{u}_1^{(k:i)}$ and $\boldsymbol{u}_1^{(k:j)}$ computed by Eqs. (5.22) and (5.23), respectively. (**a**) $\boldsymbol{u}_1^{(k:i)}$ (**b**) $\boldsymbol{u}_1^{(k:j)}$, (**c**) scatterplot of (**a**) and (**b**)

are coincident enough to recognize features with mutual correlations, i.e., $i \leq N_1$ and $j \leq M_1$, respectively. Thus as long as considering feature selection, replacing type I tensor with type II tensor does not cause any problems.

Then we need to see if two vectors,

$$\boldsymbol{u}_1^{(k;i)} = X^{(ik)} \times_i \boldsymbol{u}_1^{(i)} \tag{5.22}$$

$$\boldsymbol{u}_1^{(k;j)} = X^{(jk)} \times_j \boldsymbol{u}_1^{(j)} \tag{5.23}$$

are coincident with each other and reflect k dependence when $\boldsymbol{u}_1^{(i)}$ and $\boldsymbol{u}_1^{(j)}$ are computed from type II tensor (matrix), Eq. (5.21). Figure 5.7 shows $\boldsymbol{u}_1^{(k:i)}$ and $\boldsymbol{u}_1^{(k:j)}$. They are not only coincident with each other, but also reflecting k dependence in Eqs. (5.17) and (5.18), respectively. Thus, replacing type I tensor with type II, at least in the present case, does not likely cause any problems.

5.7 Summary

In this chapter, we proposed feature section using TD, named TD based unsupervised FE. TD based unsupervised FE can outperform conventional supervised method when the number of samples is much less than the number of features and true classification is a complex function of apparent labeling. We also further extended the concept of tensor such that we can make use of TD based unsupervised FE even when only matrices are given. As a bi-product, we come to be able to select features with mutual correlations even when conventional pairwise correlation analysis fails. Nothing shown in this chapter are proven, but are only demonstrated by synthetic data set. Nonetheless, we will see that TD based unsupervised FE can work very well when it is applied to real examples, i.e., the applications toward bioinformatics in the later part of this book.

Reference

1. Taguchi, Y.H.: Tensor decomposition-based unsupervised feature extraction applied to matrix products for multi-view data processing. PLoS One **12**(8), e0183933 (2017). https://doi.org/10.1371/journal.pone.0183933

Part III
Applications to Bioinformatics

In this part, I explain the main purpose of this book, i.e., applications of PCA or TD based unsupervised FE to bioinformatics. Although I know that readers might not be very interested in biology, because data analyzed are real numbers formatted as matrices and tensors, methods themselves should be able to be applied to other data sets than biology. Starting from the introduction of fundamental knowledge required in order to understand examples presented in this part, various applications of PCA and TD based unsupervised FE will be discussed.

Chapter 6
Applications of PCA Based Unsupervised FE to Bioinformatics

I do not need any other reason to be born than being your friend.
Rikka Takarada, SSSS.GRIDMAN, Season 1, Episode 11

6.1 Introduction

PCA is an old technology. It has been invented more than a 100 years ago. Thus many might think that it is nothing but textbook level matter (in other words, nothing new to be worthwhile being investigated might not exist anymore). Especially, because modernized many non-linear methods have been proposed, people think that no linear methods can have any superiority toward these advanced technologies. In spite of such a general belief, PCA still might be an effective method. In this chapter, I propose to make use of PCA for unsupervised feature selection. The word "unsupervised feature selection" might sound like discrepancy. If so, please look at the following. I am sure that you can understand what I mean by this word and might start to think that PCA is still an effective method and is worthwhile investigating further.

6.2 Some Introduction to Genomic Science

Although it is unrealistic to fully explain fundamental genome biology required to understand the contents in this chapter, I will try to outline very basic points here to help readers to understand. Readers who would like to understand the contents more deeply should consult with fully mentioned textbooks, e.g., Genome 4th Edition [7].

Y-h. Taguchi, *Unsupervised Feature Extraction Applied to Bioinformatics*, Unsupervised and Semi-Supervised Learning,
https://doi.org/10.1007/978-3-030-22456-1_6

6.2.1 Central Dogma

Although it has become a little bit old fashioned, the so-called central dogma still remains a gold standard in genome science. Central dogma says that any functional proteins are translated from mRNA (translation) which is transcribed from DNA (transcription), not vice versa. Thus, fundamentally, study of DNA is an essential part of genome science. DNA is the abbreviation of deoxyribonucleic acid, which is a long chain of sequence composed of only four kinds of molecules: cytosine, guanine, adenine, and thymine, which are often abbreviated as using the first letters of words: C, G, A, and T. DNA is located in the nuclei of cells, which functions as information transporter between generations as well as acts as information resources from which cellular activities are decided. The way by which DNA stores information is digital and is in some sense similar to digital information in modernized computer or information science; it is fitted to be investigated with information science. This similarity between DNA and information science is a key factor from which bioinformatics was born.

DNA takes the form of double helix, which is generated by the pairing of two complementary DNA sequences. Among four molecules that form DNA, T, C, G, and A, A binds to T and G binds to C. Thus two DNA sequences that form double helix store the same information, like positive films and negative films in photography.

The objects fitted to be studied by information science in genome biology are not only DNA but mRNA and protein as well. mRNA is an abbreviation of messenger RNA and RNA is an abbreviation of ribonucleic acid. RNA is a partial copy of lengthy DNA sequence whose total length is as many as three billion (3×10^9) base pairs (in the case of human being). Only difference between DNA and RNA other than length is that uracil (U) is used instead of T in RNA; thus, four molecules that form RNA are A, U, G, and C. Protein is a long polymer composed of 20 amino acids, each of which is coded using triplet of nucleic acids in RNA and DNA sequence; these triplets are called as codon. Because the number of total codon is as many as $4^3 = 64$ while total number of amino acids used for generating proteins is as small as 20, multiple codons code the same amino acid. Some codons are also used as terminator that marks the point where transcription ends.

Proteins translated from mRNA form complex structure to function as blocks of organisms, enzyme that accelerates the chemical reactions, and vehicle that transports something within body. The three-dimensional (tertiary) structures are believed to be dependent upon only amino acid sequence, although the strict relationship between amino acid sequence and protein tertiary structure has not yet been known.

6.2.2 Regulation of Transcription

The mostly focused process in this and the next chapter is transcription [55]. There are multiple reasons why transcription is mostly focused.

- Because of high throughput technologies including microarray and high throughput sequencing (HTS), RNA and DNA have become the easiest parts to be measured.
- In contrast to the proteins whose tertiary structure is heavily related to the functions, the functions of RNA and DNA are primarily related to sequence only. Thus, we do not need to perform downstream analysis of the structures of RNA and DNA so much.
- Non-coding RNAs which do not have any proteins translated from them have many functions to regulate transcription itself.

Thus, DNA sequence, RNA sequence, and the amount of transcript (i.e., RNA) are mainly measured and studied extensively. Thus, the application of PCA based unsupervised FE is much easier to be applied to DNA and RNA sequence as well as the mount of transcripts.

6.2.3 The Technologies to Measure the Amount of Transcript

Measuring the amount of RNA is essentially the count of the number of RNA transcribed from DNA. There are two major methods of high throughput measurements of the amount of RNA [54]; one is microarray and the other is high throughput sequencing. Microarray is the technology that prepares numerous probes that specifically bind to individual RNAs; the amount of RNA that binds to probe is measured by photo emission from the fluorescent molecules that decorate RNA. HTS employs more direct strategy to measure RNA. HTS tries to count the number of RNA by sequencing each RNA. One point that must be taken into account is that HTS can measure only fragments of individual RNAs, not a full length one. Thus, after counting the number of fragments, each fragment must be annotated in the reference of external resources (e.g., as a part of known gene). Although there are numerous ways to sequence RNA, we are not willing to explain the details of sequencing technology. Only essential point to be explained to understand the contents in the book is that the output from microarray is real number while the output from HTS is integer. In addition to this, although output from HTS is guaranteed to be proportional to the amount of transcript, that from microarray is not. The output of microarray is often translated to logarithmic values because logarithmic values more likely obey Gaussian distribution, which is believed to be a natural outcome.

6.2.4 Various Factors that Regulate the Amount of Transcript

Although it is not fully understood yet, various factors regulate transcription [54, 55]. In this subsection, I try to explain how some factors control gene expression via regulation of transcription. Most important known factors that regulate transcription are undoubtedly transcription factors (TFs). TFs are usually composed of proteins that bind to DNA region known as prompter. TFs primarily control the transcription initiation. One possible problem from the point of data analysis is that TFs are proteins. As mentioned above, the most easiest factor to be measured is not protein but RNA. Because of that, TFs are not frequently to be targets of investigations in this and the next chapter. The second major factor that regulates transcription is methylation. If promoter region is methylated, TF is forbidden to bind to the region. As a result, the transcription of RNAs whose promoter is methylated is disturbed. In addition to this, DNA methylation is heritable during DNA replication that takes place in cell duplication. Thus DNA methylation can affect transcription for longer period than other factors. The additional factors that can regulate transcription in the post transcription process is microRNA (miRNA). miRNAs are RNAs not translated to proteins but have functions; their functions are to destroy RNAs before translation takes place. Each miRNA can identify each target mRNA by the complementary binding to 8 bp length seed region within $3'$ untranslated region (UTR) of mRNA (the term $3'$ is used to identify which edge of mRNA is targeted). UTR is region of mRNA that are not translated to protein. Although there are more factors that can affect transcription, DNA methylation and miRNA expression are mostly the factors analyzed in this and the forthcoming chapters. mRNA that is not translated to protein.

6.2.5 Other Factors to Be Considered

Some other factors that can affect transcription will be discussed time to time. Single nucleotide polymorphism (SNP) is the replacement of single nucleotide in DNA. Although there are many reasons that cause SNP, it is primarily caused by miss-duplication of DNA during cell division. Until now, although SNP is primarily considered to alter amino acid sequence of protein, it can also affect transcription. For example, SNP in promoter region or $3'$ UTR region can affect the binding between TF and DNA or that between miRNA and mRNA, thus affect the transcription. Although it is not extensively investigated, SNP and transcription are mutually interacted.

Histone modification is another factor that regulates transcription. Histone is protein around which DNA winds. This process is necessary in order that long DNA chain does not get tangled up. DNA that tightly winds around histone cannot be transcribed because no TFs can bind to it. Because histone modification that means that small molecules bind to histone tale can affect how tightly DNA can wind round histone, histone modification is additional factor that can affect transcription.

Finally, although it is not so frequently analyzed, proteome and metabolome can be treated. Proteome is a set of protein translated. Their amount can be causes or outcome of transcription. Metabolome is a set of compounds generated as a consequence of chemical reaction to which some proteins take place as enzyme. Thus, metabolome is, indirectly, affected by transcription.

Integrated analysis of these factors is often annotated as multi-omics data analysis, because it integrates genome, transcriptome, proteome, metabolome, i.e., several "-ome" data sets.

6.3 Biomarker Identification

Although PCA based unsupervised FE is applied to various bioinformatics topics, we would like to start from identification of biomarker; biomarker is a kind of disease marker that can tell you about your healthy status. When you can take health check, various factors are measured from blood and urine. You will be warned if some of the measured components have non-standard values. Identification of biomarkers is very important to facilitate diagnosis, as medical knowledge is not required. In this sense, most readers are not considered to be medical professionals, so identifying biomarkers is likely to be the most understandable to readers. Thus, beginning to explain the identification of biomarkers that require less medical knowledge, readers who are not medical experts may not be as stressful.

6.3.1 Biomarker Identification Using Circulating miRNA

Circulating miRNA means miRNAs that circulate in the body. For example, blood miRNA is a typical circulating miRNA. The reason why biomarkers are searched within circulating miRNA is as follows. At first, obtaining circulating miRNA is less painful than getting tissue miRNAs that are expected to be more likely directly related to diseases than blood miRNA. In order to obtain tissue miRNA, one needs surgery or needle biopsy that inevitably injures patients body and results in some pain. In order to get blood, there need to be also needle but with less pain. Thus, if we can find useful disease biomarker in the blood, it is very convenient. On the other hand, identification of disease biomarker using circulating miRNA is more challenging than that using tissue miRNA, because circulating miRNA reflects whole body state that is not always related to specific disease. Thus, from the data science point of view, identification of disease biomarker using circulating miRNA might be challenging and interesting.

6.3.1.1 Biomarker Identification Using Serum miRNA

As the first example, we consider serum miRNAs [56]. Serum is the liquid component of blood that does not include either blood vessels or clotting factors. Serum is also supposed to contain all proteins (other than those contributing to blood clotting), electrolytes, antibodies, antigens, hormones, and any exogenous substances. Thus, it is suitable to search biomarker in it.

Table 6.1 List of serum miRNAs samples

k	Group	Number of samples (M_k)
0	Controls	70
1	Lung cancer	32
2	Prostate cancer	23
3	Melanoma	35
4	Wilms tumors	5
5	Ovarian cancer	15
6	Gastric cancers	13
7	Pancreatic ductal adenocarcinoma	45
8	Other pancr. tumors and diseases	48
9	Pancreatitis	38
10	Chronic obstructive pulmonary disease	24
11	Periodontitis	18
12	Sarcoidosis	45
13	Acute myocardial infarction	20
14	Multiple sclerosis	23

Here we make use of serum miRNA data set that is publicly available [24]. It includes serum miRNAs measurements for 14 diseases and healthy controls (Table 6.1). Although it does not always include enough number of samples in individual diseases in the recent standards (because it was 6 years ago when I performed this study), because I believe that it is a good intuitive example from which the explanation starts, I introduce the application of PCA based unsupervised FE to them. The expression of miRNAs was measured by microarray technology. It includes only 863 human miRNAs, because it is an old study. Nowadays, more number of human miRNAs are identified. For example, the most recent miRBase [25] (http://www.mirbase.org/index.shtml, version 22), which is a primary miRNA database that is periodically updated, includes as many as 1917 pre-miRNAs, each of which usually includes two complementary miRNAs (Thus, the most updated version includes c.a. 4000 miRNAs). The full data set of used gene expression profiles is available from Gene Expression Omnibus (GEO) [44] with GEO ID, GSE31568.

Although I am not interested in describing how to retrieve gene expression from GEO, I briefly introduce about it. GEO includes multiple format of gene expression: typically processed (normalized) one and raw one. The former is the one after the correction assuming some hypothesis, e.g., background correction. As mentioned above, microarray measures gene expression with light emission. Thus, measurement of gene expression by microarray is quite indirect. In order to compensate the errors and biases introduced by this technology, gene expression is often corrected based upon some assumption. Nevertheless, as can be seen in the below, PCA based unsupervised FE can make use of raw (unprocessed) data quite successfully (throughout the application of PCA and TD based unsupervised FE, it will not be very usual to use processed data).

Then, also in this case, I downloaded raw data set, GSE31568_raw.txt.gz.[1] This file includes all miRNA expression listed in Table 6.1 as one file. The first row excluding header line that includes GEO ID of individual samples annotates distinction between controls and diseases. Then we generated gene expression profiles as a form of matrix, $x_{ij}^{(k)} \in \mathbb{R}^{863\times(M_0+M_k)}$, that represents ith miRNA expression of jth sample where $M_0(=70)$ and $M_k, 1 \leq k \leq 14$ are the number of controls and the kth disease samples, respectively.

In order to apply PCA based unsupervised FE to $x_{ij}^{(k)}$, PCA is applied to it such that PC scores, $\boldsymbol{u}_\ell^{(k)} \in \mathbb{R}^{863}$, are attributed to miRNAs and PC loading, $\boldsymbol{v}_\ell^{(k)} \in \mathbb{R}^{M_0+M_k}$, are attributed to samples. Unfortunately, we cannot identify PC loadings associated with distinction between healthy controls and patients. Then, empirically, we employ the following strategy to select miRNAs used for biomarkers. At first, compute length, r_i, of PC score as

$$r_i = \sqrt{\sum_{\ell=1}^{2} u_{\ell i}^2}. \tag{6.1}$$

Then top ranked 10 miRNAs with larger r_i are selected. Table 6.2 shows the list of miRNAs selected for each of 14 pairs composed of controls and patients of one of 14 diseases. Interestingly, miRNAs selected in each of 14 pairs are heavily overlapped. In spite of that 140 miRNAs are selected in total, there are only twelve miRNAs. Nine out of twelve miRNA are selected in all of fourteen pairs of control and patients.

Although it is interesting that selected miRNAs are highly overlapped between fourteen diseases, because no PC loading exhibits distinction between controls and diseases, it might not be related to biology at all. In order to see this, we try to make use of these miRNAs selected in order to discriminate between controls and diseases. If they can, they are considered to be disease biomarkers.

In order that, we employ the following strategy. Instead of full size miRNA expression profile matrix, $x_{ij}^{(k)} \in \mathbb{R}^{863\times(M_0+M_k)}$, we prepare reduced miRNA expression profile, $x_{ij}^{(k)'} \in \mathbb{R}^{10\times(M_0+M_k)}$ that includes selected 10 miRNAs only. Then PCA is applied to $x_{ij}^{(k)'}$ again in order to get PC loading, $\boldsymbol{v}_\ell^{(k)'} \in \mathbb{R}^{M_0+M_k}$, attributed to samples. Then the first L PC loading, $\boldsymbol{v}_\ell^{(k)'}, \ell \leq L$, are used to linear discriminant analysis (LDA) in order to discriminate between controls and diseases.

Here LDA is a classical method to discriminate between multiple classes using linear algebra. In order to perform LDA, we need to compute several variables. Then new variable $y_j \in \mathbb{R}^{M_0+M_k}$ is defined as

$$y_j = \boldsymbol{a} \times_\ell \left(\boldsymbol{v}_j^{(k)'} - \left\langle \boldsymbol{v}_j^{(k)'} \right\rangle_j\right) = \boldsymbol{a} \times_\ell \delta\boldsymbol{v}_j^{(k)'} \tag{6.2}$$

[1] ftp://ftp.ncbi.nlm.nih.gov/geo/series/GSE31nnn/GSE31568/suppl/GSE31568_raw.txt.gz.

Table 6.2 Twelve miRNAs selected by applying PCA based unsupervised FE to each of pairs of controls and the kth disease in Table 6.1. ○: selected, ×: not selected

k(diseases)	1	2	3	4	5	6	7	8	9	10	11	12	13	14	Suffix
miR-425	○	○	○	○	○	○	○	○	○	○	○	○	○	○	5p
miR-191	○	○	○	○	○	○	○	○	○	○	○	○	○	×	5p
miR-185	○	○	○	○	○	○	○	○	○	○	○	○	○	○	5p
miR-140-3p	○	○	○	○	○	○	○	○	○	○	○	○	○	○	3p
miR-15b	○	○	○	○	○	○	○	○	○	○	○	○	○	○	5p
miR-16	○	○	○	○	○	○	○	○	○	○	○	○	○	○	5p
miR-320a	○	○	○	○	○	○	○	○	○	○	○	○	○	○	
miR-486-5p	○	○	○	○	○	○	○	○	○	○	○	○	○	○	5p
miR-92a	○	○	○	○	○	○	○	○	○	○	○	○	○	○	3p
miR-19b	○	×	○	×	×	×	○	×	×	×	×	×	×	○	3p
miR-106b	×	○	×	○	○	○	×	○	○	○	○	×	○	○	5p
miR-30d	×	×	×	×	×	×	×	×	×	×	×	○	×	×	5p

Suffix suggested that coincident with most recent miRBase v. 22

with deciding $\boldsymbol{a} \in \mathbb{R}^L$ such that y_j discriminates controls and diseases where

$$\boldsymbol{v}_j^{(k)\prime} = \left(v^{(k)\prime}{}_{1j}, v^{(k)\prime}{}_{2j}, \ldots, v^{(k)\prime}{}_{Lj}\right). \tag{6.3}$$

In order to decide $\boldsymbol{a}$, we need to compute in-class centroid as

$$\langle y_j \rangle_j^{(k)} = \begin{cases} \frac{1}{M_k} \sum_{j=1}^{M_k} y_{M_0+j} & k \neq 0 \\ \frac{1}{M_0} \sum_{j=1}^{M_0} y_j & k = 0 \end{cases} \tag{6.4}$$

which is also written as

$$\langle y_j \rangle_j^{(k)} = \begin{cases} \boldsymbol{a} \times_\ell \left\langle \delta \boldsymbol{v}_j^{(k)\prime} \right\rangle_j^{(k)} & k \neq 0 \\ \boldsymbol{a} \times_\ell \left\langle \delta \boldsymbol{v}_j^{(0)\prime} \right\rangle_j^{(0)} & k = 0 \end{cases}. \tag{6.5}$$

The task is maximizing the difference between in-class centroid

$$\begin{aligned} \triangle^{(k)} &= \left(\langle y_j \rangle_j^{(k)} - \langle y_j \rangle_j^{(0)} \right)^2 && (6.6) \\ &= \boldsymbol{a} \times_\ell \left[\left\{ \left\langle \delta \boldsymbol{v}_j^{(k)\prime} \right\rangle_j^{(k)} - \left\langle \delta \boldsymbol{v}_j^{(0)\prime} \right\rangle_j^{(0)} \right\} \times^0 \left\{ \left\langle \delta \boldsymbol{v}_j^{(k)\prime} \right\rangle_j^{(k)} - \left\langle \delta \boldsymbol{v}_j^{(0)\prime} \right\rangle_j^{(0)} \right\} \right] \times_{\ell'} \boldsymbol{a} && (6.7) \\ &\equiv \boldsymbol{a} \times_\ell \varSigma_B \times_{\ell'} \boldsymbol{a} && (6.8) \end{aligned}$$

relative to summation of in-class variances

$$\begin{aligned} \triangle^{(0,k)} &= \left\langle \left(y_j - \langle y_{j'} \rangle_{j'}^{(k)} \right)^2 \right\rangle_j^{(k)} + \left\langle \left(y_j - \langle y_{j'} \rangle_{j'}^{(0)} \right)^2 \right\rangle_j^{(0)} && (6.9) \\ &= \boldsymbol{a} \times_\ell \left[\left\{ \delta \boldsymbol{v}_j^{(k)\prime} - \left\langle \delta \boldsymbol{v}_j^{(k)\prime} \right\rangle_j^{(k)} \right\} \times^0 \left\{ \delta \boldsymbol{v}_j^{(k)\prime} - \left\langle \delta \boldsymbol{v}_j^{(k)\prime} \right\rangle_j^{(k)} \right\} \right] \times_{\ell'} \boldsymbol{a} && (6.10) \\ &+ \boldsymbol{a} \times_\ell \left[\left\{ \delta \boldsymbol{v}_j^{(0)\prime} - \left\langle \delta \boldsymbol{v}_j^{(0)\prime} \right\rangle_j^{(0)} \right\} \times^0 \left\{ \delta \boldsymbol{v}_j^{(0)\prime} - \left\langle \delta \boldsymbol{v}_j^{(0)\prime} \right\rangle_j^{(0)} \right\} \right] \times_{\ell'} \boldsymbol{a} && (6.11) \\ &\equiv \boldsymbol{a} \times_\ell \varSigma_W \times_{\ell'} \boldsymbol{a} && (6.12) \end{aligned}$$

It is known that this task can be performed by maximizing

$$L(\boldsymbol{a}, \lambda) = \triangle^{(k)} - \lambda \left(\triangle^{(0,k)} - 1 \right) \tag{6.13}$$

with respect to $\boldsymbol{a}$ and λ, which is also known as method of Lagrange multipliers. It is equivalent to maximize $\triangle^{(k)}$ with keeping $\triangle^{(0,k)} = 1$. In order to find $\boldsymbol{a}$ that maximizes $L(\boldsymbol{a}, \lambda)$, we require that derivatives of $L(\boldsymbol{a}, \lambda)$ with respect to $\boldsymbol{a}$ must be zero.

$$\frac{\partial L(\boldsymbol{a}, \lambda)}{\partial \boldsymbol{a}} = 2\left(\Sigma_B \times_{\ell'} \boldsymbol{a} - \lambda \Sigma_W \times_{\ell'} \boldsymbol{a}\right) = 0. \tag{6.14}$$

This is equivalent to eigenvalue problem

$$\Sigma_W^{-1} \Sigma_B \boldsymbol{a} = \lambda \boldsymbol{a} \tag{6.15}$$

and $\boldsymbol{a}$ can be obtained as the first eigenvector. LDA can be performed to find y_0 such that the distinction between two sets, $y_j < y_0$ and $y_j > y_0$, is maximally coincident with distinction between controls and diseases.

Table 6.3 shows the performance measured using leave one out cross validation (LOOCV). In LOOCV, one of $M_0 + M_k$ samples is removed from computing LDA, and y_j for removed one is computed by Eq. (6.4) using obtained $\boldsymbol{a}$. Then, it is discriminated if $y_j > y_0$ or $y_j < y_0$. This procedure is repeated for all $M_0 + M_k$ samples.

The reason why LOOCV is required is as follows. If LDA is performed considering all samples, it cannot be said to be true prediction since we know the classification of the sample whose classification is tried to predict. In real situation, biomarker must predict sample classification without knowing the answer. Thus LDA should be performed excluding a sample of which classification is tried to be predicted.

Table 6.3 Various performance achieved by LDA (with LOOCV) using PC loading computed by 10 miRNAs selected by PCA based unsupervised FE

k	Group	L	Accuracy	Specificity	Sensitivity	Precision
1	Lung cancer	5	0.784	0.800	0.750	0.632
2	Prostate cancer	5	0.806	0.800	0.826	0.576
3	Melanoma	10	0.867	0.857	0.886	0.756
4	Wilms tumors	7	0.867	0.886	0.600	0.273
5	Ovarian cancer	6	0.800	0.786	0.867	0.464
6	Gastric cancers	9	0.806	0.800	0.826	0.576
7	Pancreatic ductal adenocarcinoma	2	0.765	0.743	0.800	0.667
8	Other pancr. tumors and diseases	7	0.814	0.771	0.875	0.724
9	Pancreatitis	8	0.933	0.786	0.921	0.700
10	Chronic Obstructive Pulmonary Disease	2	0.713	0.671	0.833	0.465
11	Periodontitis	10	0.807	0.814	0.778	0.519
12	Sarcoidosis	10	0.835	0.800	0.889	0.741
13	Acute myocardial infarction	7	0.789	0.900	0.757	0.964
14	Multiple sclerosis	10	0.892	0.871	0.957	0.710

In Table 6.3, there are many performance measures. Here I briefly explain them based upon confusion matrix (Table 4.8) as

$$\text{Accuracy} = \frac{TP + TN}{TP + TN + FP + FN}, \tag{6.16}$$

$$\text{Specificity} = \frac{TN}{TN + FP}, \tag{6.17}$$

$$\text{Sensitivity} = \frac{TP}{TP + FN}, \tag{6.18}$$

$$\text{Precision} = \frac{TP}{TP + FP}. \tag{6.19}$$

Accuracy measures the ratio of the number of correctly predicted samples to the number of total samples. Specificity measures the ratio of the number of correctly predicted control samples to the number of control samples. Sensitivity measures the ratio of the number of correctly predicted disease samples to the number of disease samples. Precision measures the ratio of the number of correctly predicted disease samples to the number of samples predicted as diseases.

Generally, the performance in Table 6.3 is quite well if we consider the performance is achieved in the fully unsupervised manner. This suggests that PCA based unsupervised FE can be useful even when it is applied to the real applications.

One might wonder if this performance must be evaluated based upon the comparisons with other methods. Before starting to discuss this point, I would like to point out one important point specific to this application. In this application, selecting miRNAs as small as possible is important, because measuring more miRNAs costs more in practical applications. In addition to this, the selected miRNAs should not be dependent upon sets of samples considered. If the best selected miRNAs vary from samples to samples, it becomes useless. From this point of view, PCA based unsupervised FE is superior to other supervised methods. As mentioned above, we can select miRNAs using all samples even including samples whose classification is tried to predict because we did not use classification of samples at all. In the real application, we can do as follows. Suppose we have both samples with known classification and those without known classification. Then apply PCA to all samples including both. Select top 10 miRNAs using distanced computed with the first and the second PC scores shown in Eq. (6.1). PC loading is recomputed using selected 10 miRNAs. These all processes can be done without knowing sample classifications at all.

Actually, Keller et al. [24] failed to select a set of fixed 10 miRNAs, because they needed to excluded samples to be predicted. This results in distinct set of miRNAs selected depending upon the samples excluded. Thus, before comparing performance by other methods with those by PCA based unsupervised FE, primarily we have to know if other methods can select stable feature selection without strong sample dependency.

In order to evaluate stability we define the stability test as follows.

1. Select randomly 90% of samples within control M_0 samples and disease M_k samples, respectively.
2. Apply PCA to $x_{ij} \in \mathbb{R}^{N \times 0.9(M_0+M_k)}$.
3. Select top 10 miRNAs using r_i defined in Eq. (6.1).
4. Repeat the process over independent 100 trials and count miRNAs selected in all 100 trials

When applying this stability test to PCA based unsupervised FE, although there are 140 miRNAs selected for pairwise 14 discrimination where 10 miRNAs are selected, 129 miRNAs are always selected when the above stability test is applied to PCA based unsupervised FE. Thus, feature selection with PCA based unsupervised FE is quite stable.

Next we apply stability test to t test which Keller et al. [24] employed. In this case, in step 3, P-values computed by t test are used for selecting miRNAs instead of r_i. Then only 40 miRNAs among 140 selected miRNAs are always selected. This means that t test is quite inferior to PCA based unsupervised FE from the point of stability.

In order to confirm the superiority of PCA based unsupervised FE towards other supervised methods from the point of stability, we also apply stability test to significance analysis of microarrays (SAM) [65], gene selection based on a mixture of marginal distributions (gsMMD) [35], ensemble recursive feature elimination (RFE) [1]. The performance of these advanced supervised methods from the point of stability is quite disappointing. Among 140 miRNAs selected, only 30, 5, 1, 1, 0 miRNAs are always selected when stability test is applied to SAM, up- and downregulation by gsMMD, RFE, ensemble RFE. It is quite obvious that more advanced methods proposed to achieve better discrimination are inferior to PCA based unsupervised FE from the point of stability.

We cannot emphasize too much the importance of stability of feature selection here, although it is generally overlooked. As one can see in the below, PCA based unsupervised FE is always outstanding over the conventional supervised methods from this point of view, stability.

In order to clarify if this superiority of PCA based unsupervised FE is because of its unsupervised nature, we try here additional unsupervised method, unsupervised feature filtering (UFF) [67]. UFF is SVD based unsupervised method. Because SVD is in some sense equivalent to PCA as mentioned in the earlier part of this book, UFF has similar theoretical base to that of PCA based unsupervised FE. UFF makes use of entropy computed by SVD. Entropy H is defined as

$$\rho_i = \frac{\lambda_i^2}{\sum_{i=1}^N \lambda_i^2} \tag{6.20}$$

$$H = -\frac{1}{\log N} \sum_{i=1}^N \rho_i \log \rho_i \tag{6.21}$$

where N is the number of feature (in this example, the number of miRNAs). λ_i is singular value when SVD is applied to x_{ij}. H represents how complicated structure x_{ij} has. When λ_i is constant, i.e., there are no structures at all, $\rho_i = \frac{1}{N}$ and $H = 1$. On the other hand, when $\lambda_i \neq 0$ only for one specific i, because $\rho_i = 1$ and $\rho_{i'} = 0, i' \neq i$, $H = 0$. In UFF we compute H without ith feature as

$$H_i = -\frac{1}{\log N} \sum_{i' \neq i} \rho_{i'} \log \rho_{i'}. \tag{6.22}$$

Then we have selected top 10 miRNAs having larger $\Delta H_i = H - H_i$. Interestingly, stability test applied to UFF results in 111 always selected miRNAs among 140 miRNAs. This number is comparative with 129 miRNAs achieved by PCA based unsupervised FE. Thus, the reason why PCA based unsupervised FE outperformed other conventional supervised methods from the point of stability is likely because of unsupervised nature.

Finally, we discuss the difference between two unsupervised methods: PCA based unsupervised FE and UFF. In UFF, SVD must be repeated as many as times equal to the number of features, which can often become 10^4 in the case that mRNAs are considered as a feature. On the other hand, PCA based unsupervised FE requires PCA only once. Thus computationally, UFF is far more challenging than PCA based unsupervised FE. Thus as far as these two methods achieve competitively, there are no needs to employ UFF than PCA based unsupervised FE.

Although the readers might be primarily interested in statistical methods themselves, not in biology, I briefly explain how we can evaluate the outcome also using domain knowledge, i.e., the knowledge is outside the statistical analysis and only in the biology. It is also important that the outcome driven from statistical methods is coincident with the domain knowledge from the biological point of view, because the coincidence with domain knowledge supports the reliability of statistical methods employed.

Although it is not mathematical, the so-called literature search is a powerful method. Simply searching database for the coincidence, one can easily get evidences that support outcome. Among the diseases listed in Table 6.1 there are multiple cancers included (lung cancer, prostate cancer, melanoma, Wilms tumor, ovarian cancer, gastric cancer, pancreatic ductal adenocarcinoma). Thus, it is not a bad idea to seek database with the words e.g., “cancer” and the name of specific miRNAs. The most useful database for this purpose is pubmed[2] that corrects titles and abstract of the papers published in major biological journals. With the search of “cancer” and “miR-425,” the readers can easily find that the miR-425 is known to be oncogenic, i.e., expressive in cancer. Thus, inclusion of miR-425 into one of biomarkers for diseases including many cancers is reasonable.

[2] https://www.ncbi.nlm.nih.gov/pubmed/.

On the other hand, it is not so straightforward. Since we have employed PCA and LDA that are linear methods in order to select and construct biomarker, we can easily evaluate if the expression of miR-425 contributes positively or negatively to identify disease samples besides normal control.

From Eq. (2.21),

$$\boldsymbol{v}_\ell^{(k)'} = \frac{1}{\lambda'_\ell} X^{(k)'T} \boldsymbol{u}_\ell^{(k)'} \tag{6.23}$$

where λ'_ℓ is the singular value which is obtained by square root of the ℓth eigenvalue computed by PCA. $X^{(k)'}$ is the matrix whose component is $x_{ij}^{(k)'} \in \mathbb{R}^{10\times(M_0+M_k)}$, $\boldsymbol{u}_\ell^{(k)'} \in \mathbb{R}^{10}$ is the PC score computed by applying PCA to X'.

$$v_{\ell j}^{(k)'} = \frac{1}{\lambda'_\ell} \boldsymbol{x}_j^{(k)'} \times_i \boldsymbol{u}_\ell^{(k)'} \tag{6.24}$$

where $\boldsymbol{x}_j^{(k)'} = \left(x_{1j}^{(k)'}, \ldots, x_{10j}^{(k)\,'}\right)$.

$$y_j = \boldsymbol{a} \times_\ell \left\{ \left(\boldsymbol{x}_j^{(k)'} - \left\langle \boldsymbol{x}_j^{(k)'} \right\rangle_j \right) \times_i U^{(k)'} \right\} \tag{6.25}$$

where

$$U^{(k)'} = \left(\frac{\boldsymbol{u}_1^{(k)'}}{\lambda'_1}, \ldots, \frac{\boldsymbol{u}_L^{(k)'}}{\lambda'_L} \right) \in \mathbb{R}^{10\times L} \tag{6.26}$$

Then we can compute the contribution from the ith miRNA to y_j as

$$y_{ij} = \left(\boldsymbol{a} \times_\ell \boldsymbol{u}_i^{(k)'} \right) \cdot \left(x_{ij}^{(k)'} - \left\langle x_{ij}^{(k)'} \right\rangle_j \right) \tag{6.27}$$

where

$$\boldsymbol{u}_i^{(k)'} = \left(\frac{u_{1i}^{(k)'}}{\lambda'_1}, \ldots, \frac{u_{Li}^{(k)'}}{\lambda'_L} \right) \in \mathbb{R}^L \tag{6.28}$$

When $y_j > y_0$ corresponds to disease, i with $\boldsymbol{a} \times_\ell \boldsymbol{u}_i^{(k)'} > 0$ is considered to contribute to disease positively, because upregulation of ith miRNA in jth sample enhances the tendency that the jth sample is identified as disease sample.

Figure 6.1 shows $\boldsymbol{a} \times_\ell \boldsymbol{u}_i^{(k)'}$ whose signs are assigned such that upregulation of ith miRNA in jth sample enhances the tendency that the jth sample is identified as disease sample. In contrast to expectation, miR-425 identified as oncogenic has

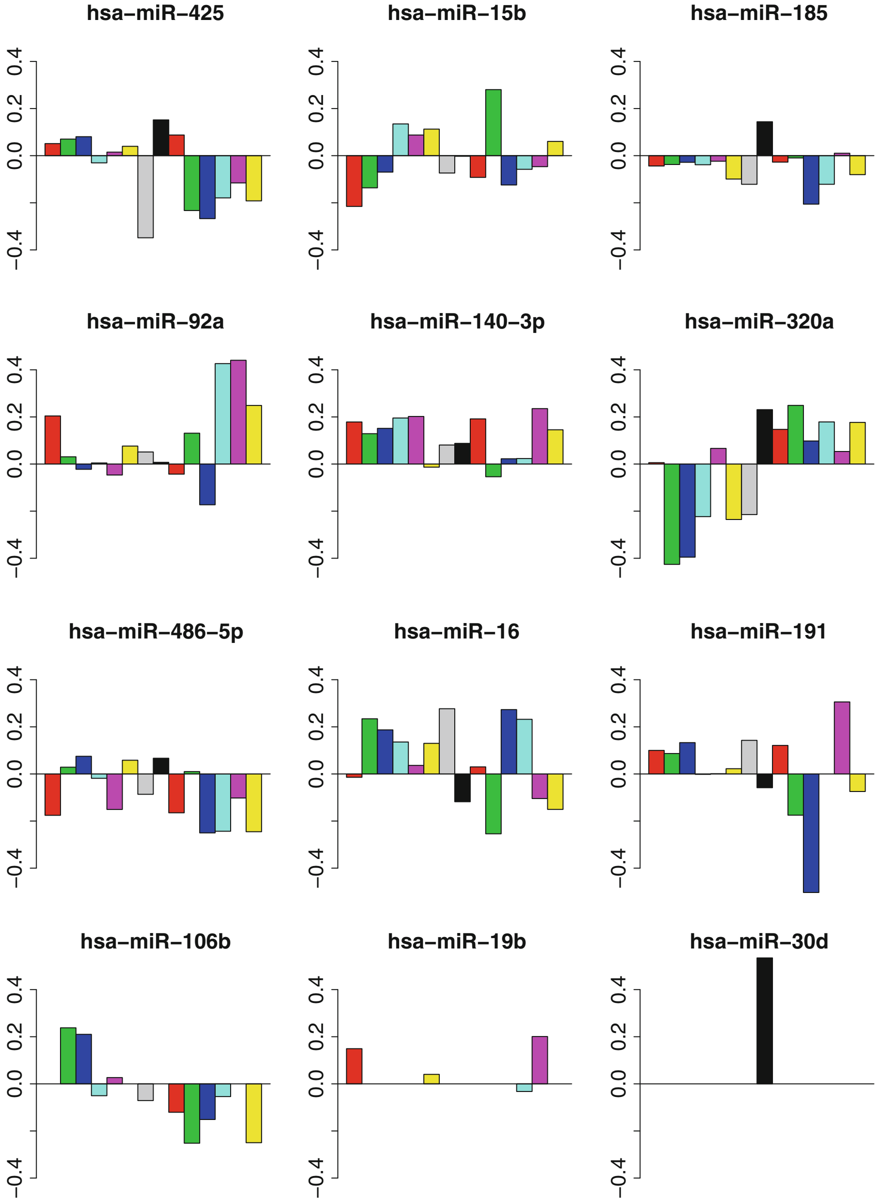

Fig. 6.1 The contribution of the ith miRNA in the jth sample toward each disease, $\boldsymbol{a} \times_\ell \boldsymbol{u}_i^{(k)\prime}$, whose sign is assigned such that upregulation contributes to identification that jth sample is identified as disease. From left to right, diseases are lung cancer (red), other pancreatic tumors and diseases (green), pancreatitis (blue), ovarian cancer (cyan), COPD (pink), ductal pancreatic cancer (yellow), gastric cancer (gray), sarcoidosis (black), prostate cancer (red), acute myocardial infarction (green), periodontitis (blue), multiple sclerosis (cyan), melanoma (pink), and Wilms tumor (yellow)

mainly negative values. Thus, although inclusion of miR-425 as disease biomarker is reasonable, the effect is opposite to the expectation. This suggests that consulting to domain knowledge is very useful to validate the outcome from statistical analysis. This observation can be a start point why serum miRNA can have opposite sign to that in tissues which really contributes to diseases. Although we are not willing to discuss this point comprehensively, after further literature search, miR-486 is tumor suppressor, miR-92a and miR-106b are oncogenic.

I would like to emphasize that the present strategy that relates $\boldsymbol{a} \times_\ell \boldsymbol{u}_i^{(k)\prime}$ to the outcome is helpful to interpret the functions of individual features. Thus, it should be employed in any other data science research.

Another strategy that validates outcome obtained statistically is more biology oriented in the sense that it makes use of biological knowledge fully. As mentioned above, miRNAs have their own targets whose numbers range from tens to hundreds. Because targeted mRNAs have their own functions, miRNAs can be validated along the biological concepts if their target mRNAs functions are evaluated. It is called enrichment analysis. Suppose that in total there are N genes among which N_1 genes' mRNAs are targeted by a specific miRNA. On the other hand, suppose that there is a set of N_2 genes that share some specific function. In this situation, suppose that there are $N_{12}(\leq N_1, N_2)$ genes that not only are targeted by the considered miRNAs but also have the specific function. Then Fisher's exact test checks if the number of overlap is more than that of those by accident or not. In order to perform Fisher's exact test, we need to make the table that represents this situation. Assuming that whether an mRNA is targeted by the miRNA or not is not related to whether the mRNA has the function or not, Fisher found [14] that the situation shown in Table 6.4 occurs with the probability

$$P(N_{12}) = \frac{(N-N_1)!N_1!(N-N_2)!N_2!}{(N-N_1-N_2+N_{12})!(N_2-N_{12})!(N_1-N_{12})!N_{12}!} \tag{6.29}$$

P-values can be computed by summing up probability equation (6.29) for N_{12} larger than real observation. Fisher's exact test can evaluate the accidental probability that the miRNA's target mRNAs are associated with the specific function. If P-values corrected with multiple comparison criterion (e.g., BH criterion) is small enough, we can insist that the specific miRNA is likely related to this function. This can be done by uploading a set of miRNAs to DIANA-miRPath [68], a web server that automatically evaluates these probabilities. In order to upload each miRNA listed

Table 6.4 Various performance achieved by LDA (with LOOCV) using PC loading computed by 10 miRNAs selected by PCA based unsupervised FE

k	mRNAs without a function	mRNAs with a function	Total
mRNAs not targeted by a miRNA	$N-N_1-N_2+N_{12}$	N_2-N_{12}	$N-N_1$
mRNAs targeted by a miRNA	N_1-N_{12}	N_{12}	N_1
Total	$N-N_2$	N_2	N

Table 6.5 KEGG pathway enrichment analysis by DIANA-miRPath for 12 miRNAs listed in Table 6.1

Rank	KEGG pathway	Adjusted	Number of	
		P-value	Genes	miRNAs
1.	Proteoglycans in cancer (hsa05205)	2.96×10^{-14}	120	12
12.	Prostate cancer (hsa05215)	1.35×10^{-6}	60	12
14.	Glioma (hsa05214)	9.41×10^{-6}	41	12
15.	Chronic myeloid leukemia (hsa05220)	1.12×10^{-5}	48	12
16.	Renal cell carcinoma (hsa05211)	1.36×10^{-5}	45	12
22.	Pathways in cancer (hsa05200)	4.49×10^{-5}	201	12
25.	Colorectal cancer (hsa05210)	1.34×10^{-4}	39	12
26.	Small cell lung cancer (hsa05222)	1.78×10^{-4}	54	12
31.	Pancreatic cancer (hsa05212)	3.59×10^{-4}	43	12
34.	Non-small cell lung cancer (hsa05223)	4.24×10^{-4}	35	12
36.	Central carbon metabolism in cancer (hsa05230)	4.83×10^{-3}	39	12
37.	Endometrial cancer (hsa05213)	5.62×10^{-3}	31	12
40.	Melanoma (hsa05218)	8.04×10^{-3}	39	12
43.	Transcriptional misregulation in cancer (hsa05202)	9.42×10^{-3}	90	12
44.	Bladder cancer (hsa05219)	9.77×10^{-3}	25	12
60.	Acute myeloid leukemia (hsa05221)	2.67×10^{-2}	33	11
61.	Thyroid cancer (hsa05216)	3.00×10^{-2}	17	12

Twelve cancer related pathways among total 61 pathways detected are listed. The number of genes is that of genes included in the union set of genes targeted by at least one of 12 miRNAs. The number of miRNAs is that of miRNAs whose target genes are included in the pathway

in Table 6.1, one needs to add suffix such that it is adapted to the most recent miRBase and “hsa” to specify species. For example, instead of uploading “miR-425,” one must upload the name of “miR-425-5p.” “miR-320a” must be uploaded as without suffix, “miR-320a.” The option that specifies miRNA target gene data base is “Tarbase.”

Table 6.5 is the result when considering Kyoto Encyclopedia of Genes and Genomes (KEGG) [23] pathway that evaluates genes based upon metabolic paths that describe chemical reactions mediated via proteins coded by genes. Among 68 pathways associated with adjusted P-values less than 0.05, as many as 17 cancer related pathways are included. This also supports the reliability of selected 12 miRNAs by PCA based unsupervised PCA.

6.3.2 *Circulating miRNAs as Universal Disease Biomarker*

In this section, occasionally, miRNAs used for biomarker that identifies if multiple diseases are highly overlapped. It is the next question if it is occasional or not. In order to see this, we need to see if miRNAs selected in this section can diagnose other diseases. For this purpose, we have collected miRNA expression of other diseases from various studies [57]. We have collected seven blood miRNA expressions from the GEO: Alzheimer's disease (AD) (GSE46579) [26], carcinoma (GSE37472) [30], coronary artery disease (CAD) (GSE49823), nasopharyngeal carcinoma (NPC) (GSE43329), HCC (GSE50013) [41], breast cancer (BC) (GSE41922) [8], and acute myeloid leukemia (AML) (GSE49665) [38] (Table 6.6). This is really a heterogeneous data set. Not only collected diseases but also resources as well as methods include multiple ones. Thus it is suitable to check if 12 miRNAs can work as robust universal disease biomarker.

The procedure is almost similar. Excluding identification of 10 miRNAs using PCA based unsupervised FE, 12 miRNAs are considered to be chosen in common for seven diseases. Then, PC loading $\boldsymbol{v}_\ell^{(k)\prime}$ for kth disease is computed with applying PCA to $x_{ij}{}' \in \mathbb{R}^{12\times(M_0+M_k)}$. Then optimal top L $\boldsymbol{v}_\ell^{(k)\prime}$ is used for discriminating patients from controls with LDA. Performance is evaluated by LOOCV. Table 6.7 shows the performance towards seven diseases. The disease-wise mean performance (Accuracy = 0.791, Sensitivity = 0.785, Specificity = 0.800) is almost the same as (even a little bit better than) that in the previous study (Accuracy = 0.784, Sensitivity = 0.750, Specificity = 0.800) [56]. This suggests that identification of 12 miRNAs universally for 12 diseases is not accidental, but they are truly useful for identification of wide range of diseases from healthy people. Thus, I named them as universal disease biomarker (UDB). The possibility of UDB is not

Table 6.6 List of blood miRNA expression profiles used in validation for 12 miRNAs in Table 6.1 as a universal disease biomarker

	Diseases			
	Alzheimer	Carcinoma	CAD	NPC
GEO ID	GSE46579	GSE37472	GSE49823	GSE43329
Number of miRNAs	502	565	746	886
Total samples	70	56	26	50
Disease samples	48	30	13	31
Healthy control samples	22	26	13	19
Methodology	HTS	qPCR	RT-PCR	Microarray
Source	Whole blood	Peripheral serum	Plasma sample	Plasma sample
GEO ID	GSE50013	GSE41922	GSE49665	
Number of miRNAs	231	274	128	
Total samples	40	54	65	
Disease samples	20	32	52	
Healthy control samples	20	22	13	
Methodology	RT-PCR	RT-PCR	Microarray	
Source	Plasma sample	Pre-operative serum	Peripheral blood	

Table 6.7 Performance of PCA based LDA using 12 miRNAs in Table 6.1 toward seven diseases with LOOCV

Diseases	Accuracy	Sensitivity	Specificity	L
AD	0.829	0.833	0.818	8
Carcinoma	0.768	0.730	0.800	11
CAD	0.846	0.846	0.846	3
NPC	0.740	0.806	0.632	12
HCC	0.700	0.700	0.700	9
BC	0.870	0.813	0.955	3
AML	0.784	0.769	0.846	8
Mean	0.791	0.785	0.800	–
Mean of previous study [56]	0.784	0.750	0.800	–

The "Mean of previous study" corresponds to the mean over the performance in Table 6.3.
L: optimal number of PC loading used for LDA

frequently recognized. Nevertheless, because blood miRNAs can reflect whole body status, they can be UDB that can diagnose multiple diseases. Actually, we very recently [58] identified 107 blood miRNAs that can successfully discriminate familial amyotrophic lateral sclerosis, sporadic amyotrophic lateral sclerosis, healthy controls, and gene mutation holders. Among twelve miRNAs identified here, as many as nine miRNAs (miR-30d, miR-19b, miR-106b, miR-425, miR-185, miR-191, miR-92a, miR-16, and miR-140-3p) are included in the 107 miRNAs. Nine out of twelve might not look like large enough, because 107 miRNAs are selected from as many as 3391 miRNAs [58], the fact that selected 107 miRNAs has nine overlaps with twelve miRNAs is highly significant ($P = 4.5 \times 10^{-4}$ by Fisher's exact test). Identification of UDB using circulating miRNAs should be searched more extensively and seriously.

6.3.3 Biomarker Identification Using Exosomal miRNAs

In the previous subsubsection, we have shown that serum biomarker can discriminate various diseases from normal controls. In this section, we would like to demonstrate that blood miRNA can even work as disease progression biomarker. miRNAs considered are those in exosome.

Exosome is a small vehicle composed of lipid bilayer membrane. It is released from cells and includes various compounds originated from cells inside. As a result, exosome is a good target by which we can know the state inside cells. The functions of exosome are not yet fully understood. Although some reports say that exosome is used to transfer some compounds from cells to cells, what the purpose is specifically is not yet understood.

Recently, exosome is considered to be a candidate as biomarker, because it can carry something out of cell inside. It is also reported that some cancers make use of functions of exosome. These suggest that compounds in exosome can reflect the change inside cells coincident with disease initiation and progression. Exosome also includes miRNAs originated from cells and are circulating in the blood. Thus, exosomal miRNAs are good targets from which disease biomarkers are generated.

The targeted diseases are liver diseases, which are classified as hepatitis. Hepatitis is a kind of chronic inflammation disease caused by various causes. Hepatitis itself is not lethal, but it becomes cirrhosis of the liver earlier or later, and finally results in deadly liver cancer. Thus, treatment of hepatitis before cirrhosis of the liver is critically important. Thus inference of hepatitis progression is very important. On the other hand, because suitable therapy varies dependent upon disease causes, it is also very important to diagnose disease cause. Therefore, the aim of constructing biomarker is not only discrimination between healthy controls and hepatitis, but also constructing biomarker that can discriminate hepatitis having different causes and progression stages. Thus, the more advanced biomarker than that we have identified in the previous subsubsection is required.

The data set is downloaded from GEO with GEO ID GSE33857 [33] (Table 6.8). This data set includes three hepatitis: one caused by hepatitis B virus (HBV) infection, one caused by hepatitis C virus (HCV) infection, and nonalcoholic steatohepatitis (NASH). The microarray used for these measurements includes 887 miRNAs. Because each miRNA is measured by multiple probes, the number of probes included is 14,192. Because feature selection below is performed not in individual miRNAs base but in probe base, it is obvious that the number of features (14,192) is much larger than the number of samples (104 for primary set).

Figure 6.2 illustrates the analysis flow of discrimination between CHB, CHC, NASH, and healthy controls (unshaded part) for the primary set.

1. Expression profiles, $x_{ij} \in \mathbb{R}^{N \times (M_k + M_{k'})}$, of $i$the miRNA and jth samples with kth and k'th disease or normal sample with the number of samples M_k and $M_{k'}$, respectively.
2. Apply PCA to x_{ij} such that PC loading, $\boldsymbol{v}_\ell \in \mathbb{R}^{M_k + M_{k'}}$, is attributed to samples.
3. Apply categorical regression analysis

$$v_{\ell j} = a_\ell + \sum_{s \in \{k,k'\}} b_{\ell s} \delta_{sj} \tag{6.30}$$

Table 6.8 List of exosome miRNA expression profiles used in this study

CHC	CHB	NASH	normal
Primary sets			
64	4	12	24
Validation sets			
31	12	8	–

CHB chronic hepatitis B, *CHC* chronic hepatitis C, *NASH* Nonalcoholic steatohepatitis

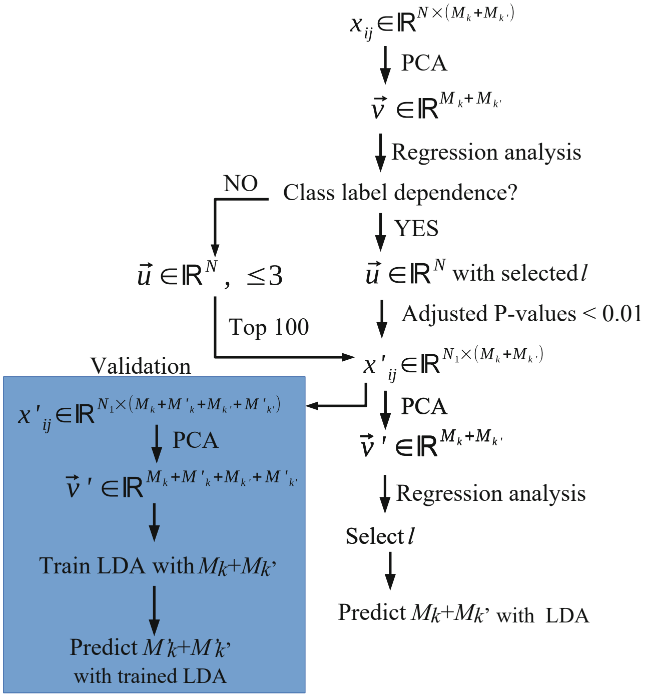
$x_{ij} \in \mathbb{R}^{N \times (M_k + M_{k'})}$
PCA
$\vec{v} \in \mathbb{R}^{M_k + M_{k'}}$
Regression analysis
NO
Class label dependence?
YES
$\vec{u} \in \mathbb{R}^N$, ≤ 3
$\vec{u} \in \mathbb{R}^N$ with selected l
Top 100
Adjusted P-values < 0.01
Validation
$x'_{ij} \in \mathbb{R}^{N_1 \times (M_k + M_{k'})}$
$x'_{ij} \in \mathbb{R}^{N_1 \times (M_k + M'_k + M_{k'} + M'_{k'})}$
PCA
PCA
$\vec{v}' \in \mathbb{R}^{M_k + M'_k + M_{k'} + M'_{k'}}$
$\vec{v}' \in \mathbb{R}^{M_k + M_{k'}}$
Regression analysis
Train LDA with Mk+Mk'
Select l
Predict Mk+Mk' with LDA
Predict $M'k$+$M'k$'
with trained LDA

Fig. 6.2 Flowchart of discrimination between diseases using exosomal miRNAs. The performance obtained with following this flowchart is in Table 6.10

to $\boldsymbol{v}_\ell$ and attribute P-values to ℓs. P-values are adjusted by BH criterion and ℓs associated with adjusted P-values less than 0.05 are selected (the cases without ℓs that pass this filtering will be discussed later).

4. Attribute P-value to ith miRNA as

$$P_i = P_{\chi^2}\left[> \sum_\ell \left(\frac{u_{\ell i}}{\sigma_\ell} \right)^2 \right] \tag{6.31}$$

where the summation is taken over ℓs associated with adjusted P-values less than 0.05 and σ_ℓ is the standard deviation of $u_{\ell i}$.

5. ith miRNA associated with adjusted P-values less than 0.01 are selected. With using only selected N_1 miRNAs, expression profile, $x_{ij}{}' \in \mathbb{R}^{N_1 \times (M_k + M_{k'})}$, are composed.
6. PCA is again applied to $x_{ij}{}'$ and $\boldsymbol{v}_\ell{}' \in \mathbb{R}^{(M_k + M_{k'})}$ are obtained. Categorical regression is applied to $\boldsymbol{v}_\ell{}'$ as

$$v_{\ell j}{}' = a_\ell{}' + \sum_{s \in \{k, k'\}} b_{\ell s}{}' \delta_{sj} \tag{6.32}$$

and ℓs with adjusted P-values less than 0.05 are used for LDA.

7. kth and k'th diseases or normal samples are discriminated with LDA using ℓs selected. LOOCV is employed for the cross validation.

There is one problem in the above process. When features are selected, it is forbidden to use the information of samples to be discriminated. Nevertheless, in Eqs. (6.30) and (6.32), all of the class labeling are used.

In order to see if exclusion of one sample to be discriminated (because we employ LOOCV) can alter the selected miRNAs, we perform the following. When PC loading is selected using Eqs. (6.30) and (6.32), one of $M_k + M_{k'}$ samples is removed and P-values are recomputed and adjusted to select PC loading. Table 6.9 is the result for 100 trials. As can be seen, only three pairs, CHC vs normal, CHB vs CHC, and NASH vs CHC, out of six possible pairs among four classes, CHB, CHC, NASH and normal controls, have non-zero selected PC loading in Eq. (6.30) (Please note, if no PC loading is selected in Eq. (6.30), the process is terminated and Eq. (6.32) is not performed). As expected, PC loading is selected with high stability for these three pairs. Thus, we decide to select PC loading shown in bold in Table 6.9 for these three pairs.

Table 6.10 shows the confusion matrices of the discrimination between CHC, CHB, NASH, and normal controls. For these three pairs, CHC vs normal, CHB vs CHC, and NASH vs CHC, performance is relatively well.

For other three pairs without CHC, i.e., CHB versus NASH, CHB versus normal, NASH versus normal, because there is no PC loading associated with adjusted P-values less than 0.05 (the "NO" branch to the question "Class label dependence?" in Fig. 6.2), we cannot select miRNAs using Eq. (6.31). Instead, we attribute P-values to miRNAs with Eq. (6.31) using $1 \leq \ell \leq 3$. Then top 100 miRNAs with smaller P-values are selected even if they are not significantly small. PC loading, $\boldsymbol{v}_{\ell}{}'$ with

Table 6.9 Frequencies of PC loading selected via Eqs. (6.30) and (6.32) when one of samples are sequentially excluded among 100 trials

CHC vs normal						
ℓ	**1**	**2**	**3**	27		
Eq. (6.30)	88	88	88	1		
Eq. (6.32)	88	50	88	—		
CHB vs CHC						
ℓ	**2**	**3**				
Eq. (6.30)	20	68				
ℓ	**1**	3	4	**5**	6	12
Eq. (6.32)	68	1	1	67	3	1
NASH vs CHC						
ℓ	**1**	**2**	**3**			
Eq. (6.30)	12	76	76			
ℓ	**1**	**3**	**4**			
Eq. (6.32)	76	76	76			

ℓs not shown are not selected. PC loading shown in bold is selected and used for selection of miRNA probes

Table 6.10 Confusion matrix of discrimination between CHB, CHC, NASH, and normal controls

Primary set[a]								
Predict	CHC	Normal	Predict	CHC	CHB	Predict	CHC	NASH
CHC	64	4	CHC	62	1	CHC	63	2
Normal	0	20	CHB	2	3	NASH	1	10
P-values	3.46×10^{-16}			7.80×10^{-4}			7.40×10^{-10}	
Odds ratio	∞			71.4			234.2	
Primary set[b]								
Predict	CHB	NASH	Predict	CHB	Normal	Predict	NASH	Normal
CHB	2	3	CHB	2	9	NASH	9	7
NASH	2	9	Normal	2	15	Normal	2	17
P-values	5.55×10^{-1}			1.00×10^{0}			8.79×10^{-3}	
Odds ratio	2.78			1.63			10.1	
Validation set								
Predict	CHB	NASH	Predict	CHC	CHB	Predict	CHC	NASH
CHB	18	6	CHC	74	3	CHC	73	8
NASH	4	12	CHB	21	17	NASH	22	12
P-values	3.21×10^{-3}			1.90×10^{-7}			2.24×10^{-3}	
Odds ratio	8.42			19.3			4.89	

Columns: True, Rows: Prediction. P-values are computed by Fisher's exact test

[a] N_1 probes are selected based upon significance.

[b] Top $N_1 (= 100)$ probes with smaller P-values are selected without considering significance.

applying PCA to $x_{ij}{}' \in \mathbb{R}^{10 \times (M_k + M_{k'})}$. Using $\boldsymbol{v}_\ell{}'$, $1 \leq \ell \leq 3$, LDA is performed. The results for these three pairs are also shown in Table 6.10. Performance for CHB is not good.

In Table 6.11, we list miRNAs selected. As in the case of serum miRNAs, they are highly overlapped. Thus, as miRNAs in serum, exosomal miRNAs have potential to be UDB, too.

Finally, we try to validate the suitability of selected miRNAs in Table 6.11 using validation set in Table 6.8. The procedure is as follows (shaded part in Fig. 6.2).

1. We construct expression profiles of selected N_1 probes listed in Table 6.11, $x_{ij}{}' \in \mathbb{R}^{N_1 \times (M_k + M'_k + M_{k'} + M'_{k'})}$, where M'_k and $M'_{k'}$ are the number of samples in validation set (Table 6.8) of kth and k'th disease or control samples.
2. PC loading $\boldsymbol{v}_\ell{}'$ is computed with applying PCA to $x_{ij}{}'$.
3. $\boldsymbol{a}$ in Eq. (6.2) is computed using only $\boldsymbol{v}_\ell{}'$ (ℓs used are the same as listed in Table 6.9 for Eq. (6.32)) of $M_k + M_{k'}$ samples in primary set. In other words, $\triangle^{(k)}$ and $\triangle^{(0,k)}$ are computed using only $M_k + M_{k'}$ samples in primary set.
4. Using obtained $\boldsymbol{a}$, y_j for $M'_k + M'_{k'}$ samples in validation set is computed using Eq. (6.2).
5. $M'_k + M'_{k'}$ samples in validation set are discriminated between k and k' using obtained y_j.

Table 6.11 List of miRNAs included in N_1 probes selected in order to compute $\boldsymbol{v}_\ell{}'$ (Fig. 6.2) with applying PCA to $x_{ij}{}' \in \mathbb{R}^{N_1 \times (M_k + M_{k'})}$

miRNAs	CHC vs normal	CHB vs CHC	NASH vs CHC	CHB vs NASH	CHB vs normal	NASH vs normal
N_1	176	140	170	100	100	100
miR-638	○	○	○	○	○	○
miR-320c	○	○	○	○	○	○
miR-486-5p	○	○	○	○	○	○
miR-451	○	○	○	○	○	○
miR-1974_v14.0	○	○	○	○	○	○
miR-1246	○	○	○	○	○	○
miR-720	○	○	○	○	○	
miR-762	○	○	○		○	○
miR-630	○	○	○	○		○
miR-92a	○	○	○		○	
miR-1275	○	○	○			
miR-1225-5p	○		○			
miR-1207-5p	○		○			
miR-1202	○					
miR-22		○		○		
miR-532-3p		○				
miR-1202			○		○	
miR-122		○				
miR-1306		○				
miR-34b		○				
miR-16		○				
miR-1					○	
miR-1271					○	

The exclusion of $M'_k + M'_{k'}$ samples in validation set for computing $\boldsymbol{a}$ is required in step 3, because we should not use any information about to which category samples in validation set belong; this information is not available in the real situation. On the other hand, their expression profiles themselves are allowed to be used for computing $\boldsymbol{v}_\ell{}'$, because we have miRNA expression of validation set in advance even if we do not know about labeling.

Table 6.10 also shows the results for these validation sets. The performance is pretty good. Interestingly, CHB samples that cannot be well discriminated in primary samples are well discriminated in the validation sample, in spite of that it is usually expected that performance in validation set decreases than training set. This suggests that probe selection by PCA based supervised FE can work pretty well even if the number of samples available is small as demonstrated in synthetic data set in the previous chapter. In conclusion, exosomal miRNA has the ability to

Table 6.12 Number of samples having specific inflammation and fibrosis levels in CHC samples

Inflammation	1	2	3	Fibrosis	0	1	2	3
Number	36	18	9	Number	3	33	16	12

diagnose not only disease but also cause of diseases, because it can discriminate among CHB, CHC, and NASH, which is hepatitis caused by different causes.

Next, we would like to see if exosomal miRNA can diagnose hepatitis progression. There are two features that describe hepatitis progression, inflammation and fibrosis. Because hepatitis is a chronic inflammation, there might be no need to explain why inflammation describes hepatitis progression. On the other hand, fibrosis is not so direct measure. As mentioned above, hepatitis develops to cirrhosis. Cirrhosis is fibrosis of liver. Thus, it is reasonable to consider fibrosis progression to be disease progression measure of hepatitis. Both inflammation and fibrosis are diagnosed for some CHC samples using integer grade.

Table 6.12 shows the frequency of inflammation and fibrosis grade levels diagnosed. In order to infer these levels using exosomal miRNAs, we do as follows:

1. PCA is applied to $x_{ij} \in \mathbb{R}^{N \times M_k}$ where M_k is the total number of CHC samples with inflammation or fibrosis diagnoses (Table 6.12). Unfortunately, we cannot identify any PC loading, $\boldsymbol{v}_\ell \in \mathbb{R}^{M_k}$, that is significantly associated with inflammation or fibrosis levels.
2. After attributing P_is to miRNAs using Eq. (6.31) with $\ell \leq 3$, top 100 probes with smaller P_is are selected.
3. PCA is applied to miRNA expression profile including only selected 100 probes, $x_{ij}{}' \in \mathbb{R}^{100 \times M_k}$.
4. The obtained $\boldsymbol{v}_\ell{}', \ell \leq 2$ as well as patient ages are used for LDA. In this case, ages must be considered together with miRNA expression in order to get significant results.

Table 6.13 shows the confusion matrices between predicted and true inflammation and fibrosis. Although the number of used miRNAs increases to twice, it is still as many as $\sim$10, which is less than 5% of total number of miRNAs in the array, 887. In order to see if they are significant, we compute correlation coefficient between true and predicted inflammation and fibrosis levels. Although the correlation is not very high, they are associated with significant P-values ($P = 0.02$, see page 112 for how to compute P-values attributed to correlation coefficients). Thus, we can expect that exosomal miRNAs can diagnose hepatitis progression together with patients' ages.

Multi-Class LDA Here we need to explain how LDA for two classes can be extended to multi-classes because discrimination of inflammation or fibrosis levels require multi-classes discrimination. At first, $\triangle^{(k)}$ in Eq. (6.6) and $\triangle^{(0,k)}$ in Eq. (6.9) are replaced with

Table 6.13 Confusion matrices between true (columns) and predicted (rows) inflammation and fibrosis levels. Correlation coefficients with associated P-values as well as 21 miRNAs to which top 100 probes are attributed are listed

True								
Inflammation				Fibrosis				
Prediction	1	2	3	Prediction	0	1	2	3
1	28	10	4	0	1	2	0	0
2	5	6	2	1	2	23	9	6
3	3	2	3	2	0	3	5	2
				3	0	5	2	4
	Corr. = 0.29, $P = 0.02$				Corr. = 0.30, $P = 0.02$			

miR-1225-5p miR-1275 miR-638 miR-320c miR-197_v14.0 miR-194* miR-630 miR-720 miR-300 miR-1179 miR-373 miR-1181 miR-1246 miR-320d miR-532-3p miR-518d-3p miR-34b miR-664 miR-668 miR-147 miR-664*

$$\triangle^{\text{inter}} = \sum_{k \neq k'} \left(\langle y_j \rangle_j^{(k)} - \langle y_j \rangle_j^{(k')} \right)^2 \tag{6.33}$$

and

$$\triangle^{\text{intra}} = \sum_k \left\langle \left(y_j - \langle y_{j'} \rangle_{j'}^{(k)} \right)^2 \right\rangle_j^{(k)} \tag{6.34}$$

respectively. Then we get Eq. (6.15) with modified Σ_W and Σ_B. In contrast to the two classes discrimination, we need the first S eigenvectors, $\boldsymbol{a}_p$, $p \leq S$, for S classes discrimination. Then y_j^ps are attributed to jth sample with substituting $\boldsymbol{a}_p$ to $\boldsymbol{a}$ in Eq. (6.2). $\boldsymbol{y}_j$ is defined as

$$\boldsymbol{y}_j = \left(y_j^1, y_j^2, \ldots, y_j^S \right) \tag{6.35}$$

and kth class centroid vector $\left\langle \boldsymbol{y}_j \right\rangle_j^{(k)}$ is computed as in Eq. (6.4). The distance between jth sample and kth centroid

$$d_{kj} = \left| \boldsymbol{y}_j - \left\langle \boldsymbol{y}_j \right\rangle_j^{(k)} \right| \tag{6.36}$$

is computed. Finally, jth sample is classified into the kth class having the smallest d_{jk} among S classes. □

In conclusion, we have found that exosomal miRNAs can not only discriminate between healthy controls and hepatitis patients, but also diagnose hepatitis progression. The advantage of the usage of PCA based unsupervised FE is that we can reduce the number of probes down to $\sim 10^2$ from 14,192. As for the number of miRNAs, it is $\sim$10 among 887 total miRNAs. Considering that it is the results of unsupervised methods, it is remarkable and demonstrates usefulness of PCA based unsupervised FE in the real application.

6.4 Integrated Analysis of mRNA and miRNA Expression

In the previous section, circulating miRNA can be an effective biomarker. As mentioned above, miRNAs can affect the biological processes through targeting mRNAs. Thus, considering miRNA and miRNA expression might be more effective to understand biological systems.

6.4.1 Understanding Soldier's Heart From the mRNA and miRNA

Soldier's heart means that veterans often have heart problems without any physiological abnormalities. Thus, it is believed to be post traumatic stress disorder (PTSD) driven disorder. PTSD is a mental disorder caused by life-threatening stresses, e.g., experiences in battlefields or encounters to disaster. Even after the stresses passed out, human beings sometimes have mental problems, not to be fully relaxed. PTSD not only affects mental sides, but also affects physical sides. In this sense, it is critically important to know how life-threatening stress causes gene expression anomaly in heart. In this subsection, we would like to fulfill this requirement with analyzing miRNA and mRNA expression profiles in stressed mice hearts [59].

Table 6.14 lists 48 samples for which mRNA and miRNA expression profiles are measured. These are downloaded from GEO ID GSE52875; the file GSE52875_RAW.tar including individual 48 raw data files is downloaded. Individual 48 files whose file names start from "GSM" are loaded into R via read.csv function, and "gProcessedSignal" columns in each file are collected as one data.frame. All probes having ControlType=0 are excluded for the further analyses.

Here we would like to emphasize the difficulty of feature selection in this case. In the case of discrimination between diseases and healthy control, miRNAs should be expressed distinctly between two classes. Even diagnosing disease progression, the direction among multiple classes is clear; inflammation and fibrosis should

Table 6.14 Number of samples in miRNA and mRNA expression profiles of stressed mice hearts

Rest period	1 day				1 day	10 days	
Stress expose period	1 day	2 days	3 days	10 days	5 days		42 days
Control/Stressed	0/4	4/4	0/4	4/4	4/4	4/4	4/4

increase as disease progressed. In contrast to these cases where how expression is expected to differ is more or less clear, how miRNA expression differs between 12 classes (5 controls and 7 stressed samples) is unclear. Of course, although miRNA expression should differ between corresponding controls and stressed samples, pairwise comparisons between five pairs of stressed samples and controls might not be a good idea, because individual comparison might identify non-overlapping sets of mRNAs and miRNAs. Because the aim of this study is to identify disease causing mRNAs and miRNAs, identification of sets of non-overlapping mRNAs and miRNAs is not desirable. Thus, how we can identify mRNAs and miRNAs that contribute to diseases is not an easy problem.

Here, we apply PCA based unsupervised FE to mRNA expression and miRNA expression separately. We denote mRNA and miRNA expression as $x_{ij}^{\text{mRNA}} \in \mathbb{R}^{59305\times 48}$ and $x_{kj}^{\text{miRNA}} \in \mathbb{R}^{2640\times 48}$, respectively. Although the total number of mRNAs measured is as many as 37,890, since some mRNAs are measured by multiple probes, the total number of probes, 59,305, is much larger than the total number of mRNAs. Although there are only 660 miRNAs measured, because they are measured by as many as four probes, total number of probes is 2640. Although x_{ij}^{mRNA} is standardized, i.e., $\sum_i x_{ij}^{\text{mRNA}} = 0$, $\sum_i \left(x_{ij}^{\text{mRNA}}\right)^2 = 59{,}305$, x_{kj}^{miRNA} are not. PCA is applied to x_{ij}^{mRNA} and x_{kj}^{miRNA} such that PC loading $\boldsymbol{v}_\ell^{\text{mRNA}} \in \mathbb{R}^{48}$ and $\boldsymbol{v}_\ell^{\text{miRNA}} \in \mathbb{R}^{48}$ are attributed to 48 samples.

In order to see which PC loading is associated with distinction among 12 classes, $1 \leq s \leq 12$, we apply categorical regression analysis

$$v_{\ell j}^{\text{mRNA}} = a_\ell^{\text{mRNA}} + \sum_{s=1}^{12} b_{\ell j}^{\text{mRNA}} \delta_{sj} \tag{6.37}$$

$$v_{\ell j}^{\text{miRNA}} = a_\ell^{\text{miRNA}} + \sum_{s=1}^{12} b_{\ell j}^{\text{miRNA}} \delta_{sj} \tag{6.38}$$

where $a_\ell^{\text{mRNA}}, b_\ell^{\text{mRNA}}, b_\ell^{\text{miRNA}}, b_\ell^{\text{miRNA}}$ are the regression coefficients. P-values are attributed to PC loading and corrected by BH criterion. As a result, PC loading with $\ell = 1, 2, 4, 10$ for mRNA and $\ell = 1, 2$ for miRNA has adjusted P-values less than 0.05. Figures 6.3 and 6.4 show the boxplots of PC loading, $\boldsymbol{v}_\ell^{\text{mRNA}}$, $\ell = 1, 2, 4, 10$ and those of PC loading, $\boldsymbol{v}_\ell^{\text{miRNA}}$, $\ell = 1, 2$, respectively. It is obvious that PCA can successfully identify PC loading associated with dependence upon 12 classes for mRNA and miRNA. It might be difficult to identify such complicated dependence with conventional supervised methods, because we need to specify the dependence upon class labeling in advance, for supervised methods.

Although PCA can identify PC loading that is coincident with twelve classes, the problem is if these coincidences are biologically reasonable or not. In order to discuss this point, we need domain knowledge. As mentioned above, primary function of miRNA is to destroy mRNA. Thus, miRNA expression should be negatively correlated to mRNA expression. Hence, PC loading that corresponds

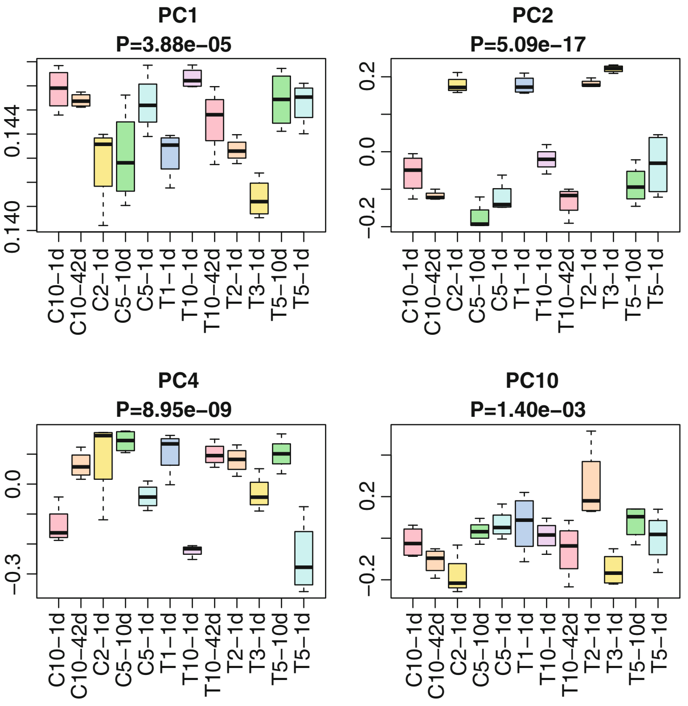

Fig. 6.3 The first, second, fourth, and tenth PC loading, $\boldsymbol{v}_{\ell}^{\text{mRNA}}$, $\ell = 1, 2, 4, 10$, to which adjusted P-values less than 0.05 are attributed. P-values above each plot are adjusted ones. Labels of classes: C: control, T: stressed, the numbers adjusted to T or C: period of stress, XXd: days of rest. See Table 6.14, too. Coloring is just for visibility and does not correspond to experimental conditions

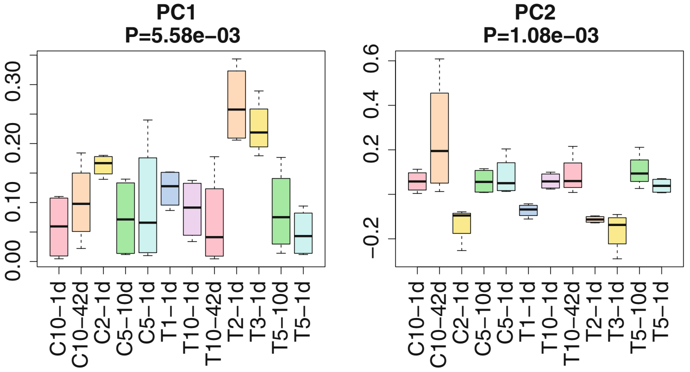

Fig. 6.4 The first and second PC loading, $\boldsymbol{v}_{\ell}^{\text{miRNA}}$, $\ell = 1, 2$, to which adjusted P-values less than 0.05 are attributed. P-values above each plot are adjusted ones. Labels of classes: C: control, T: stressed, the numbers adjusted to T or C: period of stress, XXd: days of rest. See Table 6.14, too. Coloring is just for visibility and does not correspond to experimental conditions

to these two should as well. Figure 6.5a shows the scatterplot of the first PC loading between miRNA and mRNA attributed to 48 samples. The correlation coefficients are -0.37 with associated P-value of 9.54×10^{-3}. Thus, as expected, v_{1j}^{mRNA} and v_{1j}^{miRNA} are significantly correlated. In order to further confirm the biological reliability, summation over four replicates taken. Then the correlation between

$$\left\langle v_{1j}^{\text{mRNA}} \right\rangle_j^{(s)} = \frac{1}{4} \sum_{j \in s} v_{1j}^{\text{mRNA}} \tag{6.39}$$

and

$$\left\langle v_{1j}^{\text{miRNA}} \right\rangle_j^{(s)} = \frac{1}{4} \sum_{j \in s} v_{1j}^{\text{miRNA}} \tag{6.40}$$

is computed (Fig. 6.5b). If the negative correlation between miRNA and mRNA is biologically reliable, taking summation over four replicates within each class, k, should enhance the negative correlation. As expected, the correlation coefficient decreases (absolute value increases) from -0.37 to -0.71 while associated P-value decrease (from $P = 9.54 \times 10^{-3}$ to $P = 6.28 \times 10^{-3}$); significance increases. Because the number of observations decreases from 48 to 12, it is reasonable even if P-value associated with correlation coefficient increases (becomes less significant). In spite of that, P-value actually decreases; this suggests that negative correlation between miRNA and mRNA is likely biologically reliable. Table 6.15 shows the correlation coefficients between other PC loading. Other than pairs including v_{10j}^{mRNA},

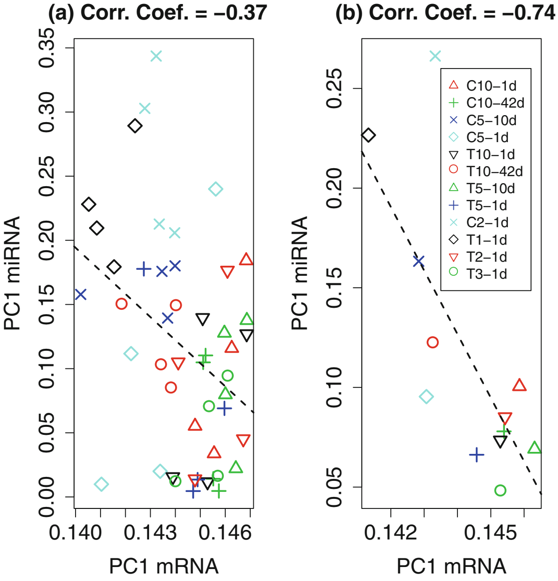

Fig. 6.5 Scatterplot between PC loading, (**a**) v_{1j}^{mRNA} and v_{1j}^{miRNA} (**b**) $\left\langle v_{1j}^{\text{mRNA}} \right\rangle_j^{(s)}$ and $\left\langle v_{1j}^{\text{miRNA}} \right\rangle_j^{(s)}$. Correlation coefficients are (**a**) -0.37, $P = 9.54 \times 10^{-3}$, (**b**) -0.74, $P = 6.28 \times 10^{-3}$

Table 6.15 Correlation coefficients between $v^{\text{mRNA}}_{\ell j}$, $\ell = 1, 2, 4, 10$ and $v^{\text{miRNA}}_{\ell j}$, $\ell = 1, 2$, and those between $\left\langle v^{\text{mRNA}}_{\ell j} \right\rangle^{(s)}_j$, $\ell = 1, 2, 4, 10$ and $\left\langle v^{\text{miRNA}}_{\ell j} \right\rangle^{(s)}_j$, $\ell = 1, 2$

$v^{\text{mRNA}}_{\ell j}$	$v^{\text{miRNA}}_{\ell j}$		$\left\langle v^{\text{mRNA}}_{\ell j} \right\rangle^{(s)}_j$	$\left\langle v^{\text{miRNA}}_{\ell j} \right\rangle^{(s)}_j$	
ℓ	1	2	ℓ	1	2
1	−0.37	0.65	1	−0.73	0.78
2	0.64	−0.62	2	0.80	−0.83
4	0.12	−0.21	4	0.30	−0.26
10	0.13	0.07	10	0.15	0.09

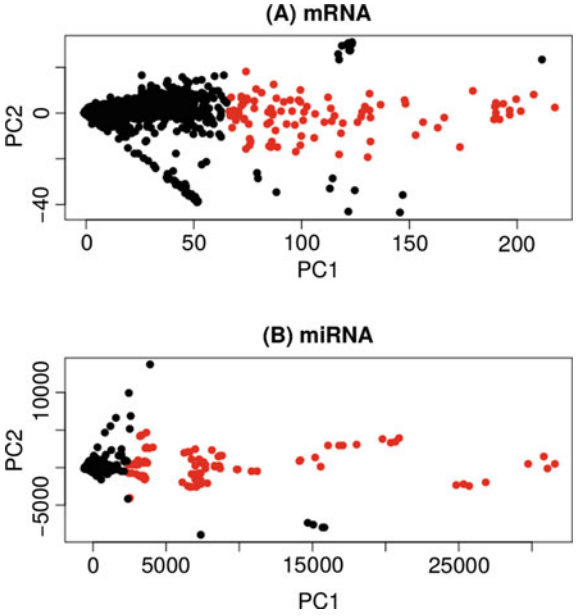

Fig. 6.6 Scatterplots of PC scores attributed to (**a**) mRNA, $\boldsymbol{u}^{\text{mRNA}}_{\ell}$, $\ell = 1, 2$,and (**b**) miRNA, $\boldsymbol{u}^{\text{miRNA}}_{\ell}$, $\ell = 1, 2$. Red dots are selected for further analysis

all pairs of PC loading between miRNA and mRNA have at least one pair associated with negative correlation. This suggests that PCA has the ability to identify expected negative correlations between miRNA and mRNA; in spite of that, no requirements for negative correlations are assumed during the selection of PC loading. This suggests that PCA has the ability to identify biologically reasonable PC loading in an unsupervised manner.

Next, in order to identify mRNAs and miRNAs that contributed to PTSD mediated heart disease, because the first two PC loading has stronger mutual correlations between miRNA and mRNA (Table 6.15) that are coincident with the miRNA function that destroys mRNA, we show scatterplots of $\boldsymbol{u}^{\text{mRNA}}_{\ell}$ and $\boldsymbol{u}^{\text{miRNA}}_{\ell}$ (Fig. 6.6). It is obvious that the first PC scores have more contributions. Thus, I decided to select miRNA and mRNA using the first PC scores. Nevertheless, the second PC loading is positively correlated with the first ones (Table 6.15), mRNAs and miRNAs having larger contribution to the second one should be excluded. The problem is that miRNAs and mRNAs having large contribution to the second PC score should be excluded. In order to estimate this, we select top 100 mRNAs and miRNAs simultaneously having the first PC score, u_{1j}^{mRNA} or u_{1j}^{miRNA}, whose absolute values are larger (i.e., highly ranked) and the second PC score, u_{2j}^{mRNA} or u_{2j}^{miRNA}, whose absolute values are less than a threshold value D. Figure 6.7 shows how D affects the selection of top 100 mRNAs and miRNAs. We can see that too small D heavily affects the selection while large enough D affects less. Then we decide to select $D = 20$ for mRNAs and $D = 5000$ for miRNAs, respectively. As a result, 27 miRNAs (mmu-miR-451, -22, -133b, -709, -126-3p, -30c, -29a, -143, -24, -23b, -133a, -378, -30b, -29b, -125b-5p, -675-5p, -16, -26a, -30e, -1983, -691, -23a, -690, -207, and -669l, and mmu-let-7b and -7g) and 59 mRNAs (Table 6.16) are associated with at least one of the selected probes.

We use seed matching to identify miRNA target genes, with the so-called 7mer-m8 [48] detecting exact matches to positions 2-8 of mature miRNAs (seed + position 8). Among the 59 mRNAs, 24 are targeted by at least one of the 27 selected miRNAs. In addition, 47 pairs of miRNAs and miRNA target genes are identified. In total, there are 45/47 negative correlation coefficients between miRNAs and miRNA target genes. We also examine the significance of correlation coefficients, with 26/47 pairs (more than half) associated with significant correlations (significance is judged if P-values adjusted by BH criterion is less than 0.05 or not. Two positive correlations are judged insignificant, because only negative correlation is biologically meaningful. See page 112 for how to compute P-values attributed to correlation coefficients), and confirm negative correlation between miRNAs and miRNA target genes.

Next, we try to see if mRNAs and miRNAs selected are distinctly expressed between stressed and control samples. Because only five experimental conditions have both stressed and control samples (Table 6.14), we consider only these five conditions. For mRNA, logarithmic ratio between stressed and control samples

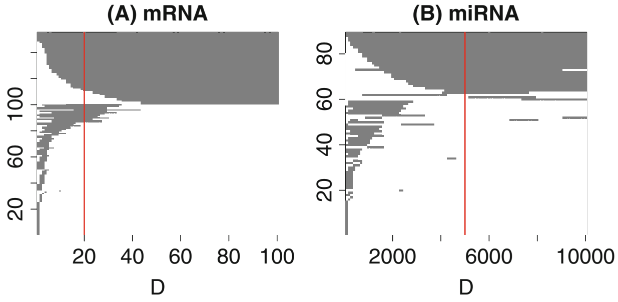

Fig. 6.7 Dependence of selected (**a**) mRNAs and (**b**) miRNAs upon D, which is a threshold value to exclude mRNAs and miRNAs having too large contribution to the second PC score. Horizontal axis: D, Vertical axis: arbitrary gene ID. Gray: selected, white: not selected. Vertical red lines indicated employed "D"

Table 6.16 Selected 59 mRNAs

Refseq	Gene symbol	Refseq	Gene symbol
NM_010859	Myl3	NM_007450	SLC25A4
NM_001083955	Hba-a2	NM_001164248	Tpm1
NM_001164171	Myh6	NM_010861	Myl2
NM_009943	Cox6a2	NM_008218	Hba-a1
NM_013593	Mb	NM_001177307	Aldoa
NM_011619	Tnnt2	NM_144886	Exosc2
NM_008084	Gapdh	NM_009944	Cox7a1
NM_175329	Chchd10	NM_001033435	Milr1
NM_010174	Fabp3	NM_001161419	Atp5g1
NM_016774	Atp5b	NM_008617	Mdh2
NM_024166	Chchd2	NM_011540	Tcap
NM_007747	Cox5a	NM_024223	CRIP2
NM_194341	SYNRG	NM_175015	Atp5g3
NM_008220	Hbb-bt	NM_009941	Cox4i1
NM_009429	TPT1	NM_008653	Mybpc3
NM_027519	medag	NM_027862	Atp5h
NM_009964	Cryab	NM_009406	Tnni3
NM_001100116	1700047I17Rik2	NM_026701	Pbld1
NM_023312	Ndufa13	NM_026614	Tnni3
NM_025352	Uqcrq	NM_198415	Ckmt2
NM_170759	Zfp628	NM_029816	2610028H24Rik
NM_019883	UBA52	NM_025641	Uqcrh
NM_007505	Atp5a1	NM_177369	Myh8
NM_010888	Ndufs6	NM_007751	Cox8b
NM_010239	Fth1	NM_010212	Fhl2
NM_173011	Idh2	NM_007475	Rplp0
NM_023374	Sdhb	NM_053071	Cox6c
NM_025983	Atp5e	NM_080633	Aco2
NM_018858	Pebp1	NM_031165	Hspa8
NM_020582	Atp5j2		

$$\log\left(\frac{x^{\mathrm{mRNA}}_{ij_q}}{x^{\mathrm{mRNA}}_{ij'_q}}\right) \tag{6.41}$$

for ith mRNA in selected 59 mRNAs is computed. Here $(j_q, j'_q), q \leq 4$ are the four pairs of stressed and control samples. Then, we apply t test to a set of $59 \times 4 = 236$ computed logarithmic ratio to see if their mean value is significantly positive or negative. Table 6.17 shows the P-values. In not all but some conditions, between control and stressed samples, mRNA expression is expressed differently for selected 59 mRNAs. Because PCA based unsupervised FE does not require the distinct expression between control and stressed samples, these suggest that PCA

Table 6.17 P-vales computed by t tests applied to logarithmic ratio, Eq. (6.41)

Rest period	2 days	5 days		10 days	
Stress expose period	1 day	1 day	10 days	1 day	42 days
PCA based unsupervised FE					
Control < stress	6.79×10^{-14}	7.41×10^{-8}	0.77	1.0	0.03
Control > stress	1.0	1.0	0.22	2.35×10^{-8}	0.97
Categorical regression					
Control < stress	6.28×10^{-9}	5.71×10^{-23}	0.80	1.0	7.37×10^{-6}
Control > stress	1.0	1.0	0.20	2.01×10^{-4}	1.00
BAHSIC					
Control < stress	1.00	1.00	1.00	1.0	1.05×10^{-3}
Control > stress	6.97×10^{-4}	7.98×10^{-10}	5.45×10^{-15}	5.43×10^{-4}	1.00

based unsupervised FE can identify genes expressed distinctly between control and stressed samples in an unsupervised manner.

Unfortunately, logarithmic ratio, Eq. (6.41), does not work well for miRNA expression profile. Thus, I propose alternative. First, we apply t test to kth miRNA in one of five experimental conditions between four control samples and four stressed samples. We compute P-values, P_k, that rejects the null hypothesis that means of four replicates are equal between control samples and stressed samples towards alternative hypothesis that means of four replicates in control samples are less than means of four replicates in stressed samples. Then, a set of logarithmic P-values, $\log P_k$, are compared between selected 27 miRNAs and other miRNAs by t test if mean $\log P_k$ is distinct between selected 27 miRNAs and others (Table 6.18). This test can address significant P-values to all five experimental conditions for which both stressed and control samples are available.

PCA based unsupervised FE successfully identified mRNAs and miRNAs, which are negatively and mutually correlated and distinctly expressed between some pairs of control and stressed samples. Nevertheless, if other methods can perform similarly, the usefulness of PCA based unsupervised FE is limited. Thus, it might be important to compare the performance with other popular or conventional methods.

The first conventional methods tried is categorical regression analysis.

$$x_{ij}^{\text{mRNA}} = a_i + \sum_{s=1}^{12} b_{is}\delta_{sj} \tag{6.42}$$

and

$$x_{kj}^{\text{miRNA}} = a_k + \sum_{s=1}^{12} b_{ks}\delta_{sj} \tag{6.43}$$

Table 6.18 P-values were computed by t tests; It was applied to logarithmic P-value, log P_k between 27 selected miRNAs and other miRNAs applied to logarithmic P-value, log P_k, P-value is the probability that rejects null hypothesis that means of four replicates are equal between controls and stressed samples. The alternative hypothesis is that mean of four replicates in control samples is less than that of stressed samples

Rest period	2 days	5 days		10 days	
Stress expose period	1 day	1 day	10 days	1 day	42 days
PCA based unsupervised FE					
Control > Stress	1.98×10^{-5}	1.0	1.00	1.0	1.0
Control < Stress	1.0	3.15×10^{-13}	4.39×10^{-4}	1.02×10^{-3}	5.67×10^{-4}
Categorical regression					
Control > Stress	0.98	0.07	0.49	2.21×10^{-3}	0.4
Control < Stress	0.02	0.93	0.51	0.99	0.6
BAHSIC					
Control > Stress	2.93×10^{-3}	0.98	0.49	0.91	0.96
Control < Stress	1.00	0.02	0.51	0.09	0.04

If mean log P_k in selected 27 miRNAs is less than that in other miRNAs, the amount by which mean miRNA expression of control samples are less than stressed samples in 27 miRNAs is greater than that in other miRNAs and vice versa

where summation is taken over twelve classes, $1 \leq s \leq 12$. Top ranked 100 probes with smaller P-values computed by categorical regression are selected. 23 mRNAs and 73 miRNAs are associated with top ranked 100 probes, respectively. Although there are 181 pairs of miRNAs and miRNA target genes identified by seed match, only 37 pairs are associated with significant negative correlations. 37/181 is much less than that for PCA based unsupervised FE, 45/47. Table 6.17 shows the results for t test applied to logarithmic ratio of 23 mRNAs selected by categorical regression analysis. The performance is, at most, comparative with PCA based unsupervised FE in Table 6.17. Nonetheless, the performance for identification of miRNA expressed distinctly between control and stressed samples is obviously less significant than that of PCA based unsupervised FE (Table 6.18). Thus, in average, the ability of categorical regression analysis to identify negatively correlated pairs of miRNAs and miRNAs that are expressed distinctly between control and stressed samples is less than that of PCA based unsupervised FE.

In addition to the comparison with categorical regression analysis, I try another more advanced FE, backward elimination using Hilbert-Schmidt norm of the cross-covariance operator (BAHSIC) [45]. HSIC is the evaluation of coincidence between features and class labeling based upon inner product. Inner product of feature vectors between jth and j'th samples is defined as

$$\boldsymbol{x}_j \times_i \boldsymbol{x}_{j'} \tag{6.44}$$

where

$$\boldsymbol{x}_j = \left(x_{1j}, x_{2j}, \ldots, x_{ij}, \ldots, x_{Nj}\right) \tag{6.45}$$

and

$$\boldsymbol{x}_{j'} = \left(x_{1j'}, x_{2j'}, \ldots, x_{ij}, \ldots, x_{Nj'}\right). \tag{6.46}$$

Similarly, inner product of class labeling vectors,

$$\boldsymbol{\delta}_j = \left(\delta_{1j}, \delta_{2j}, \ldots, \delta_{sj}, \ldots, \delta_{Sj}\right) \tag{6.47}$$

and

$$\boldsymbol{\delta}_{j'} = \left(\delta_{1j'}, \delta_{2j'}, \ldots, \delta_{sj'}, \ldots, \delta_{Sj'}\right) \tag{6.48}$$

can be defined as

$$\boldsymbol{\delta}_j \times_s \boldsymbol{\delta}_{j'}. \tag{6.49}$$

Coincidence between $\boldsymbol{x}_j \times_i \boldsymbol{x}_{j'}$ and $\boldsymbol{\delta}_j \times_s \boldsymbol{\delta}_{j'}$ means that larger (smaller) $\boldsymbol{x}_j \times_i \boldsymbol{x}_{j'}$ should be associated with larger (smaller) $\boldsymbol{\delta}_j \times_s \boldsymbol{\delta}_{j'}$. HSIC can qualitatively evaluate this coincidence as

$$\begin{aligned}\| C_{sj} \|_{HS}^2 = &\left\langle \boldsymbol{x}_j \times_i \boldsymbol{x}_{j'} \cdot \boldsymbol{\delta}_j \times_s \boldsymbol{\delta}_{j'} \right\rangle_{jj'} + \left\langle \boldsymbol{x}_j \times_i \boldsymbol{x}_{j'} \right\rangle_{jj'} \left\langle \boldsymbol{\delta}_j \times_s \boldsymbol{\delta}_{j'} \right\rangle_{jj'} \\ &-2 \left\langle \left\langle \boldsymbol{x}_j \times_i \boldsymbol{x}_{j''} \right\rangle_{j''} \left\langle \boldsymbol{\delta}_{j'} \times_s \boldsymbol{\delta}_{j''} \right\rangle_{j''} \right\rangle_{jj'}\end{aligned} \tag{6.50}$$

where the last term is added such that $\| C_{sj} \|_{HS}^2 = 0$ when features and class labeling are totally independent. $\langle \cdot \rangle_{jj'}$ is the average over j and j'. BAHSIC makes use of HSIC for FE. One of N features is excluded from the computation when HSIC is computed. Then, a feature associated with the least decreased HSIC is removed. Then the process is repeated until the desired number of features remain. In order to accelerate the process, not one but more features (e.g., top 10%) are eliminated before HSIC is recomputed for further feature elimination. BAHSIC is applied to miRNA and miRNA expression with eliminating top 10% until 100 features remain.

The 100 probes selected by BAHSIC are associated with 37 mRNAs and 47 miRNAs, respectively. Although there are 169 pairs of miRNAs and miRNA target genes identified by seed match, only 73 pairs are associated with significant negative correlations. Although 73/169 is better than 37/181 by categorical regression, it is much less than that for PCA based unsupervised FE, 45/47. Table 6.17 shows the results for t test applied to logarithmic ratio of 37 mRNAs selected by BAHSIC. The performance is better than PCA based unsupervised FE in Table 6.17. Nonetheless, the performance for identification of miRNA expressed distinctly between control and stressed samples is obviously less significant than that of PCA based unsupervised FE (Table 6.18). Thus, in average, the ability of BAHSIC to identify negatively correlated pairs of miRNAs and miRNAs that are expressed distinctly between control and stressed samples is less than that of PCA based unsupervised FE.

The advantage of PCA based unsupervised FE towards categorical regression and BAHSIC is in some sense obvious. Categorical regression and BAHSIC can identify mRNAs and miRNAs with significant category dependence. Thus, negative correlation between miRNAs and mRNAs cannot be guaranteed. On the other hand, PCA based unsupervised FE can provide PC loading by which we can see if negative correlation is persisted. Thus, although PCA based unsupervised FE itself is unsupervised method, because there are opportunities that we can screen mRNAs and miRNAs with considering additional information (in this case, negative correlation), PCA based unsupervised FE is more manageable method than other two methods.

Next, we compare the stability of FE among these three methods (Table 6.19). Because all 12 classes (Table 6.14) are composed of four replicates, stability test is performed with eliminating one of four replicates randomly for all 12 classes. Then, stability test is applied to three FEs and outcome is summed up over 100 independent trials. For PCA based unsupervised FE, 78 probes associated with mRNAs and 27 probes associated miRNAs are always selected, respectively. There are only ten probes associated with mRNAs that are not always selected. In addition to this, no other probes that are associated with miRNAs are selected. This means, independent of the ensemble, 27 miRNAs are always selected. In contrast to the performance achieved by PCA based unsupervised FE, for categorical regression analysis, 24 probes associated mRNAs and eight probes associated miRNAs are always selected, respectively. Nevertheless, there are as many as 122 probes associated with mRNAs and selected only once. 33 and 29 probes associated with miRNAs were selected only once and twice, respectively. Thus, it is obvious that stability of categorical regression as feature selection tool is much less than PCA based unsupervised FE. For BAHSIC, no probes for mRNAs and 63 probes for miRNAs are always selected, respectively. There are 31 probes associated with miRNAs not selected always. Thus, it is again obvious that stability of BAHSIC as feature selection tool is much less than PCA based unsupervised FE. As a result, from the point of stability, PCA based unsupervised FE outperforms categorical regression analysis and BAHSIC.

Finally, we evaluate selected genes biologically. Because readers might not be so interested in biological background, I present here only one evaluation. As has been done in biological validation of circulating miRNAs biomarker, enrichment analysis is an easy way to evaluate obtained mRNAs. In contrast to the evaluation of miRNAs, we have list of genes. Thus we can upload genes to the Database for Annotation, Visualization and Integrated Discovery (DAVID) [21] that evaluates sets of genes by enrichment analysis. We upload 24, 21, and 37 mRNAs that are selected by PCA based unsupervised FE, categorical regression analysis, and BAHSIC and are also simultaneously targeted by 27, 73, and 47 miRNAs selected by these individual three methods (that is, the most confident set of mRNAs based upon the integrated analysis of mRNA and miRNA expression by these three methods).

Table 6.19 The frequency of probes associated with mRNAs and miRNAs, selected by either PCA based unsupervised FE, categorical regression, or BAHSIC, among 100 independent trials

Stability analysis of PCA based unsupervised FE																				
mRNA																				
Frequency	1	8	32	36	41	43	73	89	98	99	100									
Number of probes	1	1	1	1	1	1	1	1	1	1	**78**									
miRNA																				
Frequency	100																			
Number of probes	**27**																			
Stability analysis of categorical regression based FE																				
mRNA																				
Frequency	1	2	3	4	5	6	7	8	9	10	11	12	13	14	15	16	17	18	19	20
Number of probes	122	61	25	17	15	18	8	9	10	6	6	13	7	6	7	4	4	2	5	1
Frequency	21	22	23	24	25	26	27	28	29	30	31	32	33	34	36	37	39	40	42	43
Number of probes	7	1	6	5	2	4	6	3	5	5	2	2	3	3	5	3	4	2	4	1
Frequency	44	45	46	47	48	49	50	51	55	57	58	60	62	63	65	67	68	71	72	74
Number of probes	1	1	4	2	1	3	2	2	1	1	1	1	1	1	1	1	1	1	1	1
Frequency	75	77	78	79	82	83	84	87	88	90	94	95	96	97	99	100				
Number of probes	1	1	1	3	1	4	1	1	2	1	2	1	1	2	3	**24**				
miRNA																				
Frequency	1	2	3	4	5	6	7	8	9	10	11	12	13	14	15	16	17	18	19	20
Number of probes	33	29	15	17	3	10	5	8	9	7	2	1	2	4	1	5	2	2	6	1
Frequency	21	22	23	24	25	26	27	28	29	30	31	32	33	35	36	37	38	39	40	41
Number of probes	2	4	1	5	3	2	4	2	2	4	3	1	1	3	1	1	1	4	3	5
Frequency	42	43	44	46	47	48	49	50	52	53	55	56	57	59	60	61	66	67	68	70
Number of probes	2	1	2	2	3	1	2	2	2	1	2	3	2	1	4	1	2	2	2	1
Frequency	71	74	76	77	78	80	81	82	83	84	86	87	88	89	91	93	95	100		
Number of probes	1	2	1	1	1	1	1	1	2	2	1	5	1	2	3	2	2	**8**		

Stability analysis of BAHSIC																
mRNA																
Frequency	1	2	3	4	5	6	7	8	9	10	11	12	13	14		
Number of probes	2133	886	474	280	197	136	84	55	41	14	7	6	4	1		
miRNA																
Frequency	1	3	4	20	21	25	32	40	41	43	45	60	61	62	69	70
Number of probes	2	1	1	1	3	1	1	1	1	1	1	1	1	1	1	1
Frequency	73	74	75	77	79	82	86	87	90	93	95	96	97	98	99	100
Number of probes	3	2	1	3	6	1	1	1	1	1	1	1	3	2	3	**68**

Bold numbers are the number of probes always selected (i.e., 100 times)

Table 6.20 KEGG pathway enriched by 24 mRNAs targeted by 27 miRNAs, identified by DAVID

KEGG pathway	Number of genes	%	P -values	Adjusted P-values
Cardiac muscle contraction	7	30.4	2.30×10^{-9}	3.20×10^{-8}
Parkinson's disease	7	30.4	5.80×10^{-8}	4.10×10^{-7}
Oxidative phosphorylation	6	26.1	2.30×10^{-6}	1.10×10^{-5}
Alzheimer's disease	6	26.1	1.20×10^{-5}	4.20×10^{-5}
Huntington's disease	6	26.1	1.20×10^{-5}	3.50×10^{-5}

Number of genes are genes included in pathway, % is the ratio genes included in pathway among 24 mRNAs. P-values and those adjusted by BH criterion were provided by DAVID.

Table 6.20 shows the results for mRNAs selected by PCA based unsupervised FE. These are KEGG pathways related heart disease and neurodegenerative diseases. It is quite reasonable because PTSD mediated heart disease should be associated with both heart and brain problems. On the other hand, no KEGG pathway enrichment is obtained by uploading mRNAs selected by categorical regression or BAHSIC. These results suggest that PCA based unsupervised FE can outperform categorical regression and BAHSIC also from the biological point of view.

6.4.2 Identifications of Interactions Between miRNAs and mRNAs in Multiple Cancers

In the previous subsection, we decided to select 100 probes in advance. As a result, this decision works pretty well. On the other hand, it is also possible to decide the number of features selected in fully data driven way. In actuality, when genes (or miRNAs) are selected based upon expression profile, it is very usual to select genes based upon if these are differentially expressed genes (DEGs) or not. Although there are no definition about what DEGs are, two criteria are often employed.

Statistical significance Several statistical tests are applied to check if genes are differently expressed between two classes.

Fold change (FC) The ratio of amount of expression between two classes.

Because most of the statistical tests are scale invariant, i.e., even if the amount expression is globally doubled, significance does not change. This scale invariance is unlikely true, because gene expressed twice should have more important functions. In order to compensate this difficulty, FC is employed. Generally speaking, DEGs associated with more FC and more significance are better to be selected. On the other hand, the employment of two independent criteria can cause uncertainty. There can be several choices on how to balance two criteria.

This problem is critical for the selection of pairs of miRNAs and mRNAs. When identifying mRNAs and miRNAs pairs, we require

- miRNAs should be DEG between control and treated samples.
- mRNAs should be DEG between control and treated samples.
- miRNAs and mRNAs should be mutually negatively correlated.

Because these three requirements are independent, finding miRNAs and mRNAs pairs fulfilling these three conditions is not an easy task. Simply applying these three criteria parallelly to mRNAs and miRNAs might result in no intersections between those satisfying each of three conditions. Especially, significant negative correlations are hard to achieve because of too many pairs. Typically, the number of miRNAs is 10^3 while the number of mRNAs is 10^4. Thus, the number of pairs is as many as 10^7. This means that, if multiple comparison correction is considered, P-values must be smaller than $10^{-2} \times 10^{-7} = 10^{-9}$, which is unlikely satisfied especially when large enough number of samples are not available. Nevertheless, if the number of candidate mRNAs and miRNAs is reduced in advance by identifying DEGs for miRNAs and mRNAs, required P-values associated with correlation between miRNAs and mRNAs can be much larger. For example, we can reduce the number of miRNAs and mRNAs down to 10^2 and 10^3, respectively, required minimum P-values can increase up to $10^{-2} \times 10^{-5} = 10^{-7}$. Then the combination of P-values and FC for DEGs identification is often optimized without any proper reasons such that desired number of negatively correlated miRNAs and mRNAs pairs can be identified. Table 6.21 is a partial list of identification criteria of DEGs for mRNAs and miRNAs. It is obvious that there is no de facto standard.

In this subsection, I would like to show [50] that employment of PCA based unsupervised FE enables us to identify mutually negatively correlated pairs of miRNAs and mRNAs that are expressive differently between controls and treated samples

Table 6.21 A part of significant DEG identification for mRNAs and miRNAs

	Significance criteria		
Cancer	miRNA	mRNA	References
HCC	FDR ≤ 0.01; $\log_2$ FC ≥ 1		[13]
NSCLC	FDR < 0.1 by SAM		[29]
ESCC	From preceding studies	FC > 1.5	[69]
	FDR < 0.05	FC > 3;FDR < 0.001	[71]
	FDR < 0.05		[31]
PC	None		[72]
CRC	FDR < 0.05		[15]
CC	FC > 1.2; FDR< 0.1		[27]
BC	miRtest [4]	No description	[6]
PDA	FDR* < 0.05; $\mid \log \text{FC} \mid > 1$		[28]

Preceding studies

HCC hepatocellular carcinoma, *NSCLC* non-small cell lung cancer, *ESCC* esophageal squamous-cell carcinomas, *PC* prostate cancer, *CRC* Colorectal cancer, *CC* Colon cancer, *BC* breast cancer, *PDA* Pancreatic ductal adenocarcinoma

*Bonferroni's correction-adjusted P-value

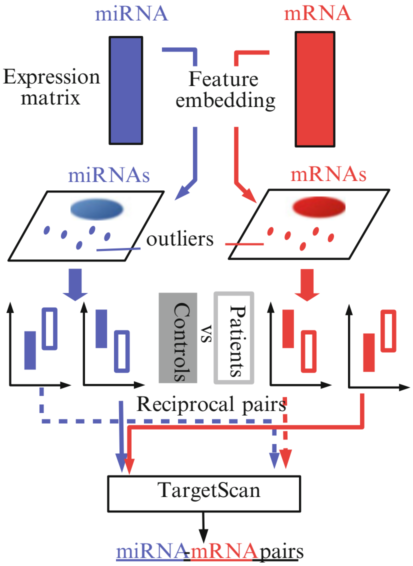

Fig. 6.8 Schematic figure that illustrates how to identify miRNAs–mRNAs pairs from expression profile using PCA based unsupervised FE. PCA is applied to miRNAs and mRNAs profiles such that PC scores, $\boldsymbol{u}_\ell^{\text{miRNA}}$ and $\boldsymbol{u}_\ell^{\text{mRNA}}$, are attributed to miRNAs and mRNAs, respectively. P-values are computed using χ^2 distribution as in Eqs. (6.52) and (6.51). mRNAs and miRNAs associated with adjusted P-values less than 0.01 are selected. Then, mRNAs and miRNAs expressed distinctly between normal tissues and cancers are selected as outliers. miRNA–mRNA pairs are identified by TargetScan among these mRNA and miRNAs with reciprocal relationship (i.e., mRNAs upregulated and miRNAs downregulated in cancer or mRNAs downregulated and miRNAs upregulated in cancer)

with the unified criterion for multiple cancers, in contrast to the various criteria depending upon the cancers as shown in Table 6.21. Figure 6.8 illustrates how to identify miRNA-mRNA pairs from expression profiles. Table 6.22 summarizes the results identified by PCA based unsupervised FE.

The more detailed procedure is as follows. Suppose we have mRNA expression profile, $\boldsymbol{x}^{\text{mRNA}} \in \mathbb{R}^{N_1 \times M_1}$, and miRNA expression profile, $\boldsymbol{x}^{\text{miRNA}} \in \mathbb{R}^{N_2 \times M_2}$. Here, N_1 and N_2 are the number of mRNAs (probes) and miRNAs (probes), respectively. M_1 and M_2 are the number of samples of mRNAs profiles and miRNAs profiles, respectively. PCA is applied to mRNAs and miRNAs profiles, and PC loading, $\boldsymbol{v}_\ell^{\text{mRNA}} \in \mathbb{R}^{N_1}$ and $\boldsymbol{v}_\ell^{\text{miRNA}} \in \mathbb{R}^{N_2}$ are obtained. Then $\boldsymbol{v}_\ell^{\text{mRNA}} \in \mathbb{R}^{N_1}$ and $\boldsymbol{v}_\ell^{\text{miRNA}} \in \mathbb{R}^{N_2}$ associated with significant distinction between normal tissues and cancers (P-values computed by t test must be less than 0.05) are selected as shown in "ℓ(P-value)s used for FE" of Table 6.22. After identifying PC loading used for FE, P-values are attributed to ith mRNA and miRNAs as

Table 6.22 Summary of the investigated mRNA and miRNA expressions

		Number of samples		Number of probes		
Cancers	GEO ID	Tumors	Controls	Selected	Non-selected	$\ell(P\text{-value})$s used for FE
HCC						
mRNA	GSE45114	24	25	269	22,963	2 (7.5×10^{-9}), 3 (7.2×10^{-5}), 4 (2.1×10^{-6})
miRNA	GSE36915	68	21	58	1087	1 (9.6×10^{-8}), 3 (3.2×10^{-16}), 4 (8.5×10^{-10})
NSCLC						
mRNA	GSE18842	46	45	1098	53,504	1 (5.5×10^{-10}), 2 (3.9×10^{-30}), 3 (1.04×10^{-2})
miRNA	GSE15008	187	174	268	3428	1 (8.0×10^{-5}), 2 (2.4×10^{-10}), 3 (1.3×10^{-2}), 4 (1.4×10^{-20}), 5 (4.6×10^{-30}), 6 (3.0×10^{-2})
ESCC						
mRNA	GSE38129	30	30	189	22,088	3 (2.1×10^{-18})
miRNA	GSE13937	76	76	37	1217	2 (2.8×10^{-5}), 3 (3.9×10^{-2}), 4 (7.8×10^{-3}), 5 (2.0×10^{-4}), 6 (3.7×10^{-6}), 7 (4.2×10^{-2})
Prostate cancer						
mRNA	GSE21032	150	29	399	43,020	3 (5.4×10^{-15})
miRNA	GSE64318	27	27	23	700	1 (2.0×10^{-2}), 2 (9.3×10^{-3}), 4 (1.4×10^{-3})
Colon/colorectal cancer						
mRNA	GSE41258	186	54	309	21,974	1 (6.2×10^{-4}), 2 (2.1×10^{-2}), 3 (3.7×10^{-2}), 4 (5.1×10^{-23}), 5 (2.1×10^{-2})
miRNA	GSE48267	30	30	12	839	5 (2.2×10^{-15})
Breast cancer						
mRNA	GSE29174	110	11	980	33,600	2 (3.3×10^{-20}), 3 (8.0×10^{-21}), 4 (1.1×10^{-6}), 5 (2.5×10^{-2})
miRNA	GSE28884	173	16	18	2258	1 (4.9×10^{-10}), 2 (4.0×10^{-11})

Probes identified and not identified by PCA-based unsupervised FE are denoted as selected and non-selected, respectively. ℓs are PC scores used for computation of P-values, Eqs. (6.51) and (6.52). P-values associated with ℓs are computed by applying t test to PC loading to test if it is distinct between normal tissues and cancers

$$P_i^{\text{mRNA}} = P_{\chi^2}\left[> \sum_{\ell}\left(\frac{u_{\ell i}^{\text{mRNA}}}{\sigma_{\ell}^{\text{mRNA}}}\right)^2\right] \tag{6.51}$$

and

$$P_i^{\text{miRNA}} = P_{\chi^2}\left[> \sum_{\ell}\left(\frac{u_{\ell i}^{\text{miRNA}}}{\sigma_{\ell}^{\text{miRNA}}}\right)^2\right] \tag{6.52}$$

Table 6.23 Summary of the biological validation of identified pairs

Cancer	HCC	NSCLC	ESCC	PC	CCC/CC	BC
Number of pairs	21	311	4	32	8	37
Pairs with previous studies	19	270	4	19	7	32
Number of pairs in starbase	9	144	2	12	3	17

“Pairs with previous studies” suggest that mRNA and miRNA are reported to be related to cancers to which these pairs are identified. “Number of pairs in starbase” suggests the number of pairs included in any cancers in starbase. More detailed information is available in Tables S1–S18 [50]

where summation is taken over ℓs selected (Table 6.22). miRNAs and mRNAs associated with BH criterion adjusted P-values less than 0.01 are selected.

In order to identify reliable mRNAs and miRNAs pairs among selected mRNAs and miRNAs, the following procedures are further performed. In order to fulfill the requirement of reciprocal relationship between miRNAs and mRNAs expression, mRNAs and miRNAs up/downregulated in cancers compared with normal tissue are identified. This has been done by applying t test. Obtained P-values are adjusted by BH criterion and mRNAs and miRNAs associated with adjusted P-values less than 0.05 are selected. Reciprocal pairs of miRNAs and miRNAs, i.e., upregulated miRNAs and downregulated mRNAs or upregulated mRNAs and downregulated miRNAs are compared with pairs included in TargetScan [2] that stores list of miRNA target mRNAs. In order to do this, Predicted_Targets_Info file that is supposed to include all of human conserved targets is obtained and all pairs included in this file remain as final candidate miRNAs and mRNAs. Table 6.23 summarizes the biological validation of identified pairs. Most of the pairs in seven cancers other than PC are composed of miRNAs and mRNAs that are previously reported to be related to cancers to which miRNAs and mRNAs are identified. We also check if pairs are in starbase [70] that stores the information of miRNA-mRNA pair. Generally, half of pairs are included in starbase. This suggests that PCA based unsupervised FE can identify limited number of mRNAs and miRNAs between which biologically reliable reciprocal pairs can be identified. In this regard, PCA based unsupervised FE is more effective than the standard strategy that requires combinatorial usage of statistical test and FC. In addition to this, we can employ unified criterion that adjusted P-values must be less than 0.01. To the best of my knowledge, no other methods can perform identification of reliable number of miRNAs and mRNAs by the unified criterion valuable for as many as six cancers, i.e., six cancers listed in Table 6.23 other than PC.

6.5 Integrated Analysis of Methylation and Gene Expression

As can be seen in the previous section, integrated analysis of mRNAs and miRNAs can give us the more reliable identification of mRNAs than selecting mRNAs based upon only the criterion of DEG. Thus, it is better to consider something other than miRNA expression together with mRNA expression. One possible candidate is DNA methylation which is known to suppress mRNA expression.

6.5.1 Aberrant Promoter Methylation and Expression Associated with Metastasis

Metastasis is a developed stage of cancer. After metastasis takes place, cancer cell starts to leave from original location where cancer initiates, to migrate to all over the body and to grow there. Thus, once metastasis starts, therapy of cancer becomes drastically difficult. Therefore, suppressing progression to metastasis is critically important in cancer therapy. In this regard, we try to identify critical genes for cancer progression to metastasis based upon the integrated analysis of mRNA expression and promoter methylation [66]. Table 6.24 shows the number of samples used in this study (files, GSE52143_series_matrix.txt.gz and GSE52144_series_matrix.txt.gz in series matrix session in GEO are used for mRNA expression profiles and promoter methylation profiles, respectively). There are two cell lines for which pre-/post-metastasis samples available. Thus, there are four classes. Two and three biological replicates are for methylation and mRNA, respectively. Before starting analysis, I would like to emphasize the difficulty of the analysis. First of all, there are only three and two biological replicates for mRNA expression profiles and promoter methylation profiles, respectively, while there are as many as 33,297 probes and 27,578 probes for mRNA expression profiles and methylation profiles, respectively. This means that identification of DEG and differentially methylated site (DMS) is not easy.

We apply PCA to mRNA expression profile, $x_{ij}^{\mathrm{mRNA}} \in \mathbb{R}^{33297\times 12}$, and promoter methylation profiles, $x_{kj}^{\mathrm{methyl}} \in \mathbb{R}^{27578\times 8}$. Then we get PC loading attributed to mRNA and miRNA samples, $\boldsymbol{v}_{\ell}^{\mathrm{mRNA}}$ and $\boldsymbol{v}_{\ell}^{\mathrm{methyl}}$, respectively. Figure 6.9 shows the obtained PC loading. The first PC loading does not exhibit any sample dependence. Thus, it is not useful to identify DEG and DMS. The second PC loading exhibits some sample dependence. Nevertheless, it is coincident with the distinction between cell lines. The third PC loading exhibits the distinction between pre- and post-metastasis as

Table 6.24 Samples used in this study

Cell lines	A549		HTB56		Total
Metastasis	Pre	Post	Pre	Post	
mRNA	3	3	3	3	12
methylation	2	2	2	2	8

pre: before metastasis, post: after metastasis. Numbers are the number of biological replicates. mRNAs expression profiles and promoter methylation profiles are obtained via GEO ID: GSE52143 and GSE52144, respectively

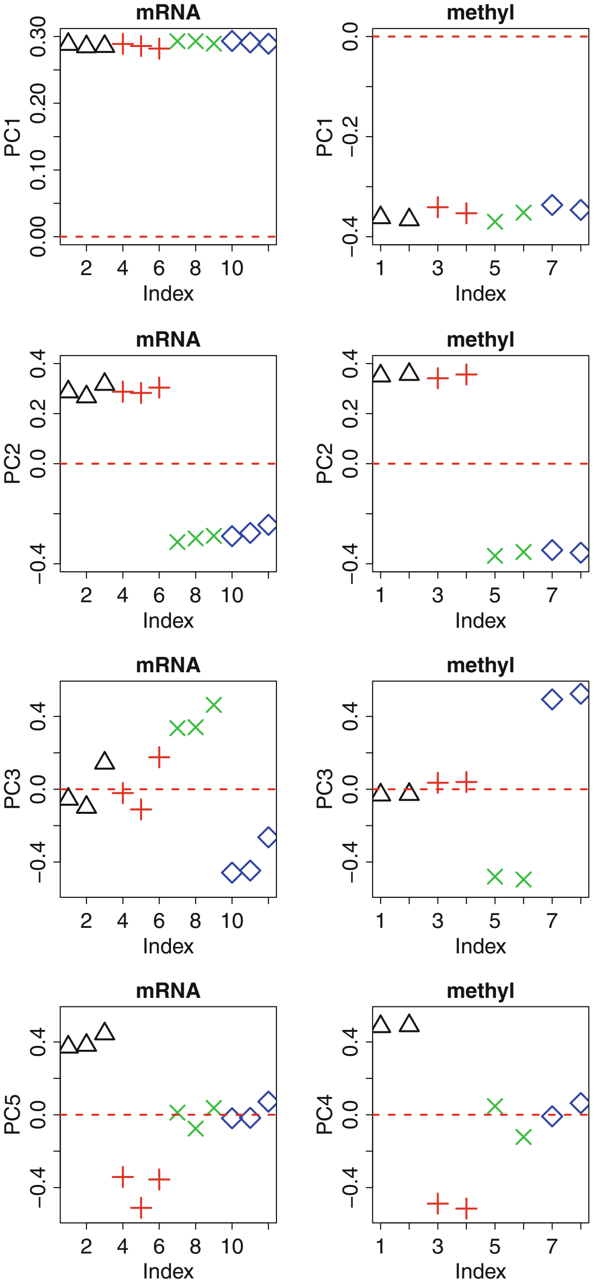

Fig. 6.9 PC loading obtained by applying PCA to mRNA expression and promoter methylation. Open triangle: A549 cell line pre-metastasis, red plus symbol: A549 cell line post-metastasis, green cross symbol: HTB56 cell line pre-metastasis, blue diamond: HTB56 cell line post-metastasis. Left column: the first, second, third, and fifth PCs for mRNA. Right column: the first, second, third, and fourth PCs for promoter methylation

expected, but only for HTB56 cell lines. The fifth PC loading for mRNA and the fourth PC loading for methylation exhibit the distinction between pre- and post-metastasis as expected, but again only for A549 cell lines.

We attribute P-values to probe using corresponding PC scores using χ^2 distribution as

$$P_i^\ell = P_{\chi^2}\left[> \left(\frac{u_{\ell i}^{\mathrm{mRNA}}}{\sigma_\ell^{\mathrm{mRNA}}} \right)^2 \right], \ell = 2, 3, 5 \tag{6.53}$$

and

$$P_k^\ell = P_{\chi^2}\left[> \left(\frac{u_{\ell k}^{\mathrm{miRNA}}}{\sigma_\ell^{\mathrm{miRNA}}} \right)^2 \right], \ell = 2, 3, 4. \tag{6.54}$$

P-values are adjusted by BH criterion. Then probes associated with adjusted P-values less than 0.01 are selected. Table 6.25 lists the number of probes selected. At least, for all cases, PCA based unsupervised FE can identify probes with significant P-values.

Because we are aiming to perform integrated analysis of mRNA expression and promoter methylation, it is important to see if genes selected for mRNA expression and promoter methylation are significantly overlapped. In order to do this, mRNA probes and methylation probes are converted to list of genes to which probes are attributed (the correspondence between probes and genes is available as files GPL6244-24073.txt and GPL8490-65.txt in GEO). Table 6.26 shows the confusion matrix and the results of Fisher's exact test. For both cases, PCA based unsupervised FE identifies mRNAs and promoter methylation sites with significant overlaps. On the other hand, the overlap of genes associated with the progression from pre- to post-metastasis is much less than those associated with distinction between two cell lines. PCA based unsupervised FE is powerful enough method to detect this slight overlap.

Figure 6.10 shows the scatterplot of PC loading shown in Fig. 6.9, which is averaged over within each of four classes. PC loading other than the first PC loading is mutually correlated between mRNA and methylation. This is coincident with Table 6.26 where significant overlap of selected genes between mRNA expression and promoter methylation is detected.

In order to confirm the superiority of PCA based unsupervised FE towards conventional supervised methods, we apply t test as follows.

Table 6.25 The number of probes selected using P-values computed by Eqs. (6.53) and (6.54)

	mRNA			Methylation		
ℓ	2	3	5	2	3	4
Number of selected probes	422	261	248	512	369	270

ℓ: PCs used for FES

Table 6.26 Confusion matrices and associated with P-values and odds ratio

Distinction between cell lines					
	Methylation ($\ell = 2$)	Not selected	Selected	P-value	Odds ratio
mRNA	Not selected	13,065	340	1.39×10^{-24}	7.12
($\ell = 2$)	Selected	286	53		
Distinction between pre- and post-metastasis for HTB56 cell line					
	Methylation ($\ell = 3$)	Not selected	Selected	P-value	Odds ratio
mRNA	Not selected	13,252	313	0.04	2.24
($\ell = 3$)	Selected	170	9		
Distinction between pre- and post-metastasis for A549 cell line					
	Methylation ($\ell = 4$)	Not selected	Selected	P-value	Odds ratio
mRNA	Not selected	13,402	232	0.01	3.33
($\ell = 5$)	Selected	104	6		

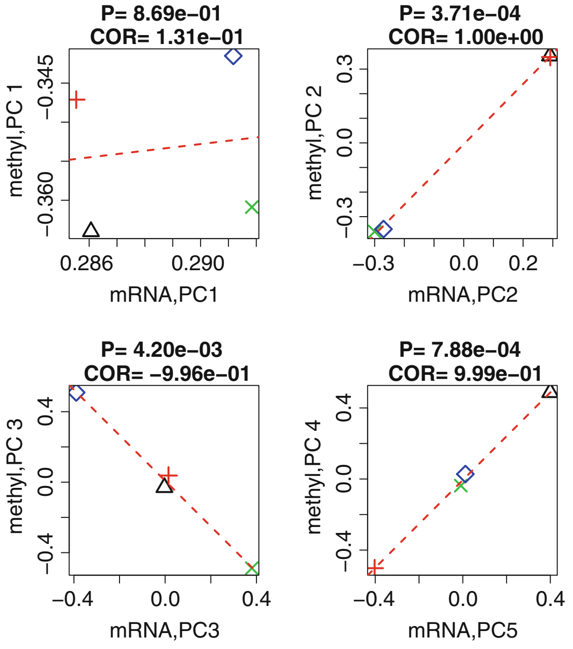

Fig. 6.10 Scatterplot of PC loading in Fig. 6.9 averaged within four classes. Broken straight lines are linear regression. Open triangle: A549 cell line pre-metastasis, red plus symbol: A549 cell line post-metastasis, green cross symbol: HTB56 cell line pre-metastasis, blue diamond: HTB56 cell line post-metastasis

1. Six samples in A549 cell lines vs six samples in HTB56 cell lines for mRNA expression.
2. Four samples in A549 cell lines vs four samples in HTB56 cell lines for promoter methylation.
3. Three samples in pre-metastasis vs three samples in post-metastasis for A549 mRNA expression.
4. Two samples in pre-metastasis vs two samples in post-metastasis for A549 promoter methylation.

5. Three samples in pre-metastasis vs three samples in post-metastasis for HTB56 mRNA expression.
6. Two samples in pre-metastasis vs two samples in post-metastasis for HTB56 promoter methylation.

Among the above comparisons, 3. 4. and 6. Has no probes associated with adjusted P-values less than 0.01. Comparison 5. has only 5 probes associated with adjusted P-values less than 0.01. Thus, t test is useless for the identification of mRNAs and promoter methylation distinct between pre- and post-metastasis. Comparison 1. and 2. have 7074 and 2186 probes associated with adjusted P-values less than 0.01. Nevertheless, there are not significant overlaps between genes to which these probes are attributed ($P = 0.57$ and odds ratio is as small as 0.97). In addition to this, we also apply categorical regression analysis assuming four classes to mRNA expression and promoter methylation independently. It identifies 7501 and 6573 probes, respectively. Nevertheless, odds ratio of overlap detection between genes associated with identified probes is 0.67, which is even smaller than the expectation, 1.0, for random selections. Thus, PCA based unsupervised FE can outperform conventional supervised methods.

Finally, we need to validate identified genes biologically as usual. We upload 15 genes shown in Table 6.27 to the molecular signatures database (MSigDB) [47] with specifying "C2: curated gene sets," which is composed of "CGP: chemical and genetic perturbations," "CP: Canonical pathways," "CP:BIOCARTA: BioCarta gene sets," "CP:KEGG: KEGG gene sets," and "CP:REACTOME: Reactome gene sets." Tables 6.28 show the results. In total, as many as 46 gene sets are significantly overlapped with uploaded 15 genes (false discovery rate (FDR) q-values are less than 0.05). Twenty seven out of 46 gene sets are directly related to tumors and cancers (asterisked). The fact that more than half of identified gene sets are cancer and tumor related demonstrates the ability of PCA based unsupervised FE that can select biologically reliable gene sets. In addition to this, it is rare that as small as 15 genes have such huge number of enriched terms, because P-values computed by enrichment analysis have tendency to increase, i.e., to become less significant, as the number of genes is smaller. This suggests that PCA based unsupervised FE has the ability to identify small number of critical genes also from the biological point of view.

6.5.2 *Epigenetic Therapy Target Identification Based upon Gene Expression and Methylation Profile*

As mentioned in the previous subsection, cancer therapy is always difficult. In order to challenge this difficult task, other than usual therapies, epigenetic therapy recently collects many researchers' interest, because epigenetic is expected to affect cancer initiation and progression [40]. Thus, conversely, modifying epigenetic profile might contribute to the cancer therapy [3]. One possible difficulty of epigenetic

Table 6.27 List of nine genes chosen for the distinction between metastasis of HTB56 cell lines in common between mRNA expression and promoter methylation, and six genes chosen for the distinction between metastasis of A549 cell lines in common between mRNA expression and promoter methylation

Refseq ID	Gene symbol	Gene name
Distinction between pre- and post-metastasis for HTB56 cell line		
NM_153608	ZNF114	Zinc finger protein 114
NM_152457	ZNF597	Zinc finger protein 597
NM_152753	scube3	Signal peptide, CUB domain and EGF like domain containing 3
NM_000793	DIO2	Deiodinase, iodothyronine type II
NM_002145	HOXB2	Homeobox B2
NM_032040	CCDC8	Coiled-coil domain containing 8
NM_004613	TGM2	Transglutaminase 2
NM_001275	CHGA	Chromogranin A
NM_006762	LAPTM5	Lysosomal protein transmembrane 5
Distinction between pre- and post-metastasis for A549 cell line		
NM_000201	ICAM1	Intercellular adhesion molecule 1
NM_005562	LAMC2	Laminin subunit gamma 2
NM_002996	CX3CL1	C-X3-C motif chemokine ligand 1
NM_020182	PMEPA1	Prostate transmembrane protein, androgen induced 1
NM_004633	IL1R2	Interleukin 1 receptor type 2
NM_022164	TINAGL1	Tubulointerstitial nephritis antigen like 1

therapy is identification of target genes. In contrast to small molecule drug that has target proteins to which small molecule binds, epigenetic therapy generally targets the alteration of epigenetic profiles, e.g., promoter methylation and histone modification. Thus, it is unclear which genes are targeted by individual epigenetic therapy. Because PCA based unsupervised FE has the ability to identify DEGs associated with methylation alteration, PCA based unsupervised FE is expected to be fitted to detect genes targeted by epigenetic therapy.

In this data set, we analyze mRNA expression and methylation profiles before and after reprogramming, which means to add pluripotency to differentiated cells, of various cancer cell lines. Here, pluripotency is the ability of cells that can differentiate into any kind of cells. The reason why we analyze gene expression profiles of reprogrammed cells is because methylation profiles altered during reprogramming and associated with altered mRNA expression is the potential target of epigenetic therapy. The data set we analyze [60] is taken from GEO with ID GSE35913. They consist of eight cell lines, H1 (ES cell), H358 and H460 (NSCLC), IMR90 (human Caucasian fetal lung fibroblast), iPCH358, iPCH460, iPSIMR90 (reprogrammed cell lines), and piPCH358 (re-differentiated iPCH358) with three biological replicates. In total, there were three replicates × 8 cell lines × 2 properties (gene expression and promoter methylation) = 48 samples. It is a typical multi-class

Table 6.28 Enrichment analysis by MSigDB

Gene set name	#1	Description	#2	k/K	P	Q
BOYAULT_LIVER_CANCER_SUBCLASS_G5_DN	27	* Down-regulated genes in hepatocellular carcinoma (HCC) subclass G5, defined by unsupervised clustering.	3	0.1111	2.97E−08	1.42E−04
KHETCHOUMIAN_TRIM24_TARGETS_UP	47	* Retinoic acid-responsive genes up-regulated in hepatocellular carcinoma (HCC) samples of TRIM24 knockout mice.	3	0.0638	1.64E−07	3.92E−04
ONDER_CDH1_TARGETS _2_DN	464	* Genes down-regulated in HMLE cells (immortalized nontransformed mammary epithelium) after E-cadhedrin (CDH1) knockdown by RNAi.	4	0.0086	3.20E−06	2.78E−03
RASHI_RESPONSE_TO_IONIZING_RADIATION_2	127	Cluster 2: late ATM dependent genes induced by ionizing radiation treatment.	3	0.0236	3.35E−06	2.78E−03
KRISHNAN_FURIN _TARGETS_UP	12	Genes up-regulated in naive T lymphocytes lacking FURIN : Cre-Lox knockout of FURIN in CD4+ cells.	2	0.1667	3.43E−06	2.78E−03
KIM_RESPONSE_TO_TSA_AND_DECITABINE_UP	129	* Genes up-regulated in glioma cell lines treated with both decitabine and TSA.	3	0.0233	3.51E−06	2.78E−03
DARWICHE_SQUAMOUS_CELL_CARCINOMA_UP	146	* Genes up-regulated in squamous cell carcinoma (SCC) compared to normal skin.	3	0.0205	5.09E−06	3.09E−03
DARWICHE_PAPILLOMA_RISK_HIGH_UP	147	* Genes up-regulated during skin tumor progression from normal skin to high risk papilloma.	3	0.0204	5.19E−06	3.09E−03
PETROVA_ENDOTHELIUM_LYMPHATIC_VS_BLOOD_DN	162	Genes down-regulated in BEC (blood endothelial cells) compared to LEC (lymphatic endothelial cells).	3	0.0185	6.95E−06	3.68E−03

(continued)

Table 6.28 (continued)

Gene set name	#1	Description	#2	k/K	P	Q
SMID_BREAST_CANCER _BASAL_UP	648	* Genes up-regulated in basal subtype of breast cancer samples.	4	0.0062	1.19E−05	5.69E−03
AFFAR_YY1_TARGETS _UP	214	Genes up-regulated in MEF cells (embryonic fibroblast) expressing 25% of YY1.	3	0.014	1.60E−05	6.52E−03
BOQUEST_STEM _CELL_DN	216	Genes down-regulated in freshly isolated CD31- (stromal stem cells from adipose tissue) versus the CD31+ (non-stem) counterparts.	3	0.0139	1.64E−05	6.52E−03
WONG_ADULT_TISSUE _STEM_MODULE	721	The ‘adult tissue stem’ module: genes coordinately up-regulated in a compendium of adult tissue stem cells.	4	0.0055	1.82E−05	6.65E−03
SENESE_HDAC1_AND _HDAC2_TARGETS_UP	238	* Genes up-regulated in U2OS cells (osteosarcoma) upon knockdown of both HDAC1 and HDAC2 by RNAi.	3	0.0126	2.19E−05	7.17E−03
HOLLERN_SOLID_NODULAR _BREAST_TUMOR_DN	30	* Genes that have low expression in mammary tumors of solid nodular histology.	2	0.0667	2.26E−05	7.17E−03
KOINUMA_TARGETS_OF _SMAD2_OR_SMAD3	824	Genes with promoters occupied by SMAD2 or SMAD3 in HaCaT cells (keratinocyte) according to a ChIP-chip analysis.	4	0.0049	3.06E−05	8.58E−03
SHIN_B_CELL _LYMPHOMA_CLUSTER_8	36	* Cluster 8 of genes distinguishing among different B lymphocyte neoplasms.	2	0.0556	3.27E−05	8.64E−03
HELLER_SILENCED_BY_METHYLATION_UP	282	* Genes up-regulated in at least one of three multiple myeloma (MM) cell lines treated with the DNA hypomethylating agent decitabine (5-aza-2’-deoxycytidine).	3	0.0106	3.64E−05	9.12E−03
PHONG_TNF_RESPONSE _NOT_VIA_P38	337	* Genes whose expression changes in Calu-6 cells (lung cancer) by TNF were not affected by p38 inhibitor LY479754.	3	0.0089	6.17E−05	1.44E−02

VILIMAS_NOTCH1 _TARGETS_UP	52	Genes up-regulated in bone marrow progenitors by constitutively active NOTCH1.	2	0.0385	6.86E−05	1.44E−02
SCHUETZ_BREAST_CANCER _DUCTAL_INVASIVE_UP	351	* Genes up-regulated in invasive ductal carcinoma (IDC) relative to ductal carcinoma in situ (DCIS, non-invasive).	3	0.0085	6.97E−05	1.44E−02
KRIEG_HYPOXIA _VIA_KDM3A	53	* Genes dependent on KDM3A for hypoxic induction in RCC4 cells (renal carcinoma) expressing VHL.	2	0.0377	7.13E−05	1.44E−02
NABA_MATRISOME	1028	Ensemble of genes encoding extracellular matrix and extracellular matrix-associated proteins	4	0.0039	7.25E−05	1.44E−02
PID_TXA2PATHWAY	57	Thromboxane A2 receptor signaling	2	0.0351	8.25E−05	1.57E−02
PHONG_TNF _TARGETS_UP	63	* Genes up-regulated in Calu-6 cells (lung cancer) at 1 h time point after TNF treatment.	2	0.0317	1.01E−04	1.85E−02
PID_INTEGRIN1 _PATHWAY	66	Beta1 integrin cell surface interactions	2	0.0303	1.11E−04	1.93E−02
SATO_SILENCED_BY_METHYLATION_IN_PANCREATIC_CANCER_1	419	* Genes up-regulated in the pancreatic cancer cell lines (AsPC1, Hs766T, MiaPaCa2, Panc1) but not in the non-neoplastic cells (HPDE) by decitabine (5-aza-2'-deoxycytidine).	3	0.0072	1.18E−04	1.93E−02
TURASHVILI_BREAST_NORMAL_DUCTAL_VS_LOBULAR_UP	68	Genes up-regulated in normal ductal and normal lobular breast cells.	2	0.0294	1.18E−04	1.93E−02
DELYS_THYROID _CANCER_UP	443	* Genes up-regulated in papillary thyroid carcinoma (PTC) compared to normal tissue.	3	0.0068	1.39E−04	2.20E−02
RADMACHER_AML _PROGNOSIS	78	* The 'Bullinger validation signature' used to validate prediction of prognostic outcome of acute myeloid leukemia (AML) patients with a normal karyotype.	2	0.0256	1.55E−04	2.38E−02

(continued)

Table 6.28 (continued)

Gene set name	#1	Description	#2	k/K	P	Q
HELLEBREKERS_SILENCED _DURING_TUMOR_ANGIOGENESIS	80	* Genes down-regulated in tumor-conditioned vs quiescent endothelial cells and up-regulated upon treatment with decitabine and TSA.	2	0.025	1.63E−04	2.38E−02
LIEN_BREAST_CARCINOMA _METAPLASTIC_VS_DUCTAL_UP	83	* Genes up-regulated between two breast carcinoma subtypes: metaplastic (MCB) and ductal (DCB).	2	0.0241	1.75E−04	2.38E−02
SANA_TNF _SIGNALING_UP	83	Genes up-regulated in five primary endothelial cell types (lung, aortic, iliac, dermal, and colon) by TNF.	2	0.0241	1.75E−04	2.38E−02
KIM_GLIS2 _TARGETS_UP	84	Partial list of genes up-regulated in the kidney of GLIS2 knockout mice compared to the wild type.	2	0.0238	1.80E−04	2.38E−02
RASHI_RESPONSE_TO_IONIZING_ RADIATION_6	84	Cluster 6: late responding genes activated in ATM deficient but not in the wild type tissues.	2	0.0238	1.80E−04	2.38E−02
KANG_IMMORTALIZED _BY_TERT_UP	89	Up-regulated genes in the signature of adipose stromal cells (ADSC) immortalized by forced expression of telomerase (TERT).	2	0.0225	2.02E−04	2.60E−02
ENK_UV_RESPONSE_KERATINOCYTE_ UP	530	Genes up-regulated in NHEK cells (normal epidermal keratinocytes) after UVB irradiation.	3	0.0057	2.35E−04	2.94E−02
BASSO_CD40 _SIGNALING_UP	101	* Genes up-regulated by CD40 signaling in Ramos cells (EBV negative Burkitt lymphoma).	2	0.0198	2.60E−04	3.17E−02
SMID_BREAST_CANCER_LUMINAL_B_DN	564	* Genes down-regulated in the luminal B subtype of breast cancer.	3	0.0053	2.82E−04	3.36E−02
GHANDHI_DIRECT _IRRADIATION_UP	110	Genes significantly (FDR $<$ 10%) up-regulated in IMR-90 cells (fibroblast) in response to direct irradiation.	2	0.0182	3.08E−04	3.58E−02

WANG_ESOPHAGUS_CANCER_VS_NORMAL_UP	121	* Up-regulated genes specific to esophageal adenocarcinoma (EAC) relative to normal tissue.	2	0.0165	3.72E−04	4.22E−02
BUYTAERT_PHOTODYNAMIC_THERAPY_STRESS_DN	637	* Genes down-regulated in T24 (bladder cancer) cells in response to the photodynamic therapy (PDT) stress.	3	0.0047	4.03E−04	4.46E−02
ZHONG_SECRETOME_OF_LUNG_CANCER_AND_FIBROBLAST	132	* Proteins secreted in co-culture of LKR-13 tumor cells (non-small cell lung cancer, NSCLC) and MLg stroma cells (fibroblasts).	2	0.0152	4.43E−04	4.79E−02
PANGAS_TUMOR_SUPPRESSION_BY_SMAD1_AND_SMAD5_UP	134	* Genes up-regulated in ovarian tumors from mouse models for the BMP SMAD signaling (gonad specific double knockout of SMAD1 and SMAD5).	2	0.0149	4.56E−04	4.83E−02
PROVENZANI _METASTASIS_DN	136	* Genes down-regulated in polysomal and total RNA samples from SW480 cells (primary colorectal carcinoma, CRC) compared to the SW620 cells (lymph node metastasis from the same individual).	2	0.0147	4.70E−04	4.86E−02

#1 : # genes in gene set (K) #2: # genes in overlap (k), P: p-value, Q: FDR q-value. Cancer or tumor related terms are asterisked. “XE−Y” means $X \times 10^{-Y}$

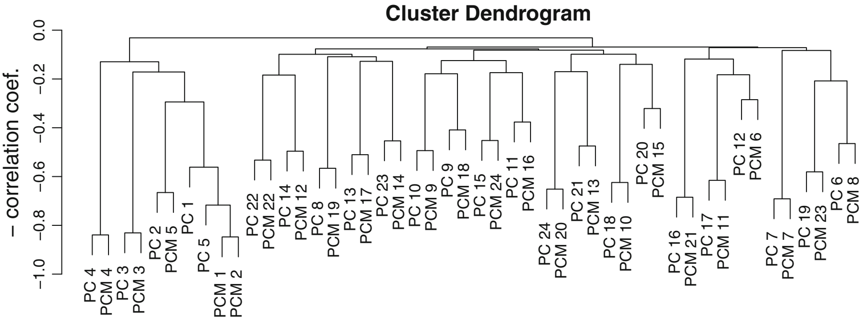

Fig. 6.11 Hierarchical clustering (UPGMA) applied to set of 24 $\boldsymbol{v}_\ell^{\text{mRNA}}$ (labeled as PCℓ) and 24 $\boldsymbol{v}_\ell^{\text{methyl}}$ (labeled as PCMℓ) with using negative signed Pearson's correlation coefficients as distance. $\boldsymbol{v}_\ell^{\text{mRNA}}$ and $\boldsymbol{v}_\ell^{\text{methyl}}$ for $\ell = 3$ and 4, i.e., four edges on the left end, are paired with high correlations

data set, because there is no clear one-to-one correspondence. Then we apply PCA based unsupervised FE as well as categorical regression analysis to this data set.

First, PCA is applied to mRNA expression, $x_{ij}^{\text{mRNA}} \in \mathbb{R}^{47321 \times 24}$, and methylation profiles, $x_{kj}^{\text{methyl}} \in \mathbb{R}^{25728 \times 24}$, and compute PC loading, $\boldsymbol{v}_\ell^{\text{mRNA}} \in \mathbb{R}^{24}$ and $\boldsymbol{v}_\ell^{\text{methyl}} \in \mathbb{R}^{24}$, which are attributed to samples. In order to perform integrated analysis of mRNA expression and methylation profile, we need to know pairs of PC loading of mRNA expression and promoter methylation associated with reciprocal relationship. For this purpose, we apply unweighted pair group method using arithmetic average (UPGMA) to set of 24 $\boldsymbol{v}_\ell^{\text{mRNA}}$ and 24 $\boldsymbol{v}_\ell^{\text{methyl}}$ with using negative signed Pearson's correlation coefficients as distance. Figure 6.11 shows the result of UPGMA. It is obvious that $\boldsymbol{v}_3^{\text{mRNA}}$ and $\boldsymbol{v}_3^{\text{methyl}}$, and $\boldsymbol{v}_4^{\text{mRNA}}$ and $\boldsymbol{v}_4^{\text{methyl}}$, are paired with high correlations (correlation coefficient $\sim$ 0.9). Figure 6.12 shows the selected PC loading. It is obvious that they have dependence upon eight classes. Especially, it is remarkable that four classes that represent reprogrammed cells ("iPCH358," "iPCH460," "iPSIMR90," and "piPCH358") have almost same values. Thus, mRNAs and methylation associated with these PC loading likely exhibit the distinction between pre- and post-reprogramming.

The algorithm of UPGMA is as follows. Suppose there are N features to be clustered and pairwise distances $d_{ii'} \in \mathbb{R}^{N \times N}$ between ith and i'th features are available.

1. Find a pair i and i' with minimum distance $d_{ii'}$.
2. Merge i and i' into a newly generated *pseudo* feature i''.
3. Compute pairwise distance between i'' and $i_0 \neq i, i'$s as

$$d_{i''i_0} = \frac{d_{ii_0} + d_{i'i_0}}{2} \tag{6.55}$$

4. If there are more than one features, go back to step 1.

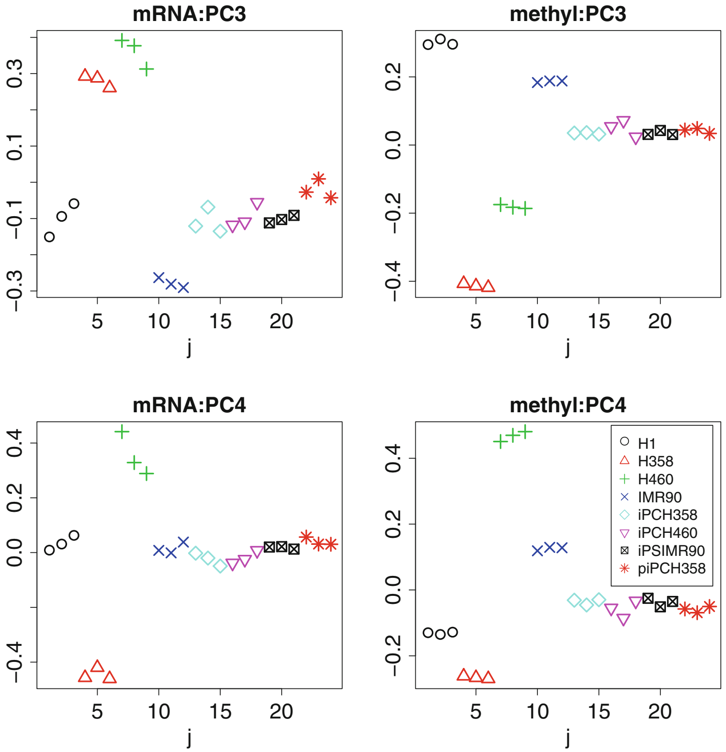

Fig. 6.12 PC loading, v_ℓ^{mRNA} and v_ℓ^{methyl} for $\ell = 3, 4$

Table 6.29 The number of probes selected using P-values computed by Eqs. (6.53) and (6.54)

	mRNA		Methylation	
ℓ	3	4	3	4
Number of selected probes	283	310	200	199

In order to confirm the stability of the selection of pairs $\ell = 3, 4$, we systematically remove one of 24 samples and apply UPGMA to 23 samples. Although $\ell = 3, 4$ are not always clustered together, four PC loading that are most similar to PC loading $\ell = 3$ or 4 when all 24 samples are used are always clustered together. Thus, the selection of $\ell = 3, 4$ as features clustered together is robust.

Then we attribute P-values to probes using corresponding PC scores using χ^2 distribution as Eqs. (6.53) and (6.54) where ℓs listed beside these equations are replaced with $\ell = 3, 4$. P-values are adjusted by BH criterion. Then probes associated with adjusted P-values less than 0.05 are selected. Table 6.29 lists the number of probes selected. At least, for all cases, PCA based unsupervised FE can identify probes with significant P-values.

Because we are aiming to perform integrated analysis of mRNA expression and promoter methylation, it is important to see if genes selected for mRNA expression

Table 6.30 Confusion matrices and associated with P-values and odds ratio

	Methylation	Not selected	Selected	P-value	Odds ratio
PCA based unsupervised FE: $\ell = 3$					
mRNA	Not selected	13,118	191	0.04	2.25
	Selected	274	9		
PCA based unsupervised FE: $\ell = 4$					
mRNA	Not selected	13,092	190	0.05	2.06
	Selected	301	9		
Categorical regression					
mRNA	Not selected	1180	6294	3.79×10^{-3}	0.87
	Selected	1080	5038		

and promoter methylation are significantly overlapped. In order to do this, mRNA probes and methylation probes are converted to the list of genes to which probes are attributed (the correspondence between probes and genes is available as files GPL8490-65.txt in GEO). Table 6.30 shows the confusion matrix and the results of Fisher's exact test. For both cases, PCA based unsupervised FE identifies mRNAs and promoter methylation sites with significant overlaps. We also apply categorical regressions and found that 11,332 and 5038 probes are associated with adjusted P-values less than 0.05 for mRNA expression and promoter methylation. On the other hand, the overlap of genes associated with categorical regression analysis has odds ratio less than 1.0 (0.87), which suggests that overlaps are less than random selection (the small P-value assigned means that overlap is significantly *less* than that expected when the selection is random). Thus, categorical regression analysis fails to identify genes associated with aberrant mRNA expression and promoter methylation simultaneously. PCA based unsupervised FE is a powerful enough method to detect this slight overlap.

Finally, we need to validate identified genes biologically. We upload 18 genes shown in Table 6.31 to MSigDB [47] with specifying "C2: curated gene sets." In total, as many as 85 gene sets are significantly overlapped with uploaded 18 genes (false discovery rate (FDR) q-values are less than 0.05). It takes three tables to display 46 gene sets (Tables 6.28 show the results). If we list all 85 gene sets here, it will take more than six tables which is simply annoying. Thus, we are not willing to list all of them here. Forty five out of 86 gene sets are listed because they are directly related to tumors and cancers. "C2: curated gene sets" is composed of "CGP: chemical and genetic perturbations," "CP: Canonical pathways," "CP:BIOCARTA: BioCarta gene sets," "CP:KEGG: KEGG gene sets," and "CP:REACTOME: Reactome gene sets." The fact that more than half of identified gene sets are cancer and tumor related demonstrates the ability of PCA based unsupervised FE that can select biologically reliable gene sets. In addition to this, P-values computed by enrichment analysis generally has tendency to increase as the number of genes is smaller. Thus, it is rare that as small as 18 genes have such huge number of enriched gene sets. This suggests that PCA based unsupervised FE

Table 6.31 List of nine genes chosen by PCA based unsupervised FE with $\ell = 3, 4$ in common between mRNA expression and promoter methylation (Table 6.30)

Refseq ID	Gene symbol	Gene name
$\ell = 3$		
NM_213606	SLC16A12	Solute carrier family 16 member 12
NM_004321	KIF1A	Kinesin family member 1A
NM_015881	DKK3	Dickkopf WNT signaling pathway inhibitor 3
NM_014220	TM4SF1	Transmembrane 4 L six family member 1
NM_003012	SFRP1	Secreted frizzled related protein 1
NM_019102	HOXA5	Homeobox A5
NM_001458	FLNC	Filamin C
NM_201525	ADGRG1	Adhesion G protein-coupled receptor G1
NM_001992	F2R	Coagulation factor II thrombin receptor
$\ell = 4$		
NM_000393	COL5A2	Collagen type V alpha 2 chain
NM_002727	SRGN	Serglycin
NM_005558	LAD1	Ladinin 1
NM_012307	EPB41L3	Erythrocyte membrane protein band 4.1 like 3
NM_005562	LAMC2	Laminin subunit gamma 2
NM_000993	RPL31	Ribosomal protein L31
NM_201525	ADGRG1	Adhesion G protein-coupled receptor G1
NM_004360	CDH1	Cadherin 1
NM_002354	EPCAM	Epithelial cell adhesion molecule

has the ability to identify small number of critical genes also from the biological point of view.

Before closing this subsection, we would like to add a few biological supportive evidences that 18 genes in Table 6.31 likely include genes targeted by epigenetic therapy more directly.

The first evidence is the comparison with cell lines resistant to epigenetic therapy [32]. Histone deacetylase (HDAC) inhibitor is one of the promising epigenetic therapies. Histone acetylation is generally believed to accelerate gene transcription. Thus, deacetylation is supposed to deactivate genes. In this regard, HDAC inhibitor suppresses the deactivation of genes by histone deacetylase. Miyanaga et al. [32] compared various cell lines to determine whether they were resistant to HDAC inhibitors. We investigated SFRP1 expression, which is in Table 6.31, between HDAC inhibitor-resistant cell lines and non-resistant cell lines for adenocarcinoma and squamous cell carcinoma and found different levels of SFRP1 expression (Table 6.32). SFRP1 expression is likely targeted by HDAC inhibitor because its expression decreases in cells resistant to HDAC inhibitor that should reactivate target genes. On the other hand, DKK3 which is also in Table 6.31 is not consistently affected by HDAC inhibitor. Thus, SFRP1 is more likely to be a HDAC inhibitor target in cancer therapy than DKK3 although both are in selected 18 genes (Table 6.31).

Table 6.32 Gene expression difference between no-resistant and resistant-cell lines to HDAC inhibitor as well as alteration of histone acetylation treated by HDAC inhibitor

Gene expression				
Adenocarcinoma				
		P-value	Non-resistant cell lines	Resistant cell lines
SFRP1		4.64×10^{-4}	611.06	> 92.60
DKK3		6.73×10^{-2}	263.27	> 30.59
Squamous cell carcinoma				
SFRP1		7.42×10^{-3}	304.53	> 49.53
DKK		4.61×10^{-1}	261.38	< 506.25
Histone modification (H3K9K14ac)				
	Cell line	P-value	0 h	2 h
SFRP1	(A549)	2.90×10^{-2}	−1.29	< -0.52
	(H1299)	4.06×10^{-2}	−2.51	< -1.85
	(CL1-1)	8.71×10^{-1}	−1.38	< -1.34
DKK3	(A549)	6.19×10^{-1}	−1.17	< -1.01
	(H1299)	1.98×10^{-3}	−1.70	< -0.48
	(CL1-1)	1.48×10^{-1}	−0.59	> -1.13
SALL4	(A549)	1.71×10^{-3}	−2.44	< -1.05
	(H1299)	5.23×10^{-1}	−2.62	> -2.86
	(CL1-1)	1.03×10^{-4}	0.997	> -0.59

The second evidence is the alteration of histone acetylation by HDAC inhibitor shown in Table 6.32; HDAC inhibitor reduces the histone acetylation of SFRP1 [61] for A549 and H1299 cell lines that are generated from non-small cell lung cancer (NSCLC), from which H358 and H640 whose gene expression and methylation level are analyzed in this study are generated. DKK3 and SALL4 are less consistently affected by HDAC inhibitor than SFRP1 for these two cell lines. On the other hand, when HDAC inhibitor is used for CL1-1 cell lines that are generated from cervix are not consistent at all for SFRP1, SALL4, and DKK3. Thus, SFRP1 is most likely a target of epigenetic therapy toward NSCLC. In conclusion, PCA based unsupervised FE is an effective method to integrate methylation profile and mRNA expression as in the integrated analysis of mRNA and miRNA expression.

6.5.3 *Identification of Genes Mediating Transgenerational Epigenetics Based upon Integrated Analysis of mRNA Expression and Promoter Methylation*

Transgenerational epigenetics (TGE) [63] is one of the recently established but important topics on evolution. Because of central dogma, it is generally believed that only heritable information is stored in DNA sequence. On the other hand, there might be some other ways that transfer information intergenetically. Epigenetics that means alteration of genome without changing DNA sequence might transfer information intergenetically. If so, it can be an alternative important factor that can contribute to evolution. In spite of that, TGE is not completely understood.

One possible way to study TGE is to study the effect of endocrine disruptors towards embryo. The reason is as follows. First of all, expose of embryo to endocrine disruptors is known to cause some disease. Thus, at least, we can expect to detect the effect of it no matter what it is. Second, by preparing the clone animals, we can guarantee that expose to endocrine disruptors does not alter DNA sequence. Third, by considering F3 generation, we can expect that DNA is not directly exposed to endocrine disruptor (Fig. 6.13). Skinner et al. [43] performed this kind of experiments. We apply PCA based unsupervised FE to their data set [49]. Data set analyzed is downloaded from GEO with GEO ID GSE59511. Table 6.33 shows the list of files used in this study. E13 and E16 correspond to 13 days and 16 days after the fertilization, respectively. Eight mRNA expression profiles, $x_{ij}^{\text{mRNA}} \in \mathbb{R}^{27342\times 8}$, are further converted to $\tilde{x}_{ij}^{\text{mRNA}} \in \mathbb{R}^{27342\times 8}$ as

$$\tilde{\boldsymbol{x}}_i^{\text{mRNA}} = \begin{pmatrix} \tilde{x}_{i1}^{\text{mRNA}} \\ \tilde{x}_{i2}^{\text{mRNA}} \\ \tilde{x}_{i3}^{\text{mRNA}} \\ \tilde{x}_{i4}^{\text{mRNA}} \\ \tilde{x}_{i5}^{\text{mRNA}} \\ \tilde{x}_{i6}^{\text{mRNA}} \\ \tilde{x}_{i7}^{\text{mRNA}} \\ \tilde{x}_{i8}^{\text{mRNA}} \end{pmatrix} = \begin{pmatrix} \frac{\text{E13 control rep 1}}{\text{E13 treated rep 1}} \\ \\ \frac{\text{E13 control rep 2}}{\text{E13 treated rep 2}} \\ \\ \frac{\text{E13 control rep 2}}{\text{E13 treated rep 1}} \\ \\ \frac{\text{E13 control rep 1}}{\text{E13 treated rep 2}} \\ \\ \frac{\text{E16 control rep 1}}{\text{E16 treated rep 1}} \\ \\ \frac{\text{E16 control rep 2}}{\text{E16 treated rep 2}} \\ \\ \frac{\text{E16 control rep 2}}{\text{E16 treated rep 1}} \\ \\ \frac{\text{E16 control rep 1}}{\text{E16 treated rep 2}} \\ \end{pmatrix} \tag{6.56}$$

because we cannot get PC loading distinct between E13 and E16 otherwise and promoter methylation is provided as ratio by the original studies' researchers. Methylation profiles, $x_{kj}^{\text{methyl}} \in \mathbb{R}^{14162\times 6}$, are used as it is, because it is provided as ratio between control and treated samples.

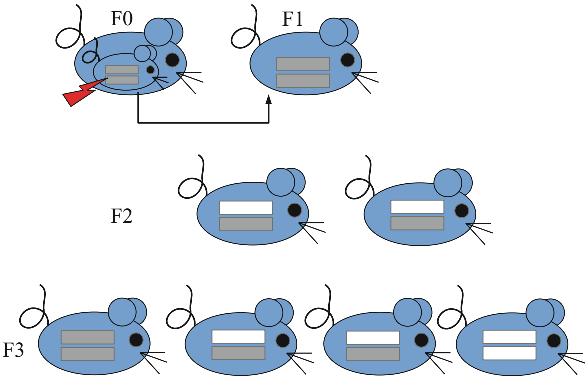

Fig. 6.13 F1 generation is exposed to endocrine disruptor during F0 generation is pregnant (red thunder mark). In F1 generation, both chromosomes are directly affected by endocrine disruptor (gray rectangular). In F2 generation, all chromosome is a pair of chromosome affected directly by endocrine disruptor (gray rectangular) and that not affected directly by endocrine disruptor (white rectangular). In F3 generation, one fourth individuals (right end one) have no chromosomes affected directly by endocrine disruptor (white rectangular)

Table 6.33 List of files used in this study

GSE43559 (gene expression)		GSE59510 (promoter methylation)	
GEO ID	Description	GEO ID	Description
GSM1065332	PGC E13 F3-Control biological rep1	GSM1438556	E16-Vip2/Cip2
GSM1065333	PGC E13 F3-Control biological rep2	GSM1438557	E13-Vip2/Cip1
GSM1065334	PGC E13 F3-Vinclozolin biological rep1	GSM1438558	E13-Vip1/Cip1
GSM1065335	PGC E13 F3-Vinclozolin biological rep2	GSM1438559	E16-Vip1/Cip1
GSM1065336	PGC E16 F3-Control biological rep1	GSM1438560	E16-Vip2/Cip1
GSM1065337	PGC E16 F3-Control biological rep2	GSM1438561	E13-Vip2/Cip2
GSM1065338	PGC E16 F3-Vinclozolin biological rep1		
GSM1065339	PGC E16 F3-Vinclozolin biological rep2		

PCA is applied to $\tilde{x}_{ij}^{\text{mRNA}}$ and x_{kj}^{methyl} and PC loading, $\boldsymbol{v}_\ell^{\text{mRNA}} \in \mathbb{R}^8$ and $\boldsymbol{v}_\ell^{\text{methyl}} \in \mathbb{R}^6$ attributed to samples are obtained. After investigation of obtained PC loading, we find that $\boldsymbol{v}_2^{\text{mRNA}}$ and $\boldsymbol{v}_1^{\text{methyl}}$ have distinction between E13 and E16 (Fig. 6.14).

P-values are attributed to probes using χ^2 distribution as

$$P_i = P_{\chi^2}\left[> \left(\frac{u_{2i}^{\text{mRNA}}}{\sigma_2^{\text{mRNA}}} \right)^2 \right], \tag{6.57}$$

and

$$P_k = P_{\chi^2}\left[> \left(\frac{u_{1k}^{\text{methyl}}}{\sigma_1^{\text{methyl}}} \right)^2 \right]. \tag{6.58}$$

Fig. 6.14 (**a**) v_2^{mRNA} (**b**)v_1^{methyl}. P-values are computed by t test. Black open circle: E13, red open circle: E16

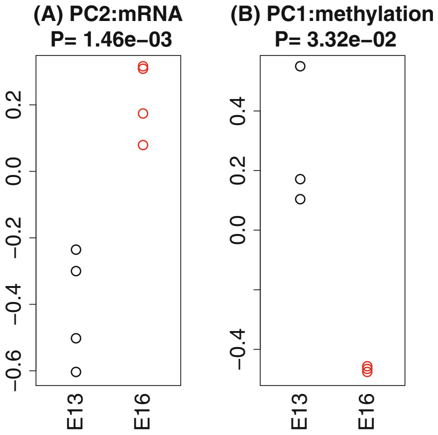

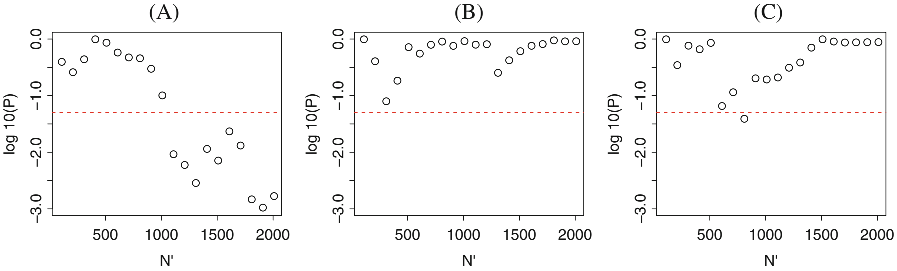

Fig. 6.15 P-values computed by Fisher's exact that evaluates overlap between top N' selected genes of mRNA and methylation by (**a**) PCA based unsupervised FE, (**b**) t test, (**c**) limma. Horizontal broken line indicates $P = 0.05$

Unfortunately, no probes for methylation are associated with adjusted P-values less than 0.05. Thus, we give up evaluating probes with P-values. Instead, we decide to evaluate probes using overlap between mRNA and methylation. That is, we select top N' probes with smaller P-values computed by Eqs. (6.57) and (6.58) for mRNA and methylation, respectively. Then compute P-values with applying Fisher's exact test to evaluate overlaps of genes to which top N' probes are attributed for mRNA and methylation. Annotation of mRNA probes is available in the file GPL6247-249.txt. Annotation of methylation probes is in methylation profile files themselves.

In order to evaluate the number of genes chosen in common between mRNA and methylation, we also compute P-values attributed to probes by two additional methods; t test and Linear Models for Microarray Data (limma) [37]. Although limma is a simple linear regression analysis using logarithmic values, it is known to work pretty well for DEG identification. Figure 6.15 shows the dependence of P-values computed by Fisher's exact test upon N' that is the number of top ranked genes with smaller P-values computed by PCA based unsupervised FE, t test, and limma. In contrast to PCA based unsupervised FE which has P-values less than 0.05 for $N' > 1000$, t test does not fulfill this criterion $N' \leq 2000$ while more advanced limma can have only one N' associated with $P < 0.05$. Thus, from the point of integrated analysis of mRNA and methylation, PCA based unsupervised FE outperforms other two conventional or popular methods for DEG identification.

Although PCA based unsupervised FE successfully integrates mRNA expression and methylation profiles, if genes chosen in common between mRNA expression and methylation are not biologically valid, it is useless. In order to evaluate genes chosen in common between mRNA expression and methylation profiles, we upload 63 genes (Table 6.34) selected by PCA based unsupervised FE when $N' = 1100$, which is minimum N' associated with $P < 0.05$, to DAVID. Table 6.35 lists gene ontology (GO) terms identified by DAVID. Here, GO terms [62] are composed of human curated list of genes supposed to have biological concepts about biological process (BP), cellular components (CC), and molecular function (MF). Most enriched GO terms are related to olfactory receptor activity, which is known to be related to TGE [42]. Thus, not only PCA based unsupervised FE can identify common genes between mRNA and methylation, but also identified GO terms are reasonable. PCA based unsupervised FE is successful from the biological point of view, too.

6.6 Time Development Analysis

Analysis of temporal data set is another important topic of not only data science but also bioinformatics. For example, periodic motion often plays critical role in biology. Typical examples where periodic motions play critical roles include heartbeats, circadian rhythm, and cell division cycle. For all of them, keeping the stability of periodicity is critically important. Thus, identification of genes that can contribute to periodic motion is also critical. Another example is development or disease progression. It is also important which genes drive these processes. From the viewpoint of feature selection, the task is similar to those mentioned in the previous sections: to identify genes having time dependence. The only difference is that there is no clear definition of what the time dependences. In some sense, it is very close to clustering. If we can find a set of genes that share similar time dependence, it might be the evidence that these are critical time dependence. The definition of periodicity is also unclear. Only definition of periodicity is that some function of time t, $f(t)$, should satisfy the condition that $f(t + T) = f(t)$ for all t in order to be a periodic function of period T. Nevertheless, because the time points measured are limited, it is usual that there are no pairs of points between whose time interval is exactly T. In this case, sinusoidal regression is often employed, in spite of that it is not guaranteed to capture all kinds of periodic motions because not all periodic functions are sinusoidal.

In the following subsections, we will demonstrate how effective is to employ PCA based unsupervised FE in order to identify genes with time dependence. As mentioned above, it is quite difficult to assume the time dependent functional form to identify time dependent genes in advance. Because of this difficulty, unsupervised

Table 6.34 63 mRNAs selected by PCA based unsupervised FE

Refseq mRNA	Gene symbol	Description
NM_021866	CCR2	C-C motif chemokine receptor 2
NM_001000650	Olr624	Olfactory receptor 624
NM_001109617	PRAMEF27	PRAME family member 27
NM_017061	LOX	Lysyl oxidase
NM_012523	CD53	Cd53 molecule
NM_001033998	ITGAL	Integrin subunit alpha L
NM_022866	SLC13A3	Solute carrier family 13 member 3
NM_001109383	ANGPTL1	Angiopoietin-like 1
NM_001109118	ELOVL2	ELOVL fatty acid elongase 2
NM_001111269	LOC689064	Beta-globin
NM_001000551	Olr218	Olfactory receptor 218
NM_001107660	CAR1	Carbonic anhydrase I
NM_023968	npy2r	Neuropeptide Y receptor Y2
NM_053994	PDHA2	Pyruvate dehydrogenase (lipoamide) alpha 2
NM_001111321	Vom2r80	Vomeronasal 2 receptor, 80
NM_020104	MYL1	Myosin, light chain 1
NM_001000646	Olr635	Olfactory receptor 635
NM_001001071	Olr862	Olfactory receptor 862
NM_001000648	Olr633	Olfactory receptor 633
NM_001109218	RGD1565355	Similar to fatty acid translocase/CD36
NM_001000600	Olr796	Olfactory receptor 796
NM_001013952	LOC300308	Similar to hypothetical protein 4930509O22
NM_013025	CCL3	C-C motif chemokine ligand 3
NM_001000566	Olr542	Olfactory receptor 542
NM_022218	CMKLR1	Chemerin chemokine-like receptor 1
NM_013158	DBH	Dopamine beta-hydroxylase
NM_001109374	LRRTM1	Leucine rich repeat transmembrane neuronal 1
NM_021853	kcnt1	Potassium sodium-activated channel subfamily T member 1
NM_175586	TAAR7B	Trace amine-associated receptor 7b
NM_001008946	Vom1r29	Vomeronasal 1 receptor 29
NM_001047891	RGD1310507	Similar to RIKEN cDNA 1300017J02
NM_001008947	Vom1r34	Vomeronasal 1 receptor 34
NM_020071	FGB	Fibrinogen beta chain
NM_001080938	Tas2r124	Taste receptor, type 2, member 124
NM_012909	AQP2	Aquaporin 2
NM_030856	LRRN3	Leucine rich repeat neuronal 3
NM_001099492	Vom2r19	Vomeronasal 2 receptor, 19
NM_013149	AHR	Aryl hydrocarbon receptor
NM_001011892	SERPINF2	Serpin family F member 2
NM_001012224	NFE2	Nuclear factor, erythroid 2
NM_001013177	Sult1c2a	Sulfotransferase family, cytosolic, 1C, member 2a

(continued)

Table 6.34 (continued)

Refseq mRNA	Gene symbol	Description
NM_053843	FCGR2A	Fc fragment of IgG, low affinity IIa, receptor
NM_001106056	TRIM52	Tripartite motif-containing 52
NM_001000523	Olr1381	Olfactory receptor 1381
NM_001007729	PF4	Platelet factor 4
NM_001000080	Olr1583	Olfactory receptor 1583
NM_001107036	MPO	Myeloperoxidase
NM_022696	HAND2	Heart and neural crest derivatives expressed 2
NM_001001053	Olr545	Olfactory receptor 545
NM_001024805	Hbe2	Hemoglobin, epsilon 2
NM_001000384	Olr408	Olfactory receptor 408
NM_001001362	Olr1059	Olfactory receptor 1059
NM_138537	LOC171573	Spleen protein 1 precursor
NM_001000896	Olr1726	Olfactory receptor 1726
NM_134326	ALB	Albumin
NM_001001017	Olr1143	Olfactory receptor 1143
NM_017105	BMP3	Bone morphogenetic protein 3
NM_012893	ACTG2	Actin, gamma 2, smooth muscle, enteric
NM_001000619	Olr727	Olfactory receptor 727
NM_001012112	ANKRD9	Ankyrin repeat domain 9
NM_001001114	Olr1701	Olfactory receptor 1701
NM_001108651	HEBP1	Heme binding protein 1
NM_001014222	Dmrtc1c1	DMRT-like family C1c1

Table 6.35 GO terms detected by DAVID

Category	Term	Count	%	P-value	Benjamini
GOTERM_BP_DIRECT	GO:0007186 G-protein coupled receptor signaling pathway	26	41.3	8.52×10^{-10}	3.57×10^{-7}
GOTERM_BP_DIRECT	GO:0050911 detection of chemical stimulus involved in sensory perception of smell	16	25.4	3.00×10^{-5}	6.26×10^{-3}
GOTERM_CC_DIRECT	GO:0016021 integral component of membrane	33	52.4	2.35×10^{-4}	2.07×10^{-2}
GOTERM_CC_DIRECT	GO:0072562 blood microparticle	5	7.94	5.80×10^{-4}	2.55×10^{-2}
GOTERM_MF_DIRECT	GO:0004984 olfactory receptor activity	16	25.4	5.83×10^{-5}	6.91×10^{-3}
GOTERM_MF_DIRECT	GO:0004930 G-protein coupled receptor activity	17	27.0	7.26×10^{-5}	4.31×10^{-3}

%: the ratio of genes annotated, Benjamini: P-values corrected by BH criterion nature of PCA based unsupervised FE works quite well. Let's start to try to identify genes that can drive cell division cycle.

6.6.1 Identification of Cell Division Cycle Genes

Cell division cycle is the primary process of living organisms. There are no living organisms that do not perform cell division, because only through cell division, living organism can develop or make the descendants. Thus, maintenance of stability of cell division cycle is quite critical. In this sense, identification of cell division cycle genes is very important for understanding living materials. Fortunately, studying cell division cycle is not difficult, because cell division can be observed even using unicellular organisms, which can often be cultured in Petri dish. Although cell structure of unicellular organisms like bacteria generally differs from that of multicellular organisms like human beings, fortunately there are some unicellular organisms that share the cell structure with multicellular organisms, e.g., yeast. Because of this ease of experiment, there is a long history of study of cell division cycles.

In this subsection, we try to reanalyze gene expression profiles of yeast during mitotic cell division cycle (i.e., normal cell division cycle that is not related to reproductive processes) [51]. One possible obstacle of this experiment is synchronization. In natural state, individual yeasts perform cell division cycle with randomized phase. In other words, cell division always takes place in some individual yeast cells. Under such a condition, measuring gene expression might not exhibit any periodicity at all. In order to avoid such a situation, all yeast cells must be synchronized before experiments start. And almost only one possible way to perform synchronization is arresting cell cycle [22]. There are multiple ways to arrest cell cycle, e.g. the usage of mutant or cutting off the food supply. Cell cycle arresting has one problem; after cell cycle releasing arresting, cell cycles start to be desynchronized; living organisms have no benefits for cell cycle synchronization, which gradually vanishes and return to randomized phase. If desynchronization is rapid, there are no ways to observe gene expression of cell division cycle for longer period. This results in again typical large p small n problem, i.e., small number of time points (often less than 100) versus huge number of genes (a few thousands).

The first data set we analyze is yeast metabolic cycle [64]. Gene expression profile, $x_{ij} \in \mathbb{R}^{9335 \times 36}$ composed of 36 times points and 9335 genes. Thirty six time points are supposed to be composed of three cycles based upon external observations. Thus, it corresponds to the observation over three cycles. It can be downloaded as a file GSE3431_series_matrix.txt from GEO ID GSE3431. PCA is applied to x_{ij} and PC loading $\boldsymbol{v}_\ell \in \mathbb{R}^{36}$ is attributed to time points. Figure 6.16 shows the $\boldsymbol{v}_\ell, \ell = 2, 3$. As expected, they are coincident with three periodic cycles. Although we never use the assumption that they are periodic motions, PCA correctly identifies periodic motions. In addition to this, time dependence of periodic motion is far from sinusoidal motion that is usually assumed. Furthermore, the functional

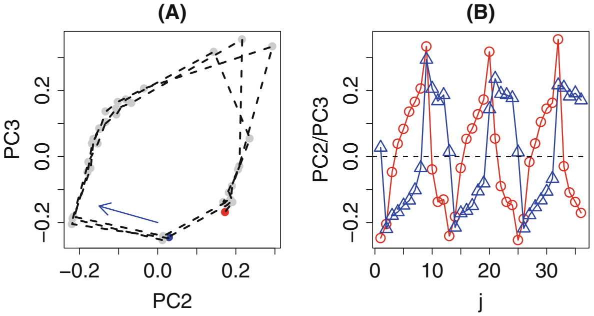

Fig. 6.16 (**a**) The scatterplot of $\boldsymbol{v}_\ell, \ell = 2, 3$. Blue filled circle, $j = 1$, red filled circle: $j = 36$, gray filled circle : $1 < j < 36$. Horizontal axis: $\ell = 2$ and vertical axis: $\ell = 3$. (**b**) Time dependence of PC loading $\boldsymbol{v}_\ell, \ell = 2, 3$. Blue: $\ell = 2$, red:$\ell = 3$

shape of $\boldsymbol{v}_2$ and $\boldsymbol{v}_3$ differs from each other so much. Although individual genes are expected to have time dependence of functional form of linear combination of $\boldsymbol{v}_2$ and $\boldsymbol{v}_3$, these apparently differ from each other because of complete different functional form of $\boldsymbol{v}_2$ and $\boldsymbol{v}_3$. Thus it completely differs from sinusoidal function for which each gene shares same functional form excluding the time shift. This suggests the limitation of employment of sinusoidal function to recognize periodic nature within gene expression. No fitting of specific functional forms to gene expression cannot identify periodic genes correctly.

In order to identify cell cycle regulated genes, we attribute P-values to ith genes using χ^2 distribution as

$$P_i = P_{\chi^2}\left[> \sum_{\ell=2}^{3} \left(\frac{u_{\ell i}}{\sigma_\ell}\right)^2 \right], \tag{6.59}$$

P_is are adjusted by BH criterion. Then we found that 298 probes are associated with adjusted P-values less than 0.01 (Fig. 6.17).

It is not easy to evaluate selected genes without biological consideration, because the functional form of PC loading, $\boldsymbol{v}_\ell, \ell = 2, 3$, is not a simple mathematical function. One possible evaluation is linear regression analysis that tests if selected genes are periodic or not. Then we perform two linear regression analyses,

$$x_{ij} = a_i + \sum_{\ell=2}^{3} b_{i\ell} v_{\ell j} \tag{6.60}$$

and

$$x_{ij} = a'_i + b'_{i1} \sin\left(\frac{2\pi j}{12}\right) + b'_{i2} \cos\left(\frac{2\pi j}{12}\right) \tag{6.61}$$

to selected 298 probes where $a_i, b_{i\ell}, a'_i, b'_{i1}, b'_{i2}$ are regression coefficients. Attributed P-values are corrected by BH criterion, and the largest (i.e., the least significant) adjusted P-values are 0.004 and 0.01, respectively. Thus, PCA based

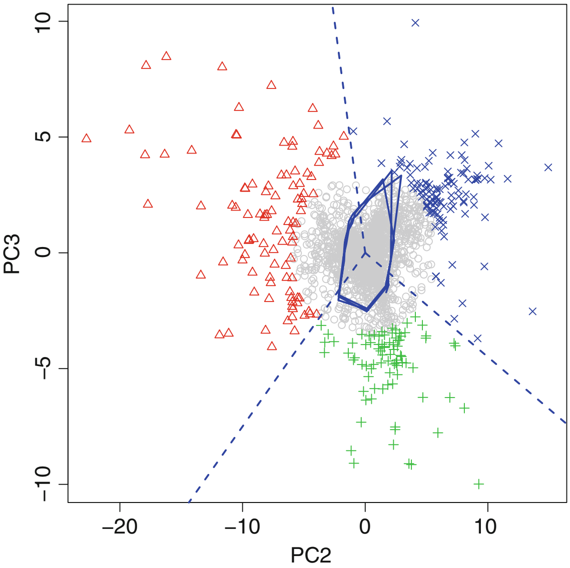

Fig. 6.17 Scatterplot of PC scores, $\boldsymbol{u}_\ell, \ell = 2, 3$. Points colored other than gray are selected 298 probes. Points displayed with red, green, and blue marks are three clusters identified by K-means assuming three clusters to $\boldsymbol{u}_\ell, \ell = 2, 3$

unsupervised FE can correctly identify genes having period 12 in fully unsupervised manner.

One might wonder how we identify $\ell = 2, 3$ for periodic function without assuming periodicity. We plot $\boldsymbol{v}_\ell$ and $\boldsymbol{v}_{\ell'}$ and identify if they form limit cycle. In order to evaluate the amount that each trajectory is limit cycle, we compute winding number, which counts how many times each orbit moves round the origin anti-clockwise direction (Fig. 6.18). It is obvious that $\boldsymbol{v}_\ell, \ell = 2, 3$ exhibit most clear limit cycle. Because identification of limit cycle does not require the knowledge about the periodicity in advance, we can identify $\boldsymbol{v}_\ell, \ell = 2, 3$ in fully unsupervised manner. One possible bi-product of winding number analysis is the identification of periodic motion other than period of 12. $\boldsymbol{v}_\ell, \ell = 2, 4$ exhibit period doubling (eight letter shaped). Sinusoidal regression that assumes specific period cannot identify these motions. It is another advantage of using unsupervised methods.

It is also possible to select genes based upon linear regression analysis. We compare the performance of linear regression analysis with that by PCA based unsupervised FE, by applying Eqs. (6.60) and (6.61) to not selected 298 but all gene expression profiles. P-values are attributed to all genes with linear regression analysis and obtained P-values are adjusted by BH criterion. Then we select gene associated adjusted P-values less than 0.01. This results in as many as 5598 genes by Eq. (6.60) and 4676 genes by Eq. (6.61), respectively, both of which are more than half of total number of genes, 9335. Because it is too many, it is better to be screened based upon additional criterion. Nevertheless, no suitable criteria as FC when two classes are clearly defined are known for the detection of periodic motion. Thus, reduction of number of genes is not straightforward. Because PCA

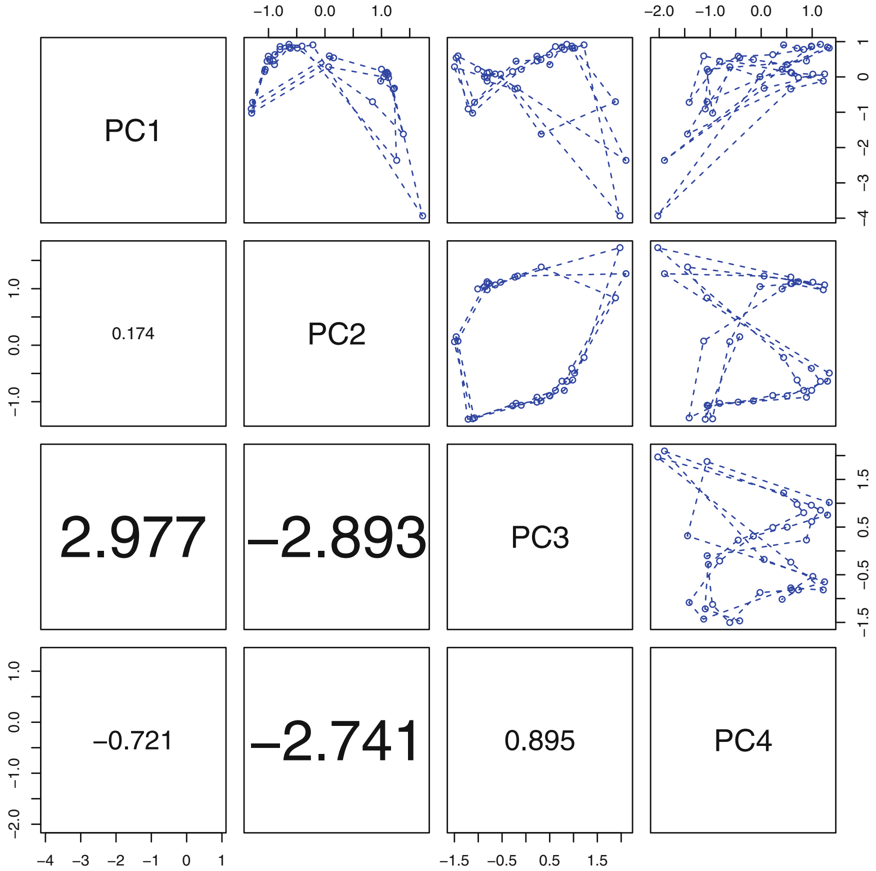

Fig. 6.18 Upper triangle: Scatterplot of PC loading, $\boldsymbol{v}_\ell, 1 \leq \ell \leq 4$. Lower triangle: winding number (anti-clockwise direction is positive)

based unsupervised FE can identify as small as 298 probes only with P-values, it is more convenient than gene selection based upon linear regression analysis.

Finally, we would like to evaluate genes associated with the selected 298 probes biologically. Tu et al. [64] identified cell cycle regulated genes using linear regression analysis, Eq. (6.61), which they call sinusoidal regression. Then, classify them into three classes based upon the similarity of functional forms, with visual inspection of time course expression. They also recognized that these three classes are associated with specific biological function. In order to see if these three classes are reproduced in the present results, we apply K-means to selected 298 probes with $\boldsymbol{u}_\ell, \ell = 2, 3$. Three colored clusters in Fig. 6.17 correspond to three clusters obtained by K-means. Genes associated with probes in three clusters are separately uploaded to DAVID. Table 6.36 lists the significant KEGG pathway enrichment. Green and blue crosses in Fig. 6.17 correspond to two classes to which

Table 6.36 GO CC terms detected for genes in Fig. 6.17 by DAVID

Category	Term	Count	%	P-value	Benjamini
Red triangles in Fig. 6.17					
GOTERM_CC_DIRECT	GO:0005739 mitochondrion	36	42.4	4.11×10^{-6}	2.40×10^{-4}
GOTERM_CC_DIRECT	GO:0005886 plasma membrane	21	24.7	8.24×10^{-6}	2.43×10^{-4}
GOTERM_CC_DIRECT	GO:0005618 cell wall	8	9.4	4.27×10^{-5}	8.40×10^{-4}
GOTERM_CC_DIRECT	GO:0005777 peroxisome	8	9.4	9.57×10^{-5}	1.40×10^{-3}
GOTERM_CC_DIRECT	GO:0005576 extracellular region	9	10.6	1.46×10^{-4}	1.72×10^{-3}
GOTERM_CC_DIRECT	GO:0005741 mitochondrial outer membrane	8	9.4	3.82×10^{-4}	3.75×10^{-3}
GOTERM_CC_DIRECT	GO:0071944 cell periphery	13	15.3	3.96×10^{-4}	$3.33. \times 10^{-3}$
GOTERM_CC_DIRECT	GO:0005782 peroxisomal matrix	4	4.7	7.07×10^{-4}	5.02×10^{-3}
GOTERM_CC_DIRECT	GO:0009277 fungal-type cell wall	8	9.4	1.07×10^{-3}	7.03×10^{-3}
Green crosses in Fig. 6.17					
GOTERM_CC_DIRECT	GO:0005739 mitochondrion	48	71.6	1.27×10^{-19}	8.64×10^{-18}
GOTERM_CC_DIRECT	GO:0005758 mitochondrial intermembrane space	17	25.4	3.13×10^{-16}	1.13×10^{-14}
GOTERM_CC_DIRECT	GO:0005743 mitochondrial inner membrane	20	29.9	3.08×10^{-12}	6.99×10^{-11}
GOTERM_CC_DIRECT	GO:0070469 respiratory chain	6	9.0	5.71×10^{-7}	9.70×10^{-6}
GOTERM_CC_DIRECT	GO:0005759 mitochondrial matrix	11	16.4	1.12×10^{-6}	1.53×10^{-5}
GOTERM_CC_DIRECT	GO:0005750 mitochondrial respiratory chain complex III	5	7.5	4.29×10^{-6}	4.86×10^{-5}
GOTERM_CC_DIRECT	GO:0005749 mitochondrial respiratory chain complex II, succinate dehydrogenase complex (ubiquinone)	4	6.0	7.01×10^{-5}	6.81×10^{-4}
GOTERM_CC_DIRECT	GO:0000788 nuclear nucleosome	4	6.0	1.04×10^{-4}	8.86×10^{-4}
GOTERM_CC_DIRECT	GO:0042645 mitochondrial nucleoid	5	7.5	1.24×10^{-4}	9.36×10^{-4}
GOTERM_CC_DIRECT	GO:0005618 cell wall	6	9.0	8.74×10^{-4}	5.92×10^{-3}

(continued)

Table 6.36 (continued)

Category	Term	Count	%	P-value	Benjamini
GOTERM_CC_DIRECT	GO:0045261 proton-transporting ATP synthase complex, catalytic core F(1)	3	4.5	1.19×10^{-3}	7.31×10^{-3}
GOTERM_CC_DIRECT	GO:0005576 extracellular region	7	10.4	1.28×10^{-3}	7.24×10^{-3}
GOTERM_CC_DIRECT	GO:0031298 replication fork protection complex	4	6.0	3.15×10^{-3}	1.64×10^{-3}
GOTERM_CC_DIRECT	GO:0000786 nucleosome	3	4.48	4.14×10^{-3}	2.00×10^{-2}
Blue crosses in Fig. 6.17					
GOTERM_CC_DIRECT	GO:0030529 intracellular ribonucleoprotein complex	54	65.1	6.94×10^{-49}	3.89×10^{-47}
GOTERM_CC_DIRECT	GO:0005840 ribosome	52	62.7	2.29×10^{-46}	6.42×10^{-45}
GOTERM_CC_DIRECT	GO:0022625 cytosolic large ribosomal subunit	31	37.3	1.27×10^{-32}	2.36×10^{-31}
GOTERM_CC_DIRECT	GO:0005622 intracellular	37	44.6	6.58×10^{-32}	9.21×10^{-31}
GOTERM_CC_DIRECT	GO:0022627 cytosolic small ribosomal subunit	21	25.3	1.22×10^{-21}	1.37×10^{-20}
GOTERM_CC_DIRECT	GO:0005737 cytoplasm	65	78.3	1.73×10^{-12}	1.62×10^{-11}
GOTERM_CC_DIRECT	GO:0015935 small ribosomal subunit	9	10.8	4.05×10^{-11}	3.24×10^{-10}
GOTERM_CC_DIRECT	GO:0030687 preribosome, large subunit precursor	10	12.1	4.07×10^{-6}	2.85×10^{-5}
GOTERM_CC_DIRECT	GO:0030686 90S preribosome	9	10.8	1.33×10^{-5}	8.29×10^{-5}
GOTERM_CC_DIRECT	GO:0031429 box H/ACA snoRNP complex	3	3.6	1.88×10^{-3}	1.05×10^{-3}

%: the ratio of genes annotated, Benjamini: P-values corrected by BH criterion mitochondrial and ribosomal GO cellular component (CC) terms are enriched, respectively. Red triangles in Fig. 6.17 are not very clear, but it is enriched by the GO CC term of cell walls, which is deeply related to cell division. Thus, it is coincident. Therefore, K-means clustering applied to 298 probes identified by PCA based unsupervised FE reproduces the biological clusters of genes reported by Tu et al. [64].

Another example of yeast cell division cycle to which PCA based unsupervised FE is applied is data set stored in Cyclebase [39]. Cyclebase collected gene expression profiles of four species, one plant (*Arabidopsis thaliana*), two yeasts (*Saccharomyces cerevisiae*, *Schizosaccharomyces pombe*), and human (*Homo sapiens*). For the yeast that we analyze in the present study, *S. cerevisiae*, there are eight time course data sets available, one of which is excluded because there are only prescreened genes included. Profiles are available as a file budding_experiments.tsv, which is downloadable from Cyclebase. Because PCA based unsupervised FE tries to identify genes as outliers, we need all genes before screening, otherwise we cannot identify outliers because of lack of non-outlier genes. As a result, we apply PCA based unsupervised FE to remaining seven gene expression profiles (Figs. 6.19 and 6.20).

In contrast to Fig. 6.18, not all trajectories exhibit clear limit cycles. In that case, we select pairs of PC loading associated with largest absolute winding numbers for gene selection (the pairs of PCs selected are shown in captions in Figs. 6.19 and 6.20). Then, using selected pairs of PC loading, (ℓ, ℓ'), P-values are attributed to ith gene as

$$P_i = P_{\chi^2}\left[> \sum_{\ell_1=\ell,\ell'} \left(\frac{u_{\ell_1 i}}{\sigma_{\ell_1}} \right)^2 \right] \tag{6.62}$$

P_i is adjusted by BH criterion. Genes associated with P-values less than 0.05 are selected (Fig. 6.21). For each of seven expression profiles, PCA based unsupervised FE identify more than 100 genes. In order to evaluate selected genes, we see how much they are overlapped, because the selected genes should be largely overlapped between seven set of genes if they are biologically valid. As in Fig. 6.21, 37 genes are chosen in common at least six among seven experiments. If considering that the total number of genes is at least several thousands (depending on microarrays used in individual experiments), this coincidence is too strong to occur accidentally. Thus, as far as coincidence is concerned, PCA based unsupervised FE is successful.

In order to see if other supervised methods can similarly achieve sufficient coincidence between seven experiments, we apply sinusoidal regression to gene expression profile, x_{ij}, as

$$x_{ij} = a_i + b_{i1} \sin\left(\frac{2\pi j}{T}\right) + b_{i2} \cos\left(\frac{2\pi j}{T}\right). \tag{6.63}$$

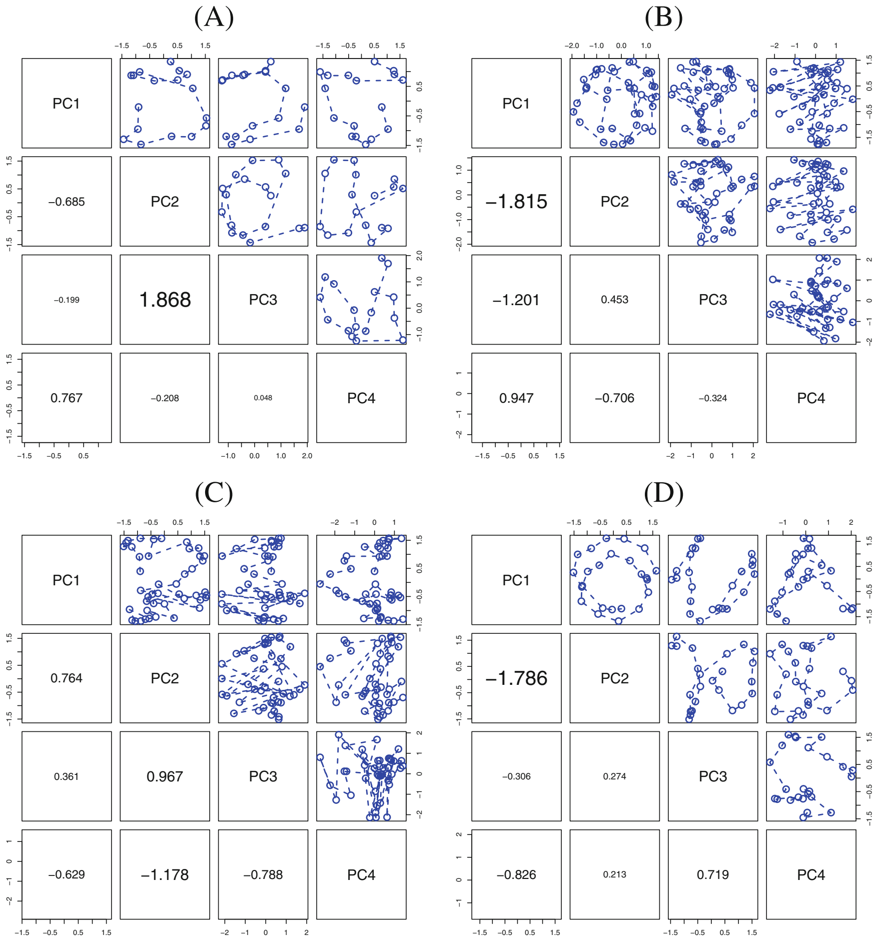

Fig. 6.19 Scatterplot of PC loading, $\boldsymbol{v}_\ell, 1 \leq \ell \leq 4$ for Cyclebase. (ℓ, ℓ') denotes PC used for gene selection. (**a**) Cho et al. [11], $(\ell, \ell') = (2, 3)$. (**b**) Granovskaia et al. [17], G1 phase arrest by α-factor,$(\ell, \ell') = (1, 2)$. (**c**) Granovskaia et al. [17], G1 phase arrest by temperature-sensitive cdc28-13 mutant cells, $(\ell, \ell') = (2, 4)$. (**d**) Pramila et al. [34], α-Factor synchronization, $(\ell, \ell') = (1, 2)$. Other notations are the same as Fig. 6.18

One problem is the decision of period T. For five out of seven experiments, because the periods are denoted in Table 1 [16], we employ these values. For Fig. 6.19b and c, because no information is available, we decide T with visual inspection of $\boldsymbol{v}_\ell$ and $\boldsymbol{v}_{\ell'}$. P-values obtained by sinusoidal regression are adjusted by BH criterion. Then genes associated with adjusted P-values less than 0.05 are selected (Table 6.37). Although sinusoidal regression also can identify large enough number of cell cycle regulated genes, the number of selected genes varies from experiments to experiments. In order to evaluate the amount of coincidence among

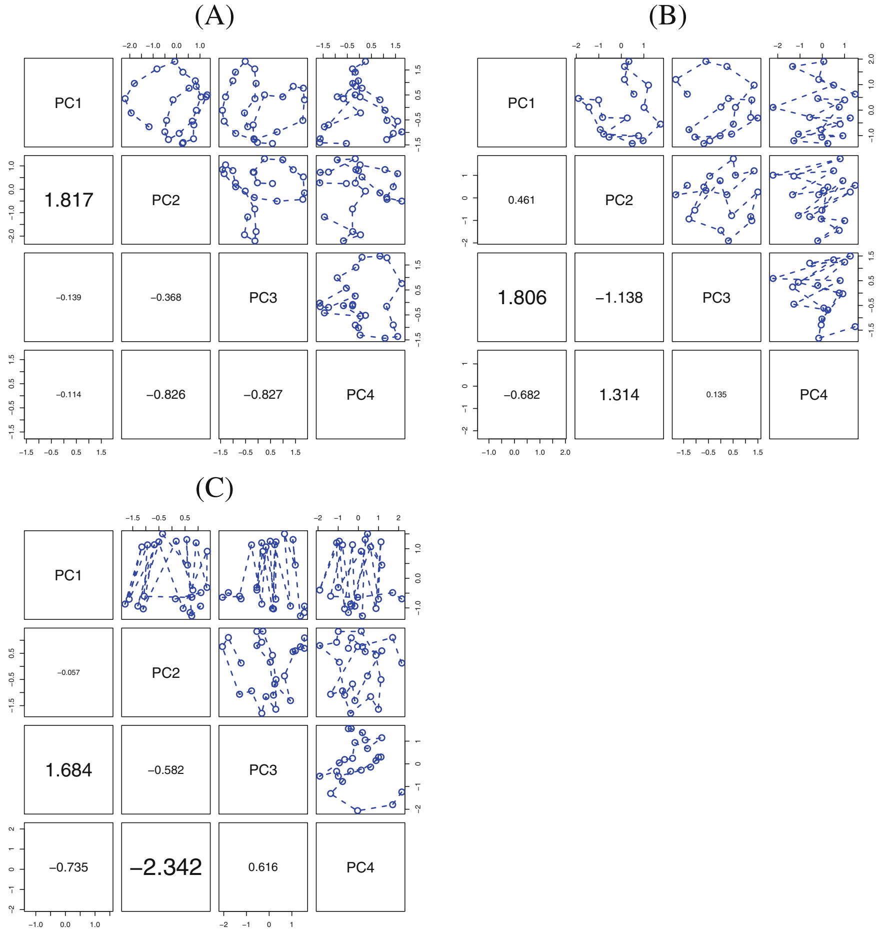

Fig. 6.20 (**a**) Pramila et al. [34], α-Factor synchronization: α38 data, $(\ell, \ell') = (1, 2)$. (**b**) Spellman et al. [46], α factor arrest, $(\ell, \ell') = (1, 3)$. (**c**) Spellman et al. [46], arrest of a cdc15 temperature-sensitive mutant. $(\ell, \ell') = (2, 4)$. Other notations are the same as Fig. 6.19

seven experiments, we select top 150 genes with smaller P-values. Then, as small as 12 genes are selected in at least six among seven experiments. Thus, PCA based unsupervised FE can identify more common genes among seven experiments.

Finally, we evaluate 37 genes (Table 6.38) selected by PCA based unsupervised FE biologically. Because DAVID does not identify any significant terms when 37 genes selected by PCA based unsupervised FE are uploaded, we instead employ YeastMine [5] (Table 6.39), which includes more carefully curated biological terms specifically for yeast. For comparisons, 36 top ranked genes in Cyclebase (Tables 6.38 and 6.40) and 40 genes selected by sinusoidal regression, Eq. (6.63), in

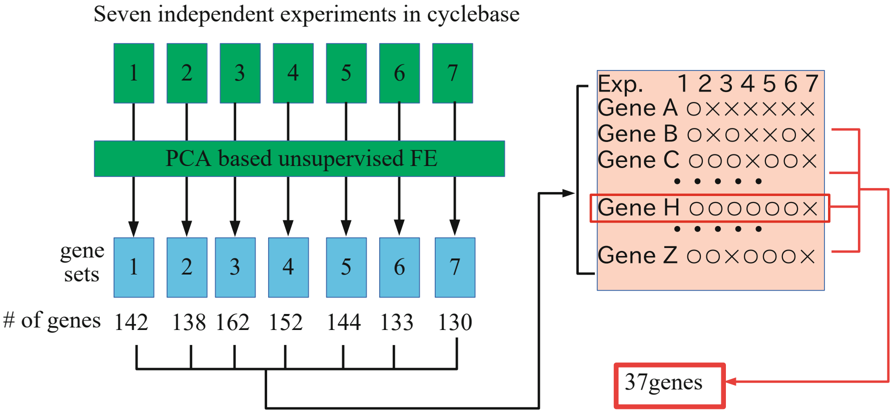

Fig. 6.21 The results of PCA based unsupervised FE applied to seven yeast cell division cycle gene expression in Cyclebase. Experiments one to seven correspond to Fig. 6.19a–d and Fig. 6.20e–g, in this order

Table 6.37 The number of genes selected using P-values computed by Eq. (6.63)

	Experiments						
	1	2	3	4	5	6	7
Number of genes measured	6214	6378	6378	6102	6145	6075	5673
Number of time points	17	41	44	24	24	18	24
Period T	8	14	20	12	12	9	10
Number of selected genes	364	3624	1164	1790	1951	298	354

at least five among seven experiments (from Tables 6.38, 6.39, 6.40 and 6.41) are also uploaded.

Venn diagram of three gene sets is in Fig. 6.22. At most, one third of genes are chosen in common. Thus, these three gene sets are quite distinct. It is also obvious that 37 genes selected by PCA based unsupervised FE are most significantly enriched by the cell cycle related genes. Thus, from the biological point of view, PCA based unsupervised FE outperforms Cyclebase as well as conventional sinusoidal regression.

In conclusion, although applications are limited to yeast cell division cycle, PCA based unsupervised FE obviously has the superior ability to identify periodic genes in fully unsupervised manner.

6.6.2 Identification of Disease Driving Genes

As can be seen in the section that describes biomarker identification (Sect. 6.4), disease alters gene expression. Gene expression is also associated with disease

Table 6.38 Genes selected by PCA based unsupervised FE, Cyclebase, and sinusoidal regression

Methods	Genes
PCA based unsupervised FE	AIM34, ALK1, **AXL2**, CDC5, CLB1, CLB2, CLB6, CLN1, **CLN2**, **CSI2**, EGT2, **GAS3**, GIN4, **HHO1**, HHT1, HOF1, HST3, **HTA1**, **HTA2**, **KCC4**, MCD1, MMR1, **MNN1**, MSH2, **MSH6**, **PDS1**, PHO3, **POL30**, **PRY2**, RAD27, **RFA1**, RNR1, SFG1, SRC1, SWI5, **TOS4**, YOX1
Cyclebase	AIM34, **AXL2**, BUD3, **CLN2**, **CSI2**, **GAS3**, **HHO1**, HHT1, HMLALPHA2, **HTA1**, **HTA2**, HTB1, HTB2, **KCC4**, MATALPHA2, MCD1, **MNN1**, MRC1, **MSH6**, NRM1, **PDS1**, **POL30**, **PRY2**, **RFA1**, SRC1, SVS1, **TOS4**, TOS6, YRF1-1, YRF1-2, YRF1-3, YRF1-4, YRF1-5, YRF1-6, YRF1-7, YRF1-8
Sinusoidal regression	ALK1, ASF1, **AXL2**, BUD3, CDC21, CDC9, **CLN2**, **CSI2**, DSN1, ERP3, **GAS3**, HHF1, HHF2, **HHO1**, HHT2, **HTA1**, **HTA2**, HTB1, HTB2, **KCC4**, MCM5, **MNN1**, MSA1, MSH2, **MSH6**, NRM1, NUF2, **PDS1**, **POL30**, **PRY2**, RAD27, **RFA1**, RFA2, RSR1, SGO1, SML1, SPC98, TOF2, **TOS4**, WTM2

Genes in bold are 15 genes chosen in common over three methods

Table 6.39 Top five GO BP term/publication enrichments reported by YeastMine in 37 genes identified by PCA based unsupervised FE

PCA based unsupervised FE			
GO BP term		p-Value	#
Cell cycle	[GO:0007049]	5.32×10^{-10}	24
Cell cycle process	[GO:0022402]	3.08×10^{-8}	21
Mitotic cell cycle	[GO:0000278]	4.45×10^{-8}	17
Mitotic cell cycle process	[GO:1903047]	2.23×10^{-7}	16
Cell division	[GO:0051301]	1.02×10^{-6}	15
Publication	PMID	p-Value	#
Clustering time-varying gene expression profiles using scale-space signals			
	[16452778]	9.74×10^{-24}	20
Serial regulation of transcriptional regulators in the yeast cell cycle			
	[11572776]	6.14×10^{-17}	16
Identification of a core set of signature cell cycle genes whose relative order of time to peak expression is conserved across species			
	[22135306]	6.34×10^{-12}	10
Identification of sparsely distributed clusters of cis-regulatory elements in sets of co-expressed genes			
	[15155858]	3.71×10^{-10}	9
Computational reconstruction of transcriptional regulatory modules of the yeast cell cycle			
	[17010188]	4.17×10^{-10}	12

#: number of genes associated with GO BP terms or mentioned in the publications. PMID: PubMed ID

Table 6.40 Top five GO BP term/publication enrichments reported by YeastMine in 36 top ranked genes by Cyclebase

Cyclebase			
GO BP term		p-Value	#
Chromosome organization	[GO:0051276]	1.13×10^{-8}	20
Telomere maintenance via recombination	[GO:0000722]	3.34×10^{-8}	8
DNA metabolic process	[GO:0006259]	3.50×10^{-8}	19
Telomere maintenance	[GO:0000723]	2.07×10^{-6}	9
Anatomical structure homeostasis	[GO:0060249]	2.07×10^{-6}	9
Publication	PMID	p-Value	#
Genome-wide array-CGH analysis reveals YRF1 gene copy number variation that modulates genetic stability in distillery yeasts			
	[26384347]	9.74×10^{-24}	20
Transcriptional effects of the potent enediyne anti-cancer agent Calicheamicin gamma(I)(1)			
	[11880039]	1.11×10^{-11}	7
Linking DNA replication checkpoint to MBF cell-cycle transcription reveals a distinct class of G1/S genes			
	[22333912]	2.32×10^{-11}	11
Mcm1p-induced DNA bending regulates the formation of ternary transcription factor complexes			
	[12509445]	2.35×10^{-11}	8
A genetic screen for yeast genes induced by sustained osmotic stress			
	[12868060]	1.82×10^{-10}	7

#: number of genes associated with GO BP terms or mentioned in the publications. PMID: PubMed ID

progression (Sect. 6.3.3). In this sense, it is not surprising even if we can identify a set of genes that describes disease progression well. In this subsection, we try to identify genes that discriminate time developments between dengue fever (DF) and dengue hemorrhagic fever (DHF) [18]. DF is usually non-lethal mosquito-borne virus disease. Nevertheless, it rarely develops to lethal DHF. Because DHF usually develops only after remission of DF, it is supposed that if DHF develops from DF is dependent upon the patients status. In spite of that, it is unclear what kind of difference decides if DHF develops after patients start to recover from DF. In this subsection, we try to apply PCA based unsupervised FE to patients blood gene expression profiles in order to identify which genes are related to DHF developments.

Table 6.41 Top five GO BP term/publication enrichments reported by YeastMine in 40 genes identified by sinusoidal regression, Eq. (6.63)

Sinusoidal regression			
GO BP term		p-Value	#
Cell cycle	[GO:0007049]	4.45×10^{-10}	26
Cell cycle process	[GO:0051276]	3.27×10^{-8}	22
Chromosome organization	[GO:0006259]	5.07×10^{-8}	21
Cellular response to DNA damage stimulus	[GO:0006974]	5.85×10^{-8}	17
Chromatin assembly or disassembly	[GO:0006333]	7.32×10^{-7}	9
Publication	PMID	p-Value	#
Clustering time-varying gene expression profiles using scale-space signals.			
	[16452778]	8.69×10^{-23}	20
Histone h3 exerts a key function in mitotic checkpoint control.			
	[19917722]	3.69×10^{-15}	9
Regulation of cell cycle-dependent gene expression in yeast.			
	[2201678]	5.846×10^{-15}	11
Molecular biology. Nucleosomes help guide yeast gene activity.			
	[15961637]	6.85×10^{-14}	8
Brownian dynamics simulation of directional sliding of histone octamers caused by DNA bending.			
	[16802969]	6.85×10^{-14}	8

#: number of genes associated with GO BP terms or mentioned in the publications. PMID: PubMed ID

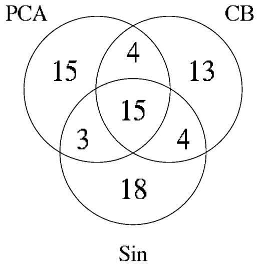

Fig. 6.22 Venn diagram of genes in Table 6.38. PCA: PCA based unsupervised FE, CB: Cyclebase, Sin: sinusoidal fitting

In this subsection, we apply PCA based unsupervised FE to five DF patients blood gene expression profiles in order to identify genes that make DHF develop. Five data sets analyzed are shown in Table 6.42 (Data sets 1–5) [52]. These five data sets are quite distinct. In data set 1, which is composed of four classes, there are healthy controls (HC), acute patients (AC), DF and DHF patients. On the other hand, in data set 2, which is also composed of four classes, three are Acute and Convalescent patients, both of which are composed of DF and DHF patients. In the following, we would like to demonstrate that starting the analysis of these quite distinct two data sets, genes chosen in common between two data sets can describe distinct time development between DF and DHF. In order to show this, we apply PCA based unsupervised FE to data sets 1 and 2, and identify genes for both data sets. Then, using genes chosen in common, we try to see how selected genes describe distinct time developments between DF and DHF, using data sets 3–5.

At first, we apply PCA to data set 1, $x_{ij} \in \mathbb{R}^{54715 \times 56}$, and 2, $x_{ij} \in \mathbb{R}^{23454 \times 30}$, after standardization, $\sum_i x_{ij} = 0$ and $\sum_i x_{ij}^2 = N$ where N is the number of probes, 54,715 and 23,454, respectively. Selection of PCs used for gene selection is not straightforward, because no single PC can discriminate four classes in Table 6.42. Upper triangles of Fig. 6.23 shows the PC loading, $\boldsymbol{v}_\ell, 1 \leq \ell \leq 4$ for data set 1 and 2. With visual inspection, we decide to employ $\ell = 2, 3$ for both data set because this combination is most coincident with clear clusters coincident with class labels. On the other hand, it is obvious that there are no PC loading that discriminate between DHF and DF. Two clusters are coincident with only the distinction between sample with and without symptom. In order to support this decision quantitatively, we perform LDA, Eq. (6.2), assuming two classes and compute accuracy, Eq. (6.16) (lower triangles of Fig. 6.23). It is obvious that $\ell = 2, 3$ achieves the highest accuracy.

Then we attribute P-values to probes assuming χ^2 distribution as

Table 6.42 List of samples included in data set 1, 2, 3, 4, and 5

Data set 1 (GSE51808)	Affymetrix HT HG-U133+ PM array plate			
	Healthy Controls (HC)	Acute Patients (AC)	DF	DHF
	9	19	18	10

Data set 2 (GSE13052)	Sentrix HumanRef-8 expression BeadChip		
	Acute	Convalescent	
Uncomplicated (DF)	10	5	
DSS* (DHF)	9	6	

Data set 3 (GSE25001)	Illumina HumanRef-8 v2.0 expression Beadchip			
	Acute	0-1	Disease (Fever)	Follow up
DF	56	32	31	16
DHF	24	12	20	18

Data set 4 (GSE43777-GPL570)	Affymetrix human genome U133 Plus 2.0 array							
	G0	G1	G2	G3	G4	G5	G6	G7
DF	0	2	5	8	9	5	11	12
DHF	0	0	3	8	10	5	11	12
Data set 5 (GSE43777-GPL201)	Affymetrix human HG-focus target array							
DF	2	5	21	18	22	22	24	45
DHF	0	0	0	1	3	1	1	3

DSS: Dengue Shock Syndrome. GSE51808: RMA normalization was performed using Expression Console software. GSE13052: Intensity was acquired using Beadstudio software Intensity was background normalized (Subtract the background value). GSE25001: Data was normalized by Beadstudio software. GSE43777: RMA normalization was performed using Expression Console software. For more details, see papers that reported these data sets

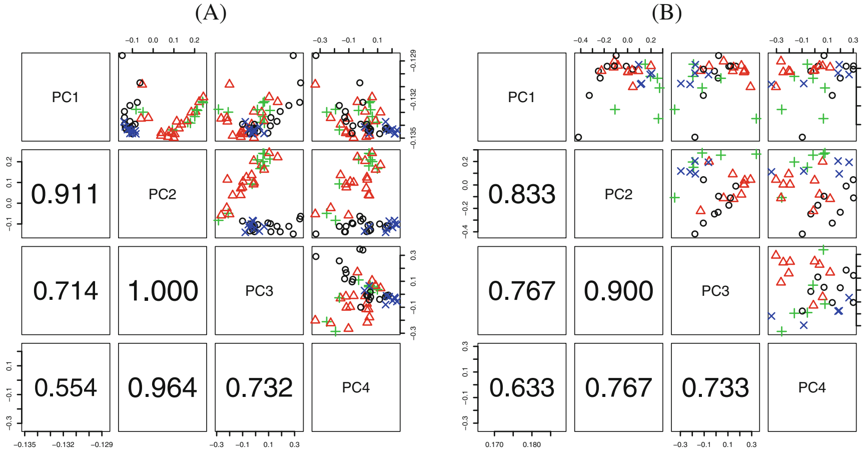

Fig. 6.23 Upper triangle: Scatterplot of PC loading, $\boldsymbol{v}_\ell$, $1 \le \ell \le 4$, for (**a**) Data set 1, open circle: Convalescent Patient, red triangle: Dengue Fever, green plus symbol: Dengue Hemorrhagic, blue cross symbol: Healthy control, (**b**) Data set 2, open circle: acute DSS, red triangle: acute uncomplicated, green plus symbol: convalescent DSS, blue cross symbol: convalescent uncomplicated. Lower triangle: accuracy of two classes (with and without symptom) discrimination. (**a**) Open circle + blue cross symbol vs red triangle + green plus symbol, (**b**) open circle + red triangle vs green plus symbol + blue cross symbol

$$P_i = P_{\chi^2}\left[> \sum_{\ell=2}^{3} \left(\frac{u_{\ell i}}{\sigma_\ell} \right)^2 \right]. \tag{6.64}$$

P-values are adjusted by BH criterion and probes associated with adjusted P-values less than 0.01 are selected. As a result, 879 and 275 probes are selected for data set 1 and 2, respectively (Fig. 6.24). Considering the fact that total number of probes are 10^4 while the number of selected probes are about 10^2, the regions where selected probes (red dots) distribute is very huge and selected probes are really outliers. The number of genes included in common in both sets of selected genes as many as 46 (Table 6.43). In order to check if as many as 46 chosen in common genes can occur accidentally, we apply Fisher's exact test (Table 6.44). It is obvious that 46 genes are too large to occur accidentally.

In order to see if other conventional supervised feature selection methods can work similarly, we test three methods, limma, categorical regression analysis, and significance analysis of microarrays (SAM) [65], which is t test modified so as to be fitted to microarray analysis. These three tests are performed under the two assumptions of either four classes or two classes. Two classes are assumed to be those with and without symptom, as shown in the caption of Fig. 6.23. Probes with adjusted P-values less than 0.01 are selected. Table 6.45 shows the results. Because the numbers of probes identified in data set 1 are too large, no methods are useful to select small enough number of genes chosen in common between two data sets.

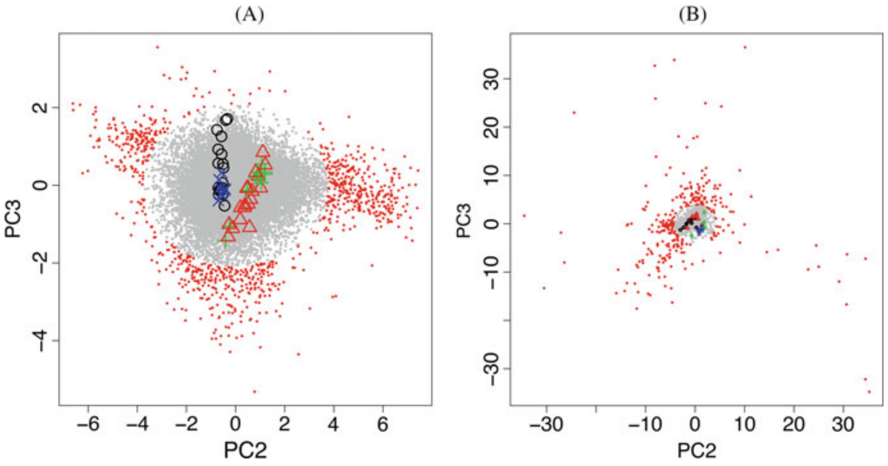

Fig. 6.24 PC score, $\boldsymbol{u}_\ell, \ell = 2, 3$, for (**a**) data set 1 and (**b**) data set 2. Gray dots: not selected probes, red dots: selected dots. Colored marks are PC loading, as shown in Fig. 6.23

Table 6.43 Forty six and forty one genes common between 879 and 275 genes selected by PCA based unsupervised FE and categorical regression

46 genes associated with probes chosen in common by PCA based unsupervised FE
FBXO7 MX1 LY6E **IFI27** TNFSF10 OAS1 CDC20 GYPC **PI3** FCGR3A HBA1 HBA2 HBG1 HBG2 IFI44L IFIT3 CCR1 FPR1 STAT2 ISG15 OASL CD38 TNFRSF17 CXCR1 ZBP1 HBB IFI35 MKRN1 APOBEC3A ALAS2 IL1RN RSAD2 ASCC2 IFIT2 **ADIPOR1** SLC25A37 OAS3 SDF2L1 TMEM140 FKBP11 HERC5 ITM2C TXNDC5 STRADB **SLC25A39** EPSTI1
41 genes associated with probes chosen in common by categorical regression
FBXO7 PSMB2 LGALS1 NMT1 TMX2 LRRC41 IDH3A BAG1 **IFI27** UBE2S ATOX1 **PI3** BAK1 MRPL28 CHAF1B HAGH PSMD11 XPNPEP1 TSPAN5 GART RTN1 YARS SLC43A3 **ADIPOR1** DCXR MRPS18A SIL1 DPP3 GPN2 TESC KCTD14 GMPPB CAMK1D TACO1 OSBP2 STRADB **SLC25A39** EHD4 TRIM69 HAVCR2 SESN3

Bold genes are common

Table 6.44 Confusion matrices and associated P-values and odds ratio

	Data set 1	Not selected	Selected	P-value	Odds ratio
PCA based unsupervised FE					
Data set 2	Not selected	13,574	186	2.17×10^{-22}	7.51
	Selected	447	46		
Categorical regression (2 classes)					
Data set 2	Not selected	13,680	185	5.73×10^{-16}	5.50
	Selected	551	41		

Although this definitely suggests the superiority towards these three conventional methods, we can make use of them with taking into account the results of PCA based unsupervised FE. PCA based unsupervised FE has already shown that 879 and 275 probes are large enough to have reasonable number of common genes between

Table 6.45 Number of genes identified by SAM, limma, and categorical regression

Data set	Sam		Limma		Categorical regression	
	Two classes	Four classes	Two classes	Four classes	Two classes	Four classes
1	17,680	16,647	54,715[a]	13,506	15,447	13,941
2	2427	865	21,795	20,629	679	581

Two classes mean “DHF+DF” vs “CP+HC” for data set 1 (GSE51808) and “Acute” vs “Convalescent” for data set 2 (GSE13052)

[a] All probes

two data sets. Thus, we select top ranked 879 and 275 probes based upon P-values computed by one of three methods in order to compare the performance with PCA based unsupervised FE. SAM attributed $P = 0$ to more than 879 genes in data set 1. Thus we cannot select top ranked 870 genes in data set 1 by SAM. Although limma allowed us to identify specified top ranked genes, the number of common probes is a few. Thus, neither SAM not limma can compete with PCA based unsupervised FE. Categorical regression analysis identifies 32 and 41 probes in common between 879 and 275 probes for two classes and four classes cases, respectively. As many as 41 genes (Table 6.43) chosen in common is highly significant (Table 6.44). Thus, categorical regression is comparable with PCA based unsupervised FE.

These two sets of genes selected by PCA based unsupervised FE and by categorical regression analysis are quite distinct. There are only five genes chosen in common between two sets. In order to see which gene set is better, we need to evaluate them biologically. For this purpose, we employ data set 3 (Table 6.42). We apply PCA to either 46 genes selected by PCA based unsupervised FE or 41 genes selected by categorical regression in data set 3. If selected genes are reasonable, samples with distinct labels should be separately located in the plane spanned by PC loading. Figure 6.25 shows that scatterplot of PC loading obtained by applying PCA to either 46 genes selected by PCA based unsupervised FE or 41 genes selected by categorical regression in data set 3. There are four disease stages in data set 3; acute, [0-1] (0 or 1 days after the symptom), DIS (disease), and FOLLOWUP (after remission). For both cases, disease progression can be seen in this order. It is also interesting, in later stage, DHF and DF are distinct to some extent. In order to further validate two gene sets, we apply t test to see how distinct DHF and DF are quantitatively. Table 6.46 shows the result. DHF and DF are more distinct when genes selected by PCA based unsupervised FE are used. Thus, PCA based unsupervised FE selected more reasonable gene than categorical regression.

Basically, we believe that the above performance is good enough to demonstrate the superiority of PCA based unsupervised FE over the conventional supervised methods. Nevertheless, we would like to emphasize the robustness of the selected 46 genes by applying PCA to additional data set, data sets 4 and 5 (Table 6.42). Figure 6.26 shows the scatterplots of PC loading, $\boldsymbol{v}_\ell, \ell = 2, 3$, obtained by applying PCA to data set 4 and 5 with only 46 genes (Table 6.43) selected with PCA based unsupervised FE applied to data set 1 and 2. The V letter shape seen in Fig. 6.25 is conserved for two data sets, too, although the distinction between DHF and DF

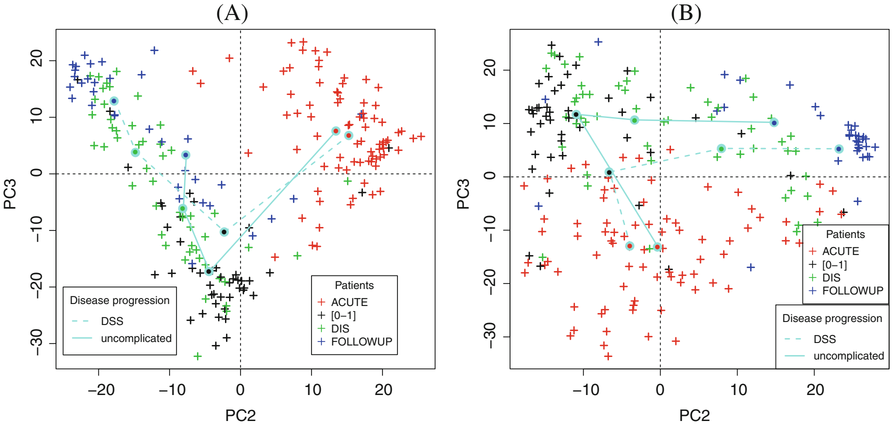

Fig. 6.25 Scatterplot of PC loading $\boldsymbol{v}_\ell, \ell = 2, 3$, obtained by applying PCA to data set 3 using only genes selected by PCA based unsupervised FE or categorical regression to data set 1 and 2. (**a**) PCA based unsupervised FE (**b**) Categorical regression

Table 6.46 P-values computed by t test applied to the distinction of the second and the third PC scores between "DSS" and "uncomplicated" patients in Fig. 6.25

	ACUTE	[0-1]	DIS	FOLLOWUP
PCA based unsupervised FE				
PC2	2.14×10^{-1}	5.62×10^{-1}	7.87×10^{-3}	4.15×10^{-3}
PC3	7.23×10^{-1}	1.07×10^{-1}	6.41×10^{-3}	9.73×10^{-3}
Categorical regression				
PC2	1.24×10^{-1}	2.78×10^{-1}	8.84×10^{-4}	4.00×10^{-2}
PC3	$9, 16 \times 10^{-1}$	1.26×10^{-2}	5.48×10^{-2}	6.49×10^{-2}

is weaker. This is possibly because the number of samples is smaller (12 samples in G7 stage of data set 4 while 16 or 18 samples in follow-up stage of data set 3). Nevertheless, in G7 stage, the second PC loading, v_{2j}, is still significantly distinct ($P = 0.05$ and 0.04 with a t test and Wilcoxon signed-rank sum test, respectively). Because 46 genes selected for data set 1 and data set 2 are valid to describe disease progression in three independent data sets, data sets 3 to 5, 46 genes in Table 6.43 should be key genes that describe the distinction between DF and DHF.

In conclusion, PCA based unsupervised FE has superior ability to identify limited number of genes that can describe DHF progression.

6.7 Gene Selection for Single Cell RNA-seq

Single cell RNA high throughput sequencing (scRNA-seq) is a newly developed technology. scRNA-seq can measure RNA expression in single cell base [20]. In

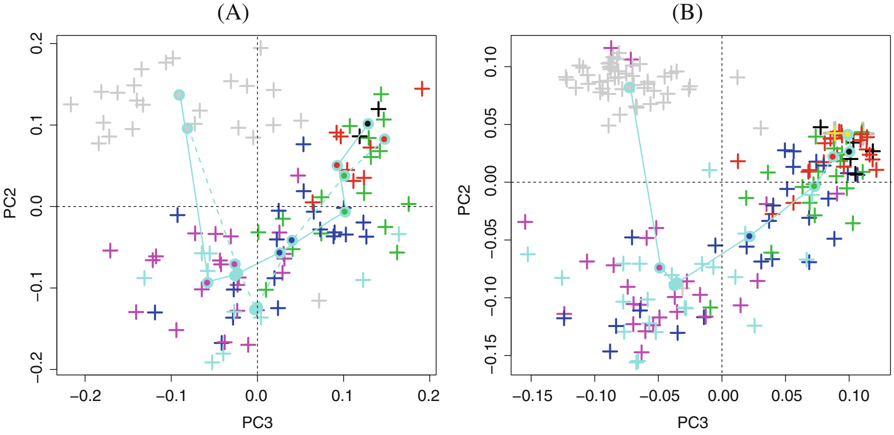

Fig. 6.26 Scatterplot of PC loading, $\boldsymbol{v}_\ell$, $\ell = 2, 3$, obtained by applying PCA to data set 4 (**a**) and 5 (**b**), using only 46 genes (Table 6.43) selected by PCA based unsupervised FE applied to data set 1 and 2. The correspondence between the colored crosses (+) and disease progression are black (stage G1), red (stage G2), green (stage G3), blue (stage G4), cyan (stage G5), magenta (stage G6), and gray (stage G7). Cyan solid and broken lines correspond to DF and DHF, respectively

contrast to the usual HTS that can measure gene expression profile only in tissue base, scRNA-seq can measure gene expression profile within individual cells.

From the data science point of view, scRNA-seq is distinct from conventional tissue based gene expression measurements in the following two points:

Larger number of samples In contrast to the conventional tissue based measurements, because the number of samples is as many as number of cells, it can be as large as 10^3.

Missing labeling Because geometrical information of individual cell within tissue is missing during the process of library preparation, samples (cells) are not basically labeled.

Because of these two primary differences, applying PCA based unsupervised FE to scRNA-seq is challenging. As emphasized many times, PCA based unsupervised FE is invented to be applied to large p small n problem. It is interesting to see if PCA based unsupervised FE is useful even if the number of samples increases up to 10^3. On the other hand, missing labeling is advantageous over PCA based unsupervised FE, because it is designed to be fitted to unlabeled samples. Because of these pros and cons, it is unclear if PCA based unsupervised FE is applicable to scRNA-seq.

In this section, we apply PCA based unsupervised FE to an scRNA-seq data set [53]. scRNA-seq data is downloaded from GEO with GEO ID GSE76381. It includes human embryo ventral midbrain cells between 6 and 11 weeks of gestation, mouse ventral midbrain cells at six developmental stages between E11.5 to E18.5, Th+ neurons at P19-P27, and fluorescence activated cell sorting (FACS)-sorted putative dopaminergic neurons at P28-P56 from Slc6a3-Cre/tdTomato mice. That is, it includes data set of brain development of human and mouse. The purpose of the analysis is to understand what is common between human and mouse brain development, based upon gene expression analysis. PCA based unsupervised FE is applied to these data sets separately. Here E denotes the number of days after fertilization while P denotes postnatal days.

Usually, the first step is to identify which PC loading exhibits the desired class dependence. Nevertheless, for scRNA-seq data, because no labeling is available for samples, it is impossible to find which PC loading reflects something to be searched. Then, we decide to select the first L PC scores, $\boldsymbol{u}_\ell$, $\ell \leq L$, and attribute P-values to gene i assuming χ^2 distribution as

$$P_i = P_{\chi^2}\left[> \sum_{\ell=1}^{L} \left(\frac{u_{\ell i}}{\sigma_\ell}\right)^2 \right]. \tag{6.65}$$

P-values are corrected by BH criterion and genes associated with adjusted P-values less than 0.01 are selected. The problem is how to decide L. In this case, we select the smallest L such that selected genes are as many as a few hundreds. Then, we find that 116 and 118 genes are selected if $L = 2$ and $L = 3$ for human and mouse, respectively.

The first evaluation of these two sets of selected genes is the amount of overlap between them. Among 116 selected human genes and 118 mouse genes, as many as 53 genes are chosen in common (Table 6.47). Unfortunately, in contrast to the

Table 6.47 Fifty three genes common between 116 human and 118 mice genes selected by PCA based unsupervised FE

53 genes associated with probes chosen in common by PCA based unsupervised FE
ACTB ACTG1 ATP5E CALM2 COX7C EEF1A1 FAU FTH1 H2AFZ H3F3B HMGB1 HMGB2 HMGN2 HSP90AA1 HSP90AB1 MALAT1 MAP1B MARCKS MEG3 NGFRAP1 PABPC1 PPIA PTMA RPL18A RPL23 RPL24 RPL32 RPL35 RPL38 RPL39 RPL4 RPLP1 RPLP2 RPS12 RPS13 RPS16 RPS20 RPS24 RPS25 RPS28 RPS29 RPS3 RPS5 RPS6 RPSA SPARC STMN1 STMN2 SUMO2 TMSB10 TMSB4X TUBA1A TUBA1B
44 genes associated with probes chosen in common by highly variable genes
ALDH1A1 APLN CARTPT CAV1 CCL2 CCL3 CCL4 CD93 CLDN5 COL4A1 COL4A2 CRABP1 CSF1R CX3CR1 DBH FLT1 FN1 HPGDS ICAM2 IGFBP3 IGFBP7 IL1B ITM2A KDR NEFM NPY NTS P2RY12 PF4 PLEK RGS5 SLC2A1 SLC38A5 SLC6A2 SLC6A4 SLC7A1 SLC7A5 SNCG SPARCL1 SPP1 SRGN SST TPH2 VWF
21 genes associated with probes chosen in common by bimodal genes
AP2B1 AP2M1 ASH1L EIF4B FXR1 G3BP1 HNRNPH2 IK ILF3 MIDN NMT1 OCIAD1 PNN PPIG PRPF6 PSMD11 RPS15 SETD5 SRP72 TAX1BP1 WAC
76 genes associated with probes chosen in common by dpFeature
ACTG1 ALDH1A1 ANK3 ARL6IP1 ATP1A2 ATP5E B2M BASP1 BGN CALD1 CALM2 CCL3 CCL4 CCNB1 CDK1 CELF4 CENPF CKS1B CKS2 CLDN5 COL4A1 COL4A2 COX7A2 COX7C CRMP1 CST3 CYR61 DCX DPYSL2 DPYSL3 DNRB EEF1A1 ELAVL2 ELAVL4 ESAM ETS1 FABP5 FABP7 FAU FGFBP3 FLT1 FN1 FOS FSTL1 GAP43 GNB2L1 GNG11 GPM6A GPM6B GRIA2 GSTP1 H2AFZ H3F3B HES1 HMGB1 HMGB2 HMGN2 HN1 HSP90AA1 IGFBP7 INA ITM2A KCNQ1OT1 KIF5C KPNA2 LGALS1 MALAT1 MAP1B MAP2 MEG3 MIAT MLLT11 MYL12A MYL6 NCAM1 NDUFA4

Table 6.48 Confusion matrices and associated *P*-values and odds ratio

PCA based unsupervised FE					
Human	Mouse	Not selected	Selected	*P*-value	Odds ratio
	Not selected	19,819	63	2.21×10^{-91}	255.00
	Selected	65	53		
Highly variable genes					
Data set 2	Data set 1	Not selected	Selected	*P*-value	Odds ratio
	Not selected	19,705	124	7.13×10^{-54}	54.97
	Selected	127	44		
Bimodal genes					
Data set 2	Data set 1	Not selected	Selected	*P*-value	Odds ratio
	Not selected	19,621	179	1.00×10^{-15}	12.85
	Selected	179	21		
dpFeature					
Data set 2	Data set 1	Not selected	Selected	*P*-value	Odds ratio
	Not selected	19,676	124	1.03×10^{-105}	96.98
	Selected	124	76		

microarray, there are no definite number of "total genes" for scRNA-seq. Thus, tentatively, we assume that there are 20,000 genes for mouse and human. Table 6.48 shows the confusion matrix and the result of Fisher's exact test. In any case, overlap is highly significant.

In order to compare the performance with other methods, first we consider highly variable genes [9]. The procedure of how to perform highly variable genes is as follows. First we perform regression analysis

$$\log_{10}\left(\frac{\sqrt{\langle x_{ij}^2\rangle_j - \langle x_{ij}\rangle_j^2}}{\langle x_{ij}\rangle_j}\right) = \frac{1}{2}\log_{10}\left(\frac{\beta}{\langle x_{ij}\rangle_j} + \alpha\right) + \epsilon_i \tag{6.66}$$

where α and β are regression coefficients and ϵ_i is residual. *P*-values are attributed to genes, i, assuming χ^2 distribution as

$$P_i = P_{\chi^2}\left[> \left(\frac{\epsilon_i}{\sigma'}\right)^2\right]. \tag{6.67}$$

P-values are corrected by BH criterion. Genes associated with adjusted *P*-values less than 0.01 are selected. We identify 168 human genes and 171 mouse genes between which 44 genes are chosen in common (Table 6.47). Although it is a little bit less significant than PCA based unsupervised FE, it is still highly significant (Table 6.48).

Next, we compare PCA based unsupervised FE with bimodal genes [12]. Bimodal genes are selected based upon the *P*-values computed by Hartigan's dip test, which rejects the null hypothesis that the distribution is unimodal [19]. The concept behind bimodal genes is that if gene expression of a gene is unimodal, it is unlikely that the expression is coincident with the distinction between two classes. We attribute P-values to genes using this test. P-values are adjusted by BH criterion. Then genes associated with adjusted P-values less than 0.01 are selected. As a result, 11,344 human and 10,849 mouse genes are selected. Thus, it is obvious that bimodel genes are too many. In order to see the coincidence between the two gene sets, we select top ranked 200 human and mouse genes based upon P-value computed by Hartigan's dip test. This results in as small as 21 genes chosen in common (Table 6.47). Thus, as far as consistency between human and mouse is concerned, bimodel genes are inferior to either PCA based unsupervised FE or highly variable genes (Table 6.48).

Finally, we compare PCA based unsupervised FE with dpFeature [36], which was proposed very recently as an advanced tool to select genes in scRNA-seq. It selects 13,775 human and 13,362 mouse genes. Thus it cannot select reasonable number of genes. In order to verify consistency between human and mouse, we selected top ranked 200 genes and compare them. Then there are 76 common genes (Table 6.47). The significance is comparable with PCA based unsupervised FE (Table 6.48).

Although biological validations of selected genes using enrichment analysis are available elsewhere [53], I am not willing to discuss about it in detail here, because coincidence between mouse and human can be a biological evaluation to some extent; the results by enrichment analysis also support the superiority of PCA based unsupervised FE to other three methods. In addition to this, Chen et al. [10] evaluated biologically multiple gene selection methods applicable to scRNA-seq using enrichment analysis; they concluded that PCA based unsupervised FE is at least competitively good with other compared methods.

In conclusion, PCA based unsupervised FE is at least comparable with other popular or conventional methods.

6.8 Summary

In this chapter, I demonstrated how we can make use of PCA based unsupervised FE in the application to bioinformatics, especially, in the field of feature selection. In all application examples, PCA is applied such that PC loading, $\boldsymbol{v}_\ell$, is attributed to samples while PC score, $\boldsymbol{u}_\ell$, is attributed to features (genes, miRNAs). The next step is to investigate PC loading, $\boldsymbol{v}_\ell$, in order to identify ℓs used for computing P-values. This step is the most difficult. The simplest case is to apply linear regression analysis to PC loading and to identify which PC loading is coincident with class labeling. Nevertheless, it is not always possible. When class labeling is missing or no PC loading is coincident with class labeling, simply $\ell \leq L$ is employed (in this case, there are no definite ways to decide L). In some case, we need to find a set of ℓs that are coincident with class labeling. In this case, we need to draw scatterplot of PC loading, $\boldsymbol{v}_\ell$. When we aim to perform integrated analysis, e.g., that between miRNAs and mRNAs or that between methylation and mRNAs, the coincidence of PC loading between these two. When samples are shared between two, correlation coefficients and hierarchical clustering using correlation coefficients are useful. If samples are not shared, we need to investigate PC loading with more additional information, e.g., down/upregulated in treated samples towards control samples simultaneously between these two features. Thus, although PCA based unsupervised FE is powerful method, in contrast to other machine learning technique, we need more deep understanding of data to be analyzed. This can be pros or cons of PCA based unsupervised FE.

References

1. Abeel, T., Helleputte, T., de Peer, Y.V., Dupont, P., Saeys, Y.: Robust biomarker identification for cancer diagnosis with ensemble feature selection methods. Bioinformatics **26**(3), 392–398 (2009). https://doi.org/10.1093/bioinformatics/btp630
2. Agarwal, V., Bell, G.W., Nam, J.W., Bartel, D.P.: Predicting effective microRNA target sites in mammalian mRNAs. eLife **4** (2015). https://doi.org/10.7554/elife.05005
3. Ahuja, N., Sharma, A.R., Baylin, S.B.: Epigenetic therapeutics: a new weapon in the war against cancer. Annu. Rev. Med. **67**(1), 73–89 (2016). https://doi.org/10.1146/annurev-med-111314-035900
4. Artmann, S., Jung, K., Bleckmann, A., Beissbarth, T.: Detection of simultaneous group effects in microRNA expression and related target gene sets. PLoS One **7**(6), e38365 (2012)
5. Balakrishnan, R., Park, J., Karra, K., Hitz, B.C., Binkley, G., Hong, E.L., Sullivan, J., Micklem, G., Michael Cherry, J.: Yeastminełn integrated data warehouse for saccharomyces cerevisiae data as a multipurpose tool-kit. Database **2012**, bar062 (2012). http://dx.doi.org/10.1093/database/bar062
6. Bleckmann, A., Leha, A., Artmann, S., Menck, K., Salinas-Riester, G., Binder, C., Pukrop, T., Beissbarth, T., Klemm, F.: Integrated miRNA and mRNA profiling of tumor-educated macrophages identifies prognostic subgroups in estrogen receptor-positive breast cancer. Mol. Oncol. **9**(1), 155–166 (2015)
7. Brown, T.A.: Genomes 4, 4th edn. Garland Science, New York (2017). https://www.crcpress.com/Genomes-4/Brown/p/book/9780815345084
8. Chan, M., Liaw, C.S., Ji, S.M., Tan, H.H., Wong, C.Y., Thike, A.A., Tan, P.H., Ho, G.H., Lee, A.S.G.: Identification of circulating MicroRNA signatures for breast cancer detection. Clin. Cancer Res. **19**(16), 4477–4487 (2013). https://doi.org/10.1158/1078-0432.ccr-12-3401
9. Chen, H.I.H., Jin, Y., Huang, Y., Chen, Y.: Detection of high variability in gene expression from single-cell RNA-seq profiling. BMC Genet. **17**(7), 508 (2016). https://doi.org/10.1186/s12864-016-2897-6
10. Chen, B., Lau, K.S., Herring, C.A.: pyNVR: investigating factors affecting feature selection from scRNA-seq data for lineage reconstruction. Bioinformatics (2018). https://dx.doi.org/10.1093/bioinformatics/bty950
11. Cho, R.J., Campbell, M.J., Winzeler, E.A., Steinmetz, L., Conway, A., Wodicka, L., Wolfsberg, T.G., Gabrielian, A.E., Landsman, D., Lockhart, D.J., Davis, R.W.: A genome-wide transcriptional analysis of the mitotic cell cycle. Mol. Cell **2**(1), 65–73 (1998). https://doi.org/10.1016/s1097-2765(00)80114-8
12. DeTomaso, D., Yosef, N.: Fastproject: a tool for low-dimensional analysis of single-cell rna-seq data. BMC Bioinf. **17**(1), 315 (2016). https://doi.org/10.1186/s12859-016-1176-5
13. Ding, M., Li, J., Yu, Y., Liu, H., Yan, Z., Wang, J., Qian, Q.: Integrated analysis of miRNA, gene, and pathway regulatory networks in hepatic cancer stem cells. J. Transl. Med. **13**, 259 (2015)

14. Fisher, R.A.: On the interpretation of χ^2 from contingency tables, and the calculation of p. J. R. Stat. Soc. **85**(1), 87 (1922). https://doi.org/10.2307/2340521
15. Fu, J., Tang, W., Du, P., Wang, G., Chen, W., Li, J., Zhu, Y., Gao, J., Cui, L.: Identifying microRNA-mRNA regulatory network in colorectal cancer by a combination of expression profile and bioinformatics analysis. BMC Syst. Biol. **6**, 68 (2012)
16. Gauthier, N.P., Larsen, M.E., Wernersson, R., de Lichtenberg, U., Jensen, L.J., Brunak, S., Jensen, T.S.: Cyclebase.orgł comprehensive multi-organism online database of cell-cycle experiments. Nucleic Acids Res. **36**(Suppl. 1), D854–D859 (2008). http://dx.doi.org/10.1093/nar/gkm729
17. Granovskaia, M.V., Jensen, L.J., Ritchie, M.E., Toedling, J., Ning, Y., Bork, P., Huber, W., Steinmetz, L.M.: High-resolution transcription atlas of the mitotic cell cycle in budding yeast. Genome Biol. **11**(3), R24 (2010). https://doi.org/10.1186/gb-2010-11-3-r24
18. Gubler, D.J.: Dengue and dengue hemorrhagic fever. Clin. Microbiol. Rev. **11**(3), 480–496 (1998). https://doi.org/10.1128/cmr.11.3.480
19. Hartigan, J.A., Hartigan, P.M.: The dip test of unimodality. Ann. Stat. **13**(1), 70–84 (1985). https://doi.org/10.1214/aos/1176346577
20. Hwang, B., Lee, J.H., Bang, D.: Single-cell RNA sequencing technologies and bioinformatics pipelines. Exp. Mol. Med. **50**(8) (2018). https://doi.org/10.1038/s12276-018-0071-8
21. Jiao, X., Sherman, B.T., Huang, D.W., Stephens, R., Baseler, M.W., Lane, H.C., Lempicki, R.A.: DAVID-WS: a stateful web service to facilitate gene/protein list analysis. Bioinformatics **28**(13), 1805–1806 (2012). https://doi.org/10.1093/bioinformatics/bts251
22. Juanes, M.A.: Methods of Synchronization of Yeast Cells for the Analysis of Cell Cycle Progression, pp. 19–34. Springer, New York (2017). https://doi.org/10.1007/978-1-4939-6502-1_2
23. Kanehisa, M., Furumichi, M., Tanabe, M., Sato, Y., Morishima, K.: KEGG: new perspectives on genomes, pathways, diseases and drugs. Nucleic Acids Res. **45**(D1), D353–D361 (2016). https://doi.org/10.1093/nar/gkw1092
24. Keller, A., Leidinger, P., Bauer, A., ElSharawy, A., Haas, J., Backes, C., Wendschlag, A., Giese, N., Tjaden, C., Ott, K., Werner, J., Hackert, T., Ruprecht, K., Huwer, H., Huebers, J., Jacobs, G., Rosenstiel, P., Dommisch, H., Schaefer, A., Müller-Quernheim, J., Wullich, B., Keck, B., Graf, N., Reichrath, J., Vogel, B., Nebel, A., Jager, S.U., Staehler, P., Amarantos, I., Boisguerin, V., Staehler, C., Beier, M., Scheffler, M., Büchler, M.W., Wischhusen, J., Haeusler, S.F.M., Dietl, J., Hofmann, S., Lenhof, H.P., Schreiber, S., Katus, H.A., Rottbauer, W., Meder, B., Hoheisel, J.D., Franke, A., Meese, E.: Toward the blood-borne miRNome of human diseases. Nat. Methods **8**(10), 841–843 (2011). https://doi.org/10.1038/nmeth.1682
25. Kozomara, A., Griffiths-Jones, S.: miRBase: annotating high confidence microRNAs using deep sequencing data. Nucleic Acids Res. **42**(D1), D68–D73 (2014). http://dx.doi.org/10.1093/nar/gkt1181
26. Leidinger, P., Backes, C., Deutscher, S., Schmitt, K., Mueller, S.C., Frese, K., Haas, J., Ruprecht, K., Paul, F., Stähler, C., Lang, C.J., Meder, B., Bartfai, T., Meese, E., Keller, A.: A blood based 12-miRNA signature of Alzheimer disease patients. Genome Biol. **14**(7), R78 (2013). https://doi.org/10.1186/gb-2013-14-7-r78
27. Li, X., Gill, R., Cooper, N.G., Yoo, J.K., Datta, S.: Modeling microRNA-mRNA interactions using PLS regression in human colon cancer. BMC Med. Genet. **4**, 44 (2011)
28. Liu, P.F., Jiang, W.H., Han, Y.T., He, L.F., Zhang, H.L., Ren, H.: Integrated microRNA-mRNA analysis of pancreatic ductal adenocarcinoma. Genet. Mol. Res. **14**(3), 10288–10297 (2015)
29. Ma, L., Huang, Y., Zhu, W., Zhou, S., Zhou, J., Zeng, F., Liu, X., Zhang, Y., Yu, J.: An integrated analysis of miRNA and mRNA expressions in non-small cell lung cancers. PLoS ONE **6**(10), e26502 (2011)
30. MacLellan, S.A., Lawson, J., Baik, J., Guillaud, M., Poh, C.F.Y., Garnis, C.: Differential expression of miRNAs in the serum of patients with high-risk oral lesions. Cancer Med. **1**(2), 268–274 (2012). https://doi.org/10.1002/cam4.17
31. Meng, X.R., Lu, P., Mei, J.Z., Liu, G.J., Fan, Q.X.: Expression analysis of miRNA and target mRNAs in esophageal cancer. Braz. J. Med. Biol. Res. **47**(9), 811–817 (2014)

32. Miyanaga, A., Gemma, A., Noro, R., Kataoka, K., Matsuda, K., Nara, M., Okano, T., Seike, M., Yoshimura, A., Kawakami, A., Uesaka, H., Nakae, H., Kudoh, S.: Antitumor activity of histone deacetylase inhibitors in non-small cell lung cancer cells: development of a molecular predictive model. Mol. Cancer Ther. **7**(7), 1923–1930 (2008). http://mct.aacrjournals.org/content/7/7/1923
33. Murakami, Y., Toyoda, H., Tanahashi, T., Tanaka, J., Kumada, T., Yoshioka, Y., Kosaka, N., Ochiya, T., Taguchi, Y.H.: Comprehensive miRNA expression analysis in peripheral blood can diagnose liver disease. PLoS One **7**(10), e48366 (2012). https://doi.org/10.1371/journal.pone.0048366
34. Pramila, T., Wu, W., Miles, S., Noble, W.S., Breeden, L.L.: The forkhead transcription factor hcm1 regulates chromosome segregation genes and fills the s-phase gap in the transcriptional circuitry of the cell cycle. Genes Dev. **20**(16), 2266–2278 (2006). http://genesdev.cshlp.org/content/20/16/2266.abstract
35. Qiu, W., He, W., Wang, X., Lazarus, R.: A marginal mixture model for selecting differentially expressed genes across two types of tissue samples. Int. J. Biostat. **4**(1) (2008). https://doi.org/10.2202/1557-4679.1093
36. Qiu, X., Mao, Q., Tang, Y., Wang, L., Chawla, R., Pliner, H.A., Trapnell, C.: Reversed graph embedding resolves complex single-cell trajectories. Nat. Methods **14**(10), 979–982 (2017). https://doi.org/10.1038/nmeth.4402
37. Ritchie, M.E., Phipson, B., Wu, D., Hu, Y., Law, C.W., Shi, W., Smyth, G.K.: Limma powers differential expression analyses for rna-sequencing and microarray studies. Nucleic Acids Res. **43**(7), e47 (2015). http://dx.doi.org/10.1093/nar/gkv007
38. Rommer, A., Steinleitner, K., Hackl, H., Schneckenleithner, C., Engelmann, M., Scheideler, M., Vlatkovic, I., Kralovics, R., Cerny-Reiterer, S., Valent, P., Sill, H., Wieser, R.: Overexpression of primary microRNA 221/222 in acute myeloid leukemia. BMC Cancer **13**(1) (2013). https://doi.org/10.1186/1471-2407-13-364
39. Santos, A., Wernersson, R., Jensen, L.J.: Cyclebase 3.0: a multi-organism database on cell-cycle regulation and phenotypes. Nucleic Acids Res. **43**(D1), D1140–D1144 (2015). http://dx.doi.org/10.1093/nar/gku1092
40. Sharma, S., Kelly, T.K., Jones, P.A.: Epigenetics in cancer. Carcinogenesis **31**(1), 27–36 (2009). https://doi.org/10.1093/carcin/bgp220
41. Shen, J., Wang, A., Wang, Q., Gurvich, I., Siegel, A.B., Remotti, H., Santella, R.M.: Exploration of genome-wide circulating MicroRNA in hepatocellular carcinoma: MiR-483-5p as a potential biomarker. Cancer Epidemiol. Biomark. Prev. **22**(12), 2364–2373 (2013). https://doi.org/10.1158/1055-9965.epi-13-0237
42. Skinner, M.K.: Environmental stress and epigenetic transgenerational inheritance. BMC Med. **12**(1) (2014). https://doi.org/10.1186/s12916-014-0153-y
43. Skinner, M.K., Haque, C.G.B.M., Nilsson, E., Bhandari, R., McCarrey, J.R.: Environmentally induced transgenerational epigenetic reprogramming of primordial germ cells and the subsequent germ line. PLOS One **8**(7), 1–15 (2013). https://doi.org/10.1371/journal.pone.0066318
44. Soboleva, A., Yefanov, A., Evangelista, C., Robertson, C.L., Lee, H., Kim, I.F., Phillippy, K.H., Marshall, K.A., Tomashevsky, M., Holko, M., Serova, N., Zhang, N., Sherman, P.M., Ledoux, P., Davis, S., Wilhite, S.E., Barrett, T.: NCBI GEO: archive for functional genomics data setsłpdate. Nucleic Acids Res. **41**(D1), D991–D995 (2012). https://dx.doi.org/10.1093/nar/gks1193
45. Song, L., Smola, A., Gretton, A., Bedo, J., Borgwardt, K.: Feature selection via dependence maximization. J. Mach. Learn. Res. **13**(May), 1393–1434 (2012)
46. Spellman, P., Sherlock, G., Zhang, M., Iyer, V., Anders, K., Eisen, M., Brown, P., Botstein, D., Futcher, B.: Comprehensive identification of cell cycle-regulated genes of the yeast saccharomyces cerevisiae by microarray hybridization. Mol. Biol. Cell **9**(12), 3273–3297 (1998)
47. Subramanian, A., Tamayo, P., Mootha, V.K., Mukherjee, S., Ebert, B.L., Gillette, M.A., Paulovich, A., Pomeroy, S.L., Golub, T.R., Lander, E.S., Mesirov, J.P.: Gene set enrichment analysis: a knowledge-based approach for interpreting genome-wide expression profiles. Proc. Natl. Acad. Sci. **102**(43), 15545–15550 (2005). https://doi.org/10.1073/pnas.0506580102

48. Taguchi, Y.H.: Inference of target gene regulation by miRNA via mirage server. In: Wan, J. (ed.) Introduction to Genetics: DNA Methylation, Histone Modification and Gene Regulation, chap. 9, pp. 175–200. iConcept Press, Kowloon (2013)
49. Taguchi, Y.H.: Identification of aberrant gene expression associated with aberrant promoter methylation in primordial germ cells between e13 and e16 rat f3 generation vinclozolin lineage. BMC Bioinf. **16**(18), S16 (2015). https://doi.org/10.1186/1471-2105-16-S18-S16
50. Taguchi, Y.H.: Identification of more feasible MicroRNA–mRNA interactions within multiple cancers using principal component analysis based unsupervised feature extraction. Int. J. Mol. Sci. **17**(5), 696 (2016). https://doi.org/10.3390/ijms17050696
51. Taguchi, Y.H.: Principal component analysis based unsupervised feature extraction applied to budding yeast temporally periodic gene expression. BioData Min. **9**(1), 22 (2016). https://doi.org/10.1186/s13040-016-0101-9
52. Taguchi, Y.H.: Principal components analysis based unsupervised feature extraction applied to gene expression analysis of blood from dengue haemorrhagic fever patients. Sci. Rep. **7**(1) (2017). https://doi.org/10.1038/srep44016
53. Taguchi, Y.H.: Principal component analysis-based unsupervised feature extraction applied to single-cell gene expression analysis. In: Intelligent Computing Theories and Application, pp. 816–826. Springer International Publishing, Cham (2018). https://doi.org/10.1007/978-3-319-95933-7_90
54. Taguchi, Y.H.: Comparative transcriptomics analysis. In: Ranganathan, S., Gribskov, M., Nakai, K., Schönbach, C. (eds.) Encyclopedia of Bioinformatics and Computational Biology, pp. 814–818. Academic, Oxford (2019). http://www.sciencedirect.com/science/article/pii/B9780128096338201635
55. Taguchi, Y.H.: Regulation of gene expression. In: Ranganathan, S., Gribskov, M., Nakai, K., Schönbach, C. (eds.) Encyclopedia of Bioinformatics and Computational Biology, pp. 806–813. Academic, Oxford (2019). http://www.sciencedirect.com/science/article/pii/B9780128096338206675
56. Taguchi, Y.H., Murakami, Y.: Principal component analysis based feature extraction approach to identify circulating microRNA biomarkers. PLoS One **8**(6), e66714 (2013). https://doi.org/10.1371/journal.pone.0066714
57. Taguchi, Y.H., Murakami, Y.: Universal disease biomarker: can a fixed set of blood microRNAs diagnose multiple diseases? BMC. Res. Notes **7**(1), 581 (2014). https://doi.org/10.1186/1756-0500-7-581
58. Taguchi, Y.H., Wang, H.: Exploring microrna biomarker for amyotrophic lateral sclerosis. Int. J. Mol. Sci. **19**(5) (2018). http://www.mdpi.com/1422-0067/19/5/1318
59. Taguchi, Y.H., Iwadate, M., Umeyama, H.: Principal component analysis-based unsupervised feature extraction applied to in silico drug discovery for posttraumatic stress disorder-mediated heart disease. BMC Bioinf. **16**(1), 139 (2015). https://doi.org/10.1186/s12859-015-0574-4
60. Taguchi, Y.H., Iwadate, M., Umeyama, H.: SFRP1 is a possible candidate for epigenetic therapy in non-small cell lung cancer. BMC Med. Genom. **9**(1), 28 (2016). https://doi.org/10.1186/s12920-016-0196-3
61. Tang, Y.A., Wen, W.L., Chang, J.W., Wei, T.T., Tan, Y.H.C., Salunke, S., Chen, C.T., Chen, C.S., Wang, Y.C.: A novel histone deacetylase inhibitor exhibits antitumor activity via apoptosis induction, f-actin disruption and gene acetylation in lung cancer. PLoS One **5**(9), e12417 (2010). https://doi.org/10.1371/journal.pone.0012417
62. The Gene Ontology Consortium: The Gene Ontology Resource: 20 years and still GOing strong. Nucleic Acids Res. **47**(D1), D330–D338 (2018). https://dx.doi.org/10.1093/nar/gky1055
63. Tollefsbol, T. (ed.): Transgenerational Epigenetics. Elsevier, San Diego (2014). https://doi.org/10.1016/c2012-0-02853-0
64. Tu, B.P.: Logic of the yeast metabolic cycle: temporal compartmentalization of cellular processes. Science **310**(5751), 1152–1158 (2005). https://doi.org/10.1126/science.1120499

65. Tusher, V.G., Tibshirani, R., Chu, G.: Significance analysis of microarrays applied to the ionizing radiation response. Proc. Natl. Acad. Sci. **98**(9), 5116–5121 (2001). https://doi.org/10.1073/pnas.091062498
66. Umeyama, H., Iwadate, M., Taguchi, Y.H.: TINAGL1 and B3GALNT1 are potential therapy target genes to suppress metastasis in non-small cell lung cancer. BMC Genomics **15**(9), S2 (2014). https://doi.org/10.1186/1471-2164-15-S9-S2
67. Varshavsky, R., Gottlieb, A., Horn, D., Linial, M.: Unsupervised feature selection under perturbations: meeting the challenges of biological data. Bioinformatics **23**(24), 3343–3349 (2007). http://dx.doi.org/10.1093/bioinformatics/btm528
68. Vlachos, I.S., Zagganas, K., Paraskevopoulou, M.D., Georgakilas, G., Karagkouni, D., Vergoulis, T., Dalamagas, T., Hatzigeorgiou, A.G.: DIANA-miRPath v3.0: deciphering microRNA function with experimental support. Nucleic Acids Res. **43**(W1), W460–W466 (2015). https://doi.org/10.1093/nar/gkv403
69. Wu, B., Li, C., Zhang, P., Yao, Q., Wu, J., Han, J., Liao, L., Xu, Y., Lin, R., Xiao, D., Xu, L., Li, E., Li, X.: Dissection of miRNA-miRNA interaction in esophageal squamous cell carcinoma. PLoS One **8**(9), e73191 (2013)
70. Yan, X., Chen, X., Liang, H., Deng, T., Chen, W., Zhang, S., Liu, M., Gao, X., Liu, Y., Zhao, C., Wang, X., Wang, N., Li, J., Liu, R., Zen, K., Zhang, C.Y., Liu, B., Ba, Y.: miR-143 and miR-145 synergistically regulate ERBB3 to suppress cell proliferation and invasion in breast cancer. Mol. Cancer **13**(1), 220 (2014). https://doi.org/10.1186/1476-4598-13-220
71. Yang, Y., Li, D., Yang, Y., Jiang, G.: An integrated analysis of the effects of microRNA and mRNA on esophageal squamous cell carcinoma. Mol. Med. Rep. **12**(1), 945–952 (2015)
72. Zhang, W., Edwards, A., Fan, W., Flemington, E.K., Zhang, K.: miRNA-mRNA correlation-network modules in human prostate cancer and the differences between primary and metastatic tumor subtypes. PLoS One **7**(6), e40130 (2012)

Chapter 7
Application of TD Based Unsupervised FE to Bioinformatics

May my wish never come true.
Rikka Takarada, SSSS.GRIDMAN, Season 1, Episode 12

7.1 Introduction

Because of continuous price reduction of multiomics data measurements, including gene expression, promoter methylation, SNP, histone modification, and miRNA expression, more number of experimental conditions come to be considered. For example, if gene expression is measured for various tissues of patients, gene expression has better to be formatted, not in matrix, but in tensor, as patients vs tissue vs genes. In this case, TD rather than PCA is a suitable technology to apply. On the other hand, in the previous chapter, we aimed various integrated analysis, e.g., miRNA and mRNA expression, mRNA expression and methylation, mRNA expression of two species. If genes or features are shared in the integrated analysis, generation of case I or II tensor and application of TD to it is a suitable treatment. In the following, we introduce some application of TD based unsupervised FE to either of these cases.

7.2 PTSD Mediated Heart Diseases

The first example to be processed as tensor form is PTSD mediated heart diseases. Although this disease has already been analyzed in the previous chapter (Sect. 6.4.1), the data set analyzed there includes only one tissue, heart. Nonetheless, if one would like to understand how PTSD mediates heart disease, we need to know gene expression of both heart and brain. Fortunately, there is a such kind of data set. In this section, I would like to demonstrate the usefulness of TD based unsupervised FE applied to gene expression of multiple tissues aiming to understand PTSD mediated heart disease based upon the recent publication [24].

Y-h. Taguchi, *Unsupervised Feature Extraction Applied to Bioinformatics*,
Unsupervised and Semi-Supervised Learning,
https://doi.org/10.1007/978-3-030-22456-1_7

Table 7.1 Samples used in this study

Stress, days	5		10			5		10	
Rest period	24 h	1.5 w	24 h	6w		24 h	1.5 w	24 h	6w
AY	3,2	5,4	3,4	3,4	HC	3,5	4,5	5,4	4,5
MPFC	4,5	5,5	3,4	4,4	SE	3,2	2,3	3,3	3,3
ST	5,5	5,5	5,4	4,4	VS	5,5	5,5	3,4	5,4
Blood	5,5	5,5	4,5	4,5	Heart	5,5	4,5	5,5	5,5
Hemibrain	5,5	4,5	5,5	5,5	Spleen	5,5	5,5	5,4	5,5

Numbers before/after comma are control/treated samples. *h* hours, *w* weeks, *AY* amygdala, *HC* hippocampus, *MPFC* medial prefrontal cortex, *SE* septal nucleus, *ST* striatum, *VS* ventral striatum

The data set analyzed is composed of the following samples (Table 7.1). It includes ten tissues under eight experimental conditions. This data set is formatted as a five-mode tensor, $x_{ij_1j_2j_3j_4} \in \mathbb{R}^{43699\times 2\times 10\times 2\times 3}$, of the ith probe, subjected to j_1th treatment ($j_1 = 1$: control, $j_1 = 2$: treated [stress-exposed] samples), in the j_2th tissue [$j_2 = 1$: amygdala (AY), $j_2 = 2$: hippocampus (HC), $j_2 = 3$: medial prefrontal cortex (MPFC), $j_2 = 4$: septal nucleus (SE), $j_2 = 5$: striatum (ST), $j_2 = 6$: ventral striatum (VS), $j_2 = 7$: blood, $j_2 = 8$: heart, $j_2 = 9$: hemibrain, $j_2 = 10$: spleen], with the j_3th stress duration ($j_3 = 1$: 10 days, $j_3 = 2$: 5 days) and j_4th rest period after application of stress ($j_4 = 1$: 1.5 weeks, $j_4 = 2$: 24 h, $j_4 = 3$: 6 weeks). Zero values are assigned to missing observations (e.g., measurements at 6 weeks after a 5-day period of stress are not available).

HOSVD algorithm (Fig. 3.8) is applied to $x_{ij_1j_2j_3j_4}$ as

$$x_{ij_1j_2j_3j_4} = \sum_{\ell_5=1}^{43699} \sum_{\ell_1=1}^{2} \sum_{\ell_2=1}^{10} \sum_{\ell_3=1}^{2} \sum_{\ell_4=1}^{3} G(\ell_1, \ell_2, \ell_3, \ell_4, \ell_5) u^{(j_1)}_{\ell_1 j_1} u^{(j_2)}_{\ell_2 j_2} u^{(j_3)}_{\ell_3 j_3} u^{(j_4)}_{\ell_4 j_4} u^{(i)}_{\ell_5 i} \tag{7.1}$$

where $u^{(i)}_{\ell_5 i} \in \mathbb{R}^{43699\times 43699}$, $u^{(j_1)}_{\ell_1 j_1} \in \mathbb{R}^{2\times 2}$, $u^{(j_2)}_{\ell_2 j_2} \in \mathbb{R}^{10\times 10}$, $u^{(j_3)}_{\ell_3 j_3} \in \mathbb{R}^{2\times 2}$, and $u^{(j_4)}_{\ell_4 j_4} \in \mathbb{R}^{3\times 3}$ are singular value vectors and $G(\ell_1, \ell_2, \ell_3, \ell_4, \ell_5) \in \mathbb{R}^{43699\times 2\times 10\times 2\times 3}$ is a core tensor.

We need to specify which singular value vector attributed to genes, $\boldsymbol{u}^{(i)}_{\ell_1}$, is used for gene selection. For this purpose, we investigate other singular value vectors, $\boldsymbol{u}^{(j_k)}_{\ell_k}$, $1 \leq k \leq 4$. One of the important points is tissue specificity. What I would like to find is a set of genes expressive in common between heart and brain. Because $1 \leq j \leq 6$ and $j = 9$ correspond to brain and $j = 8$ corresponds to heart, we need to find $\boldsymbol{u}^{(j_2)}_{\ell_2}$ expressive in common $j = 1, 2, \cdots, 6, 8, 9$. Figure 7.1 shows the singular value vectors, $\boldsymbol{u}^{(j_2)}_{\ell_2}$, $1 \leq \ell_2 \leq 10$. Although no $\boldsymbol{u}^{(j_2)}_{\ell_2}$ fully satisfies this requirement, $\boldsymbol{u}^{(j_2)}_{4}$ relatively fulfills this requirement. $\boldsymbol{u}^{(j_2)}_{4}$ are negatively signed in common for $j = 1, 2, 8, 9$ that correspond to AY, HC, heart, and hemibrain. Especially, because AY and HC are very important in PTSD [14], it is promising that we can get singular value vector expressive in common AY, HC, and heart.

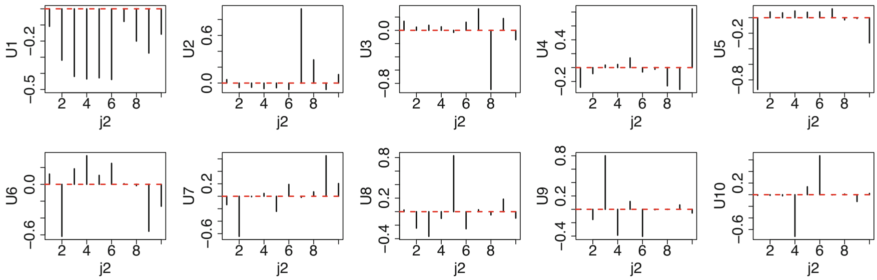

Fig. 7.1 Singular value vectors, $\boldsymbol{u}_{\ell_2}^{(j_2)}$, $1 \le \ell_2 \le 10$. Red horizontal broken lines show baseline

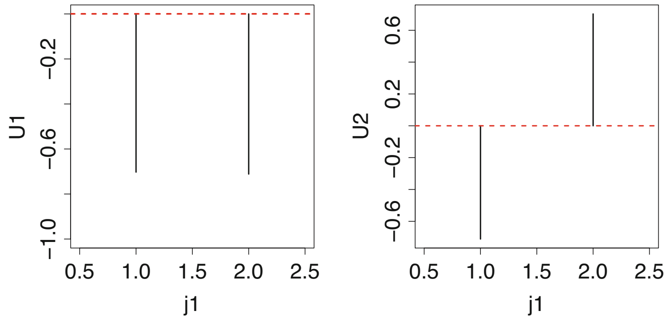

Fig. 7.2 Singular value vectors, $\boldsymbol{u}_{\ell_1}^{(j_1)}$, $\ell_1 = 1, 2$. Red horizontal broken lines show baseline

The next important requirement is that control and stressed samples should be oppositely expressive. This means, $u_{\ell_1 1}^{(j_1)} = -u_{\ell_1 2}^{(j_1)}$. This requirement is easy to fulfill because $u_{\ell_1 1}^{(j_1)} = -u_{\ell_1 2}^{(j_1)}$ or $u_{\ell_1 1}^{(j_1)} = u_{\ell_1 2}^{(j_1)}$ must be satisfied when there are only two classes and mean is zero. Figure 7.2 shows the singular value vectors, $\boldsymbol{u}_{\ell_1}^{(j_1)}$, $\ell_1 = 1, 2$. As expected, $\ell_1 = 2$ corresponds to the reversed sign between control and stressed samples.

Because there are no known pre-defined desirable properties for experimental conditions, i.e. stress and rest period, we should find $G(2, 4, \ell_3, \ell_4, \ell_5)$ with the larger absolute values. Table 7.2 shows the top ranked G with larger absolute values. Then we can find that $\ell_5 = 1, 4, 11$ are associated with $G(2, 4, \ell_3, \ell_4, \ell_5)$ with the larger absolute values. Thus we decided to attribute P-values using $\ell_5 = 1, 4, 11$ with assuming χ^2 distribution as

$$P_i = P_{\chi^2}\left[> \sum_{\ell_5 = 1,4,11} \left(\frac{u_{\ell_5 i}}{\sigma_{\ell_5}} \right)^2 \right]. \tag{7.2}$$

P-values are corrected by BH criterion and 801 probes associated with adjusted P-values less than 0.01 are selected.

Table 7.2 Top-ranked $G(\ell_1 = 2, \ell_2 = 4, \ell_3, \ell_4, \ell_5)$ with greater absolute values

ℓ_3	ℓ_4	ℓ_5	$G(2, 4, \ell_3, \ell_4, \ell_5)$
1	1	11	−35.0
1	1	1	−30.8
2	2	1	−30.3
2	3	4	−30.0
2	3	1	28.7
2	2	4	28.5

Table 7.3 Thirteen combinations of tissues and experimental conditions where the selected 801 probes are differentially expressed between stress-exposed and control samples

Stress duration	10 days		5 days	
Rest period	24 h	6 weeks	24 h	1.5 weeks
AY		○		○
HC		○	○	○
MPFC		○		
Heart	○			○
Hemibrain			○	○
Spleen		○	○	○

MPFC: medial prefrontal cortex. ○: associated with P-values that are computed by t test, adjusted by BH criterion and less than 0.01

The first validation of selected 801 probes is to see if these are expressed distinctly between control and stressed samples, selectively on only heart and brain. In order to confirm this, we apply t test to the selected 801 probes between control and stressed samples for all combination of tissues, rest and stressed period. P-values are corrected by BH criterion and conditions associated with adjusted P-values less than 0.01 are considered to be expressed distinctly and significantly between control and stressed samples. Table 7.3 shows the results. The selected 801 genes are expressed distinctly between control and stressed samples, selectively in heart, HC, and AY (it is also in spleen, because it is oppositely expressed toward heart, HC, and AY as shown in Fig. 7.1).

Here we would like to emphasize the difficulty of gene selection in this data set. As mentioned above, what we are aiming is quite abstract, i.e., "genes expressive in common between brain and heart as well as distinctly between control and stressed samples." As a result, we realize that common expression between AY, HC, and heart is possible (with the investigation of $\boldsymbol{u}_4^{(j_2)}$ in Fig. 7.1). Generally, it is impossible to know this combination in advance. When no clear purpose is given in advance, supervised methods cannot perform well while unsupervised methods can.

In order to see how well other conventional supervised methods perform, we test three methods, SAM, limma, and categorical regression analysis. The first example to be compared with TD based unsupervised FE is categorical regression analysis. For the data set shown in Table 7.1, the only possible way to apply categorical regression is to treat it as 80 classes (10 tissues vs four experimental conditions vs control and stressed samples). Although it is better to consider the pair of control and stressed samples, it is impossible. Typically, although ratio might be taken, because

Table 7.4 Results of gene selection based on categorical regression

Adjusted P-values	$P > 0.01$	$P < 0.01$	$P > 0.05$	$P < 0.05$	$P > 0.1$	$P < 0.1$
Number of probes	2222	41,157	1986	41,713	1839	41,860

P-values are adjusted by BH criterion

Table 7.5 Results by SAM

	Delta	p0	False	Called	FDR
1	0.1	0.011	38,538.08	43,379	0.0094
2	11.4	0.011	0.02	5424	3.9e−08
3	22.7	0.011	0	323	0
4	34.0	0.011	0	40	0
5	45.2	0.011	0	7	0
6	56.5	0.011	0	4	0
7	67.8	0.011	0	2	0
8	79.1	0.011	0	1	0
9	90.3	0.011	0	1	0
10	101.6	0.011	0	1	0

p0 is the ratio of the null hypothesis, FDR corresponds to the adjusted P-values. Called is the number of genes that break the null hypothesis. Expected number of false positives is False × FDR × p0

it is not paired samples, i.e., there is no one-to-one correspondence, we cannot take ratio. Table 7.4 shows the result of categorical regression analysis. Because of treatment as 80 classes, genes associated with any kind of distinction are detected (i.e., associated with significantly small adjusted P-values). As a result, almost all genes are judged as distinct between some combinations. It is obvious that this result is not desirable for our purpose, "genes expressive in common between brain and heart distinctly between control and stressed samples," at all, because of lack of specificity. To screen these genes, we need some additional criterion that TD based unsupervised FE does not require. Thus, TD based unsupervised is more fitted to the present purpose than categorical regression.

Next, we apply SAM with assuming 80 classes to the data set shown in Table 7.1. Table 7.5 shows the result of SAM. $p0$, which represents the contribution of null hypothesis that no distinction exist among 80 classes, is 1%. This means, almost all genes are distinctly expressive in either of these combinations. Although FDR corresponds to the adjusted P-values, it is clear that all genes are associated with FDR less than 0.01. Although this conclusion itself is coincident with that of categorical regression, in this sense SAM is not useful to select "genes expressive in common between brain and heart distinctly between control and stressed samples," either.

Finally, we apply limma to the data set shown in Table 7.1. Fortunately, limma enables us to select genes that are distinct between any pairs of controls and samples. Thus, we apply limma in two ways. One assumes 80 classes (case A in Table 7.6) and the other assumes 40 classes (case B in Table 7.6) composed of forty (10

Table 7.6 Results of gene selection based on limma

Adjusted P-values	$P > 0.01$	$P < 0.01$	$P > 0.05$	$P < 0.05$	$P > 0.1$	$P < 0.1$
	Case A : not considering differential expression					
Number of probes	0	43,379	0	43,379	0	43,379
	Case B: considering differential expression					
Number of probes	25,992	17,387	17,745	25,634	13,542	29,837

P-values are adjusted by limma itself

Table 7.7 KEGG pathway enrichment by the 457 genes identified by TD based unsupervised FE

Category	Term	Genes count	%	P-value	Adjusted P-value
KEGG_PATHWAY	Ribosome	57	12.8	8.4×10^{-58}	1.0×10^{-55}
KEGG_PATHWAY	Parkinson's disease	48	10.8	3.6×10^{-33}	2.2×10^{-31}
KEGG_PATHWAY	Oxidative phosphorylation	47	10.5	1.7×10^{-32}	6.9×10^{-31}
KEGG_PATHWAY	Alzheimer's disease	50	11.2	2.5×10^{-28}	7.5×10^{-27}
KEGG_PATHWAY	Huntington's disease	48	10.8	3.6×10^{-26}	8.6×10^{-25}
KEGG_PATHWAY	Cardiac muscle contraction	30	6.7	2.4×10^{-21}	4.8×10^{-20}
KEGG_PATHWAY	Glycolysis/ gluconeogenesis	10	2.2	1.5×10^{-3}	2.6×10^{-2}

Adjusted P-values are by BH criterion

tissues vs four experimental conditions) pairwise combinations between control and stress samples. Possibly because of its advanced feature, limma successfully denies the detection of genes expressive distinct among any pairs of 80 classes (case A). Nevertheless, limma still detects too many positives in 40 pairwise comparisons (case B). As expected, because of lack of well-defined screening criterion, three supervised methods are useless to find "genes expressive in common between brain and heart as well as distinctly between control and stressed samples." In conclusion, none of the three conventional supervised methods are as useful as TD based unsupervised FE for the present purpose.

Although TD based unsupervised FE successfully identifies genes expressive distinct between control and stressed samples in tissue specific manner (Table 7.3), if it is biologically useless, it cannot be considered to be successful. In order to evaluate selected probes biologically, we try to identify protein coding genes associated with these 801 probes. Then, we find 457 genes (because of lack of space, we cannot list all of 457 genes, which is available as Additional file 5 [24], if the readers are particularly interested in them). We upload 457 genes to DAVID. The result is quite promising. Table 7.7 shows the enriched KEGG pathway associated with adjusted P-values less than 0.05. They include four neurodegenerative diseases as well as one cardiac problem. Thus, they are quite suitable to be candidate genes that cause PTSD mediated heart diseases as those in Table 6.20 where PTSD mediated heart disease is investigated by PCA based unsupervised FE.

7.3 Drug Discovery From Gene Expression

Drug discovery is time-consuming and expensive processes. It starts from preparing as many small molecules as possible. Then, tries to find one effective to target diseases by exhausted search. The number of initially prepared molecule can be 10^4; testing this many number of compounds causes huge amount of money and long period. If we can reduce the number of initial candidate small molecules to one tenth, it benefits so much to reduce the time and cost required.

In this sense, the so-called in silico drug discovery develops with much expectation to fulfill this requirement. In silico drug discovery is aiming to identify candidate small molecules without *wet* experiments. With making full use of recently developed computational power, including CPU with high speed computing, huge storage that can store massive information as well as recently developed machine learning technique, in silico drug discovery enables us to prepare set of more promising candidate small molecules as drugs.

Traditionally, there are two main streams of in silico drug discovery. One is ligand-based drug design [1] (LBDD) and the other is structure-based drug design [3] (SBDD). LBDD is aiming to identify new candidate drug compounds based upon the similarity with known drugs. LBDD has huge varieties depending upon how similarity is defined. The advantage of LBDD is that it has more trust, i.e. larger probability to find true drug compounds, and requires smaller computational resources than SBDD. The disadvantage of LBDD is that it requires the information of known drugs and fails to find new drug candidates that lack similarity with known drug. On the contrary, SBDD has the advantage that it can predict new candidate drugs without the information of known drugs. The disadvantage of SBDD is that it requires massive computation, because it must execute docking simulation between drug candidate compounds and target proteins. Another disadvantage of SBDD is that it needs protein tertiary structure to which individual candidate drug compounds must bind. Experimental measurements of protein tertiary structure itself are difficult tasks. Although it has become much easier because of the invention of cryo-electron microscopy [10] than before, it still needs to pay much amount of money and time. When there are no protein tertiary structures available, protein tertiary structure itself must be computationally predicted [6]. The prediction inevitably has inaccuracy that affects the prediction of binding affinity of small molecules.

In order to compensate these disadvantages of LBDD and SBDD, the third option is recently proposed: drug design from gene expression [5]. Post-treatment gene expression can be used to screen candidate compounds for their ability to induce the target phenotype. This approach is very useful once post-treatment gene expression is available. In this section, we try to make use of TD based unsupervised FE to predict new drug target with analyzing post-treatment gene expression [27].

Post-treatment gene expression is obtained from LINCS [20]. L1000 is highly reproducible, comparable to RNA sequencing, and suitable for computational inference of the expression levels of 81% of non-measured transcripts. Gene expression profile is available in GEO with GEO ID GSE70138. Table 7.8 summarizes the gene expression profiles. They include 13 cell lines to which 100–300 compounds (denoted as "all compounds") are treated. One problem of this data set is that it includes only 978 genes' expression profiles, because it is measured by Luminex scanners. Gene expression profiles in individual cell lines are formatted as tensor, $x_{ijk} \in \mathbb{R}^{978 \times 6 \times K}$; i denotes gene (probe), j denotes dose density of drug compound, and k stands for individual compounds among K total number of compounds that correspond to "all compounds" in Table 7.8. HOSVD algorithm (Fig. 3.8) is applied as

$$x_{ijk} = \sum_{\ell_1=1}^{978} \sum_{\ell_2=1}^{6} \sum_{\ell_3=1}^{K} G(\ell_1, \ell_2, \ell_3) u_{\ell_1 i}^{(i)} u_{\ell_2 i}^{(j)} u_{\ell_3 k}^{(k)} \tag{7.3}$$

where $\boldsymbol{u}_{\ell_1}^{(i)} \in \mathbb{R}^{978}$, $\boldsymbol{u}_{\ell_2}^{(j)} \in \mathbb{R}^{6}$, $\boldsymbol{u}_{\ell_3}^{(k)} \in \mathbb{R}^{K}$, are the singular value vectors, and $G(\ell_1, \ell_2, \ell_3) \in \mathbb{R}^{978 \times 6 \times K}$ is a core tensor.

The first step is to identify genes whose expression is altered by drug treatment. In order that, we try to identify which $\boldsymbol{u}^{(j)}$ has monotonic dependence upon dose

Table 7.8 The number of the inferred compounds and inferred genes associated with significant dose-dependent activity

Cell lines	BT20	HS578T	MCF10A	MCF7	MDAMB231	SKBR3
Tumor	Breast					
Inferred genes	41	57	42	55	41	46
Inferred compounds	4	3	2	6	5	6
All compounds	110	106	106	108	108	106
Predicted targets	418	576	476	480	560	423

Cell lines	A549	HCC515	HA1E	HEPG2	HT29	PC3
Tumor	Lung		Kidney	Liver	Colon	Prostate
Inferred genes	45	46	48	54	50	63
Inferred compounds	8	5	7	2	2	9
All compounds	265	270	262	269	270	270
Predicted targets	428	352	423	396	358	439

Cell lines	A375
Tumor	Melanoma
Inferred genes	43
Inferred compounds	6
All compounds	269
Predicted targets	421

The target proteins predicted by means of the comparison with the data showing upregulation of the expression of individual genes ("predicted targets") are also shown

The full list of inferred genes and predicted targets is available in Additional file 7 [27]. Inferred compounds are presented in Table 7.9. "All compounds" rows represent the total number of compounds used for the treatment of each cell line density. Figure 7.3 shows $\boldsymbol{u}^{(j)}_{\ell_2}$, $1 \leq \ell_2 \leq 3$ for 13 cell lines listed in Table 7.8. It is obvious that $\boldsymbol{u}^{(j)}_{2}$ shows almost linear dependence upon dose independent of cell lines. The next task is to identify $G(\ell_1, 2, \ell_3)$ with larger absolute values in order

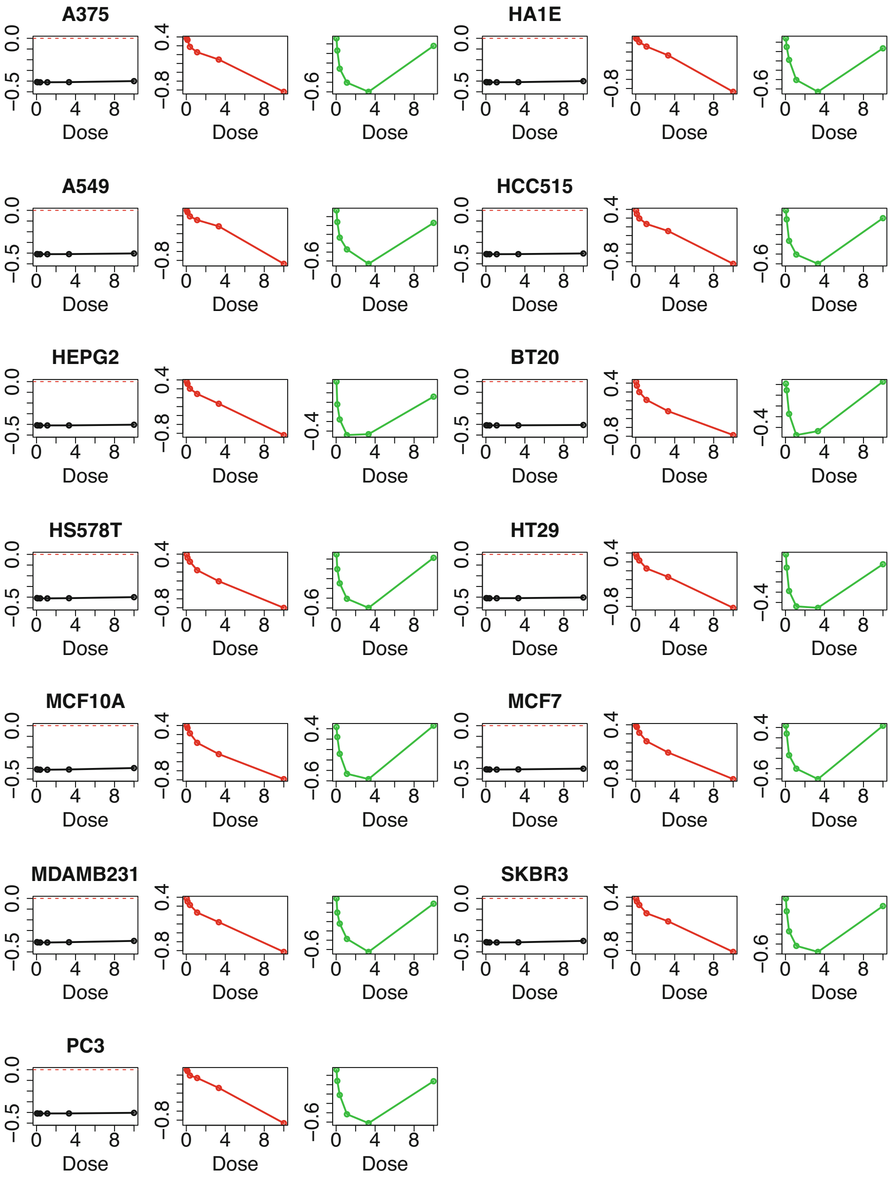

Fig. 7.3 Singular value vectors, $\boldsymbol{u}^{(j)}_{\ell_2}$, $1 \leq \ell_2 \leq 3$. Red horizontal broken lines indicates baseline. Black: $\ell_2 = 1$, red: $\ell_2 = 2$, green: $\ell_2 = 3$

to decide which $\boldsymbol{u}_{\ell_1}^{(i)}$ and $\boldsymbol{u}_{\ell_3}^{(k)}$ are used for selecting the combinations of genes and compounds that commit linear dose dependence. Because

$$G(\ell_1 \leq 6, \ell_2 \leq 6, \ell_3 \leq 6) = \frac{\sum_{\ell_1 \leq 6, \ell_2 \leq 6, \ell_3 \leq 6} G(\ell_1, \ell_2, \ell_3)^2}{\sum_{\ell_1, \ell_2, \ell_3} G(\ell_1, \ell_2, \ell_3)^2} \tag{7.4}$$

exceeds 0.95 for almost all cell lines, it is decided to employ $(\ell_1 \leq 6, \ell_2 = 2, \ell_3 \leq 6)$ components for FE. Nonetheless, in the case of PC3 cells, $(\ell_1 \leq 8, \ell_2 = 2, \ell_3 \leq 8)$, as an exception, are used for FE because the eighth component is found to have non-negligible contributions in this cell line.

To identify the genes and compounds associated with a significant dose-dependent activity, it is assumed that $u_{\ell_1 \leq 6, i}$ and $u_{\ell_3 \leq 6, k}$ follow independent normal distributions and P-values are attributed to the ith gene and the kth compounds using a χ^2 distribution,

$$P_i = P_{\chi^2}\left[> \sum_{\ell_1 \leq 6} \left(\frac{u_{\ell_1 i}^{(i)}}{\sigma_{\ell_1}} \right)^2 \right] \tag{7.5}$$

and

$$P_k = P_{\chi^2}\left[> \sum_{\ell_3 \leq 6} \left(\frac{u_{\ell_3 k}^{(k)}}{\sigma_{\ell_3}} \right)^2 \right] \tag{7.6}$$

where σ_{ℓ_1} and σ_{ℓ_3} are the standard deviations of $u_{\ell_1 i}^{(i)}$ and $u_{\ell_3 k}^{(k)}$, respectively. For PC3 cells, $\ell_1 \leq 8$ and $\ell_3 \leq 8$ are used in the above equations. $P_{\chi^2}[> x]$ is the cumulative probability that the argument is greater than x assuming a χ^2 distribution with eight degrees of freedom for PC3 cell lines and with six degrees of freedom for other cell lines. P_i and P_k are adjusted by means of the BH criterion, and compounds and genes associated with the adjusted P-value lower than 0.01 are selected as those associated with a significant dose-dependent cellular response. The number of selected genes and compounds are listed as “inferred genes” and “inferred compounds” in Table 7.8, respectively. The above process is illustrated in Fig. 7.4.

The next task is to identify proteins to which selected compounds bind. “inferred genes” in Table 7.8 do not correspond to the proteins to which selected compounds bind, because they are the genes whose mRNA expression is altered because of drug treatment. Usually, mRNA expression of proteins to which selected compounds bind is not altered because of drug treatment. Thus we need to infer proteins targeted by drug treatment. In order that, we need additional external information that lists the genes whose mRNA expression is altered because of a gene perturbation. Then if “inferred genes” matched with genes mRNA expression is altered because of the gene perturbation, we infer the perturbed gene as target protein (Fig. 7.5).

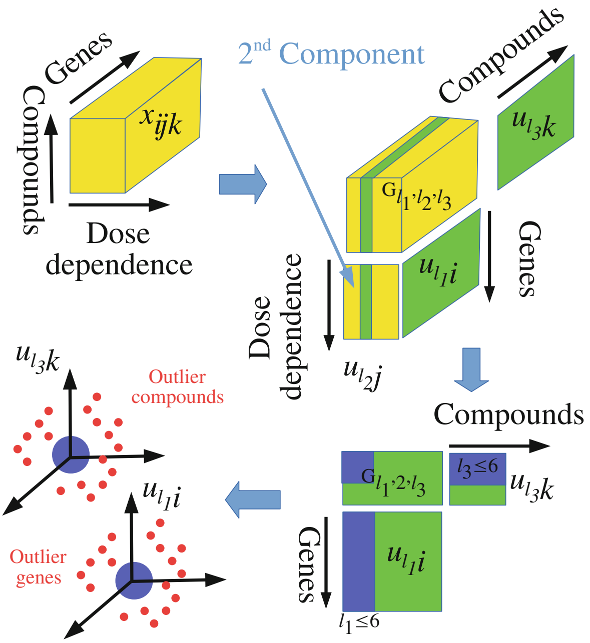

Fig. 7.4 Starting from gene expression profile formatted as tensor, x_{ijk}, singular value vectors, $\boldsymbol{u}^{(i)}_{\ell_1}, \boldsymbol{u}^{(j)}_{\ell_2}$, and $\boldsymbol{u}^{(k)}_{\ell_3}$, are obtained. After identifying $\ell_2 = 2$ as associated with linear dose dependence (see Fig. 7.3), $\ell_1 \leq 6$ and $\ell_3 \leq 6$ are decided to be used for FE because of larger contribution defined in Eq. (7.4). Genes i and compounds k are selected using $\boldsymbol{u}^{(i)}_{\ell_1}, \ell_1 \leq 6, \boldsymbol{u}^{(k)}_{\ell_3}, \ell_3 \leq 6$

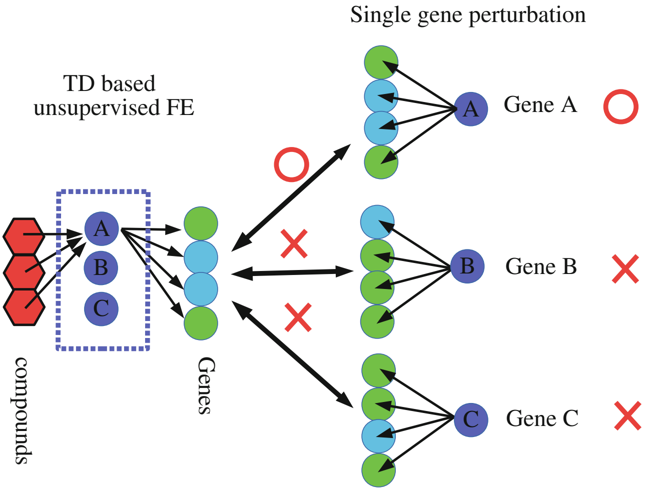

Fig. 7.5 After the drug (red hexagon) treatments, we can detect mRNAs with altered expression (filled cyan circle) along with those without altered expression (filled green circle). We have no information about proteins (circled A, B, and C). List of genes with altered expression can be compared with genes with altered expression when genes A, B, or C is perturbed. Then, we can identify compounds that might bind to protein A, because the list of genes whose mRNA expression is altered are common

There can be multiple resources from which we can retrieve the list of genes whose mRNA expression is altered because of single gene perturbation. Here we employ Enrichr [11] that collects multiple data resources in order to perform various enrichment analyses. After uploading "inferred genes" to Enrichr, we list genes associated with adjusted P-values less than 0.01 in the category of "Single gene Perturbations from GEO up." Their number corresponds to the number of "predicted targets" in Table 7.8. This strategy is especially efficient for LINCS data set that includes only expression of 978 genes. Employing the strategy in Fig. 7.5, we can identify target proteins not included in these 978 genes.

Next we would like to evaluate if our prediction is correct, i.e., if "inferred compounds" bind to "predicted targets." In principle, it is impossible to check the accuracy of our prediction without experiments. Thus, instead of executing experiments, we compare our prediction with known list of target proteins of drug compounds. For this purpose, we employ two information resources, drug2gene.com [19] and DSigDB [33]. Table 7.9 shows the results of Fisher's exact test that evaluates overlaps between "predicted targets" and known target proteins of "inferred compounds." If P-values computed by Fisher's exact test is less than 0.05, it is significant (no correction considering multiple comparisons). It is obvious that in most of the cases, our prediction significantly overlaps with known target proteins of drug compounds. Thus, TD based unsupervised FE can be used for in silico drug discovery from gene expression.

It is also interesting that "inferred compounds" are largely overlapped among cell lines. Because two to nine compounds are identified in each of 13 cell lines, the total number of identified compounds can be several tens. Nevertheless, the number of compounds listed in Table 7.9 is as small as 19. In some sense, it might be an evidence that our strategy is correct. It is reasonable that anti-cancer drugs are effective to multiple cancers. Thus, large overlap of "inferred compounds" between distinct cell lines makes sense. On the other hand, analyses based upon distinct gene expression profiles unlikely results in largely overlapped results without any biological reasons. Possibly, the result shown in Table 7.9 are trustable.

Although we employed single gene perturbation to infer target proteins from the list of genes with altered expression caused by drug treatment, any other database that can describe gene interaction should be usable. As an alternative, we try "PPI Hub Proteins" in Enrichr instead of "Single gene Perturbations from GEO up." The primary difference between "PPI Hub Proteins" and "Single gene Perturbations from GEO up" is the number of genes included. "PPI Hub Proteins" includes only a few hundred genes, while "Single gene Perturbations from GEO up" includes a few thousand genes. This suggests that the results using "PPI Hub Proteins" might be less significant. Table 7.10 lists the results of Fisher's exact test of the comparison between predicted targets based upon "PPI Hub Proteins" and drug2gene.com database. In contrast to the expectation, all cases have significant overlap with drug2gene.com. This supports our expectation that any kind of gene–gene interaction is usable together with TD based unsupervised FE for *in silico* drug discovery from gene expression.

Table 7.9 Compound–gene interactions presented in Table 7.8 that significantly overlap with interactions described in two data sets

Compounds	(1)	(2)	(3)	(4)	(5)	(6)	(7)	(8)	(9)	(10)	(11)	(12)	(13)
Dabrafenib													○ ○
Dinaciclib							○ ○	○ ○	○ ○	○ ○	○ ○	○ ○	○ ○
CGP-60474			○ ×	○ ×	○ ×	○ ×	○ ×		○ ×			○ ×	○ ○
LDN-193189	○ ○				○ ○								○ ○
OTSSP167							– ○	– ○		– ○		– ○	– ○
WZ-3105		– ○		– ○	– ○		– ○	– ○	– ○			– ○	– ○
AT-7519				○ ○		○ ○		○ ○	○ ○			○ ○	
BMS-387032				○ ○		○ ○	○ ○		○ ○				
JNK-9L									○ ○				
Alvocidib	○ –	○ –	○ –	○ –	○ –	○ –			○ –				
GSK-2126458							– –					– –	
NVP-BEZ235							○ ×					○ ×	
Torin-2							× ○					× ○	
NVP-BGT226					– –			– –			– –	– –	
QL-XII-47	– –												
Celastrol	○ –												
A443654		○ ○		○ ○									
NVP-AUY922					× –	○ –							
Radicicol						○ –							

For each compound in the table, the upper row: the drug2gene.com data set is used for comparisons [19], the lower row: the DSigDB data set is used for comparisons [33]. Columns represent cell lines used in the analysis: (1) BT20, (2) HS578T, (3) MCF10A, (4) MCF7, (5) MDAMB231, (6) SKBR3, (7) A549, (8) HCC515, (9) HA1E,(10) HEPG2, (11) HT29, (12) PC3, (13) A375

○: a significant overlap between the data sets ($P < 0.05$); ×: no significant overlap between the data sets; –: no data; blank: no significant dose–response relation is identified. The confusion matrix and a full list of genes chosen in common are available in Additional file 3 [27].

Table 7.10 A significant overlap demonstrated between compound–target interactions presented in Table 7.8 and drug2gene.com

Compounds	(1)	(2)	(3)	(4)	(5)	(6)	(7)	(8)	(9)	(10)	(11)	(12)	(13)
										○	○	○	
CGP-60474			○	○	○	○	○		○			○	○
LDN-193189					○								
AT-7519				○		○		○	○			○	
BMS-387032				○		○	○		○				
Alvocidib		○	○	○	○	○			○				
NVP-BEZ235												○	
Celastrol	○												
A443654		○		○									
NVP-AUY922					○	○							
Radicicol						○							

In this case, the "PPI Hub Proteins" category in Enrichr is used. Labels (1) to (13) represent the same cell lines as described in Table 7.9

The full list of confusion matrices and genes chosen in common is available in Additional file 3 [27]

It might be useful to demonstrate how more direct and simple approach fails. One possible alternative simpler way is to apply linear regression

$$x_{ijk} = a_{ik} + b_{ik} D_j \tag{7.7}$$

where D_j is the jth dose density and a_{ik} and b_{ik} are regression coefficients. Then simply select i and k associated with more significant P-values as in the case of TD based unsupervised FE. In order to show that it cannot give us the reasonable set of is and ks, we apply Eq. (7.7) to A375 cell lines ((13) in Tables 7.8, 7.9, and 7.10) as an example. After correcting P-values that Eq. (7.7) gives by BH criterion, we find that all compounds have adjusted P-values less than 0.01 with at least one of the genes while all genes have adjusted P-values less than 0.01 with at least one of the compounds. Thus, by simply requesting "adjusted P-values less than 0.01" as in the case of TD based unsupervised FE, we cannot screen either genes or compounds. We can still try to select "top ranked" genes or compounds. In order to show that this cannot work well either, we apply two distinct criteria to select "top ranked" compounds as

- Select top ranked 10 compounds having larger number of genes associated with adjusted P-values less than 0.01.
- Suppose P_{ik} is P-value that Eq. (7.7) gives. Select top ranked 10 compounds having smaller $\sum_i \log P_{ik}$.

These two criteria rank compounds with more significant correlation with genes through dose density in some sense. The result is a bit disappointing (Table 7.11). Only three of top 10 compounds are chosen in common. This suggests that it is not

Table 7.11 Compounds selected by P-values that Eq. (7.7) gives, for A375 cell line ((13) in Tables 7.8, 7.9, and 7.10)

Compounds selected
Criterion 1
chelerythrine chloride, TGX-221, lapatinib, AS-601245, PIK-93, **canertinib**, LDN-193189, MK-2206, PF-04217903, **DCC-2036**
Criterion 2
ALW-II-49-7, AZ20, BI-2536, **canertinib**, celastrol, **chelerythrine chloride**, CHIR-99021, **DCC-2036**, dovitinib, GSK-1904529A

Bold ones are chosen in common

easy to select compounds in robust way simply based upon P-values that Eq. (7.7) gives. Thus, TD based unsupervised FE is much better strategy without no additional criterion than adjusted P-values than selection based upon P-values that Eq. (7.7) gives.

Before ending this section, I would like to mention briefly why the results of TD based unsupervised FE differ from that based upon linear regression, Eq. (7.7), so much in spite of that both TD based unsupervised FE and linear regression try to find the combinations of genes and compounds associated with dose dependence. As can be seen in Fig. 7.3, $\boldsymbol{u}_2^{(j)}$ used for FE is not simple linear function of dose density. In spite of that, the dependence of $\boldsymbol{u}_2^{(j)}$ upon dose density is quite universal, in other words, independent of cell lines. TD is the only method that can successfully identify this universal (independent of cell lines) functional form. There are no other ways to find it in advance. This cannot be achieved by any other supervised method, because any supervised method cannot avoid assuming something contradictory to this universal functional form. Because of this superiority, TD based unsupervised FE can achieve good performance shown in Tables 7.9 and 7.10.

7.4 Universarity of miRNA Transfection

miRNA transfection is a popular method that finds miRNA target genes experimentally. Nevertheless, some doubt arises if transfected miRNA can work similar to endogenous miRNAs [9], because it causes various unexpected effects that cannot be seen by upregulation of endogenous miRNAs. Because the aim of miRNA transfection experiments is to find miRNA target genes, only genes downregulated by the transfection are searched. Nevertheless, it is quite usual to find that many mRNAs are upregulated because of transfection. These upregulated mRNAs are usually ignored, because it is not interpretable from the knowledge about conventional miRNA functions. On the other hand, Jin et al. [9] argued that miRNA transfection can cause non-specific changes in gene expression. To the best of my knowledge, there are no studies that try to identify these non-specific effects in more positive points of view.

In this section, using TD based unsupervised FE, we are aiming to study how universal these non-specific gene expression alterations by miRNA transfections are. In order that, we collect multiple studies where multiple miRNA transfection experiments are performed. In individual studies, genes whose expression is altered in common over multiple miRNA transfection experiments are tried to be identified. Then it is checked if genes identified in individual studies are common over multiple studies. If so, sequence-nonspecific off-target regulation of mRNA does really exist and might play some critical roles in biology, too.

The identification of genes altered in common by sequence-nonspecific off-target regulation caused by miRNA transfection can be performed by TD based unsupervised FE as follows [26]. In usual application of TD based unsupervised FE, singular value vectors associated with desired sample dependence, e.g., distinction between patients and healthy controls, are searched to identify genes associated with such a dependence. On the contrary, in the present application, we are aiming to seek singular value vectors "not" associated with the distinction between transfected miRNAs, because lack of transfected miRNA dependence might be the evidence that gene expression alteration caused by miRNA expression toward these genes is because of sequence-nonspecific off-target regulation, no matter what the biological reasons that cause it are. Table 7.12 lists 11 studies including the gene expression profiles collected for the analysis in this study. It is obvious that they are quite diverse. Not only used cell lines but also transfected miRNAs differ from

Table 7.12 Eleven studies conducted for this analysis

Exp	GEO ID	Cell lines (cancer)	miRNA	Misc	Methods
1	GSE26996	BT549 (breast cancer)	miR-200a/b/c		PCA
2	GSE27431	HEY (ovarian cancer)	miR-7/128	mas5	PCA
3	GSE27431	HEY (ovarian cancer)	miR-7/128	plier	PCA
4	GSE8501	Hela (cervical cancer)	miR-7/9/122a/128a/132/133a /142/148b/181a		TD
5	GSE41539	CD1 mice	cel-miR-67, hsa-miR-590-3p, hsa-miR-199a-3p		PCA
6	GSE93290	multiple	miR-10a-5p, 150-3p/5p, 148a-3p/5p, 499a-5p, 455-3p		TD
7	GSE66498	multiple	miR-205/29a/144-3p/5p, 210,23b,221/222/223		TD
8	GSE17759	EOC 13.31 microglia cells	miR-146a/b	(KO/OE)	TD
9	GSE37729	HeLa	miR-107/181b	(KO/OE)	TD
10	GSE37729	HEK-293	miR-107/181b	(KO/OE)	TD
11	GSE37729	SH-SY5Y	181b	(KO/OE)	TD

More detailed information on how to process individual experiments in these eleven studies is available in Appendix. Methods: PCA or TD based unsupervised FE is used experiments to experiments. Both KO (knock out) and OE (over expression) are considered. Thus, if there are genes chosen in common among these eleven studies, it is quite likely caused by sequence-nonspecific off-target regulation.

Because of their diversity, not only TD based unsupervised FE but also PCA based unsupervised FE is used. If the number of samples used for individual transfection in individual experiments does not match with one another, multiple experiments in which distinct miRNAs are transfected are hardly formulated in tensor forms. In these cases, PCA based unsupervised FE is employed instead. In the following, individual data set and how to format them in either matrix or tensor is discussed in a little bit detail in Appendix.

Table 7.13 shows the results. In spite of the heterogeneous data sets analyzed, they are highly consistent with one another. Thus, there might be some universal mechanisms that cause sequence-nonspecific off-target regulation.

From the data science point of view, it is important to see if other methods can derive the set of genes associated with the same amount of consistency among 11 studies listed in Table 6.12. For the comparison, we select t test. What we aim is essentially to find genes expressed distinctly between control and transfected samples. This kind of two class comparisons can be done by t test, too. In order to see if t test is inferior to TD and PCA based unsupervised FE, t test is applied to 11 studies. In this analysis, samples in individual studies are divided into two classes: samples to which no miRNAs (or mock miRNA) were transfected and samples to which miRNAs were transfected. Two-sided t test is applied to individual 11 studies. Then, obtained P-values are adjusted by BH criterion. Then, probes associated with adjusted P-values less than 0.01 are selected (Table 7.14). The result is a little bit disappointing. For five out of 11 studies, t test cannot identify any differently expressed genes. On the other hand, the numbers of selected genes vary from 35 to 11,060, which is contrast to the range of number of genes selected by PCA or TD based unsupervised FE, $\sim 10^2$ (Table 7.13). These numbers are unlikely biologically trustable. This possibly shows the failure of methodology.

In order to further demonstrate the inferiority of t test to TD or PCA based unsupervised FE, we try to reproduce the results of PCA or TD based unsupervised FE in Table 7.13. Since the number of genes selected by t test is often 0 (Table 7.14), the same number of top ranked genes with smaller P-values as those in PCA or TD based unsupervised FE are selected in individual experiments based upon P-values computed by t test even though P-values are not significant. It is obvious that the selected genes by t test are less coincident with each other than the selected genes by PCA or TD based unsupervised FE (Table 7.13) because odds ratios are smaller and P-values are larger. Thus, also from the point of coincidence between 11 studies, t test is inferior to TD or PCA based unsupervised FE.

Although PCA or TD based unsupervised FE successfully identifies sets of genes highly coincident between heterogeneous eleven studies, if they are not biologically reasonable, they are useless. In order to see biological values of selected genes, we here show one evaluation, although many evaluations were performed in my published paper [26] (I am not willing to show all of them here, because it might be simply boring).

Table 7.13 Fisher's exact test for coincidence among 11 miRNA transfection studies for PCA or TD based unsupervised FE and *t* test

Exp.		1	2	3	4	5	6	7	8	9	10	11
	#	232	711	747	441	123	292	246	873	113	104	120
PCA or TD based unsupervised FE												
1	232		4.14e−19	6.59e−22	3.96e−41	4.12e−71	9.41e−70	2.90e−60	1.34e−17	1.15e−27	6.84e−26	2.66e−07
2	711	7.68		0.00	1.89e−18	4.93e−27	5.59e−20	2.69e−32	4.62e−13	9.23e−16	8.66e−12	1.37e−03
3	747	8.30	345.52		3.63e−20	7.96e−21	5.70e−12	1.82e−27	9.52e−12	1.18e−14	1.01e−12	3.90e−06
4	441	18.23	5.19	5.34		6.14e−41	1.01e−34	1.44e−69	4.61e−11	2.16e−30	4.09e−28	1.35e−10
5	123	53.86	9.04	7.27	17.48		2.9e−179	1.27e−63	6.24e−15	3.16e−25	2.37e−17	4.69e−09
6	292	61.50	8.15	5.52	17.71	204.39		3.53e−53	2.57e−15	6.65e−22	1.65e−12	5.60e−05
7	246	20.27	5.35	4.67	12.39	20.11	22.03		6.91e−42	1.77e−36	4.50e−31	2.78e−14
8	873	18.61	7.22	6.51	8.29	15.61	18.53	20.73		1.81e−07	1.37e−06	2.76e−02
9	113	39.34	9.87	8.77	25.98	32.44	34.90	21.94	16.02		3.7e−125	9.27e−18
10	104	40.29	8.22	8.27	26.64	23.34	20.86	21.56	15.18	517.87		6.82e−16
11	120	10.15	3.19	4.43	9.19	11.55	8.11	8.28	4.92	19.57	18.70	
t test												
1	232		4.96e−04	8.49e−01	2.59e−01	6.35e−01	1.00e+00	5.40e−01	1.00e+00	4.08e−01	6.45e−01	6.68e−01
2	711	2.56		6.40e−69	1.38e−02	1.25e−01	1.55e−01	9.36e−03	1.00e+00	1.00e+00	3.76e−01	1.00e+00
3	747	0.80	10.49		8.65e−01	5.28e−01	3.76e−01	2.47e−01	7.79e−01	7.75e−01	5.30e−01	1.00e+00
4	441	1.55	1.90	0.89		6.58e−01	1.00e+00	4.31e−01	1.26e−01	2.71e−01	2.56e−01	1.00e+00
5	123	0.00	0.00	0.36	1.39		1.13e−22	1.00e+00	3.86e−01	1.00e+00	1.00e+00	1.00e+00
6	292	0.77	1.83	0.32	0.72	27.05		3.71e−01	1.00e+00	1.00e+00	1.00e+00	1.00e+00
7	246	1.16	0.48	0.71	1.22	0.67	0.31		4.47e−01	1.83e−01	7.60e−02	2.04e−01
8	873	0.64	1.00	1.17	2.15	2.09	0.00	0.46		1.59e−01	4.54e−01	1.27e−03
9	113	0.00	0.81	0.60	0.00	0.00	0.00	0.25	2.91		1.18e−03	4.07e−01
10	104	0.00	0.32	0.35	1.75	0.00	0.00	0.00	1.68	5.56		6.37e−01
11	120	1.31	0.78	0.88	0.97	0.00	0.00	1.69	6.87	0.00	0.00	

Upper triangle: P-value, lower triangle: odds ratio. #: number of genes selected in individual studies. "Xe−Y" means that "$X \times 10^{-Y}$"

Table 7.14 The number of genes selected by *t* test

Studies	1	2	3	4	5	6	7	8	9	10	11
Samples	6:6	3:4	6:4	18:18	2:2	16:16	19:19	18:18	6:12	6:12	4:4
Selected genes	11,060	0	0	0	0	35	280	55	5949	5730	0

Two numbers besides colon are the number of control and transfected samples, respectively

Table 7.15 is the result for KEGG pathway enrichment by uploading selected genes to Enrichr. It is obvious that not only there are many significant enrichment but also they are highly coincident between 11 studies. Thus, coincidence of selected genes between eleven studies shown in Table 7.13 is also biologically reasonable. In this sense, PCA or TD based unsupervised FE can identify biologically meaningful genes chosen in common between heterogeneous studies including various miRNAs transfected to various cell lines. Universal nature detected has seemingly biological importance, too.

7.5 One-Class Differential Expression Analysis for Multiomics Data Set

In general, there are two kinds of biological experiments, in vivo and in vitro. In vivo means real biological experiments using living organisms, e.g., animals and plants. Nevertheless, in vivo cannot be said as very economical, because it wastes whole body even when we are interested in a specific tissue. For example, even if you are interested in liver disease, in vivo experiments require to cultivate a whole body. You may wonder if only liver can be separately cultivated, it would be more effective. In vivo experiments recently have tendency to be avoided from the ethical point of view, too, because they kill numerous animals. In vitro experiments can fulfill these requirements more or less. in vitro makes use of cell lines, which is an immortalized cell that is often made out of cancer cells. Once cell line is established, you can do any kind of experiments in vitro using cell lines. Because cell lines can be cultivated even in a dish, it is definitely cost effective and does not kill any animals.

One possible problem of in vitro is the lack of control samples. It is known that cell lines differ from the tissue cells from which cell lines are established. Thus, usually cell lines are compared between not treated and treated ones. Characterizing immortalized cell lines themselves is not an easy task.

In this section, we propose the method that can characterize cancer cell line from gene expression without comparing with something [22]. In this criterion, genes are expressive in common over multiple cancer subtypes are searched and are considered to be characteristic gene expression of cancer cell line. In this regard, TD based unsupervised FE used to identify expressed gene in common over multiple miRNAs transfection studies in the previous section is employed again.

Table 7.15 In each of 11 studies, 20 top-ranked significant KEGG pathways whose associated genes significantly match some genes selected for each experiment are identified

Exp	#	(i)	(ii)	(iii)	(iv)	(v)	(vi)	(vii)	(viii)	(ix)	(x)
1	(232)	31/137	7/168	10/142	6/133	9/55	9/193			7/169	8/203
	[10]	3.69e−29	3.18e−02	1.66e−04	3.45e−02	1.02e−06	6.85e−03			3.18e−02	3.01e−02
2	(711)	36/137	18/168	14/142	12/133	13/55				16/169	18/203
	[12]	3.43e−19	1.48e−03	1.05e−02	3.20e−02	5.92e−06				8.12e−03	8.12e−03
3	(747)	23/137	15/168			14/55				18/169	19/203
	[15]	3.58e−07	1.94e−02			1.20e−06				2.02e−03	4.78e−03
4	(441)	50/137	15/168	19/142	18/133	6/55	19/193	7/78	12/151	9/169	
	[10]	2.92e−45	1.91e−04	3.97e−08	6.42e−08	2.49e−02	3.40e−06	2.74e−02	4.44e−03	1.29e−01	
5	(123)	9/137						8/78		6/169	8/203
	[23]	2.97e−06						6.08e−07		4.29e−03	3.03e−04
6	(292)	45/137	20/168	19/142	18/133	4/55	19/193	11/78	12/151		
	[14]	1.35e−46	3.32e−11	2.27e−11	4.00e−11	7.95e−02	2.24e−09	4.90e−07	4.87e−05		

7	(246)	40/137	9/168	10/142	9/133		11/193	4/78	7/151		6/203
	[7]	5.61e−42	6.60e−03	5.80e−04	1.32e−03		1.16e−03	2.57e−01	6.31e−02		4.52e−01
8	(873)	75/137	30/168	32/142	32/133		36/193	14/78	24/151	25/169	
	[24]	5.59e−63	2.09e−09	9.32e−13	1.89e−13		7.51e−12	1.39e−04	1.62e−06	3.11e−06	
9	(113)	18/137	11/168	12/142	10/133	6/55	12/193	4/78	11/151		
	[20]	8.24e−18	7.10e−08	1.66e−09	8.42e−08	8.85e−06	2.96e−08	6.64e−03	2.96e−08		
10	(104)	11/137	8/168	9/142	8/133	5/55	10/193		8/151		
	[20]	1.98e−08	6.68e−05	3.23e−06	1.71e−05	1.56e−04	3.23e−06		3.60e−05		
11	(120)	6/137		4/142		5/55					5/203
	[3]	9.04e−03		8.49e−02		2.98e−03					6.83e−02

Thus, the following KEGG pathways are most frequently ranked within the top 20. “Xe−Y” means that “$X \times 10^{-Y}$”

(i) Ribosome:hsa03010, (ii) Alzheimer’s disease:hsa05010, (iii) Parkinson’s disease:hsa05012, (iv) Oxidative phosphorylation:hsa00190, (v) Pathogenic *Escherichia coli* infection:hsa05130, (vi) Huntington’s disease:hsa05016, (vii) Cardiac muscle contraction:hsa04260, (viii) Nonalcoholic fatty liver disease (NAFLD):hsa04932, (ix) Protein processing in endoplasmic reticulum:hsa04141, and (x) Proteoglycans in cancer:hsa05205. (numbers):gene, [numbers]:KEGG pathways associated with adjusted P-values less than 0.01. Upper rows in each exp: (the number of genes coinciding with the genes selected for each experiment)/(genes listed in Enrichr in each category). Lower rows in each exp: adjusted P-values provided by Enrichr

In addition to this, TD based unsupervised FE is used as a tool that integrates omics data. The data set used is downloaded from DBTSS [21], which is a database of transcriptional start sites (TSS), and includes RNA-seq, TSS-seq, and ChIP-seq (histone modification, H3K27ac). These are observed in 26 NSCLC subtype cell lines using HTS technology; DBTSS also stores various omics data set measured on various cell lines and living organisms.

Before starting analysis, we briefly explain the difference among TSS-seq, RNA-seq, and ChIP-seq. As it name says, TSS-seq tries to sequence RNA transcribed from the region around TSS. Thus, TSS-seq basically counts how many times transcription starts. On the other hand, RNA-seq counts the fragments taken from any part of whole RNA. In this sense, RNA-seq counts the total amount of RNA transcribed. Generally, TSS-seq and RNA-seq are positively correlated, although there are no known functional forms that relate between these two, because the function is affected by many factors, e.g., individual genes have various length and some genes are long while others are short. If longer genes are more transcribed, the ratio RNA-seq to TSS-seq becomes larger. In addition to this, individual genes have isoforms, each of which has different length. This mechanism is called as an alternative splicing. If more number of longer isoforms are transcribed from each gene, it also contributes to the increased RNA-seq/TSS-seq ratio. Although there are many detailed points that must be considered in order to relate RNA-seq to TSS-seq, there is one clear point; TSS-seq and RNA-seq should be positively correlated. Thus, seeking genes associated with both more TSS-seq counts and RNA-seq counts can reduce the possibility that genes are wrongly identified as being upregulated or downregulated, e.g., because of technical issues like miss amplification.

ChIP-seq is a different technology that detects to which part of DNA the protein binds. Although I do not explain the details of the relationship between DNA and proteins that bind to it, basically DNA binding protein can control the rate of transcription. ChIP-seq can study this relationship by considering DNA binding protein. Histone modification is more advanced feature. In order to suppress the self-entanglements of lengthy DNA, long DNA string is wrapped around protein core called histone. Because tightly wrapped DNA is hardly transcribed, how tightly DNA is wrapped around histone can affect the amount of transcription drastically. On the other hand, affinity between histone and DNA can be affected by chemical modification of histone. Among various histone modification, acetylation of histone tail is supposed to enhance the transcription by reducing the affinity between DNA and histone. As a result, considering histone modification (H3K27ac) together with RNA-seq and TSS-seq can further reduce the possibility of wrongly identified up/downregulated genes. In the following, we try to seek genes simultaneously associated with the increased TSS-seq, RNA-seq, and ChIP-seq that measureds H3K27ac counts.

When formatting RNA-seq, TSS-seq, and ChIP-seq measurement data into tensor form, how we can practically perform this is a problem. Fundamentally, although it is possible to perform it in single nucleotide base, it results in too huge tensor that requires too large memory to manage. In this case, it is better to employ coarse graining approach that takes average over local chromosome regions. The problem is how long regions should be. If the length of the region is too large, each region includes more than one (protein coding) genes. Then, increased or decreased counts within each region might reflect more than one genes. This will result in low interpretability. On the other hand, if the length of the region is too short, individual (protein coding) genes are expressed over multiple region. It again results in low interpretability. Thus, there should be somewhat optimal length of region. In this section, I try 25,000 nucleotides as a length of region. Generally, the average length of protein is $\sim 10^2$. Because one amino acid is coded by three-nucleotide (codon), a length of region that codes individual protein coding genes should be at most $\sim 10^3$. The regions that code protein coding genes are typically composed of both exon and intron, which correspond to translated and non-translated regions, respectively. Thus, the region of DNA that codes individual genes might be doubled. It is still expected not to exceed $\sim 10^3$ so much. In actuality, some literature reported that average length of DNA regions that code human protein coding genes is still a little bit shorter than $\sim 10^4$ [8]. Nevertheless, if the region over which TSS-seq, RNA-seq and ChiP-seq count data is averaged is as long as expected length of DNA region that codes individual protein coding genes, boundaries between averaging region might frequently fall into the mid of the DNA region that codes individual protein coding region. Thus, the length of region averaging counts data should be a few times longer than expected length of DNA region that codes individual protein coding region. Based upon these considerations, 25,000 nucleotides region over which TSS-seq, RNA-seq, and ChIP-seq counts are averaged is proposed.

In the data set having a type “human lung adenocarcinoma cell line 26 cell line” in inhouse data category, RNA-seq, TSS-seq, and ChIP-seq data are used. Among ChIP-seq data, only the H3K27ac is used (H3K27ac means that K27 position of the 3rd histone (H3) is acetlyated). Counts are averaged over chromosomal regions fragmented to regions of length of 25,000 nucleotides. Tensors are generated for each chromosome separately. Then, tensor is the form of $x_{ijk} \in \mathbb{R}^{N \times 26 \times 3}$, where N is the total number of regions of the length of 25,000 nucleotides within each chromosome, j stands for 26 cell lines, and k stands for counts of TSS-seq, RNA-seq, and ChIP-seq. HOSVD algorithm, Fig. 3.8, is applied to x_{ijk} as

$$x_{ijk} = \sum_{\ell_1=1}^{N} \sum_{\ell_2=1}^{26} \sum_{\ell_3=1}^{3} G(\ell_1, \ell_2, \ell_3) u_{\ell_1 i}^{(i)} u_{\ell_2 j}^{(j)} u_{\ell_3 k}^{(k)} \tag{7.8}$$

where $u_{\ell_1 i}^{(i)} \in \mathbb{R}^{N \times N}$, $u_{\ell_2 j}^{(j)} \in \mathbb{R}^{26 \times 26}$, and $u_{\ell_3 k}^{(k)} \in \mathbb{R}^{3 \times 3}$ are singular value matrices and $G(\ell_1, \ell_2, \ell_3) \in \mathbb{R}^{N \times 26 \times 3}$ is a core tensor.

First, we need to find $\boldsymbol{u}_{\ell_2}^{(j)}$ that is independent of 26 cell lines and $\boldsymbol{u}_{\ell_3}^{(k)}$ that is independent of RNA-seq, TSS-seq, and ChIP-seq. Figure 7.6 shows $\boldsymbol{u}_1^{(j)}$. Excluding X chromosome, it is highly independent of 26 cell lines. Then we decide to employ $\ell_2 = 1$. Figure 7.7 shows $\boldsymbol{u}_1^{(k)}$. They are highly independent of TSS-seq, RNA-seq, and ChIP-seq. Then we decide to employ $\ell_3 = 1$.

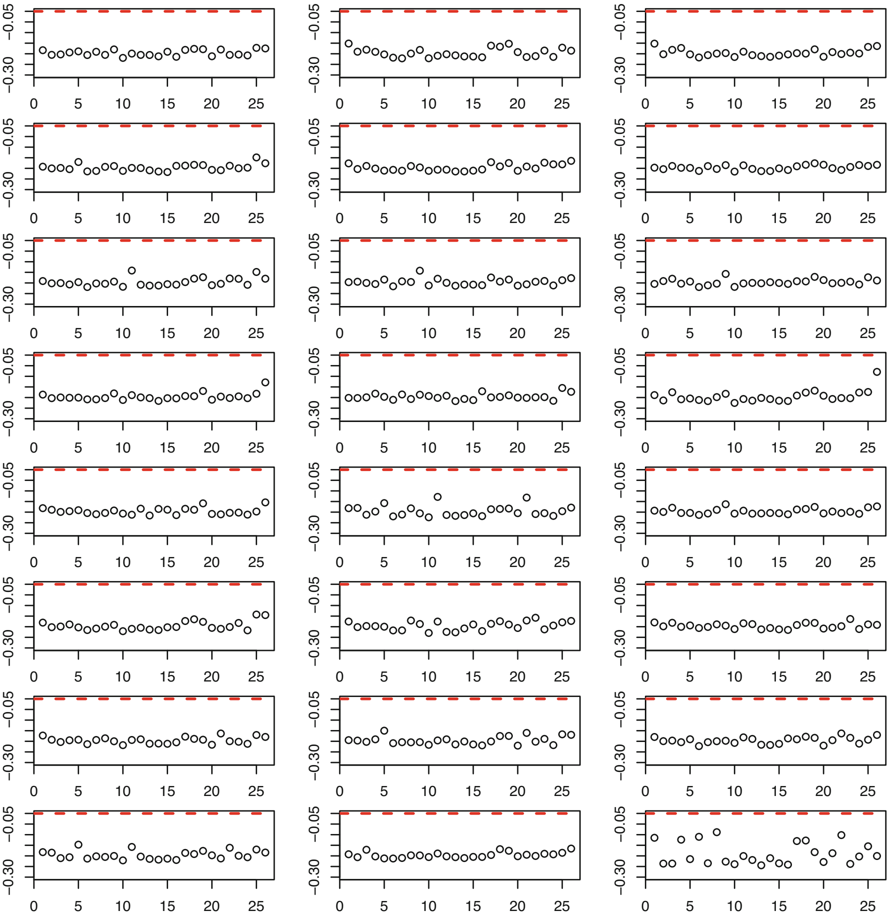

Fig. 7.6 $\boldsymbol{u}_1^{(j)}$. The first row, from left to right, chromosome 1, 2, 3, the second row, from left to right, chromosome 4, 5, 6 , and so on. The last row, from left to right, chromosome 22, X, Y. Red broken line is baseline

Then we try to find which $G(\ell_1, 1, 1)$ has the largest absolute value and find that $G(1, 1, 1)$ has always the largest absolute values independent of chromosome. Thus, $\boldsymbol{u}_1^{(i)}$ is used to attributed P-value to regions as

$$P_i = P_{\chi^2}\left[> \left(\frac{u_{1i}^{(i)}}{\sigma_1}\right)^2\right]. \tag{7.9}$$

P-values are collected from 24 chromosome and are corrected by BH criterion. Then 826 regions associated with adjusted P-values less than 0.01 are selected. 826 is very small compared with the total number of regions; because the total number

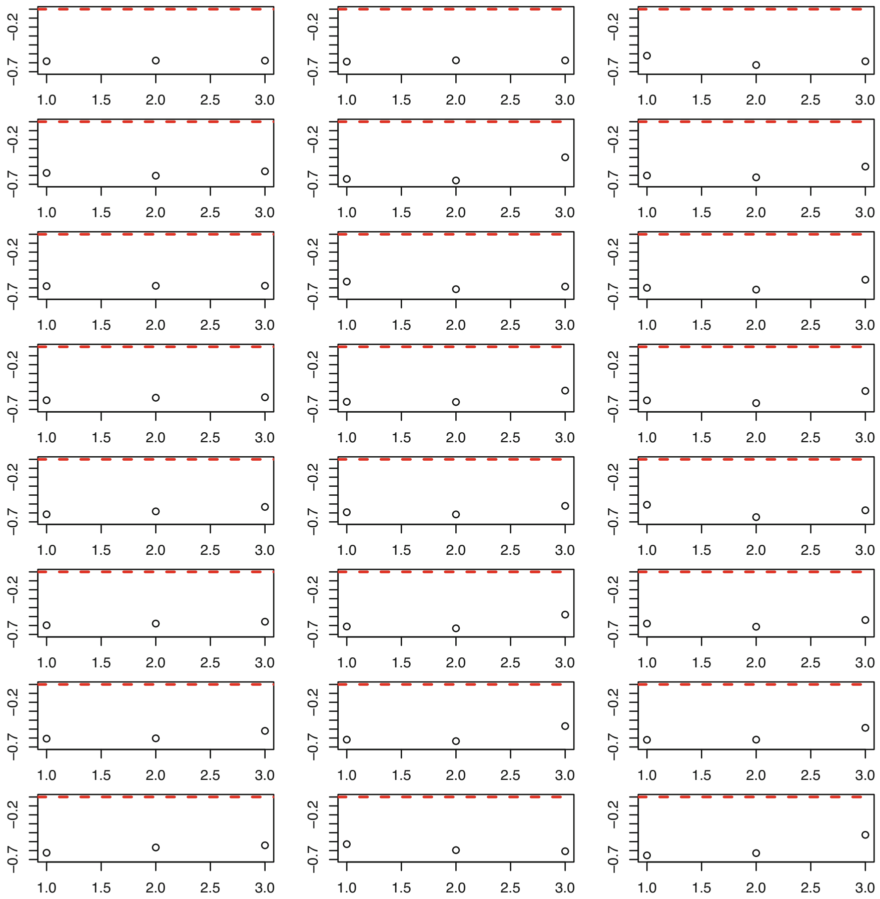

Fig. 7.7 $\boldsymbol{u}_1^{(k)}$. The first row, from left to right, chromosome 1, 2, 3, the second row, from left to right, chromosome 4, 5, 6, and so on. The last row, from left to right, chromosome 22, X, Y. Red broken line is baseline

of regions is about $3 \times 10^9/2.5 \times 10^4 \sim 10^5$ where 3×10^9 is the total length of human genome while 2.5×10^4 is the length of individual regions, 826 corresponds to as little as 0.8% of regions. This is reasonable because only a few percentages of genome code protein coding genes.

In order to validate these selected regions, we upload 1741 Entrez genes associated with these 826 regions to DAVID. Entrez genes are gene ID manually curated gene unique ID that is integer number [12]. Table 7.16 lists the KEGG pathway enrichment associated with adjusted P-values less than 0.05. At a glance, they do not look like related to cancers. Nevertheless, some of them are cancer related terms. For example, the relationship between “antigen processing and presentation” and cancer is often discussed [4]. Parkinson’s disease is often reported to be related

Table 7.16 KEGG pathway enrichment by the 1741 Entrez genes identified by TD based unsupervised FE

Category	Term	Genes count	%	P-value	Adjusted P-value
KEGG_PATHWAY	Ribosome	73	4.2	9.8×10^{-38}	2.7×10^{-35}
KEGG_PATHWAY	Spliceosome	39	2.2	6.2×10^{-10}	8.4×10^{-8}
KEGG_PATHWAY	Protein processing in endoplasmic reticulum	41	2.4	8.0×10^{-8}	7.3×10^{-6}
KEGG_PATHWAY	Antigen processing and presentation	22	1.3	8.0×10^{-6}	5.5×10^{-4}
KEGG_PATHWAY	Pathogenic Escherichia coli infection	17	1.0	1.7×10^{-5}	9.2×10^{-4}
KEGG_PATHWAY	Parkinson's disease	30	1.7	9.6×10^{-5}	4.3×10^{-3}
KEGG_PATHWAY	Biosynthesis of antibiotics	39	2.2	1.6×10^{-4}	6.3×10^{-3}
KEGG_PATHWAY	Oxidative phosphorylation	26	1.5	1.0×10^{-3}	3.5×10^{-2}
KEGG_PATHWAY	Bacterial invasion of epithelial cells	18	1.0	1.2×10^{-3}	3.6×10^{-2}
KEGG_PATHWAY	Alzheimer's disease	30	1.7	1.7×10^{-3}	4.6×10^{-2}

Adjusted P-values are by BH criterion

to lung cancer [30]. Although we are not willing to discuss fully about the relations between the detected KEGG pathway enrichment and NSCLC, it is obvious that TD based unsupervised FE can detect set of genes including those related to NSCLC.

Although it is better to evaluate the performance of TD based unsupervised FE based upon the comparison with other methods, it is not easy because there are no control samples to be compared. Thus, alternatively we select genes based upon the ratio of standard deviation to average over 26 cell lines, because the smaller ratio of variance to mean might suggest smaller variability between 26 cell lines. For each of TSS-seq, RNA-seq, and ChIP-seq, we select top 5% regions with smaller ratio. Then regions chosen in common among TSS-seq, RNA-seq, and ChIP-seq are collected; we find that 2041 Entrez genes are included in these regions chosen in common. This number, 2041, is comparative with 1741 that is the number of Entrez genes selected by TD based unsupervised FE. Thus, uploading these to DAVID is a suitable test to see if TD based unsupervised FE is superior to this alternative method. Then we find that only two KEGG pathways, "Spliceosome" and "Ubiquitin mediated proteolysis" are associated with adjusted P-values less than 0.05. This suggests that TD based unsupervised FE can identify far more biologically reasonable set of genes than this alternative approach.

7.6 General Examples of Case I and II Tensors

Before demonstrating individual cases using case I and case II tensor in detail, we demonstrate various cases briefly based upon the recent publication [23]. As shown in Table 5.3, matrices or low mode tensor can be combined to generate (higher mode) tensor. In this section, we demonstrate how the combinations shown in Table 5.3 work to select genes critical to the diseases or phenomena considered.

7.6.1 Integrated Analysis of mRNA and miRNA

Integrated analysis of mRNA and miRNA was also performed by PCA based unsupervised FE (Sect. 6.4), which is once applied to mRNA and miRNA separately. Then obtained two sets of PC loading attributed to sample were investigated to seek those sharing common nature between two sets. After that, corresponding PC scores attributed to mRNA and miRNA were used for FE. On the contrary, in the application of TD based unsupervised FE to the integrated analysis of mRNA and miRNA, mRNA and miRNA expression profiles are integrated in advance.

The analyzed data set is composed of mRNA and miRNA profiles which were measured for multi-class breast cancer samples including normal breast tissues [7]. mRNA and miRNA expression profiles of multi-omics data are downloaded from GEO using GEO ID GSE28884. At first, GSE28884_RAW.tar is downloaded and expanded. For mRNA, 161 files whose names ended by the string "c.txt.gz" are used. Each file is loaded into R by read.csv command and the second column named "M" is employed as mRNA expression values. Probes not associated with Human Genome Organisation (HUGO) gene names are discarded and 13,393 probes remain. One hundred and sixty one files whose names end by the string "geo.txt.gz" are used for miRNA expression profiles; mRNA expression profiles of the corresponding samples are also used. Each file is loaded into R by read.csv command and the second column ("Count") is summed using the same third column ("Annotation") values. If the resulting total sum is less than 10, it is discarded and not used for further analysis.

Because the 161 samples are shared between miRNA and mRNA expression profiles, the multi-omics data corresponds to case I data (Table 5.3). TD based unsupervised FE is applied to the data set in order to identify disease critical genes and latent relations between miRNA and mRNA, whose expression profiles are $x_{i_1 j}^{\text{mRNA}} \in \mathbb{R}^{13393 \times 161}$ and $x_{i_2 j}^{\text{miRNA}} \in \mathbb{R}^{755 \times 161}$, respectively. They can be formatted as case I tensor as

$$x_{i_1 i_2 j} = x_{i_1 j}^{\text{mRNA}} x_{i_2 j}^{\text{miRNA}}. \tag{7.10}$$

HOSVD, Fig. 3.8, is applied to $x_{i_1 i_2 j}$ as

$$x_{i_1 i_2 j} = \sum_{\ell_1=1}^{13393} \sum_{\ell_2=1}^{755} \sum_{\ell_3=1}^{161} G(\ell_1, \ell_2, \ell_3) u_{\ell_1 i_1}^{(i_1)} u_{\ell_2 i_2}^{(i_2)} u_{\ell_3 j}^{(j)} \tag{7.11}$$

where $u_{\ell_1 i_1}^{(i_1)} \in \mathbb{R}^{13393 \times 13393}$,$u_{\ell_2 i_2}^{(i_2)} \in \mathbb{R}^{755 \times 755}$ and $u_{\ell_3 j}^{(j)} \in \mathbb{R}^{161 \times 161}$ are singular value matrices and $G(\ell_1, \ell_2, \ell_3) \in \mathbb{R}^{13393 \times 755 \times 161}$ is a core tensor.

First we need to seek singular value vectors, $\boldsymbol{u}_{\ell_3}^{(j)} \in \mathbb{R}^{161}$, with significant cancer subtype dependence. Figure 7.8 shows boxplots of $\boldsymbol{u}_{\ell_3}^{(j)}, 1 \leq \ell_3 \leq 5$; it is obvious that these singular value vectors have significant class (cancer subtypes) dependence. The next step is to find $G(\ell_1, \ell_2, 1 \leq \ell_3 \leq 5)$ with larger absolute values. Table 7.17 shows the top ranked $G(\ell_1, \ell_2, 1 \leq \ell_3 \leq 5)$s; there are clearly only $1 \leq \ell_1 \leq 5$ and $1 \leq \ell_2 \leq 2$, respectively. Thus, P-values are attributed to i_1 and i_2 using $u_{\ell_1 i_1}^{(i_1)}, 1 \leq \ell_1 \leq 5$ and $u_{\ell_2 i_2}^{(i_2)}, 1 \leq \ell_1 \leq 2$, respectively, as

$$P_{i_1} = P_{\chi^2}\left[> \sum_{\ell_1=1}^{5} \left(\frac{u_{\ell_1 i_1}^{(i_1)}}{\sigma_{\ell_1}} \right)^2 \right], \tag{7.12}$$

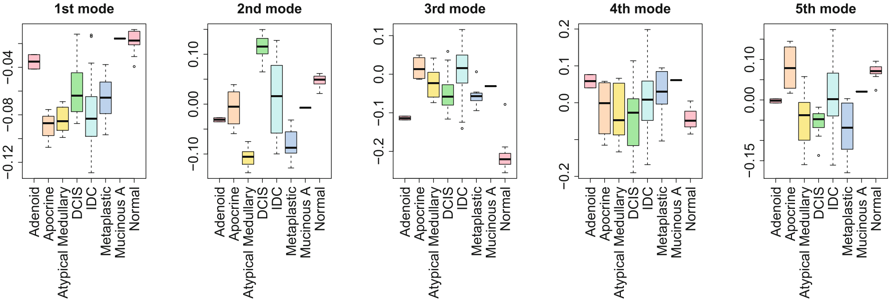

Fig. 7.8 Boxplot of $\boldsymbol{u}_{\ell_3}^{(j)}, 1 \leq \ell_3 \leq 5$ when HOSVD is applied as Eq. (7.11). P-values computed by categorical regression. 1st: 2.39×10^{-5}, 2nd: 5.83×10^{-14}, 3rd: 1.36×10^{-24}, 4th: 2.58×10^{-2}, 5th: 2.12×10^{-5}

Table 7.17 Top ranked 10 $G(\ell_1, \ell_2, 1 \leq \ell_3 \leq 5)$s with larger absolute values among $1 \leq \ell_1, \ell_2, \ell_3 \leq 10$ in Eq. (7.11)

ℓ_1	1	2	4	3	5
ℓ_2	1	1	1	1	1
ℓ_3	1	2	4	3	5
$G(\ell_1, \ell_2, \ell_3)$	1.67×10^5	-1.03×10^5	7.48×10^4	-6.64×10^4	6.23×10^4
ℓ_1	3	1	3	2	1
ℓ_2	2	2	1	2	2
ℓ_3	3	3	5	3	2
$G(\ell_1, \ell_2, \ell_3)$	3.00×10^4	-2.87×10^4	-2.33×10^4	-2.02×10^4	-1.48×10^4

$$P_{i_2} = P_{\chi^2}\left[> \sum_{\ell_2=1}^{2} \left(\frac{u_{\ell_2 i_2}^{(i_2)}}{\sigma_{\ell_2}} \right)^2 \right]. \tag{7.13}$$

Computed P-values are adjusted by BH criterion; i_1s and i_2s associated with adjusted P-values less than 0.01 are selected. Then, 426 mRNA probes and 7 miRNAs are selected, respectively.

In order to evaluate selected 426 mRNAs biologically, we upload these mRNAs to DAVID. Then we can find numerous enrichment. Tables 7.18 and 7.19 show the results of GO term enrichment (adjusted P-values less than 0.05). BP is related to biological feature, CC is related to the location within cell, and MF is function of gene as molecules. Although we are not willing to summarize all of them, most of them are reasonably related to cancers, e.g., immune related or cell surface enrichment. Thus TD based unsupervised FE is likely successful to identify cancer related genes.

In order to demonstrate superiority of type I tensor, we also employ type II tensor as

$$x_{i_1 i_2} = \sum_j x_{i_1 i_2 j}. \tag{7.14}$$

Table 7.18 GO BP enrichment by the 426 ensembl genes identified by TD based unsupervised FE

Category	Term	Genes count	%	P-value	Adjusted P-value
GOTERM_BP_DIRECT	Immune response	36	11.4	2.7×10^{-14}	5.6×10^{-11}
GOTERM_BP_DIRECT	Signal transduction	57	18.1	5.1×10^{-12}	5.3×10^{-9}
GOTERM_BP_DIRECT	Type I interferon signaling pathway	10	3.2	1.8×10^{-6}	1.2×10^{-3}
GOTERM_BP_DIRECT	Collagen catabolic process	10	3.2	1.8×10^{-6}	1.2×10^{-3}
GOTERM_BP_DIRECT	Positive regulation of cell proliferation	25	7.9	3.2×10^{-6}	1.3×10^{-3}
GOTERM_BP_DIRECT	Cell–cell signaling	18	5.7	3.1×10^{-6}	1.6×10^{-3}
GOTERM_BP_DIRECT	Response to estradiol	11	3.5	4.8×10^{-6}	1.6×10^{-3}
GOTERM_BP_DIRECT	Defense response to virus	14	4.4	8.0×10^{-6}	2.3×10^{-3}
GOTERM_BP_DIRECT	B cell receptor signaling pathway	8	2.5	4.5×10^{-5}	1.1×10^{-2}
GOTERM_BP_DIRECT	Positive regulation of cAMP metabolic process	4	1.3	1.1×10^{-4}	2.4×10^{-2}
GOTERM_BP_DIRECT	Response to peptide hormone	7	2.2	1.2×10^{-4}	2.4×10^{-2}

(continued)

Table 7.18 (continued)

Category	Term	Genes count	%	P-value	Adjusted P-value
GOTERM_BP_DIRECT	Negative regulation of apoptotic process	21	6.7	1.9×10^{-4}	2.6×10^{-2}
GOTERM_BP_DIRECT	Defense response	8	2.5	1.8×10^{-4}	2.6×10^{-2}
GOTERM_BP_DIRECT	T cell activation	7	2.2	1.7×10^{-4}	2.7×10^{-2}
GOTERM_BP_DIRECT	T cell differentiation	6	1.9	1.7×10^{-4}	2.8×10^{-2}
GOTERM_BP_DIRECT	Skeletal system development	11	3.5	1.7×10^{-4}	3.1×10^{-2}
GOTERM_BP_DIRECT	Chemokine-mediated signaling pathway	8	2.5	2.6×10^{-4}	3.3×10^{-2}
GOTERM_BP_DIRECT	Mast cell activation	4	1.3	2.9×10^{-4}	3.4×10^{-2}
GOTERM_BP_DIRECT	Adaptive immune response	11	3.5	3.1×10^{-4}	3.5×10^{-2}
GOTERM_BP_DIRECT	Cell surface receptor signaling pathway	15	4.8	4.0×10^{-4}	4.2×10^{-2}
GOTERM_BP_DIRECT	Cellular response to interferon-alfa	4	1.3	4.3×10^{-4}	4.3×10^{-2}
GOTERM_BP_DIRECT	Inflammatory response	18	5.7	4.5×10^{-4}	4.3×10^{-2}
GOTERM_BP_DIRECT	Apoptotic process	23	7.3	5.2×10^{-4}	4.5×10^{-2}
GOTERM_BP_DIRECT	Humoral immune response	7	2.2	5.0×10^{-4}	4.6×10^{-2}
GOTERM_BP_DIRECT	Positive regulation of neutrophil chemotaxis	5	1.6	5.5×10^{-4}	4.6×10^{-2}
GOTERM_BP_DIRECT	Collagen fibril organization	6	1.9	6.0×10^{-4}	4.8×10^{-2}
GOTERM_BP_DIRECT	Proteolysis	21	6.7	6.4×10^{-4}	4.9×10^{-2}

Adjusted P-values are by BH criterion

Applying SVD to $x_{i_1 i_2}$, we get singular value vectors $u^{(i_1)}_{\ell_1 i_1} \in \mathbb{R}^{13393 \times 161}$ and $u^{(i_2)}_{\ell_2 i_2} \in \mathbb{R}^{755 \times 161}$. In order to select singular vector used for FE, we need to know dependence upon classes (in this case, cancer subtype). In order that, we need singular value vectors attributed to samples. It is computed as Eqs. (5.12) and (5.13),

$$u^{j;i_1}_{\ell_1 j} = \sum_{i_1=1}^{13393} x_{i_1 j} u^{(i_1)}_{\ell_1 i_1} \tag{7.15}$$

$$u^{j;i_2}_{\ell_2 j} = \sum_{i_2=1}^{755} x_{i_2 j} u^{(i_2)}_{\ell_2 i_2} \tag{7.16}$$

Figure 7.9 shows boxplot of $u^{j;i_1}_{\ell_1 j}$ and $u^{j;i_2}_{\ell_2 j}$ for $1 \le \ell_3 \le 5$. It is obvious that these singular value vectors have significant class (cancer subtypes) dependence.

Thus, P-values are attributed to i_1 and i_2 using $u^{(i_1)}_{\ell_1 i_1}$ and $u^{(i_2)}_{\ell_2 i_2}$ for $1 \le \ell_3 \le 5$, respectively, as

Table 7.19 GO CC and MF enrichment by the 426 ensembl genes identified by TD based unsupervised FE

Category	Term	Genes count	%	P-value	Adjusted P-value
GOTERM_CC_DIRECT	Extracellular space	84	26.7	1.60×10^{-26}	4.90×10^{-24}
GOTERM_CC_DIRECT	Extracellular region	82	26	3.10×10^{-20}	4.80×10^{-18}
GOTERM_CC_DIRECT	Extracellular exosome	97	30.8	9.00×10^{-13}	9.20×10^{-11}
GOTERM_CC_DIRECT	External side of plasma membrane	23	7.3	1.00×10^{-11}	7.70×10^{-10}
GOTERM_CC_DIRECT	Cell surface	23	7.3	1.20×10^{-4}	7.40×10^{-3}
GOTERM_CC_DIRECT	Extracellular matrix	15	4.8	4.80×10^{-4}	1.80×10^{-2}
GOTERM_CC_DIRECT	Multivesicular body	5	1.6	4.40×10^{-4}	1.90×10^{-2}
GOTERM_CC_DIRECT	Anchored component of membrane	9	2.9	6.20×10^{-4}	2.10×10^{-2}
GOTERM_CC_DIRECT	Cytosol	80	25.4	4.20×10^{-4}	2.10×10^{-2}
GOTERM_MF_DIRECT	Protein homodimerization activity	34	10.8	8.60×10^{-7}	4.90×10^{-4}
GOTERM_MF_DIRECT	RAGE receptor binding	5	1.6	2.90×10^{-5}	5.50×10^{-3}
GOTERM_MF_DIRECT	Chemokine activity	8	2.5	2.40×10^{-5}	6.70×10^{-3}
GOTERM_MF_DIRECT	CXCR3 chemokine receptor binding	4	1.3	5.40×10^{-5}	7.60×10^{-3}
GOTERM_MF_DIRECT	Receptor binding	18	5.7	2.00×10^{-4}	1.90×10^{-2}
GOTERM_MF_DIRECT	Serine-type endopeptidase activity	15	4.8	2.00×10^{-4}	2.20×10^{-2}
GOTERM_MF_DIRECT	Protein binding	187	59.4	2.90×10^{-4}	2.30×10^{-2}
GOTERM_MF_DIRECT	Identical protein binding	28	8.9	4.00×10^{-4}	2.80×10^{-2}

Adjusted P-values are by BH criterion

$$P_{i_1} = P_{\chi^2}\left[> \sum_{\ell_1=1}^{5} \left(\frac{u_{\ell_1 i_1}^{(i_1)}}{\sigma_{\ell_1}} \right)^2 \right], \tag{7.17}$$

$$P_{i_2} = P_{\chi^2}\left[> \sum_{\ell_2=1}^{5} \left(\frac{u_{\ell_2 i_2}^{(i_2)}}{\sigma_{\ell_2}} \right)^2 \right]. \tag{7.18}$$

P-values are adjusted by BH criterion. i_1 and i_2 associated with adjusted P-values less than 0.01 are selected. Then, 374 mRNA probes and 21 miRNAs are selected.

In order to validate selected 374 mRNAs, we upload these mRNAs to DAVID. Then we can find numerous enrichment. Table 7.20 shows the results of GO term enrichment (adjusted P-values less than 0.05) as in Tables 7.18 and 7.19. Thus, although the number of enrichment decreases than that in the type I tensor, still there are many cancer related GO terms. Thus, type II tensor approach is still valid enough biologically.

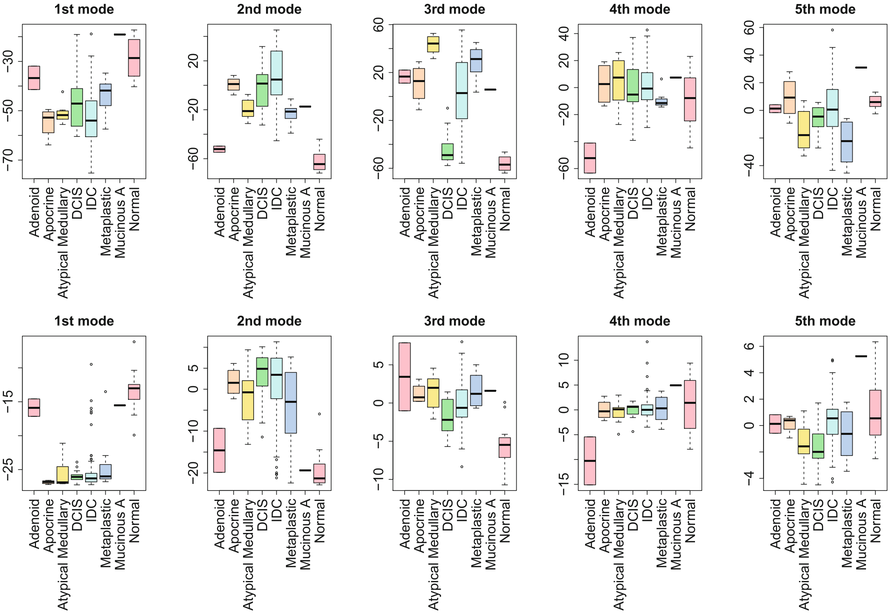

Fig. 7.9 Boxplot of $u_{\ell_1 j}^{j;i_1}$ (upper row) and $u_{\ell_2 j}^{j;i_2}$ (lower row) for $1 \leq \ell_3 \leq 5$ computed by Eqs. (7.15) and (7.16). P-values computed by categorical regression. Upper, 1st: 4.07×10^{-11}, 2nd: 4.36×10^{-22}, 3rd: 2.03×10^{-23}, 4th: 4.14×10^{-4}, 5th: 1.57×10^{-4}. Lower, 1st: 3.36×10^{-27}, 2nd: 3.91×10^{-13}, 3rd: 7.39×10^{-9}, 4th: 9.32×10^{-5}, 5th: 2.82×10^{-5}

Finally, in order to emphasize the superiority of TD based unsupervised FE to conventional supervised methods, we apply categorical regression analysis to mRNAs expression,

$$x_{i_1 j} = a_{i_1} + \sum_s b_{i_1 s} \delta_{js} \tag{7.19}$$

where a_{i_1} and $b_{i_1 s}$ are the regression coefficients. Based upon the results by categorical regression analysis, because too many 16,917 mRNAs probes are associated with adjusted P-values less than 0.01, we instead upload top ranked 500 mRNAs with smaller P-values to DAVID. As a result, only one GO CC enrichment, cytoplasm, associated with adjusted P-values less than 0.05, 1.9×10^{-3}, is detected. Although more advanced methods than categorical regression might achieve better performance, this drastic decrease of the number of detected GO terms enrichment demonstrates the superiority over conventional supervised method. In this sense, TD based unsupervised FE is outstanding, no matter which of type I or type II tensor is used.

Table 7.20 GO BP, CC and MF enrichment by the 374 ensembl genes identified by TD based unsupervised FE for type II tensor

Category	Term	Genes count	%	P-value	Adjusted P-value
GOTERM_BP_DIRECT	Response to estradiol	15	5.1	2.50×10^{-10}	5.00×10^{-7}
GOTERM_BP_DIRECT	Collagen catabolic process	11	3.7	8.20×10^{-8}	5.50×10^{-5}
GOTERM_BP_DIRECT	Skeletal system development	15	5.1	5.60×10^{-8}	5.70×10^{-5}
GOTERM_BP_DIRECT	Positive regulation of cell proliferation	26	8.8	2.10×10^{-7}	1.10×10^{-4}
GOTERM_BP_DIRECT	Collagen fibril organization	8	2.7	2.90×10^{-6}	1.20×10^{-3}
GOTERM_BP_DIRECT	Extracellular matrix organization	15	5.1	4.40×10^{-6}	1.30×10^{-3}
GOTERM_BP_DIRECT	Extracellular matrix disassembly	10	3.4	4.10×10^{-6}	1.40×10^{-3}
GOTERM_BP_DIRECT	Ossification	10	3.4	6.20×10^{-6}	1.60×10^{-3}
GOTERM_BP_DIRECT	Signal transduction	40	13.5	1.50×10^{-5}	3.30×10^{-3}
GOTERM_BP_DIRECT	Cell–cell signaling	15	5.1	8.00×10^{-5}	1.50×10^{-2}
GOTERM_BP_DIRECT	Response to peptide hormone	7	2.4	7.60×10^{-5}	1.50×10^{-2}
GOTERM_BP_DIRECT	Regulation of branching involved in prostate gland morphogenesis	4	1.40	1.40×10^{-4}	2.20×10^{-2}
GOTERM_BP_DIRECT	Mammary gland alveolus development	5	1.7	1.40×10^{-4}	2.40×10^{-2}
GOTERM_BP_DIRECT	Cellular response to hypoxia	9	3.0	1.80×10^{-4}	2.50×10^{-2}
GOTERM_BP_DIRECT	Immune response	19	6.4	2.10×10^{-4}	2.80×10^{-2}
GOTERM_BP_DIRECT	Proteolysis	21	7.1	2.30×10^{-4}	2.80×10^{-2}
GOTERM_BP_DIRECT	Aging	11	3.7	4.00×10^{-4}	4.60×10^{-2}
GOTERM_CC_DIRECT	Extracellular space	89	30.1	6.10×10^{-33}	1.80×10^{-30}
GOTERM_CC_DIRECT	Extracellular region	80	27.0	2.60×10^{-21}	3.90×10^{-19}
GOTERM_CC_DIRECT	Extracellular matrix	27	9.1	8.60×10^{-13}	8.60×10^{-11}
GOTERM_CC_DIRECT	Extracellular exosome	91	30.7	1.90×10^{-12}	1.40×10^{-10}
GOTERM_CC_DIRECT	Proteinaceous extracellular matrix	21	7.1	7.00×10^{-9}	4.10×10^{-7}

(continued)

Table 7.20 (continued)

Category	Term	Genes count	%	P-value	Adjusted P-value
GOTERM_CC_DIRECT	Cell surface	24	8.1	1.20×10^{-5}	6.20×10^{-4}
GOTERM_CC_DIRECT	Basement membrane	8	2.7	2.20×10^{-4}	9.20×10^{-3}
GOTERM_CC_DIRECT	Cytosol	75	25.3	4.20×10^{-4}	1.50×10^{-2}
GOTERM_MF_DIRECT	Growth factor activity	12	4.1	7.60×10^{-5}	6.70×10^{-3}
Category	Term	Genes count	%	P-value	Adjusted P-value
GOTERM_MF_DIRECT	Heparin binding	12	4.1	6.80×10^{-5}	7.20×10^{-3}
GOTERM_MF_DIRECT	Collagen binding	8	2.7	5.50×10^{-5}	7.20×10^{-3}
GOTERM_MF_DIRECT	Calcium ion binding	28	9.5	5.30×10^{-5}	9.30×10^{-3}
GOTERM_MF_DIRECT	Protein binding	178	60.1	3.90×10^{-5}	1.00×10^{-2}
GOTERM_MF_DIRECT	RAGE receptor binding	5	1.7	2.10×10^{-5}	1.10×10^{-2}
GOTERM_MF_DIRECT	Protein homodimerization activity	26	8.8	4.40×10^{-4}	3.20×10^{-2}
GOTERM_MF_DIRECT	Identical protein binding	26	8.8	6.30×10^{-4}	3.20×10^{-2}
GOTERM_MF_DIRECT	Serine-type peptidase activity	7	2.4	5.70×10^{-4}	3.30×10^{-2}
GOTERM_MF_DIRECT	Insulin-like growth factor I binding	4	1.4	8.60×10^{-4}	3.40×10^{-2}
GOTERM_MF_DIRECT	Extracellular matrix structural constituent	7	2.4	8.00×10^{-4}	3.40×10^{-2}
GOTERM_MF_DIRECT	Metalloendopeptidase activity	9	3.0	5.50×10^{-4}	3.60×10^{-2}
GOTERM_MF_DIRECT	Fibronectin binding	5	1.7	8.00×10^{-4}	3.80×10^{-2}
GOTERM_MF_DIRECT	Serine-type endopeptidase activity	13	4.4	1.10×10^{-3}	3.90×10^{-2}
GOTERM_MF_DIRECT	Protein kinase binding	16	5.4	1.40×10^{-3}	4.90×10^{-2}

Adjusted P-values are by BH criterion

7.6.2 Temporally Differentially Expressed Genes

Although type I and type II tensor approaches achieved good performance in integrated analysis of multi-class multi-omics data set in the previous section, it is better if we can demonstrate yet another example to which TD based unsupervised FE can achieve better performance. In this subsection, we try to identify genes temporally expressed distinctly between two classes.

The first data set analyzed is the comparison of NSCLC cell line H1975, with and without EGF treatment [2]. EGF is a gene supposed to accelerate cell growth and is known to be expressive frequently in cancers. Thus, EGF treatment is expected to activate cancer cell lines. The data set is composed of two mRNA expression profile, $x_{ij_1}^{\text{control}} \in \mathbb{R}^{39937 \times 13}$ and $x_{ij_2}^{\text{EGF}} \in \mathbb{R}^{39937 \times 15}$, which are gene expressions of cell lines without and with EGF treatment, respectively. j_1 and j_2 represent time points after the treatment (Table 7.21). Because they share genes, $x_{ij_1}^{\text{control}}$ and $x_{ij_2}^{\text{EGF}}$ can be converted to case II type I tensor as

$$x_{ij_1j_2} = x_{ij_1}^{\text{control}} x_{ij_2}^{\text{EGF}}. \tag{7.20}$$

HOSVD, Fig. 3.8, is applied to $x_{ij_1j_2}$ as

$$x_{ij_1j_2} = \sum_{\ell_1=1}^{13} \sum_{\ell_2=1}^{15} \sum_{\ell_3=1}^{39937} G(\ell_1, \ell_2, \ell_3) u_{\ell_1 j_1}^{(j_1)} u_{\ell_2 j_2}^{(j_2)} u_{\ell_3 i}^{(i)} \tag{7.21}$$

At first, we need to find singular value vectors $\boldsymbol{u}_{\ell_1}^{(j_1)} \in \mathbb{R}^{13}$ and $\boldsymbol{u}_{\ell_2}^{(j_2)} \in \mathbb{R}^{15}$ that exhibit distinct temporal expression between them. Figure 7.10 shows time development of $\boldsymbol{u}_{\ell_1}^{(j_1)}$ and $\boldsymbol{u}_{\ell_2}^{(j_2)}$ for $\ell_1 = \ell_2 = 1, 2$. Here the components of singular value vectors sharing the time points are averaged within individual vectors, $u_{\ell_1 j_1}^{(j_1)}$. It is obvious that $\boldsymbol{u}_1^{(j_1)}$ and $\boldsymbol{u}_1^{(j_2)}$ do not exhibit any time dependence while $\boldsymbol{u}_2^{(j_1)}$ and $\boldsymbol{u}_2^{(j_2)}$ do. Thus, there is a possibility that genes associated with $\boldsymbol{u}_2^{(j_1)}$ and $\boldsymbol{u}_2^{(j_2)}$ also exhibit the temporal difference between control and EGF treated cells.

In order to select genes associated with $\boldsymbol{u}_2^{(j_1)}$ and $\boldsymbol{u}_2^{(j_2)}$, we need to find $G(\ell_1, \ell_2, \ell_3)$, $\ell_1 = 2$ or $\ell_2 = 2$ having larger absolute values; $G(2, 1, 2)$ and $G(1, 2, 2)$ have larger absolute values (Table 7.22). Thus we decide to use $\boldsymbol{u}_2^{(i)}$ for FE. P-values are attributed to i as

Table 7.21 List of samples in EGF treatment experiments

Time points (h)	0	0.5	1	2	4	6	8	12	18	24	48
Control	3	1	1	1	1	1	0	0	0	2	3
EGF treated	0	2	1	1	1	1	1	1	1	3	3

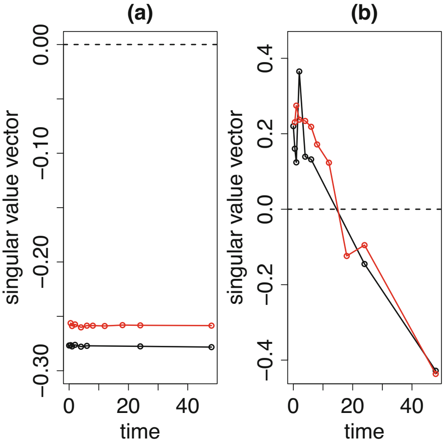

Fig. 7.10 Singular value vectors, Eq. (7.21). (**a**) $\boldsymbol{u}_1^{(j_1)}$ (black) and $\boldsymbol{u}_1^{(j_2)}$ (red). (**b**) $\boldsymbol{u}_2^{(j_1)}$ (black) and $\boldsymbol{u}_2^{(j_2)}$(red)

Table 7.22 Top ranked 10 $G(\ell_1, \ell_2, \ell_3)$s with larger absolute values among in Eq. (7.21)

ℓ_1	1	2	1	3	1
ℓ_2	1	1	2	1	3
ℓ_3	1	2	2	3	4
$G(\ell_1, \ell_2, \ell_3)$	-4.03×10^4	-1.56×10^3	1.49×10^3	1.05×10^3	-5.79×10^2
ℓ_1	4	2	5	1	4
ℓ_2	1	1	1	4	1
ℓ_3	5	3	6	6	4
$G(\ell_1, \ell_2, \ell_3)$	4.24×10^2	4.16×10^2	3.25×10^2	3.19×10^2	-2.62×10^2

$$P_i = P_{\chi^2}\left[> \left(\frac{u_{2i}^{(i)}}{\sigma_2}\right)^2 \right]. \tag{7.22}$$

P-values are corrected by BH criterion and genes associated with adjusted P-values less than 0.01 are selected. Then 552 mRNA probes are selected.

Next, we need to see if the selected 552 mRNA probes really exhibit temporal difference between control and EGF treated cells. For this purpose, we compute correlation coefficient between

$$\left(x_{i1}^{\text{control}}, \ldots, x_{i13}^{\text{control}}, x_{i1}^{\text{EGF}}, \ldots, x_{i15}^{\text{EGF}}\right) \tag{7.23}$$

and

$$\left(u_{2,1}^{(j_1)}, \ldots, u_{2,13}^{(j_1)}, u_{2,1}^{(j_2)}, \ldots, u_{2,15}^{(j_2)}\right) \tag{7.24}$$

to see if 552 selected genes are coincident with $\boldsymbol{u}_2^{(j_1)}$ and $\boldsymbol{u}_2^{(j_2)}$. Figure 7.11a shows the histogram of correlation coefficients. Because there are two peaks at ±1, it is obvious that gene expression of selected 552 mRNA probes is highly coincident with $\boldsymbol{u}_2^{(j_1)}$ and $\boldsymbol{u}_2^{(j_2)}$.

Before comparing 552 genes directly between control and EGF treated cells, we need shift and scale individual gene expression profiles such that they have same baseline and amplitude. In order that, we apply the following linear regression

$$u_{2j_1}^{(j_1)} = a_i x_{ij_1}^{\text{control}} + b_i \tag{7.25}$$

$$u_{2j_2}^{(j_2)} = a_i x_{ij_2}^{\text{EGF}} + b_i \tag{7.26}$$

where a_i and b_i are the regression coefficients. Because regression coefficients are shared between control and EGF treated ones, this does not reduce the difference between these two. Then, we compare $a_i x_{ij_1}^{\text{control}} + b_i$ and $a_i x_{ij_2}^{\text{EGF}} + b_i$ of selected 552 mRNA probes (Fig. 7.11b). Not all, but the comparisons of five out of seven time points excluding two time points, 4 and 24 h, after the EGF treatment are associated with P-values less than 0.05. Thus, TD based unsupervised FE has the ability to select genes associated with temporal distinction.

Next, we try to see if type II tensor approach works as well. Because case II tensor share the feature whose number is generally much larger than the number of samples, type II tensor where shared dimension is summed up can result in much smaller number of components. Type II tensor is defined as

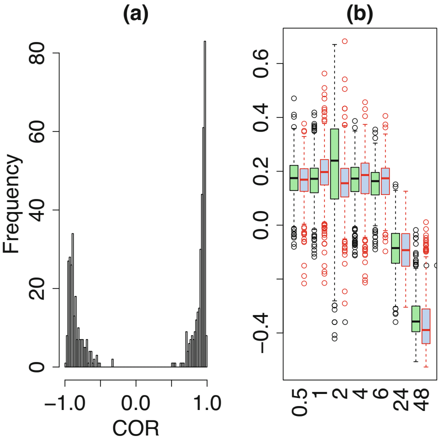

Fig. 7.11 (**a**) Histogram of correlation coefficients between Eqs. (7.23) and (7.24) for case II type I tensor, Eq. (7.20). (**b**) Boxplot of Eqs. (7.25) (black boxes filled with green) and (7.26) (red boxes filled with blue) for case II type I tensor, Eq. (7.20). P-values computed by t test: 0.5 h:2.83×10^{-2}, 1 h:6.81×10^{-8}, 2 h:5.63×10^{-12}, 4 h:3.5×10^{-1}, 6 h:4.83×10^{-2}, 24 h:5.0×10^{-1}, 48 h:1.70×10^{-6}

$$x_{j_1 j_2} = \sum_{i=1}^{39937} x_{i j_1 j_2}. \tag{7.27}$$

where $x_{ij_1j_2}$ is defined in Eq. (7.20). The number of components in $x_{j_1j_2} \in \mathbb{R}^{13\times 15}$ is $13 \times 15 = 195$, which is as small as 1/39937 of the number of components in $x_{ij_1j_2} \in \mathbb{R}^{39937\times 13\times 15}$. Thus, if type II tensor approach works as well, it is very effective. SVD is applied to $x_{j_1j_2}$ as

$$x_{j_1 j_2} = \sum_{\ell} \lambda_\ell u^{(j_1)}_{\ell j_1} u^{(j_2)}_{\ell j_2} \tag{7.28}$$

Figure 7.12 shows the $\boldsymbol{u}^{(j_1)}_\ell$ and $\boldsymbol{u}^{(j_2)}_\ell$ for $\ell = 1, 2$. Basically, it looks similar to Fig. 7.10. Thus we decide to employ $\ell = 2$ for FE. Then, singular value vectors attributed to i can be computed as Eq. (5.14),

$$u^{i;j_1}_{\ell i} = \sum_{j_1=1}^{13} x^{\text{control}}_{ij_1} u^{(j_1)}_{\ell j_1} \tag{7.29}$$

$$u^{i;j_2}_{\ell i} = \sum_{j_2=1}^{15} x^{\text{EGF}}_{ij_2} u^{(j_2)}_{\ell j_2} \tag{7.30}$$

Thus P-values are also attributed to i in two ways as

$$P^{j_1}_i = P_{\chi^2}\left[> \left(\frac{u^{(i;j_1)}_{2i}}{\sigma_2} \right)^2 \right], \tag{7.31}$$

$$P^{j_2}_i = P_{\chi^2}\left[> \left(\frac{u^{(i;j_2)}_{2i}}{\sigma'_2} \right)^2 \right]. \tag{7.32}$$

P-values are corrected by BH criterion. mRNA probes associated with adjusted P-values less than 0.01 are selected. Then, 482 and 487 mRNA probes, between which 396 mRNA probes are chosen in common, are selected using $P^{j_1}_i$ and $P^{j_2}_i$, respectively. Thus, in some sense, type II tensor approach can give the results coincident between two approximations of singular value vectors attributed to i using Eqs. (7.29) and (7.30), respectively.

Next, we need to see if the 396 mRNA probes chosen in common really exhibit temporal difference between control and EGF treated cells as in the case of type I tensor approach. The correlation coefficient between Eqs. (7.23) and (7.24) is computed again to see the coincidence between gene expression and singular value vectors (Fig. 7.13a). It is obvious that the peaks at ±1 is much steeper than that in

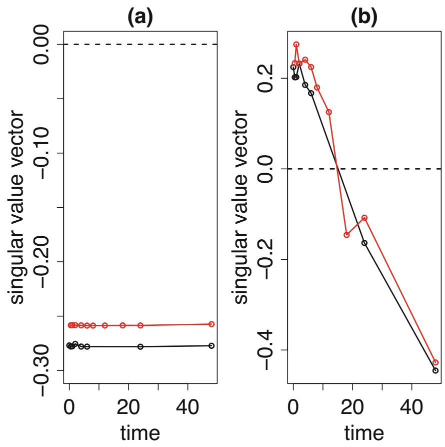

Fig. 7.12 Singular value vectors, Eq. (7.28). (**a**) $\boldsymbol{u}_1^{(j_1)}$ (black) and $\boldsymbol{u}_1^{(j_2)}$ (red). (**b**) $\boldsymbol{u}_2^{(j_1)}$ (black) and $\boldsymbol{u}_2^{(j_2)}$(red)

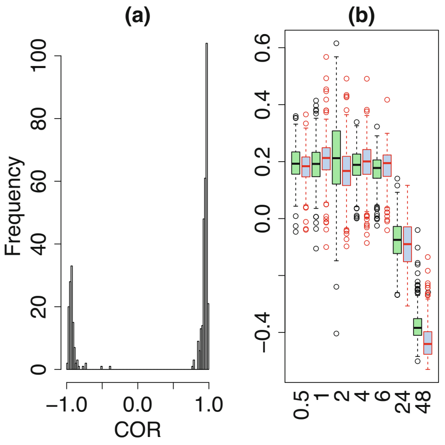

Fig. 7.13 (**a**) Histogram of correlation coefficients between Eqs. (7.23) and (7.24) for case II type II tensor, Eq. (7.27). (**b**) Boxplot of Eqs. (7.25) (black boxes filled with green) and (7.26) (red boxes filled with blue) for case II type II tensor, Eq. (7.27). P-values computed by t test: 0.5 h:1.68×10^{-2}, 1 h:2.56×10^{-5}, 2 h: 3.83×10^{-7}, 4 h:9.14×10^{-2}, 6 h:7.30×10^{-4}, 24 h:2.36×10^{-2}, 48 h:5.55×10^{-38}

Fig. 7.11a. This suggests that type II tensor approach might be better than type I tensor approach in spite of the smaller computational resources required.

In order to confirm the superiority of type II tensor approach, we again apply linear regression Eqs. (7.25) and (7.26) replacing singular value vectors with those obtained by type II tensor (Fig. 7.13b). Because six among seven time points excluding 4 h after the EGF treatment are associated with P-values less than 0.05, type II tensor approach is superior to type I tensor approach.

Finally, in order to validate 552 and 396 mRNA probes selected by type I and II tensor approaches, respectively, we upload RefSeq mRNA IDs associated with these probes to DAVID. Table 7.23 lists the KEGG pathways identified by DAVID for type I and II tensor approach. Although common five KEGG pathways are associated with adjusted P-values less than 0.05, P-values for type II tensor approach are smaller than those for type I tensor approach. Because P-values are more likely smaller for more number of genes uploads, smaller P-values attributed to KEGG

Table 7.23 KEGG pathways identified by DAVID for genes associated with 552 (upper numbers) and 396 (lower numbers) miRNA probes selected using type I, Eq. (7.20), and II, Eq. (7.27), tensor approach

Category	Term	Count	%	P-value	Adjusted P-value
KEGG_PATHWAY	Cell cycle	29 28	9.0 12.1	7.2×10^{-24} 3.7×10^{-29}	1.0×10^{-21} 3.2×10^{-27}
KEGG_PATHWAY	Oocyte meiosis	14 14	4.3 6.0	7.6×10^{-8} 1.4×10^{-10}	5.5×10^{-6} 5.8×10^{-9}
KEGG_PATHWAY	DNA replication	8 9	2.5 3.9	2.8×10^{-6} 3.2×10^{-9}	1.4×10^{-4} 9.3×10^{-8}
KEGG_PATHWAY	Progesterone-mediated oocyte maturation	8 9	2.5 3.9	9.2×10^{-4} 4.0×10^{-6}	3.3×10^{-2} 8.6×10^{-5}
KEGG_PATHWAY	p53 signaling pathway	7 6	2.2 2.6	1.2×10^{-3} 7.7×10^{-4}	3.5×10^{-2} 1.3×10^{-2}

Adjusted P-values are by BH criterion

pathways by type II tensor approach where less number of genes are selected suggest the superiority of type II tensor approach from the biological point of view.

Although type II approach is better than type I approach in this specific example, because it is highly dependent upon data sets analyzed, it is difficult to know in advance which is better.

7.7 Gene Expression and Methylation in Social Insects

As the first example of the application of case I tensor approach, we employ the multi-omics analysis of social insects. Social insects, e.g., ants and bees, are known to have castes where distinct phenotypes appear in spite of shared genome. Thus, it is interesting to know what drives differentiation between castes.

One possible scenario is the alteration of epigenome [29], because epigenome has plasticity that can mediate differentiation between castes. Most typical caste is composed of queen and worker. The former, queen, concentrates on reproduction while the latter, workers, serve to maintain colony. In spite of their strict difference of phenotype, they are often known to be relatives. Thus, they share genome to some extent with having distinct phenotype. This suggests that epigenome can play potential roles in the differentiation of caste.

In this section, we try to identify genes associated with differential expression and methylation between caste, especially queens and workers [25], because such genes are potential candidates that can mediate distinct phenotypes between castes. In order that, we employ TD based unsupervised FE that can integrate multi-omics data sets. The data set analyzed [16] is composed of two insect species, bee (*P.*

Table 7.24 Number of samples in social insect study [16]

	Methylation			mRNA	
Caste	Control	Queen	Worker	Queen	Worker
P. canadensis	1	3	3	4	6
D. quadriceps	1	3	3	7	6

canadensis) and ant (*D. quadriceps*). Table 7.24 shows the number of samples available from GEO with GEO ID GSE59525. As can be seen, it is a typical large p small n data set.

Because the amount of gene expression is measured by the unit of Reads Per Kilobase of exon per Million mapped reads (RPKM), it is used as it is. Because the gene expression profile of *P. canadensis* was $\log_2$-ratio converted, it is expanded to the original one as 2^x where x is gene expression. On the other hand, we would like to employ case II tensor format (Table 5.3) where genes are shared. Thus we need to convert methylation profiles to be attributed to individual genes. In order that, assuming m_{s_1} and m_{s_2} are methylation and nonmethylation values, respectively, at locus s, then the relative methylation within the ith gene can be defined as

$$\frac{\sum_{s \in i} m_{s_1}}{\sum_{s \in i} \left(m_{s_1} + m_{s_2}\right)} \tag{7.33}$$

where $\sum_{s \in i}$ is taken over s bases within DNA sequences corresponding to the ith gene body; the reason why methylation not in promoter region but in the gene body is summed up and is attributed to genes is because gene body methylation is believed to affect gene expression in insects [32]. Relative methylation profile is formatted as

$$x_{ik}^{\text{metyl, bee}} \in \mathbb{R}^{N \times 7}, \tag{7.34}$$

$$x_{ik}^{\text{metyl, ant}} \in \mathbb{R}^{N \times 7}, \tag{7.35}$$

where N is the number of genes. $k = 1$ corresponds to control samples. $2 \leq k \leq 4$ and $5 \leq k \leq 7$ correspond to queens and workers, respectively. On the other hand, mRNA expression is formatted as

$$x_{ij}^{\text{mRNA, bee}} \in \mathbb{R}^{N \times 10}, \tag{7.36}$$

$$x_{ij}^{\text{mRNA, ant}} \in \mathbb{R}^{N \times 13}. \tag{7.37}$$

where $1 \leq j \leq 4$ and $5 \leq j \leq 10$ for bee correspond to queens and workers, respectively, while $1 \leq j \leq 7$ and $8 \leq j \leq 13$ for ant correspond to queens and workers, respectively. Then case II tensor is generated as

$$x_{ijk}^{\text{bee}} = x_{ij}^{\text{mRNA, bee}} x_{ik}^{\text{metyl, bee}}, \tag{7.38}$$

$$x_{ijk}^{\text{ant}} = x_{ij}^{\text{mRNA, ant}} x_{ik}^{\text{metyl, ant}}, \tag{7.39}$$

where $x_{ijk}^{\text{bee}} \in \mathbb{R}^{N\times 10\times 7}$ and $x_{ijk}^{\text{ant}} \in \mathbb{R}^{N\times 13\times 7}$. HOSVD, Fig. 3.8, is applied to x_{ijk}^{bee} and x_{ijk}^{ant} as

$$x_{ijk}^{\text{bee}} = \sum_{\ell_1=1}^{N}\sum_{\ell_2=1}^{10}\sum_{\ell_3=1}^{7} G(\ell_1,\ell_2,\ell_3) u_{\ell_1 i}^{\text{bee}(i)} u_{\ell_2 j}^{\text{bee}(j)} u_{\ell_3 k}^{\text{bee}(k)} \tag{7.40}$$

$$x_{ijk}^{\text{ant}} = \sum_{\ell_1=1}^{N}\sum_{\ell_2=1}^{13}\sum_{\ell_3=1}^{7} G(\ell_1,\ell_2,\ell_3) u_{\ell_1 i}^{\text{ant}(i)} u_{\ell_2 j}^{\text{ant}(j)} u_{\ell_3 k}^{\text{ant}(k)} \tag{7.41}$$

where $u_{\ell_1 i}^{\text{bee}(i)} \in \mathbb{R}^{N\times N}$, $u_{\ell_2 j}^{\text{bee}(j)} \in \mathbb{R}^{10\times 10}$, $u_{\ell_3 k}^{\text{bee}(k)} \in \mathbb{R}^{7\times 7}$, $u_{\ell_1 i}^{\text{ant}(i)} \in \mathbb{R}^{N\times N}$, $u_{\ell_2 j}^{\text{ant}(j)} \in \mathbb{R}^{13\times 13}$, and $u_{\ell_3 k}^{\text{ant}(k)} \in \mathbb{R}^{7\times 7}$.

Next, as usual, we need to find which singular value vectors are coincident with the distinction between queens and workers. Figures 7.14a and b, 7.15a and b show singular value vectors associated with highest distinction between queens and workers. Unfortunately, singular value vectors of methylation do not exhibit small enough P-values to be significant. Nevertheless, because selected genes might exhibit significant distinct expression between queens and workers, we continue the procedure. We seek $G(\ell_1, 1, 3)$ for *P. canadensis* and $G(\ell_1, 1, 5)$ for *D. quadriceps* with larger absolute values.

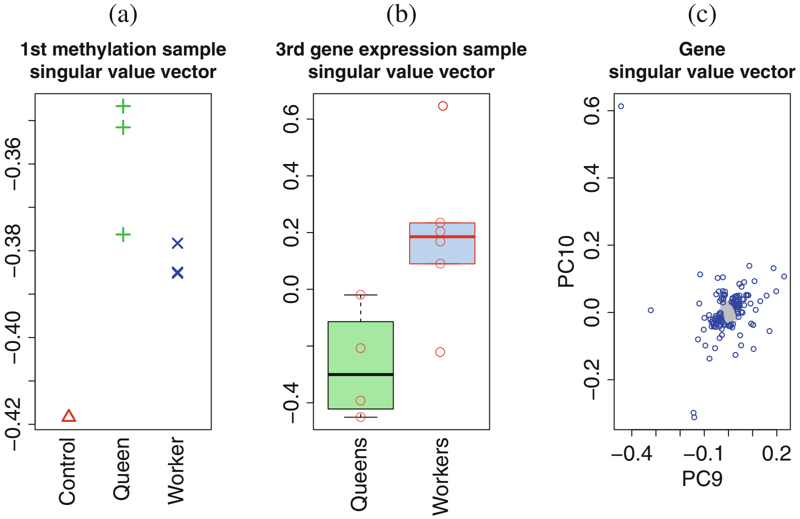

Fig. 7.14 Singular value vectors for *P. canadensis*. P-values are computed by t test between queens and workers. (**a**) $\boldsymbol{u}_1^{\text{bee}(k)}$, $P = 1.1 \times 10^{-1}$ (**b**) $\boldsymbol{u}_3^{\text{bee}(j)}$, $P = 1.65 \times 10^{-2}$ (**c**) $\boldsymbol{u}_{\ell_1}^{\text{bee}(i)}$, $\ell_1 = 9, 10$. Blue open circles are selected genes

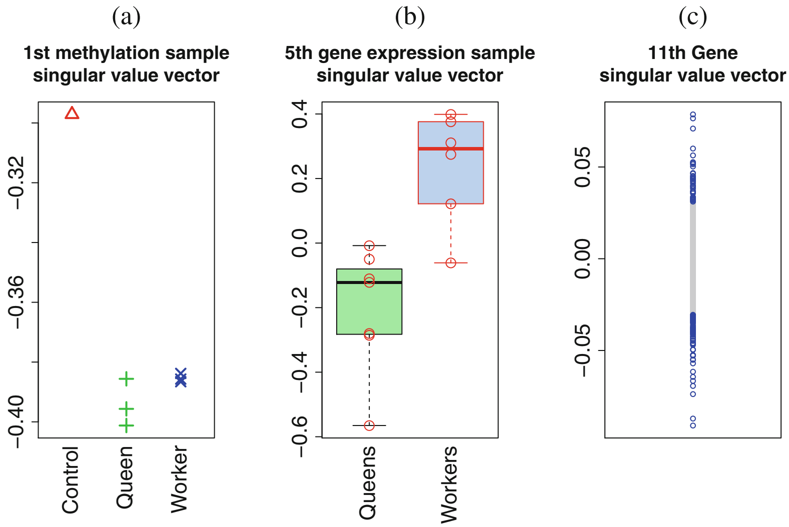

Fig. 7.15 Singular value vectors for *D. quadriceps*. P-values are computed by t test between queens and workers. (**a**) $\boldsymbol{u}_1^{\text{ant}(k)}$, $P = 1.9 \times 10^{-1}$ (**b**) $\boldsymbol{u}_5^{\text{ant}(j)}$, $P = 1.25 \times 10^{-3}$ (**c**) $\boldsymbol{u}_{11}^{\text{ant}(i)}$. Blue open circles are selected genes

Table 7.25 The top 10 core tensors, G, with large absolute values

P. canadensis		*D. quadriceps*	
ℓ_1	$G(\ell_1, 1, 3)$	ℓ_1	$G(\ell_1, 1, 5)$
9	−79.8	11	−54.8
10	75.4	12	4.1
7	−61.4	25	3.4
11	38.4	2	−2.9
5	−23.4	23	2.8
4	−16.0	9	2.4
12	−11.9	20	−2.2
1	−5.4	8	2.2
13	5.4	10	−1.7
6	−4.5	22	−1.4

Table 7.25 lists the top ranked Gs with larger absolute values. Then we decide that $\boldsymbol{u}_{\ell_1}^{\text{bee}(i)}$, $\ell_1 = 9, 10$ and $\boldsymbol{u}_{11}^{\text{ant}(i)}$ are used for FE (Figs. 7.14c and 7.15c). P-values are attributed to ith gene as

$$P_i^{\text{bee}} = P_{\chi^2}\left[> \sum_{\ell_1=9}^{10} \left(\frac{u_{\ell_1 i}^{\text{bee}(i)}}{\sigma_{\ell_1}} \right)^2 \right], \tag{7.42}$$

and

Table 7.26 Statistical tests of the differences (between queens and workers) in gene expression and methylation

		t	Wilcox	KS
P. canadensis	Gene expression	1.71×10^{-3}	1.89×10^{-2}	0.08
	Methylation	1.74×10^{-4}	5.06×10^{-3}	1.02×10^{-3}
D. quadriceps	Gene expression	2.73×10^{-12}	9.05×10^{-12}	4.41×10^{-11}
	Methylation	0.3757	0.7163	0.4413

The genes identified by TD-based unsupervised FE are analyzed by *t* (the *t* test), Wilcox (the Wilcoxon rank sum test), and KS (the Kolmogorov–Sinai test), all two-sided

$$P_i^{\text{ant}} = P_{\chi^2}\left[> \left(\frac{u_{11i}^{\text{ant}(i)}}{\sigma_{11}}\right)^2\right], \tag{7.43}$$

P-values are adjusted by BH criterion. Genes associated with adjusted P-values less than 0.01 are selected. As a result, 133 and 128 genes are selected for *P. canadensis* and *D. quadriceps*, respectively.

The point is if selected genes are associated with distinct gene expression and methylation between queens and workers simultaneously. Then we apply three statistical tests to 133 genes and 128 genes between queens and workers (Table 7.26). Selected genes exhibit simultaneous distinct gene expression and methylation between queens and workers for *P. canadensis*, but not for *D. quadriceps*. Thus selected genes can be potential factors that can mediate caste differentiation for *P. canadensis*, but not for *D. quadriceps*. Although we are not sure the lack of detection for *D. quadriceps* is because of biological reason or failure of our methodology, at least, our purpose is achieved for *P. canadensis*. In order to clarify this point, we need to continue research.

In order to see if conventional supervised methods can do this, we apply *t* test to gene expression and promoter methylation to find genes that exhibit significant distinction between queens and workers. As a result, two genes for distinct gene expression between queens and workers for *D. quadriceps* are associated with adjusted P-vales less than 0.01. This poor performance is because of small number of samples. Thus, TD based unsupervised FE has the ability to find significant genes for large p small n problem, for which conventional supervised method fails.

Before closing this section, we would like to validate selected genes from the biological point of view. Because these two insects are not included in popular enrichment servers, e.g. DAVID or Enrichr, instead we download list of GO terms,[1] PCAN.v01.GO.tsv for *P. canadensis* and DQUA.v01.GO.tsv for *D. quadriceps*. Fisher's exact test is performed in order to evaluate enrichment and computed P-values are corrected by BH criterion. GO terms associated with adjusted P-values less than 0.05 are searched. There are three GO terms, Lipid transporter activity

[1] Paper Wasp and Dinosaur Ant Project. Accessed 15 Jan. 2019. http://wasp.crg.eu/download.html.

(GO:0005319), Lipid particle (GO:0005811), and Lipid transport (GO:0006869) enriched in 133 genes selected for *P. canadensis*, while there are no GO terms enriched in 128 genes selected for *D. quadriceps*. This might be reasonable because 128 genes selected for *D. quadriceps* are not associated with distinct methylation between queens and workers (Table 7.26). Anyway, 133 genes selected for *P. canadensis*, which is simultaneously associated with distinct gene expression and methylation between queens and workers, are associated with a few GO term enrichment. Thus, at least for *P. canadensis*, TD based unsupervised FE is useful also from the biological point of view.

7.8 Drug Discovery From Gene Expression: II

In Sect. 7.3, we have already shown that TD based unsupervised FE successfully identifies compounds that affect gene expression in dose-dependent manner and their target proteins from only gene expression profiles in fully unsupervised manner. Nevertheless, it is strictly restricted to cancers because gene expression profiles are measured in cancer cell lines. The identifying drug compounds that are effective to other diseases requires additional gene expression profiles treated by compounds in specific diseases, e.g., model animals or cell lines originated from the disease. Thus in the manner in Sect. 7.3, the effectiveness of methods is quite limited.

In this section, with using case II tensor where genes are shared between two matrices or tensors, we try to identify disease effective drugs without measuring gene expression repeatedly for individual diseases. The study design is as follows (Fig. 7.16). $x_{ij_1j_2}$ is the ith gene expression profiles of animals treated by j_1 compound at the time point j_2 after the treatment. x_{ij_3} is the human gene expression profile of gene i at j_3th patients or healthy control. Case II tensor $x_{ij_1j_2j_3}$ is generated as

$$x_{ij_1j_2j_3} = x_{ij_1j_2}x_{ij_3} \tag{7.44}$$

HOSVD algorithm, Fig. 3.8, is applied to $x_{ij_1j_2j_3}$ as

$$x_{ij_1j_2j_3} = \sum_{\ell_1=1}^{N_1}\sum_{\ell_2=1}^{N_2}\sum_{\ell_3=1}^{N_3}\sum_{\ell_4=1}^{N_4} G(\ell_1,\ell_2,\ell_3,\ell_4)u_{\ell_1j_1}^{(j_1)}u_{\ell_2j_2}^{(j_2)}u_{\ell_3j_3}^{(j_3)}u_{\ell_4i}^{(i)} \tag{7.45}$$

Then, $\boldsymbol{u}_{\ell_2}^{(j_2)}$ that exhibits time dependence and $\boldsymbol{u}_{\ell_3}^{(j_3)}$ that exhibits distinction between healthy controls and patients are searched. After identifying ℓ_2 and ℓ_3, ℓ_1 and ℓ_4 associated with $G(\ell_1,\ell_2,\ell_3,\ell_4)$ with larger absolute values are selected. Once, ℓ_1 and ℓ_4 are selected, P-values are attributed to i and j_1 as

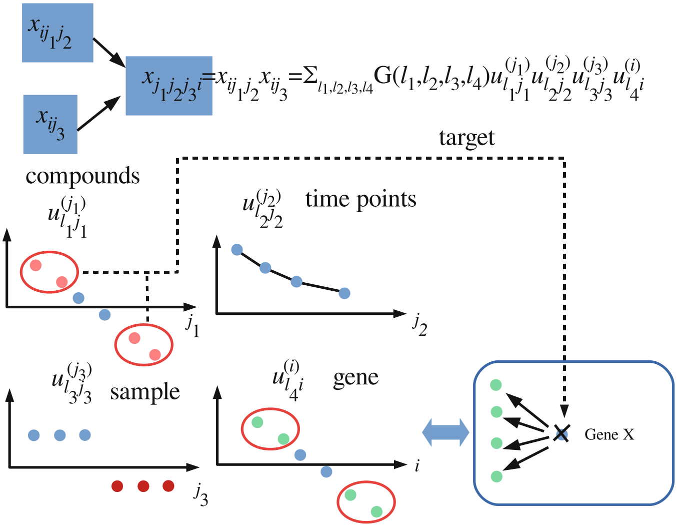
$x_{ij_1j_2}$
x_{ij_3}
$x_{j_1j_2j_3i}=x_{ij_1j_2}x_{ij_3}=\Sigma_{l_1,l_2,l_3,l_4}G(l_1,l_2,l_3,l_4)u^{(j_1)}_{l_1j_1}u^{(j_2)}_{l_2j_2}u^{(j_3)}_{l_3j_3}u^{(i)}_{l_4i}$
target
compounds
$u^{(j_1)}_{l_1j_1}$
j_1
$u^{(j_2)}_{l_2j_2}$ time points
j_2
$u^{(j_3)}_{l_3j_3}$ sample
j_3
$u^{(i)}_{l_4i}$ gene
i
Gene X

Fig. 7.16 Integrated analysis of gene expression profile of drug treated animals, $x_{ij_1j_2}$ and human gene expression profiles of patients and healthy control, x_{ij_3}. i: genes, j_1: compounds, j_2: time point after the treatment, j_3: human samples

$$P_i = P_{\chi^2}\left[> \left(\frac{u_{\ell_4 i}}{\sigma_{\ell_4}}\right)^2\right], \tag{7.46}$$

and

$$P_{j_1} = P_{\chi^2}\left[> \left(\frac{u_{\ell_1 j_1}}{\sigma_{\ell_1}}\right)^2\right]. \tag{7.47}$$

P-values are corrected by BH criterion and i and j_1 associated with adjusted P-values less than 0.01 (filled pink circles and filled light green circles surrounded by pink oval in Fig. 7.16) are supposed to be selected. Target proteins are decided by the comparison with external databases (as shown in Fig. 7.5). This process results in the set of drug candidates compounds and candidate target proteins. Figure 7.17 and Table 7.27 summarize the process till selection of singular value vectors attributed to genes and compounds. There are six diseases analyzed: heart failure, PTSD, acute lymphoblastic leukemia (ALL), diabetes, renal carcinoma, and cirrhosis. In some cases, modes of case II tensors are more than four because human gene expression profiles are represented as not matrices but tensors.

Gene expression profiles of model animals are downloaded from DrugMatrix [15] where rats are treated as model animals and gene expression profiles of various tissues are extracted. Corresponding human or rat disease expression profiles are downloaded from GEO. For heart failure, human disease heart failure

Table 7.27 A summary of TDs and identification of various singular value vectors for identification of candidate drugs and genes used to find genes encoding drug target proteins

	Tensors				
Diseases	DrugMatrix	Disease	Generated	Core tensor	Singular value vectors
Heart failure	$x_{ij_1j_2}$ $\in \mathbb{R}^{N_4 \times N_1 \times N_2}$	x_{ij_3} $\in \mathbb{R}^{N_4 \times N_3}$	$x_{ij_1j_2j_3}$ $\in \mathbb{R}^{N_4 \times N_1 \times N_2 \times N_3}$	$G(\ell_1\ell_2\ell_3\ell_4)$ $\in \mathbb{R}^{N_1 \times N_2 \times N_3 \times N_4}$	$u^{(j_k)}_{\ell_k, j_k}, k \le 3, u^{(i)}_{\ell_4, i} \in \mathbb{R}^{N_k \times N_k}$ $(N_1, N_2, N_3, N_4) = (218, 4, 313, 3937)$
Selected				$\ell_1 = 2; \ell_2 = 2; \ell_3 = 2, 3; \ell_4 = 21, 25, 27, 28, 33, 36, 37, 41, 42, 48$	
PTSD rat model	$x_{ij_1j_2}$ $\in \mathbb{R}^{N_6 \times N_1 \times N_2}$	$x_{ij_3j_k}, k = 4, 5$ $\in \mathbb{R}^{N_6 \times N_3 \times N_k}$	$x_{ij_1j_2j_3j_4j_5}$ $\in \mathbb{R}^{N_6 \times N_1 \times N_2 \times N_3 \times N_4 \times N_5}$	$G(\ell_1\ell_2\ell_3\ell_4\ell_5\ell_6)$ $\in \mathbb{R}^{N_1 \times N_2 \times N_3 \times N_4 \times N_5 \times N_6}$	$u^{(j_k)}_{\ell_k, j_k}, k \le 5, u^{(i)}_{\ell_6, i} \in \mathbb{R}^{N_k \times N_k}$ $(N_1, N_2, N_3, N_4, N_5, N_6) = (22, 4, 2, 15, 15, 7501)$
Selected				$\ell_1 = 2; \ell_2 = 2; \ell_3 = 1; \ell_4 = \ell_5 = 3; \ell_6 = 75, 77, 81, 83, 84, 85, 89, 90, 102$	
ALL	$x_{ij_1j_2}$ $\in \mathbb{R}^{N_5 \times N_1 \times N_2}$	$x_{ij_3j_4}$ $\in \mathbb{R}^{N_5 \times N_3 \times N_4}$	$x_{ij_1j_2j_3j_4}$ $\in \mathbb{R}^{N_5 \times N_1 \times N_2 \times N_3 \times N_4}$	$G(\ell_1\ell_2\ell_3\ell_4\ell_5)$ $\in \mathbb{R}^{N_1 \times N_2 \times N_3 \times N_4 \times N_5}$	$u^{(j_k)}_{\ell_k, j_k}, k \le 4, u^{(i)}_{\ell_5, i} \in \mathbb{R}^{N_k \times N_k}$ $(N_1, N_2, N_3, N_4, N_5) = (77, 4, 4, 74, 2597)$
Selected				$\ell_1 = 2, 3, 5, 6, 9, 10; \ell_2 = 3; \ell_3 = 4; \ell_5 = 1, 2, 3, 5$	
Diabetes	$x_{ij_1j_2}$ $\in \mathbb{R}^{N_4 \times N_1 \times N_2}$	x_{ij_3} $\in \mathbb{R}^{N_4 \times N_3}$	$x_{ij_1j_2j_3}$ $\in \mathbb{R}^{N_4 \times N_1 \times N_2 \times N_3}$	$G(\ell_1\ell_2\ell_3\ell_4)$ $\in \mathbb{R}^{N_1 \times N_2 \times N_3 \times N_4}$	$u^{(j_k)}_{\ell_k, j_k}, k \le 3, u^{(i)}_{\ell_4, i} \in \mathbb{R}^{N_k \times N_k}$ $(N_1, N_2, N_3, N_4) = (253, 4, 69, 3489)$
Selected				$\ell_1 = 2; \ell_2 = 2; \ell_3 = 1, 4; \ell_4 = 1, 4$	
Renal carcinoma	$x_{ij_1j_2}$ $\in \mathbb{R}^{N_4 \times N_1 \times N_2}$	x_{ij_3} $\in \mathbb{R}^{N_4 \times N_3}$	$x_{ij_1j_2j_3}$ $\in \mathbb{R}^{N_4 \times N_1 \times N_2 \times N_3}$	$G(\ell_1\ell_2\ell_3\ell_4)$ $\in \mathbb{R}^{N_1 \times N_2 \times N_3 \times N_4}$	$u^{(j_k)}_{\ell_k, j_k}, k \le 3, u^{(i)}_{\ell_4, i} \in \mathbb{R}^{N_k \times N_k}$ $(N_1, N_2, N_3, N_4) = (253, 4, 202, 4036)$
Selected			$\ell_1 = 2; \ell_2 = 2; \ell_3 = 13, 15, 30, 33, 35; \ell_4 = 186, 215, 233, 244, 251, 269, 274, 309, 312, 318$		
Cirrhosis	$x_{ij_1j_2}$ $\in \mathbb{R}^{N_4 \times N_1 \times N_2}$	x_{ij_3} $\in \mathbb{R}^{N_4 \times N_3}$	$x_{ij_1j_2j_3}$ $\in \mathbb{R}^{N_4 \times N_1 \times N_2 \times N_3}$	$G(\ell_1\ell_2\ell_3\ell_4)$ $\in \mathbb{R}^{N_1 \times N_2 \times N_3 \times N_4}$	$u^{(j_k)}_{\ell_k, j_k}, k \le 3, u^{(i)}_{\ell_4, i} \in \mathbb{R}^{N_k \times N_k}$ $(N_1, N_2, N_3, N_4) = (355, 4, 216, 3961)$
Selected				$\ell_1 = 2; \ell_2 = 2; \ell_3 = 2, 6; 2 \le \ell_4 \le 10$	

In all cases, ℓ_1 stands for singular value vectors of compounds, whereas ℓ_k with the last (largest) k denotes gene singular value vectors. ℓ_2 stands for singular value vectors of time points in DrugMatrix data. The remaining singular value vectors correspond to sample singular value vectors depending on the properties of gene expression profiles of diseases. See also Fig. 7.17 for the corresponding data

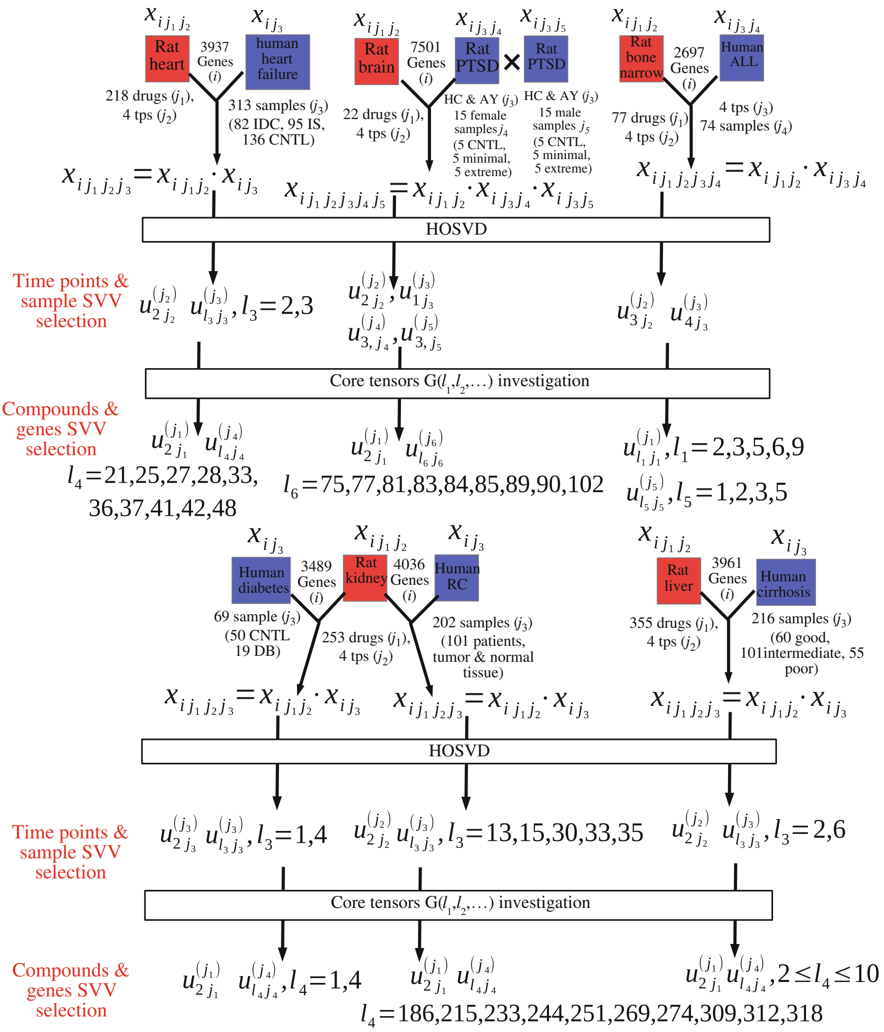
$x_{ij_1j_2}$
Rat heart
3937 Genes (i)
x_{ij_3}
human heart failure
218 drugs (j_1), 4 tps (j_2)
313 samples (j_3) (82 IDC, 95 IS, 136 CNTL)
$x_{ij_1j_2j_3}=x_{ij_1j_2}\cdot x_{ij_3}$
$x_{ij_1j_2}$
Rat brain
7501 Genes (i)
$x_{ij_3j_4}$
Rat PTSD
×
$x_{ij_3j_5}$
Rat PTSD
22 drugs (j_1), 4 tps (j_2)
HC & AY (j_3) 15 female samples j_4 (5 CNTL, 5 minimal, 5 extreme)
HC & AY (j_3) 15 male samples j_5 (5 CNTL, 5 minimal, 5 extreme)
$x_{ij_1j_2j_3j_4j_5}=x_{ij_1j_2}\cdot x_{ij_3j_4}\cdot x_{ij_3j_5}$
$x_{ij_1j_2}$
Rat bone narrow
2697 Genes (i)
$x_{ij_3j_4}$
Human ALL
77 drugs (j_1) 4 tps (j_2)
4 tps (j_3) 74 samples (j_4)
$x_{ij_1j_2j_3j_4}=x_{ij_1j_2}\cdot x_{ij_3j_4}$
HOSVD
Time points & sample SVV selection
$u^{(j_2)}_{2j_2}\ u^{(j_3)}_{l_3j_3}, l_3=2,3$
$u^{(j_2)}_{2j_2}, u^{(j_3)}_{1j_3}$
$u^{(j_4)}_{3,j_4}, u^{(j_5)}_{3,j_5}$
$u^{(j_2)}_{3j_2}\ u^{(j_3)}_{4j_3}$
Core tensors G(l_1,l_2,…) investigation
Compounds & genes SVV selection
$u^{(j_1)}_{2j_1}\ u^{(j_4)}_{l_4j_4}$
l_4=21,25,27,28,33, 36,37,41,42,48
$u^{(j_1)}_{2j_1}\ u^{(j_6)}_{l_6j_6}$
l_6=75,77,81,83,84,85,89,90,102
$u^{(j_1)}_{l_1j_1}, l_1=2,3,5,6,9$
$u^{(j_5)}_{l_5j_5}, l_5=1,2,3,5$
x_{ij_3}
Human diabetes
3489 Genes (i)
$x_{ij_1j_2}$
Rat kidney
4036 Genes (i)
x_{ij_3}
Human RC
69 sample (j_3) (50 CNTL 19 DB)
253 drugs (j_1), 4 tps (j_2)
202 samples (j_3) (101 patients, tumor & normal tissue)
$x_{ij_1j_2j_3}=x_{ij_1j_2}\cdot x_{ij_3}$
$x_{ij_1j_2j_3}=x_{ij_1j_2}\cdot x_{ij_3}$
$x_{ij_1j_2}$
Rat liver
3961 Genes (i)
x_{ij_3}
Human cirrhosis
355 drugs (j_1), 4 tps (j_2)
216 samples (j_3) (60 good, 101intermediate, 55 poor)
$x_{ij_1j_2j_3}=x_{ij_1j_2}\cdot x_{ij_3}$
HOSVD
Time points & sample SVV selection
$u^{(j_3)}_{2j_3}\ u^{(j_3)}_{l_3j_3}, l_3=1,4$
$u^{(j_2)}_{2j_2}\ u^{(j_3)}_{l_3j_3}, l_3=13,15,30,33,35$
$u^{(j_2)}_{2j_2}\ u^{(j_3)}_{l_3j_3}, l_3=2,6$
Core tensors G(l_1,l_2,…) investigation
Compounds & genes SVV selection
$u^{(j_1)}_{2j_1}\ u^{(j_4)}_{l_4j_4}, l_4=1,4$
$u^{(j_1)}_{2j_1}\ u^{(j_4)}_{l_4j_4}$
l_4=186,215,233,244,251,269,274,309,312,318
$u^{(j_1)}_{2j_1}u^{(j_4)}_{l_4j_4}, 2\le l_4\le 10$

Fig. 7.17 Schematics that illustrate the procedure of TD-based unsupervised FE applied to the various disease and DrugMatrix data sets. SVV: singular value vector. Selected four time points (tps) are 1/4, 1, 3, and 5 days after treatment

gene expression profiles and rat heart gene expression profiles treated by drugs are used. For PTSD, stressed mouse brain gene expression profiles and rat brain gene expression profiles treated by drugs are used. For ALL, drug treated rat and ALL human patients bone marrow gene expression profiles are used. For diabetes and renal carcinoma, drug treated rat kidney gene expression profiles are used. Diabetes and renal carcinoma human patients kidney gene expression profiles are used for diabetes and renal carcinoma, respectively. For cirrhosis, drug treated rat

Table 7.28 The number of genes, drugs, and target proteins identified by TD based unsupervised FE

			Predicted target	
Disease	Inferred genes	Inferred compounds	Up	Down
Heart failure	274	43	556	449
PTSD	374	6	578	548
ALL	24	2	91	57
Diabetes	65	14	186	140
Renal carcinoma	225	14	229	177
Cirrhosis	132	27	510	488

liver gene expression profiles and cirrhosis human liver expression profiles are used. See appendix for more details.

After selecting genes and drugs, genes are uploaded to Enrichr for target protein identification. Genes enriched (adjusted P-values less than 0.01) in “Single gene perturbation GEO up” and “Single gene perturbation GEO down” are selected as target proteins. This process is similar to that illustrated in Fig. 7.5. Table 7.28 summarizes the number of identified genes, compounds, and target proteins.

In order to validate the relationship between drugs and target proteins predicted, we compare them with DINIES [31] that stores known protein–drug interactions. We upload drugs one by one to DENIES with parameters “chemogenomic approach” and “with learning on all DBs” and can get list of target proteins. They are merged into a list of proteins because individual proteins can be targeted by multiple drugs. The obtained set of target proteins are compared with predicted targets in Table 7.28. Here total proteins considered is limited to genes included in “Single_Gene_Perturbations_from_GEO_all_list” of Enrichr. Table 7.29 shows the results of evaluation by Fisher’s exact test and χ^2 test. Ten out of twelve are evaluated as significant (P-values less than 0.05) by either Fisher’s exact test or χ^2 test. This suggests that TD based unsupervised FE can be used for the prediction of target protein and diseases of drugs only from gene expression profile, in fully unsupervised manner in the sense that it does not require any pre-knowledge about disease–drug or protein–drug interaction.

7.9 Integrated Analysis of miRNA Expression and Methylation

Unsupervised method is often useful when applied to something for which no pre-knowledge is available. For example, two kinds of omics data might be correlated with unknown reasons. To search this kind of hidden (latent) relationship, unsupervised method is critically useful. In this section, we propose the application

Table 7.29 Fisher's exact test (P_F) and the uncorrected χ^2 test (P_{χ^2}) of known drug target proteins regarding the inference of the present study

		Single gene perturbations from GEO up					Single gene perturbations from GEO down				
		F	T	P_F	P_{χ^2}	RO	F	T	P_F	P_{χ^2}	RO
Heart failure	F	521	517	3.4×10^{-4}	3.9×10^{-4}	3.02	628	416	1.3×10^{-3}	7.3×10^{-4}	2.61
	T	13	39				19	33			
PTSD	F	500	560	3.8×10^{-2}	3.1×10^{-2}	2.67	532	529	6.1×10^{-3}	4.5×10^{-3}	3.81
	T	6	18				5	19			
ALL	F	979	89	2.7×10^{-1}	3.0×10^{-1}	2.19	1009	57	1.0×10^{0}	–	–
	T	10	2				12	0			
Diabetes	F	889	177	1.2×10^{-2}	7.1×10^{-3}	3.00	936	130	3.6×10^{-4}	2.0×10^{-5}	5.13
	T	15	9				14	10			
Renal carcinoma	F	847	219	2.0×10^{-2}	1.2×10^{-2}	2.75	895	169	4.3×10^{-2}	2.2×10^{-2}	2.64
	T	14	10				16	8			
Cirrhosis	F	572	490	1.1×10^{-2}	8.1×10^{-3}	2.91	595	467	1.6×10^{-3}	1.1×10^{-3}	3.81
	T	8	20				7	21			

Rows: known drug target proteins (DINIES). Columns: Inferred drug target proteins using "Single Gene Perturbations from GEO up" or "Single Gene Perturbations from GEO down." OR: odds ratio

of case I type II tensor to investigate relationship between miRNA expression and methylation, between which no direct relationships are biologically expected.

Promoter methylation of genes targeted by miRNAs can of course affect expression of these genes. Nevertheless, there seem to be no biological reasons that promoter methylation of genes targeted by miRNAs affects the expression of these miRNAs themselves or vice versa. Thus, if we can find any correlations between these two, it might be a starting point of finding new biological points of view.

In this section, we make use of TCGA data set [28]. The data set we analyze is composed of eight normal ovarian tissue samples and 569 tumor samples. Our data set includes expression data on 723 miRNAs as well as promoter methylation profiles of 24,906 genes. They are formatted as matrices

$$x_{ij}^{\text{methyl}} \in \mathbb{R}^{24906 \times 577} \tag{7.48}$$

$$x_{kj}^{\text{miRNA}} \in \mathbb{R}^{723 \times 577} \tag{7.49}$$

They are converted to case I tensor because they share samples as

$$x_{ijk} = x_{kj}^{\text{miRNA}} x_{ij}^{\text{methyl}} \tag{7.50}$$

Usually, HOSVD, Fig. 3.8, is supposed to be applied to x_{ijk} as

$$x_{ijk} = \sum_{\ell_1=1}^{24906} \sum_{\ell_2=1}^{577} \sum_{\ell_3=1}^{723} G(\ell_1, \ell_2, \ell_3) u^{(i)}_{\ell_1 i} u^{(j)}_{\ell_2 j} u^{(k)}_{\ell_3 k}. \tag{7.51}$$

Unfortunately, x_{ijk} is too huge to apply HOSVD directly. Thus, instead, we derive type II tensor as

$$x_{ik} = \sum_{j=1}^{577} x_{ijk}. \tag{7.52}$$

Now it is a matrix. Thus we can apply PCA to it. Then we can have PC score $\boldsymbol{u}_\ell \in \mathbb{R}^{723}$ attributed to miRNA and PC loading $\boldsymbol{v}_\ell \in \mathbb{R}^{24906}$ attributed to methylation. The singular value vectors attributed to sample j are computed in two ways as Eq. (5.15)

$$u^{(j;k)}_{\ell j} = \sum_k u_{\ell k} x^{\text{miRNA}}_{kj}, \tag{7.53}$$

$$u^{(j;i)}_{\ell j} = \sum_i v_{\ell i} x^{\text{methyl}}_{ij}. \tag{7.54}$$

The first thing to check is if there are any ℓs such that $\boldsymbol{u}^{(j;k)}_\ell \in \mathbb{R}^{577}$ and $\boldsymbol{u}^{(j;i)}_\ell \in \mathbb{R}^{577}$ satisfy the following requirements simultaneously;

- $\boldsymbol{u}^{(j;i)}_\ell$ and $\boldsymbol{u}^{(j;k)}_\ell$ are significantly correlated.
- $\boldsymbol{u}^{(j;k)}_\ell$ is expressed distinctly between healthy controls ($j \leq 8$) and patients ($j > 8$).
- $\boldsymbol{u}^{(j;i)}_\ell$ is expressed distinctly between healthy controls ($j \leq 8$) and patients ($j > 8$).

In order to validate these requirements visually, we show scatterplot for $1 \leq \ell \leq 9$ (Fig. 7.18). More or less all nine scatterplots look like satisfying the above requirements simultaneously. In order to select $\boldsymbol{u}_\ell$ and $\boldsymbol{v}_\ell$ used for miRNA and gene selection, respectively, we need to identify which ℓ satisfies the above requirements best. In order that, we propose several measures. First, we select miRNAs and genes. P-values are attributed as

$$P_k = P_{\chi^2}\left[> \left(\frac{u_{\ell k}}{\sigma_\ell}\right)^2\right], \tag{7.55}$$

$$P_i = P_{\chi^2}\left[> \left(\frac{v_{\ell i}}{\sigma'_\ell}\right)^2\right]. \tag{7.56}$$

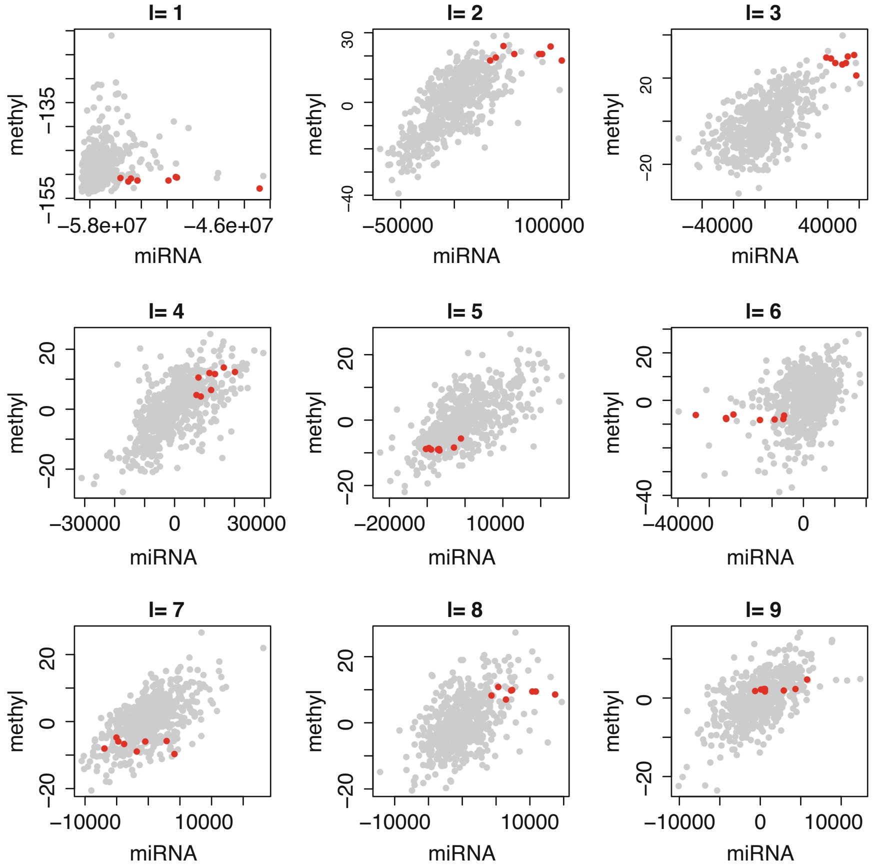

Fig. 7.18 Scatterplots of $\boldsymbol{u}_\ell^{(j;k)}$ (horizontal) and $\boldsymbol{u}_\ell^{(j;i)}$ (vertical) for $1 \le \ell \le 9$. Red filled circle: eight normal controls ($j \le 8$), gray filled circles: ovarian cancer patients ($j > 8$)

P-values are adjusted by BH criterion and i and k associated with adjusted P-values less than 0.01 are selected. Then we require genes and miRNA selected similar to the above requirements as

- Selected genes and miRNAs are significantly correlated.
- Selected miRNAs are expressed distinctly between normal controls ($j \le 8$) and patients ($j > 8$).
- Selected genes are methylated distinctly between normal controls ($j \le 8$) and patients ($j > 8$).

In order that, we compute the followings:

(a) Correlation coefficient between $\boldsymbol{u}_\ell^{(j;i)}$ and $\boldsymbol{u}_\ell^{(j;k)}$.
(b) P-value attributed to the above correlation coefficients.

(c) P-values computed by t test that evaluates if $\boldsymbol{u}_\ell^{(j;k)}$ is distinct between normal control ($j \leq 8$) and patients ($j > 8$).
(d) P-values computed by t test that evaluates if $\boldsymbol{u}_\ell^{(j;i)}$ is distinct between normal control ($j \leq 8$) and patients ($j > 8$).
(e) Ratio of significantly correlated pairs of genes and miRNAs selected.
(f) Ratio of miRNA associated with adjusted P-values computed by t test that evaluates if selected miRNAs are expressed distinctly between normal control ($j \leq 8$) and patients ($j > 8$).
(g) Ratio of genes associated with adjusted P-values computed by t test that evaluates if selected genes are methylated distinctly between normal control ($j \leq 8$) and patients ($j > 8$).
(h) The number of selected miRNAs.
(i) The number of selected genes.

Here significant correlation is evaluated if associated BH criterion adjusted P-values are less than 0.01 (see page 112 for how to compute P-values attributed to correlation coefficients). Table 7.30 shows the result. $\ell = 3$ seems to be the best, because $\ell = 3$ is the best for the sixth and the seventh measures and the second best in the fifth measure; the fifth, sixth, and seventh measures are important because they are direct evaluations of selected genes and miRNAs. Because the number of selected genes and miRNAs do not vary depending on ℓ so much, it is the best to select $\ell = 3$. Because more than 88% of genes and miRNAs and their pairs satisfy the desired requirements in the above (88% is the smallest ratio (percentage) among requirements from (e) to (g) in Table 7.30), TD based unsupervised FE can be considered to have ability to select miRNAs and genes satisfying desired requirements mentioned above.

In order to see if other supervised methods can identify set of genes and miRNAs satisfying desired requirements, i.e., selected genes are methylated distinctly between healthy control and patients, miRNAs selected are expressed distinctly between healthy controls and patients, selected genes and miRNAs are significantly correlated, we apply t test to select genes methylated distinctly between healthy

Table 7.30 Measures that evaluate which ℓ satisfies the desired requirements best

ℓ	(a)	(b)	(c)	(d)	(e)	(f)	(g)	(h)	(i)
1	0.187	6.35×10^{-6}	6.25×10^{-3}	4.42×10^{-7}	–	**1.000**	–	2	0
2	**0.718**	$\mathbf{1.95 \times 10^{-92}}$	1.28×10^{-4}	1.21×10^{-11}	**0.944**	0.571	0.834	7	241
3	0.628	1.49×10^{-64}	$\mathbf{3.06 \times 10^{-8}}$	5.55×10^{-10}	0.884	**1.000**	**0.905**	7	284
4	0.649	2.45×10^{-70}	6.15×10^{-5}	1.02×10^{-4}	0.539	0.714	0.597	7	273
6	0.348	6.76×10^{-18}	1.68×10^{-3}	$\mathbf{5.71 \times 10^{-17}}$	0.350	0.375	0.674	8	132
7	0.624	1.27×10^{-63}	2.00×10^{-1}	7.65×10^{-7}	0.365	0.400	0.758	5	293
8	0.500	8.60×10^{-38}	1.33×10^{-4}	5.89×10^{-13}	0.274	0.833	0.775	6	231
9	0.593	3.50×10^{-56}	6.44×10^{-2}	3.35×10^{-5}	0.182	0.667	0.681	3	251

The number in the first row corresponds to the alphabetical list in the main text
Bold numbers are the best values within each category

controls and patients and miRNA expressed distinctly between healthy controls and patients. P-values are attributed to miRNAs and genes and adjusted by BH criterion. Then, 214 miRNAs and 19,395 genes associated with adjusted P-values less than 0.01 are selected. In order to see how much ratio of significantly correlated pairs among total $241 \times 19395 = 4{,}829{,}355$ pairs is, we compute correlation coefficients between them and attribute P-values to these pairs (see page 112 for how to compute P-values attributed to correlation coefficients). P-values are corrected by BH criterion and 555,391 pairs are associated with adjusted P-values less than 0.01. Because this is as small as 11.5% of 4829,355 pairs, t test is inferior to TD based unsupervised FE to identify genes and miRNAs satisfying desired requirements.

This poor performance might be because of the too many genes and miRNAs selected. P-values given by t test have strong tendency to reduce its value when many samples are available. In this example, because as many as 575 samples are available, even gene and miRNAs associated with small distinction are associated with small enough P-values. In order to avoid this difficulty, we reduce the number of genes and miRNAs selected by t test as many as those by TD based unsupervised FE, by selecting to ranked seven miRNA and 284 methylation probes attributed to genes based upon P-values computed by t test. Then among $7 \times 284 = 1967$ pairs, as small as 50 pairs are associated with adjusted P-values less than 0.01 attributed to correlation coefficient. Thus, only 2.5% of 1967 pairs are significantly correlated. Thus, the ratio decreases instead of increasing in opposed to the expectation.

It might be possible to select genes and miRNAs starting from identifying significantly correlated pairs before finding genes and miRNAs distinct between healthy control and patients. Then correlation coefficients are computed among all pairs of genes and miRNAs. P-values are attributed to correlation coefficient (see page 112 for how to compute P-values attributed to correlation coefficients) and are corrected by BH criterion. Then among $24{,}906 \times 723 = 18{,}007{,}038$ pairs, 1,197,772 pairs are associated with adjusted P-values less than 0.01. Unfortunately, these pairs include all genes and miRNAs. Thus, starting from pairs significantly correlated is not an effective strategy. This poor performance achieved by t test as well as correlation analysis demonstrates the difficulty of identifying gene and miRNAs satisfying desired requirement, i.e., selected genes are methylated distinctly between healthy control and patients, miRNAs selected are expressed distinctly between healthy controls and patients, selected genes and miRNAs are significantly correlated, which is easily achieved by TD based unsupervised FE.

Before closing this section, genes and miRNA selected should be biologically evaluated, too. First, 240 gene symbols associated with 284 probes are uploaded to DAVID (Table 7.31). At a glance, although it does not look deeply related to cancers, detailed investigation can alter this impression. This data is about ovarian cancer. The most major subtype is surface epithelial-stromal tumor which is known to be associated with keratinization [13]. Thus, the detection of keratinization as the most enriched term is reasonable, while the third enriched one is also related to keratinization. Because the fifth one, epidermis development, is the parent term of keratinization, it is also understandable.

Table 7.31 GO BP enrichment by the 274 gene symbols identified by TD based unsupervised FE for ovarian cancer data from TCGA

Category	Term	Genes count	%	P-value	Adjusted P-value
GOTERM_BP_DIRECT	Keratinization	14	6.2	9.3E−15	1.1E−11
GOTERM_BP_DIRECT	Peptide cross-linking	14	6.2	1.7E−14	9.6E−12
GOTERM_BP_DIRECT	Keratinocyte differentiation	15	6.6	2.8E−13	1.1E−10
GOTERM_BP_DIRECT	Acute-phase response	7	3.1	6.4E−6	1.8E−3
GOTERM_BP_DIRECT	Epidermis development	9	4.0	8.0E−6	1.8E−3

Adjusted P-values are by BH criterion

Next, the selected seven miRNAs are uploaded to DIANA-mirpath for the evaluation (Fig. 7.19). It is obvious that they are enriched with various cancers. Thus, the selected seven miRNAs are supposed to be related to cancers.

In conclusion, TD based unsupervised FE successfully identifies reasonable genes and miRNAs also from the biological point of view.

7.10 Summary

Because TD based unsupervised FE was more recently proposed than PCA based unsupervised FE, the examples of applications of TD based unsupervised FE introduced in this chapter are very limited. In spite of that, it still covers wide range of applications tried in the previous chapter using PCA based unsupervised FE: analysis of time course data set, integrated analysis of multi-omics data set, and identification of disease causing genes. In addition to this, it has new application target, e.g., application to in silico drug discovery.

The general procedure of application of TD based unsupervised FE is as follows. If there are no tensors available, generate case I or case II tensor of type I. Occasionally, it might be requires to generate type II tensor in order to reduce the required computational memory. If generated type II tensor is matrix, apply PCA. If not, apply HOSVD. If type II tensor is employed, generate missing singular value vectors by multiplying original tensor to obtained singular value vectors. Seek singular value vectors attributed to samples coincident with desired property, e.g., distinction between controls and treated samples. Then, in order to select singular value vectors attributed to features used for FE, core tensor is investigated. Singular value vectors that share core tensor with larger absolute values with singular value vectors attributed to samples associated with desired properties are selected. P-values are attributed to features using selected singular value vectors attributed to features with assuming χ^2 distributions. P-values are corrected by BH criterion and features associated with adjusted P-values less than 0.01.

This general procedure can be applied to wide range of bioinformatics topics depending upon what kind of singular value vectors attributed to samples are selected. In this sense, TD based unsupervised FE is expected to be applicable to wider range of biological problems other than those treated in this chapter.

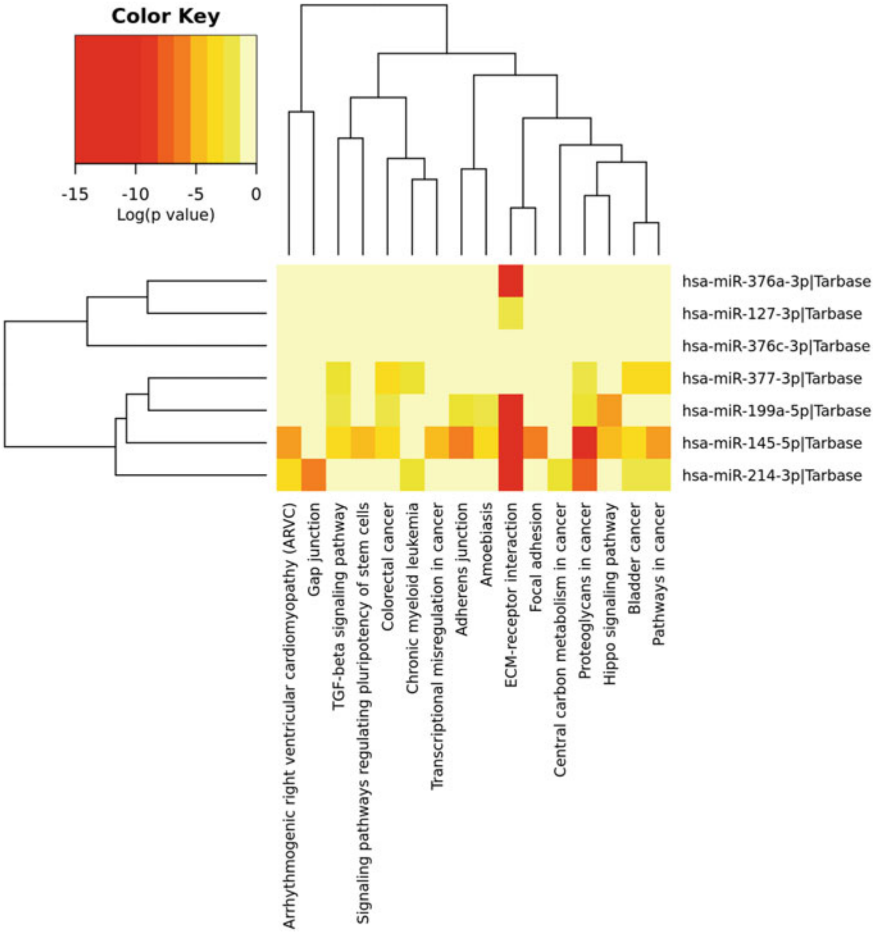

Fig. 7.19 Heatmap that summarize the results of DIANA-mirpath for the selected seven miRNAs, with specifying "pathways union" option

Appendix

Universarity of miRNA Transfection

Study 1

This data set includes transfection of three miRNAs, miR-200a, 200b, and 200c. The number of probes in microarray is as many as 43,376. For each of three, two paired experiments of treated and control samples. Treated and control sample measurement is performed by one microarray. Thus these two must be retrieved from it (columns annotated as gProcessedSignal and rProcessedSignal). Then, it is possible to make a tensor, $x_{ij_1j_2j_3} \in \mathbb{R}^{43376\times3\times2\times2}$ where i stands for probes, j_1 stands for miRNAs, j_2 stands for two replicates, and j_3 stands for control vs treated samples. Nevertheless, it is not suitable for this specific case. If the number of components is two, automatically the two components of singular value vectors are $u_j = u_{j'}$ and $u_j = -u_{j'}$ where j and j' are each of two categories. The present purpose is to see if the components independent of category exist. This means, the setup that always results in the components independent of category is not good. Therefore, in this specific case, we format mRNA expression profiles as $x_{ij} \in \mathbb{R}^{43,376\times12}$ where $1 \leq j \leq 6$ and $7 \leq j \leq 12$ are control and treated samples, respectively. PCA is applied to x_{ij} such that PC score, $\boldsymbol{u}_\ell \in \mathbb{R}^{43376}$, and PC loading, $\boldsymbol{v}_\ell \in \mathbb{R}^{12}$, are attributed to probes and samples, respectively. As a result, we find that $\boldsymbol{v}_2$ represents distinct expression between control and treated samples, but independent of miRNAs transfected (Fig. 7.20). This suggests that there are non-negligible number of mRNAs affected by sequence-nonspecific off-target regulation. P-values are attributed to probes using the second PC score $\boldsymbol{u}_2$ with assuming χ^2 distribution as

$$P_i = P_{\chi^2}\left[> \left(\frac{u_{2i}}{\sigma_2}\right)^2\right]. \tag{7.57}$$

P-values are corrected by BH criterion and probes associated with adjusted P-values less than 0.01 are selected.

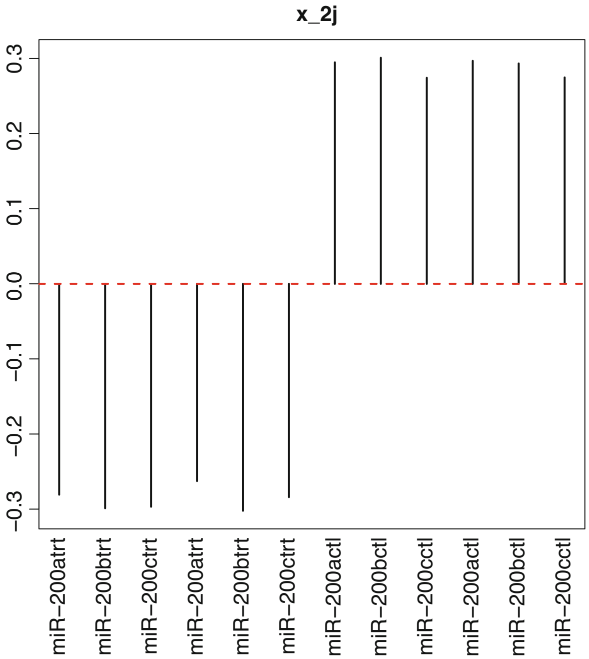

Fig. 7.20 The second PC loading, $\boldsymbol{v}_2$, obtained by PCA applied to x_{ij} made out of study 1

Study 2

This data set includes two miR-7 transfection experiments, two miR-128 transfection experiments, and three control experiments, normalized by mas5 procedure [17]. As mentioned in the beginning of the previous chapter, microarray technology measures photo emission of hybridized probes. Thus, various normalization procedures are applied. mas5 is one of such popular procedures, although I do not intend to explain mas5 in more detail, because it is beyond the scope of this textbook. Because of unmatched number of experiments of treated and control samples, they are difficult to be formatted in tensor. Thus it is instead formatted as matrix, $x_{ij} \in \mathbb{R}^{54675 \times 7}$, where $j = 1, 2$ corresponds to miR-7 transfection $j = 3, 4$ corresponds to miR-128 transfection and $5 \leq j \leq 7$ correspond to control samples. PCA is applied to x_{ij} such that PC score, $\boldsymbol{u}_\ell \in \mathbb{R}^{54675}$, and PC loading, $\boldsymbol{v}_\ell \in \mathbb{R}^7$, are attributed to probes and samples, respectively. The result is a bit disappointing. In contrast to Fig. 7.20, we cannot find any PC loading that is constant independent of miRNAs transfected. Figure 7.21 shows the second PC loading, $\boldsymbol{v}_2$, which exhibits opposite signs between miR-7 transfection and miR-128 transfection. In spite of that, Fig. 7.21 still suggests the possibility of sequence-nonspecific off-target regulation. As mentioned previously, the only canonical function of miRNA is to downregulate target mRNAs. With only this function, it is impossible to assign opposite signs toward controls between miR-7 and miR-128 transfection as shown in Fig. 7.21. Downregulation can result in only same signs towards controls. At least, either of miR-7 or miR-128 transfection must be associated with sequence-nonspecific off-target regulation that can cause upregulation. Thus, we keep the selection of the second PC loading and assign P-values to probes as Eq. (7.57).

Fig. 7.21 The second PC loading, $\boldsymbol{v}_2$, obtained by PCA applied to x_{ij} made out of study 2

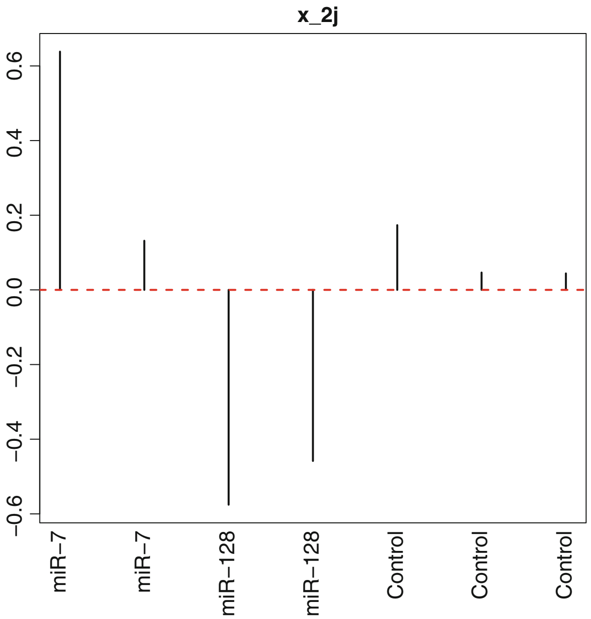

P-values are corrected by BH criterion and probes associated with adjusted P-values less than 0.01 are selected.

Study 3

This data set includes two miR-7 transfection experiments, two miR-128 transfection experiments, and six control experiments, normalized by plier procedure [18]. Plier is yet another procedure that normalizes microarray, although I do not intend to explain plier in more detail, because it is beyond the scope of this textbook. Because number of experiments of treated and control samples, they are difficult to be formatted in tensor. Thus it is instead as matrix, $x_{ij} \in \mathbb{R}^{54675 \times 10}$, where $j = 1, 2$ corresponds to miR-7 transfection $j = 3, 4$ corresponds to miR-128 transfection and $5 \leq j \leq 10$ correspond to control samples. PCA is applied to x_{ij} such that PC score, $\boldsymbol{u}_\ell \in \mathbb{R}^{54675}$, and PC loading, $\boldsymbol{v}_\ell \in \mathbb{R}^{10}$, are attributed to probes and samples, respectively. The result is similar to study 2. In contrast to Fig. 7.20, we cannot find any PC loading that is constant independent of miRNAs transfected. Figure 7.22 shows the second PC loading, $\boldsymbol{v}_2$, which exhibits opposite signs between miR-7 transfection and miR-128 transfection. As in the study 2, we keep the selection of the second PC loading and assign P-values to probes as Eq. (7.57). P-values are corrected by BH criterion and probes associated with adjusted P-values less than 0.01 are selected.

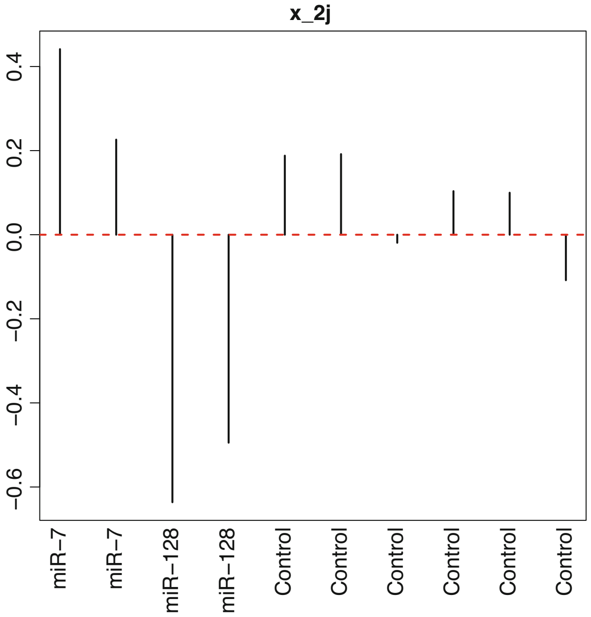

Fig. 7.22 The second PC loading, $\boldsymbol{v}_2$, obtained by PCA applied to x_{ij} made out of study 3

Study 4

This data set includes two replicates of nine transfected miRNAs (miR-7/9/122a/128a/132/133a/142/148b/181a) and corresponding 18 control samples. Thus, the total number of samples is 36. This is successfully formatted as tensor, $x_{ijk} \in \mathbb{R}^{23651 \times 18 \times 2}$ where i stands for probes, j stands for nine miRNAs transfection times two biological replicates, and k is control and treated samples. We apply HOSVD algorithm, Fig. 3.8, to x_{ijk} as

$$x_{ijk} = \sum_{\ell_1=1}^{23651} \sum_{\ell_2=1}^{18} \sum_{\ell_3=1}^{2} G(\ell_1, \ell_2, \ell_3) u_{\ell_1 i}^{(i)} u_{\ell_2 j}^{(j)} u_{\ell_3 k}^{(k)} \tag{7.58}$$

where $\boldsymbol{u}_{\ell_1}^{(i)} \in \mathbb{R}^{23651}, \boldsymbol{u}_{\ell_2}^{(j)} \in \mathbb{R}^{18}, \boldsymbol{u}_{\ell_3}^{(k)} \in \mathbb{R}^2$ are singular value vectors and $G(\ell_1, \ell_2, \ell_3) \in \mathbb{R}^{23651 \times 18 \times 2}$ is a core tensor. Now we need to find $\boldsymbol{u}_{\ell_3}^{(k)}$ satisfying $u_{\ell_3 1}^{(k)} = -u_{\ell_3 2}^{(k)}$; $\ell_3 = 2$ turns out to satisfy this requirement. On the other hand, we need to find $\boldsymbol{u}_{\ell_2}^{(j)}$ satisfying $u_{\ell_2 j}^{(j)}$ = constant; $\ell_2 = 1$ turns out to satisfy this requirement (Fig. 7.23). After investigating which $G(\ell_1, 1, 2)$ has the largest absolute value, we find that $\ell_1 = 6$. P-values are attributed to probes using the sixth PC score $\boldsymbol{u}_6^{(i)}$ with assuming χ^2 distribution as

$$P_i = P_{\chi^2}\left[> \left(\frac{u_{6i}^{(i)}}{\sigma_6} \right)^2 \right]. \tag{7.59}$$

P-values are corrected by BH criterion and probes associated with adjusted P-values less than 0.01 are selected.

Study 5

This data set includes four profiles to which mock and cel-miR-67 miR-509/199a-3p are transfected. We format it to matrix $x_{ij} \in \mathbb{R}^{41539 \times 4}$. PCA is applied to x_{ij} and the second PC loading, $\boldsymbol{v}_2$, is selected as that exhibits distinction between mock + cel-miR-67 and miR-509/199a-3p (Fig. 7.24). Although outcome cannot be said very promising, because $\boldsymbol{v}_2$ is best fitted with the requirement, P-values are attributed to probes using Eq. (7.57). P-values are corrected by BH criterion and probes associated with adjusted P-values less than 0.01 are selected.

Study 6

This data set includes transfection of eight miRNAs, miR-10a-5p, 150-3p/5p, 148a-3p/5p, 499a-5p, 455-3p. The number of probes in microarray is as many as 62,976. The number of samples is 16 composed of combination of miRNAs and cell lines.

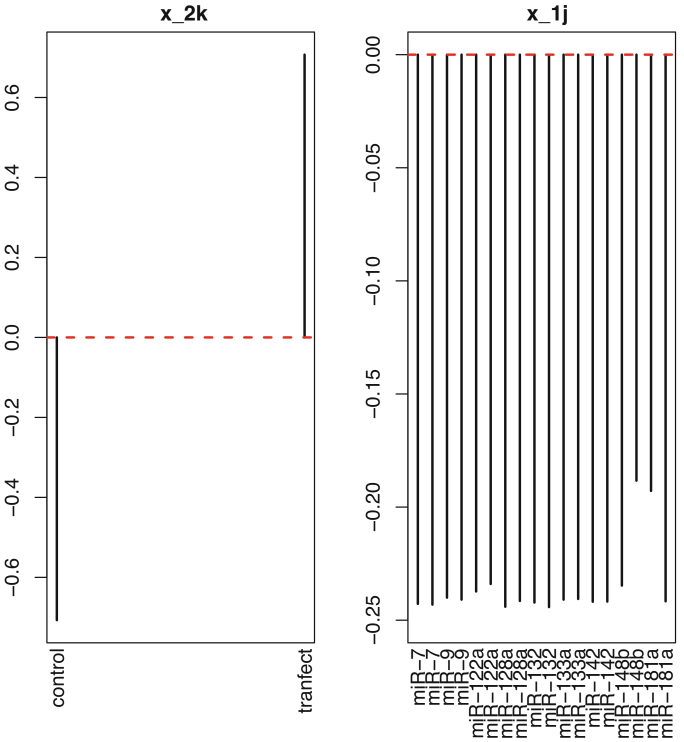

Fig. 7.23 The second singular value vector, $\boldsymbol{u}_2^{(k)}$, attributed to control and treated samples, and the first singular value vector, $\boldsymbol{u}_1^{(j)}$, attributed to miRNAs and replicates, obtained by HOSVD applied to x_{ijk} made out of study 4

Not all miRNAs are used equally. For each of 16, two paired experiments of treated and control samples. Treated and control sample measurement is performed by one microarray. Thus these two must be retrieved from it (columns annotated as gProcessedSignal and rProcessedSignal). This is successfully formatted as tensor, $x_{ijk} \in \mathbb{R}^{62976 \times 16 \times 2}$ where i stands for probes, j stands for combinations of eight miRNAs transfection and cell lines, and k is control and treated samples. We apply HOSVD algorithm, Fig. 3.8, to x_{ijk} as

$$x_{ijk} = \sum_{\ell_1=1}^{62976} \sum_{\ell_2=1}^{16} \sum_{\ell_3=1}^{2} G(\ell_1, \ell_2, \ell_3) u_{\ell_1 i}^{(i)} u_{\ell_2 j}^{(j)} u_{\ell_3 k}^{(k)} \tag{7.60}$$

where $\boldsymbol{u}_{\ell_1}^{(i)} \in \mathbb{R}^{62976}, \boldsymbol{u}_{\ell_2}^{(j)} \in \mathbb{R}^{16}, \boldsymbol{u}_{\ell_3}^{(k)} \in \mathbb{R}^2$ are singular value vectors and $G(\ell_1, \ell_2, \ell_3) \in \mathbb{R}^{62976 \times 16 \times 2}$ is a core tensor. Now we need to find $\boldsymbol{u}_{\ell_3}^{(k)}$ satisfying

Fig. 7.24 The second PC loading, $\boldsymbol{v}_2$, obtained by PCA applied to x_{ij} made out of study 5

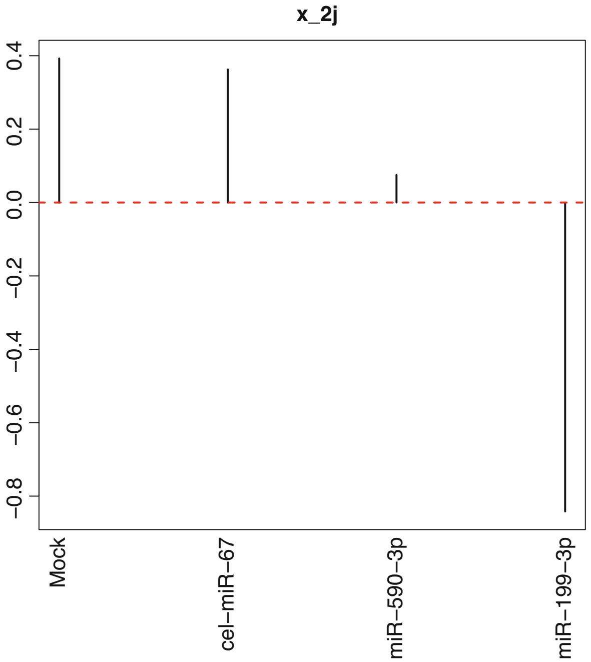

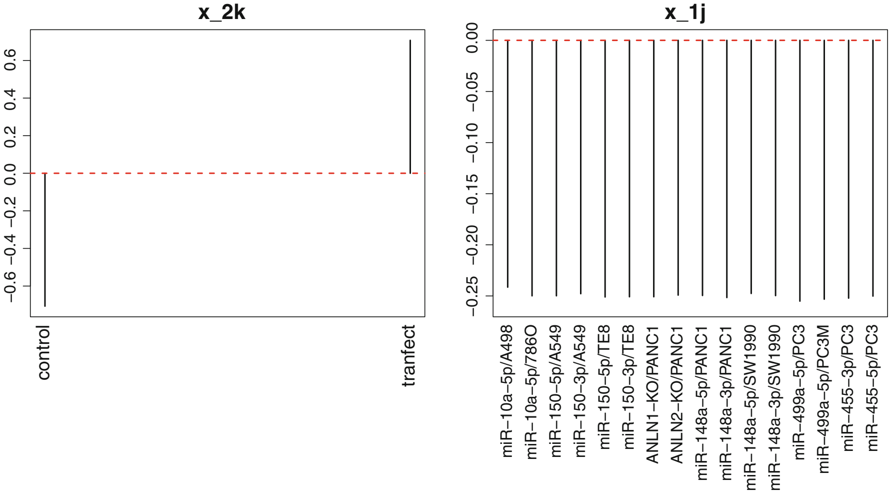

Fig. 7.25 The second singular value vector, $\boldsymbol{u}_2^{(k)}$, attributed to the various combinations of control and cell lines, and the first singular value vector, $\boldsymbol{u}_1^{(j)}$, attributed to miRNAs and replicates, obtained by HOSVD applied to x_{ijk} made out of study 6

$u_{\ell_3 1}^{(k)} = -u_{\ell_3 2}^{(k)}$; $\ell_3 = 2$ turns out to satisfy this requirement. On the other hand, we need to find $\boldsymbol{u}_{\ell_2}^{(j)}$ satisfying $u_{\ell_2 j}^{(j)}$ = constant; $\ell_2 = 1$ turns out to satisfy this requirement (Fig. 7.25). After investigating which $G(\ell_1, 1, 2)$ has the largest absolute value, we find that $\ell_1 = 7$. P-values are attributed to probes using the seventh PC score $\boldsymbol{u}_7^{(i)}$ with assuming χ^2 distribution as

$$P_i = P_{\chi^2}\left[> \left(\frac{u_{7i}^{(i)}}{\sigma_7} \right)^2 \right]. \tag{7.61}$$

P-values are corrected by BH criterion and probes associated with adjusted P-values less than 0.01 are selected.

Study 7

This data set includes transfection of nine miR-205/29a/144-3p/5p, 210, 23b, 221/222/223. The number of probes in microarray is as many as 62,976. The number of samples is 19 composed of combination of miRNAs and cell lines. Not all miRNAs are used equally. For each of 19, two paired experiments of treated and control samples. Treated and control sample measurement is performed by one microarray. Thus these two must be retrieved from it (columns annotated as gProcessedSignal and rProcessedSignal). This is successfully formatted as tensor, $x_{ijk} \in \mathbb{R}^{62976 \times 19 \times 2}$ where i stands for probes, j stands for combinations of eight miRNAs transfection and cell lines, and k is control and treated samples. We apply HOSVD algorithm, Fig. 3.8, to x_{ijk} as

$$x_{ijk} = \sum_{\ell_1=1}^{62976} \sum_{\ell_2=1}^{19} \sum_{\ell_3=1}^{2} G(\ell_1, \ell_2, \ell_3) u_{\ell_1 i}^{(i)} u_{\ell_2 j}^{(j)} u_{\ell_3 k}^{(k)} \tag{7.62}$$

where $\boldsymbol{u}_{\ell_1}^{(i)} \in \mathbb{R}^{62976}, \boldsymbol{u}_{\ell_2}^{(j)} \in \mathbb{R}^{19}, \boldsymbol{u}_{\ell_3}^{(k)} \in \mathbb{R}^2$ are singular value vectors and $G(\ell_1, \ell_2, \ell_3) \in \mathbb{R}^{62976 \times 19 \times 2}$ is a core tensor. Now we need to find $\boldsymbol{u}_{\ell_3}^{(k)}$ satisfying $u_{\ell_3 1}^{(k)} = -u_{\ell_3 2}^{(k)}$; $\ell_3 = 2$ turns out to satisfy this requirement. On the other hand, we need to find $\boldsymbol{u}_{\ell_2}^{(j)}$ satisfying $u_{\ell_2 j}^{(j)}$ = constant; $\ell_2 = 1$ turns out to satisfy this requirement (Fig. 7.26). After investigating which $G(\ell_1, 1, 2)$ has the larger absolute values, we find that $\ell_1 = 2, 3$. P-values are attributed to probes using the second and third PC scores $\boldsymbol{u}_{\ell_1}^{(i)}, \ell_1 = 2, 3$ with assuming χ^2 distribution as

$$P_i = P_{\chi^2}\left[> \sum_{\ell_1=2}^{3} \left(\frac{u_{\ell_1 i}^{(i)}}{\sigma_{\ell_1}} \right)^2 \right]. \tag{7.63}$$

P-values are corrected by BH criterion and probes associated with adjusted P-values less than 0.01 are selected.

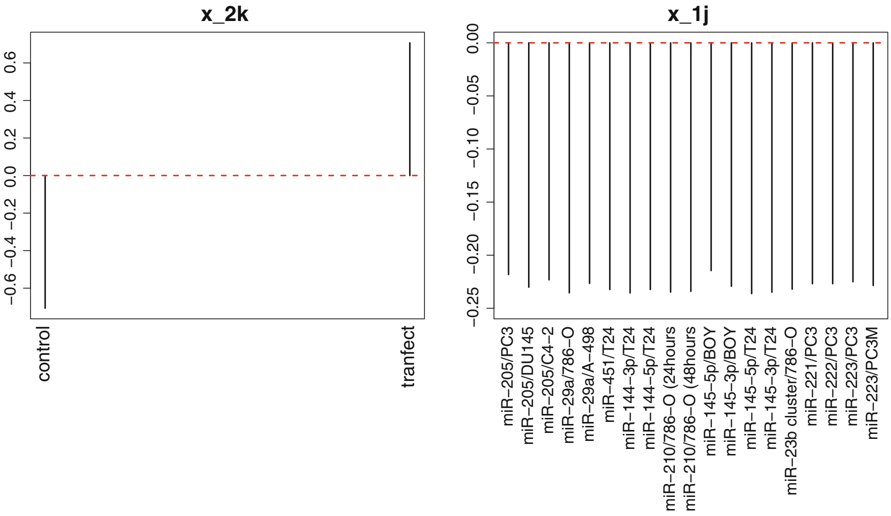

Fig. 7.26 The second singular value vector, $\boldsymbol{u}_2^{(k)}$, attributed to control and treated samples, and the first singular value vector, $\boldsymbol{u}_1^{(j)}$, attributed to the combinations of miRNAs and cell lines, obtained by HOSVD applied to x_{ijk} made out of study 7

Study 8

This data set includes transfection of two miRNAs, miR-146a/b. The number of probes in microarray is as many as 43,379. The number of samples is 18 composed of six miR-146a OE, four miR-146b OE, and eight miR-146a KO. For each of 19, two paired experiments of treated and control samples. Treated and control sample measurement is performed by one microarray. Thus these two must be retrieved from it (columns annotated as gProcessedSignal and rProcessedSignal). This is successfully formatted as tensor, $x_{ijk} \in \mathbb{R}^{43379 \times 18 \times 2}$ where i stands for probes, j stands for combinations of eight miRNAs transfection and cell lines, and k is control and treated samples. We apply HOSVD algorithm, Fig. 3.8, to x_{ijk} as

$$x_{ijk} = \sum_{\ell_1=1}^{43379} \sum_{\ell_2=1}^{18} \sum_{\ell_3=1}^{2} G(\ell_1, \ell_2, \ell_3) u_{\ell_1 i}^{(i)} u_{\ell_2 j}^{(j)} u_{\ell_3 k}^{(k)} \tag{7.64}$$

where $\boldsymbol{u}_{\ell_1}^{(i)} \in \mathbb{R}^{43379}, \boldsymbol{u}_{\ell_2}^{(j)} \in \mathbb{R}^{18}, \boldsymbol{u}_{\ell_3}^{(k)} \in \mathbb{R}^2$ are singular value vectors and $G(\ell_1, \ell_2, \ell_3) \in \mathbb{R}^{43379 \times 18 \times 2}$ is a core tensor. Now we need to find $\boldsymbol{u}_{\ell_3}^{(k)}$ satisfying $u_{\ell_3 1}^{(k)} = -u_{\ell_3 2}^{(k)}$; $\ell_3 = 2$ turns out to satisfy this requirement. On the other hand, we need to find $\boldsymbol{u}_{\ell_2}^{(j)}$ satisfying $u_{\ell_2 j}^{(j)}$ = constant; $\ell_2 = 1$ turns out to satisfy this requirement (Fig. 7.27). After investigating which $G(\ell_1, 1, 2)$ has the largest absolute value, we find that $\ell_1 = 5$. P-values are attributed to probes using the fifth

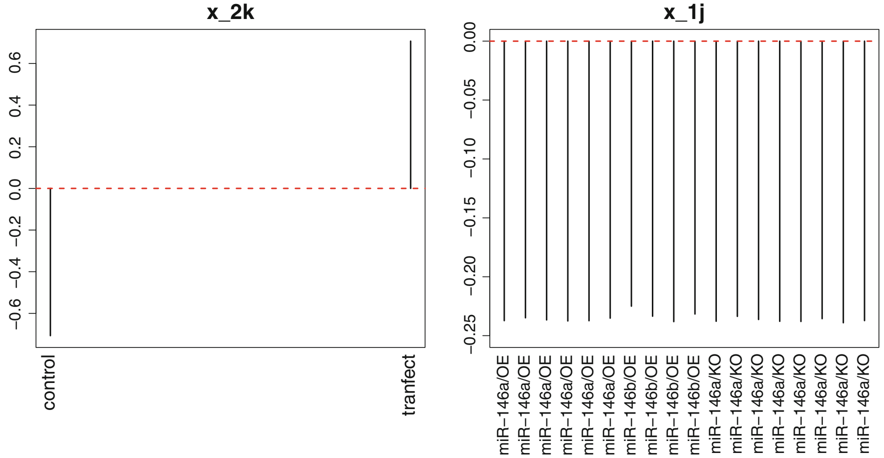

Fig. 7.27 The second singular value vector, $\boldsymbol{u}_2^{(k)}$, attributed to control and treated samples, and the first singular value vector, $\boldsymbol{u}_1^{(j)}$, attributed to miRNAs and replicates, obtained by HOSVD applied to x_{ijk} made out of study 8

PC score $\boldsymbol{u}_5^{(i)}$ with assuming χ^2 distribution as

$$P_i = P_{\chi^2}\left[> \left(\frac{u_{5i}^{(i)}}{\sigma_5} \right)^2 \right]. \tag{7.65}$$

P-values are corrected by BH criterion and probes associated with adjusted P-values less than 0.01 are selected.

Study 9

This data set includes transfection of two miRNAs, miR-107/181b. transfected to HeLa cell lines. The number of probes in microarray is as many as 9987. The number of samples is 18 composed of six controls, two anti-miR-107, four miR-107, two anti-miR-181b, and four miR-181b transfected samples. This is successfully formatted as tensor, $x_{ijk} \in \mathbb{R}^{9987 \times 16 \times 3}$ where i stands for probes, j stands for replicates, and k is control, miR-107 and miR-181b. We apply HOSVD algorithm, Fig. 3.8, to x_{ijk} as

$$x_{ijk} = \sum_{\ell_1=1}^{9987} \sum_{\ell_2=1}^{6} \sum_{\ell_3=1}^{3} G(\ell_1, \ell_2, \ell_3) u_{\ell_1 i}^{(i)} u_{\ell_2 j}^{(j)} u_{\ell_3 k}^{(k)} \tag{7.66}$$

Fig. 7.28 The second singular value vector, $\boldsymbol{u}_2^{(k)}$, attributed to control, miR-107 and miR-181b transfection, and the first singular value vector, $\boldsymbol{u}_1^{(j)}$, attributed to miRNAs and replicates, obtained by HOSVD applied to x_{ijk} made out of study 9

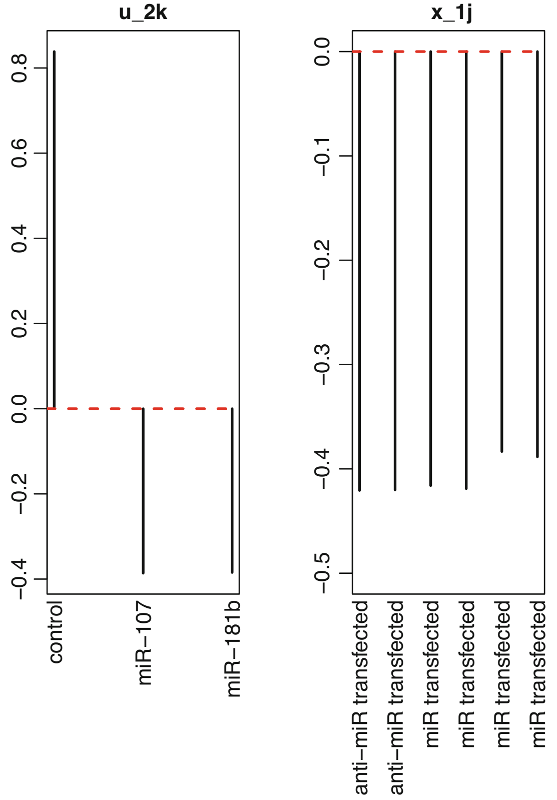

where $\boldsymbol{u}_{\ell_1}^{(i)} \in \mathbb{R}^{9987}, \boldsymbol{u}_{\ell_2}^{(j)} \in \mathbb{R}^6, \boldsymbol{u}_{\ell_3}^{(k)} \in \mathbb{R}^3$ are singular value vectors and $G(\ell_1, \ell_2, \ell_3) \in \mathbb{R}^{9987\times6\times3}$ is a core tensor. Now we need to find $\boldsymbol{u}_{\ell_3}^{(k)}$ satisfying $u_{\ell_3 1}^{(k)} = -u_{\ell_3 2}^{(k)} = -u_{\ell_3 3}^{(k)}$; $\ell_3 = 2$ turns out to satisfy this requirement. On the other hand, we need to find $\boldsymbol{u}_{\ell_2}^{(j)}$ satisfying $u_{\ell_2 j}^{(j)}$ = constant; $\ell_2 = 1$ turns out to satisfy this requirement (Fig. 7.28). After investigating which $G(\ell_1, 1, 2)$ has the largest absolute value, we find that $\ell_1 = 2$. P-values are attributed to probes using the second PC score $\boldsymbol{u}_2^{(i)}$ with assuming χ^2 distribution as Eq. (7.57). P-values are corrected by BH criterion and probes associated with adjusted P-values less than 0.01 are selected.

Study 10

Everything is the same as study nine other than that transfected cell line is HEK 293 cell line (see Fig. 7.29 for singular value vectors selected).

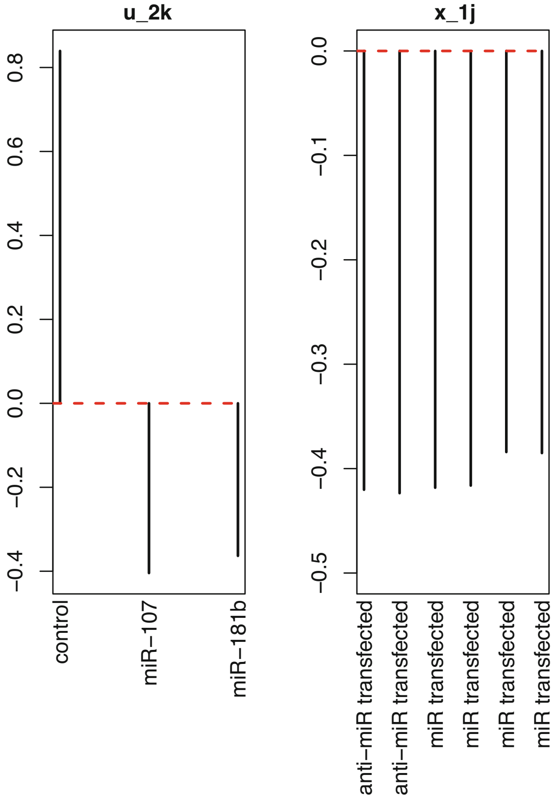

Fig. 7.29 The second singular value vector, $\boldsymbol{u}_2^{(k)}$, attributed to control, miR-107 and miR-181b transfection, and the first singular value vector, $\boldsymbol{u}_1^{(j)}$, attributed to miRNAs and replicates, obtained by HOSVD applied to x_{ijk} made out of study 10

Study 11

This data set includes transfection of a miRNA, miR-181b transfected to SH-SY5Y cell line. The number of probes in microarray is as many as 9987. The number of samples is eight composed of four controls, two anti-miR-181b, and two miR-181b transfected samples. This is successfully formatted as tensor, $x_{ijk} \in \mathbb{R}^{9987 \times 4 \times 2}$ where i stands for probes, j stands for replicates, and k is control and miR-181b. We apply HOSVD algorithm, Fig. 3.8, to x_{ijk} as

$$x_{ijk} = \sum_{\ell_1=1}^{9987} \sum_{\ell_2=1}^{4} \sum_{\ell_3=1}^{2} G(\ell_1, \ell_2, \ell_3) u_{\ell_1 i}^{(i)} u_{\ell_2 j}^{(j)} u_{\ell_3 k}^{(k)} \tag{7.67}$$

where $\boldsymbol{u}_{\ell_1}^{(i)} \in \mathbb{R}^{9987}, \boldsymbol{u}_{\ell_2}^{(j)} \in \mathbb{R}^4, \boldsymbol{u}_{\ell_3}^{(k)} \in \mathbb{R}^2$ are singular value vectors and $G(\ell_1, \ell_2, \ell_3) \in \mathbb{R}^{9987 \times 4 \times 2}$ is a core tensor. Now we need to find $\boldsymbol{u}_{\ell_3}^{(k)}$ satisfying $u_{\ell_3 1}^{(k)} = -u_{\ell_3 2}^{(k)}$; $\ell_3 = 2$ turns out to satisfy this requirement. On the other hand, we need to find $\boldsymbol{u}_{\ell_2}^{(j)}$ satisfying $u_{\ell_2 j}^{(j)}$ = constant; $\ell_2 = 1$ turns out to satisfy

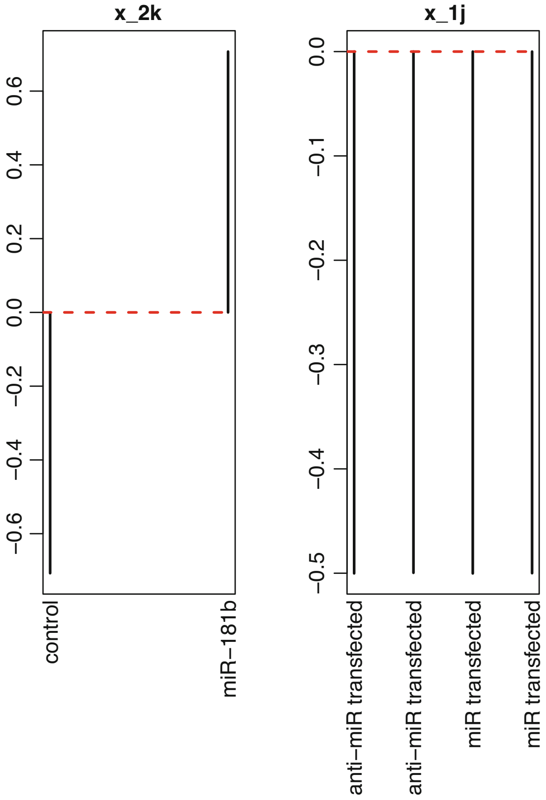

Fig. 7.30 The second singular value vector, $\boldsymbol{u}_2^{(k)}$, attributed to control and miR-181b transfection, and the first singular value vector, $\boldsymbol{u}_1^{(j)}$, attributed to miRNAs and replicates, obtained by HOSVD applied to x_{ijk} made out of study 11

this requirement (Fig. 7.30). After investigating which $G(\ell_1, 1, 2)$ has the largest absolute value, we find that $\ell_1 = 2$. P-values are attributed to probes using the second PC score $\boldsymbol{u}_2^{(i)}$ with assuming χ^2 distribution as Eq. (7.57). P-values are corrected by BH criterion and probes associated with adjusted P-values less than 0.01 are selected.

Drug Discovery From Gene Expression: II

Heart Failure

Human gene expression profiles are downloaded from GEO with GEO ID 57345. File used is GSE57345-GPL11532_series_matrix.txt.gz. Rat heart gene expression profiles are downloaded from GEO with GEO ID GSE59905. Files used are GSE59905-GPL5426_series_matrix.txt.gz, and GSE59905-GPL5425_series_matrix.txt.gz. 3937 genes are shared between human and rat. Case II tensor, $x_{ij_1j_2j_3}$, is generated as

$$x_{ij_1j_2j_3} = x_{ij_1j_2}x_{ij_3}. \tag{7.68}$$

HOSVD algorithm, Fig. 3.8, is applied to $x_{ij_1j_2j_3}$.

At first, we try to find $\boldsymbol{u}_{\ell_3}^{(j_3)}$ associated with significant distinction between three classes, healthy control, idiopathic dilated cardiomyopathy, ischemic stroke, by applying categorical regression

$$u_{\ell_3j_3}^{(j_3)} = a_{\ell_3} + \sum_{s=1}^{3} b_{\ell_3s}\delta_{j_3s} \tag{7.69}$$

P-values computed by categorical regression are corrected by BH criterion. Then we found that $\ell_3 = 2, 3, 5, 17, 313$ are associated with adjusted P-values less than 0.01, raw P-values of which are 1.65×10^{-17}, 1.00×10^{-39}, 1.29×10^{-4}, 4.97×10^{-6} and 1.554×10^{-4}. Among them we select $\ell_3 = 2, 3$ because they have more contribution than others. Figure 7.31a shows the $\boldsymbol{u}_{\ell_3}^{(j_3)}$, $1 \leq \ell_3 \leq 3$.

Next we try to identify $\boldsymbol{u}_{\ell_2}^{(j_2)}$ associated with significant time dependence. Figure 7.31b shows the $\boldsymbol{u}_{\ell_2}^{(j_2)}$, $1 \leq \ell_2 \leq 4$. The correlation coefficients between $\boldsymbol{u}_{\ell_2}^{(j_2)}$ and (1/4,1,3,5) are −0.72, −0.82, 0.51, and −0.09. Then $\ell_2 = 2$ with largest absolute value is selected. Then we need to find $\boldsymbol{u}_{\ell_1}^{(j_1)}$ and $\boldsymbol{u}_{\ell_4}^{(i)}$ associated with larger absolute $G(\ell_1, 2, 2, \ell_4)$ or $G(\ell_1, 2, 3, \ell_4)$ in order to select compounds j_1 and genes i associated with time dependence and distinction between patients and healthy controls simultaneously. In order that, we list top 20 $G(\ell_1, 2, 2, \ell_4)$ or $G(\ell_1, 2, 3, \ell_4)$ (Table 7.32). Because G gradually decreases, we cannot select specific cut off. Thus, tentatively, we select ℓ_1 and ℓ_4 associated with top 10 Gs; $\ell_1 = 2$ and $\ell_4 = 21, 25, 27, 28, 33, 36, 37, 38, 41, 42$. Figure 7.31c shows $\boldsymbol{u}_2^{(j_1)}$. Forty three outlier drugs, $\left|u_{2j_1}^{(j_1)}\right| > 0.1$, blue parts, are selected, by visual inspection, because P-values computed from $\boldsymbol{u}_2^{(j_1)}$ and corrected by BH criterion cannot be less than 0.01. On the other hand, P-values are attributed to ith gene as

$$P_i = P_{\chi^2}\left[> \sum_{\ell_4=21,25,27,28,33,36,37,38,41,42} \left(\frac{u_{\ell_4 i}}{\sigma_{\ell_4}}\right)^2 \right] \tag{7.70}$$

P-values are corrected by BH criterion and 274 genes associated with adjusted P-values less than 0.01 are selected.

PTSD

PTSD model rat amygdala and hippocampus gene expression are downloaded from GEO with GEO ID GSE60304. A file GSE60304_series_matrix.txt.gz is used. Gene expression profiles of the brain for drug treatments of rats are

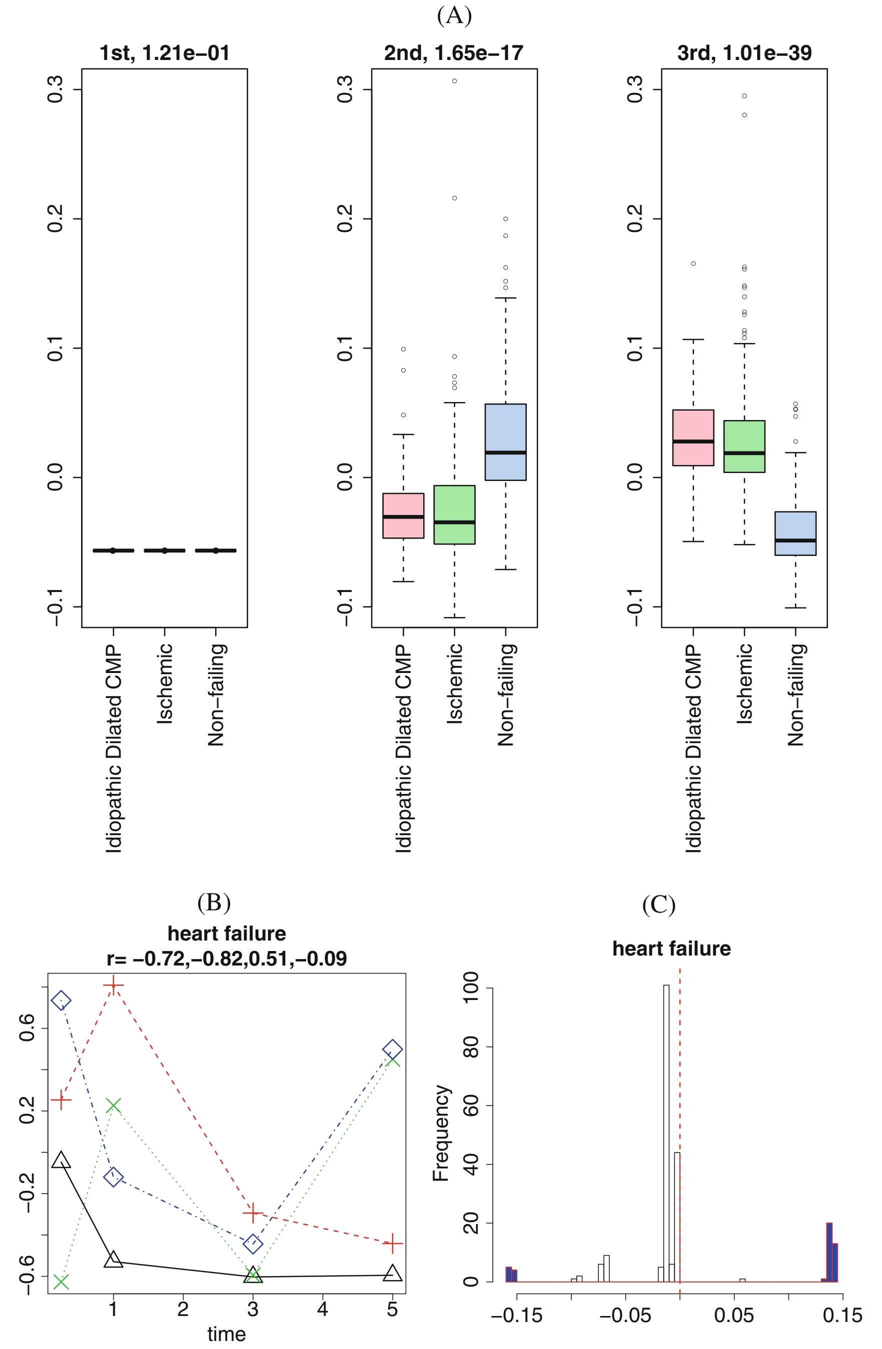

Fig. 7.31 (**a**) $\boldsymbol{u}^{(j_3)}_{\ell_3}$, $1 \leq \ell_3 \leq 3$, P-values are computed by categorical regression, Eq. (7.69). (**b**) $\boldsymbol{u}^{(j_2)}_{\ell_2}$, $1 \leq \ell_2 \leq 4$, open triangle: $\ell_2 = 1$, red plus symbol: $\ell_2 = 2$, green cross symbol: $\ell_2 = 3$, blue diamond: $\ell_2 = 4$. r: correlation coefficient. (**c**) Histogram of $\boldsymbol{u}^{(j_1)}_2$. Blue parts are selected ones. Vertical red broken line is 0

Table 7.32 Top 20 $G(\ell_1, 2, 2, \ell_4)$ or $G(\ell_1, 2, 3, \ell_4)$

Rank	1	2	3	4	5	6	7	8	9	10
ℓ_1	2	2	2	2	2	2	2	2	2	2
ℓ_3	2	3	2	2	3	3	2	3	3	2
ℓ_4	27	38	33	28	41	37	21	36	42	25
$G(\ell_1, 2, \ell_3, \ell_4)$	66.2	−43.7	40.7	−40.2	38.2	−31.6	28.5	−26.8	−26.2	−26.2

Rank	11	12	13	14	15	16	17	18	19	20
ℓ_1	2	2	2	2	2	2	2	2	2	2
ℓ_3	2	3	2	2	3	3	2	2	2	3
ℓ_4	40	29	31	39	32	33	26	11	18	31
$G(\ell_1, 2, \ell_3, \ell_4)$	−25.5	25.2	−22.6	21.8	20.7	−19.7	−19.5	−18.2	−17.3	15.4

downloaded from GEO with GEO ID GSE59895. Files used are GSE59895-GPL5425_series_matrix.txt.gz and GSE59895-GPL5426_series_matrix.txt.gz. Case II tensor, $x_{ij_1j_2j_3j_4j_5}$, is generated as

$$x_{ij_1j_2j_3j_4j_5} = x_{ij_1j_2}x_{ij_3j_4}x_{ij_3j_5}. \tag{7.71}$$

HOSVD algorithm, Fig. 3.8, is applied to $x_{ij_1j_2j_3j_4j_5}$.

In order to identify $\boldsymbol{u}_{\ell_4}^{(j_4)}$ and $\boldsymbol{u}_{\ell_5}^{(j_5)}$ associated with three classes, control samples, minimal behavioral response samples, and extreme behavioral response samples, by applying categorical regression,

$$u_{\ell j_4}^{(j_4)} = a_\ell + \sum_{s=1}^{3} b_{\ell s}\delta_{j_4 s} \tag{7.72}$$

$$u_{\ell j_5}^{(j_5)} = a_\ell + \sum_{s=1}^{3} b_{\ell s}\delta_{j_5 s} \tag{7.73}$$

where regression coefficients are shared between $\ell_4 = \ell_5 = \ell$. P-values computed by categorical regression are corrected by BH criterion. Then, only $\ell = 3$ is associated with adjusted P-values less than 0.05 (Fig. 7.32a).

Next we try to identify $\boldsymbol{u}_{\ell_2}^{(j_2)}$ associated with significant time dependence. Figure 7.32b shows the $\boldsymbol{u}_{\ell_2}^{(j_2)}$, $1 \le \ell_2 \le 4$. The correlation coefficients between $\boldsymbol{u}_{\ell_2}^{(j_2)}$ and (1/4,1,3,5) are $-0.75, -0.81, -0.30$, and 0.50. Then $\ell_2 = 2$ with largest absolute value is selected. Then we need to find $\boldsymbol{u}_{\ell_1}^{(j_1)}$ and $\boldsymbol{u}_{\ell_6}^{(i)}$ associated with larger absolute $G(\ell_1, 2, \ell_3, 3, 3, \ell_6)$ in order to select compounds j_1 and genes i associated with time dependence and distinction between patients and healthy controls simultaneously. In order that, we list top 20 $G(\ell_1, 2, \ell_3, 3, 3, \ell_6)$ (Table 7.33). Because G gradually decreases, we cannot select specific cut off. Thus, tentatively, we select ℓ_1 and ℓ_4 associated with top 10 Gs; $\ell_1 = 2$ and

Table 7.33 Top 20 $G(\ell_1, 2, \ell_3, 3, 3, \ell_6)$

Rank	1	2	3	4	5	6	7	8	9	10
ℓ_1	2	2	2	2	2	2	2	2	2	2
ℓ_3	1	1	1	1	1	1	1	1	1	1
ℓ_6	81	84	88	77	85	75	83	90	90	102
$G(\ell_1, 2, \ell_3, 3, 3, \ell_6)$	−0.133	0.112	0.110	−0.078	0.075	−0.075	0.074	0.069	0.069	−0.063

Rank	11	12	13	14	15	16	17	18	19	20
ℓ_1	2	2	2	2	2	2	2	2	2	2
ℓ_3	1	1	2	2	2	1	2	2	1	2
ℓ_6	76	80	94	76	128	285	86	286	92	282
$G(\ell_1, 2, \ell_3, 3, 3, \ell_6)$	−0.063	0.062	0.054	−0.054	−0.053	−0.052	0.048	0.047	0.045	0.045

$\ell_6 = 75, 77, 81, 83, 84, 85, 88, 89, 90, 102$. Figure 7.32c shows $\boldsymbol{u}_2^{(j_1)}$. Six outlier drugs, $u_{2j_1}^{(j_1)} < -0.2$ and $u_{1j_1}^{(j_1)} < -0.15$, blue parts, are selected, by visual inspection, because P-values computed from $\boldsymbol{u}_2^{(j_1)}$ and corrected by BH criterion cannot be less than 0.01. On the other hand, P-values are attributed to ith gene as

$$P_i = P_{\chi^2}\left[> \sum_{\ell_6=75,77,81,83,84,85,88,89,90,102} \left(\frac{u_{\ell_6 i}}{\sigma_{\ell_6}}\right)^2 \right] \tag{7.74}$$

P-values are corrected by BH criterion and 374 genes associated with adjusted P-values less than 0.01 are selected.

ALL

Bone marrow gene expression profiles of drug treated rats are downloaded from GEO with GEO ID GSE59894, and ALL human bone marrow gene expression is from GEO with GEO ID GSE67684. Used files are GSE67684-GPL570_series_matrix.txt.gz, GSE67684-GPL96_series_matrix.txt.gz, GSE59894-GPL5425_series_matrix.txt.gz, and GSE59894-GPL5426_series_matrix.txt.gz. In this case both gene expression profiles are time dependent. ALL human bone marrow gene expression profiles are measured at four times points, 0, 8, 15, and 33 days after a remission induction therapy. Case II tensor, $x_{ij_1j_2j_3j_4}$ is obtained as

$$x_{ij_1j_2j_3j_4} = x_{ij_1j_2}x_{ij_3j_4} \tag{7.75}$$

HOSVD algorithm, Fig. 3.8, is applied to $x_{ij_1j_2j_3j_4}$.

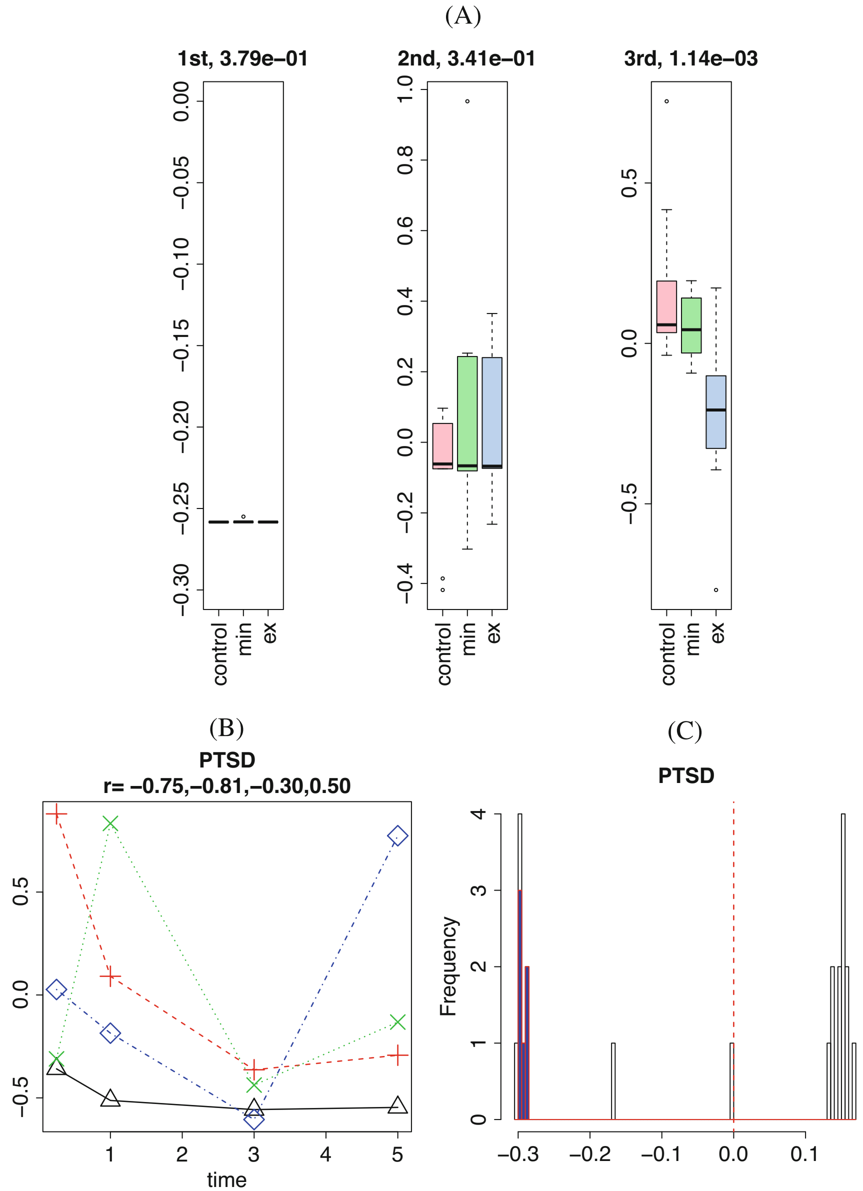

Fig. 7.32 (**a**) $\boldsymbol{u}_{\ell_3}^{(j_3)}$, $1 \leq \ell_3 \leq 3$, P-values are computed by categorical regression, Eqs. (7.72) and (7.73). (**b**) $\boldsymbol{u}_{\ell_2}^{(j_2)}$, $1 \leq \ell_2 \leq 4$, open triangle: $\ell_2 = 1$, red plus symbol: $\ell_2 = 2$, green cross symbol: $\ell_2 = 3$, blue diamond: $\ell_2 = 4$. r: correlation coefficient. (**c**) Histogram of $\boldsymbol{u}_2^{(j_1)}$. Blue parts are selected ones. Vertical red broken line is 0

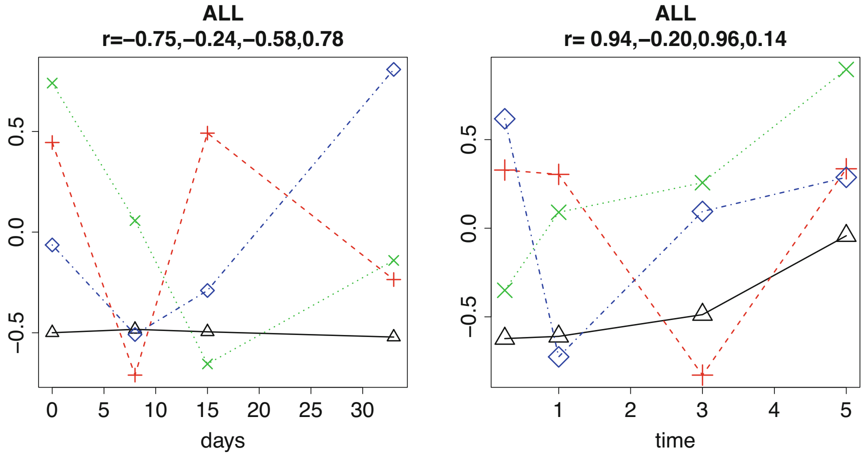

Fig. 7.33 (**a**) $\boldsymbol{u}^{(j_3)}_{\ell_3}$, $1 \leq \ell_3 \leq 4$, (**b**) $\boldsymbol{u}^{(j_2)}_{\ell_2}$, $1 \leq \ell_2 \leq 4$, open triangle: $\ell_2 = 1$, red plus symbol: $\ell_2 = 2$, green cross symbol: $\ell_2 = 3$, blue diamond: $\ell_2 = 4$. r: correlation coefficient

We compute correlation coefficients between $\boldsymbol{u}^{(j_3)}_{\ell_3}$ and days after a remission induction therapy, we decide to select $\ell_3 = 4$ because it has the largest absolute value of correlation coefficient (Fig. 7.33a).

Next we try to identify $\boldsymbol{u}^{(j_2)}_{\ell_2}$ associated with significant time dependence. Figure 7.33b shows the $\boldsymbol{u}^{(j_2)}_{\ell_2}$, $1 \leq \ell_2 \leq 4$. The correlation coefficients between $\boldsymbol{u}^{(j_2)}_{\ell_2}$ and (1/4,1,3,5) are 0.94, −0.20, 0.96, and 0.14. Then $\ell_2 = 3$ with largest absolute value is selected. Then we need to find $\boldsymbol{u}^{(j_1)}_{\ell_1}$ and $\boldsymbol{u}^{(i)}_{\ell_5}$ associated with larger absolute $G(\ell_1, 3, 4, \ell_4, \ell_5)$ in order to select compounds j_1 and genes i associated with time dependence and distinction between patients and healthy controls simultaneously. In order that, we list top 20 $G(\ell_1, 3, 4, \ell_4, \ell_5)$ (Table 7.34). For ℓ_1 and ℓ_5, we decide to select those associated with top 10 Gs. As a result, $\ell_1 = 2, 3, 5, 6, 9, 10$ and $\ell_5 = 1, 2, 3, 5$ are selected. P-values are attributed to j_1 and i as

$$P_{j_1} = P_{\chi^2}\left[> \sum_{\ell_1=2,3,5,6,9,10} \left(\frac{u_{\ell_1 i}}{\sigma_{\ell_1}}\right)^2 \right], \tag{7.76}$$

$$P_i = P_{\chi^2}\left[> \sum_{\ell_5=1,2,3,5} \left(\frac{u_{\ell_5 i}}{\sigma_{\ell_5}}\right)^2 \right]. \tag{7.77}$$

P-values are corrected by BH criterion and two compounds and 24 genes associated with adjusted P-values less than 0.01 are selected.

Table 7.34 Top 20 $G(\ell_1, 3, 4, \ell_4, \ell_5)$

Rank	1	2	3	4	5	6	7	8	9	10
ℓ_1	3	5	2	3	10	9	6	3	2	9
ℓ_4	4	4	4	7	4	4	4	5	4	4
ℓ_5	1	1	1	5	3	3	1	5	2	2
$G(\ell_1, 3, 4, \ell_4, \ell_5)$	260.6	−40.2	40.6	−20.9	20.7	20.4	−19.9	−18.0	16.8	−15.0

Rank	11	12	13	14	15	16	17	18	19	20
ℓ_1	8	6	14	3	3	13	12	2	1	3
ℓ_4	4	4	4	8	2	4	4	4	4	2
ℓ_5	6	4	2	5	5	4	2	3	4	1
$G(\ell_1, 3, 4, \ell_4, \ell_5)$	−13.9	13.3	13.2	−12.8	12.3	11.6	11.4	11.3	10.5	−10.5

Diabetes

Drug treated rat kidney gene expression profiles are downloaded from GEO with GEO ID GSE59913. Human diabetic kidney gene expression profile are downloaded from GEO with GEO ID GSE30122. Files used are GSE59913-GPL5425_series_matrix.txt.gz, GSE59913-GPL5426_series_matrix.txt.gz, and GSE30122_series_matrix.txt.gz. Case II tensor, $x_{ij_1j_2j_3}$, is generated as

$$x_{ij_1j_2j_3} = x_{ij_1j_2}x_{ij_3}. \tag{7.78}$$

HOSVD algorithm, Fig. 3.8, is applied to $x_{ij_1j_2j_3}$.

At first, we try to find $\boldsymbol{u}_{\ell_3}^{(j_3)}$ associated with significant distinction between four classes, normal human glomeruli, normal human kidney, normal human tubuli, and diabetic human kidney, by applying categorical regression

$$u_{\ell_3 j_3}^{(j_3)} = a_{\ell_3} + \sum_{s=1}^{4} b_{\ell_3 s}\delta_{j_3 s} \tag{7.79}$$

P-values computed by categorical regression are corrected by BH criterion. Then we found that $\ell_3 = 1, 4$ are associated with adjusted P-values less than 0.01, raw P-values of which are 2.69×10^{-9} and 1.66×10^{-9} and are selected. Figure 7.34a shows the $\boldsymbol{u}_{\ell_3}^{(j_3)}$, $1 \le \ell_3 \le 4$.

Next we try to identify $\boldsymbol{u}_{\ell_2}^{(j_2)}$ associated with significant time dependence. Figure 7.34b shows the $\boldsymbol{u}_{\ell_2}^{(j_2)}$, $1 \le \ell_2 \le 4$. The correlation coefficients between $\boldsymbol{u}_{\ell_2}^{(j_2)}$ and (1/4,1,3,5) are −0.60, −0.85, 0.53, and 0.20. Then $\ell_2 = 2$ with largest absolute value is selected. Then we need to find $\boldsymbol{u}_{\ell_1}^{(j_1)}$ and $\boldsymbol{u}_{\ell_4}^{(i)}$ associated with larger absolute $G(\ell_1, 2, 1, \ell_4)$ or $G(\ell_1, 2, 4, \ell_4)$ in order to select compounds j_1 and genes i associated with time dependence and distinction between patients and

Table 7.35 Top 20 $G(\ell_1, 2, 1, \ell_4)$ or $G(\ell_1, 2, 4, \ell_4)$

Rank	1	2	3	4	5	6	7	8	9	10
ℓ_1	2	2	3	4	4	3	9	11	2	4
ℓ_3	1	4	1	1	4	4	1	1	1	1
ℓ_4	1	4	1	1	4	4	48	59	42	42
$G(\ell_1, 2, \ell_3, \ell_4)$	−1410	955	−75	74	−53	51	38	34	−34	34

Rank	11	12	13	14	15	16	17	18	19	20
ℓ_1	2	9	2	9	11	9	6	11	9	4
ℓ_3	4	1	1	1	1	4	1	1	4	1
ℓ_4	40	29	31	39	32	33	26	11	18	31
$G(\ell_1, 2, \ell_3, \ell_4)$	−33	33	−32	31	31	−30	−30	−29	−29	28

healthy controls simultaneously. In order that, we list top 20 $G(\ell_1, 2, 1, \ell_4)$ or $G(\ell_1, 2, 4, \ell_4)$ (Table 7.35). Because top two Gs are outstandingly large, we select $\ell_1 = 2$ and $\ell_4 = 1, 4$ associated with top two Gs.

Figure 7.34c shows $\boldsymbol{u}_2^{(j_1)}$. Fourteen outlier drugs, $u_{2j_1}^{(j_1)} > 0.13$, blue parts, are selected, by visual inspection, because P-values computed from $\boldsymbol{u}_2^{(j_1)}$ and corrected by BH criterion cannot be less than 0.01. On the other hand, P-values are attributed to ith gene as

$$P_i = P_{\chi^2}\left[> \sum_{\ell_4=1,4} \left(\frac{u_{\ell_4 i}}{\sigma_{\ell_4}}\right)^2 \right] \tag{7.80}$$

P-values are corrected by BH criterion and 65 genes associated with adjusted P-values less than 0.01 are selected.

Renal Carcinoma

Drug treated rat kidney gene expression profiles are downloaded from GEO with GEO ID GSE59913. Human renal cancer gene expression profile are downloaded from GEO with GEO ID GSE40435. Files used are GSE59913-GPL5425_series_matrix.txt.gz, GSE59913-GPL5426_series_matrix.txt.gz, and GSE40435_series_matrix.txt.gz. Case II tensor, $x_{ij_1j_2j_3}$, is generated as

$$x_{ij_1j_2j_3} = x_{ij_1j_2} x_{ij_3}. \tag{7.81}$$

HOSVD algorithm, Fig. 3.8, is applied to $x_{ij_1j_2j_3}$.

At first, we try to find $\boldsymbol{u}_{\ell_3}^{(j_3)}$ associated with significant distinction between two classes, normal and cancer kidney, by applying categorical regression

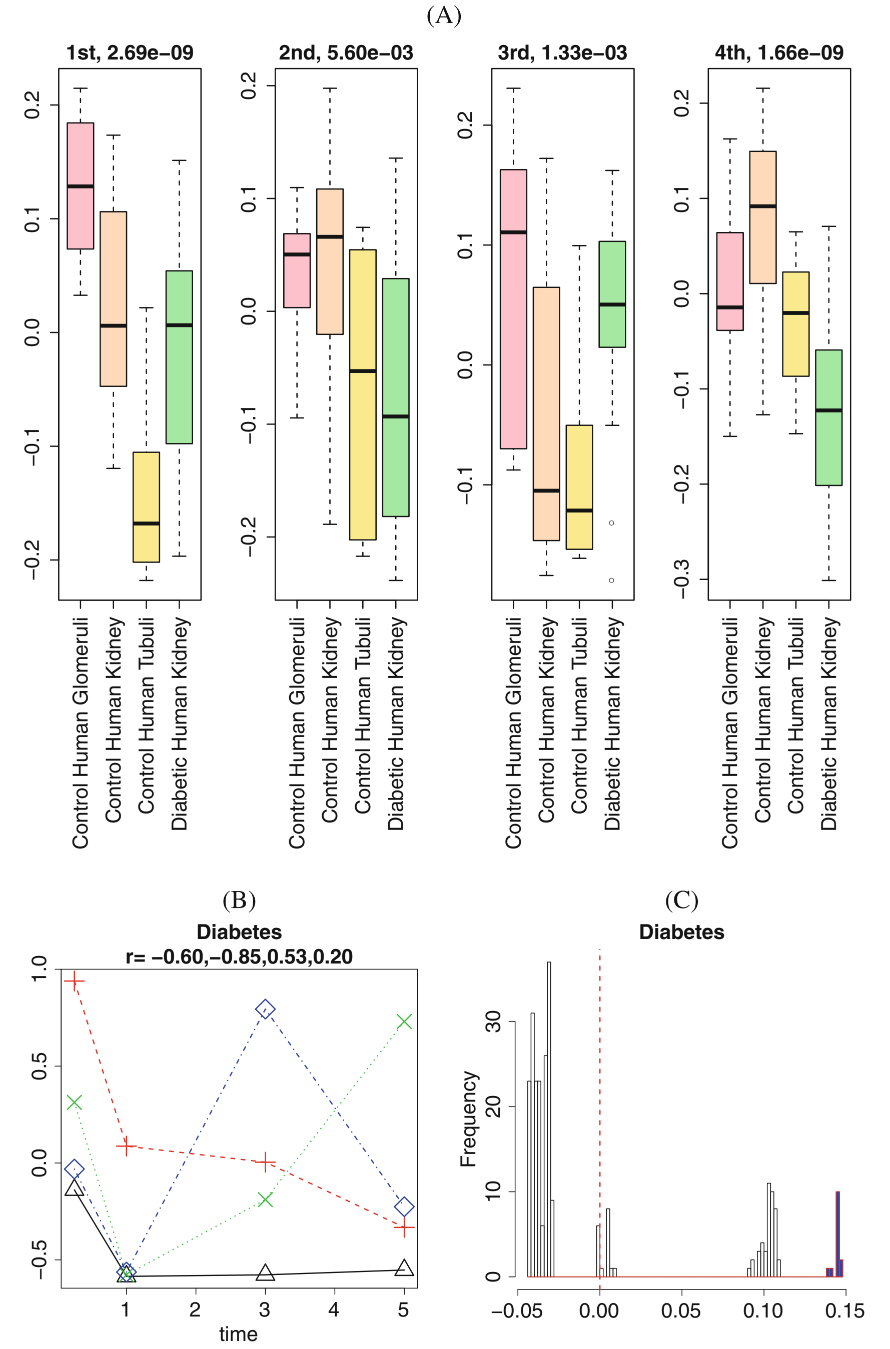

Fig. 7.34 (**a**) $\boldsymbol{u}^{(j_3)}_{\ell_3}$, $1 \le \ell_3 \le 4$, P-values are computed by categorical regression, Eq. (7.79). (**b**) $\boldsymbol{u}^{(j_2)}_{\ell_2}$, $1 \le \ell_2 \le 4$, open triangle: $\ell_2 = 1$, red plus symbol: $\ell_2 = 2$, green cross symbol: $\ell_2 = 3$, blue diamond: $\ell_2 = 4$. r: correlation coefficient. (**c**) Histogram of $\boldsymbol{u}^{(j_1)}_2$. Blue parts are selected ones. Vertical red broken line is 0

$$u^{(j_3)}_{\ell_3 j_3} = a_{\ell_3} + \sum_{s=1}^{2} b_{\ell_3 s}\delta_{j_3 s} \tag{7.82}$$

P-values computed by categorical regression are corrected by BH criterion. Then we found that $\ell_3 = 13, 15, 30, 33, 35$ are associated with adjusted P-values less than 0.05, raw P-values of which are 3.4×10^{-4}, 1.1×10^{-3}, 2.7×10^{-4}, 1.1×10^{-4}, and 2.4×10^{-4} and are selected. Figure 7.35a shows the $\boldsymbol{u}^{(j_3)}_{\ell_3}$, $\ell_3 = 13, 15, 30, 33, 35$.

Next we try to identify $\boldsymbol{u}^{(j_2)}_{\ell_2}$ associated with significant time dependence. Figure 7.35b shows the $\boldsymbol{u}^{(j_2)}_{\ell_2}$, $1 \leq \ell_2 \leq 4$. The correlation coefficients between $\boldsymbol{u}^{(j_2)}_{\ell_2}$ and (1/4,1,3,5) are -0.60, -0.84, 0.54, and 0.21. Then $\ell_2 = 2$ with largest absolute value is selected. Then we need to find $\boldsymbol{u}^{(j_1)}_{\ell_1}$ and $\boldsymbol{u}^{(i)}_{\ell_4}$ associated with larger absolute $G(\ell_1, 2, \ell_3, \ell_4)$, $\ell_3 = 13, 15, 30, 33, 35$ in order to select compounds j_1 and genes i associated with time dependence and distinction between patients and healthy controls simultaneously. In order that, we list top 20 $G(\ell_1, 2, \ell_3, \ell_4)$, $\ell_3 = 13, 15, 30, 33, 35$ (Table 7.36). For top 20 Gs, it is always that $\ell_1 = 2$. On the other hand, because G gradually changes, we cannot decide threshold values. Thus, we tentatively decide that $\ell_4 = 186, 215, 233, 244, 251, 269, 274, 309, 312, 318$ associated with top 10 Gs.

Figure 7.35c shows $\boldsymbol{u}^{(j_1)}_2$. Fourteen outlier drugs, $u^{(j_1)}_{2j_1} > 0.13$, blue parts, are selected, by visual inspection, because P-values computed from $\boldsymbol{u}^{(j_1)}_2$ and corrected by BH criterion cannot be less than 0.01. On the other hand, P-values are attributed to ith gene as

$$P_i = P_{\chi^2}\left[> \sum_{\ell_4 = 186,215,233,244,251,269,274,309,312,318} \left(\frac{u_{\ell_4 i}}{\sigma_{\ell_4}}\right)^2\right] \tag{7.83}$$

Table 7.36 Top 20 $G(\ell_1, 2, \ell_3, \ell_4)$, $\ell_3 = 13, 15, 30, 33, 35$

Rank	1	2	3	4	5	6	7	8	9	10
ℓ_1	2	2	2	2	2	2	2	2	2	2
ℓ_3	13	13	13	13	15	15	13	13	13	15
ℓ_4	215	269	233	186	309	312	251	244	274	318
$G(\ell_1, 2, \ell_3, \ell_4)$	5.63	−5.30	5.08	−5.06	−4.84	4.78	4.66	4.61	4.57	−4.56

Rank	11	12	13	14	15	16	17	18	19	20
ℓ_1	2	2	2	2	2	2	2	2	2	2
ℓ_3	13	15	15	15	15	13	15	13	13	15
ℓ_4	289	399	336	206	363	255	375	219	342	297
$G(\ell_1, 2, \ell_3, \ell_4)$	−4.53	4.43	4.37	4.24	−4.19	−4.05	4.04	−3.97	−3.88	3.86

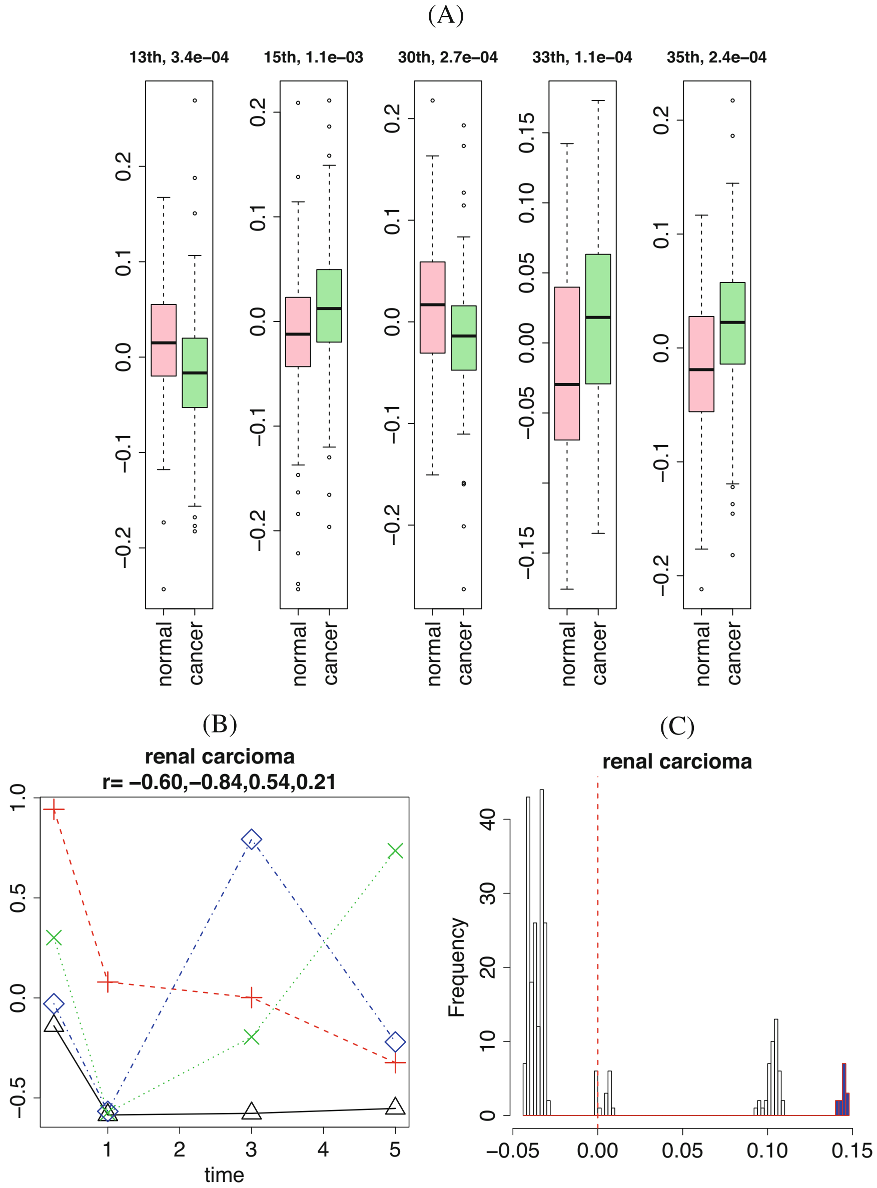

Fig. 7.35 (**a**) $\boldsymbol{u}_{\ell_3}^{(j_3)}$, $\ell_3 = 13, 15, 30, 33, 35$, P-values are computed by categorical regression, Eq. (7.85). (**b**) $\boldsymbol{u}_{\ell_2}^{(j_2)}$, $1 \leq \ell_2 \leq 4$, open triangle: $\ell_2 = 1$, red plus symbol: $\ell_2 = 2$, green cross symbol: $\ell_2 = 3$, blue diamond: $\ell_2 = 4$. r: correlation coefficient. (**c**) Histogram of $\boldsymbol{u}_2^{(j_1)}$. Blue parts are selected ones. Vertical red broken line is 0

P-values are corrected by BH criterion and 225 genes associated with adjusted P-values less than 0.01 are selected.

Cirrhosis

Drug treated rat liver gene expression profiles are downloaded from GEO with GEO ID GSE59923. Cirrhosis patient human liver gene expression profile is downloaded from GEO with GEO ID GSE15654. File used are GSE15654_series_matrix.txt.gz, GSE59923-GPL5424_series_matrix.txt.gz, GSE59923-GPL5425_series_matrix.txt.gz, and GSE59923-GPL5426_series_matrix.txt.gz. Case II tensor, $x_{ij_1j_2j_3}$, is generated as

$$x_{ij_1j_2j_3} = x_{ij_1j_2}x_{ij_3}. \tag{7.84}$$

HOSVD algorithm, Fig. 3.8, is applied to $x_{ij_1j_2j_3}$.

At first, we try to find $\boldsymbol{u}_{\ell_3}^{(j_3)}$ associated with significant distinction between three classes, good, intermediate, and poor prognosis, by applying categorical regression

$$u_{\ell_3 j_3}^{(j_3)} = a_{\ell_3} + \sum_{s=1}^{3} b_{\ell_3 s}\delta_{j_3 s} \tag{7.85}$$

P-values computed by categorical regression are corrected by BH criterion. Then we found that $\ell_3 = 2, 6$ are associated with adjusted P-values less than 0.01, raw P-values of which are 2.3×10^{-14} and 1.0×10^{-9} and are selected. Figure 7.36a shows the $\boldsymbol{u}_{\ell_3}^{(j_3)}, \ell_3 = 2, 6$.

Next we try to identify $\boldsymbol{u}_{\ell_2}^{(j_2)}$ associated with significant time dependence. Figure 7.36b shows the $\boldsymbol{u}_{\ell_2}^{(j_2)}, 1 \leq \ell_2 \leq 4$. The correlation coefficients between $\boldsymbol{u}_{\ell_2}^{(j_2)}$ and (1/4,1,3,5) are $-0.56, -0.78, 0.52$ and 0.36. Then $\ell_2 = 2$ with largest absolute value is selected. Then we need to find $\boldsymbol{u}_{\ell_1}^{(j_1)}$ and $\boldsymbol{u}_{\ell_4}^{(i)}$ associated with larger absolute $G(\ell_1, 2, \ell_3, \ell_4), \ell_3 = 2, 6$ in order to select compounds j_1 and genes i associated with time dependence and distinction between patients and healthy controls simultaneously. In order that, we list top 20 $G(\ell_1, 2, \ell_3, \ell_4), \ell_3 = 2, 6$ (Table 7.37). For top 20 Gs, it is always that $\ell_1 = 2$. On the other hand, because G gradually changes, we cannot decide threshold values. Thus, we tentatively decide to select $2 \leq \ell_4 \leq 10$ associated with top 10 Gs.

Figure 7.36c shows $\boldsymbol{u}_2^{(j_1)}$. Twenty seven outlier drugs, $\left|u_{2j_1}^{(j_1)}\right| > 0.075$, blue parts, are selected, by visual inspection, because P-values computed from $\boldsymbol{u}_2^{(j_1)}$ and corrected by BH criterion cannot be less than 0.01. On the other hand, P-values are attributed to ith gene as

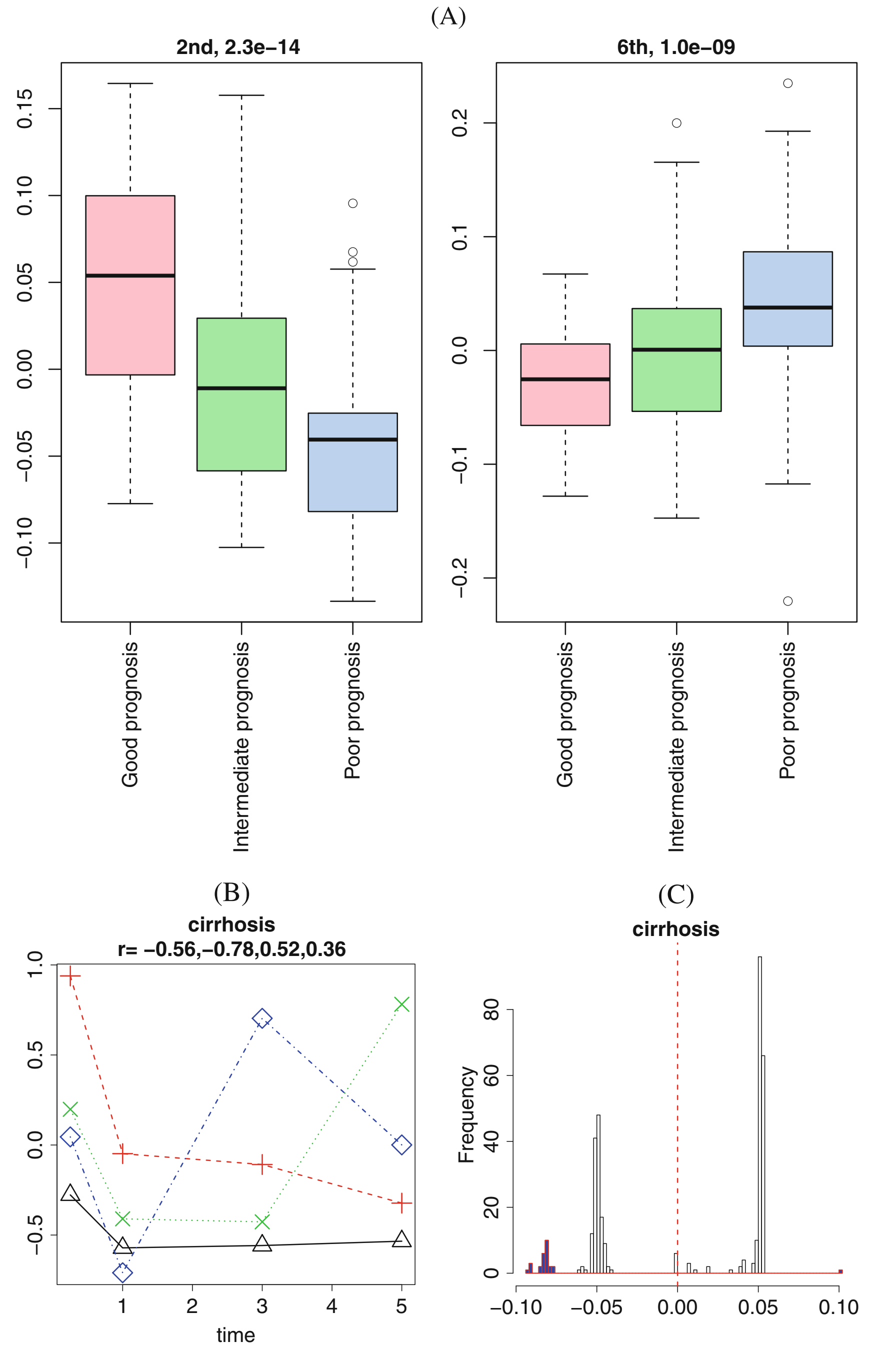

Fig. 7.36 (**a**) $\boldsymbol{u}^{(j_3)}_{\ell_3}$, $\ell_3 = 2, 6$, P-values are computed by categorical regression, Eq. (7.85). (**b**) $\boldsymbol{u}^{(j_2)}_{\ell_2}$, $1 \leq \ell_2 \leq 4$, open triangle: $\ell_2 = 1$, red plus symbol: $\ell_2 = 2$, green cross symbol: $\ell_2 = 3$, blue diamond: $\ell_2 = 4$. r: correlation coefficient. (**c**) Histogram of $\boldsymbol{u}^{(j_1)}_2$. Blue parts are selected ones. Vertical red broken line is 0

Table 7.37 Top 20 $G(\ell_1, 2, \ell_3, \ell_4)$, $\ell_3 = 2, 6$

Rank	1	2	3	4	5	6	7	8	9	10
ℓ_1	2	2	2	2	2	2	2	2	2	2
ℓ_3	2	6	6	6	6	6	2	6	2	2
ℓ_4	2	8	7	6	9	10	6	5	4	3
$G(\ell_1, 2, \ell_3, \ell_4)$	−945	310	278	194	−123	93	77	−76	−73	−67

Rank	11	12	13	14	15	16	17	18	19	20
ℓ_1	2	2	2	2	2	2	2	2	2	2
ℓ_3	6	6	6	6	6	6	6	2	6	2
ℓ_4	4	11	12	17	13	3	16	7	23	5
$G(\ell_1, 2, \ell_3, \ell_4)$	−59	49	43	40	33	−32	−31	27	25	−23

$$P_i = P_{\chi^2}\left[> \sum_{2 \le \ell_4 \le 10} \left(\frac{u_{\ell_4 i}}{\sigma_{\ell_4}} \right)^2 \right] \qquad (7.86)$$

P-values are corrected by BH criterion and 132 genes associated with adjusted P-values less than 0.01 are selected.

References

1. Acharya, C., Coop, A., Polli, J.E., MacKerell, A.D.: Recent advances in ligand-based drug design: relevance and utility of the conformationally sampled pharmacophore approach. Curr. Comput. Aided Drug Des. **7**(1), 10–22 (2011). https://doi.org/10.2174/157340911793743547
2. Albrecht, M., Stichel, D., Müller, B., Merkle, R., Sticht, C., Gretz, N., Klingmüller, U., Breuhahn, K., Matthäus, F.: TTCA: an R package for the identification of differentially expressed genes in time course microarray data. BMC Bioinf. **18**(1), 33 (2017). https://doi.org/10.1186/s12859-016-1440-8
3. Anderson, A.C.: The process of structure-based drug design. Chem. Biol. **10**(9), 787–797 (2003). https://doi.org/10.1016/j.chembiol.2003.09.002. http://www.sciencedirect.com/science/article/pii/S1074552103001947
4. Bandola-Simon, J., Roche, P.A.: Dysfunction of antigen processing and presentation by dendritic cells in cancer. Mol. Immunol. (2018). http://www.sciencedirect.com/science/article/pii/S0161589018301044
5. Evans, W.E., Guy, R.K.: Gene expression as a drug discovery tool. Nat. Genet. **36**(3), 214–215 (2004). https://doi.org/10.1038/ng0304-214
6. Farhadi, T.: Advances in protein tertiary structure prediction. Biomed. Biotechnol. Res. J. (BBRJ) **2**(1), 20 (2018). https://doi.org/10.4103/bbrj.bbrj_94_17
7. Farazi, T.A., Horlings, H.M., ten Hoeve, J.J., Mihailovic, A., Halfwerk, H., Morozov, P., Brown, M., Hafner, M., Reyal, F., van Kouwenhove, M., Kreike, B., Sie, D., Hovestadt, V., Wessels, L.F., van de Vijver, M.J., Tuschl, T.: MicroRNA sequence and expression analysis in breast tumors by deep sequencing. Cancer Res. **71**(13), 4443–4453 (2011). http://cancerres.aacrjournals.org/content/71/13/4443
8. Jareborg, N., Birney, E., Durbin, R.: Comparative analysis of noncoding regions of 77 orthologous mouse and human gene pairs. Genome Res. **9**(9), 815–824 (1999). http://genome.cshlp.org/content/9/9/815.abstract

9. Jin, H.Y., Gonzalez-Martin, A., Miletic, A.V., Lai, M., Knight, S., Sabouri-Ghomi, M., Head, S.R., Macauley, M.S., Rickert, R.C., Xiao, C.: Transfection of microRNA mimics should be used with caution. Front. Genet. **6**, 340 (2015). https://www.frontiersin.org/article/10.3389/fgene.2015.00340
10. Jonic, S., Vénien-Bryan, C.: Protein structure determination by electron cryo-microscopy. Curr. Opin. Pharmacol. **9**(5), 636–642 (2009). https://doi.org/10.1016/j.coph.2009.04.006
11. Lachmann, A., Rouillard, A.D., Monteiro, C.D., Gundersen, G.W., Jagodnik, K.M., Jones, M.R., Kuleshov, M.V., McDermott, M.G., Fernandez, N.F., Duan, Q., Jenkins, S.L., Koplev, S., Wang, Z., Ma'ayan, A.: Enrichr: a comprehensive gene set enrichment analysis web server 2016 update. Nucleic Acids Res. **44**(W1), W90–W97 (2016).https://dx.doi.org/10.1093/nar/gkw377
12. Maglott, D., Ostell, J., Pruitt, K.D., Tatusova, T.: Entrez gene: gene-centered information at NCBI. Nucleic Acids Res. **39**(suppl_1), D52–D57 (2011). http://dx.doi.org/10.1093/nar/gkq1237
13. Merritt, M.A., Cramer, D.W.: Molecular pathogenesis of endometrial and ovarian cancer. Cancer Biomark. **9**(1–6), 287–305 (2011). https://doi.org/10.3233/cbm-2011-0167
14. Moustafa, A.A., Gilbertson, M.W., Orr, S.P., Herzallah, M.M., Servatius, R.J., Myers, C.E.: A model of amygdala-hippocampal-prefrontal interaction in fear conditioning and extinction in animals. Brain Cogn. **81**(1), 29–43 (2013). http://www.sciencedirect.com/science/article/pii/S0278262612001418
15. National Toxicology Program: DrugMatrix (2010). https://ntp.niehs.nih.gov/drugmatrix/index.html
16. Patalano, S., Vlasova, A., Wyatt, C., Ewels, P., Camara, F., Ferreira, P.G., Asher, C.L., Jurkowski, T.P., Segonds-Pichon, A., Bachman, M., González-Navarrete, I., Minoche, A.E., Krueger, F., Lowy, E., Marcet-Houben, M., Rodriguez-Ales, J.L., Nascimento, F.S., Balasubramanian, S., Gabaldon, T., Tarver, J.E., Andrews, S., Himmelbauer, H., Hughes, W.O.H., Guigó, R., Reik, W., Sumner, S.: Molecular signatures of plastic phenotypes in two eusocial insect species with simple societies. Proc. Natl. Acad. Sci. **112**(45), 13970–13975 (2015). https://www.pnas.org/content/112/45/13970
17. Pepper, S.D., Saunders, E.K., Edwards, L.E., Wilson, C.L., Miller, C.J.: The utility of mas5 expression summary and detection call algorithms. BMC Bioinf. **8**(1), 273 (2007). https://doi.org/10.1186/1471-2105-8-273
18. Qu, Y., He, F., Chen, Y.: Different effects of the probe summarization algorithms PLIER and RMA on high-level analysis of affymetrix exon arrays. BMC Bioinf. **11**(1), 211 (2010). https://doi.org/10.1186/1471-2105-11-211
19. Roider, H.G., Pavlova, N., Kirov, I., Slavov, S., Slavov, T., Uzunov, Z., Weiss, B.: Drug2gene: an exhaustive resource to explore effectively the drug-target relation network. BMC Bioinfor. **15**(1), 68 (2014). https://doi.org/10.1186/1471-2105-15-68
20. Subramanian, A., Narayan, R., Corsello, S.M., Peck, D.D., Natoli, T.E., Lu, X., Gould, J., Davis, J.F., Tubelli, A.A., Asiedu, J.K., Lahr, D.L., Hirschman, J.E., Liu, Z., Donahue, M., Julian, B., Khan, M., Wadden, D., Smith, I.C., Lam, D., Liberzon, A., Toder, C., Bagul, M., Orzechowski, M., Enache, O.M., Piccioni, F., Johnson, S.A., Lyons, N.J., Berger, A.H., Shamji, A.F., Brooks, A.N., Vrcic, A., Flynn, C., Rosains, J., Takeda, D.Y., Hu, R., Davison, D., Lamb, J., Ardlie, K., Hogstrom, L., Greenside, P., Gray, N.S., Clemons, P.A., Silver, S., Wu, X., Zhao, W.N., Read-Button, W., Wu, X., Haggarty, S.J., Ronco, L.V., Boehm, J.S., Schreiber, S.L., Doench, J.G., Bittker, J.A., Root, D.E., Wong, B., Golub, T.R.: A next generation connectivity map: L1000 platform and the first 1,000,000 profiles. Cell **171**(6), 1437–1452.e17 (2017). https://doi.org/10.1016/j.cell.2017.10.049. http://www.sciencedirect.com/science/article/pii/S0092867417313090
21. Suzuki, A., Kawano, S., Mitsuyama, T., Suyama, M., Kanai, Y., Shirahige, K., Sasaki, H., Tokunaga, K., Tsuchihara, K., Sugano, S., Nakai, K., Suzuki, Y.: DBTSS/DBKERO for integrated analysis of transcriptional regulation. Nucleic Acids Res. **46**(D1), D229–D238 (2018). http://dx.doi.org/10.1093/nar/gkx1001

22. Taguchi, Y.H.: One-class differential expression analysis using tensor decomposition-based unsupervised feature extraction applied to integrated analysis of multiple omics data from 26 lung adenocarcinoma cell lines. In: 2017 IEEE 17th International Conference on Bioinformatics and Bioengineering (BIBE), pp. 131–138 (2017). https://doi.org/10.1109/BIBE.2017.00-66
23. Taguchi, Y.H.: Tensor decomposition-based unsupervised feature extraction applied to matrix products for multi-view data processing. PLoS One **12**(8), 1–36 (2017). https://doi.org/10.1371/journal.pone.0183933
24. Taguchi, Y.H.: Tensor decomposition-based unsupervised feature extraction identifies candidate genes that induce post-traumatic stress disorder-mediated heart diseases. BMC Med. Genom. **10**(4), 67 (2017).https://doi.org/10.1186/s12920-017-0302-1
25. Taguchi, Y.H.: Tensor decomposition-based and principal-component-analysis-based unsupervised feature extraction applied to the gene expression and methylation profiles in the brains of social insects with multiple castes. BMC Bioinfor. **19**(4), 99 (2018). https://doi.org/10.1186/s12859-018-2068-7
26. Taguchi, Y.H.: Tensor decomposition-based unsupervised feature extraction can identify the universal nature of sequence-nonspecific off-target regulation of MRNA mediated by microRNA transfection. Cells **7**(6) (2018). http://www.mdpi.com/2073-4409/7/6/54
27. Taguchi, Y.H.: Drug candidate identification based on gene expression of treated cells using tensor decomposition-based unsupervised feature extraction for large-scale data. BMC Bioinfor. **19**(13), 388 (2019). https://doi.org/10.1186/s12859-018-2395-8
28. Tomczak, K., Czerwińska, P., Wiznerowicz, M.: The Cancer Genome Atlas (TCGA): an immeasurable source of knowledge. Contemp. Oncol. **19**, 68–77 (2015).http://dx.doi.org/10.5114/wo.2014.47136
29. Weiner, S.A., Toth, A.L.: Epigenetics in social insects: a new direction for understanding the evolution of castes. Genet. Res. Int. **2012**, 1–11 (2012). https://doi.org/10.1155/2012/609810
30. Xie, X., Luo, X., Xie, M., Liu, Y., Wu, T.: Risk of lung cancer in Parkinson's disease. Oncotarget **7**(47) (2016). https://doi.org/10.18632/oncotarget.12964
31. Yamanishi, Y., Kotera, M., Moriya, Y., Sawada, R., Kanehisa, M., Goto, S.: DINIES: drug-target interaction network inference engine based on supervised analysis. Nucleic Acids Res. **42**(W1), W39–W45 (2014). http://dx.doi.org/10.1093/nar/gku337
32. Yan, H., Bonasio, R., Simola, D.F., Liebig, J., Berger, S.L., Reinberg, D.: DNA methylation in social insects: How epigenetics can control behavior and longevity. Annu. Rev. Entomol. **60**(1), 435–452 (2015). https://doi.org/10.1146/annurev-ento-010814-020803. PMID: 25341091
33. Yoo, M., Shin, J., Kim, J., Ryall, K.A., Lee, K., Lee, S., Jeon, M., Kang, J., Tan, A.C.: DSigDB: drug signatures database for gene set analysis. Bioinformatics **31**(18), 3069–3071 (2015). http://dx.doi.org/10.1093/bioinformatics/btv313

Appendix A
Various Implementations of TD

A.1 Introduction

Because TD is not a major technology, it might not be easy to find implementation of TDs. Thus, we list a few of implementations in various platforms.

A.2 R

R is a major language used for data science. It has various implementations of TD.

A.2.1 rTensor

It is a part of CRAN. `rTensor`[1] can be installed via standard install command, `install.packages`. It includes the following:

- `hosvd` that executes Tucker decomposition using HOSVD algorithm.
- `cp` that executes CP decomposition.
- `tucker` that executes Tucker decomposition using HOOI algorithm.

[1] https://cran.r-project.org/web/packages/rTensor/index.html.

Y-h. Taguchi, *Unsupervised Feature Extraction Applied to Bioinformatics*,
Unsupervised and Semi-Supervised Learning,
https://doi.org/10.1007/978-3-030-22456-1

A.2.2 ttTensor

It is a part of CRAN. `ttTensor`[2]

- `TTSVD` that executes tensor train decomposition.

A.3 Python

Python is a script language, which is recently adopted to machine learning.

A.3.1 HOTTBOX

HOTTBOX: Higher Order Tensors ToolBOX[3]

- `HOSVD` that executes Tucker decomposition using HOSVD algorithm.
- `CPD` that executes CP decomposition.
- `HOOI` that executes Tucker decomposition using HOOI algorithm.
- `TTSVD` that executes tensor train decomposition.

A.4 MATLAB

MATLAB is a software that aims matrix manipulations.

A.4.1 Tensor Toolbox

Tensor Toolbox[4]

- `hosvd` that executes Tucker decomposition using HOSVD algorithm.
- `cp_als` that executes CP decomposition.
- `tucker_als` that executes Tucker decomposition using HOOI algorithm.

[2] https://cran.r-project.org/web/packages/ttTensor/index.html.

[3] https://hottbox.github.io/stable/index.html.

[4] http://www.tensortoolbox.org.

A.5 julia

julia is a script language that mainly aims statistical analysis.

A.5.1 TensorDecompositions.jl

TensorDecompositions.jl[5] is a package that aims tensor decompositions.

- `hosvd` that executes Tucker decomposition using HOSVD algorithm.
- `candecomp` that executes CP decomposition.

A.6 TensorFlow

TensorFlow is a library for deep learning.

A.6.1 t3f

t3f[6] is a package that aims tensor train decomposition.

[5] https://github.com/yunjhongwu/TensorDecompositions.jl.

[6] https://github.com/Bihaqo/t3f.

Appendix B
List of Published Papers Related to the Methods

Here is a comprehensive list of my papers where I applied PCA and TD based unsupervised FE to various topics in genomic science. Some of them were also cited in the preceding individual chapters.

References

1. Ishida, S., Umeyama, H., Iwadate, M., Taguchi, Y.H.: Bioinformatic screening of autoimmune disease genes and protein structure prediction with FAMS for drug discovery. Protein Pept. Lett. **21**(8), 828–39 (2014). http://dx.doi.org/10.2174/09298665113209990052
2. Kinoshita, R., Iwadate, M., Umeyama, H., Taguchi, Y.H.: Genes associated with genotype-specific DNA methylation in squamous cell carcinoma as candidate drug targets. BMC Syst. Biol. **8**(Suppl. 1), S4 (2014). http://doi.org/10.1186/1752-0509-8-S1-S4
3. Murakami, Y., Toyoda, H., Tanahashi, T., Tanaka, J., Kumada, T., Yoshioka, Y., Kosaka, N., Ochiya, T., Taguchi, Y.H.: Comprehensive miRNA expression analysis in peripheral blood can diagnose liver disease. PLoS One **7**(10), e48366 (2012). http://doi.org/10.1371/journal.pone.004836
4. Murakami, Y., Tanahashi, T., Okada, R., Toyoda, H., Kumada, T., Enomoto, M., Tamori, A., Kawada, N., Taguchi, Y.H., Azuma, T.: Comparison of hepatocellular carcinoma miRNA expression profiling as evaluated by next generation sequencing and microarray. PLoS One **9**(9), e106314 (2014). http://doi.org/10.1371/journal.pone.0106314
5. Murakami, Y., Kubo, S., Tamori, A., Itami, S., Kawamura, E., Iwaisako, K., Ikeda, K., Kawada, N., Ochiya, T., Taguchi, Y.H.: Comprehensive analysis of transcriptome and metabolome analysis in Intrahepatic Cholangiocarcinoma and Hepatocellular Carcinoma. Sci. Rep. **5**, 16294 (2015). http://doi.org/10.1038/srep16294
6. Taguchi, Y.H.: Integrative analysis of gene expression and promoter methylation during reprogramming of a non-small-cell lung cancer cell line using principal component analysis-based unsupervised feature extraction. In: Intelligent Computing in Bioinformatics, pp. 445–455. Springer International Publishing, Cham (2014). http://doi.org//10.1007/978-3-319-09330-7_52

Y-h. Taguchi, *Unsupervised Feature Extraction Applied to Bioinformatics*,
Unsupervised and Semi-Supervised Learning,
https://doi.org/10.1007/978-3-030-22456-1

7. Taguchi, Y.H.: Identification of aberrant gene expression associated with aberrant promoter methylation in primordial germ cells between E13 and E16 rat F3 generation vinclozolin lineage. BMC Bioinf. **16**(Suppl. 18), S16 (2015). http://doi.org/10.1186/1471-2105-16-S18-S16
8. Taguchi, Y.H.: Identification of more feasible MicroRNA-mRNA interactions within multiple cancers using principal component analysis based unsupervised feature extraction. Int. J. Mol. Sci. **17**(5), 696 (2016). http://doi.org/10.3390/ijms17050696
9. Taguchi, Y.H.: microRNA-mRNA interaction identification in Wilms tumor using principal component analysis based unsupervised feature extraction. In: The 16th Annual IEEE International Conference on Bioinformatics and Bioengineering (2016). http://doi.org/10.1109/BIBE.2016.14
10. Taguchi, Y.H.: Principal component analysis based unsupervised feature extraction applied to budding yeast temporally periodic gene expression. BioData Min. **9**, 22 (2016). http://doi.org/10.1186/s13040-016-0101-9
11. Taguchi, Y.H.: Principal component analysis based unsupervised feature extraction applied to publicly available gene expression profiles provides new insights into the mechanisms of action of histone deacetylase inhibitors. Neuroepigenetics **8**, 1–18 (2016). http://doi.org/10.1016/j.nepig.2016.10.001
12. Taguchi, Y.H.: Identification of candidate drugs for heart failure using tensor decomposition-based unsupervised feature extraction applied to integrated analysis of gene expression between heart failure and DrugMatrix datasets. In: Intelligent Computing Theories and Application, pp. 517–528. Springer International Publishing, Cham (2017). http://doi.org/10.1007/978-3-319-63312-1_45
13. Taguchi, Y.H.: Identification of candidate drugs using tensor-decomposition-based unsupervised feature extraction in integrated analysis of gene expression between diseases and drugmatrix datasets. Sci. Rep. **7**(1), 13733 (2017). http://doi.org/10.1038/s41598-017-13003-0
14. Taguchi, Y.H.: One-class differential expression analysis using tensor decomposition-based unsupervised feature extraction applied to integrated analysis of multiple omics data from 26 lung adenocarcinoma cell lines. In: 2017 IEEE 17th International Conference on Bioinformatics and Bioengineering (BIBE), pp. 131–138 (2017). http://doi.org/10.1109/BIBE.2017.00-66
15. Taguchi, Y.H.: Principal components analysis based unsupervised feature extraction applied to gene expression analysis of blood from dengue haemorrhagic fever patients. Sci. Rep. **7**, 44016 (2017). http://doi.org/10.1038/srep44016
16. Taguchi, Y.H.: Tensor decomposition-based unsupervised feature extraction applied to matrix products for multi-view data processing. PLoS One **12**(8), e0183933 (2017). http://doi.org/10.1371/journal.pone.0183933
17. Taguchi, Y.H.: Tensor decomposition-based unsupervised feature extraction identifies candidate genes that induce post-traumatic stress disorder-mediated heart diseases. BMC Med. Genom. **10**(Suppl. 4), 67 (2017). http://doi.org/10.1186/s12920-017-0302-1
18. Taguchi, Y.H.: Principal component analysis-based unsupervised feature extraction applied to single-cell gene expression analysis. In: Huang, D.S., Jo, K.H., Zhang, X.L. (eds.) Intelligent Computing Theories and Application, pp. 816–826. Springer International Publishing, Cham (2018). http://doi.org/10.1007/978-3-319-95933-7_90
19. Taguchi, Y.H.: Tensor decomposition-based unsupervised feature extraction can identify the universal nature of sequence-nonspecific off-target regulation of mRNA mediated by microRNA transfection. Cells **7**(6), 54 (2018). http://doi.org/10.3390/cells7060054. http://www.mdpi.com/2073-4409/7/6/54
20. Taguchi, Y.H.: Tensor decomposition/principal component analysis based unsupervised feature extraction applied to brain gene expression and methylation profiles of social insects with multiple castes. BMC Bioinf. **19**(Suppl. 4), 99 (2018). http://doi.org/10.1186/s12859-018-2068-7

21. Taguchi, Y.H.: Drug candidate identification based on gene expression of treated cells using tensor decomposition-based unsupervised feature extraction for large-scale data. BMC Bioinf. **19**(13), 388 (2019). https://doi.org/10.1186/s12859-018-2395-8
22. Taguchi, Y.H., Murakami, Y.: Principal component analysis based feature extraction approach to identify circulating microRNA biomarkers. PLoS One **8**(6), e66714 (2013). http://doi.org/10.1371/journal.pone.0066714
23. Taguchi, Y.H., Murakami, Y.: Universal disease biomarker: can a fixed set of blood microRNAs diagnose multiple diseases? BMC. Res. Notes **7**(1), 581 (2014). http://doi.org/10.1186/1756-0500-7-581
24. Taguchi, Y.H., Ng, K.: Tensor decomposition-based unsupervised feature extraction for integrated analysis of TCGA data on microRNA expression and promoter methylation of genes in ovarian cancer. In: 2018 IEEE 18th International Conference on Bioinformatics and Bioengineering (BIBE), pp. 195–200 (2018). http://doi.org/10.1109/BIBE.2018.00045
25. Taguchi, Y.H., Wang, H.: Genetic association between amyotrophic lateral sclerosis and cancer. Genes **8**(10), 243 (2017). http://doi.org/10.3390/genes8100243. http://www.mdpi.com/2073-4425/8/10/243
26. Taguchi, Y.H., Wang, H.: Exploring microRNA biomarker for amyotrophic lateral sclerosis. Int. J. Mol. Sci. **19**(5) (2018). http://doi.org/10.3390/ijms19051318. http://www.mdpi.com/1422-0067/19/5/1318
27. Taguchi, Y.H., Wang, H.: Exploring microRNA biomarkers for Parkinson's disease from mRNA expression profiles. Cells **7**(12) (2018). http://doi.org/10.3390/cells7120245. http://www.mdpi.com/2073-4409/7/12/245
28. Taguchi, Y.H., Iwadate, M., Umeyama, H., Murakami, Y., Okamoto, A.: Heuristic principal component analysis-based unsupervised feature extraction and its application to bioinformatics. In: Big Data Analytics in Bioinformatics and Healthcare, pp. 138–162. IGI Global, Hershey (2014). http://doi.org/10.4018/978-1-4666-6611-5.ch007
29. Taguchi, Y.H., Iwadate, M., Umeyama, H.: Heuristic principal component analysis-based unsupervised feature extraction and its application to gene expression analysis of amyotrophic lateral sclerosis data sets. In: 2015 IEEE Conference on Computational Intelligence in Bioinformatics and Computational Biology (2015). http://doi.org/10.1109/CIBCB.2015.7300274
30. Taguchi, Y.H., Iwadate, M., Umeyama, H.: Principal component analysis-based unsupervised feature extraction applied to in silico drug discovery for posttraumatic stress disorder-mediated heart disease. BMC Bioinf. **16**, 139 (2015). http://doi.org/10.1186/s12859-015-0574-4
31. Taguchi, Y.H., Iwadate, M., Umeyama, H.: SFRP1 is a possible candidate for epigenetic therapy in non-small cell lung cancer. BMC Med. Genom. **9**(S1) (2016). https://doi.org/10.1186/s12920-016-0196-3
32. Taguchi, Y.H., Iwadate, M., Umeyama, H., Murakami, Y.: Principal component analysis based unsupervised feature extraction applied to bioinformatics analysis. In: Computational Methods with Applications in Bioinformatics Analysis, pp. 153–182. World Scientific, Singapore (2017). https://doi.org/10.1142/9789813207981_0008
33. Umeyama, H., Iwadate, M., Taguchi, Y.H.: TINAGL1 and B3GALNT1 are potential therapy target genes to suppress metastasis in non-small cell lung cancer. BMC Genom. **15**(Suppl. 9), S2 (2014). http://doi.org/10.1186/1471-2164-15-S9-S2

Glossary

Adjusted or corrected P-values P-values collected with considering multiple comparisons.

BH criterion One of the methods that collect P-values obtained by some statistical tests with considering multiple comparisons.

Categorical regression (analysis) Linear regression analysis that predict independent variables from class labels represented as dummy variables as dependent variables.

Cell division cycle The biological process that duplicates a cell into two. All living organisms must perform cell division, because it is the only way for them to increase the numbers.

Epigenetics The factor that can affect the amount of transcripts without modifying genomic (DNA) sequence. Typical examples are DNA methylation, histone modification, and non-coding RNAs.

Linear discriminant analysis The linear method that infers class labels from the given feature variables, which is also applicable to multiple classes.

Multiomics The integration of distinct omics data, e.g., gene expression, promoter methylation, metabolome, proteome, and SNP.

Sinusoidal regression Linear regression analysis assuming that a function obeys sinusoidal shapes.

χ^2 **distribution** The distribution that obeys sum of squared variables drawn from $\mathcal{N}(0, 1)$.

Y-h. Taguchi, *Unsupervised Feature Extraction Applied to Bioinformatics*,
Unsupervised and Semi-Supervised Learning,
https://doi.org/10.1007/978-3-030-22456-1

Solutions

Problems of Chap. 1

1.1

- book and pages
- water and temperature
- movie and running time
- stone and pieces
- human and height
- human and weight
- book and weight
- bottle and volume
- paper and thickness
- card and width

1.2 colors (red, blue, yellow, ...), nations (Japan, USA, ...), cities (Tokyo, Beijing, Paris, ...), towns (Atherton, Corte Madera, ...), foods (apple, fish, ...), names (Ben, Taro, ...), animals (lion, tiger, ...), plants (cherry, sunflower, ...), sports (baseball, football, ...), books (novel, fiction, ...)

1.3 $x+y+z$, $x-y-z$, $2x+3y-4z$, $x+y-z$, $x+2y+z$, $x-y+z$, $3z+2y+4z$, $2x+2y+2z$, $x+2y+z$, $x-y$

Y-h. Taguchi, *Unsupervised Feature Extraction Applied to Bioinformatics*,
Unsupervised and Semi-Supervised Learning,
https://doi.org/10.1007/978-3-030-22456-1

1.4

Persons	Weight
Ben	34 kg
Tom	45 kg
Mac	70 kg
Naomi	64 kg

1.5

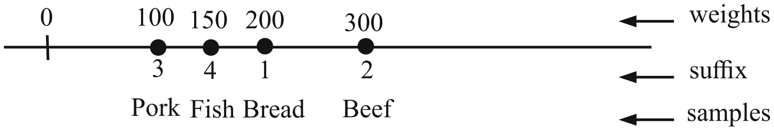

1.6 Euclidean distance between beef and bread is

$$\sqrt{(1000-100)^2+(300-200)^2} \simeq 906 \tag{B.1}$$

1.7

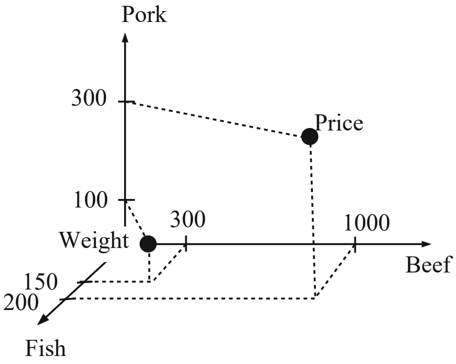

1.8

Here is a new feature, 2 × weight + 3 × price.

	Weight	Price	2 × weight + 3 × price
Bread	200	100	700
Beef	300	1000	3600
Pork	100	300	1100
Fish	150	200	900

1.9

Suppose, we would like to generate dummy vectors describing comic novels or movies as

Title	Hero	Heroine	Villain
Superman	Clark Kent	Lois Lane	Lex Luthor
Batman	Bruce Wayne	Vicki Vale	Joker
Spiderman	Peter Parker	Mary Jane Watson	Green Goblin

1.10

$$X = \begin{pmatrix} 200 & 300 & 100 & 150 \\ 1 & 10 & 3 & 2 \end{pmatrix} \tag{B.2}$$

1.11

$$\boldsymbol{x}_1 = (200, 1) \tag{B.3}$$

$$\boldsymbol{x}_2 = (300, 10) \tag{B.4}$$

$$\boldsymbol{x}_3 = (100, 3) \tag{B.5}$$

$$\boldsymbol{x}_4 = (150, 2) \tag{B.6}$$

or

$$\boldsymbol{x}_1 = (200, 300, 100, 150) \tag{B.7}$$

$$\boldsymbol{x}_2 = (1, 10, 3, 2) \tag{B.8}$$

1.12

$$X = \begin{pmatrix} 100 & 1000 & 300 & 200 \\ 200 & 300 & 100 & 150 \end{pmatrix} \tag{B.9}$$

and

$$A = \begin{pmatrix} 1 & \frac{1}{2} \\ \frac{1}{2} & 1 \end{pmatrix} \tag{B.10}$$

then

$$X' = AX = \begin{pmatrix} 200 & 1150 & 350 & 275 \\ 250 & 800 & 250 & 250 \end{pmatrix} \tag{B.11}$$

1.13

$$x_{1jk} = \begin{pmatrix} 1 & 2 & 3 \\ 4 & 5 & 6 \\ 7 & 8 & 9 \end{pmatrix} \tag{B.12}$$

$$x_{2jk} = \begin{pmatrix} 10 & 11 & 12 \\ 13 & 14 & 15 \\ 16 & 17 & 18 \end{pmatrix} \tag{B.13}$$

$$x_{3jk} = \begin{pmatrix} 19 & 20 & 21 \\ 22 & 23 & 24 \\ 25 & 26 & 27 \end{pmatrix} \tag{B.14}$$

1.14

$$X = \begin{pmatrix} 1 & 2 & 3 & 4 & 5 & 6 & 7 & 8 & 9 \\ 10 & 11 & 12 & 13 & 14 & 15 & 16 & 17 & 18 \\ 19 & 20 & 21 & 22 & 23 & 24 & 25 & 26 & 27 \end{pmatrix} \tag{B.15}$$

1.15

The three-mode tensor defined in exercise 1-13 is used as $\mathcal{X}$. A is supposed to be

$$\begin{pmatrix} 1 & 1 & 1 \\ 1 & 1 & 1 \\ 1 & 1 & 1 \end{pmatrix} \tag{B.16}$$

then

$$(A \times_i \mathcal{X})_{1jk} = (A \times_i \mathcal{X})_{2jk} = (A \times_i \mathcal{X})_{3jk} = \begin{pmatrix} 30 & 39 & 48 \\ 33 & 42 & 51 \\ 36 & 45 & 54 \end{pmatrix} \tag{B.17}$$

1.16

$$\boldsymbol{a} = (1, 2, 3) \tag{B.18}$$

and

$$\boldsymbol{b} = (4, 5, 6) \tag{B.19}$$

then

$$\boldsymbol{a} \times^0 \boldsymbol{b} = \begin{pmatrix} 4 & 5 & 6 \\ 8 & 10 & 12 \\ 12 & 15 & 18 \end{pmatrix} \tag{B.20}$$

Problems of Chap. 2

2.1

$$A = \begin{pmatrix} 0 & 1 & 0 \\ 0 & 0 & 1 \\ 1 & 0 & 0 \end{pmatrix} \tag{B.21}$$

$$B = \begin{pmatrix} 0 & 0 & 1 \\ 1 & 0 & 0 \\ 0 & 1 & 0 \end{pmatrix} \tag{B.22}$$

2.2

$$F = \begin{pmatrix} 350 & 87.5 & 400 & 400 \\ -100 & 37.5 & -250 & 425 \\ 250 & 137.5 & 400 & 450 \\ 300 & 112.5 & 450 & -225 \end{pmatrix} \tag{B.23}$$

2.3

$$U = \begin{pmatrix} -0.5 & -0.5 \\ -0.5 & -0.5 \\ 0.5 & -0.5 \\ -0.5 & 0.5 \end{pmatrix} \tag{B.24}$$

$$\Sigma = \begin{pmatrix} 2 & 0 \\ 0 & 2 \end{pmatrix} \tag{B.25}$$

$$V = \begin{pmatrix} -1 & 0 \\ 0 & -1 \end{pmatrix} \tag{B.26}$$

2.4

$$S = \begin{pmatrix} 0 & 0 & 0 & 0 \\ 0 & 0 & 0 & 0 \\ 0 & 0 & 2 & -2 \\ 0 & 0 & -2 & 2 \end{pmatrix} \tag{B.27}$$

then

$$U = \begin{pmatrix} 0 & 0 & 0 & 1 \\ 0 & 0 & 1 & 0 \\ -\frac{1}{\sqrt{2}} & \frac{1}{\sqrt{2}} & 0 & 0 \\ \frac{1}{\sqrt{2}} & \frac{1}{\sqrt{2}} & 0 & 0 \end{pmatrix} \tag{B.28}$$

and

$$SU = \begin{pmatrix} 0 & 0 & 0 & 0 \\ 0 & 0 & 0 & 0 \\ -2\sqrt{2} & 0 & 0 & 0 \\ 2\sqrt{2} & 0 & 0 & 0 \end{pmatrix} \tag{B.29}$$

2.5 They differ from each other because of mean extraction.

2.6

$$X^T U = \begin{pmatrix} \sqrt{2} & 0 & 0 & 0 \\ -\sqrt{2} & 0 & 0 & 0 \end{pmatrix} \tag{B.30}$$

Thus variance along the first direction is 4. Others are zero.

2.7 Residuals are zero.

2.8

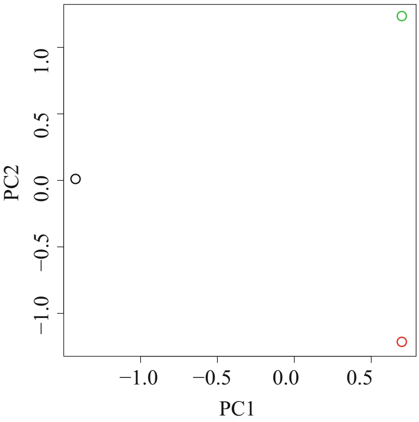

The first vs the second PC scores. Black open circle: $1 \le i \le 3$, red open circle: $4 \le i \le 6$, green open circle: $7 \le i \le 9$.

Problems of Chap. 3

3.1

Suppose $\boldsymbol{u} = (1, 1, 1)$ and $\mathcal{X}$ is a tensor whose component is $x_{ijk} = 1$. Then,

$$\mathcal{X} = \boldsymbol{u} \times^0 \boldsymbol{u} \times^0 \boldsymbol{u} \tag{B.31}$$

CP decomposition: In Eq. (3.1), $L = 1$, $\lambda_1 = 1$, $\boldsymbol{u}_1^{(i)} = \boldsymbol{u}_1^{(j)} = \boldsymbol{u}_1^{(k)} = \boldsymbol{u}$.

Tucker decomposition: In Eq. (3.2), $G(1, 1, 1) = 1$ and other Gs are zero. $\boldsymbol{u}_1^{(i)} = \boldsymbol{u}_1^{(j)} = \boldsymbol{u}_1^{(k)} = \boldsymbol{u}$. Other $\boldsymbol{u}_{\ell_1}^{(i)}, \boldsymbol{u}_{\ell_2}^{(j)}, \boldsymbol{u}_{\ell_3}^{(k)}$ are zero.

Tensor train decomposition: In Eq. (3.3), $R_1 = R_2 = 1$. $G^{(i)}(i, 1) = G^{(j)}(j, 1, 1) = G^{(k)}(k, 1) = 1$.

3.2

When we add the term with $\ell_1 = 1, \ell_2 = \ell_3 = 2$,

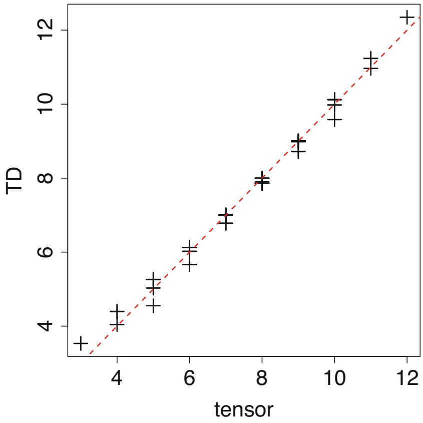

3.3

When $L = 2$,

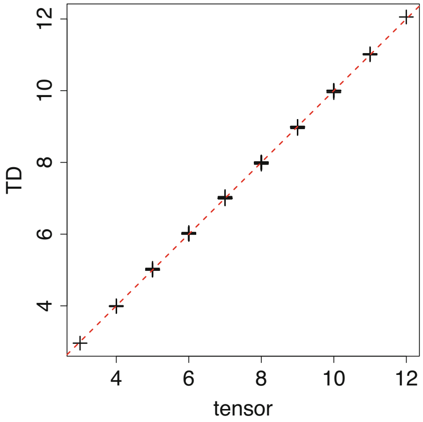

3.4 Because there are no ways to take partial summation of tensor train decomposition, we cannot draw something that corresponds to these figures.

3.5

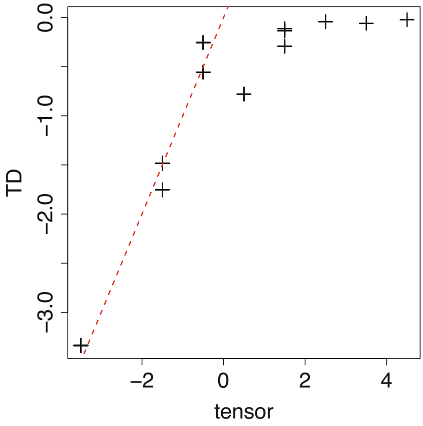

3.6

Assume

$$\mathcal{X} = \boldsymbol{a} \times^0 \boldsymbol{b} \times^0 \boldsymbol{c} \tag{B.32}$$

Then we get

$$a_1 b_1 c_1 = 1 \tag{B.33}$$

$$a_1 b_2 c_1 = 2 \tag{B.34}$$

$$a_2 b_1 c_1 = 3 \tag{B.35}$$

$$a_2 b_2 c_1 = 4 \tag{B.36}$$

$$a_1 b_1 c_2 = 5 \tag{B.37}$$

$$a_1 b_2 c_2 = 6 \tag{B.38}$$

$$a_2 b_1 c_2 = 7 \tag{B.39}$$

$$a_2 b_2 c_2 = 8 \tag{B.40}$$

From these, we get

$$a_1 = \frac{14}{(b_1 + b_2)(c_1 + c_2)} \tag{B.41}$$

$$a_2 = \frac{22}{(b_1 + b_2)(c_1 + c_2)} \tag{B.42}$$

$$b_1 = \frac{16}{(c_1+c_2)(a_1+a_2)} \tag{B.43}$$

$$b_2 = \frac{20}{(c_1+c_2)(a_1+a_2)} \tag{B.44}$$

$$c_1 = \frac{10}{(a_1+a_2)(b_1+b_2)} \tag{B.45}$$

$$c_2 = \frac{26}{(a_1+a_2)(b_1+b_2)} \tag{B.46}$$

Starting

$$\boldsymbol{a} = \boldsymbol{b} = \boldsymbol{c} = \begin{pmatrix} 1 \\ 1 \end{pmatrix} \tag{B.47}$$

In each iteration,

$$\boldsymbol{a} = \begin{pmatrix} \frac{7}{2} \\ \frac{11}{2} \end{pmatrix}, \boldsymbol{b} = \begin{pmatrix} 1 \\ 1 \end{pmatrix}, \boldsymbol{c} = \begin{pmatrix} 1 \\ 1 \end{pmatrix} \tag{B.48}$$

$$\boldsymbol{a} = \begin{pmatrix} \frac{7}{2} \\ \frac{11}{2} \end{pmatrix}, \boldsymbol{b} = \begin{pmatrix} \frac{8}{9} \\ \frac{10}{9} \end{pmatrix}, \boldsymbol{c} = \begin{pmatrix} 1 \\ 1 \end{pmatrix} \tag{B.49}$$

$$\boldsymbol{a} = \begin{pmatrix} \frac{7}{2} \\ \frac{11}{2} \end{pmatrix}, \boldsymbol{b} = \begin{pmatrix} \frac{8}{9} \\ \frac{10}{9} \end{pmatrix}, \boldsymbol{c} = \begin{pmatrix} \frac{5}{9} \\ \frac{13}{9} \end{pmatrix} \tag{B.50}$$

This is the converged solution.

3.7

$$X^{i\times(jk)} = \begin{pmatrix} 1 & 3 & 5 & 7 \\ 2 & 4 & 6 & 8 \end{pmatrix} \tag{B.51}$$

then

$$X^{i\times(jk)} \left(X^{i\times(jk)}\right)^T = \begin{pmatrix} 84 & 100 \\ 100 & 120 \end{pmatrix} = 4 \begin{pmatrix} 21 & 25 \\ 25 & 30 \end{pmatrix} \tag{B.52}$$

We would like to find eigenvalues and eigenvectors of $\begin{pmatrix} 21 & 25 \\ 25 & 30 \end{pmatrix}$. In order that, we need to solve eigen equation,

$$\begin{vmatrix} 21-\lambda & 25 \\ 25 & 30-\lambda \end{vmatrix} = 0 \tag{B.53}$$

$$(21-\lambda)(30-\lambda) - 25^2 = 0 \tag{B.54}$$

$$\lambda^2 - 51\lambda + 5 = 0 \tag{B.55}$$

$$\lambda = \frac{51 \pm \sqrt{2581}}{2} \tag{B.56}$$

On the other hand, if $\boldsymbol{u}$ is an eigenvector,

$$\begin{pmatrix} 21-\lambda & 25 \\ 25 & 30-\lambda \end{pmatrix} \begin{pmatrix} u_1 \\ u_2 \end{pmatrix} = 0 \tag{B.57}$$

then

$$u_1 = \frac{\lambda - 30}{25} u_2 \tag{B.58}$$

Since

$$\frac{\lambda - 30}{25} = \frac{-9 \pm \sqrt{2581}}{50} \tag{B.59}$$

thus

$$u_1 = \frac{-9 \pm \sqrt{2581}}{50} u_2 \tag{B.60}$$

In order that $|\boldsymbol{u}| = 1$,

$$u_1^2 + u_2^2 = 1 \tag{B.61}$$

$$\left\{ 1 + \left(\frac{-9 \pm \sqrt{2581}}{50} \right)^2 \right\} u_2^2 = 1 \tag{B.62}$$

$$u_1 = \frac{\pm 1}{\sqrt{1 + \left(\frac{-9 \pm \sqrt{2581}}{50} \right)^2}} \tag{B.63}$$

$$u_2 = \frac{\pm \frac{-9 \pm \sqrt{2581}}{50}}{\sqrt{1 + \left(\frac{-9 \pm \sqrt{2581}}{50} \right)^2}} \tag{B.64}$$

Then if we define

$$u_1^+ = \frac{1}{\sqrt{1+\left(\frac{-9+\sqrt{2581}}{50}\right)^2}} \tag{B.65}$$

$$u_2^+ = \frac{\frac{-9+\sqrt{2581}}{50}}{\sqrt{1+\left(\frac{-9+\sqrt{2581}}{50}\right)^2}} \tag{B.66}$$

$$u_1^- = \frac{1}{\sqrt{1+\left(\frac{-9-\sqrt{2581}}{50}\right)^2}} \tag{B.67}$$

$$u_2^- = \frac{\frac{-9-\sqrt{2581}}{50}}{\sqrt{1+\left(\frac{-9-\sqrt{2581}}{50}\right)^2}} \tag{B.68}$$

we can have

$$U^{(i)} = \begin{pmatrix} u_1^+ & u_1^- \\ u_2^+ & u_2^- \end{pmatrix} \tag{B.69}$$

using the representation of Eq. (3.55). With applying similar computation to

$$X^{j\times(ik)} = \begin{pmatrix} 1 & 2 & 5 & 6 \\ 3 & 4 & 7 & 8 \end{pmatrix} \tag{B.70}$$

and

$$X^{k\times(ij)} = \begin{pmatrix} 1 & 2 & 3 & 4 \\ 5 & 6 & 7 & 8 \end{pmatrix} \tag{B.71}$$

we can get $U^{(j)}$ and $U^{(k)}$ as well. Then G can be computed by

$$G = \mathcal{X} \times_{\ell_1} \left(U^{(i)}\right)^T \times_{\ell_2} \left(U^{(j)}\right)^T \times_{\ell_3} \left(U^{(k)}\right)^T \tag{B.72}$$

3.8

Equations (3.26)–(3.28) are solutions.

Index

Y-h. Taguchi, *Unsupervised Feature Extraction Applied to Bioinformatics*,
Unsupervised and Semi-Supervised Learning,
https://doi.org/10.1007/978-3-030-22456-1